Technical Report

TR-10-54

Comparative analysis of safety related site characteristics

Svensk Kärnbränslehantering AB

December 2010

Svensk Kärnbränslehantering AB
Swedish Nuclear Fuel
and Waste Management Co

Box 250, SE-101 24 Stockholm
Phone +46 8 459 84 00

ISSN 1404-0344
SKB TR-10-54
ID 1265223
Updated 2013-02

Comparative analysis of safety related site characteristics

Svensk Kärnbränslehantering AB

December 2010

Keywords: Site selection, Post-closure safety, Forsmark, Laxemar.

Update notice

The original report, dated December 2010, was found to contain both factual and editorial errors which have been corrected in this updated version. The corrected factual errors are presented below.

Updated 2013-02

Location	Original text	Corrected text
Appendix on CD – Appendix A1, page 13, Reference Smellie and Tullborg 2009	SKB R-08-11	SKB R-08-111

Preface

SKB has performed comprehensive investigations of two candidate sites for a final repository; in Forsmark (municipality of Östhammar) and in Laxemar (municipality of Oskarshamn). In June 2009 SKB decided to submit licence applications according to the Act on Nuclear Activities and the Environmental Code for a final repository at Forsmark. The license applications include comprehensive documentation to support that a KBS-3 repository at Forsmark will meet requirements in laws and regulations, including a full evaluation of long term safety.

In addition the licence applications contain documentation to motivate the selection of site for the final repository considering a wide range of siting factors. This document presents a comparative analysis of site characteristics related to long-term safety for the two candidate sites in Forsmark and in Laxemar. It supports the site selection presented and justified in the license applications for a final repository in Sweden.

This report has been edited by Johan Andersson. Several persons, within the SKB's team developing the long term safety assessment SR-Site have contributed to this report. In particular Jens-Ove Näslund (climate), Raymond Munier (earthquakes), Jan-Olof Selroos (hydrogeology), Sven Follin (hydrogeology), Ignasi Puigdomènech (chemistry), Tobias Lindborg with coworkers (surface environment) and Allan Hedin (risk assessment) have managed the supporting assessments and have provided the written input in their fields of expertise. A special thanks goes to Martin Löfgren, Niressa AB, who has edited Appendix A assessing the quality of the data used for this comparative assessment.

Stockholm, December 2010

Olle Olsson
Director of the Spent Fuel Project

Summary

This document presents a comparative analysis of site characteristics related to long-term safety for the two candidate sites for a final repository for spent nuclear fuel in Forsmark (municipality of Östhammar) and in Laxemar (municipality of Oskarshamn). The analyses performed have provided input to the site selection, from the perspective of long-term safety, and the present document constitutes the reporting of results and conclusions. Thus, the objective with this report is to:

- Present a set of analyses of factors of primary importance for assessment of site suitability with respect to long-term safety.
- Present conclusions on differences in suitability between the sites, or alternatively, state that such conclusions cannot be drawn based on this set of analyses.

A full evaluation of safety is made for a repository at the selected site in the safety assessment SR-Site /SKB 2011/, referred to as **SR-Site main report**. However, the analyses in SKB's previous safety assessment SR-Can shown to be important for long-term safety and with impacts potentially different depending on site properties are selected for re-assessment in this report, based on the updated site descriptions of Forsmark and Laxemar, together with associated updated repository layouts and designs. The basis for the comparison is thus the two equally and thoroughly assessed sites. Furthermore, the re-assessments take into account the assessment methodology evolution since SR-Can, and most of the supporting analyses for SR-Site, directly involving site specific data, are made for both sites, with the same approach and reported in joint supporting documents.

Based on experiences from SR-Can, a number of issues related to long-term safety need to be considered in the context of site comparison. Each of these factors is discussed in a dedicated chapter and overall conclusions are finally presented.

Regarding *the initial state*, the underground openings construction report /SKB 2010b/ shows that the proposed design, excavation and control procedures, will ensure that deposition tunnels and deposition holes accepted for disposal will meet the Design Premises as set out in /SKB 2009c/. However, based on the technical risk assessments presented in the Layout D2 reports it is expected that this would imply a substantially greater loss of potential deposition positions at Laxemar than at Forsmark, due to ahigher frequency of water conducting fractures at Laxemar. Furthermore, at Laxemar most deposition holes will be connected to a flowing fracture and it is expected that a large portion of the deposition tunnels would need to be grouted. At Forsmark, only few deposition holes will be connected to a flowing fracture and grouting is only expected to be needed at a few locations. Furthermore, compared to Forsmark, there would be many more accepted deposition positions that would have inflows close to the acceptability criterion and this has safety consequences.

Changing *climate conditions* may result in several phenomena that impact the Forsmark and Laxemar sites, including the formation of ice sheets and permafrost, changes in shore line displacement, surface weathering and erosion. However, the differences between the sites are not large enough to be of importance for the site selection, even if the process as such is important for the safety assessment. During cold periods without ice sheets at the sites, permafrost and freezing of ground water reach greater depths at Forsmark than at Laxemar. This is mainly due to differences in climate and in bedrock thermal properties. A larger vertical portion of the rock above the repository is subject to repeated freezing/thawing cycles at Forsmark compared to Laxemar. However, even for the most pessimistic case of, unrealistically combining all uncertainties as to favour permafrost development, freezing of free water at repository depth cannot take place at either of the sites. Furthermore, since the buffer clay would only freeze at temperatures below the freezing point of free water, buffer and backfill freezing can also be excluded at both Forsmark and Laxemar. Possible differences in potential for freezing between Laxemar and Forsmark have little significance for the potential of constructing a safe repository at any of the sites.

Rock mechanics conditions, including the potential for thermally induced spalling differ between the repository layouts adapted to the two sites. If rock stresses are high, an excavated rock surface may crack and form rock flakes in a phenomenon called spalling. Even if the initial rock stresses are not sufficient to produce spalling following excavation, there is still the possibility that spalling may occur later due to the additional thermal load. The potential occurrence of spalling is site and repository design specific, as it depends on the in situ stresses, the intact rock strength and the repository layout. The assessment of spalling potential shows that there is potential for thermally induced spalling at both sites, but the likelihood and extent of the spalling is much less at Laxemar. Spalling around deposition holes may have a considerable impact on mass exchange between flowing groundwater and the buffer as long as diffusion is the dominant transport mechanism in the buffer. However, significant releases of radionuclides from the repository only occur if advective conditions prevail in the buffer or if the canister is sheared due to earthquakes. For these conditions, the effects of spalling are insignificant. This implies that the occurrence of spalling would only affect risk to a very minor extent.

The input to the site selection process from the *hydrogeology* discipline includes relevant information extracted from the site descriptive models for Forsmark and Laxemar, respectively, and from subsequent consequence analyses. The flow-related transport performance measures may, for certain groundwater compositions affect the stability of the buffer and the canister, and are direct input for radionuclide transport calculations, and hence affect radionuclide discharge from near field and far field, as well as associated dose in biosphere and resulting risk. When the average conductive fracture frequency of the rock mass volumes between the deterministically modelled deformation zones is considered, it is observed that at Forsmark a clear distinction can be made between the rock above and below 400 m elevation, such that the rock above is significantly more fractured than below. At Laxemar, the average conductive fracture frequency at potential repository depth is much greater than at Forsmark and there is also a considerable spatial variability between different parts of considered rock mass volumes. When hydraulic characteristics at repository depth are compared in detail, it is found that Forsmark has a much lower average conductive fracture frequency (less than 0.01 m^{-1} compared to 0.06 m^{-1} to 0.23 m^{-1} at Laxemar). For the construction and operation phases, the calculated inflow at Laxemar is more than ten times larger than at Forsmark assuming a realistic grouting efficiency. The number of deposition holes with an inflow larger than 0.1 L/min during the excavation and operation phases, assuming a realistic grouting efficiency, is more than 30 times larger at Laxemar than at Forsmark. In the temperate period simulations, the Darcy flux at the deposition hole locations (for fractures intersecting deposition holes) is approximately two orders of magnitude larger at Laxemar than at Forsmark. When the flow-related transport resistance is considered, the values are higher at Forsmark than at Laxemar by approximately a factor of 30. Thus, both performance measures are more favourable at Forsmark than at Laxemar. In the glacial period simulations of an ice sheet in close proximity to the repository, the relative difference in Darcy flux at the deposition hole positions is approximately two orders of magnitude, with higher fluxes for Laxemar. In the glacial period simulations, the disturbance to the salinity field is more pronounced at Laxemar than at Forsmark. In conclusion, all hydrogeological measures and entities considered are in favour of Forsmark. However, it is noted that Laxemar exhibits slightly more favourable conditions than Forsmark concerning rock matrix characteristics (i.e. non-flow related migration parameters). The favourable properties for Laxemar in this respect are incorporated in the analysis of radionuclide transport and risk.

Chemical conditions affect the performance of a repository in a number of ways. Data on groundwater chemical compositions are needed to calculate the chemical evolution and physical stability of bentonite, the corrosion of canisters and the transport of radionuclides. In addition, the geochemical and mineralogical properties of the rocks and fracture-filling minerals will affect the transport of radionuclides and the penetration depth of dissolved oxygen in glacial meltwaters. At present, groundwater samples show lower salinity at Laxemar, when comparing the candidate repository depths of the two sites. Most future climatic changes will induce groundwater dilutions. During the next million years or so, a sea water body, similar to the Littorina or Baltic Seas is expected to cover the Forsmark site longer than the Laxemar site, due to differences in ice thickness and location of the repository sites. Furthermore, due to the low hydraulic conductivity of the repository volume at Forsmark, it is possible that the groundwater salinity at the target repository volume in Forsmark would remain at the present levels over the whole glacial cycle. In contrast, there will be a larger impact of the dilution processes resulting in lower salinities at Laxemar as a whole, and in the frac-

ture zones at Forsmark. At present the sulphide levels at Laxemar and Forsmark are not significantly different. The future evolution of sulphide concentrations is expected to be similar at both sites. The fracture filling mineral at both sites, mainly calcite, indicate a good pH buffering capacity in the fractures of both sites. The content of Fe(II) in the rock types at Laxemar is about twice as high as that at Forsmark. This can be an advantage for Laxemar with respect to the possibility of intrusion of oxygenated glacial meltwaters. However, the conceptual models of O_2 consumption by Fe(II) in the rock matrix show that the larger reducing capacity is more than compensated by lower transmissivity of the fractures at Forsmark.

Earthquake-triggered, fast shear movements along fractures intersecting a canister can affect the containment of the canister if the shear load exceeds the stated design premise regarding the canister ability to withstand shear movement, i.e. for slip exceeding 5 cm at a rate of 1 m/s or more. Glacially induced faulting occurs in glaciated regions in response to changes in the glacial load: either as a result of glacial advance (crustal loading) or deglaciation (crustal unloading). With few exceptions, glacially induced faults are unique in that they occur in regions where there is no evidence of surface rupture during historical time. In addition, these regions have no historical record of seismicity that approaches the magnitude thresholds for generating surface faulting. The potential for fault weakening and/or reactivation at the sites, as a response to future glaciations as well as the effect on a repository, should a large earthquake occur in the vicinity, has been assessed. Furthermore, the detrimental effects of a large earthquake near the repository can be avoided or considerably lessened by adaptive design involving the use of respect distance and deposition hole rejection criteria. Despite the lack of evidence for large earthquakes near the sites, such large earthquakes cannot be entirely disregarded as a risk factor. Computed stability margins of deformation zone models used to identify the zones most likely to reactivate during various periods of the glacier evolution combined with deposition hole rejection criteria, were used to assess the number of critical canister positions and thereby the contribution to radiation risk at each site. This analysis shows that despite differences in deformation zone and fracture geometries and frequencies, the difference between the sites is of the same order of magnitude as the difference due to the uncertainty in the fracture description for each site. Even though Laxemar has a lower number of critical positions compared with Forsmark, despite a generally higher fracture intensity, the difference is not sufficiently clear, given the uncertainties, to suggest that the risk of seismic impacts would be significantly less at Laxemar. The risk contribution from earthquakes is judged similar for both sites.

In order to mitigate the risk of future human intrusion, the rock suitability criteria, as set out by SKB in /Andersson et al. 2000/, requiring that the rock types in the deposition area do not have *ore potential* and do not contain such *valuable minerals* as to justify mining at a depth of hundreds of metres, has been considered. Neither of the sites has potential for ore, industrial minerals or commercial stones. It is noted that at Forsmark there are areas that bear this potential to the south-west of the candidate area, predominantly in the felsic to intermediate metavolcanic rocks. However, it is emphasised that the small iron mineralisations in this area are far away from the repository and have no current economic value. This latter judgement is also deemed to be valid in a long-term perspective.

The dose to humans and other biota is a key delivery in the safety assessment to prove that the performance fulfils the regulations. There are several site specific *biosphere aspects* that are important for the dose. The most important are the location of the discharge and the receiving ecosystem, which describes the food-chain, the land use and amounts of food and water produced and water-turnover rate. The ecosystem also affects the human utilisation and occupancy in the area where radionuclides can be released, which are important parameters in the dose assessment. The dose resulting from a unit release of a radionuclide, the landscape dose conversion factors (LDF) values, for Forsmark are very similar to calculated indicatory LDF values for Laxemar. The difference in total risk between the sites will depend on differences in radionuclide releases. However, there are some differences between the sites that can be of relevance for their comparison. The assessment indicates that the Forsmark site will be submerged under the sea or covered by ice for longer periods than Laxemar, most likely giving considerable lower doses for long time periods. Moreover, the potential for future agriculture in areas potentially affected by released radionuclides seems reduced for Forsmark.

Estimation of risk is the main output of the safety assessment. The analysis is divided into two parts: analysis of containment potential and analysis of retardation potential. The analysis shows that the safety functions for the buffer and the canister are breached for many more deposition holes at Laxemar than at Forsmark. At Forsmark only a small number of depositions holes will lose buffer material due to dilute groundwater such that advective conditions are reached. After one million years, 23 deposition holes reach advective conditions and for the initial temperate period few if any deposition holes will reach advective conditions. This yields a mean number of failed canisters of 0.087 at one million years assuming that the sulphide distribution is randomly combined with the flow rates for all the deposition holes. At Laxemar, nearly all deposition holes connected to a water conductive fracture (about 3,600 if applying the Extended Full Perimeter Criterion, EFPC, and about 4,200 if not applying EFPC) reach advective conditions in one million years, and about half of these holes reach these conditions within 100,000 years. This yields a mean number of failed canisters of 146 at one million years when the sulphide distribution is randomly combined with the flow rates for all the deposition holes.

The risk assessments thus imply that the calculated risk for Forsmark will be considerably lower than for Laxemar. This is a key result from the point of view of long-term safety, since the calculated risk is the primary acceptance measure according to Swedish regulations. Furthermore, the risk assessment for Laxemar suggests that for a repository at Laxemar, constructed according to the current reference design, the doses will exceed the regulatory limit some time after 100,000 years and eventually grow to a level comparable to that due to the background radiation. However, this does not necessarily mean that a safe repository could not be constructed at Laxemar, but then design modifications would be needed. To illustrate this option, hypothetical cases assuming that deposition holes with high Darcy fluxes could be completely avoided have also been analysed. This could in theory reduce dose, potentially enough to meet the regulatory limit. Another theoretical possibility would be to locate the repository at a depth, exceeding 700 m, where the frequency of water conducting fractures possibly is much lower than at higher elevation. However, in practice the cost in terms of losses of potential deposition holes and methodology to be developed and verified is potentially quite high.

The site descriptive models developed have good confidence for both sites. However, it must also be noted that the potential repository volume at Forsmark is more homogeneous, both in rock type distribution and in the occurrence of water conductive fractures, than the Laxemar site. This is judged to facilitate the acquirement of detailed information and development of understanding required to adopt the repository to local conditions during construction.

In summary, there are a number of safety related site characteristics for which the analyses do not show any decisive differences in terms of implications on safety, between the sites Forsmark and Laxemar. However, the frequency of water conducting fractures at repository depth is much larger at Laxemar than at Forsmark. This difference, in turn, affects the future stability of the current favourable groundwater composition, which combined with the much higher flows at Laxemar would, for the current repository design, lead to a breach in the safety functions for the buffer and the canister for many more deposition positions at Laxemar than at Forsmark. Thereby the calculated risk for Forsmark will be considerably lower than that for Laxemar. From the safety perspective, therefore, Forsmark is clearly the preferable option.

Contents

1 Introduction

This document presents a comparative analysis of site characteristics related to long-term safety for the two candidate sites for a final repository for spent nuclear fuel in Forsmark (municipality of Östhammar) and in Laxemar (municipality of Oskarshamn) from the point of view of site selection. The analyses are based on the updated site descriptions of Forsmark /SKB 2008a/ and Laxemar /SKB 2009a/, together with associated updated repository layouts and designs /SKB 2008b and SKB 2009b/. The basis for the comparison is thus two equally and thoroughly assessed sites. However, the analyses presented here are focussed on differences between the sites rather than evaluating them in absolute terms. The document serves as a basis for the site selection, from the perspective of long-term safety, in SKB's application for a final repository. A full evaluation of safety is made for a repository at the selected site in the safety assessment SR-Site /SKB 2011/, referred to as **SR-Site main report** in the following.

1.1 Objectives and scope

The objective with this report is to:

- Present a set of analyses of primary importance for assessment of site suitability with respect to long term safety.
- Present conclusions on differences in suitability between the sites, or alternatively, state that such conclusions cannot be drawn based on this set of analyses.

1.2 Identification of issues of primary importance for site suitability with respect to long-term safety

The criteria for judging the safety of the repository, are defined in regulations issued by the Swedish Radiation Safety Authority (SSM). The regulations are based on various pertinent components of framework legislation, the most important being the Nuclear Activities Act and the Radiation Protection Act. Guidance on radiation protection matters is provided by a number of international bodies, and national legislation is often, as in the case of Sweden, influenced by international recommendations. The following specific regulations are of special interest in this context:

- Protection of human health shall be demonstrated by compliance with a risk criterion that states that "the annual risk of harmful effects after closure does not exceed 10^{-6} for a representative individual in the group exposed to the greatest risk" /SSMFS 2008:37, 5 §/.
- Safety after the closure of a repository shall be maintained through a system of passive barriers /SSMFS 2008:21, 2 §/.
- The function of each barrier shall be to, in one or several ways, contribute to the containment, prevention or retardation of dispersion of radioactive substances, either directly, or indirectly by protecting other barriers in the barrier system /SSMFS 2008:21, 3§/.

Compliance to the regulations can strictly only be demonstrated by a safety assessment, as is done in **SR-Site main report**. However, experiences from the previous safety assessment SR-Can /SKB 2006a/, suggest that only a subset of all analyses included in a safety assessment really concern differences in site conditions. These mainly concern conditions for the initial state, the geosphere evolution as assessed in Chapter 9 of /SKB 2006a/ and retention in the far-field.

The analyses shown in SR-Can to be important for long-term safety and with impacts potentially different depending on site properties are selected for re-assessment in this report. The basis for this re-assessment are the updated site descriptions of Forsmark /SKB 2008a/ and Laxemar /SKB 2009a/, together with associated updated repository layouts and designs /SKB 2008b and SKB 2009b/. The basis for the comparison is thus two equally and thoroughly assessed sites. Furthermore, most of the supporting analyses for SR-Site directly involving site specific data from Forsmark, were also made for Laxemar and with the same approach. The evolution of the assessment methodology that has occurred since SR-Can is also taken into account.

1.2.1 Safety functions

SR-Can /SKB 2006a/ introduced the concept of safety functions. The safety functions and their indicators and criteria are used to structure and differentiate the evaluation of safety when the long-term evolution of the repository is evaluated. They also play a key role in the selection and analyses of scenarios. This concept has been further developed in SR-Site and some of the safety functions and the safety function indicators have evolved based on new knowledge gained. Following the definitions stated in the **SR-Site main report**, Chapter 8:

- A *safety function* is defined qualitatively as a role through which a repository component contributes to safety.
- A *safety function indicator* is a measurable or calculable quantity through which a safety function can be quantitatively evaluated.
- In order to determine whether a safety function is maintained or not, *safety function indicator criteria* are defined against which the safety function indicators can be evaluated over the time period covered by the safety assessment.

For more elaboration on these concepts, see **SR-Site main report** Chapter 8.

Since the SR-Site safety functions are a good basis for assessing the performance of the different repository subsystems, and thus also for site comparison, they are repeated here, such that easy reference to these safety functions can be made in this report. Two groups of safety functions are derived, safety functions with respect to containment and safety functions with respect to retardation, although most of the safety functions are relevant in both contexts. The safety function, and associated indicators and criteria for containment are summarised in Figure 1-1. The safety functions, and associated indicators and criteria for retardation are summarised in Figure 1-2.

1.2.2 Geosphere analyses of importance for the construction and operational stage

Rock mechanics

The **SR-Can main report** (Section 9.2.2) assessed the following mechanical processes related to the excavation and the open phase:

- Development of an Excavation Damaged Zone (EDZ) and other impacts on rock permeability (safety function R2ab).
- Spalling, (safety function R2b and also safety functions of the buffer that either directly or indirectly depend on buffer density).
- Reactivation of fractures (safety function R3b).
- Induced seismicity (safety function R3b).

Of these issues, SR-Can /SKB 2006a, Chapter 9/ showed that only the EDZ and spalling are potentially important for long-term safety. The impacts are essentially handled by adapting the repository design and layout to account for this, but some site specific differences on how this affects the initial state remains. This issue is thus potentially important for the initial state and are thus addressed in Chapter 2.

Hydraulic impacts

Repository excavation and operation imply a major impact on groundwater flow, since the excavated tunnels will be at atmospheric pressure resulting in inflow of water. The inflow will result in a redirection of flow and in changes of the groundwater flow pattern, potentially resulting in draw-down of the water table, infiltration of near-surface waters into the deeper parts of the bedrock, and in upconing of saline water from depth. The actual impacts primarily depend on the permeability distribution of the rock, the repository layout and on how tight the underground openings would be. The latter partly, in turn depends on the grouting efficiency. /SKB 2006a, Section 9.2.3/ assessed the effects of an open repository on site hydrogeological and hydrogeochemical conditions, i.e. safety functions R1 and R2.

The hydraulic impacts are primarily important for the environmental impact, whereas the long-term safety implications are limited, or at least not site specific.

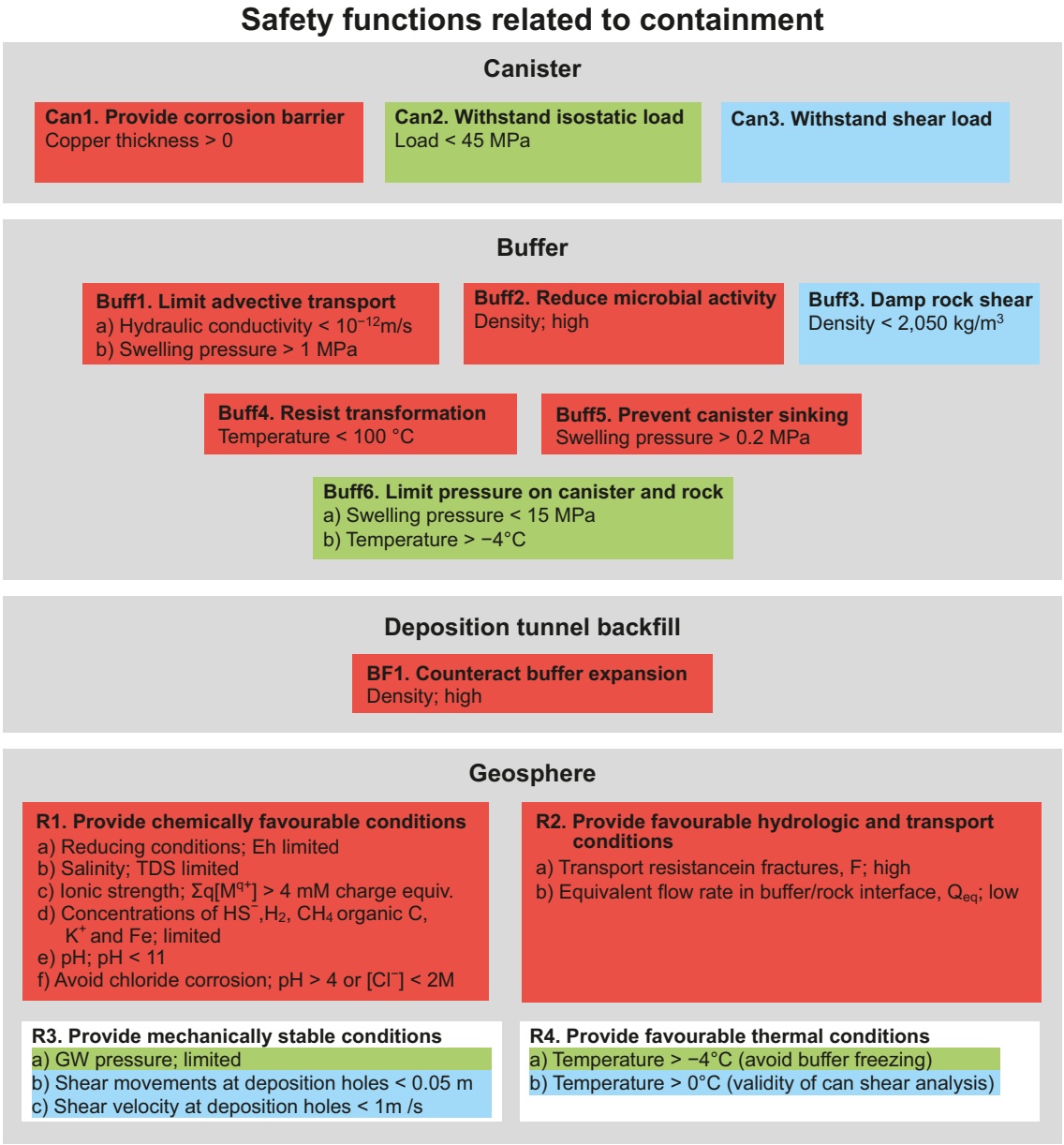

Figure 1-1. *Safety functions (bold), safety function indicators and safety function indicator criteria related to containment. Where quantitative criteria cannot be given, terms like "high", "low" and "limited" are used to indicate favourable values of the safety function indicators. The colour coding shows how the functions contribute to the canister safety functions Can1 (red), Can2 (green) and Can3 (blue). (From* ***SR-Site main report.****)*

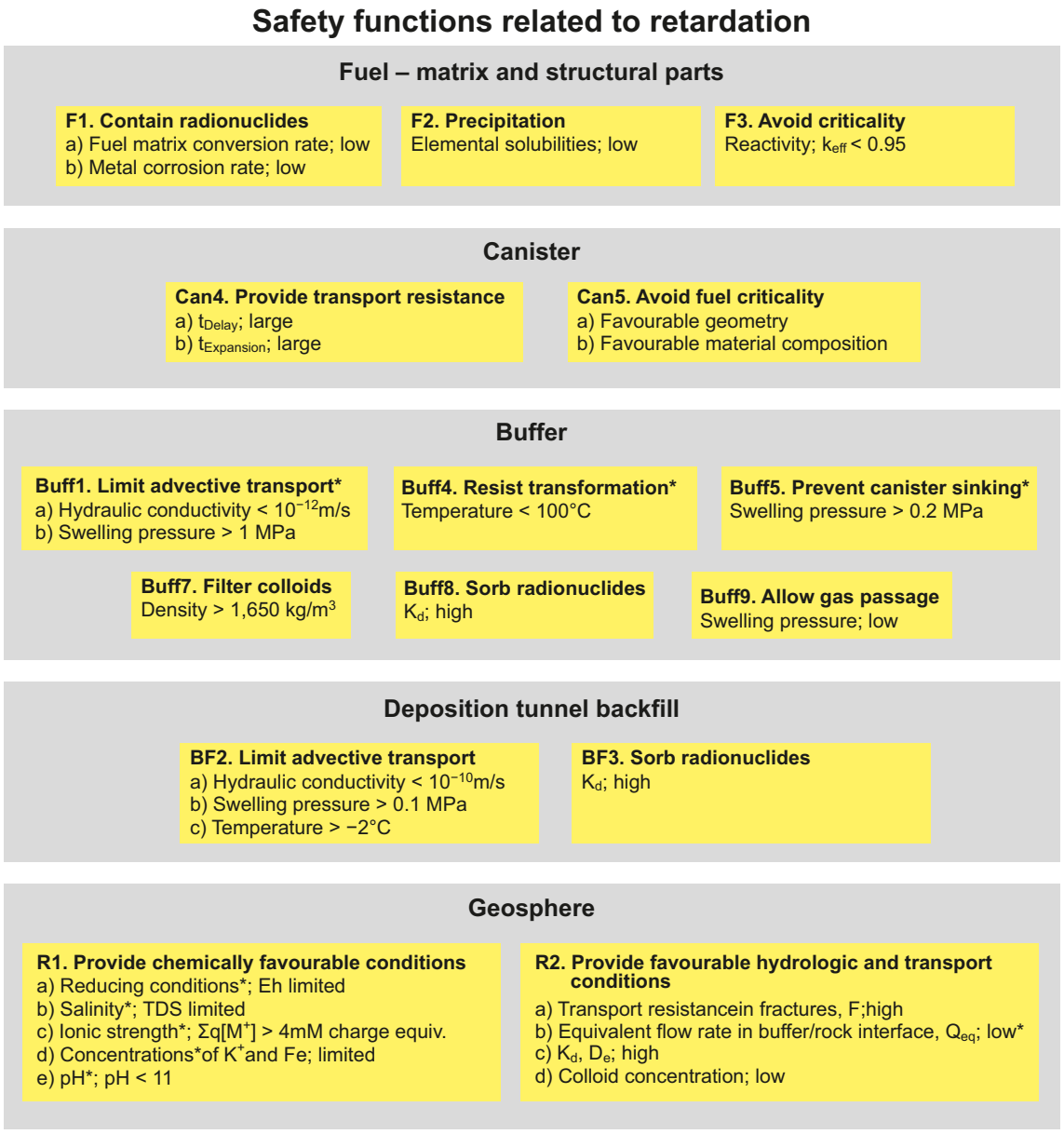

Figure 1-2. *Safety functions (bold), safety function indicators and safety function indicator criteria related to retardation. Where quantitative criteria cannot be given, terms like "high", "low" and "limited" are used to indicate favourable values of the safety function indicators. Safety functions marked with an asterisk (*) apply also to containment, see Figure 1-1. (From* ***SR-Site main report.****)*

Piping/erosion of buffer and backfill

SR-Can /SKB 2006a, Section 9.2.4/ also addressed piping and associated erosion effects in the buffer and backfill. Water inflow into the deposition holes and tunnels will take place mainly through fractures and will contribute to the wetting of the buffer and the backfill. If the inflow is localized to fractures that carry more water than the swelling bentonite can adsorb, there will be a water pressure in the fracture acting on the buffer. Since the swelling bentonite is initially a gel, with increasing density over time as water goes deeper into the bentonite, the gel may be too soft to stop the water inflow. The result may be piping in the bentonite, formation of a channel and a continuing water flow and erosion of soft bentonite gel. There will be a competition between the swelling rate of the bentonite and the flow through, and erosion rate of, the buffer.

The impacts of piping and erosion are essentially mitigated by different design measures, but site specific differences may remain. This is addressed in Chapter 2.

Chemical evolution in and around the repository

The changed hydraulic conditions, during the excavation and relatively long operational period, may alter the groundwater composition around the repository as assessed in /SKB 2006a, Section 9.2.5/. Some of these changes will be induced by the presence of the repository, but also shore-level displacements and climatic variations may cause more limited alterations. As a consequence, the salinity in some parts of the repository may decrease due to an increased infiltration of diluted waters of meteoric origin, whereas in other regions the corresponding up-coning might instead induce an increase in salinity. This involves the safety function indicators R1b and R1c.

The groundwater composition and its evolution during the operational phase may be different between the sites and these matters are discussed in Chapter 6 of this report. There are also other chemical effects, like impact of grouting, stray materials and the presence of oxygen assessed in /SKB 2006a, Section 9.2.5/. These impacts are not judged to be clearly different between the sites.

1.2.3 The initial period of temperate climate after closure

Thermal

The thermal evolution assessed in /SKB 2006a, Section 9.3.4/ concerned the thermal criterion on the buffer peak temperature, safety function indicator Buff4, that requires that this temperature does not exceed 100°C, chosen pessimistically in order to avoid, with a margin of safety, mineral transformations of the buffer.

The fulfilment of this requirement is ensured already by the repository design and layout /SKB 2009d, b/, where thermal calculations are done to determine the minimum allowed distance between deposition holes. Consequently, there is no reason to include this assessment in the current report. However, it can be noted that the generally lower thermal conductivity of the Laxemar site compared with Forsmark necessitates a larger distance between deposition holes, and thus a larger repository footprint.

Rock mechanics

SR-Can /SKB 2006a, Section 9.3.5/ assessed the following mechanical processes related to the initial temperate period after repository closure:

- Reactivation of fractures in the near field due to thermal load that could affect the mechanical stability (safety function R3b) and the fracture transmissivity in the near-field rock (safety function R2b).
- Reactivation of fractures in the far-field that could affect fracture transmissivity (safety function R2ab).
- Reactivation due to increased ridge push[1] that could affect the mechanical stability of the deposition holes (safety function R3b).
- Fracturing of the rock due to the thermal load that could affect the deposition hole geometry (safety function Buff1) and migration between buffer and rock (related to safety function R2b).
- Potential for creep deformation that could affect deposition hole geometry (related to safety function Buff1). Here the term creep is used also for cases in which the mechanical load is not constant over time, i.e. when the shear strain successively relaxes the stresses.

Of these processes only fracturing of the rock due to the thermal load (e.g. thermally induced spalling) that could affect the migration between buffer and rock (related to safety function R2b) was found to have any significance for safety. An updated assessment of this possibility is thus included in Chapter 4 of this report.

[1] Mid-ocean ridge push is a proposed mechanism for plate motion in plate tectonics.

Hydrogeology

SR-Can assessed the following hydrogeological processes related to the initial temperate period after repository closure (see /SKB 2006a, Section 9.3.6/):

- The analysis of the resaturation phase deals with effects of an initially open repository, i.e. a repository at atmospheric pressure, being water filled. The overall objective was to assess the implications of site hydrogeological and hydrogeochemical conditions on the repository saturation process, i.e. safety functions R1 and R2.
- After saturation of the repository, groundwater flow directions and magnitudes are of interest for studying transport of solutes potentially harmful to the repository, and for studying potential releases of radionuclides from defective canisters. Groundwater flow paths provide information on where in the bedrock transport would take place and where exfiltration to the biosphere occurs. Properties along flow paths provide information on transport and retention characteristics of potentially migrating radionuclides. The overall objective is to assess the implications of site hydrogeological and hydrogeochemical conditions on repository performance. Generally, this was assessed by simulating the groundwater flow, identifying migration paths and calculating travel time and transport resistance (F-factor) for these paths. Thus, the analysis is mainly related to the safety function R1 and R2ab.

Of these analyses, the assessment of flow related transport parameters was shown to be of importance for long-term safety. An update of these parameters is thus included in Chapter 5 of this report.

Chemical evolution in and around the repository

SR-Can /SKB 2006a, Section 9.3.7/ assessed the Chemical evolution in and around the repository for the initial temperate period after repository closure. The key question addressed for this period is whether the chemical environment will remain favourable after repository closure. The most important parameters are redox properties (safety function R1a) and salinity (safety function R1b and R1c). Other factors to consider are the groundwater content of potassium, sulphide and iron(II), as they might affect the chemical stability of the buffer and the canister (safety function R1d) and the effect of grouting in the geosphere and cementitous materials in the engineered barriers that could affect groundwater pH (safety function R1e).

An assessment of the chemical evolution in and around the repository for the initial temperate period after repository closure is potentially important. An update is thus included in Chapter 6 of this report.

1.2.4 Evolution for the remaining part of the reference glacial cycle

Thermal evolution

The thermal evolution during this glacial cycle is assessed in /SKB 2006a, Section 9.4.3/. The main factors of importance for repository safety in the periglacial climate domain are the permafrost and frozen depths, the depth of the isotherm at which the clay buffer freezes, the duration of permafrost or frozen conditions and the possible freezing out of salt that may result in a zone with high salinity beneath the frozen front.

SR-Can shows that the evolution of the permafrost depth is site and repository layout (depth) dependent. Such an analysis is thus potentially important as input to the site selection and is found in Chapter 3 of this report.

Rock mechanics

SR-Can /SKB 2006a, Section 9.4.4–9.4.5/, assessed the following rock mechanics processes related to the glaciation cycle:

- Reactivation of fractures that could affect fracture transmissivity in the far-field and in the near field (safety function R2b).
- Fracturing – potential for hydraulic jacking that could affect fracture transmissivity (safety function R2b).

- Potential for creep deformation that could affect the geometry of the deposition holes (safety function R3), which in turn indirectly could affect several of the buffer and canister safety functions.
- Seismicity and faulting that could imply shear movement of fractures intersecting deposition holes (safety function R3a) and also increase the transmissivity of the sheared fracture (safety function R2b).

Of these processes, only seismicity and faulting was shown to be significantly important for long-term safety. Such an analysis is thus potentially important as input to the site selection and is found in Chapter 7 of this report.

Hydrogeology

SR-Can /SKB 2006a, Section 9.4.6/, assessed the following hydrogeological issues during periods of permafrost and ice-sheet development:

- What is the maximum groundwater pressure during a glacial episode (safety function R3a)? In particular, will it be altered in such a way that the mechanical environment is not favourable?
- What is the groundwater flow during periods of permafrost and ice-sheet development (safety function R2ab)? In particular, will it be altered in such a way that the hydrological environment is not favourable?

These conditions are potentially different between the sites.

Geochemical evolution

SR-Can /SKB 2006a, Section 9.4.7/ treated the following geochemical issues for permafrost and glacial conditions:

- Evolution of salinity.
- Evolution of redox conditions.
- Evolution of concentrations of other relevant natural groundwater components.
- Effects of grouting, shotcreting and concrete on pH.

All these affect safety function R1 (Provide chemically favourable conditions). Of these, the evolution of salinity, redox and concentrations of other relevant natural groundwater components during the glacial cycle were shown to have long-term safety implications Such an analysis is thus potentially important as input to the site selection and is found in Chapter 6 of this report.

1.2.5 Containment potential and risk

Estimation of risk is the main output of the safety assessment methodology applied in SR-Site. As further described in **SR-Site main report**, Section 2.5.9, estimation of risk is Step 9 of the SR-Site assessment methodology, and it is is divided into two steps: analysis of containment potential and analysis of retardation potential.

While SR-Site encompasses a complete risk assessment for all scenarios, a more limited approach is judged sufficient for this report. For comparison between the sites it is judged fully sufficient to only compare the risk contributions arising from the scenarios that are the main contributor to risk. The assessment is made in Chapter 10.

1.2.6 Confidence in the site descriptive model

As already discussed above, only some site properties are important for the long-term safety, but the feedback from SR-Can also demonstrates the necessity to develop sufficient understanding of the processes and mechanisms governing the general evolution of the site. Nevertheless, it is necessary to assess the uncertainties and the confidence in the modelling and address whether the confidence in the site descriptive model, with its uncertainties, is sufficiently high for this intended purpose. This is discussed in Chapter 11 of this report.

1.3 Resulting issues addressed in this report

Based on the identification of issues addressed in the previous section, a number of issues related to long-term safety need to be considered in the context of site selection:

- The possibility of achieving the initial state and potential site differences relating to this such as spalling and site specific flow conditions affecting piping erosion. This is addressed in Chapter 2.
- Results from analyses of freezing of various parts of the repository during permafrost and glacial conditions and an evaluation of the impact this could have on long-term safety. This is addressed in Chapter 3.
- The possibility of preventing or reducing thermally induced spalling at the sites and an updated evaluation of the importance of this factor for safety. This is addressed in Chapter 4.
- Results from analyses of long-term hydrogeology including performance measures like the flow related transport resistance, F, advective travel times, t_w, and equivalent flow rate, Q_{eq}. Results from several conceptual models are evaluated for each site, see Chapter 5.
- The composition and evolution of salinity, redox and concentrations of other relevant natural groundwater components. This is addressed in Chapter 6.
- An updated estimate of the number of deposition holes in which canisters could be damaged by earthquakes. This is addressed in Chapter 7.
- A discussion on potential mineral resources at the sites, based on the findings from the SDMs, as this is of relevance for assessing future human actions. This is addressed in Chapter 8.
- While dilution does not have any specific safety function, as discussed in SR-Can /SKB 2006a, Section 7.1.1/ and in **SR-Site main report** Chapter 8, it is the biosphere conditions, e.g. the surface ecosystems, that determines the dose and risk consequences of potentially released radionuclides. This is addressed in Chapter 9.
- Expected results of calculated risk at the sites. This discussion is based on differences in input data and experiences from earlier calculations. This is addressed in Chapter 10.
- An evaluation of whether the confidence assessment of the Site Descriptive Models of the sites implies differences in confidence in the results of the safety assessment. This is addressed in Chapter 11.

In the following, each of these factors is discussed in a dedicated chapter and overall conclusions are finally presented in Chapter 12.

2 Achieving the initial state

2.1 Introduction

The initial state of the engineered parts of the repository system, e.g. the canister, the buffer, the backfill, the sealing and the rock excavations, is the result of the repository design, construction and quality control. These conditions are described in "production reports" /SKB 2010a/. The initial states of the geosphere and the biosphere relate to the site properties and conditions at the time of disposal and is documented in the site description reports for the two sites /SKB 2008a/ and /SKB 2009a/.

The initial state of the geosphere and biosphere, not being directly disturbed by the underground excavation, is discussed in subsequent chapters and is not further discussed here. Furthermore, most of the initial state of the engineered parts of the system (e.g. the canister, buffer, backfill and the closure) are essentially independent of site. In contrast, the underground openings, e.g. the design and location of deposition tunnels, deposition holes, as well as auxiliary parts of the repository must be adapted to the site conditions as described in detail in the underground openings construction report /SKB 2010b/. Site specific designs fulfilling stated design premises have been developed both for Forsmark /SKB 2009d/ and for Laxemar /SKB 2009b/. These aspects of the initial state are potentially important for safety.

2.2 Safety relevance

In order to ensure that the repository design and construction leads to a safe repository SKB has developed design premises with respect to long-term safety / SKB 2009c/. The purpose is to provide requirements from a long-term safety perspective, to form the basis for the development of the reference design of the repository and to justify that design. Design premises typically concern specifications of mechanical loads the barriers must withstand, restrictions on the composition of barrier materials, or acceptance criteria for underground excavations. The justification for these design premises is derived from the safety assessment SR-Can, **SR-Can main report**, complemented with a few additional analyses.

2.3 Forsmark

A site specific design for a repository at Forsmark has been developed and reported in Layout D2 Forsmark /SKB 2009d/. Furthermore, the underground openings construction report /SKB 2010b, Chapter 6/ shows that the proposed design, excavation and control procedures, will ensure that deposition tunnels and deposition holes accepted for disposal will meet the Design Premises for long-term safety. In addition, a technical risk assessment is made in the Layout D2 report addressing the risk that the loss of potential deposition positions would exceed the 23% loss that the current design can accommodate without changing the layout. The following is found /SKB 2009d, Section 9.3/:

- None of the consequences from the geohazards assessed would render the repository unsuitable for the purpose intended.
- The in situ stress conditions at the depth of the repository are not expected to cause spalling on the deposition holes, before the thermal load is applied, assuming the most likely stress conditions. However, there is uncertainty regarding this design parameter. Some data and indirect evidence point to lower stress magnitudes while other data and evidence point to higher stress magnitudes. Evaluation of all possible stress models indicates that mitigation measures in terms of deposition tunnel orientation and opening shape should be adequate for restricting the spalling to acceptable levels. Plans should be developed to reduce the uncertainty in the stress magnitudes and orientations during the construction of the access ramp and shaft.

- There is a general lack of confidence in the predicted loss of deposition hole positions due to large fractures, but the risk that the loss is underestimated is judged very low.
- There is great confidence in the overall geological and hydrogeological model for the site. It indicates that the frequency of water bearing fractures at the repository level is less than 0.01/m implying that there is on average more than 100 m between water bearing fractures.

It can thus generally be concluded that a repository constructed at Forsmark will meet the design premises for long-term safety, while also meeting SKB's capacity requirements.

2.4 Laxemar

A site specific design for a repository at Laxemar has been developed and reported in Layout D2 Laxemar /SKB 2009b/. Furthermore, although the underground openings construction report /SKB 2010b, Chapter 6/ strictly concerns the layout and design developed for Forsmark, the arguments and facts used for showing compliance with the long-term safety design premises are non-site specific. This means that the proposed design, excavation and control procedures, should ensure that deposition tunnels and deposition holes accepted for disposal will meet the Design Premises for long-term safety. However, the technical risk assessment for Laxemar, made in the Layout D2 report concludes that when applying the requirements as stated by the Design Premises, the available gross capacity of about 8,000 deposition positions cannot be judged sufficient to host a repository with 6,000 deposited canisters, without significant design changes. Furthermore, as demonstrated in Chapter 10, conformity with the design premises is not alone a guarantee for a safe repository. The following is found /SKB 2009b, Chapter 9/:

- The water inflows to many deposition holes are judged to be higher than the accepted values. This occurs most frequently in the hydraulic domain (HRD_EW007, see Figure 5-8), which in the current repository layout accounts for about 2,000 positions. The loss of positions is however high (20–30%) also in other domains. This risk can be handled primarily by avoiding HRD_EW007 and by revising the thermal dimensioning such that the remaining area is used more efficiently, although at the expense of more deposition tunnels to be constructed. Additional space, outside the currently well-investigated area may also be needed. Even considering these design changes there will be a substantial need for grouting and special technology may be needed in order to reach sufficiently small inflows. Such grouting technology has recently been developed by SKB, but further development is required to reach a level industrial application.
- The in situ stress conditions at the depth of the repository are not expected to cause spalling of the deposition holes before the thermal load is applied.
- There is a general lack of confidence in predicted loss of deposition hole positions due to large fractures, but the risk that the loss is underestimated is judged very low.

It can thus generally be concluded that a repository constructed at Laxemar could meet the design premises for long-term safety, but there is high uncertainty as to whether the current layout and design would meet SKB's capacity requirements. Furthermore, compared with Forsmark, there would be many more accepted deposition positions that would have inflows close to the acceptability criterion and this has safety consequences as assessed in Chapter 10.

2.5 Conclusion

The underground openings construction report /SKB 2010b/ shows that the proposed design, excavation and controlled procedures, will ensure that deposition tunnels and deposition holes accepted for disposal will meet the Design Premises. This applies to both sites. However, based on the technical risk assessments presented in the Layout D2 reports, sites /SKB 2008b/ and /SKB 2009b/ respectively, it is expected that this will imply a substantially greater loss of potential deposition positions at the Laxemar site, due to its high frequency of water conducting fractures, than at the Forsmark site. In addition the following can be noted:

- At Laxemar most deposition holes will be connected to a flowing fracture, whereas only a few deposition holes at Forsmark will be connected to a flowing fracture. Furthermore, compared with Forsmark, there would be many more accepted deposition positions that would have inflows close to the acceptability criterion and this has safety consequences, as assessed in Chapter 10.
- At Laxemar, it is expected that a large proportion of the deposition tunnels would need to be grouted, in order to meet inflow criteria for deposition tunnels, and such tunnel sections would be unsuitable for deposition holes. At Forsmark, such grouting is only expected to be needed at a few locations.
- At Forsmark, there is a risk that deposition holes will experience spalling after excavation, whereas no such spalling is expected at Laxemar. However, the depth of the spalling is limited, and the geometrical deviations of the deposition holes are judged to lie within the required tolerances. Furthermore, this can easily be checked prior to disposal, which means that there is no risk that canisters will be emplaced in unsuitable holes.

3 Sensitivity to climate evolution

3.1 Introduction

Changing climate conditions may result in several phenomena that have impact on the Forsmark and Laxemar sites, including the formation of ice sheets and permafrost, shore-level displacement and surface weathering and erosion. However, as will be discussed in this chapter, the *differences* between the sites are, with some exceptions, not large enough to be of importance for site selection, even if the process as such is of high importance in the safety assessment.

3.2 Safety relevance

Currently both sites experience a temperate climate domain, which apart from the impact from groundwater flow and infiltration of meteoric water will not affect a repository. However, additional impact may occur if the climate changes.

3.2.1 Effects of global warming

In the *Global warming case* analysed in SR-Site, both sites experience a warmer and wetter climate than today /Kjellström et al. 2009/. At both sites, the annual temperature range in the present climate is reduced due to the future warming being stronger in winter than in summer. The snow season is much shorter at the sites, or even totally absent. The present-day spring peak in runoff is absent and there is instead a more widespread wintertime runoff maximum related to the large amounts of precipitation for that season. In one model realisation, out of many possible, the annual mean air temperature at Forsmark, simulated for a period a few thousand years into the future, rises by 3.6°C and at Laxemar by 3.2°C (compared with the climate 1961–2000) /Kjellström et al. 2009/. This results in a mean annual air temperature at Forsmark of +8.3°C and at Laxemar +9.4°C. In the same climate simulation, the annual precipitation increases by 20–30% at Forsmark and by 15–20% at Laxemar (annual mean precipitation is just above 800 mm at Forsmark and just above 900 mm at Laxemar).

In a warmer climate, there is some difference between the sites in terms of maximum sea level rise up to year 2100 /Brydsten et al. 2009/, with a maximum value of around +3 m at Forsmark and +3.5 m at Laxemar. These numbers apply for short-term severe storm events, and also assume the worst scenario for global sea-level rise as known from the literature today. However, the difference between the sites is not large. Also in the more long-term, there are differences in shore line displacement between the sites /SKB 2006b, SKB 2010c/, mainly related to a larger amount of remaining isostatic uplift at Forsmark compared with Laxemar. Regardless of present uncertainties in future sea level rise, the Forsmark site will in the *Global warming case* eventually raise higher above sea-level than the Laxemar site /SKB 2006b, SKB 2010c/.

After some thousands of years of global warming and associated rising sea levels in the *Global warming case*, the remaining isostatic rebound is assumed to keep the sites above sea level for a long period of time /SKB 2006b, SKB 2010c/. During this time, ground water forms entirely by meteoric waters. Possible consequences of this are discussed in the geochemistry chapter (Chapter 6).

3.2.2 Maximum ice sheet thickness

During periods of future ice sheet coverage, Forsmark will experience a larger maximum ice sheet thickness than Laxemar due to the difference in geographical location. This results in that Forsmark also has a larger maximum hydrostatic pressure at repository depth. The maximum additional pressure from ice loading is c. 5 MPa higher at Forsmark than at Laxemar /SKB 2006b/. This difference is however judged to be small compared with the margin between the highest pressures and the isostatic load that the canister can withstand without global collapse, and therefore this process is not further discussed here.

3.2.3 Total time of ice sheet coverage

For glacial conditions, the total time of ice sheet coverage is longer at Forsmark than at Laxemar, with ice covering Forsmark for 24% and Laxemar for 16% of the time in the SR-Site *Reference evolution* (i.e. repetition of last glacial cycle conditions). This could affect groundwater chemistry (see Chapter 6) and doses in the biosphere (Chapter 9). In this context it is worth mentioning that cases with considerably *longer* periods of ice sheet coverage are analysed for Forsmark in SR-Site /SKB 2010c, Section 5.3/.

3.2.4 Surface weathering and erosion

Possible amounts of surface weathering and erosion in a 100,000 year and 1 million year time perspective were studied in /Olvmo 2010/ The results show that the differences between the sites are small, and therefore these processes are therefore not further discussed here.

3.2.5 Total time of sea coverage

In the *Reference evolution*, the sea covers the Forsmark site longer than the Laxemar site /SKB 2006b/, due to differences in ice sheet thickness and location of the repository sites. This could affect groundwater chemistry (Chapter 6) and doses in the biosphere (Chapter 9).

3.2.6 Permafrost and freezing

As mentioned above, a changing climate can result in that permafrost develops at the sites, i.e. that the ground water freezes and may stay frozen for long periods of time. This results in three phenomena of relevance for repository safety; i) freezing of parts of the rock above the repository ii) changes in ground water flow pattern and iii) expulsion of salt in case salt water is freezing. The SR-Site analysis of the effects of changes in ground water flow have been conducted within the hydrogeology programme, see Chapter 5. Expulsion of salt and its impact on salinity is considered in the hydrogeochemical analysis, see Chapter 6.

Climate model simulations show that during the cold ice-free periods of glacials, both sites have the necessary climatological requirements for permafrost formation /Kjellström et al. 2009/. The results also show that Forsmark may experience a climate more favourable for severe permafrost growth, resulting in more widespread and/or deeper permafrost than Laxemar. This difference is due mainly to the geographical locations of the sites.

In this context, the term “permafrost depth” is defined as the depth of the 0°C isotherm, while “freezing depth” also includes the effect of the prevailing pressure (higher pressures lowers the freezing point temperature, and hence water may stay unfrozen even if the temperature is below 0°C) and ground water salinity. In the following the two terms are used interchangeably. However, when depth values are reported, they always refer to freezing depth, since this is the relevant parameter when analyzing repository performance.

If water filled fractures and cavities are exposed to freezing temperatures, the water will freeze. The increase in volume associated with the phase change will yield a pressure on the fracture walls, which theoretically could enlarge fractures. Theoretically, this could also apply to fractures induced by the excavation work, the “EDZ”. However, if the water freezes there will be about 9% volume expansion. At the very most this implies a 9% increase of the aperture corresponding to a 30% increase of fracture transmissivity for the unrealistic case that this aperture increase would not be reversible. Such a small increase would be of no significance for safety.

If buffer erosion takes place, water filled cavities will form in the affected deposition hole. If such cavities are subject to freezing temperatures, the formation of ice may yield a pressure on the canister. Calculations made for SR-Can show that, for a relevant ambient pressure of 20 MPa (sum of swelling pressure and ground water pressure), the maximum pressure in the erosion cavity, including the freezing pressure, is 26 MPa /SKB 2006a, Section 12.4.4, Table 12-1/. For higher ambient pressures, such as under a maximum large ice sheet, see above, the high pressures prevents freezing in the cavities. Complementary studies made for SR-Site support these conclusions, see the SR-Site **Climate report**, Section 5.7 / SKB 2010c/.

Since permafrost and freezing are potentially important to repository safety, permafrost simulations have been carried out within SR-Can for both sites. The results are presented in the following two sections. 2D permafrost simulations have been conducted for Forsmark for the *Reference evolution* and for a *Severe permafrost case*, favourable for early and deep permafrost development (Figure 3-1), see the **Climate report** Sections 3.4.4 and 5.5 and /Hartikainen et al. 2010/. 2D permafrost simulations have not been performed for Laxemar. Instead, for a comparison of the sites, the 1D permafrost simulations conducted for Forsmark and Laxemar for corresponding climate cases in SR-Can /SKB 2006b/ are used. The 1D and 2D models produce very similar results at the specific locations of the repository (Figure 3-2), legitimising this approach.

3.3 Permafrost development at Forsmark

Permafrost development at Forsmark has been simulated along a 15 km long profile (Figure 3-1), for various possible climate situations. In the simulation for the *Reference evolution*, that is the repetition of reconstructed last glacial cycle conditions, the maximum freezing depth at Forsmark is c. 250 m (Figure 3-2). In the *Severe permafrost* simulation, favourable for early and deep permafrost development, the maximum freezing depth over the repository at Forsmark is c 360 m (Figure 3-3). This case describes a situation in a cold ice age climate with significantly dryer conditions than during the last glacial cycle.

Examples of the temperature distribution in bedrock and permafrost depth from the 2D simulation of the *Severe permafrost case* at Forsmark is seen in Figure 3-4. During the first thousands of years after repository closure, heat generated by the repository has a large impact on bedrock temperatures, and also on permafrost depth (Figure 3-4 upper panel). After c. 50,000 years, continuous permafrost has formed at the site, and repository heat production has declined (Figure 3-4 lower panel).

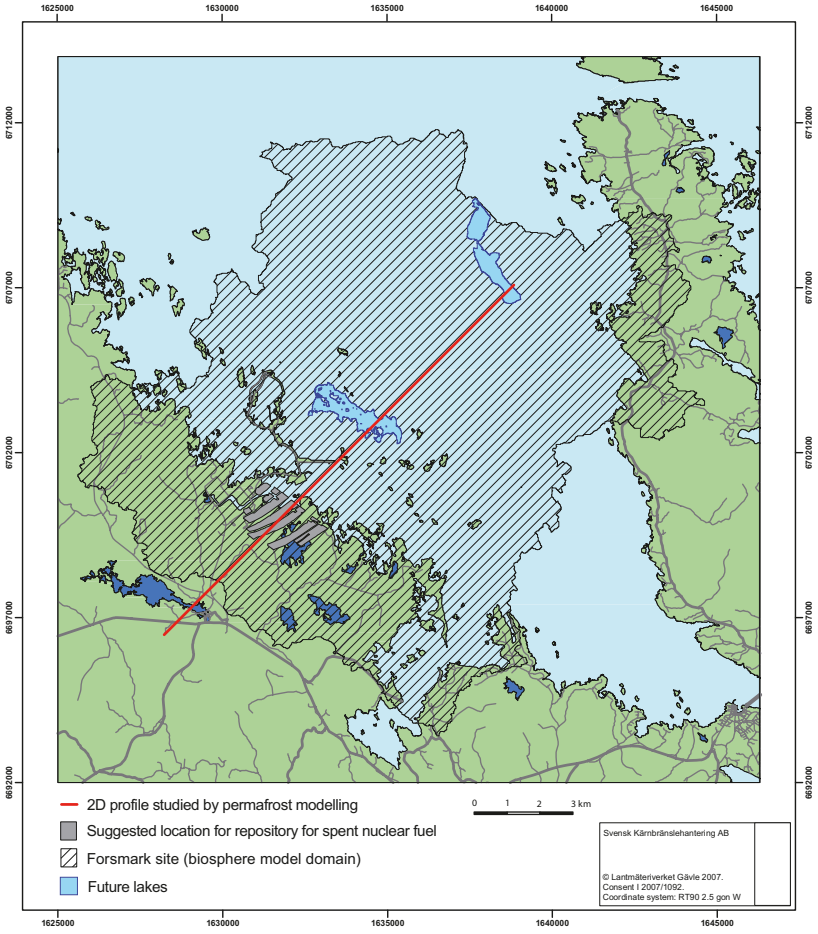

Figure 3-1. *Location of the c. 15 km long profile analysed for permafrost development in SR-Site.*

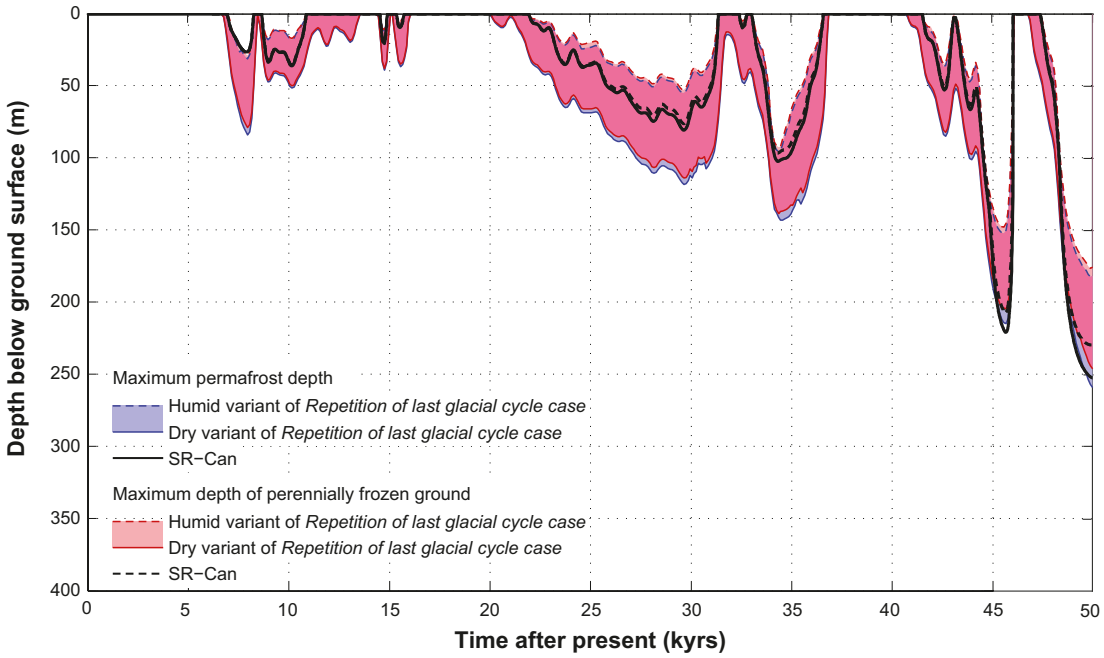

Figure 3-2. *Evolution of permafrost and perennially frozen ground depth at the Forsmark repository location for the first 50 kyrs of the reference evolution as simulated by the 2D (SR-Site) and 1D (SR-Can) permafrost models. The shaded area in blue and red represents the range obtained from the 2D modelling when considering one wet and one humid climate variant. Further uncertainties in the permafrost modelling are discussed in the* ***Climate report*** *Section 3.4.4. Both model simulations show that the maximum permafrost depth is ~250 m around 50 kyrs after present.*

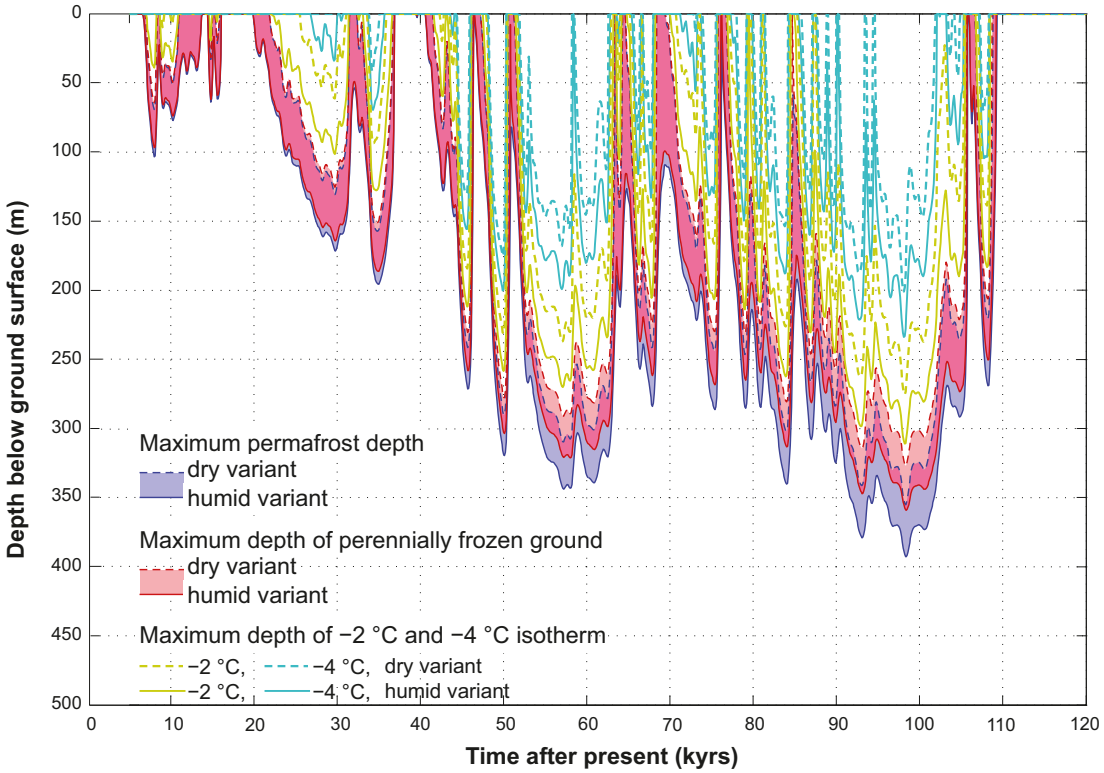

Figure 3-3. *Evolution of maximum permafrost depth, maximum depth of perennially frozen ground and maximum depth of –2 and –4°C isotherms over the repository location in Forsmark for the Severe permafrost case, see Climate report, Section 5.5. The upper permafrost surface, for periods of permafrost degradation from above, is not shown. The shaded area in blue and red represents the range when considering the dry and humid climate variants of the severe permafrost case. The darker lilac colour indicates that the results for permafrost and perennially frozen ground overlap.*

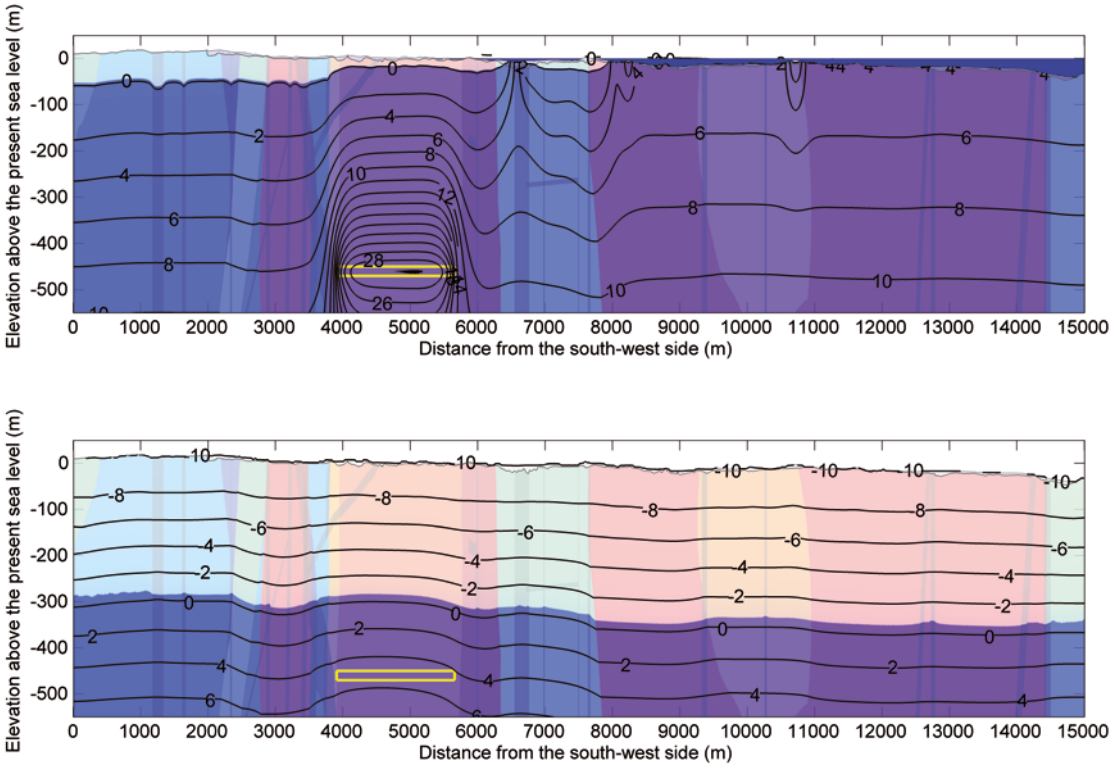

Figure 3-4. *Examples of temperature contours in (°C) and extent of frozen conditions from the 2D permafrost simulations of the Severe permafrost case (humide climate variant). The upper and lower panels show the situation 8,500 and 50,000 years after present respectively. The 0°C isotherm shows the permafrost depth, while bright colours in the upper part of the bedrock show frozen conditions and darker colours at greater depths indicate unfrozen conditions Vertically coloured areas indicate different rock domains. The repository is seen as a rectangular box at a distance of c. 5,000 m. 8,500 years after present (upper panel) the heat from the repository has a large influence on bedrock temperatures and permafrost formation.*

The 2D results further show that unfrozen sections from the surface to the depths "taliks", may form under lakes in the vicinity of a repository at Forsmark (not shown in figures here). The hydrogeological implications of this have been investigated within the hydrogeology programme, see e.g. Chapter 10 of **SR-Site main report**.

At Forsmark, in the *Reference evolution* and *Severe permafrost case*, permafrost grows progressively deeper in several phases interlaced with periods without permafrost (Figure 3-2 and 3-3). In the *Reference evolution*, the maximum freezing depth occurs just prior to the first ice sheet advance over the sites, around 50,000 years into the future (Figure 3-2). At this advanced stage, the entire landscape at Forsmark is covered by permafrost (no unfrozen taliks are present) (Figure 3-4, lower panel). In the *Severe permafrost case* the maximum freezing depth occurs later, around 90,000–100,000 years into the future (Figure 3-3).

In the upper part of the repository, ramp and shafts repeatedly experience sub-zero temperatures in both the *Reference evolution (*Figure 3-2) and in the *Severe permafrost case* (Figure 3-3).

For both the *Reference evolution* and the *Severe permafrost case*, complementary sensitivity studies were performed to cover all uncertainties related to permafrost development, including the large uncertainty in air temperature, see **Climate report** Appendix A. Also uncertainties in geothermal heat flux and other parameters related to subsurface and surface conditions were evaluated, see Climate report, Section 3.4.4 and 5.5.

The sensitivity tests of uncertainties showed that even under very pessimistic circumstances, i.e. when simultaneously setting *all* known uncertainties in the position most favourable for permafrost growth, freezing does not occur at repository depth in Forsmark, see the **Climate report** Section 5.5.

The results from this quite unrealistic combination of uncertainties, yielded a maximum depth of the uncertainty interval for freezing of 422 m, see Climate report, Section 5.5. At the same time, the uncertainty interval for the permafrost depth (defined by the 0°C isotherm) reaches a maximum depth of 463 m. It should be noted that the presence of permafrost does not mean that the ground at depth is frozen since the groundwater pressure, groundwater composition of groundwater, and the adsorptive and capillary properties of ground matter make the groundwater to freeze at temperatures below 0°C. The results further showed that the maximum depth of the uncertainty interval for the −2°C and −4°C isotherms, corresponding to the SR-Site temperature criteria used for buffer and back-fill freezing, reach 388 and 316 m.

The conclusion from a combined analysis of the *Reference glacial cycle* and the *severe permafrost case*, and taking all relevant uncertainties into account for each case, is thus that freezing of groundwater, buffer or back-fill material at repository depth will not occur at Forsmark. This is the case even when making the most pessimistic, and unrealistic, combination of uncertainties, see **SR-Site main report**.

3.4 Permafrost development at Laxemar

In the *Reference evolution* simulation made in 1D for Laxemar for SR-Can, the maximum freezing depth is 157 m (Figure 3-5, right panel). In a 1D simulation with pessimistic climate assumptions favourable for deep permafrost (corresponding to the SR-Site *Severe permafrost case* at Forsmark above), the maximum freezing depth at Laxemar is 263 m (Figure 3-6 right panel). Given the very large similarity between the 1D and 2D results of Forsmark (Figure 3-2), the 1D results for Forsmark from SR-Can / SKB 2006b/ may be used to make a comparison with the Laxemar site. Like in Forsmark, the permafrost at Laxemar in the *Reference evolution* and *Severe permafrost case*, grows progressively deeper in several phases interlaced with periods without permafrost (Figure 3-5 and 3-6). In the *Reference evolution*, the maximum freezing depth occurs just prior to the first ice sheet advance over the sites, around 50,000 years into the future (Figure 3-5 at time –70 ka). In the *Severe permafrost case,* the maximum freezing depth occurs later, around 90,000–100,000 years into the future (Figure 3-6, right panel, at time –20 krs).

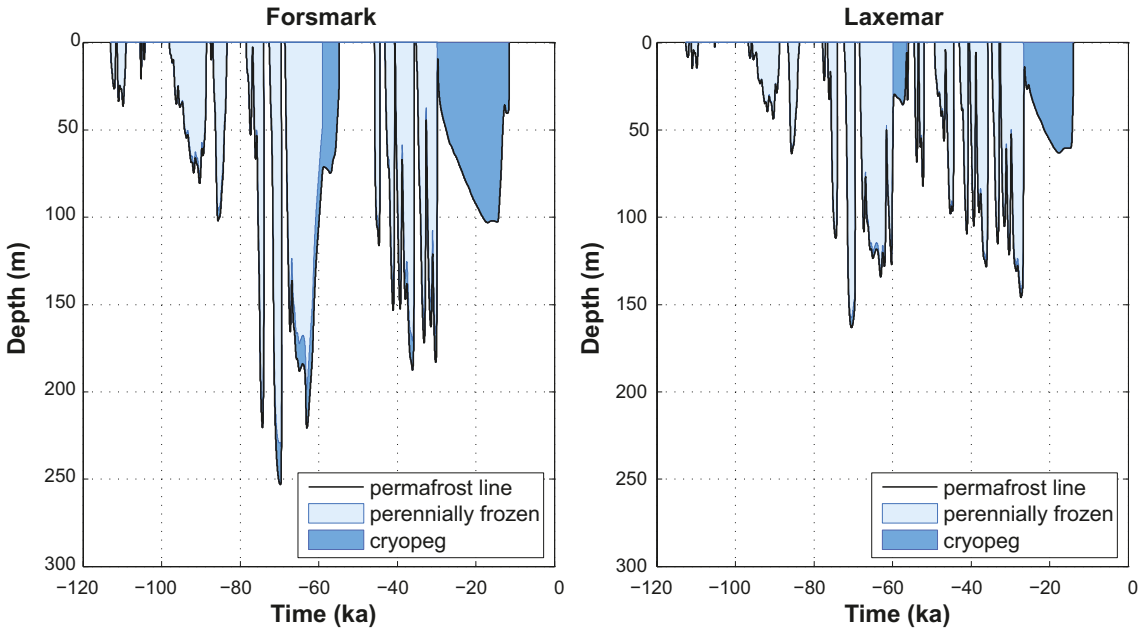

Figure 3-5. *Depth of permafrost and perennially frozen conditions at Forsmark and Laxemar for the Reference evolution from 1D modelling for SR-Can /SKB 2006b/. (The cryopeg denotes unfrozen parts of the permafrost due to high pressure). The maximum permafrost depth at Laxemar is c 160 m in the reference evolution (right panel). Note that the time scale in the figure shows times for the last glacial cycle. In order to project this into the future, 0 ka should be on the left side and +120 ka on the right.*

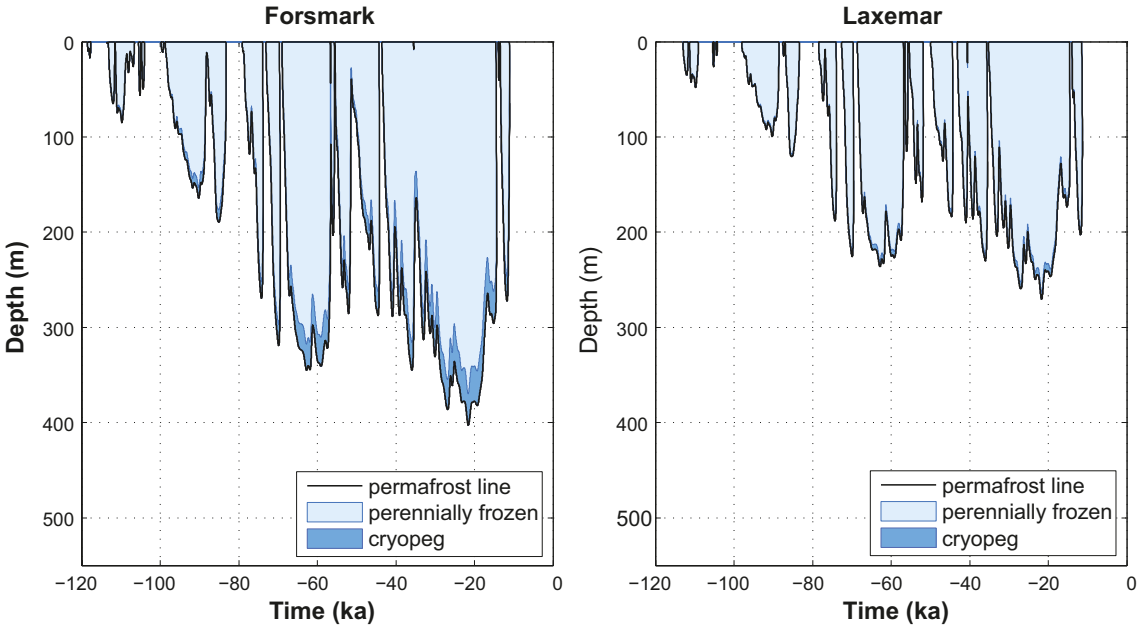

Figure 3-6. *Depth of permafrost and perennially frozen conditions at Forsmark and Laxemar for the severe permafrost case from 1D modelling for SR-Can /SKB 2006b/. (The cryopeg denotes unfrozen parts of the permafrost due to high pressure). The maximum permafrost depth in the severe permafrost case at Laxemar is c 260 m. Note that the time scale in the figure shows times for the last glacial cycle. In order to project this into the future, 0 ka should be on the left side and +120 ka on the right.*

In the upper part of the repository ramp and shafts repeatedly experience sub-zero temperatures in both the *Reference evolution (*Figure 3-5 right panel) and in the *Severe permafrost case* (Figure 3-6 right panel). In line with the above, the 1D simulations made for SR-Can shows that freezing at repository depth at Laxemar can be excluded (Figure 3-2 right panel). Given these results, and the results of the analysis of uncertainties in Forsmark (Section 3.3), it is further anticipated that there would be ample margin to freezing at Laxemar even if all uncertainties related to permafrost growth would be included.

3.5 Conclusions

In terms of changes in climate, the major difference between the sites relates to periglacial climates with permafrost, with some exceptions related to the biosphere and to ground water chemistry.

During cold periods without ice sheets at the sites, permafrost and freezing of ground water reach closer to repository depth at Forsmark than at Laxemar, even if freezing of groundwater, buffer and deposition tunnel back-fill is ruled out also in Forsmark. The difference between the sites is mainly due to differences in climate /e.g. Kjellström et al. 2009/ and differences in bedrock thermal properties /SKB 2006b/.

Freezing above repository depth

A larger vertical portion of the rock above the repository is subject to repeated freezing/thawing cycles at Forsmark than at Laxemar. In the ramp, a larger portion of the closure backfill material (from the surface and downwards) will freeze at Forsmark compared with Laxemar. This is true also for water filled bedrock fractures (including any fracturing induced by the excavation “the EDZ”). A theoretical enlargement of such fractures from repeated freeze and thaw cycles could take place along a larger portion of the ramp in Forsmark than in Laxemar.

Freezing at repository depth, except intact buffer

Even in the most pessimistic, but still feasible, situation, freezing of free water at repository depth does not take place at Forsmark. That is water in e.g. the central area, in cavities in weathered plugs, or in water filled bedrock fractures remains unfrozen. This is in line with the situation at Laxemar, where all parts of the repository at repository depth are projected to remain unfrozen at all times.

Freezing of intact buffer clay

Based on the results of SR-Can and SR-Site, the buffer clay will not freeze at repository depth at Forsmark or Laxemar, even in the most pessimistic climate case, see the **SR-Site main report**, Section 12.4. If such freezing of the buffer clay would occur, the clay would regain its properties after thawing.

Freezing in buffer erosion cavities

Freezing in buffer erosion cavities has been excluded at both Forsmark and Laxemar, even for the most pessimistic climate case analysed for the Forsmark site.

Overall conclusion

The major difference between the sites in terms climate related processes relates to freezing of various parts of the repository. Other climate related processes may give relevant differences in ground water chemistry and biosphere characteristics.

With regard to freezing the following is found:

- A larger vertical portion of the rock above the repository is subject to repeated freezing/thawing cycles at Forsmark compared to Laxemar.
- Even for the most pessimistic case of, unrealistically, combining all uncertainties as to favour permafrost development, freezing of free water at repository depth, e.g. in the central area or in cavities in weathered plugs, can not take place at Forsmark or Laxemar.
- The buffer clay will not freeze at repository depth at Forsmark or Laxemar even in the most pessimistic case of, unrealistically, combining all uncertainties as to favour permafrost development.

In conclusion, due to the lower thermal conductivity at Laxemar and its more southern position a repository at Laxemar will experience less freezing than a repository at Forsmark. The differences are, however, judged small. Since freezing of groundwater, buffer and deposition tunnel backfill is judged unrealistic at both sites, and since the impact of freezing, was it to occur, is moderate, the differences in potential for freezing between Laxemar and Forsmark have little significance for the site selection.

4 Rock mechanics impacts – thermally induced spalling

4.1 Introduction

If rock stresses are high, the rock towards an excavated rock surface may crack and form rock flakes in a phenomenon called spalling. Spalling occurs if the tangential stress at the wall reaches the spalling strength of the material (called crack initiation stress). Even if the initial rock stresses are not sufficient to produce spalling, there is still the possibility that spalling may occur later due to the additional thermal load. The potential occurrence of spalling is site and repository design specific, as it depends on the in situ stress, the intact strength, and thermal expansion behaviour of the rock, and on the repository layout.

4.2 Safety relevance

*S*palling may create a zone of substantially enhanced porosity and hydraulic conductivity. These changes may dramatically increase the mass transfer between the deposition hole and the rock, noted $Q_{eq1,}$ if the buffer is intact, as shown in SR-Can main report /SKB 2006a, Section 9.3.6/. SR-Can main report /SKB 2006a, Section 13.1 concludes that thermally induced spalling around deposition holes may have a considerable impact on mass exchange between the flowing groundwater and the buffer as long as diffusion is the dominant transport mechanism in the buffer, but such situations contribute little to risk. If advective conditions prevail in the buffer, the effects of spalling are insignificant. This means that spalling has no impact on the risk dominating conditions according to SR-Can (nor according to SR-Site), e.g. impact of rock shear due to potential earthquakes and impact of loss of buffer due to bentonite erosion.

4.3 Analysis of the potential for thermally induced spalling

The potential for thermally induced spalling has been reassessed /Hökmark et al. 2010/, using the modelling approach applied in SR-Can, but with updated site specific data and for the repository layouts developed Layout D2 Forsmark /SKB 2009d/ and Layout D2 Laxemar /SKB 2009b/.

The model calculates the tangential stress at the wall of the deposition hole resulting from in situ stress and the thermal load. This stress is in turn compared with the spalling strength of the rock. The latter is assumed to lie somewhere between 52%–62% of the Uniaxial Compressive Strength (UCS) of the rock, cf. Section 6.4 in the SR-Site Data report /SKB 2010d/ and Appendix A4.

The modelling requires the following geosphere input data:

- Rock mass elastic properties for the different scales of importance (Young's modulus E [GPa] and Poisson ratio υ).
- Rock mass density r [kg/m^3].
- Uniaxial compressive strength UCS [MPa].
- Initial, pre-mining stress magnitudes and orientations.

The modelling also needs:

- Rock mass thermal conductivity λ [W/(m·K)] and diffusivity a [m^2/s].
- Rock mass thermal expansion coefficient α [m/(m·K)].
- In situ temperature at repository depth T [°C].

These data are provided in the SR-Site Data report /SKB 2010d, Sections 6.2 and 6.4/ for Forsmark and Appendix A2 and A4 in this report for Laxemar, and fully builds on the Site descripitve models of the two sites SDM-Site Forsmak /SKB 2008a/ and SDM-Site Laxemar /SKB 2009a/. The modelling also needs repository design and layout.

In addition, SKB has conducted field tests at Äspö HRL /Glamheden et al. 2010/ to assess the potential for mitigating spalling by adding small counter pressures. However, while the tests support the possibility that the counter pressure exerted by bentonite pellets in the slit between buffer and rock wall, may suppress the spalling, current results are inconclusive. For the purpose of this assessment it is thus judged appropriate to discount the possibility that thermally induced spalling can be handled in this manner. This does not mean that efforts to handle and mitigate thermally induced spalling should not continue – only that this factor will not be considered in site comparison.

4.4 Forsmark

The thermo-mechanical analyses of the potential for spalling at Forsmark /Hökmark et al. 2010, Chapter 9/ shows that when uncertainties in mechanical properties and*in situ* stresses and their orientations are taken into account, the following conclusions can be drawn:

- The spalling strength is likely to be exceeded during the thermal phase even when the lower limit of the stress magnitudes and most favourable tunnel orientations are considered.
- For the most unfavourable stress orientation and upper limit of stress magnitudes, it is possible that the lower limit of the spalling strength (52% of UCS) will be exceeded from the tunnel floor down to a depth of around 7.9 m (both when considering the mean value and the dimensioning value of the thermal conductivity) after 50 years. The upper limit of the spalling strength (62% of UCS) will be exceeded, after 50 years, from the tunnel floor to a depth of 7.3 m (mean value of the thermal conductivity) and 7.6 m (dimensioning value of the thermal conductivity), respectively.

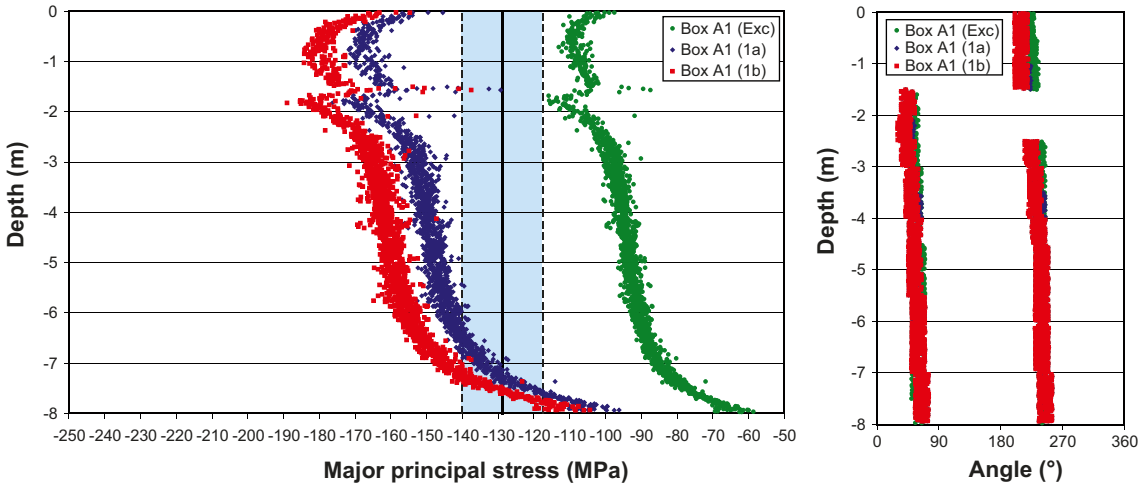

Figure 4-1. *Simulated maximum tangential stress after excavation (green) and 50 years after deposition (for two different thermal conductivities- red and blue) along deposition hole wall in Forsmark. Blue area represents interval for spalling strength. (Figure 9-8 from /Hökmark et al. 2010/.)*

4.5 Laxemar

The thermo-mechanical analyses of the potential for spalling at Laxemar /Hökmark et al. 2010, Appendix I: section I6/ shows (Figure 4-2) that for the models with mean values of the thermo-mechanical properties and *in situ* stress orientations (using the Laxemar stress model), the following conclusions can be drawn:

- The lower limit of the spalling strength (52% of the UCS) is exceeded in the two models in rock domain RSMD after about 10 years. In the other domains, the maximum stress is below the lower limit of the spalling strength.
- In the model with the highest stresses, the lower limit of the spalling strength is exceeded from about 2 m below the tunnel floor to about 6.5 m below the tunnel floor after 50 years.

These results suggest quite limited thermally induced spalling at Laxemar. However, in order to account for uncertainty in stress magnitude the assessment was also repeated for the highest stress levels measured in the region – as found in the Äspö HRL. For the models with dimensioning values of the thermo-mechanical properties and *in situ* stress orientations (using major horizontal *in situ* stress as in Äspö), the following conclusions can be drawn:

- The lower limit of the spalling strength (52% of the UCS) is exceeded in RSMA after about 5 months to 1 year. The upper limit of the spalling strength (62% of the UCS) is not exceeded in the two models but is close to 62% after 30 years.
- The lower limit of the spalling strength (52% of the UCS) is exceeded in RSMD after about 2–5 months. The upper limit of the spalling strength (62% of the UCS) is also exceeded after 2–5 years.
- The lower limit of the spalling strength (52% of the UCS) is exceeded in RSMM after 2–5 months. The upper limit of the spalling strength (62% of the UCS) is exceeded in after 2–30 years depending on location.
- In the model with the highest stresses the lower limit of the spalling strength (52% of UCS) is exceeded from the tunnel floor to a depth of about 7.5 m after 50 years. The upper limit of the spalling strength (62% of UCS) is exceeded from about 2 m to 7 m below the tunnel floor after 50 years.

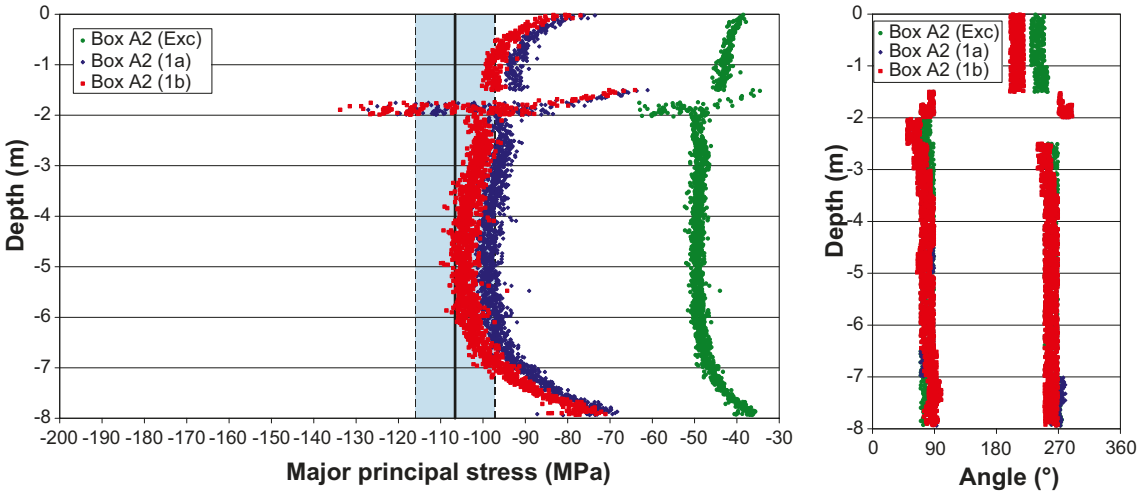

Figure 4-2. *Simulated maximum tangential stress (Laxemar in situ stress model) after excavation (green) and 50 years after deposition (for two different thermal conductivities red and blue) along deposition hole wall in Laxemar. Blue area represents interval of spalling strength. (Figure I-34 of /Hökmark et al. 2010/.)*

4.6 Conclusions

The assessment of spalling potential shows that:

- There is potential for thermally induced spalling at both sites.
- The likelihood and extent of the spalling is much less at Laxemar, especially in rock domain RSMA. The difference is largest if the Laxemar stress model, see Chapter 7 of SDM_Site Laxemar /SKB 2009a/ can be assumed to be representative of the Laxemar area, but also remains when assuming the limiting value of stress measured at the Äspö HRL.
- Taking the uncertainty spans for in situ stress orientations and magnitudes into account, there is potential for the spalling strength to be exceeded during the thermal phase to depths of around 7.9 m below the tunnel floor at both sites. This means that there is little risk that the spalled zone would reach the bottom of the deposition hole at any of the sites.

However, **SR-Site main report** shows that the only risk contribution for a repository at Forsmark occur if advective conditions prevail in the buffer or if the canister is sheared due to earthquakes. For these conditions, the effects of spalling still add little to risk. The difference in potential for spalling between the sites is thus of little relevance for site selection.

5 Hydrogeology and transport conditions

5.1 Introduction

In the present chapter, issues related to hydrogeology are presented. First, a brief summary of the Hydrogeological site understanding as expressed in the site-descriptive modelling (SDM) reports /Follin 2008, Rhén and Hartley 2009/ and references therein are provided. However, in addition to the results presented in the SDM reports, an analysis is provided where hydraulic conductivity values at repository depth, obtained from hydraulic testing, are compiled in order to make a quantitative comparison between the sites. Second, modelling results obtained as part of SR-Site for Forsmark, used in **SR-Site main report**, and result of corresponding performed for Laxemar as part of the present study, are summarised and compared. Finally, concluding remarks are given where the sites are ranked in terms of performance.

5.2 Safety relevance

The results produced by the hydrogeological modelling are used as input for several analyses in the safety assessment. Some key components are:

- Development of groundwater flow at regional, site and repository scale during the assessment period.
- Development of groundwater chemistry, specifically salinity, at the corresponding scales during the assessment period.
- Transport characteristics in terms of advective travel time and flow-related transport resistance from surface to repository depth along recharge flow paths for different time periods.
- Transport characteristics in terms of advective travel time and flow-related transport resistance from the repository to the surface along discharge flow paths for different time periods. In addition, as input to radionuclide transport calculations also the Darcy flux at deposition hole locations in the repository is needed for the corresponding time periods.

One of the main inputs to the modelling discussed above is fracture statistics and associated relevant hydraulic properties. The resulting permeability distribution of the bedrock, expressed e.g. as conductivity values on a given scale, is thus in itself already a good indicator of what subsequent modelling may yield for different applications.

5.3 Hydrogeological data and site understanding

5.3.1 Forsmark

General characteristics of the site

Forsmark is located near the coast in northern Uppland in a region that forms a part of the sub-Cambrian peneplain in south-eastern Sweden. The candidate area for site investigation is located along the shoreline of Öregrundsgrepen. It is characterised by a small-scale topography of low altitude. The north-western part of the candidate area was selected as the target area[2] for the complete site investigation work, see Figure 5-1. The hydrogeology of the bedrock is summarised in /Follin 2008/ and presented in more detail in /Follin et al. 2007a, b/ and /Follin et al. 2008/.

Table 5-1 lists the 25 cored boreholes shown Figure 5-1. These are investigated with the Posiva Flow Log (PLF) method and the Pipe String System (PSS) method. The hydraulic data acquired from these tests were used to parameterise the deterministically defined deformation zones and the fracture networks contained in the rock mass volumes in between the deformation zones. In SKB's approach to hydraulic assessment, the former are referred to as Hydraulic Conductor Domains (HCD), whereas the latter are referred to as Hydraulic Rock Mass Domains (HRD).

[2] In SDM-Site, the subareas selected for complete site investigations at Forsmark and Laxemar are referred to as the Target area and the Focus area, respectively.

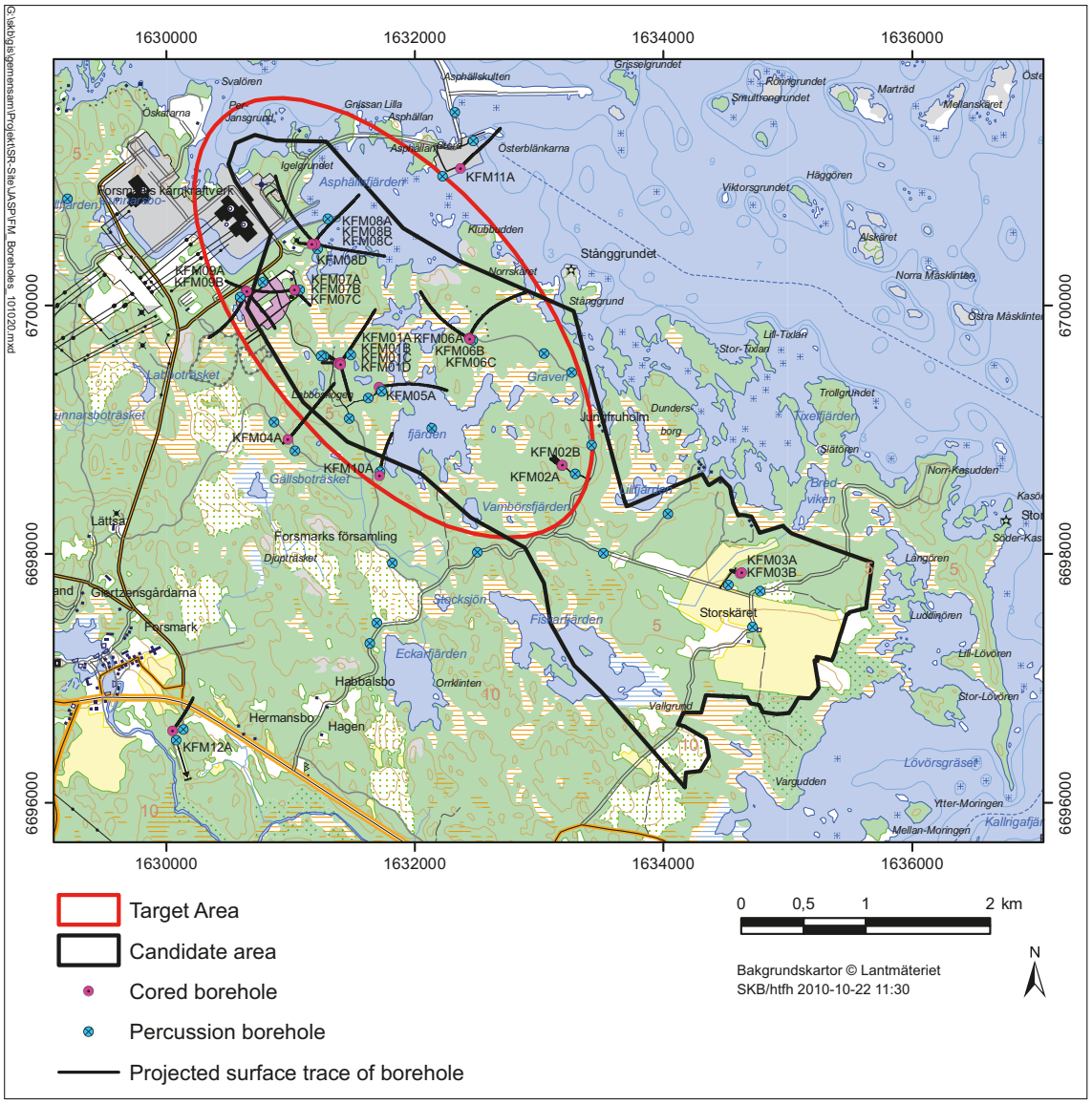

Figure 5-1. *Map showing the 25 core-drilled and the 38 percussion-drilled boreholes produced during the site investigation at Forsmark between year 2002–2007. The projection of the boreholes on the ground surface due to their inclination is also shown. The ellipse indicates the target area. (Note that the term "candidate area" might be changed in the future.) (Modified after Figure A-1 in /Follin 2008/.)*

Table 5-1. List of the cored boreholes at Forsmark tested with the PFL and PSS methods. (Modified after Table B-4 in /Follin et al. 2008/.)

Borehole	PFL	PSS	Bottom elevation of borehole (m)	Borehole	PFL	PSS	Bottom elevation of borehole (m)
KFM01A	X	X	–982	KFM07A	X		–819
KFM01B		X	–479	KFM07B		X	–238
KFM01C		X	–333	KFM07C	X		–494
KFM01D	X	X	–612	KFM08A	X	X	–759
KFM02A	X	X	–987	KFM08B		X	–166
KFM02B	X	X	–565	KFM08C	X		–781
KFM03A	X	X	–987	KFM08D	X		–751
KFM03B		X	–88	KFM09A		X	–621
KFM04A	X	X	–796	KFM09B		X	–472
KFM05A	X	X	–825	KFM10A	X	X	–338
KFM06A	X	X	–826	KFM11A	X	X	–716
KFM06B	X	X	–93	KFM12A		X	–511
KFM06C		X	–781				

The fractured rock mass volumes between the deterministically modelled deformation zones was divided into six fracture domains, FFM01–FFM06 based on the fracture frequency of *all* fractures /Olofsson et al. 2007/. The key fracture domains in the target area aimed for a deep repository; FFM01 and FFM06, occur below fracture domain FFM02, see Figure 5-2 and Figure 5-3. At Forsmark, the HRD geometries are identical to the geometries of the fracture domains.

Figure 5-4 shows examples of PFL fracture transmissivity data from four cored boreholes, KFM01D, KFM06A-8A, located at drill sites 1, 6, 7 and 8, respectively. As can be seen in the plots, the bedrock has a high frequency of conductive fractures above –200 m, whereas below –400 m the frequency of conductive fractures decreases significantly. The decrease in fracture transmissivity is not as significant as the decrease in frequency, although the highest transmissivity values are clearly observed above –200 m. These observations are commented more in detail in the text below. For the sake of clarity, it is noted that a casing is installed in the cored boreholes, which prohibits a detailed characterisation of the uppermost 100 m of bedrock with the PFL and PSS methods. Instead, the hydraulic characterisation of the uppermost 100 m of the bedrock is made with the HTHB method. A description of the three different test methods, PFL, PSS and HTHB, is found in /Follin et al. 2007a/.

Deformation zones modelled deterministically, elevation c. 0 to –1,000 m

The deduced transmissivities of the deterministically modelled deformation zones are shown in Figure 5-5. The transmissivities are coloured with regard to the orientations of the zones, where G means gently dipping. The steeply dipping zones are denoted by their strike direction. The deformation zones with no measurable flow are assigned an arbitrary low transmissivity value of $1 \cdot 10^{-10}$ m^2/s in order to make them visible on the log scale. The transmissivity data that are marked by slightly larger squares with a white cross in the centre represent data that were acquired for verification purposes, see /Follin et al. 2008/.

As can be seen in the figure, the deformation zones are hydraulically heterogeneous but there is also a significant decrease in deformation zone transmissivity with depth, where the gently dipping zones have the highest transmissivities regardless of elevation followed by the steeply dipping WNW zones.

Fractured bedrock between the deterministically modelled deformation zones, elevation c. 0 to –1,000 m

The data shown in Figure 5-6 represent PFL fracture transmissivity data acquired in the target area in the rock mass volumes between the deterministically modelled deformation zones. Above –200 m, the conductive fracture frequency is much higher than below this elevation. In fact, there are hardly any conductive fractures below –400 m. The decrease in fracture transmissivity is not as significant as the decrease in frequency, although the highest transmissivity values are clearly observed above –200 m. These observations are confirmed by the measurements conducted with the PSS method. (Table 5-1 lists the boreholes that are tested with both methods.)

It is noted that the data occurring around –450 m are observed in the cored borehole KFM02A at drill site 2, see Figure 5-1 and the lower image in Figure 5-3. This segment of KFM02A intersects the rock mass volume sandwiched in between two deformation zones, ZFMA2 and ZFMF1, and is not part of the planned repository volume. In conclusion, the fractured rock mass volumes between the deterministically modelled deformation zones look very different above and below approximately –400 m from a safety assessment point of view.

5.3.2 Laxemar

General characteristics of the site

Laxemar is located close to the coast in the northern part of Småland in a region that forms a part of the sub-Cambrian peneplain in south-eastern Sweden. The topography is fairly flat but with relatively distinct valleys. The southern part of the Laxemar Local model area was selected as the focus area for the complete site investigation work, see Figure 5-7. The hydrogeology of the bedrock is summarised in /Rhén and Hartley 2009/ and presented in more detail in /Rhén et al. 2008, Rhén et al. 2009/.

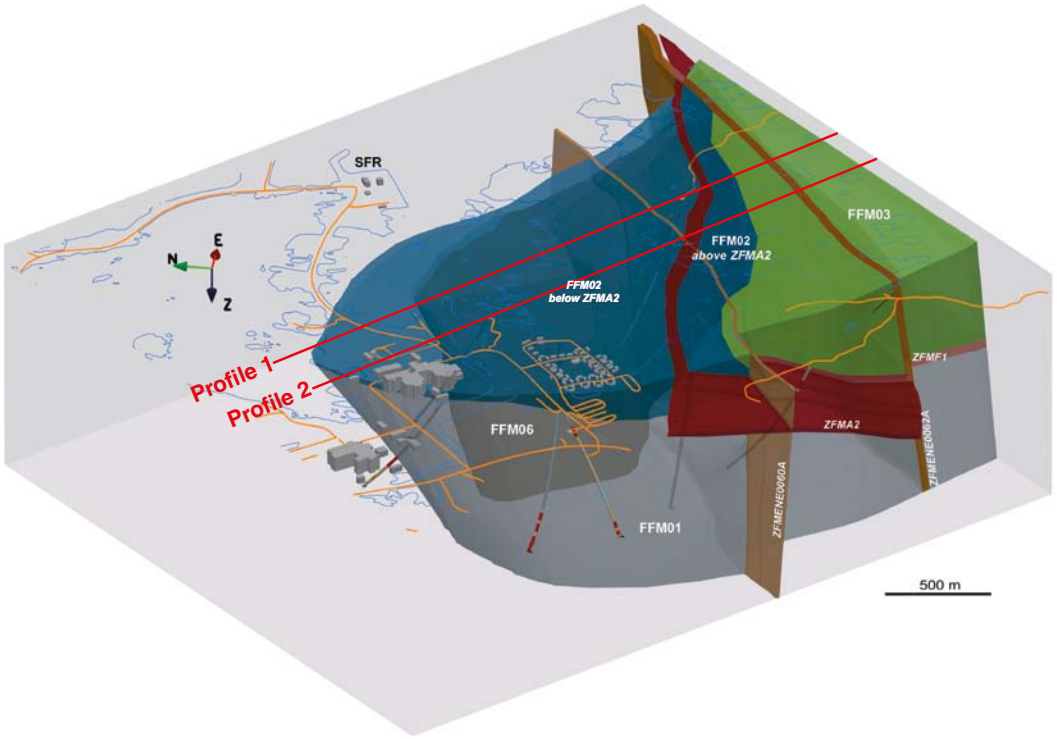

Figure 5-2. *Three-dimensional view to the east-north-east showing the relationship between deformation zone ZFMA2 (red) and fracture domains FFM01–03 and FFM06. Profile 1 and 2 are shown as cross-sections in Figure 5-3. (Source: Figure 3-11 in /Follin 2008/.)*

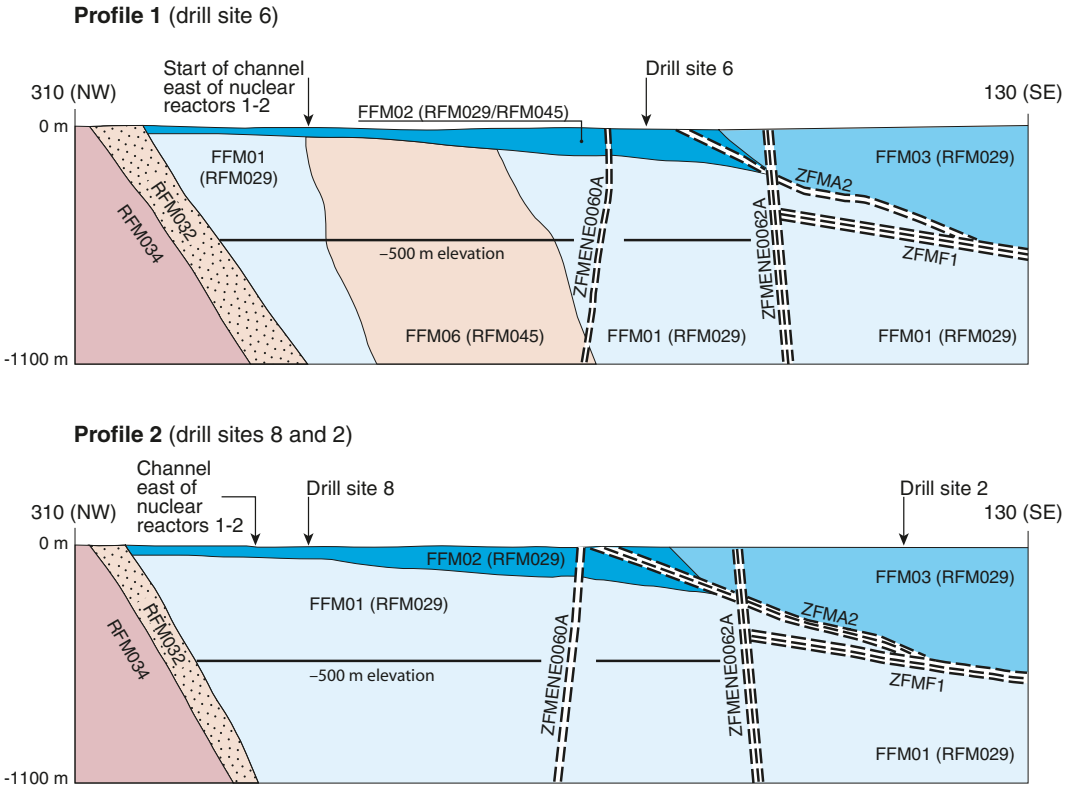

Figure 5-3. *Simplified profiles in a NW-SE direction that pass through drill sites 2 and 8 (lower profile) and drill site 6 (upper profile). (The profiles are shown in Figure 5-2) The key fracture domains FFM01,- 02 and -06 occur in the footwall of zones ZFMA2 (gently dipping) and ZFMF1 (sub-horizontal). The major steeply dipping zones ZFMENE0060A and ZFMENE0062A are also included in the profiles. (Source: Figure 3-9 in /Follin 2008/.)*

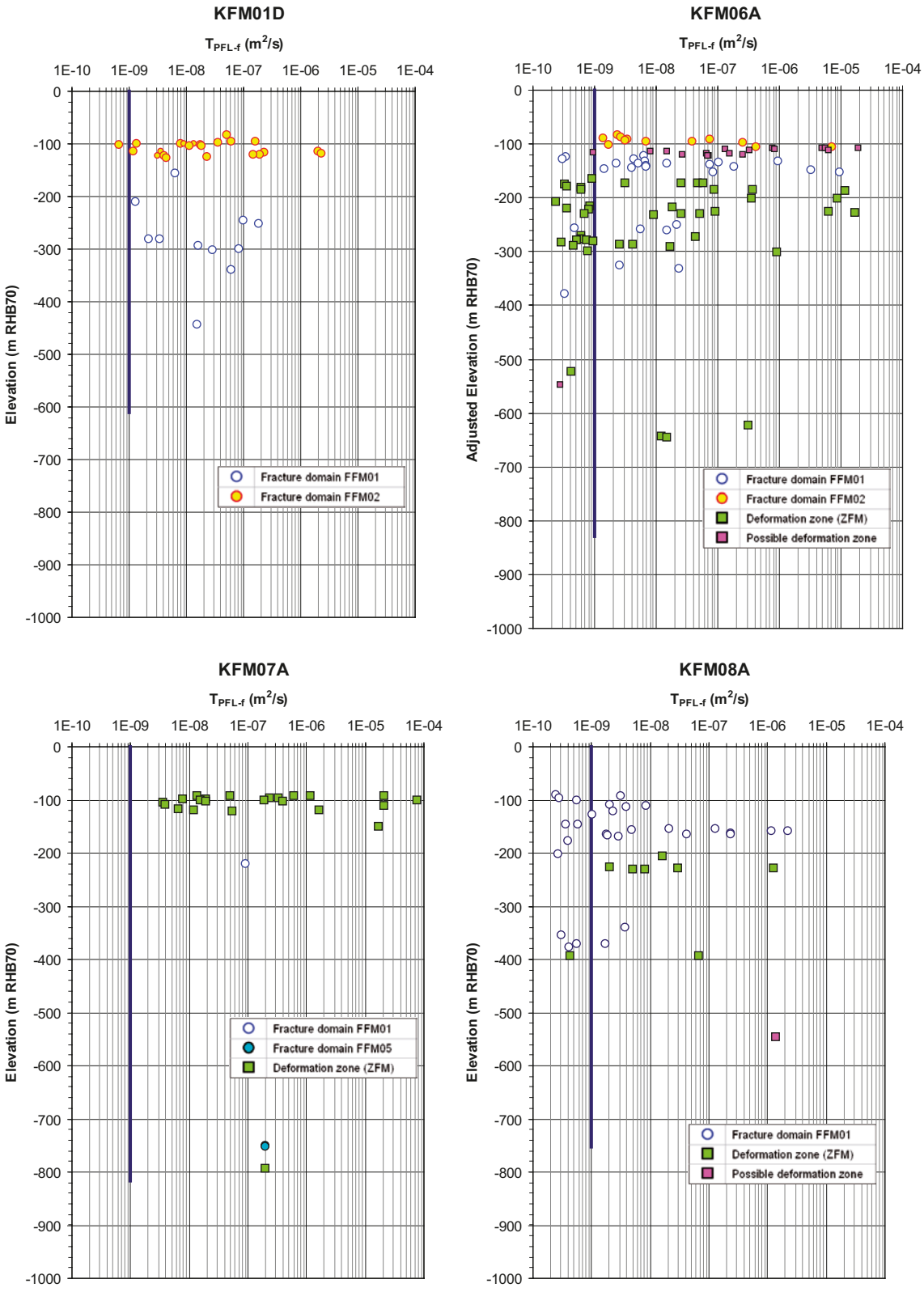

Figure 5-4. *Fracture transmissivity data from the cored boreholes KFM01D, KFM06A, KFM07A and KFM08A acquired with the PFL method. The data are coloured with regard to their structural classification and the blue lines indicate the typical threshold value reported from the investigations in the Forsmark area, 1×10^{-9} m^2/s. The lengths of the blue lines correspond to the depths investigated with the PFL method. (Source: Figure 5-2, Figure 5-7, Figure 5-8 and Figure 5-10 in /Follin et al. 2007a/.)*

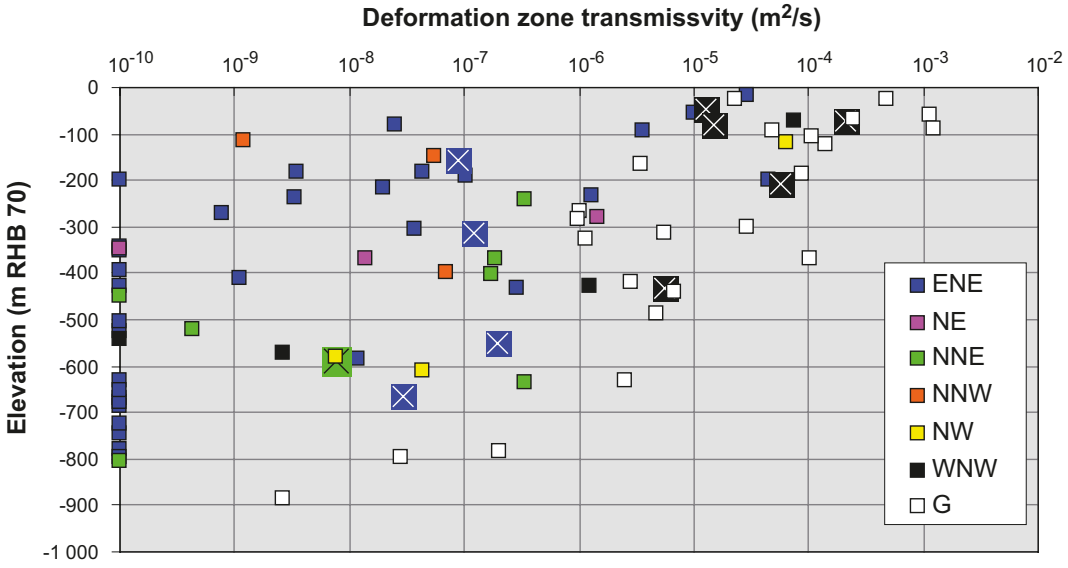

Figure 5-5. *Transmissivity data versus depth for the deterministically modelled deformation zones. The transmissivities are coloured with regard to the orientations of the deformation zones, where G means gently dipping. The steeply dipping zones are denoted by their strike direction. (Source: Figure 5-3 in /Follin 2008/.)*

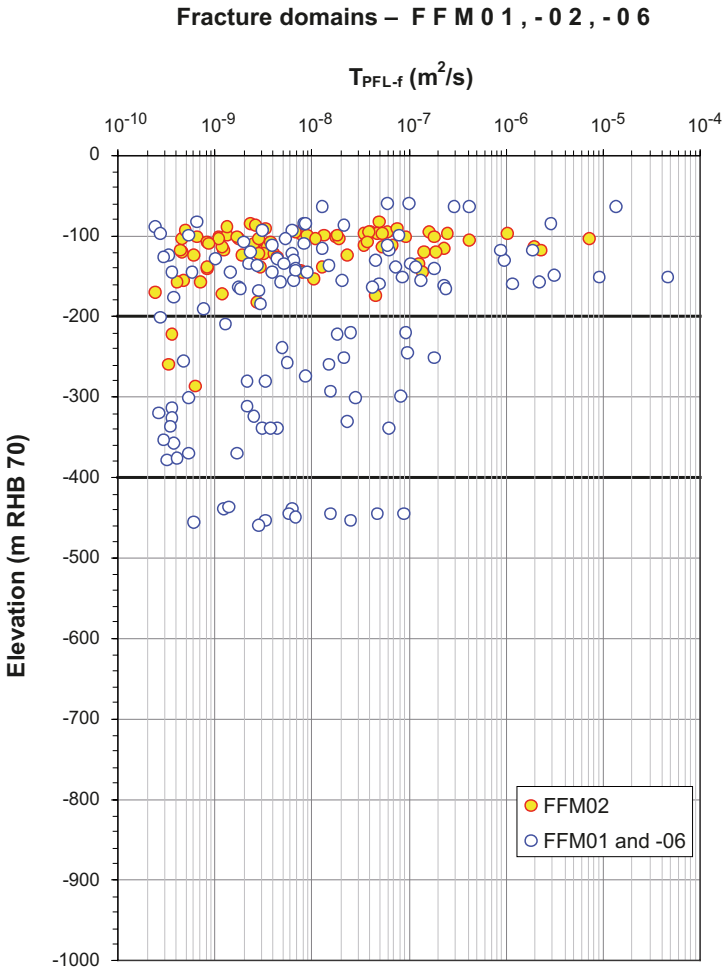

Figure 5-6. *Transmissivities of connected open fractures detected with the PFL method in boreholes KFM01A, -01D, -02A, -04A to -08A, -08C and -08D outside deformation zones within the target area (fracture domains FFM01–02 and -06). (Modified after Figure 5-12 in /Follin 2008/.)*

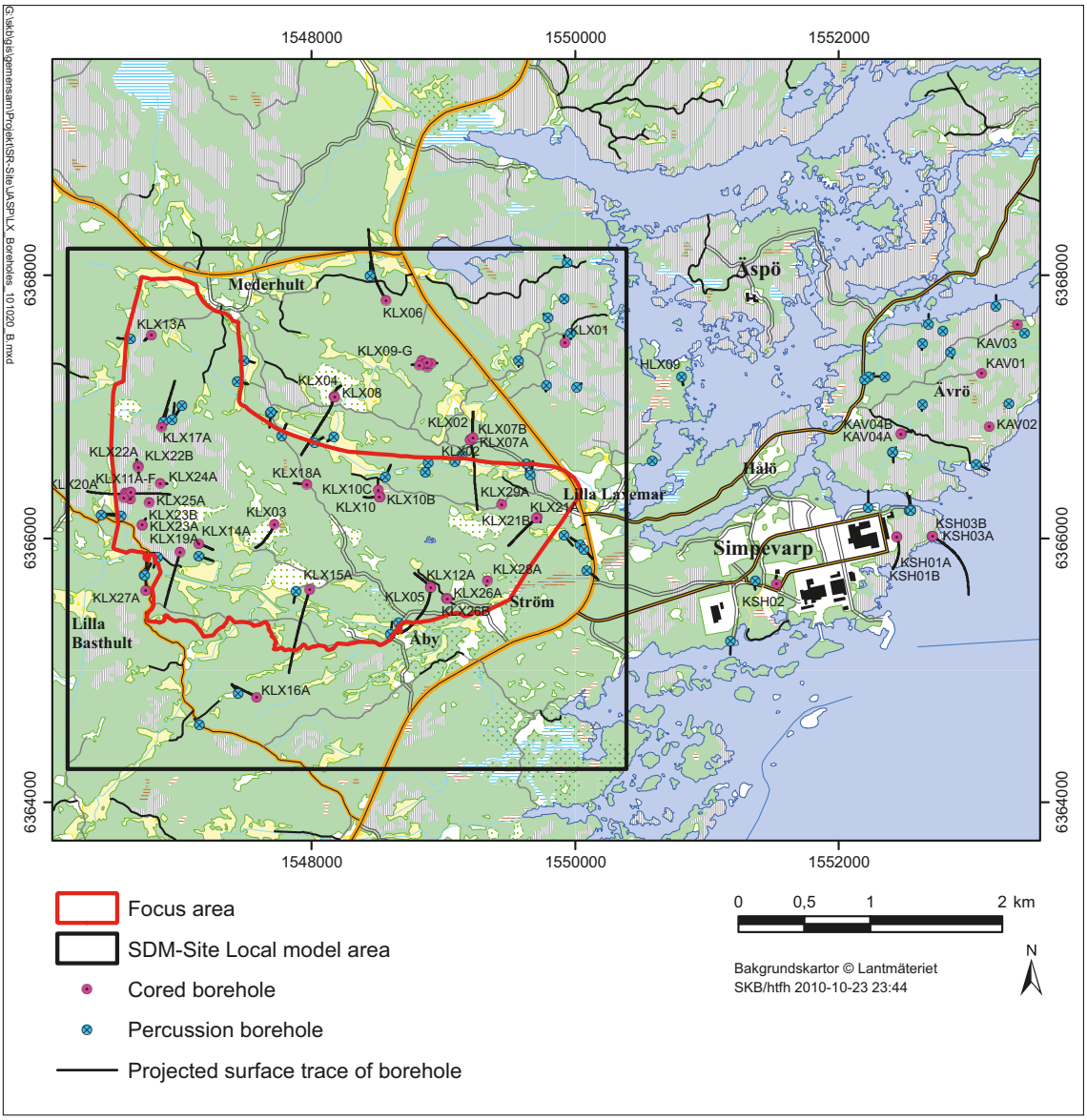

Figure 5-7. *Map showing the 46 core-drilled boreholes and the 43 percussion-drilled boreholes within the Laxemar local model area. The figure also shows boreholes within the Simpevarp model area. (Modified after Figure A1-1 and Figure A1-2 in /Rhén and Hartley 2009/.)*

Table 5-2 lists the 46 cored boreholes drilled within the Local model area, see Figure 5-7. The boreholes were investigated with the Posiva Flow Log (PLF) method and the Pipe String System (PSS) method. The hydraulic data acquired from the tests were used to parameterise the deterministically defined deformation zones (HCD) and the fracture networks contained in the rock mass volumes (HRD) in between the deformation zones.

At Laxemar, the HRDs are defined based on the spatial variability in the measured hydraulic properties, mainly the hydraulic conductivity, see /Rhén et al. 2008/ for details. Figure 5-8 and Figure 5-9 shows the key HRDs (HRD_N, HRD_EW007, HRD_C, and HRD_W) within the Local model area. The N-S cross-section indicated in Figure 5-9 is shown in Figure 5-10. The focus area covers HRD_C (north of deformation zone ZSMNW042A), HRD_W (south of deformation zone ZSMEW007C) and the southern part of HRD_EW007.

Table 5-2. List of the cored boreholes at Laxemar tested with the PFL and PSS methods. (Based on Appendix 1 in /Rhén and Hartley 2009/.)

Borehole	PFL	PSS	Bottom elevation of borehole (m)	Borehole	PFL	PSS	Bottom elevation of borehole (m)
KLX01		X[1]	–1,059	KLX11B–F	X	X[2]	Above –82
KLX02	X[1]	X	–1,669	KLX12A	X	X	–560
KLX03	X	X	–950	KLX13A	X	X	–565
KLX04	X	X	–962	KLX14A	X	X[2]	–112
KLX05	X	X	–879	KLX15A	X	X	–740
KLX06	X	X	–788	KLX16A	X	X	–371
KLX07A	X	X	–629	KLX17A	X	X	–569
KLX07B	X	X[2]	–181	KLX18A	X	X	–581
KLX08	X	X	–826	KLX19A	X	X	–649
KLX09	X	X	–844	KLX20A	X	X	–311
KLX09B–G	X	X[2]	Above –110	KLX21B	X	X	–789
KLX10	X	X	–971	KLX22A,B–KLX26A,B	X	X[2]	Above –71
KLX10B,C	X	X[2]	Above –107	KLX27A	X	X	–565
KLX11A	X	X	–909	KLX28A–KLX29A	X	X[2]	Above –59

[1] Measurements before the site investigations for SDM-Site Laxemar.
[2] Only pumping tests with long test section, generally entire borehole.

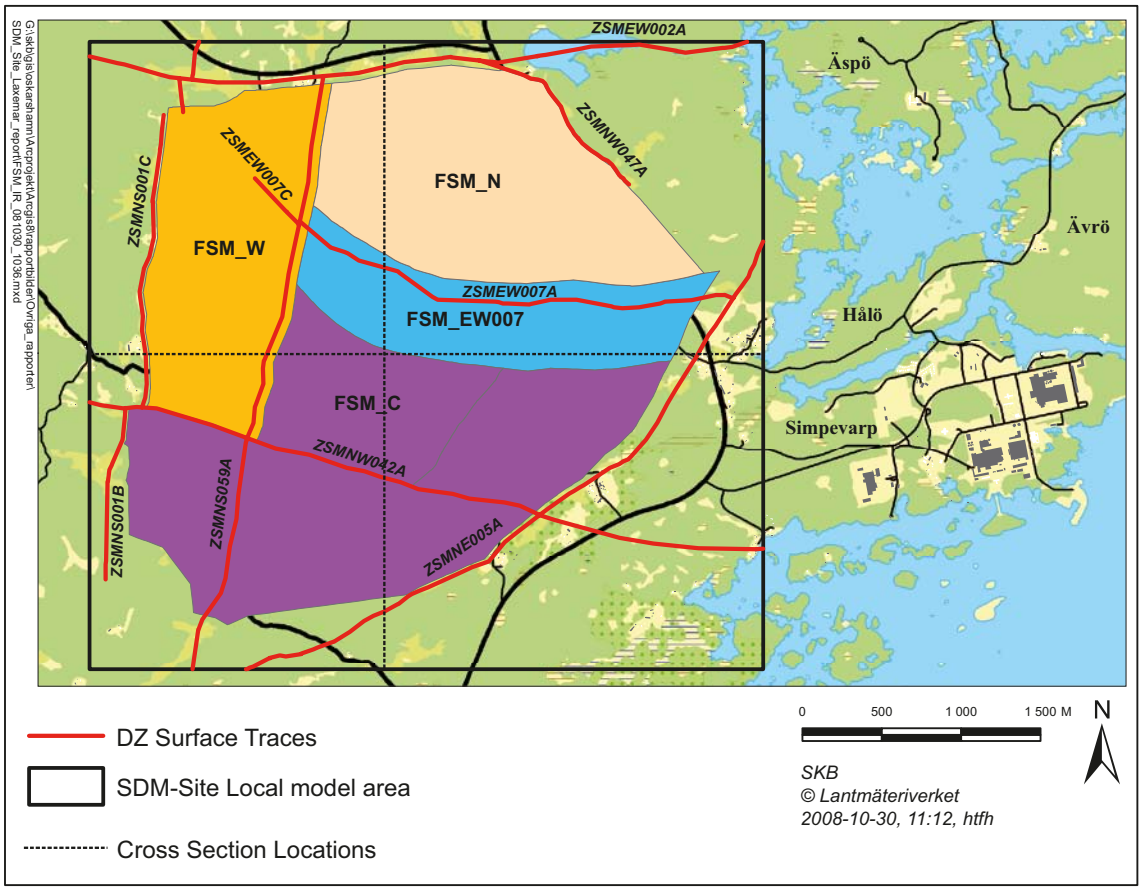

Figure 5-8. *Illustration of the SDM-Site Laxemar Hydraulic Rock mass Domain Model. (Source: Figure 5-4 in /Rhén and Hartley 2009/.)*

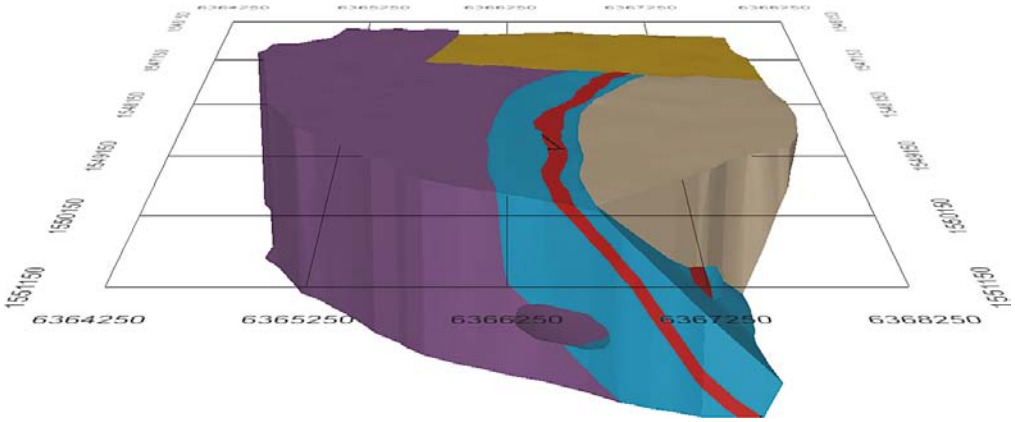

Figure 5-9. *Illustration of the SDM-Site Laxemar Hydraulic Rock Domain Model, 3D perspective view looking westward. (Source: Figure 5-6 in /Rhén and Hartley 2009/.)*

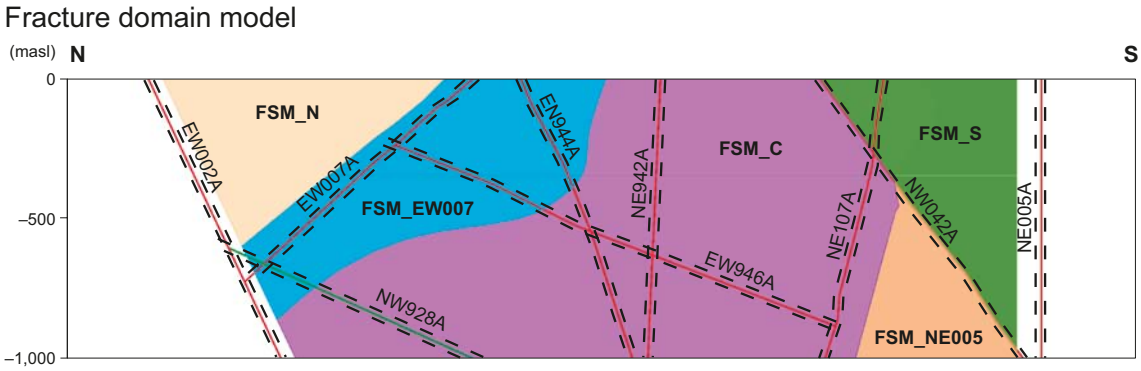

Figure 5-10. *N-S cross-section through the local model volume showing the formation of fracture domains and deterministically modelled deformation zones, cf. Figure 5-8. The length of the section is approximately 4,300 m. (Source: Figure 11-18 in /SKB 2009a/.)*

Figure 5-11 shows examples of PFL fracture transmissivity data from four core-drilled boreholes KLX05, KLX08A, KLX11A and KLX15A. As can be seen in the plots, the conductive fracture frequency is generally higher above –200 m than below this elevation. However, there is a pertinent variation in the conductive fracture frequency with depth suggesting local heterogeneities within each HRD below –200 m. The decrease in fracture transmissivity is not as significant as the decrease in fracture frequency, although the highest transmissivity values are for most parts observed above –200 m. Among the four HRDs, the frequency of conductive fractures is the highest in HRD_EW007. This will be commented more in the text below.

Deformation zones modelled deterministically, elevation c. 0 to –1,000 m

The deduced transmissivities of the deterministically modelled deformation zones are shown in Figure 5-12. As can be seen in the figure, the variability in transmissivity is large but considering mean values for the shown depth zones, the transmissivity decreases with depth. There is a tendency for the transmissivity to be positively correlated with the interpreted lineament length of the HCD and also that the steeply dipping HCDs with a E-W strike are slightly more transmissive than HCDs of other orientations, see /Rhén et al. 2008/ for details.

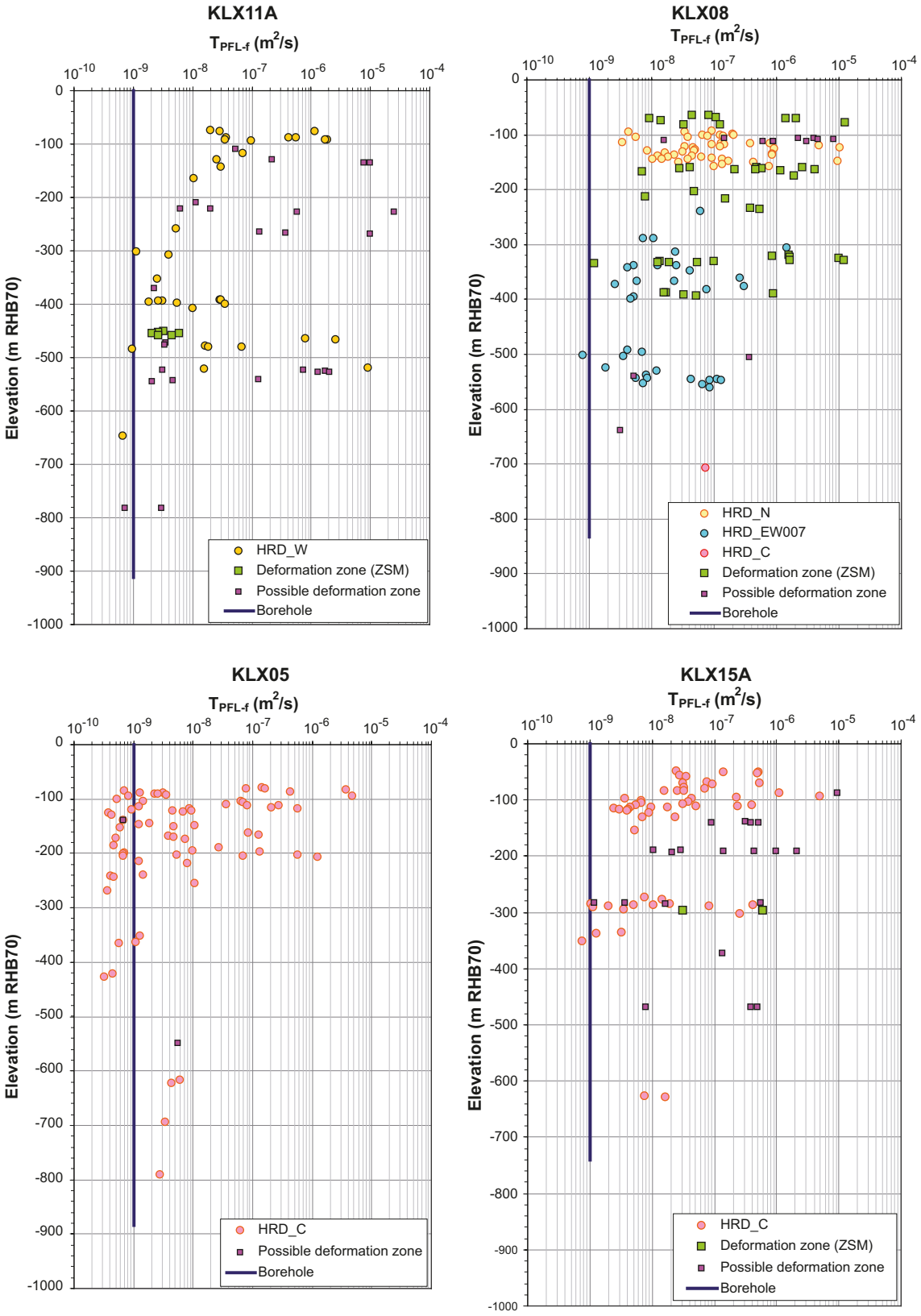

Figure 5-11. *Fracture transmissivity data in the cored boreholes KLX05, KLX08A, KLX11A and KLX15 acquired with the PFL method. The data are coloured with regard to their structural classification and the blue lines indicate the typical threshold value reported from the investigations in the Forsmark area, 1×10^{-9} m^2/s. The lengths of the blue lines correspond to the depths investigated with the PFL method. (Source: Two of figures from Figure 11-14 in SKB 2009a/.)*

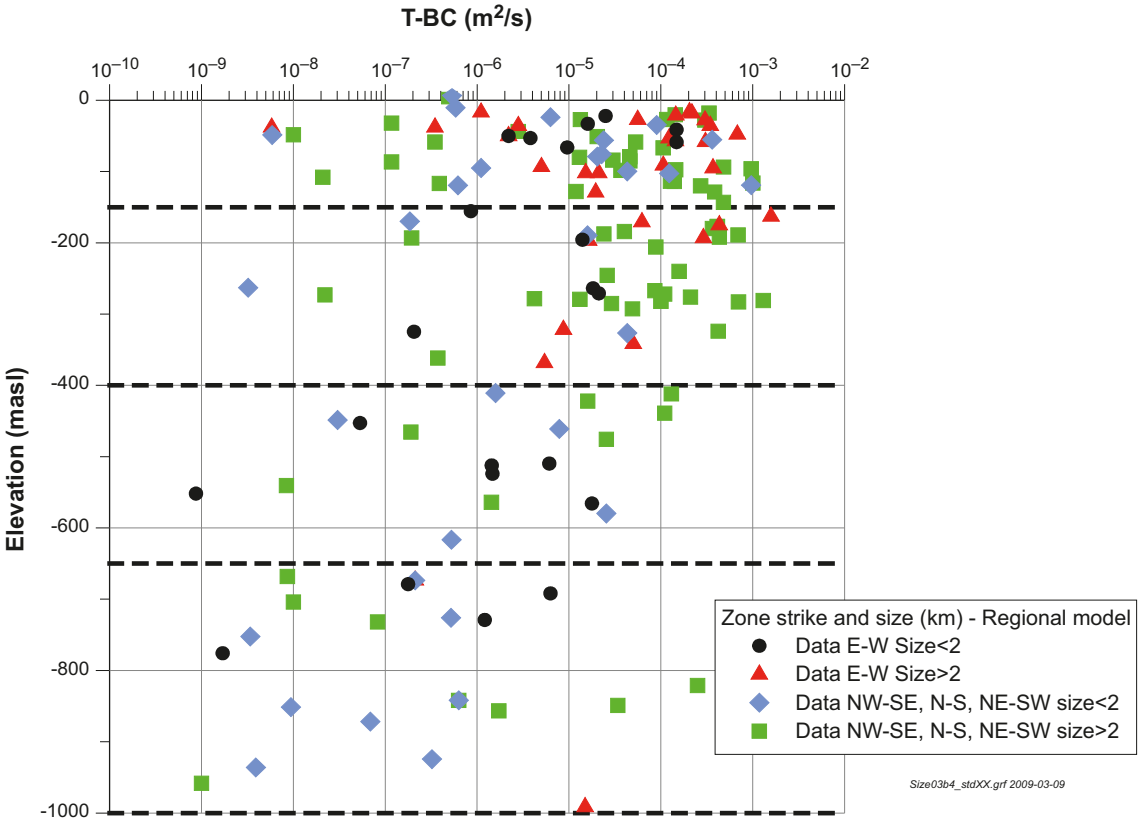

Figure 5-12. *Deformation zone transmissivity (T) versus depth taking the strike and lineament length of the zones into account. Data represent the regional model domain. (Source: Figure 5-3 in /Rhén and Hartley 2009/.)*

Fractured bedrock between the deterministically modelled deformation zones, elevation c. 0 to –1,000 m

Figure 5-13 shows hydraulic conductivity data by elevation acquired within the local model area with the PSS method using a packer spacing (test scale) of 100 m. The data represent the rock mass volumes between the deterministically modelled deformation zones. As seen in the plot, there is a significant variability in the hydraulic conductivity within each depth zone. The variability supports the irregular decrease with depth in the frequency and the transmissivity of flowing fractures shown in Figure 5-11.

5.3.3 Site comparison – data

In this section, data from the target area at Forsmark and in the focused area at Laxemar are compared. The comparison is centred on the observations made at repository depth, i.e. –400 to –700 m.

The hydraulic conductivity estimated from measurements conducted with the PSS method (K_PSS) and the conductive fracture frequency estimated from measurements using the PFL method (PFL $P_{10,corr}$) are quantities that are often used to describe the permeability of the rock mass volumes between the deterministically modelled deformation zones. The two quantities are also used in groundwater flow modelling.

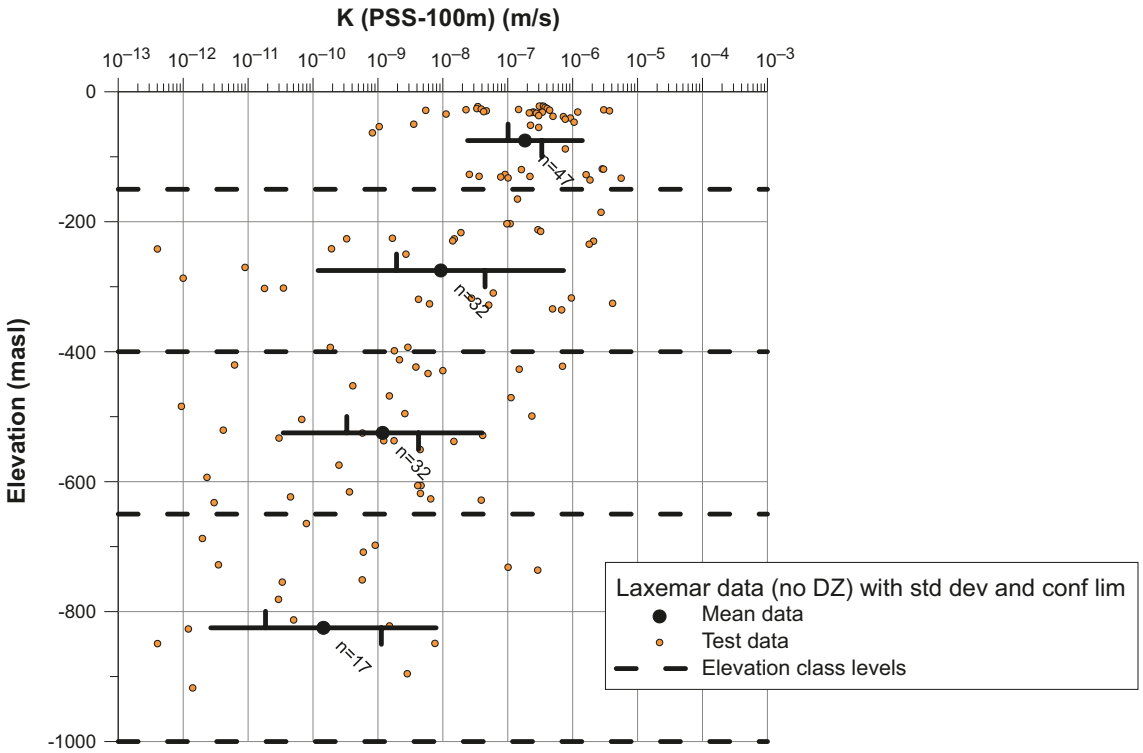

Figure 5-13. *Hydraulic conductivity (K) data by elevation acquired within the local model area with the PSS method using a packer spacing (test scale) of 100 m. The test sections are positioned between the deterministically modelled deformation zones. Three statistics are shown for each depth zone: the geometric mean of all values of K (mean of log10(K)), the 95% confidence limits for the mean of log10(K), and the ±1 standard deviation of log10(K). (Modified after Figure 5-11 in /Rhén and Hartley 2009/.)*

Figure 5-14 shows a cumulative probability plot of all $\log_{10}(K\_PSS)$ data measured with a packer spacing (test scale) [3] of 20 m in the depth interval, based on the data presented in /Selroos and Follin 2010, Figure 2-7/ and /Rhén et al. 2008/ for the two respective sites. There is a clear difference between the two distributions a large proportion of the Forsmark sample is much less conductive compared with Laxemar. Excluding data for the most conductive HRD at Laxemar, HRD_EW007, does not change this conclusion.

Table 5-3 shows average values of the conductive fracture frequencies (PFL $P_{10,corr}$) at potential repository depths within the target/focus volumes. The key part of the rock mass volume in the target area at Forsmark, FFM01 and FFM06, has a very low average conductive fracture frequency. The rock mass volume south of the target area, FFM03, also has a low average conductive fracture frequency, but higher than in FFM01 and FFM06. The average conductive fracture frequencies in HRD_C and HRD_W at Laxemar resemble that of FFM03 at Forsmark, whereas the conductive fracture frequency in HRD_EW007 is much greater.

[3] A telescopic approach is used for the single-hole hydraulic testing with the PSS method at Laxemar and Forsmark. Each borehole is measured with consecutive 100-m long, 20-m long and 5-m long packer intervals beginning with the longest packer interval. However, non-flowing 100-m long packer intervals are not studied with 20-m long packer intervals, etc. To display a cumulative plot of all 20m sections a uniform distribution of transmissivity (T) is assumed in each low-transmissive 100 m section and the corresponding five unmeasured 20m sections are a assigned a hydraulic conductivity (K) as follows; K(20m) = T(100m)/100 m.

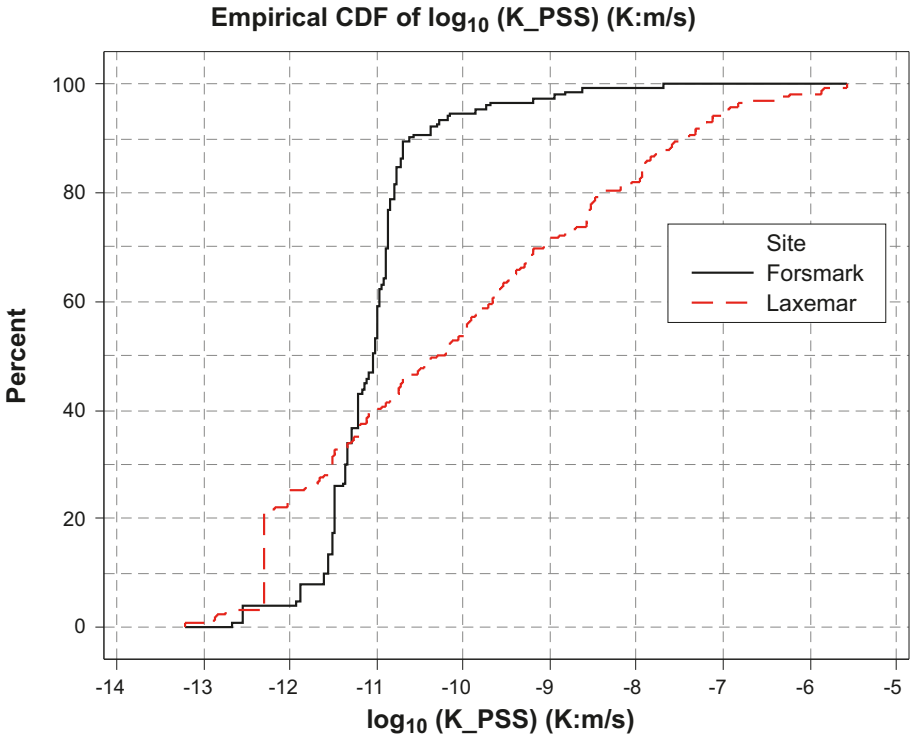

Figure 5-14. *Cumulative distribution plot of all log10(K_PSS) data measured with a packer spacing (test scale) of 20 m between elevations –400 m to –700 m within the target area at Forsmark and the focus area at Laxemar. Values lower than –10.4 are uncertain as they lie below the robust lower measurement limit for the PSS equipment, but the percent of tested sections below this limit (i.e. about 90% at Forsmark and about 50% at Laxemar) is well established.*

Table 5-3. Average values of the frequency of flowing fractures detected with the PFL method (PFL $P_{10,corr}$) in the rock mass volumes between deterministically modelled deformation zones. (Modified after Table 5-3 in /Follin 2008/ and Table 5-2 in /Rhén and Hartley 2009/.)

Site	Domain	Depth zone (m)	PFL $P_{10,corr}$ (m^{-1})	Min T (m^2/s)	Max *T* (m^2/s)
Forsmark	FFM01 and -FFM06	–400 to –1,000	< 0.01	$6.2 \cdot 10^{-10}$	$8.9 \cdot 10^{-8}$
Laxemar	HRD_EW007	–400 to –650	0.23	$7.9 \cdot 10^{-10}$	$1.8 \cdot 10^{-06}$
Laxemar	HRD_W	–400 to –650	0.06	$6.7 \cdot 10^{-10}$	$9.2 \cdot 10^{-06}$
Laxemar	HRD_C	–400 to –650	0.11	$3.3 \cdot 10^{-10}$	$1.1 \cdot 10^{-06}$

5.3.4 Non flow related transport characteristics

Migration through the fractures in the rock depends not only on the groundwater flow and its geometrical distribution, but also on the properties of the rock matrix surrounding the flow paths. Regarding the rock matrix characteristics Laxemar exhibits slightly more favourable conditions than Forsmark /Crawford 2008, Crawford and Sidborn 2008/. The site specific non-flow related transport properties are incorporated in the analysis of radionuclide transport presented in Chapter 10.

5.4 Model results for different time periods

5.4.1 Modelling methodology

The modelling methodology adopted in SR-Site and applied for the Forsmark site is described in detail in /Selroos and Follin 2010/. All results for Forsmark presented below originate from the SR-Site modelling. The same modelling methodology is adopted for the Laxemar site.

Three different modelling periods are included in the assessment. These are, with the appropriate references to the supporting model reports, given below for the Forsmark and Laxemar sites, respectively:

- The excavation and operation phase /Svensson and Follin 2010, Svensson and Rhén 2011/.
- The initial period of temperate climate after closure /Joyce et al. 2010, 2011/.
- The remaining part of the reference glacial cycle /Vidstrand et al. 2010, 2011/.

Each model representation is based on the site-descriptive models presented in /Follin 2008/ and /Rhén and Hartley 2009/, for Forsmark and Laxemar, respectively. Detailed information about the model setup is described in the individual model reports. In general, a hydrogeological base case model including a hydrogeological discrete fracture network (Hydro-DFN) model is developed within the temperate phase modelling, and is exported to the two other model applications of the other periods. Thus, the most elaborate descriptions of the developed hydrogeological base cases, and their relation to the underlying SDM-Site models, are provided in /Joyce et al. 2010, 2011/. For Laxemar, an elaborated hydrogeological discrete fracture network has been developed relative to SDM-Site for reasons discussed in /Joyce et al. 2011/. This model is fully propagated to the excavation and operation phase model, and to the glacial period model for relevant parts of the analyses.

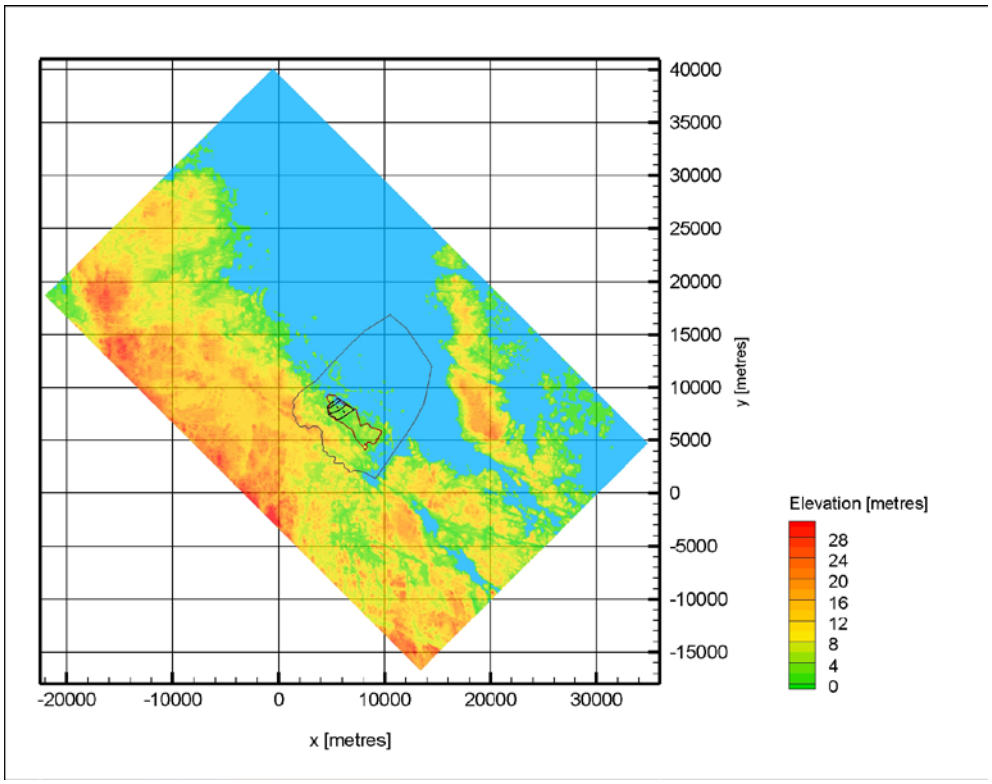

Figure 5-15. *The three model scales treated in SR-Site exemplified for the Forsmark site. These are the super-regional, regional and site/repository scales. The rectangle corresponds to the model domain on a super-regional scale, the large polygon in the centre corresponds to the model domain on a regional scale, whereas the small polygon inside the large polygon shows the location of the investigated candidate area. The repository scale model domain is located in the north-western part of the small polygon.*

It is also noted that the groundwater flow modelling in SR-Site is carried out on several scales, see Figure 5-15. The periglacial and glacial flow modelling is conducted on a super-regional scale (on the order of 10 km dimensions), but with enhanced resolution in the centre part. The temperate flow modelling is conducted on three scales; regional, site and repository, and uses a mixture of flow concepts, continuum, equivalent continuum and discrete. For instance, the regional scale modelling is identical in size and flow concept to that used in the SDM-Site modelling, whereas the repository scale modelling (on the order of 1 km dimension) utilises solely the discrete fracture network approach. The excavation and operation phase modelling is conducted on a regional scale, but have increased resolution around the repository tunnels and deposition holes.

As already mentioned, different flow concepts are used, i.e. both continuous porous medium and equivalent continuous porous medium (CPM/ECPM) models as well as discrete fracture network representations are used. All CPM/ECPM models applied for the different time periods above solve density driven flow including matrix diffusion of salt in sparsely fractured rock. The ECPM models are based on up-scaling of underlying discrete fracture network models. Discrete model representations are used within the temperate modelling at site and repository scale.

In the repository scale model, the individual deposition holes are resolved, and three different release paths are studied. These are for a fracture intersecting a deposition hole (the Q1 release path), a potential excavation damaged zone (the Q2 release path), and a path through the backfilled tunnel and into a fracture intersecting the deposition tunnel (the Q3 release path).

A variety of results are available from the different studies. Below, a subset of results of safety relevance as listed in Section 5.2, are given. All results are presented in a comparative mode, i.e. results for both sites are presented together.

5.4.2 Site comparison – modelling

Excavation and operation phases

During the excavation and operation phase, the tunnels are open and kept at atmospheric pressure. Hence, an inflow to the repository will occur. The total inflow to the repository at the sites is presented in Table 5-4 below for both grouted and ungrouted cases. The calculations are based on a fully open repository; i.e. all tunnels are open at the same time. This should be a conservative case in terms of total inflow. The grouting case is based on an assumed grouting efficiency, or threshold value, of $K=1\cdot10^{-8}$ m/s, i.e. all cells in the model in contact with a tunnel or deposition hole with a value higher than the threshold are lowered to the threshold value $K=1\cdot10^{-8}$ m/s.

It is observed that the total inflow for ungrouted conditions to the Laxemar repository is more than five times larger than that to the repository at Forsmark. Also, it is observed that while the grouting reduces the inflows by approximately a factor of four in Forsmark, the corresponding number for Laxemar is smaller than two.

Table 5-4. Total inflow (L/s) to a repository at Forsmark and at Laxemar.

Site	Case	
	Grouted	Ungrouted
Laxemar	420	793
Forsmark	31.2	133.7

Table 5-5. Inflow (L/min/100 m tunnel) to deposition holes and tunnels.

Site	Case	
	Grouted	Ungrouted
Laxemar	21.6	33.0
Forsmark	1.6	1.9

Since the repository at Laxemar, in terms of tunnel length, is larger than in Forsmark it is of interest to also analyse a normalised inflow. This analysis is based on inflow into deposition tunnels and deposition holes only. The total deposition tunnel length in the model is 54,157 m in Forsmark, and 89,331 m in Laxemar. The results are presented in Table 5-5 below. Here, total inflow to the deposition tunnels and deposition holes is expressed as total inflow rate per minute and 100 m of tunnel (for both grouted case and ungrouted cases). It is observed that the effect of grouting is reduced when the normalised inflow is studied, specifically for Forsmark. This is due to the fact that at Forsmark, the largest inflows are in the ramp and shaft in the upper part of the repository (inflow from the sheet joints). Here, grouting is more effective than in the deposition tunnels where inflows are low also without grouting.

In Table 5-6, the number of potential deposition holes that have an inflow larger than 0.1 L/min are presented for both grouted and ungrouted conditions. It is clear that the number of holes is much smaller in Forsmark than in Laxemar. It is noted that grouting slightly increases the number of deposition holes with an inflow larger than 0.1 L/min. This is due to the fact that groundwater pressure increase when the larger fractures have been grouted.

In Figure 5-16 below, the cumulative density functions for inflow to deposition holes are shown for the ungrouted case. The different shapes of the distributions are noted; for Forsmark, approximately 90% of the deposition holes have inflows below 0.01 L/min, whereas for Laxemar the distributions are much less steep.

Table 5-6. Number of deposition holes with a simulated inflow larger than 0.1 L/min.

Site	Case	
	Grouted	Ungrouted
Laxemar (8,038*)	5,113	4,211
Forsmark (6,916)	154	142

* In the CAD delivery used, 10 extra deposition positions exist relative to the correct layout.

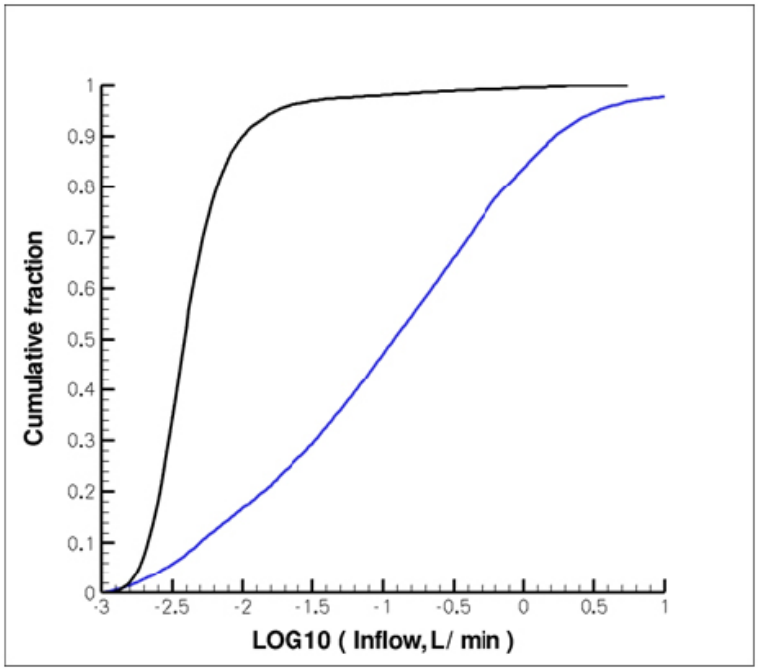

Figure 5-16. *CDF of inflow to deposition holes connected to a water conductive fracture – ungrouted case. Black colour is for Forsmark and blue is for Laxemar.*

Temperate period

During the temperate period, the repository is backfilled and water saturated. Hence, the repository structures will be part of the connected system where flow and transport can occur.

The number of deposition holes intersected by at least one fracture, and the number of deposition holes with an initial Darcy flux above a threshold value 10^{-6} m/y representing the smallest value that can be numerically resolved, see /Joyce et al. 2010/ for details), are presented in Table 5-7. For Forsmark it is observed that roughly 40% of depositions holes are connected to the network, but only roughly 30% of holes have a flow (expressed as Darcy flux) that is high enough to be numerically resolved. For Laxemar, roughly 70% of deposition holes are connected, and essentially all of these holes have a Darcy flux above the threshold value. It should be noted that these simulated inflows are consistent, and if anything higher, then the inflows estimated without numerical simulation, which were used when developing the design for the two sites /SKB 2009d/ and /SKB 2009b/ respectively, see further Chapter 2.

Figure 5-17 shows the cumulative distribution function of the Darcy flux q at deposition holes for all deposition hole positions with a flow path to the top surface of the model. (Such release paths are called Q1 release paths, see above at the end of Section 5.4.1). There is a consistency with lower Darcy fluxes

Table 5-7. Comparison of deposition hole statistics for Forsmark and Laxemar hydrogeological base cases at 2000 AD.

	Forsmark	Laxemar
Total number of deposition holes	6,916	8,031
Number of deposition holes intersected by at least one fracture	2,762 (39.9%)	5,668 (70.6%)
Number of deposition holes intersected by at least one fracture with a flow > 10^{-6} m/y	2,008 (29.0%)	5,642 (70.3%)

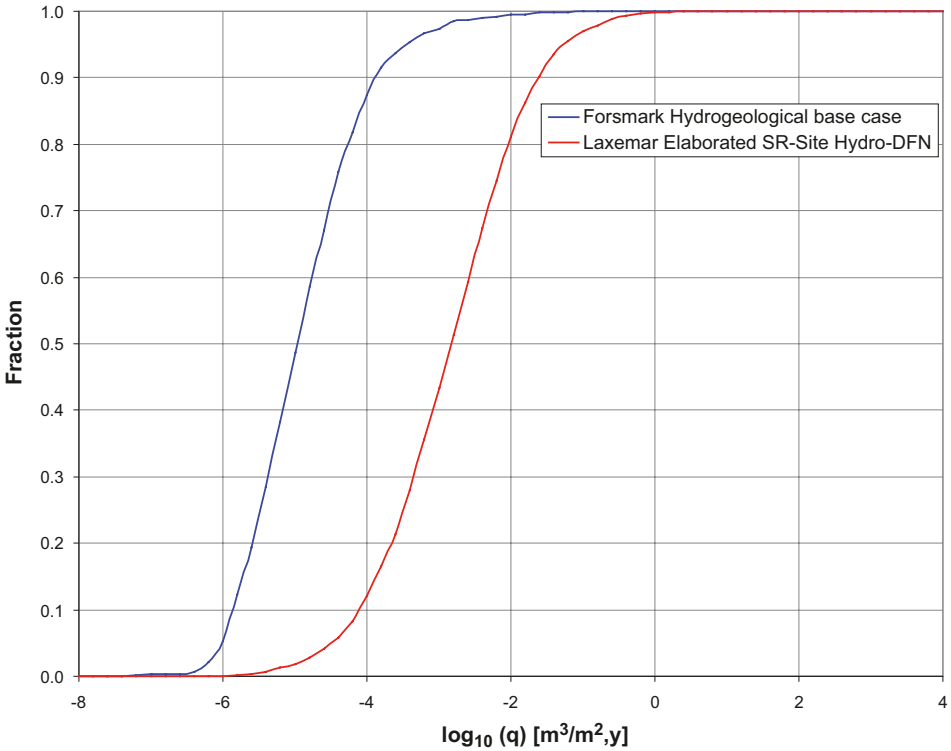

Figure 5-17. *Cumulative distribution functions of Darcy flux in deposition holes (Q1 release path) for the particles successfully reaching the model top boundary, for releases at 2000 AD from the Forsmark hydrogeological base case (blue) and the Laxemar Elaborated SR-Site Hydro-DFN (red). At Forsmark only 24% of the deposition holes have such release paths directly from the deposition holes whereas the corresponding figure at Laxemar is 60%.*

for all release paths, i.e. also for Q2 starting in a potential EDZ intersecting the depostion hole and for Q3 starting in a fracture intersecting the deposition tunnel, at Forsmark than at Laxemar. The largest difference is seen for the Q1 release path, i.e. the fracture intersecting a deposition hole. Here, the Darcy fluxes at Forsmark are smaller than at Laxemar by approximately two orders of magnitude.

The cumulative distribution functions of the flow-related transport resistance are shown in Figure 5-18 for the Q1 release path. The flow-related transport resistance is an entity integrated along flow paths from repository depth to the surface and is a measure of how much retention of transported solutes can occur along the flow path (the retention is controlled by the flow-related transport resistance and a group of nuclide specific parameters describing diffusion and sorption in the matrix). A larger value implies more retention.

For the flow-related transport resistance, Forsmark displays larger values than Laxemar for all three release paths. The values at Forsmark are slightly more than one order of magnitude larger than at Laxemar (for all release paths). The reason the difference is smaller between the different release paths for the flow-related transport resistance relative to the Darcy flux is that the flow-related transport resistance is integrated along flow paths, and hence an averaging takes place (i.e. a summation is made where the order of summed elements does not matter).

Glacial period

The primary driving force for groundwater flow at repository depth during periods of periglacial (permafrost) and glacial climate conditions is the difference in residual hydraulic pressure below the ice sheet and in front of the ice-sheet margin. The expected effects of this gradient are assessed by numerical flow modelling. The results of this modelling with relevance for long-term safety are related to the groundwater chemistry, the performance measures of groundwater flow at repository depth, and the flow-related transport parameters.

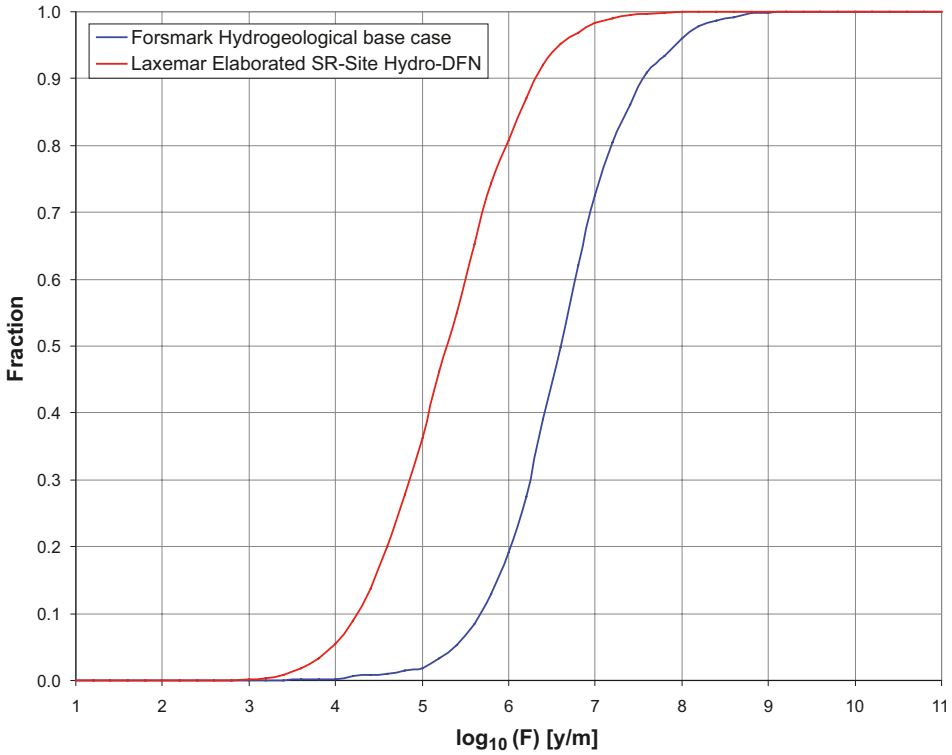

Figure 5-18. *Cumulative distribution functions of flow-related transport resistance for the particles successfully reaching the model top boundary in the Q1 path, for releases at 2000 AD from the Forsmark hydrogeological base case (blue) and the Laxemar Elaborated SR-Site Hydro-DFN (red). Furthermore, at Forsmark only 24% of the deposition holes have such release paths directly from the deposition holes whereas the corresponding figure at Laxemar is 60%.*

Below, modelling results are reported for the case with an advancing ice-sheet margin without permafrost in the periglacial area in front of the ice sheet. The three figures shown represents a situation when the ice-sheet margin is right above the repository, a location referred to as ice-front location II in the works of /Vidstrand et al. 2010, 2011/. The total number of deposition holes in these simulations is 6,916 at Forsmark and 8,031 at Laxemar.

Figure 5-19 shows a normalised cumulative density function (CDF) plot of the simulated Darcy flux q at the deposition hole positions for ice-front location II. The CDF for Forsmark is steeper and the magnitudes are approximately two orders of magnitude lower for the median compared with the CDF for Laxemar.

Figure 5-20 and Figure 5-21 show the fracture water salinity fields. The simulated disturbances caused by the glacial meltwater recharge is greater at Laxemar than at Forsmark.

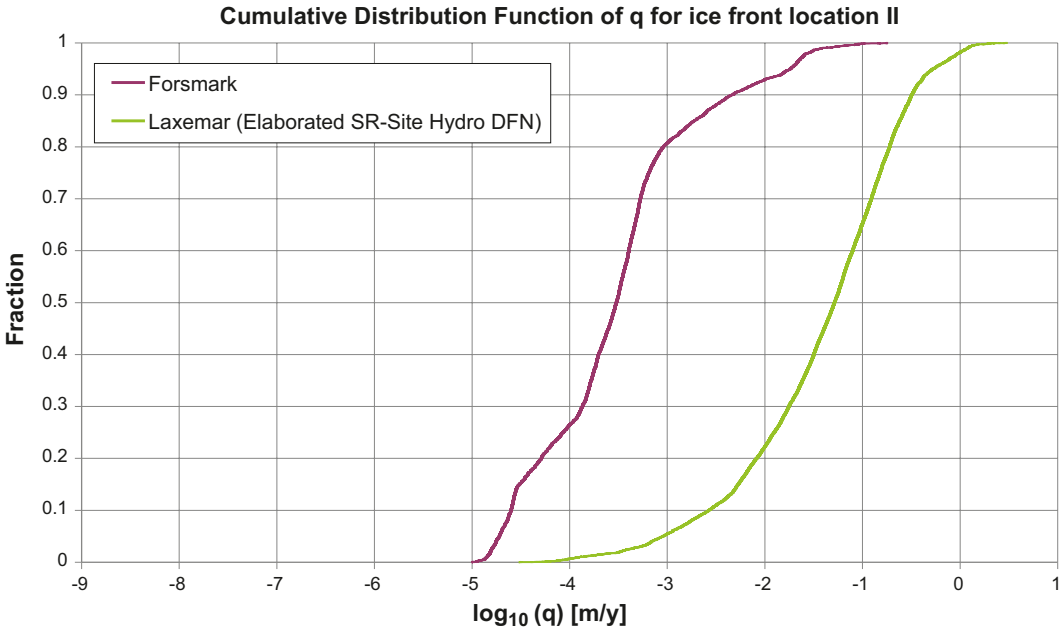

Figure 5-19. *CDF plot showing the Darcy flux at the deposition hole positions at Forsmark (6,916) and Laxemar (8,031) for ice front location II during the advance of an ice sheet without permafrost in the periglacial area in front of the ice sheet.*

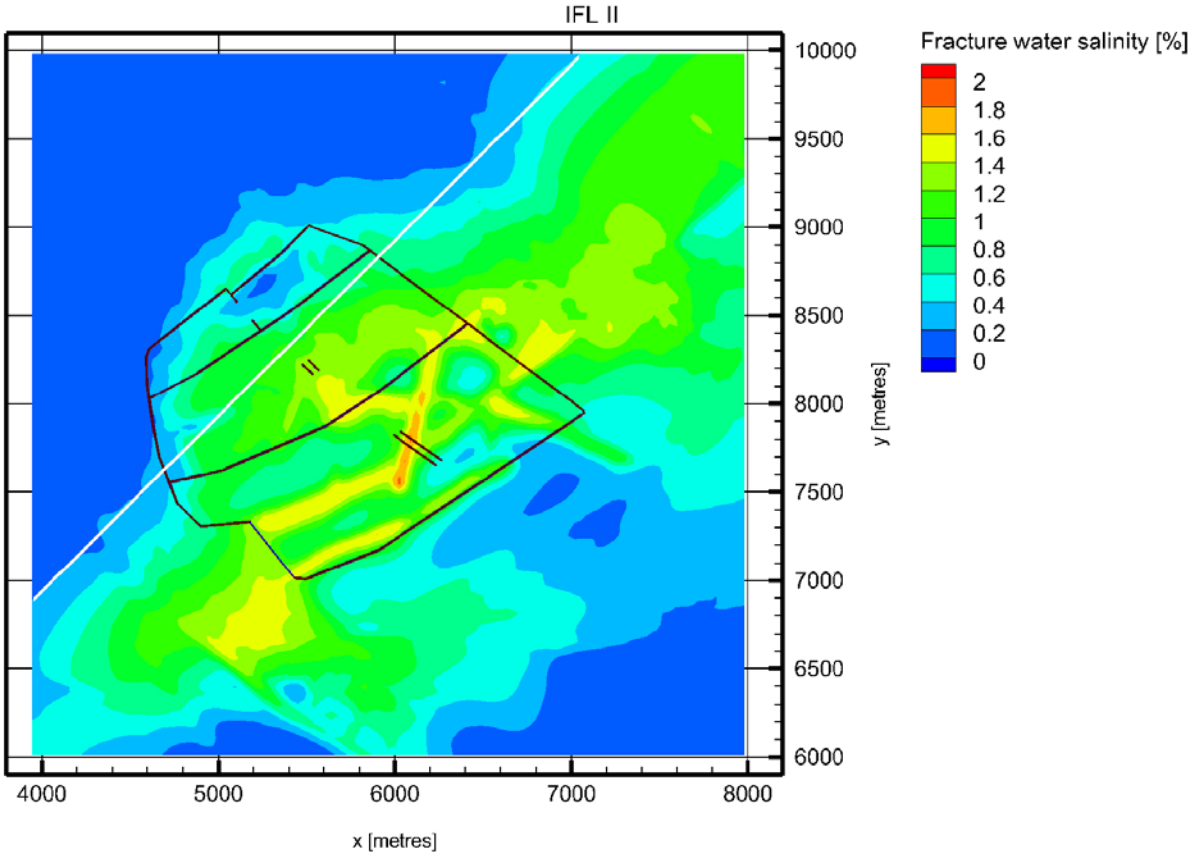

Figure 5-20. *Map showing the salinity at repository depth in Forsmark when the ice-sheet margin is at ice-front location II.*

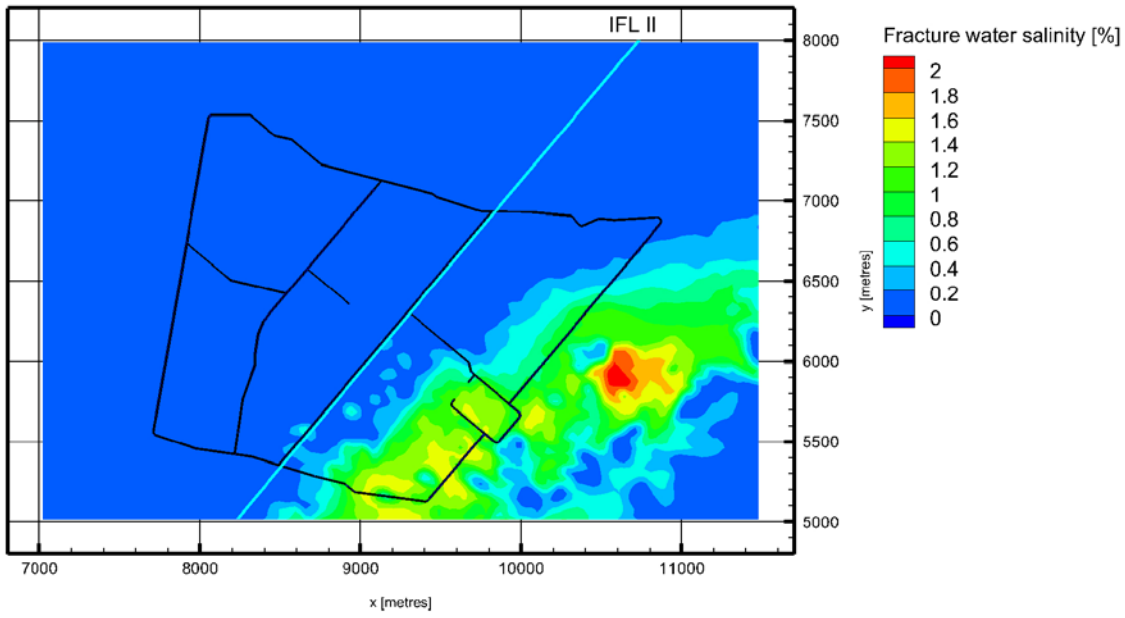

Figure 5-21. *Map showing the salinity at repository depth in Laxemar when the ice-sheet margin is at ice-front location II.*

5.5 Conclusions

In this chapter, the Forsmark and Laxemar sites are compared both in terms of data emanating from the site characterisation and the SDM-Site modelling (Section 5.3) and in terms of modelling results related to the phase of repository operation and to long-term safety (Section 5.4). Below the main findings are summarised.

- Both sites exhibit depth trends with regard to transmissivity of the deterministically modelled deformation zones. Although the lateral variability in transmissivity is quite large at both sites, the depth trend is more profound at Forsmark, where very few conducting fractures are found below –400 m elevation. At Laxemar, the average conductive fracture frequency is greater at repository depth and there is also a considerable spatial variability between different parts of considered rock mass volumes. When hydraulic characteristics at repository depth are compared in detail, it is found that Forsmark has a much lower average conductive fracture frequency (less than 0.01 m^{-1} compared to 0.06 m^{-1} to 0.23 m^{-1} at Laxemar). Also, the resulting hydraulic conductivity distributions estimated from hydraulic testing (PSS tests) indicate that Laxemar has a higher geometric mean and a larger spread in values with the high end tail showing values approximately two orders of magnitude higher than at Forsmark.
- During the construction and operation phases, the calculated inflow at Laxemar is more than ten times larger than at Forsmark assuming a realistic grouting efficiency. This is the case both when total inflows are considered, and when inflow normalised per unit tunnel length is considered.
- The number of deposition holes with an inflow larger than 0.1 L/min during the excavation and operation phases, assuming a realistic grouting efficiency, is more than 30 times larger at Laxemar than at Forsmark.
- In the temperate period simulations, the Darcy flux at the deposition hole locations (for fractures intersecting deposition holes) is approximately two orders of magnitude larger at Laxemar than at Forsmark. When the flow-related transport resistance is considered, the values are higher at Forsmark than at Laxemar by approximately one and a half orders of magnitude. Thus, both performance measures are more favourable at Forsmark than at Laxemar.
- In the glacial period simulations of an ice sheet in close proximity to the repository, the relative difference in Darcy flux at the deposition hole positions is approximately two orders of magnitude, with higher fluxes for Laxemar. The absolute values for both sites are higher by approximately one order of magnitude than the temperate period results.
- In the glacial period simulations, the disturbance to the salinity field is more pronounced at Laxemar than at Forsmark.

In conclusion, all hydrogeological measures and entities considered in this comparison are in favour of Forsmark. Regarding the rock matrix characteristics Laxemar exhibits slightly more favourable conditions than Forsmark. The site specific flow related and non-flow related transport properties are incorporated in the analysis of radionuclide transport presented in Chapter 10.

6 Chemical conditions and their evolution

6.1 Introduction

Chemical conditions affect the performance of a repository in a number of ways. Groundwater chemical compositions are needed to calculate the chemical evolution and physical stability of bentonite, the corrosion of canisters and the transport of radionuclides. In addition, the geochemical and mineralogical properties of the rocks and fracture-filling minerals will affect the transport of radionuclides and the penetration depth of dissolved oxygen in glacial meltwaters.

Groundwater compositions are mainly affected by ion-exchange, dissolution-precipitation reactions and microbial processes. The compositions are also affected by groundwater flow and mixing, which in turn is affected by changes in topography, climatic conditions, and sea level changes (shoreline displacements). It is therefore clear that a comparative analysis of the chemical conditions of the sites must include possible evolutions of such conditions with time over a glacial cycle.

Bentonite erosion has to be modelled for deposition holes where flowing groundwaters have low salinities for a given time period. Recent studies show that the important parameter is the charge concentration of groundwater cations, i.e. $\Sigma q[M^{q+}]$. In SR-Site it is considered that bentonite colloid stability is suppressed when the safety function indicator criteria is $\Sigma q[M^{q+}] > 4$ mM, see Figure 1-1. An examination of the groundwater compositions at the studied sites indicates that this criterion corresponds to salinities >0.27 g/L (>0.027 mass %).

The modelling of the chemical evolution of the bentonite in the buffer and backfill requires groundwater compositions and other variables as mentioned above. Important chemical parameters are the concentrations of Ca^{2+}, Mg^{2+}, Na^{+}, K^{+}, Fe, Cl^{-}, SO_4^{2-}, HCO_3^{-}, SiO_2(aq) and pH and Eh for groundwaters surrounding the repository.

In the case of a failed canister, the release of radionuclides to surrounding groundwaters can be limited by solubility if an insoluble solid phase is formed. Radionuclide concentration limits are calculated using a set of selected solid phases and equilibrium speciation calculations for a distribution of groundwater compositions.

To model the transport of radionuclides in the geosphere and in the buffer and backfill, K_d values (distribution coefficients) must be selected according to the groundwater salinities, carbonate concentrations, pH and redox potentials. Colloid facilitated transport of radionuclides in the geosphere requires information on the colloid concentrations and their sorption properties.

Two important parameters when modelling copper corrosion are the concentrations of either sulphide or oxygen. These corrodants either diffuse through the bentonite buffer towards the canister or, in the case of deposition boreholes where bentonite erosion has taken place, they are transported by the groundwater flow.

6.2 Safety relevance

The conclusions from the SR-Site assessment, see **SR-Site main report**, Chapter 15, is that the process of largest negative influence for the safety of the repository is the erosion of bentonite, caused by groundwaters of very low salinity, combined with canister corrosion caused by the groundwater contents of sulphide. Copper corrosion by oxygenated groundwaters is a process that could have an even larger impact, especially in deposition holes affected by erosion of bentonite, but only if oxygenated waters would reach the deposition holes. Hence, of the various groundwater chemical parameters, salinity, sulphide and oxygen contents appear to be the crucial ones from a site comparative point of view.

Salinity is mainly determined by the Ca^{2+} and Na^{+} concentrations in groundwaters occurring at Laxemar and Forsmark, as sulphide contents will be also dependent on the groundwater characteristics. On the other hand, the extent of oxygen intrusion will be dependent on the redox buffering capacity of the Laxemar and Forsmark bedrock/groundwater systems in the long-term perspective.

When establishing the chemical conditions in the bedrock only relatively few points for a relatively low number of boreholes can be sampled from any site and therefore data uncertainty and variability as well as model confidence are important points to consider.

6.3 Site data and model results for Forsmark and Laxemar

6.3.1 Salinity, Ca^{2+} and Na^{+} under temperate, periglacial and glacial periods

Present temperate conditions

Figure 6-1 shows determined Ca^{2+} and Na^{+} concentrations as a function of depth for both Laxemar and Forsmark. The data indicate that Forsmark groundwaters have a larger Ca^{2+} and Na^{+} contents at depths lower than –200 m. Furthermore, the Ca^{2+} concentrations are higher than the 2 mM safety limit for most Forsmark groundwaters while for Laxemar this is not the case. Hence, in present temperate conditions the potential for bentonite erosion is larger in Laxemar than in Forsmark.

In Forsmark there is a clear indication of groundwaters originating from the Littorina sea, especially in the fracture domain FFM03 or "hanging wall". The location of the different fracture domains is shown in Figure 5-2 and Figure 5-3. In Laxemar the Mg concentrations and the Cl/Br ratios indicate only a limited proportion of groundwaters of Littorina origin. This agrees with the maximum extent of the Littorina Sea, which was less at Laxemar than at Forsmark, see /SKB 2008a, Section 3.2 and SKB 2009a , Section 3.2/.

The analyses of the matrix porewaters in a few boreholes at each site show diffusional equilibrium with the fracture groundwaters in the more fractured volumes of rock. Rock matrix diffusion is a process that has therefore been confirmed at both sites. It may be noted that in Forsmark the matrix porewaters are generally more diluted than the fracture waters, especially in volumes of sparsely fractured rock. The number of data is however too limited to provide an explanation for this fact.

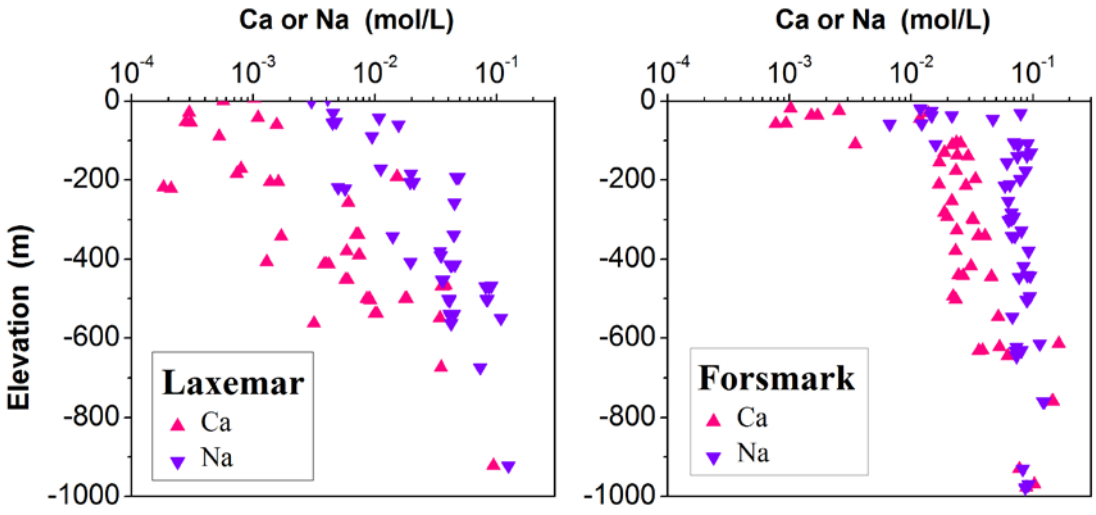

Figure 6-1. *Distribution of sodium and calcium concentrations in the groundwaters at Forsmark and Laxemar with respect to depth. The diagrams show that at Laxemar there are a few quite dilute groundwaters below 300 m depth, indicating that the risk for bentonite erosion during long-lasting temperate periods is larger at Laxemar. Data from /Laaksoharju et al. 2008, 2009/, categories 1–3. (See e.g. /SKB 2008a, Table 9-3/ for an explanation of the categories).*

During the first temperate period after repository closure, the sites are expected to undergo a continued infiltration of meteoric waters, and this will be accentuated by the larger topographic gradient as the Baltic Sea shore moves away from the sites[4] due to the geostatic uplift discussed in Section 3.2.1. The increased proportion of groundwaters of meteoric origin will result in decreased overall groundwater salinity, and this is seen in the outcome of the hydrogeological calculations described above in Section 5.4.2. The hydrogeological results are coupled with geochemical modelling, resulting in a calculated evolution of groundwater compositions for each site. Details on the geochemical modelling and its results are given in /Salas et al. 2010/ for the Forsmark site and in /Gimeno et al. 2010/ for the Laxemar site. Examples of this calculated evolution are shown in Figure 6-3 and Figure 6-4, where it may be seen that the dilution effect by the infiltration of meteoric waters down to repository depth is potentially larger at Laxemar. This is in agreement with the outcome of the comparative hydrogeological analysis of the two sites which indicates up to two orders of magnitude larger meteoric water inflow in Laxemar compared to Forsmark.

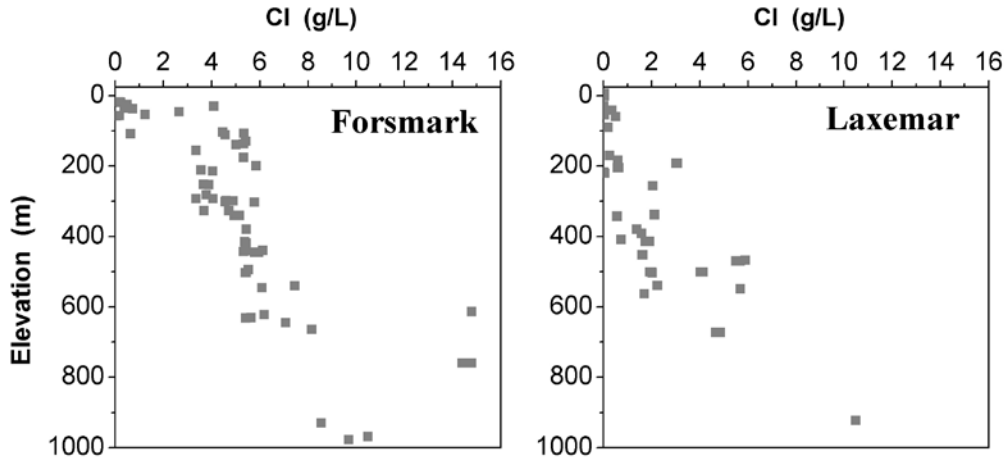

Figure 6-2. *Chloride concentrations in groundwaters at Forsmark and Laxemar as a function of depth. Data with categories 1–3 are shown /Laaksoharju et al. 2008, 2009/.*

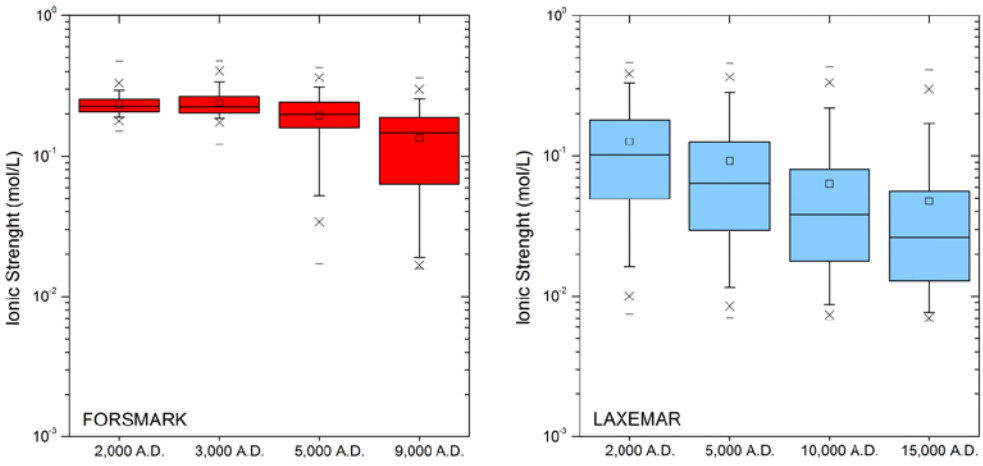

Figure 6-3. *The calculated evolution of the ionic strength during the first temperate period after the closure of hypothetical repositories at Forsmark (left) and Laxemar(right). The figures display box and whisker plots for the repository target rock volumes /Salas et al. 2010, Gimeno et al. 2010/.*

[4] Unless there is a larger and more rapid contribution from the West Antarctic ice sheet and from thermal expansion of the oceans than has been taken into account.

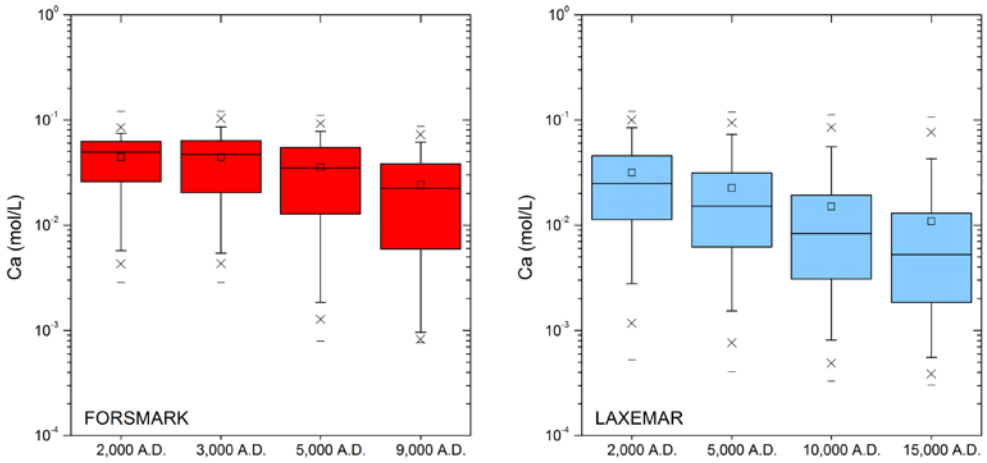

Figure 6-4. *The calculated evolution of the groundwater calcium concentrations during the first temperate period after the closure of hypothetical repositories at Forsmark (left) and Laxemar (right). The figures display box and whisker plots for the repository target rock volumes. From /Salas et al. 2010, Gimeno et al. 2010/.*

The consequence of infiltrating meteoric waters will be larger when considering the climatic alternative Global warming case presented in Section 3.2.1.

A conclusion from the present-day data at both sites and from the modelling results for the first temperate period after repository closure is that at Laxemar there is a larger potential for bentonite erosion.

Periglacial periods

Permafrost could affect the salinity of groundwaters through out-freezing of salts. Both the vertical extent of frozen ground and the initial salinity of the groundwaters will determine the magnitude of out-freeze effect At Forsmark, in the fracture domains FFM01 and FFM06, the salinity profile shows higher salinities than at Laxemar at any depth down to about 800 m, and the expected depth of permafrost is also generally larger, see Sections 3.3 and 3.4. Both factors suggest higher potential for a saline out-freezing of salts at Forsmark.

The effect of out-freezing of salts in Forsmark is evaluated in the two-dimensional modelling presented in Sections 3.3 and 3.4. The model results are described in /Hartikainen et al. 2010/ and show that when freezing is extensive, down to some hundreds of metres depth, a front of moderately higher salinity is developed. Also pockets of groundwater with high salinity may develop in the frozen rock when the freezing front advances faster than the transport of salt.

It must be noted that the displacement of the Baltic shoreline away from the repository area will induce increased penetration of meteoric waters and a general dilution of the groundwaters at both sites, excluding the parts of the target repository volume in Forsmark lacking transmissive fractures. Therefore, the effect of out-freezing of salts during a future permafrost period is not expected to be able to create as much increased salinity as it would if permafrost was to start today with the present day salinity-depth distribution of the groundwaters.

Essentially the out-freezing of salts due to permafrost is not expected to affect the performance of the repository, because the salinity levels that can be obtained through this process at repository level in both sites are not higher than ≈17.5% (3 M), which is the salinity that would be necessary to affect negatively the swelling capacity of the backfill in the repository tunnels.

Glacial periods

Figure 6-5 shows two diagrams with the calculated proportions of glacial waters in the present day groundwaters /Laaksoharju et al. 2008, 2009/. In both sites there is evidence for infiltration in the past of cold surface waters. This is based mostly on the $\delta^{18}O$ values and it is supported by other isotope data such as those for ^{36}Cl and ^{14}C. These data have been used on a multi-variate statistical

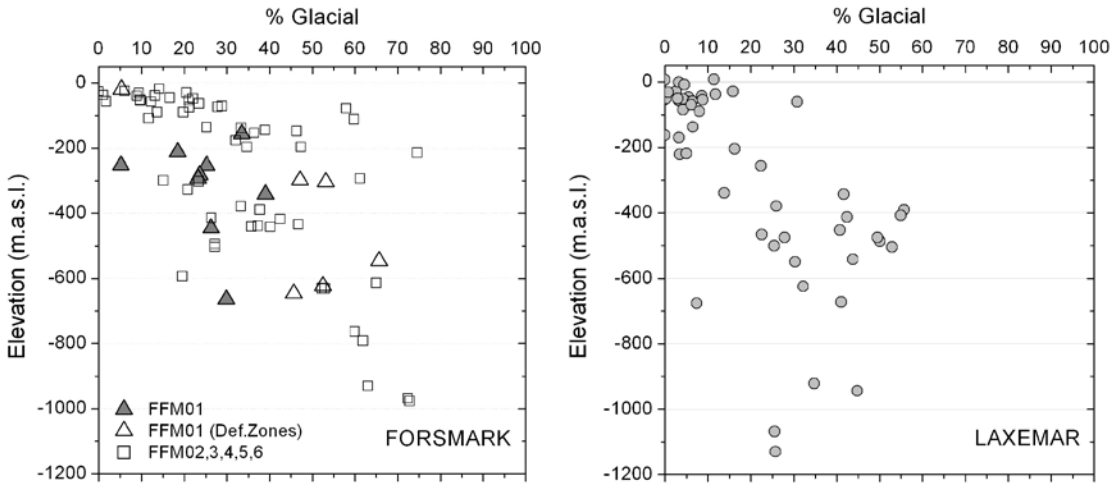

Figure 6-5. *Mixing proportions of the glacial water at Forsmark (left) and at Laxemar (right) as calculated using the present-day groundwater data /Laaksoharju et al. 2008, 2009/. In the plot for Forsmark a distinction is made for the data from the "foot wall", fracture domain FFM01, where the candidate repository is located.*

analysis of the groundwater data using the M3 code /Laaksoharju et al. 1999 and Gómez et al. 2009/, which provides a depth distribution of the glacial influence.

Hence, there is good evidence for infiltration of cold surface waters in the past. In the case of Laxemar the data indicate that these waters were introduced during the last glaciation, although the glacial waters at depths around 1 km could originate from earlier glacial periods. In the case of the target repository rock volume at Forsmark, the few available data indicate that the cold water component is in general older than the last glaciation. These waters could be either meltwaters or meteoric, although an infiltration of meltwaters during the last glaciation can not be ruled out.

The evidence for glacial meltwater intrusion is in general agreement with groundwater data from other sites in Fennoscandia and Canada. In addition, this is also in agreement with the outcome of several models of the infiltration of glacial meltwaters under an inland ice sheet. As explained in Section 5.4.2 the model for the infiltration of glacial meltwaters in Forsmark is reported in /Vidstrand et al. 2010/ and for Laxemar in /Vidstrand et al. 2011/. Typical results are shown in Figure 5-20 and Figure 5-21 respectively. It should be noted however that there is a substantial uncertainty in the hydrogeological models for the glacial period, especially at Laxemar /Vidstrand et al. 2011/, and a higher weight must be put on the indications from present day groundwaters. The hydrogeological model results suggest nevertheless a deeper and more intense penetration at Laxemar of glacial meltwaters close to the advancing ice margin, see for example Figure 5-19.

In Forsmark, the groundwater data shows that the infiltration of cold waters is, in general, older than the last glaciation, as indicated above, and the rock volume occupied by the projected repository has quite low hydraulic permeability, and therefore it could be that the dilution effect by glacial meltwaters is less pronounced. If so, then the groundwater salinities at the target repository rock volume in Forsmark could remain at the present levels over the whole of the next glacial cycles, and this would be beneficial in preventing bentonite erosion. At Laxemar as a whole, and in the fracture zones at Forsmark, a substantial infiltration of dilute meltwaters is to be expected.

6.3.2 Sulphide and related processes (microbial) and variables

Present temperate conditions

During the interpretation of the results, some degree of uncertainty has developed concerning of the sulphide concentrations from Laxemar and Forsmark. Monitoring sampling, that followed the site characterisation, indicated sulphide concentrations that were much higher at several borehole sections. Experimental data at the Microbe site at Äspö also indicated that sulphide levels increased when an experimental setup was not being sampled, see /Hallbeck and Pedersen 2008c, Figure 5/.

These discrepancies in data stimulated the start of an Äspö project to investigate the processes, mainly microbial, taking place during sampling and periods of inactivity of cored boreholes from the ground surface and in the Äspö tunnel. Preliminary results from this study suggest that in some boreholes, but not all, substantial microbial sulphate reduction takes place when the borehole is not being sampled at the isolated borehole section, in the tubings and in the stand pipe in the casing at the top of the borehole. The reason for this increased microbial activity has not yet been fully established. Although there are larger amounts of tubing and plastic parts within the isolated borehole sections in the monitoring campaign, as compared with the equipment used in the complete chemical characterisation (CCC) following borehole drilling, these increased amounts of foreign materials are similar for all the monitoring sections, while the intensity in microbial activity varies between sections.

From the preliminary results from the Äspö project, it appears that when enough deep groundwater is allowed to completely flush the borehole section and monitoring equipment, the samples collected have lower sulphide and higher iron(II) concentrations. This observation is supported by the more limited groundwater time series collected during the monitoring at the Forsmark and Laxemar sites, and this has been taken into account when evaluating the sulphide data obtained during the monitoring campaigns.

In order to avoid bias when comparing the sulphide data from the two sites, due to the fact that some borehole sections have a larger number of samples analysed, etc, a single sulphide value is selected for each investigated borehole section, with a few exceptions. The available sulphide data and the selection of values representative of the concentration in the groundwaters are discussed in /Tullborg et al. 2010a, b/. The selected 51 samples in Laxemar and 46 in Forsmark are presented in Figure 6-6. It may be seen that given the analytical and sampling uncertainties there is no significant difference between the sites. One of the samples from the monitoring campaign in Forsmark has a value above 0.1 mM (3.2 mg/L), and it may be unrealistically high, but additional time series measurements would be required in order to exclude it.

Given that sulphide may only be generated through the process of microbial sulphate reduction, it is important to look at the sulphate reducing bacteria (SRB), as well as at the concentration of sulphate and of reductants that could sustain such process. Figure 6-7 shows the numbers of sulphate reducing bacteria and Figure 6-8 displays the concentrations of sulphate at the sites. The concentrations of methane and hydrogen are shown in Figure 6-9 while the concentration of dissolved organic carbon (DOC) is illustrated in Figure 6-10.

Both sites show significant populations of sulphate reducing bacteria (SRB) as well as of all other analysed groups of microorganisms (not shown here) /Hallbeck and Pedersen 2008a, b/.

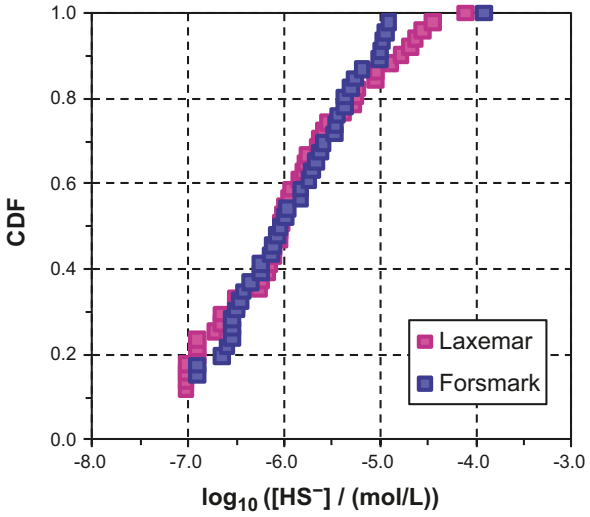

Figure 6-6. *The distribution of sulphide concentrations (in mol/L) at Forsmark and Laxemar for the samples selected as being representative in /Tullborg et al. 2010a, b/.*

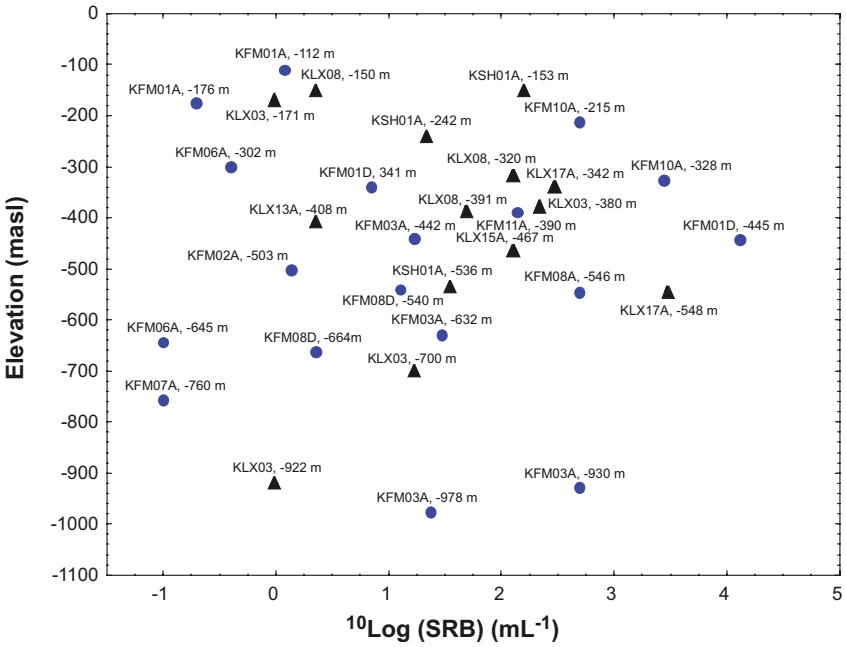

Figure 6-7. *The most probable number (MPN) of sulphate-reducing bacteria (SRB) from Forsmark and Laxemar as a function of depth. All available data are shown /Hallbeck and Pedersen 2008a, b/.*

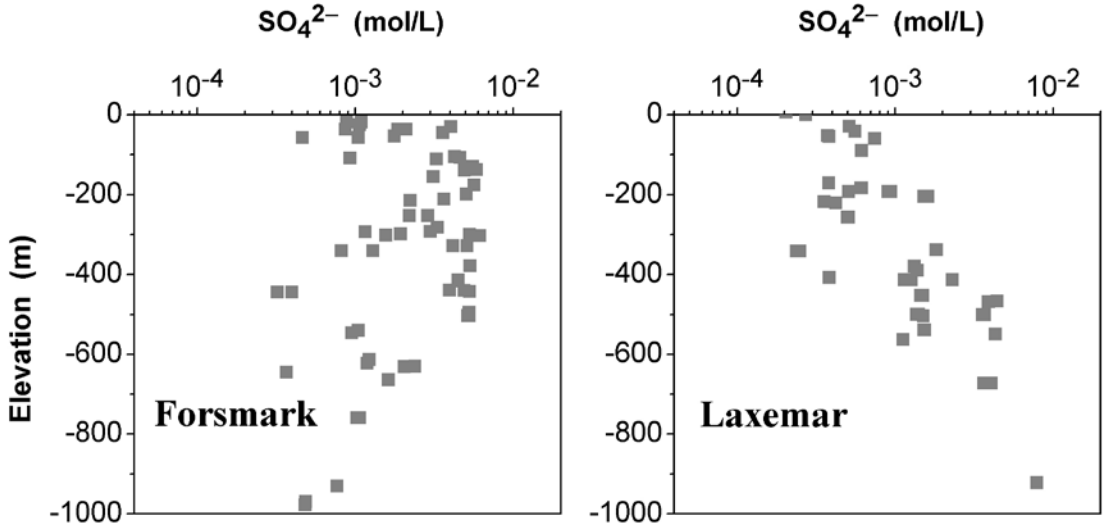

Figure 6-8. *Concentrations of sulphate in groundwaters at Forsmark and Laxemar as a function of depth. Data with categories 1–3 are shown /Laaksoharju et al. 2008, 2009/. Ocean waters have SO_4^{2-} 0.0282 mol/L while Littorina and Baltic Sea waters correspond to sulphate concentrations ≈ 0.0094 and ≈ 0.0051 mol/L, respectively.*

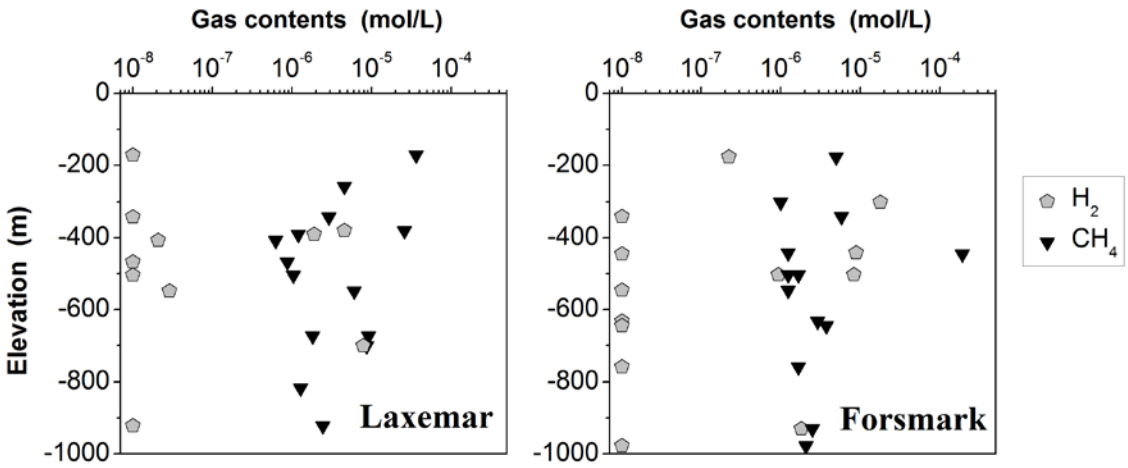

Figure 6-9. *The concentrations of methane and molecular hydrogen as a function of depth at Forsmark and Laxemar. Samples with H_2 contents below the detection limit are plotted at 10^{-8}M.*

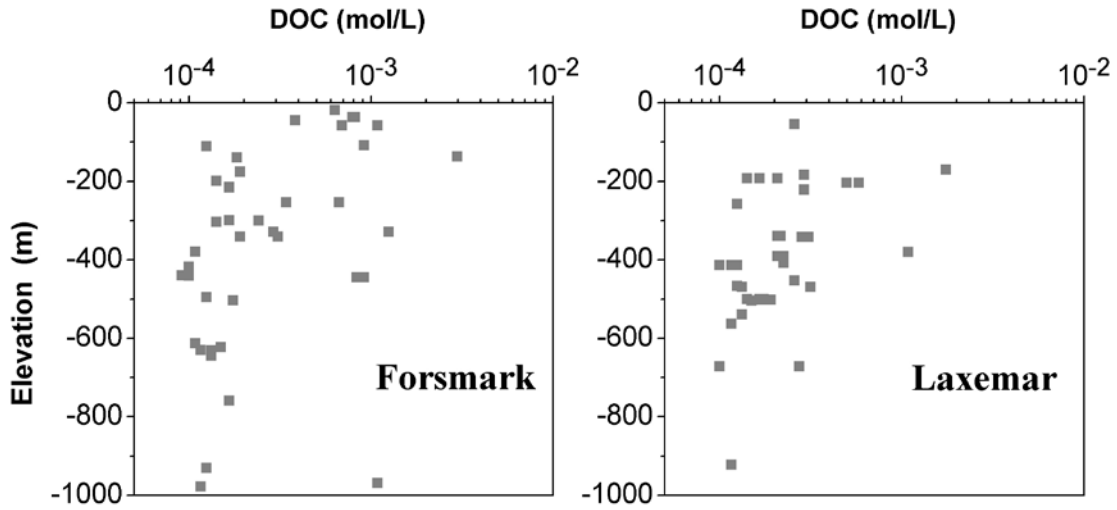

Figure 6-10. *The concentrations of dissolved organic carbon (DOC) as a function of depth at Forsmark and Laxemar. The diagrams show data with categories 1–3 /Laaksoharju et al. 2008, 2009/.*

Both sites have enough SO_4^{2-} at the sampled points to sustain microbial reduction of SO_4^{2-} to HS^-, and enough PO_4^{3-} (not shown in the figures) at most sampled points to sustain microbial life at the observed total numbers of microorganisms. Forsmark has at present much more NH_4^+ than Laxemar (not shown in the figures), and this appears to be related to the waters of Littorina Sea origin. Nevertheless, both sites have enough ammonium to sustain the observed numbers of microorganisms. Both sites have similar concentrations of dissolved organic carbon (DOC), Figure 6-10, and they are enough to sustain the observed numbers of microorganisms.

Both sites have enough CH_4 to potentially sustain anaerobic methane oxidation with concomitant sulphate reduction to sulphide. However, the presence of this group of microorganisms were not analysed for at the sites. Both sites had some observations of H_2, but they were in many cases very low, suggesting that microbes either remove hydrogen from groundwater by using it as a source of energy, or that a source of hydrogen is lacking at the sites.

It is evident from these figures that there are enough concentrations of reductants, especially as DOC, to potentially sustain a sulphate reduction and increase the concentrations of sulphide in the groundwaters at both sites. However, it has not been confirmed to date that in granitic rocks methane can be used as a reductant in the microbial reduction of sulphate, and some of the DOC will be in the form of humic acids that are only slowly degraded.

There are differences between the two sites judging from the $\delta^{34}S$ in dissolved SO_4^{2-} shown in Figure 6-11 (all $\delta^{34}S$ values are referred to the standard CDT, Canyon Diablo Troilite). The sulphur source at Laxemar for the deeper saline groundwater seems to have a different origin from that at Forsmark. The other sulphur sources (marine, sea spray and sulphide minerals) are similar at both sites. The marine signature of SO_4^{2-} is more emphasized at Forsmark mainly due to the infiltration of Littorina water. It is hard to evaluate any difference in the sulphide production over time at both sites based on the $\delta^{34}S$ data of the remaining dissolved SO_4^{2-}. However, other groundwater chemical parameters, for example Mg and Br, indicate that part of the SO_4^{2-} reduction of the Littorina component at Forsmark took place before or during the infiltration into the bedrock. When considering the whole post-glacial period, and based on all the residual $\delta^{34}S$ in SO_4^{2-}, there are no major differences in the sulphide production between the sites. But when considering only the low saline groundwaters, the $\delta^{34}S$ data of dissolved SO_4^{2-} together with the microbial data show that SO_4^{2-} reduction in these dilute groundwaters seems to be more intense at Laxemar than at Forsmark at present.

The conclusion from the present-day site data related to sulphide and sulphide production is that given the spread of the values it is not evident that any of the two sites has either significantly larger microbial populations or a larger amount of reductants available.

Periglacial periods

Sulphate reduction will be limited to those rock volumes that are unfrozen and where the production of sulphide will depend on the availability of reductants, as sulphate is expected to remain, during permafrost conditions, at the same or higher levels than under temperate conditions. In addition, sulphide levels will be controlled by the release of Fe(II) through mineral-water interactions.

There is a risk of an accumulation of gases migrating from the deeper parts of the crust and upper mantle due to reduced hydraulic permeability of the frozen upper rock layers. If the gas flow is large there would be a possibility of forming layers of methane gas hydrates. However, if taliks are present in the area they will offer a venting possibility for the upward flow of gases. The flow of gas is estimated in /Delos et al. 2010/ using the data in Figure 6-9, and it is concluded that the accumulation of CH_4 or H_2 may be ruled out for the expected lifetime of the repository at the two sites. On the other hand the downward flow of dissolved organic carbon (DOC) from the surface will decrease in cases of permafrost at the sites. As DOC is the most important reductant present in the groundwaters at the sites, this would limit the possibility of sulphate reduction in the absence of an accumulation of CH_4 and/or H_2.

It may be concluded that there are no differences in properties related to sulphide and related processes and variables during periglacial periods between the two sites.

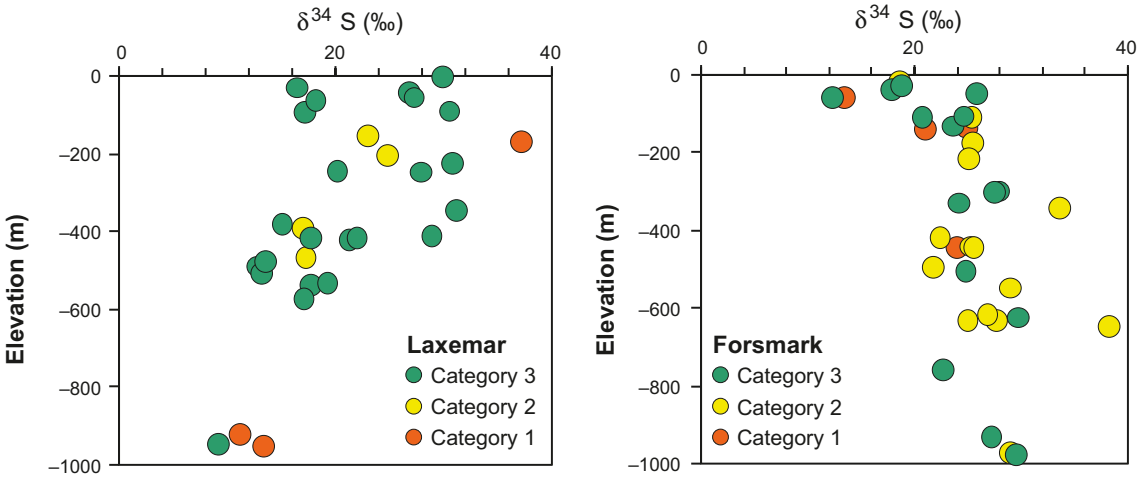

Figure 6-11. *Isotope compositions for dissolved sulphate in groundwaters at Forsmark and Laxemar as a function of depth. For marine waters $\delta^{34}S$ in sulphate is about 20‰, while sulphide from microbial SO_4^{2-} reduction has $\delta^{34}S$ < 0‰, which means that if sulphate is of marine origin, then $\delta^{34}S$ values >20‰ indicate microbial sulphate reduction.*

Glacial periods

The potential for sulphate reduction in the deeper rock under an inland ice could decrease because of low concentrations of sulphate in the groundwaters having a large proportion of meltwater component.

As for the case during permafrost conditions, in a situation where the site is completely covered by a thick inland ice sheet, there could be an accumulation of methane and hydrogen which are reductants that could be used in microbial sulphate reduction, although this can not occur in either Forsmark or Laxemar since the flow of these gases is too low /Gimeno et al. 2010/. It is expected that the infiltration of dissolved organic carbon from the surface, which is another possible reductant, would decrease noticeably at both sites.

It is possible that the infiltrating meltwater, if anoxic, could contain sulphide as a consequence of dissolution of sulphide minerals (e.g. pyrite) present in the rock that is being reworked and ground up at the bottom of the glaciers. However the solubility of sulphides is quite low and the potential for dilution from the melting ice is high.

All these effects will be of comparable magnitude at both sites. In Forsmark, the rock volume occupied by the projected repository has quite low hydraulic conductivity, and it could be that the dilution effects would be less pronounced. If so, then the sulphide concentration at the target repository volume in Forsmark could remain at the present levels over the whole glacial cycle. However, at Laxemar as a whole and in the fracture zones at Forsmark the larger dilution processes and the lower concentrations of reductants will decrease the sulphide levels, which is beneficial from the standpoint of canister corrosion.

6.3.3 Redox buffer capacity; potential for oxygen penetration; mineralogy

During temperate climate conditions there is a large reducing capacity within the soil layers and within the upper first few metres in the rock fractures. This is due to microbial activities and continuous input of organic carbon. Deeper down there is a large reducing capacity in the Fe(II) content of the fracture filling minerals (mainly in chlorite and sulphides) and in the rock matrix (mainly in biotite and sulphides).

Figure 6-12 shows that chlorite is identified in practically all fractures at both sites. Mössbauer analysis of the rocks at both sites show that the Fe(II) content in Laxemar is 2.5 to 3.5 mass %, wheras in Forsmark it is in the range 1–1.5 mass %. Thus the reducing capacity of the rock matrix at Laxemar is larger than at Forsmark.

Models of oxygen consumption by Fe(II) in the rock matrix through advection in the fractures and matrix diffusion /Sidborn et al. 2010/ show that the higher Fe(II) content in the Laxemar rocks is compensated by higher flow-related transport resistance (F-factors, related to the flow-wetted surface area available for matrix diffusion) in Forsmark, see for example Figure 5-18 .

6.3.4 Colloid concentrations under temperate, permafrost and glacial periods

In Laxemar and Forsmark colloid concentrations in waters from boreholes at varying depth have been analyzed with different methods: filtration, fractionation using membrane filters, LIBD-analysis (Laser Induced Breakdown Detection) and micro-filtration followed by scanning electron microscopy and energy-dispersive spectroscopy (SEM/EDS). The analyses show that the colloid concentration with depth at Forsmark and Laxemar are not significantly different. Most of the samples at both sites contain less than 60 µg/L with maximum analysed concentrations of ~170 µg/L at Forsmark and ~90 µg/L at Laxemar. As shown in Figure 6-1 above, practically all groundwaters analyzed have charge concentrations that exceed the critical coagulation concentration for bentonite colloids.

This indicates that natural colloid concentrations at both sites will not cause increased radionuclide transport in the case of a canister failure.

In the case of decreased groundwater salinities during a future glaciation period, colloid stability would be increased. The same situation could happen under long temperate periods of infiltration of meteoric waters. The concentration of colloids would need to become very large to have an impact on radionuclide transport. The increased colloidal stability will be of comparable magnitude at both

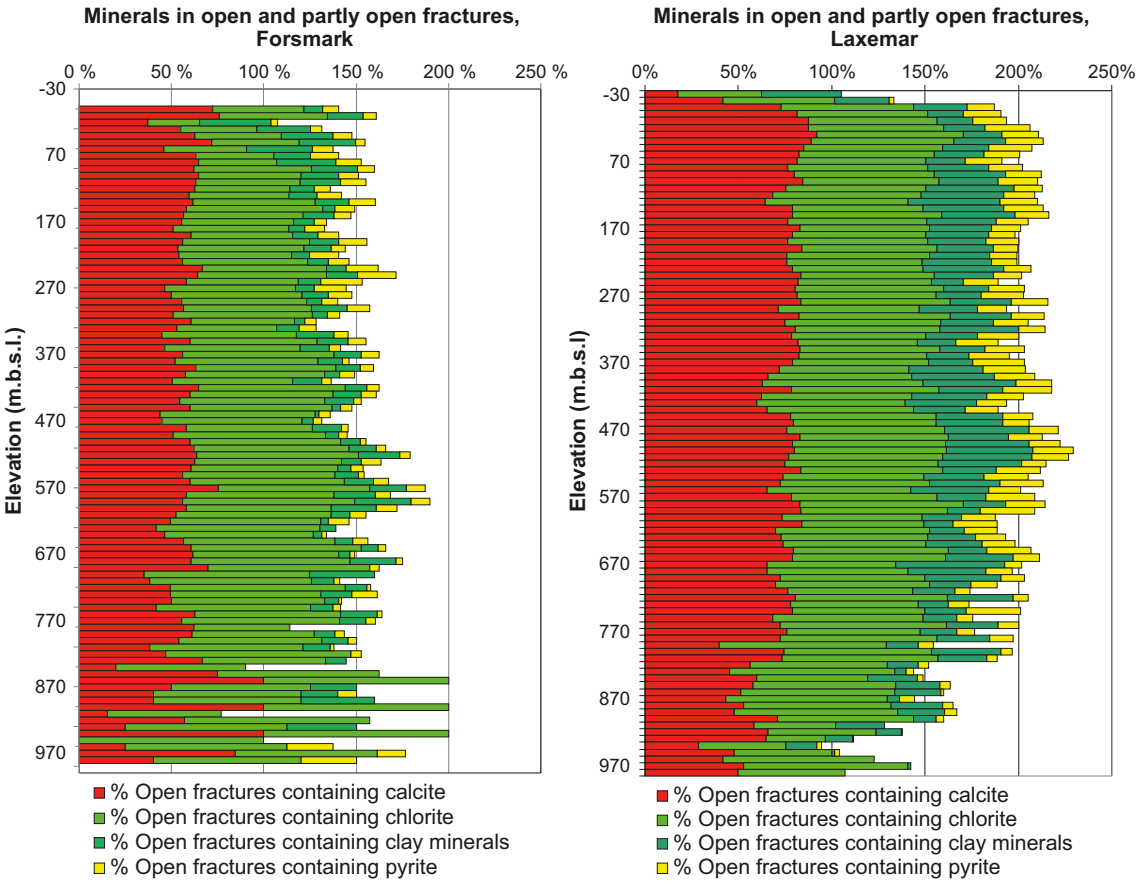

Figure 6-12. *Fracture filling minerals identified in fractures of Forsmark and Laxemar /Drake and Tullborg 2009, Sandström et al. 2008/.*

sites. In Forsmark, the rock volume occupied by the projected repository has quite low hydraulic permeability, and it could be that the dilution effects would be less pronounced. If so, then the colloid concentration at the target repository volume in Forsmark could remain at the present levels over the whole glacial cycle, while at Laxemar as a whole and in the fracture zones at Forsmark they could potentially increase during periods of enhanced recharge of meteoric or glacial melt waters.

6.3.5 Buffer capacity in relation to pH; calcite contents, etc

Figure 6-12 shows that calcite is identified in practically all fractures at both sites, despite that they have been exposed to infiltrating waters during large periods of time. This indicates a substantial pH buffering effect at both sites.

6.3.6 Confidence in the data and in the site description

In the target repository volume at Forsmark, the low hydraulic conductivity of the rock and low transmissivity of the few fractures available makes it very hard to get representative groundwater samples. In Laxemar the large number of fractures makes it difficult to obtain groundwater samples representative of the borehole section depth. In both cases it is quite difficult to have a good model of the spatial variability of groundwater chemical data, although for different reasons. The number of sampling points is sufficiently large, however, to provide a good confidence about the water types at the different depths at both sites.

In Forsmark most of the groundwater samples originate from fracture zones or more conductive rock volumes, and there is a general lack of information about the composition of the groundwaters flowing in small fractures and at large depth within the candidate repository area.

Data obtained after the site investigations in general confirm the existing conceptual models of groundwater chemistry at both sites. However in the case of sulphide, there are indications at both sites of increased microbial sulphate reduction during the monitoring period. The reasons for this apparent increase in sulphide levels are being investigated.

In addition, in Forsmark there are a few more chemistry-related data that require more investigation before they can be explained to satisfaction. For example, a very small number of fractures in the drillcores show non-altered surfaces without any fracture filling minerals, while it would be expected that some mineral alteration should have taken place. Other groundwater chemistry data that still requires further investigation is the elevated uranium concentrations in some samples at Forsmark. Although there are models and explanations for the observed uranium concentrations, more evidence would be needed to explain their limited spatial distribution, and the processes that have lead to the U-deposition. Data that might be useful are for example: characterisation of the uranium containing minerals, uranium isotopes, redox speciation, dissolved organic matter composition, etc. A more comprehensive discussion on data that should be assessed during detailed investigations at Forsmark is given in **SR-Site main report**, Section 15.6.

6.4 Conclusions

Salinity and cation concentrations

Groundwater samples show that current salinity levels at repository depth are lower at Laxemar than at Forsmark. Most expected future climatic changes will induce groundwater dilution. During the next million years or so, a sea water body, similar to the Littorina or Baltic Seas is expected to cover the Forsmark site longer than the Laxemar site, due to differences in ice thickness and location of the repository sites. Furthermore, due to the low hydraulic conductivity of the repository volume at Forsmark, it is likely that the groundwater salinity within the target repository volume in Forsmark will remain at present levels over the whole glacial cycle. In contrast, there will be a larger impact of the dilution processes resulting in lower salinities at Laxemar as a whole (and in the fracture zones at Forsmark). In short this means that conditions at Laxemar are likely to be less favourable for the stability of the bentonite buffer.

Sulphide

At present the sulphide levels at Laxemar and Forsmark are not significantly different. However, the microbial processes involved in sulphide production introduce uncertainties in the interpretation of the analytical results. The borehole sampling procedures and the microbial processes occurring in the fractures, inside the isolated borehole sections and on the equipment are under investigation.

Both sites show physical and chemical characteristics that will support sulphate reduction to sulphide. There are no important differences between the sites with respect to the conditions for sulphate reduction.

Both sites show similar average amounts and numbers of analysed biomass and microbes. However, the range is larger in Forsmark. The mean concentrations of sulphate reducing bacteria are similar at both sites.

The $\delta^{34}S$ values in the dissolved SO_4^{2-} show small differences in the sulphide production in the past. At Forsmark some sulphate reduction to sulphide seems to have taken place already in the sediments and in the Littorina Sea water prior to the infiltration into the bedrock. At Laxemar the residual $\delta^{34}S$ values in the dissolved SO_4^{2-} indicate that most of the sulphate reduction has taken place in the bedrock groundwater itself.

The future evolution of sulphide concentrations is expected to be similar at both sites. In Forsmark, the rock volume occupied by the projected repository has quite low hydraulic permeability, and it could also be that the effects on the sulphide concentrations would be less pronounced. If so, then the sulphide levels at the target repository volume in Forsmark could remain at the present levels over the whole glacial cycle, while at Laxemar as a whole, and in the fracture zones at Forsmark the larger dilution processes and the lower concentrations of reductants will decrease the sulphide levels, which is beneficial from the standpoint of canister corrosion.

Buffer capacity

Both sites have pH-buffering minerals in the fracture filling minerals, mainly calcite, indicating a good pH buffering capacity in the fractures of both sites.

The content of Fe(II) in the rocks at Laxemar is about twice as high as that at Forsmark. This can be an advantage for Laxemar in terms of potential for intrusion of oxygenated glacial meltwaters. However, the conceptual models of O_2 consumption by Fe(II) in the rock matrix show that the larger reducing capacity is more than compensated by lower transmissivity of the fractures at Forsmark.

Other aspects

As a consequence of the much lower frequency of transmissive fractures at Forsmark, confidence in the chemical conditions of the fracture groundwaters are comparably lower due to a smaller number of sampled groundwaters. However, the Laxemar site with its larger overall hydraulic conductivity, is more exposed to future changes in the groundwater chemistry at repository depth due to shoreline displacements and to climate induced changes at the surface, such as glaciation, meteoric water infiltration etc.

7 Earthquakes

7.1 Introduction

Large future earthquakes at any of the sites cannot be excluded within any time frame but are thought to be associated with glacially induced faulting. Glacially induced faulting occurs in glaciated regions in response to changes in the glacial load: either as a result of deglaciation (crustal unloading) or glacial advance (crustal loading). Such faulting is commonly referred to as "postglacial faulting" and abbreviated "PGF" although it may actually occur before the glaciation in response to an advancing ice sheet. Glacially induced faulting has been reported from northwest Europe (Norway, Sweden, Finland, Russia, Eire, and Scotland) and North America (eastern Canada, New England, and possibly California and Montana). To date, all examples of glacially induced faulting have been recorded in regions of low to moderate seismicity, namely passive margin, failed rift, or intraplate/craton environments such as Sweden. With the notable exception of the 1,989 M 6.1 Ungawa surface rupture /Adams et al. 1991/, glacially induced faults are unique in that they occur in regions where there is no evidence of surface rupture during historical time. In addition, these regions have no historical record of seismicity that approaches the magnitude thresholds for generating surface faulting.

The spectacular postglacial faults in northern Sweden are the most convincing examples of glacially induced faulting. Although there have been numerous claims of such faulting in southern Sweden /Mörner 1989, 2003/, many have been disregarded or questioned as such /SKB 1990, Carlsten and Stråhle 2000, Wänstedt 2000, Lagerbäck and Sundh 2008/. Within the framework of the site investigations, /Lagerbäck et al. 2005, 2006/ have investigated large areas in the vicinity of the sites and came to the conclusion that glacially induced faulting of larger magnitudes cannot be positively demonstrated. However, /Lagerbäck and Sundh 2008/ emphasize that their findings do not exclude the possibility of smaller earthquakes having occurred, nor do they exclude the possibility of future, large earthquakes in the investigated areas.

The potential for fault weakening and/or reactivation at the sites, as a response to future glaciations has, using simulation of advancing and retreating glaciers, been addressed by /Lund 2005, 2006/ in a series of reports to SKB whereas the effect on a repository, should a large earthquake occur in the vicinity, has been investigated in a series of reports and publications by Fälth and Hökmark /Fälth and Hökmark 2006, Fälth et al. 2007, 2008/.

The detrimental effects of a large earthquake near the repository can be avoided or considerably lessened by adaptive design involving the use of respect distance /Munier and Hökmark 2004, Munier et al. 2008/ and deposition hole rejection criteria /Munier 2006, 2007, Hedin 2008/.

Using the outcome of /Lund et al. 2009/, /Fälth et al. 2010/computed stability margins of deformation zone models to identify the zones most likely to reactivate during various periods of the glacier evolution. This, combined with deposition hole rejection criteria, was used to assess the number of critical canister positions and thereby the potential contribution to radiation risk at each site. This is elaborated further upon below.

7.2 Safety relevance

Earthquake-triggered, fast, shear movements along fractures intersecting a canister can affect the containment of the canister if the shear load exceeds the design premises of the canister, i.e. for slip exceeding 5 cm at a rate of 1 m/s or more, see **SR-Site main report**, Section 10.4.5.

7.3 Assessment of risk for earthquake triggered fast shear movements

7.3.1 Probability of future large earthquakes

The possibility of predicting future large earthquakes is naturally associated with large uncertainties, which increase with increasing time span. There is an abundance of arguments for assuming that the probability of large earthquakes at either of the site locations is low or very low during a glacial cycle. An expert elicitation project conducted by /Hora and Jensen 2005/, indicated that on average $3.0 \cdot 10^{-2}$ earthquakes of magnitude 6 or greater are estimated to occur within 5 km radius of either of the sites during a glacial cycle. The project was aimed at testing the elicitation procedure rather than providing an answer on earthquake probability and the relatively limited resources given to the experts to respond to the question is noted. However, the remarkable similarity in the experts' opinions, despite disparate approaches to the problem, is seen as an indication that the estimated probability of occurrence is likely to be realistic, given the limitations and uncertainties.

In SR-Can /SKB 2006a/, we assumed yearly frequencies between $7 \cdot 10^{-8}$ (using /La Pointe et al. 1999/) and $4 \cdot 10^{-7}$ (using /Böðvarsson et al. 2006/) earthquakes of magnitude 6 or larger within 5 km radius from the sites (Table 7-1). However, due to a relative lack of data from the sites (Figure 7-1), short time series combined with insufficient understanding of local seismicity; it is not possible to estimate site-specific earthquake probabilities which therefore must be assumed equal for the Forsmark and Laxemar sites. Figure 7-1 shows earthquakes recorded by SNSN /Böðvarsson 2002/ during the period 2002–2009.

For SR-Site, the probabilities, presented in Table 7-1, need to be rescaled to cover events of M5 or larger, due to the change of canister failure criterion from 100 mm to 50 mm /SKB 2009c/. A rough estimate, is that the frequencies change by a factor of 10 for a unit change in magnitude.

The frequencies of Table 7-1 were obtained by averaging over the area covered by the original data and rescaling to smaller areas. While this procedure is adequate for large target areas, implicitly assuming there exist structures large enough to host the earthquakes, it is necessary to address the local structural geology when applying to relatively small areas such as the sites; earthquakes are naturally anticipated to cluster along deformation zones rather than being randomly distributed over the area. In SR-Can /SKB 2006a/ we estimated the probability of any zone to host an earthquake by dividing the probability estimated for the circular area (with 5 km radius) by the number of deformation zones within that area regardless of the properties, e.g. orientation, size, etc. of the zones. This conservatism was necessary as we did not possess any information on the stress evolution during a glacial cycle and therefore had no solid arguments to exclude deformation zones unlikely to reactivate. However, the findings of /Lund et al. 2009/ were used to identify which of the deformation zones have the potential amenable for reactivation at various times during the glacial evolution. This essentially means that the earthquake probabilities are localised to fewer zones as compared to SR-Can.

7.3.2 Potential for fast shear movements

The canister is designed to withstand a shear movement of 5 cm. This means that if cumulative slip exceeding 5 cm along fracture planes that intersect the canisters can be avoided, earthquakes have no means to jeopardise the integrity of the buffer/canister package by shear load. As the maximum slip that can be hosted by a fracture is related to its size /Cowie and Scholz 1992/, we only need to ensure that canisters are not intersected by large fractures to warrant long-term safety.

Table 7-1. Yearly frequencies for magnitude 6 events or larger normalised to a circular area with radius 5 km.

Normalised frequency (y^{-1})	Reference
$3.75 \cdot 10^{-7}$	/Böðvarsson et al. 2006/
$6.83 \cdot 10^{-8}$	/La Pointe 1999, table 4-5/ (excluding Lake Vänern area)
$2.50 \cdot 10^{-7}$	Expert Elicitation project /Hora and Jensen 2005/
$3.14 \cdot 10^{-7}$	/Fenton et al. 2006/

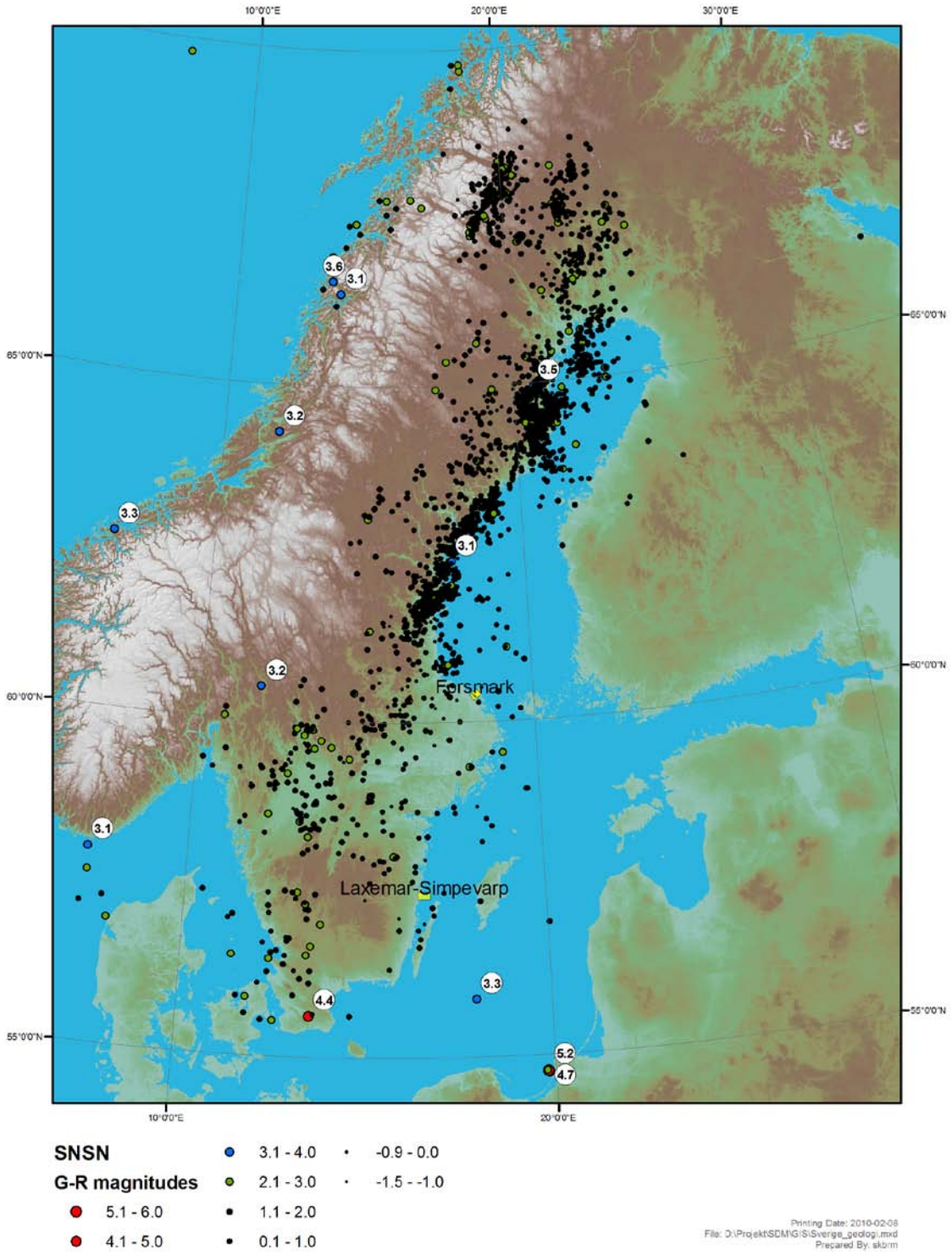

Figure 7-1. *Earthquake measured by SNSN during the period 2002–2009 /Böðvarsson 2002–2009/.*

The impact of earthquakes on target fractures was addressed by /Fälth et al. 2010/, who investigated the relations between earthquake magnitude, distance to the fault and target fracture geometry. /Fälth et al. 2010/ conclude that, provided that a distance of 600 m is kept to the boundary of deformation zones, none of the canisters within a repository will be subject to shear loads such that their integrity is jeopardised, regardless of earthquake magnitude (moment magnitudes up to M7.5 were simulated). This under the condition that fractures with radii exceeding 225 m are avoided in deposition holes. We judge such fractures will be safely detected during underground mapping /SKB 2010e/ and may hence conclude that, beyond 600 m from any deformation zone (≥ 3km), earthquakes have no practical importance to long-term safety.

In the interpretation of the simulation results, the deformation zones were divided into two categories: zones 3–5 km able to host minor earthquakes (≤ M5.5), and zones exceeding 5 km in trace length which are able to host large earthquakes (> M5.5). If both respect distances and rejection criteria /Munier 2010/ are applied, the canisters would be able to resist the impact of earthquakes located to zones intersecting portions of the repository volume. For this to be valid, however, SKB needs to ensure that (Figure 7-2):

1. No canister is placed within the damage zone of a deformation zone (fault). The damage zone of a fault is the volume of rock within which the zone may grow /Scholz 2002, Kim et al. 2004, Kim and Sanderson 2008/. This is ensured by repository design /SKB 2009b, d/ and using the site descriptive models e.g. /Stephens et al. 2007, 2008a, 2009d, Wahlgren et al. 2008/. The boundaries of the deformation zones will be delineated with further detail and less uncertainty during underground mapping and modelling.
2. No canister is intersected by any fracture that is mechanically connected (i.e. splay) to any deformation zone. The risk for this to occur is lessened by the use of 100 m respect distances /Munier and Hökmark 2004, Munier et al. 2008/ to the boundary of the deformation zone, defined to include the damage zone see e.g. /Munier et al. 2003/ for details. There is an uncertainty, however, whether this respect distance is sufficient to include all splays. Naturally, the splays are smaller than the deterministically modelled zones and ought to consist of fractures or small deformation zones with radii in the order of about 100 – 500 m. Hence most of them will be detected and characterised by underground investigations /SKB 2010e/. It is, however, imperative to, during underground investigations, pay particular attention to make sure that such splays do not intersect any deposition hole. The work of /Cosgrove et al. 2006/ is of particular importance in this context and we anticipate that ongoing detailing of the underground investigation program /SKB 2010e/ will further sharpen the identification tools.
3. Deposition hole rejection criteria are applied to the rock volumes beyond the 100 m respect distance which depend on /Fälth et al. 2010/:
   a. The size of the nearest deformation zone (i.e. the maximum size of anticipated earthquake, should it occur)
   b. The distance to the deformation zone
   c. The orientation of the fracture intersecting the deposition hole.
   d. The size of the fracture intersecting the deposition hole.

The complex task of determining the absolute size of fractures /Cosgrove et al. 2006/ can be avoided by the use of the so called FPI criteria /Munier 2010/ which constitute proxies for large fractures. In practice, therefore, the critical radii of Table 7-2 are used only to obtain a quantitative estimate of the number of critical canister positions for the few cases for which the FPI criteria may fail (see next section).

In summary, despite the lack of positive evidence for large earthquakes near the sites /Lagerbäck and Sundh 2008/, large earthquakes cannot be entirely disregarded as a risk factor. However, there are a number of countermeasures that can be taken. These are based on the properties, essentially the anticipated state of stress, the size and orientation of the deformation zones and the nature of the fracture array in the host rock.

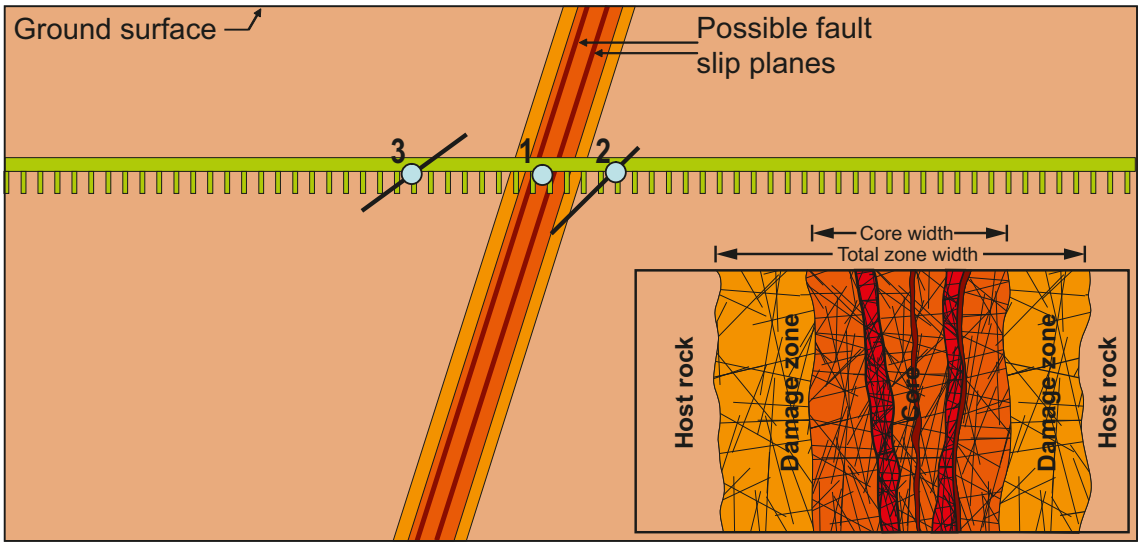

Figure 7-2. Cases to consider regarding slip across canisters. Case #1 = the canister is intersected by a deformation zone. Case #2= the canister is intersected by a splay from the deformation zone. Case #3= the canister is intersected by a large fracture at some distance from, and mechanically disconnected to, the zone.

Table 7-2. Summary of deposition hole rejection criteria/redrawn from /Fälth et al. 2010/.

Zone trace length (km)	Target fracture dip (degree)	Distance from zone (m)	Critical target fracture radius (m)
>5	0-55	100-200	62.5
>5	0-55	200-400	125
>5	0-55	400-600	160
>5	0-55	>600	225
>5	55-90	100-200	85
>5	55-90	200-400	170
>5	55-90	400-600	215
>5	55-90	>600	>300
3-5	0-55	100-200	75
3-5	0-55	200-400	150
3-5	0-55	400-600	235
3-5	0-55	>600	>300
3-5	55-90	100-200	100
3-5	55-90	200-400	200
3-5	55-90	400-600	>300

7.4 Results

The deposition hole rejection criteria are identical for Laxemar and Forsmark but the effect of their implementation naturally differs between the sites, due to local differences in deformation zone geometry (orientation), properties, fracture array properties and thermal properties (affects the canister spacings). Additionally, with current knowledge, the earthquake hazard must be assumed identical for both sites. A comparison of Laxemar and Forsmark from a long-term (one or several glacial cycles) seismic hazard perspective therefore simplifies to a comparison of the impact of deformation zones upon the repository layout in terms of respect distance(s) and the number of critical canister positions.

The discrete fracture models (DFN) provide input to the canister/fracture intersection simulation and, hence, to the assessment of earthquake effects upon the integrity of the KBS-3 system. The uncertainty of DFN models were expressed in term of alternative models, reflecting conceptual uncertainty, to encompass what we perceive as an adequate uncertainty space. All models were

propagated through all calculations to ensure that we do not underestimate the impact of earthquakes. In essence, the output is a range of the number of potentially damaged canisters from which we cautiously have chosen the largest. Details on DFN models and their alternatives is provided in the data report for SR-Site and appendix A3. Applying the full perimeter intersection criteria on site-specific deformation zone- and fracture models, /Munier 2010/ computed the number of canisters affected by various deformation zones and stress regimes, the main results of which are presented in Table 7-3 to Table 7-5 (see /Munier 2010/ for further argumentation).

7.4.3 Forsmark

In short, the number of critical canisters in Forsmark, i.e. canisters that escaped the FPI rejection criteria and are thus intersected by fractures large enough to host slips exceeding 5 cm, varies between roughly $1.0 \cdot 10^{-3}$ (for DFN model OSM + TFM and ZFMNW0017) and $1.1 \cdot 10^{-1}$ (for DFN model TCM and ZFMA2) canisters depending on DFN model, stress regime and zone assumed to reactivate seismically (Table 7-3). The reverse stress regime (Table 7-4) only affects one deformation zone, ZFMA2, and yields $1.1 \cdot 10^{-1}$ critical canisters (for DFN model TCM).

7.4.4 Laxemar

At Laxemar, only the mixed (strike slip + reverse) stress regime is applicable. The number of critical canisters (Table 7-5) lie in the range 0 (ZSMNW088A) to 5.6E-2 (ZSMNW042A). We only simulated the main DFN alternative, "BMU" in Laxemar, and to address the differences in DFN models, we ran a batch of simulations /Munier 2010/ with fewer realisations using only fracture domain FSM_C and 8.1 m canister spacing (Table 7-6). We judge the differences between the different DFN models sufficiently small, in the light of the overall uncertainties, that the impact of the DFN model can be disregarded.

Table 7-5 Number of critical canister positions assuming mixed stress regime (6,000 canister repository) at Laxemar, all fracture domains and all canister spacings. Note that only the main DFN model alternative was used for this computation from /Munier 2010/.

Table 7-3. Number of critical canister positions for various DFN models, assuming mixed stress regime (6,000 canister repository) at Forsmark.

DFN Model	# Crit. Min	# Crit. Max
OSM+TFM	$1 \cdot 10^{-03}$	$6.7 \cdot 10^{-02}$
r0-fixed	$3.5 \cdot 10^{-03}$	$4.8 \cdot 10^{-02}$
TCM	$2.3 \cdot 10^{-03}$	$1.1 \cdot 10^{-01}$
Overall	$\mathbf{1 \cdot 10^{-03}}$	$\mathbf{1.1 \cdot 10^{-01}}$

Table 7-4. Number of critical canister positions for various DFN models, assuming reverse regime (6,000 canister repository) at Forsmark.

DFN Mode	I# Crit.
OSM+TFM	$6.7 \cdot 10^{-02}$
r0-fixed	$4.8 \cdot 10^{-02}$
TCM	$1.1 \cdot 10^{-01}$

Table 7-5. Number of critical canister positions assuming mixed stress regime (6,000 canister repository) at Laxemar, all fracture domains and all canister spacings. Note that only the main DFN model alternative was used for this computation from /Munier 2010/.

Probabilistic slip, mixed (strike-slip + reverse) regime		
DFN Mode	**I# Crit. Min**	**# Crit. Max**
BMU, All domains	$0.0000 \cdot 10^{0}$	$5.638 \cdot 10^{-02}$

Table 7-6. Number of critical canister positions assuming mixed stress regime (6,000 canister repository) at Laxemar. Only one fracture domain (FSM_C) and one canister spacing (8.1 m) was simulated from /Munier 2010/. Note that the difference between "BMU" in this table and the one in Table 7-5 is due to a different number of realisations.

Model	# Crit. Min	# Crit. Max
BMU, C	0.00	$2.48 \cdot 10^{-2}$
BM, C	0.00	$1.68 \cdot 10^{-2}$
BMU_alt, C	0.00	$1.10 \cdot 10^{-2}$
BM_alt, C	0.00	$6.78 \cdot 10^{-3}$
BMU_open, C	0.00	$1.62 \cdot 10^{-2}$
Overall	**0.00**	**$2.48 \cdot 10^{-2}$**

7.5 Conclusions

Despite the lack of evidence for large earthquakes near the sites /Lagerbäck and Sundh 2008/, large earthquakes cannot be entirely disregarded as a risk factor. However, there are a number of countermeasures that can be taken. The detrimental effects of a large earthquake near the repository can be avoided or considerably lessened by adaptive design involving the use of a respect distance and deposition hole rejection criteria.

Computed stability margins of deformation zone models used to identify the zones most likely to reactivate during various periods of the glacier evolution combined with deposition hole rejection criteria, were used to assess the number of critical canister positions and thereby the potential contribution to radiological risk at each site. This analysis shows that despite differences in deformation zone and fracture geometries and frequencies, the difference between the sites is of the same order of magnitude as the difference due to the uncertainty in the fracture description for each site. Even though Laxemar has less critical canister positions as compared to Forsmark, despite a generally higher fracture intensity, the difference is not sufficiently clear, given the uncertainties, to suggest that the risk of seismic impacts would be significantly less at Laxemar. The risk contribution from earthquakes is judged similar for the two sites.

8 Mineral resources

8.1 Introduction

In order to mitigate the risk of future human intrusion, the rock suitability criteria, as set out by SKB in /Andersson et al. 2000/, set as a requirement that the rock types in the deposition area do not have ore potential and do not contain such valuable minerals as to justify mining at a depth of hundreds of metres. There is a preference for common rock types with no occurrence of valuable utility stone or industrial minerals. For the feasibility studies, this called for avoiding areas with known ore potential and heterogeneous or unusual bedrock. Furthermore, it was stipulated that, if extensive occurrence of ore-bearing minerals is encountered during the Site Investigation, the site should be abandoned.

8.2 Safety relevance

SR-Can evaluated the ore potential for the analysed sites /SKB 2006a, Section 4.3/ and propagated this to the analyses of FHA-scenarios /SKB 2006a, Section 12.10 /.

8.3 Forsmark

The ore potential at the Forsmark site is addressed in /SKB 2008a, Section 11.2.4/. It is concluded that ore potential in the coastal area in northern Uppland is correlated to the rock types and their characteristics. An assessment of the ore potential /Lindroos et al. 2004/ , came to the conclusion that there is no potential for metallic and industrial mineral deposits within the candidate area at Forsmark. A potential for iron oxide (magnetite) mineralisation was recognised in an area to the south-west of the candidate area, predominantly in the felsic to intermediate metavolcanic rocks (see Figure 8-1), but the mineral deposits are small and have been assessed to be of no current economic value.

Based on data from the islands outside the Forsmark candidate area, a new rock domain (RFM021, see Figure 11-8a in /SKB 2008a/), dominated by felsic to intermediate metavolcanic rocks, was recognised in version 1.2 of the site descriptive model. This rock domain is located north of the candidate area. There is no documented iron mineralisation in data available from the islands, but since most of this rock domain is located beneath the Baltic Sea from where relevant data are lacking, the potential for iron oxide mineralisation in rock domain RFM021 cannot be completely excluded. However, the modelling work indicates that this rock domain does not occur in the candidate volume at elevations above –1,000 m.

8.4 Laxemar

The potential for ore, industrial minerals and commercial stones of the Laxemar site has also been assessed by an experienced exploration geologist (/Lindroos 2004/). In that work, ore potential was defined as mineralisations considered worthwhile exploring today or over a longer period. It is concluded that the Simpevarp regional model area is dominated by intrusive rocks and granites, belonging to the c. 1,810–1,760 Ma generation of the Transscandinavian Igneous Belt (TIB), which by experience is more or less devoid of metallic mineralisation. The only candidate for metallic mineralisation in the Simpevarp regional model area is the c. 1,450 Ma old Götemar-type granite, which is judged to have a potential for tin (Sn) and tungsten (W), although no mineralisations of this type have so far been found.

Consequently, the whole Simpevarp regional model area may be considered as sterile concerning metallic mineralisations and ores. Furthermore, the only real potential for quarrying building- and ornamental stone is associated with the Götemar and Uthammar granite intrusions in the north and south, respectively, i.e. well outside the Laxemar subarea.

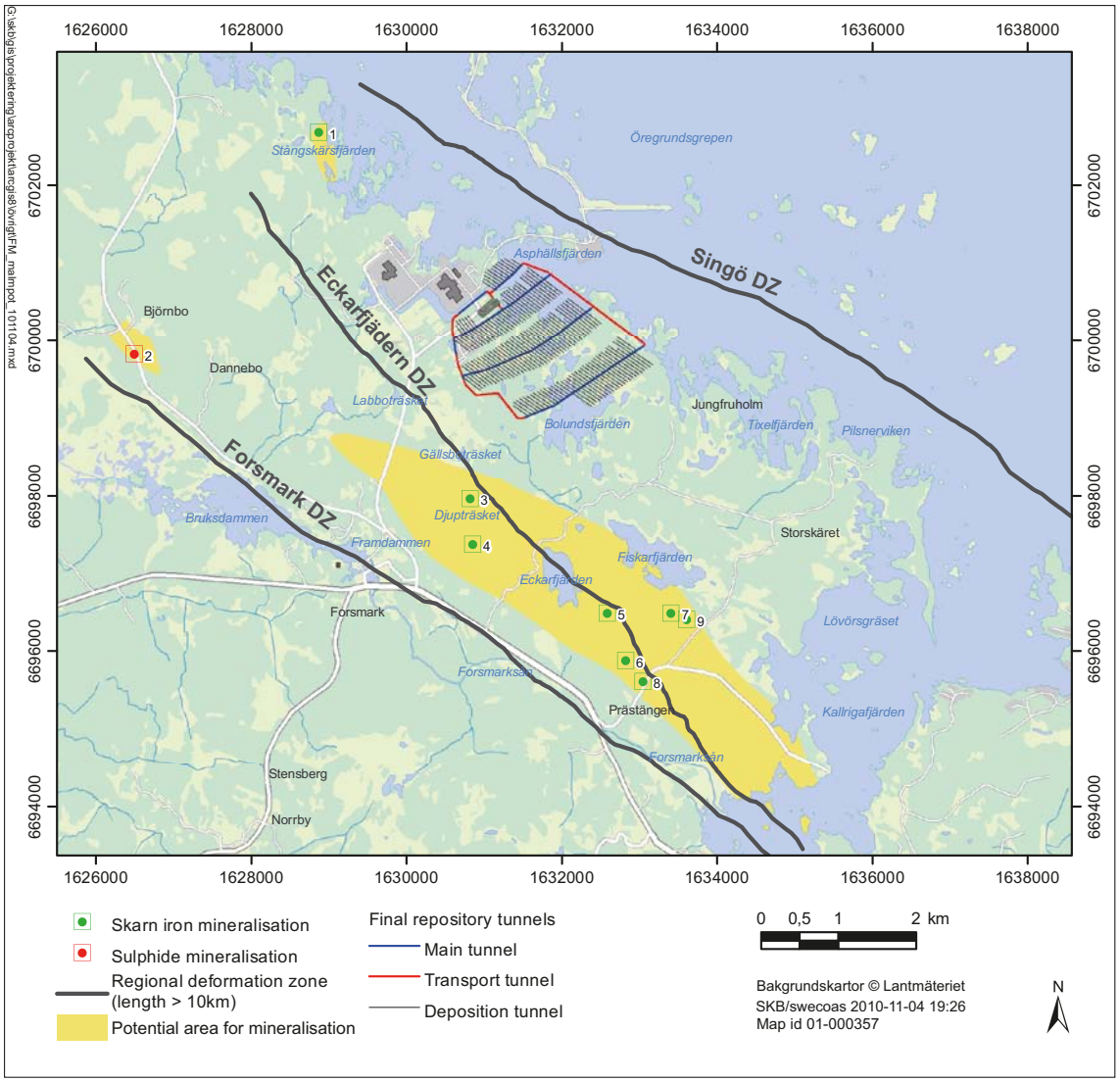

Figure 8-1. *Mineral resources map of the Forsmark area. The map shows the areas on the surface that are judged to have some exploration potential for mineral deposits (modified after /Lindroos et al. 2004/).*

8.5 Conclusions

Neither of the sites has potential for ore, industrial minerals or commercial stones. It is noted that at Forsmark there are areas that bear this potential situated to the south-west of the candidate area, predominantly in the felsic to intermediate metavolcanic rocks. However, it is emphasised that the small iron mineralisations in this area have no current economic value and this judgement is also deemed to be valid in a long-term perspective. Furthermore, the relatively large distance between the Forsmark repository and any potential mine implies that the impacts from mining activities would be low. This is also demonstrated in **SR-Site main report**, Section 14.2.7, which concludes that exploitation of the potential mineral resources in the vicinity of the Forsmark site would not impact the safety functions of the repository.

9 Surface ecosystems

9.1 Introduction

The dose to humans and other biota is one of the central estimates in the safety assessment to prove that the repository performance fulfils the regulatory requirements, as well as to judge siting and technical alternatives including optimisation of the repository. The dose to humans and other biota is dependent on several aspects. The most obvious, e.g. the inventory of hazardous substances, the integrity of the repository and the transport of radionuclides towards the surface, are handled in other sections. Other aspects are generic and not site–specific, like properties of radionuclides, decay rates, dose conversion factors for ingestion and inhalation, and individual intakes of food and water. Finally, there are several site-specific biosphere aspects that are important for the dose estimates. The most important are location of the discharge and properties of the receiving ecosystem, including food-chain characteristics, potential land use and amount of food and water produced, as well as radionuclide and water turnover. The ecosystem properties also determine the potential human utilisation and occupancy in the area where radionuclides can be released, which are important parameters in the dose assessment.

The main purposes of the safety assessment, **SR-Site main report**, are to assess the safety of a potential KBS-3 repository at Forsmark in order to support the license application, and to provide feedback to the design development and the SKB research and development programme. For the dose and risk assessments within the safety assessment, a Radionuclide Model for the biosphere (presented in detail in /Andersson 2010/) has been developed on the basis of a comprehensive site investigation programme (see /SKB 2008a/). This model is designed to handle important processes for different sites, using site-specific data.

This model has been applied in the dose assessments for Forsmark using the methodologies described in the biosphere synthesis report /SKB 2010f/ based on site specific landscape development described in the Landscape report /Lindborg 2010/, site specific parameters described in the ecosystems reports /Andersson 2010, Aquilonius 2010, Löfgren 2010/ and calculation of LDF:s /Avila et al. 2010/.

A comprehensive site investigation programme has also been carried out for the Laxemar site /SKB 2009a/. However, only limited biosphere assessments have been carried out, with the aim of obtaining an estimate of the possible impact of differences between the sites in terms of radiological consequences of a potential release to the biosphere from a future repository. This section presents a comparison between the sites, based on the SR-Site work for Forsmark and the limited study for Laxemar.

9.2 Safety relevance

From a safety assessment viewpoint, the most important endpoint is the life time risk to a representative individual of the most exposed group. In the assessments for Forsmark, the annual doses to future inhabitants of the potentially affected area, *per unit constant release rate* to all potential release areas (biosphere objects), were calculated for each radionuclide, and the maximum values of these factors over all biosphere objects and time points are referred to as *Landscape Dose Conversion Factors* (LDFs) /Avila et al. 2010/. Multiplying these factors with modelled release rates from the geosphere under different release scenarios, resulted in estimates of the annual doses used to assess compliance with the regulatory risk criterion. However, compliance with regulatory criteria is not the only indicator for site selection and therefore the comparison between the sites cannot be limited to a comparison of LDF values. Other aspects can play a role in the site selection, such as the duration of the periods when the potential exposure is the highest, the extent of the area that potentially can be affected by releases, and the viable use of potentially affected areas. Some of the differences between the sites that can be of relevance for their comparison are discussed in this chapter.

The LDF concept focuses on estimating a reasonable worst case and it also represents a fairly short period (60,000 years) of the total lifetime of the repository. Since the spatial and temporal dimensions are omitted with the concept of unit release rate, the LDF doesn't give much information about

the how low the risk may be over long time periods, and therefore the LDF only gives a realistic estimate within a limited context. For the site selection, both the maximum risk (i.e. based on LDF) as well as the long-time integrated overall risk are of importance and may differ between the sites.

In all assessments, the highest dose conversion factors are observed in periods when the affected biosphere objects are terrestrial and lake ecosystems. In periods when the affected biosphere objects are submerged under the sea the dose conversion factors are several orders of magnitude lower than for the terrestrial stage. For periods with glacial conditions the same LDF values as for the submerged period are used, although the LDFs could be even lower due to isolation and lack of food production in ice covered situations. The other climate stages give variations around one order of magnitude for the sites and climate stages. The variation is dependent on the ecosystem (i.e. food-chain), sorption of radionuclides on soils and rocks (Kd) and water turnover. The water turnover is dependent on the area/volume of the ecosystem in relation to the drainage area. The ecosystems expected to receive discharge from deep groundwater are in the lower parts of the terrain, i.e. streams, lakes, wetlands and shallow areas along the coastline. These areas often show thicker sediments and higher accumulation of organic material than more elevated areas, and may therefore be used by humans as agricultural land or for forestry. Thus, the geometry of the area, i.e. topography including bathymetry, is an important feature that affects the dose conversion factors. The geometry is mainly determined by the rock surface and thus expected to be site specific and fairly constant even over time frames of a hundred thousands years. Moreover, the geometry is the major parameter affecting the potential discharge of deep groundwater from repository depth, thus there a correlation between release areas, receiving ecosystem and water-turnover at the surface.

9.3 Forsmark

The Forsmark site is today close to the sea, but the shoreline moves continuously towards the east and around 9000 AD it is expected to be more than 10 km from the repository /SKB 2010f/. That means release from the repository either will continue to follow the shoreline or continue closer to the repository and discharge in limnic or terrestrial ecosystems, which have higher dose conversion factors than the marine ecosystem. The potential use of land for agriculture in Forsmark is restricted because the emerging land is difficult to use due to the richness in boulders and relatively modest sediment thickness /SKB 2010f/. Thus the most exposed group will be small. The topographic variation is low in Forsmark which gives future potential ecosystems that have a high water turnover.

In SR-Site, a Weichelian glacial cycle covering approximately 120 kyrs was modelled /SKB 2010c/. It showed that Forsmark will be in a glacial stage for 24% of the cycle. Thus, the repository area will be isolated from humans due to the ice thickness and the absent or sparse population with no agricultural practises.

The site will be submerged below the sea for 16% of the cycle. This gives low doses because the dose conversion factors are low during the marine period. Wells are not drilled during this period and humans will not settle in the vicinity of the release area.

The LDF values for Forsmark, reported in /Avila et al. 2010/, are illustrated in Figure 9-1. The figure shows deterministic values for a selection of radionuclides, together with mean values and percentiles (5, 25, 75 and 95) obtained from probabilistic simulations. The probabilistic results presented in Figure 9-1 include only the effect of parameter uncertainties, where mainly parameters that are generic for both sites have been considered. In the uncertainty analyses of the LDFs for Forsmark, many of the individual site-specific parameters were not treated fully probabilistically. Instead, these parameters were systematically varied as a group, since they are strongly correlated. The results from these analyses have shown that uncertainties in these parameters do not have a significant effect on the uncertainty of the LDFs /Avila et al. 2010/.

The variation of dose conversion factors over an interglacial show that the period when the site is submerged below the sea gives LDF values 3–7 orders of magnitude lower than in the terrestrial period (Figure 9-2).

9.4 Laxemar

The Laxemar site is today close to the sea and the shoreline is expected to move eastwards only to a limited extent. However, bays will be isolated in the vicinity to the site. Release from a repository at Laxemar can continue to the sea or stay closer to repository and go into terrestrial or riverine ecosystems. The terrestrial release areas are potentially favourable for agriculture due to thick sediments, and already today agricultural activities are well developed in the area. The topographic variation is high, which gives small sub-catchments and thus low water turnover in the terrestrial ecosystems.

Over the modelled Weichselian glacial cycle, Laxemar is expected to be in the glacial climate domain for 16% of the period, and the repository is expected to be submerged under the sea for 11% of the period (cf. Figure 4-7 in /SKB 2006b/).

Indicative LDF values for the Laxemar site are illustrated in Figure 9-1. It should be taken into account that the LDF values obtained for Laxemar should be seen only as indicative estimates. Although they have been obtained with the same model and approximately the same methodology as that used for Forsmark, the parameterization of the model for Laxemar has not been undertaken at the same level of detail and with the same quality control procedures as for Forsmark, see Appendix A9. Moreover, in the case of Laxemar not all potential discharge areas, but only a representative subset, have been included in the derivation of LDF values (Appendix A9).

Similar to the results for Forsmark, the variation of dose conversion factors over an interglacial show that the period when the site is submerged below the sea gives LDF values 3–7 orders of magnitude lower than in the terrestrial period (Figure 9-2).

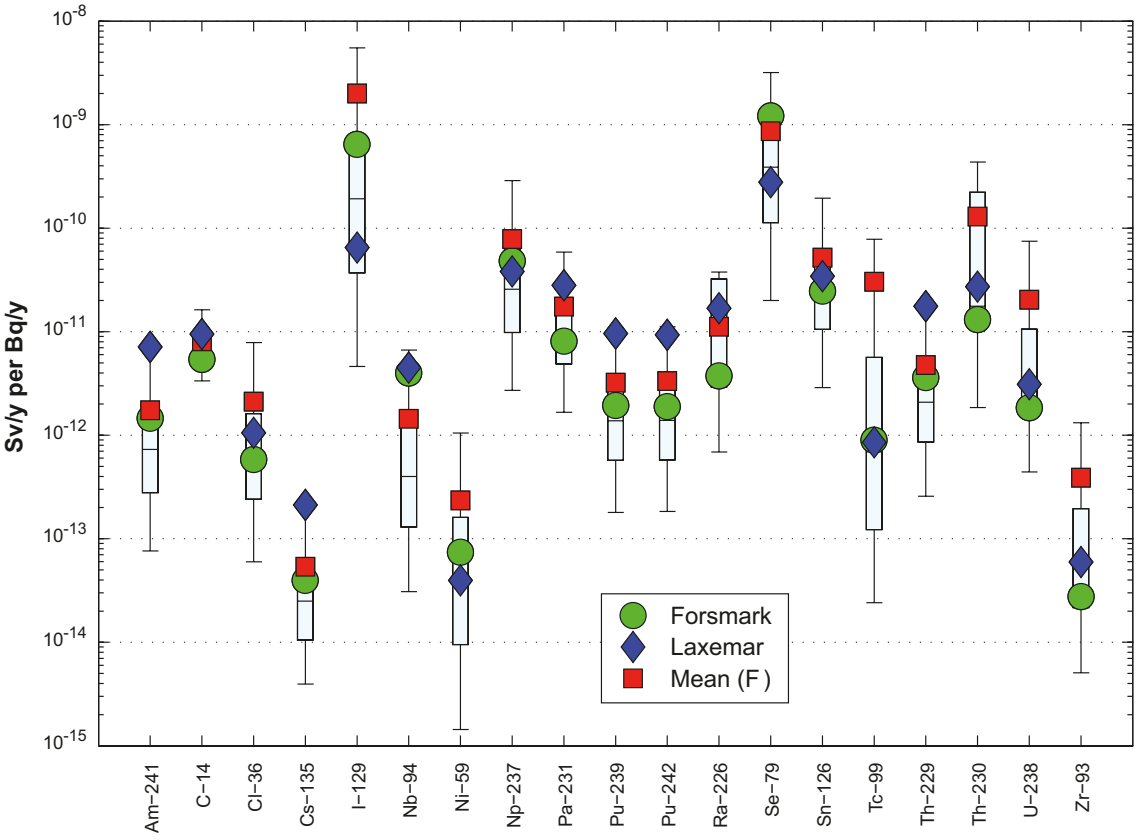

Figure 9-1. *Maximum LDF values for a selection of important radionuclides obtained from deterministic simulations for Forsmark and Laxemar. For Forsmark the mean and percentiles (5, 25, 75 and 95) obtained from probabilistic simulations are also shown.*

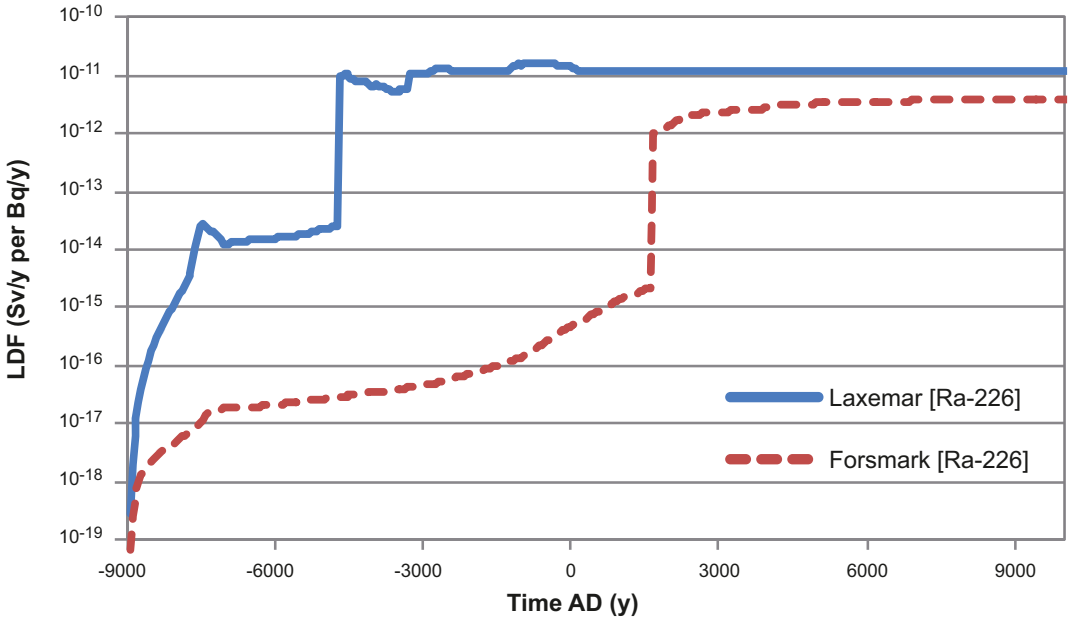

Figure 9-2. *Development of LDF for Ra-226 at Laxemar and Forsmark during an interglacial period, following the deglaciation when the site is covered by the sea and gradually develops to a coastal area and finally to land. The terrestrial period starts around -5000 AD in Laxemar and around 2000 AD in Forsmark.*

9.5 Comparison between Forsmark and Laxemar

For comparison the resulting LDFs are illustrated in Figure 9-1, where deterministic values obtained for Forsmark and Laxemar are shown for a selection of radionuclides. In the same figure, mean values and percentiles (5, 25, 75 and 95) obtained from probabilistic simulations for Forsmark are also shown. The differences in deterministic values between Forsmark and Laxemar appear marginal in comparison with the uncertainties shown by the probabilistic simulations for Forsmark. Further, no clear tendency of the LDF values for Laxemar being generally higher or lower than the values for Forsmark can be observed from these results.

In the uncertainty analyses of the LDFs for Forsmark /Avila et al. 2010/, mainly parameters that are generic for both sites have been considered. The results from an additional analysis in which the site-specific parameters were varied systematically as a group showed that uncertainties in these parameters do not have any significant effect on the uncertainty of the LDFs /Avila et al. 2010/. The variation assumed for these parameters in the uncertainty study for Forsmark will in many cases cover their variation between Forsmark and Laxemar. This therefore gives an indication that there are not expected to be any major differences in LDF values between the two sites."

The LDF values represent maximum values of doses per unit release rate to the most exposed individuals over very long periods with constant releases. They are used primarily for demonstration of compliance with quantitative regulatory criteria, which are expressed in terms of expected risk to a representative individual of the most exposed group. The comparison of LDF values for Forsmark and preliminary LDF values for Laxemar indicates that no conclusion can be drawn on significant differences between the sites. Thus, any conclusion in the comparison between Forsmark and Laxemar in terms of risk and compliance with quantitative regulatory criteria has to be based on other parts of the KBS-3 system.

From the analysis of site data it can, however, be concluded that there are other important factors in the biosphere which show differences between the sites. The Forsmark site is expected to be covered by ice for about 24% of the glacial cycle, compared with 16% for Laxemar. Exposures to humans under glacial conditions, when the site is covered by a glacial ice sheet, are unlikely. However, if they occur then humans can only be exposed to radionuclides through ingestion of sea food which is

contaminated by releases to the sea when the ice margin is situated above or close to the repository. The resulting doses in this case are expected to be lower than during terrestrial or limnic conditions, due to a larger dilution of radionuclides released to the sea.

The periods of submergence below the sea are estimated to 16% of a glacial cycle for Forsmark and 11% for Laxemar. Fluxes in the geosphere during submerged periods are lower, which would result in lower release rates to the biosphere. Moreover, the resulting doses from releases in this case are, similarly to the doses during glacial conditions, expected to be low due to a larger dilution of radionuclides (Figure 9-2). It is also unlikely that wells will be drilled during this period and that humans will settle in the vicinity of the release area. However, the shoreline displacement is much slower in Laxemar, which could lead to more permanent discharge to the sea in the vicinity of the repository at Laxemar.

The potential use of land for agriculture in areas that may be affected by released radionuclides is more restricted in Forsmark as compared to Laxemar. The emerging land in potential discharge areas in Forsmark is rich in boulders and has relatively modest sediment thickness, whereas emerging land in the fissure valleys at Laxemar has thicker sediments, which makes it more suitable for agriculture, as evidenced by today's presence of a developed agricultural practice in this area. As a result of this, the size of the potentially exposed population is lower in Forsmark than in Laxemar.

9.6 Conclusions

A comparison of LDF values for Forsmark and preliminary LDF values for Laxemar indicates that it is not possible to infer any differences between the sites in terms of compliance with quantitative regulatory criteria caused by the biosphere assessment. The potential difference between the sites in terms of total risk should be related to other parts of the KBS-3 system. However, compliance with regulatory criteria is not the only indicator for site selection and therefore the comparison between the sites cannot be limited to comparison of LDF values. Other aspects that can play a role in the site selection, such as the duration of the periods when the exposure is the highest, the extent of the area that can be potentially affected by the releases, the viable use of potentially affected areas, should also be considered. A comprehensive analysis of all relevant aspects has not been carried out, but some of the differences between the sites that can be of relevance for their comparison indicate that the Forsmark site will be submerged under sea or covered by ice for longer periods than Laxemar, most likely giving considerable lower doses for long time periods. Moreover, the potential for future agriculture in areas potentially affected by released radionuclides seems reduced for Forsmark, meaning that the size of the potentially exposed population will be smaller.

10 Containment potential, retardation and risk

10.1 Introduction and safety relevance

Estimation of risk is the main output of the safety assessment methodology applied in SR-Site. As further described in the **SR-Site main report**, Section 2.5.9, this analysis is Step 9 of the analysis and is divided into two parts: analysis of containment potential and of retardation potential.

The analysis of the containment potential is centred around the main scenario based on the analysis of the reference evolution of the repository system, see the **SR-Site main report**, Section 2.5.7. The purpose is to gain an understanding of the overall evolution of the system and of uncertainties affecting the evolution, for the scenario selection and scenario analyses that follow in the two subsequent steps. The evolution is an important basis for the later definition of a main scenario. Additional scenarios are analysed by focussing on the factors potentially leading to situations in which the safety functions of the repository, Figure 1-1, are not maintained. In most cases, these analyses are carried out by comparison with the evolution for the main scenario, meaning that they only encompass aspects of repository evolution for which the scenario in question differs from the main scenario.

The analysis of containment potential and of retardation potential encompasses calculations of radionuclide release, transport and dose impacts for potential failure modes of canisters identified for each scenario in the analysis of containment potential. The purpose is to assess the retardation properties of the system for these scenarios and to quantify risk.

For Forsmark, it is concluded in the **SR-Site main report** that the main contributor to risk is from the corrosion scenario, being the combination of loss of buffer due to ingress of dilute groundwater leading to advective conditions in some deposition holes, followed by enhanced potential for canister corrosion, which in turn leads to a few canister failures and subsequent release and transport of radionuclides. Furthermore, this risk is essentially captured within the assessment of the main scenario, although there are some risk contributions from the additional cases considered in the canister corrosion scenario. For comparison between the sites it is thus judged fully sufficient to compare the risk contributions arising from the main scenario and for the issues of loss of buffer material and canister corrosion. While there is a risk contribution also from potential future earthquakes, this risk contribution is smaller than that from the corrosion, and, as is concluded in Chapter 7, the differences in potential risk contribution from earthquakes between the sites are judged small.

10.2 Analysis of containment potential

10.2.1 Loss of buffer material

As further detailed in Section 10.3.11 of the **SR-Site main report** extensive studies of the process of colloid release from the buffer have been undertaken recently. A summary of the studies and a justification of the treatment of the process can be found in the Buffer, backfill and closure process report /SKB 2010g/. The description of the background and the development of a quantitative model is given in /Neretnieks et al. 2009/.

As discussed in Section 10.3.9 of the **SR-Site main report** a loss of 1,200 kg of buffer material from one deposition hole position will lead to cases where advective transport in the buffer needs to be considered (loss of the diffusive barrier). The rate of loss can be calculated with the model described by /Neretnieks et al. 2009/. The information needed for each canister position is:

- The duration of conditions with a groundwater composition with a positive charge of less than 4 mM, requiring a determination of the groundwater composition, in particular the concentrations of Na+ and Ca2+.
- The water velocity around a deposition hole/tunnel.
- The fracture apertures.

Forsmark

At the Forsmark site, see Chapter 6 and Sections 10.3.7 and 10.4.7 of the **SR-Site main report**, the quantity $\Sigma q[M^{q+}]$, could fall below 4 mM charge equiv. i.e. violating safety indictor criterion R1c, see Figure 1-1, for typically one percent of the deposition holes during the later parts of the initial temperate period, i.e. after about 10,000 years. This means that colloid release may occur from these holes. Furthermore, less than 2 per cent of the deposition hole positions are likely to have dilute conditions during a glacial cycle, and they will only have these conditions a fraction of the time.

Using the modelling approach described above and the flow rates from the semi correlated base case of the hydrogeological DFN model, see Chapter 5 and Section 10.3.6 of the **SR-Site main report**, the resulting distribution of erosion rates for Forsmark is seen in Figure 10-1. The figure also indicates the number of holes with advective conditions in the buffer, i.e. holes that have experienced a loss of more than 1,200 kg of buffer.

It is obvious that at Forsmark only a small number of depositions holes will reach advective conditions, even in 10^6 years. Using the EFPC rejection criterion, see Section 5.2.2 of the **SR-Site main report**, and assuming that "dilute" conditions occur 25% of the time, 23 deposition holes (out of 6,000) reach advective conditions. For the initial temperate period few if any deposition holes will reach advective conditions.

Laxemar

At the Laxemar site, see Chapter 6, the quantity $\Sigma q[M^{q+}]$, could fall below 4 mM charge equiv. i.e. violating safety indictor criterion R1c, for a majority of the deposition holes during the later parts of the temperate period, i.e. after about 10,000 years. This means that colloid release may occur from these holes. These dilute conditions are likely to persist for a large part of the glacial cycle, although more saline conditions will occur during periods when the site is covered by the sea or experiencing upconing during the glacial advance.

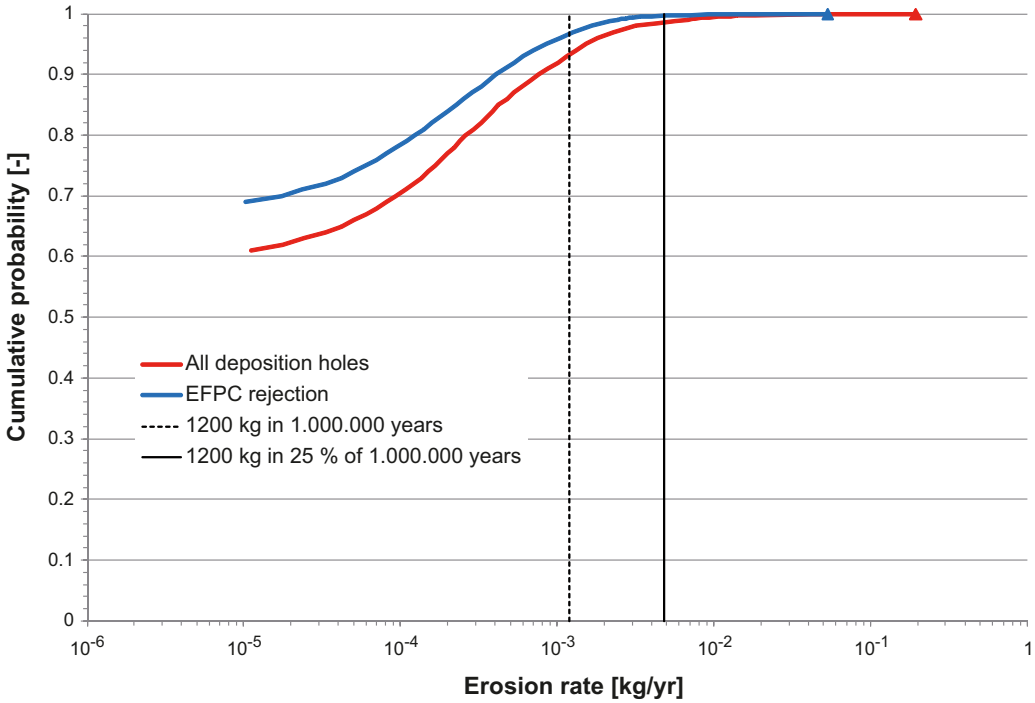

Figure 10-1. *Distribution of erosion rates at Forsmark for the semi-correlated base case of the DFN hydro model, with the EFPC rejection criterion used and for all deposition holes. The erosion rate required to achieve advective conditions in a deposition hole are given as vertical lines, for dilute conditions all the time (dashed line) and 25% of the time (solid line) in all deposition holes. It should also be noted that less than 2 per cent of the deposition hole positions are likely to have dilute conditions during a glacial cycle, and they will only have these conditions a fraction of the time.*

Using the modelling approach described above and the flow rates from the elaborated hydrogeological DFN model (see Section 5.4.1 and /Joyce et al. 2011/), the resulting distribution of erosion rates for Laxemar is shown in Figure 10-2. The figure also indicates the number of holes with advective conditions in the buffer, i.e. holes that have experienced a loss of more than 1,200 kg of buffer.

At Laxemar a large fraction of the deposition holes will eventually reach advective conditions. Even when using the EFPC rejection criterion and assuming that "dilute" conditions occur 25% of the time, nearly all deposition holes connected to a water conductive fracture (about 3,600 out of 6,000 if applying EFPC and about 4,200 out of 6,000 if not applying EFPC) reach advective conditions in one million years, and about half of these holes reach these conditions after 100,000 years.

10.2.2 Canister corrosion

The approach to assessing canister corrosion for the case of a partially eroded buffer is outlined in the **SR-Site main report**, Section 10.4.9, and is based on the approach suggested by /Neretnieks 2006/ supplemented by the Appendix in /Neretnieks et al. 2010/. In short, the corrosion rate will depend on the groundwater flux, q, through the part of the fracture that intersects the deposition hole, the geometry of the eroded buffer section, the copper shell thickness and the concentration of sulphide in the groundwater.

Erosion and subsequent corrosion is modelled probabilistically, using distributions of groundwater flow conditions from the hydrogeological DFN modelling and the sulphide distribution. In the combined erosion/corrosion calculations the time to canister failure is calculated by adding the corrosion time to the erosion time for each deposition hole with its specific flow and for a sulphide concentration randomly sampled from the sulphide distribution. The central output is the mean number of failed canisters at one million years and a list of failure times and canister positions resulting from the combination of canister specific flow rates with the sampled sulphide concentrations.

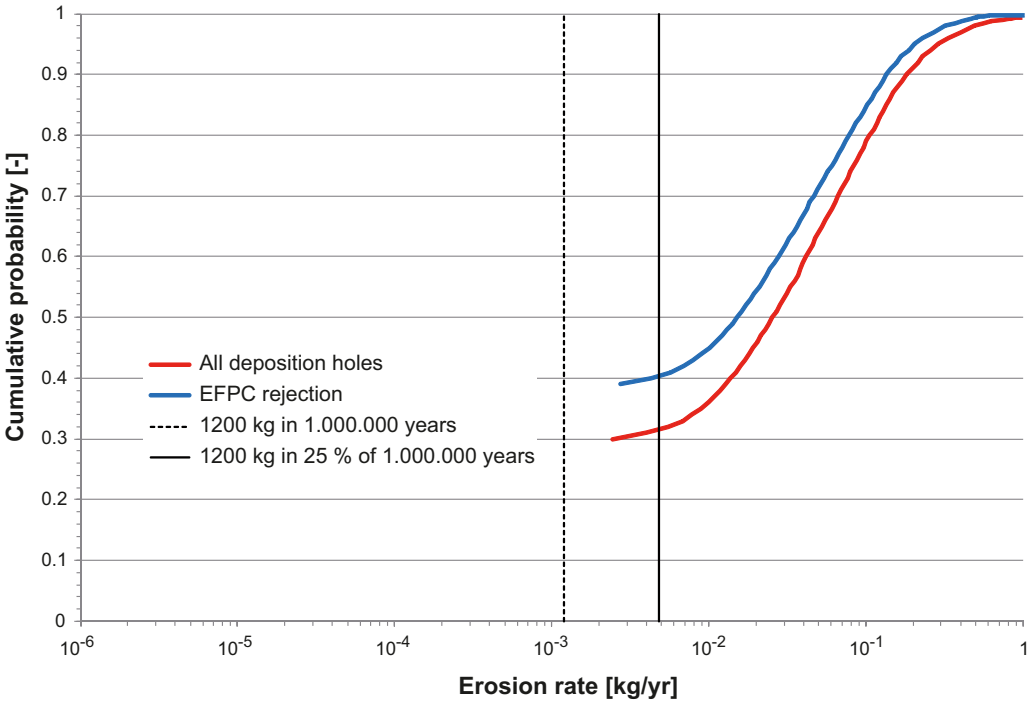

Figure 10-2. *Distribution of erosion rates at Laxemar for the semi-correlated base case of the DFN hydro model, with the EFPC rejection criterion used and without applying any rejection criterion (noted as "all deposition holes" in the figure. The erosion rate required to achieve advective conditions in a deposition hole are given as vertical lines, for dilute conditions all the time (dashed line) and 25% of the time (solid line) in all deposition holes. It should also be noted a majority of the deposition hole positions are likely to have dilute conditions already after the initial temperate period, i.e. in about 10,000 years from now.*

Forsmark

The corrosion rate distribution for the semi-correlated base case of the hydrogeological DFN model for Forsmark, see Chapter 5 and Section 10.4.6 of the **SR-Site main report**, and assuming advective conditions in all deposition holes remaining after rejection according to the EFPC criterion, is given in Figure 10-3. Here, a sulphide concentration of 10^{-5} M is assumed in all deposition holes and all incoming sulphide is assumed to attack the exposed canister surface. Also the result when disregarding EFPC rejection is shown in the figure. As can be seen from the figure, there will be no canister failures at Forsmark, even if advective conditions are assumed in all holes if the sulphide concentration is at, or below 10^{-5} M.

A proper account of the distributions of flow rates and sulphide concentrations requires a probabilistic assessment. In a base case calculation, the semi-correlated base case of the hydrogeological DFN model, deposition hole rejection according to the EFPC criterion, the sulphide concentration distribution for temperate conditions and a cautious corrosion geometry are used. The distribution of sulphide concentrations for present and future conditions at Forsmark is presented in Chapter 6. More details on the derivation of this distribution are found in Sections 10.3.7 and 10.4.7 of the **SR-Site main report**. This yields a mean number of failed canisters of 0.087 at one million years when the sulphide distribution is randomly combined with the flow rates for all the deposition holes. Only four deposition holes have sufficiently high flow rates for failure to occur within one million years and for all four, the highest concentration of sulphide is required.

Laxemar

The corrosion rate distribution for the semi-correlated base case of the hydrogeological DFN model for Forsmark, see Chapter 5, and assuming advective conditions in all deposition holes remaining after rejection according to the EFPC criterion, is given in Figure 10-4. Here, a sulphide concentration of 10^{-5} M is assumed in all deposition holes and all incoming sulphide is assumed to attack the exposed canister surface. The result when disregarding EFPC rejection is also shown in the figure. As can be seen from the figure, there will be several hundred canister failures at Laxemar for these conditions.

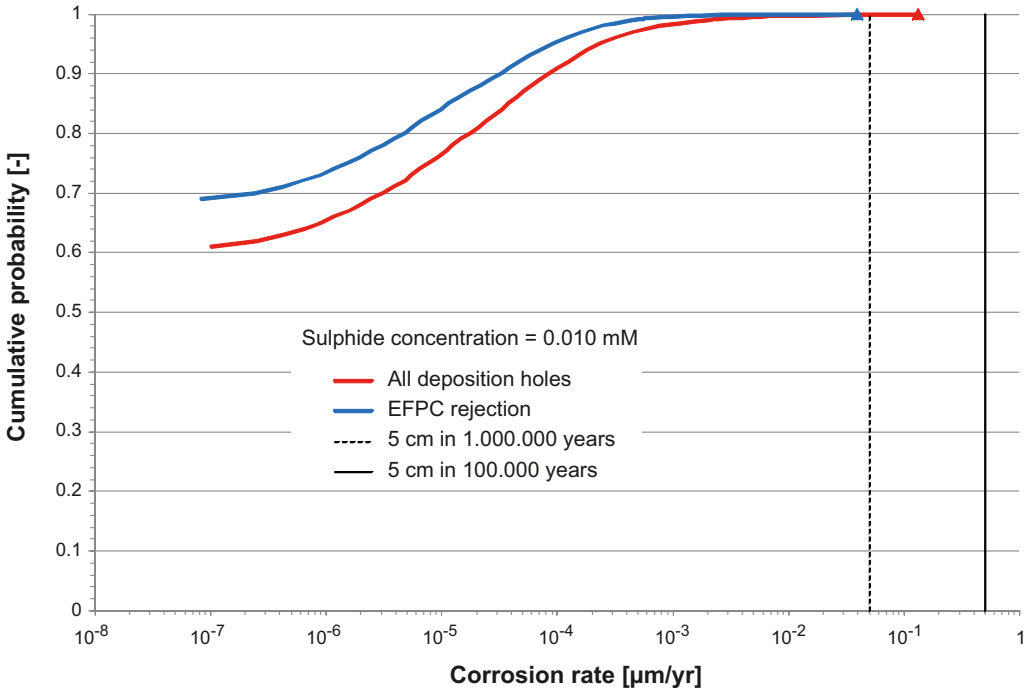

Figure 10-3. *Distribution of corrosion rates at Forsmark for the base case semi-correlated hydrogeological DFN model and assuming that all deposition holes have advective conditions. The vertical lines indicates the corrosion rates that correspond to corrosion of 47 mm copper in 10^6 (dashed line) and 10^5 (solid line) years respectively.*

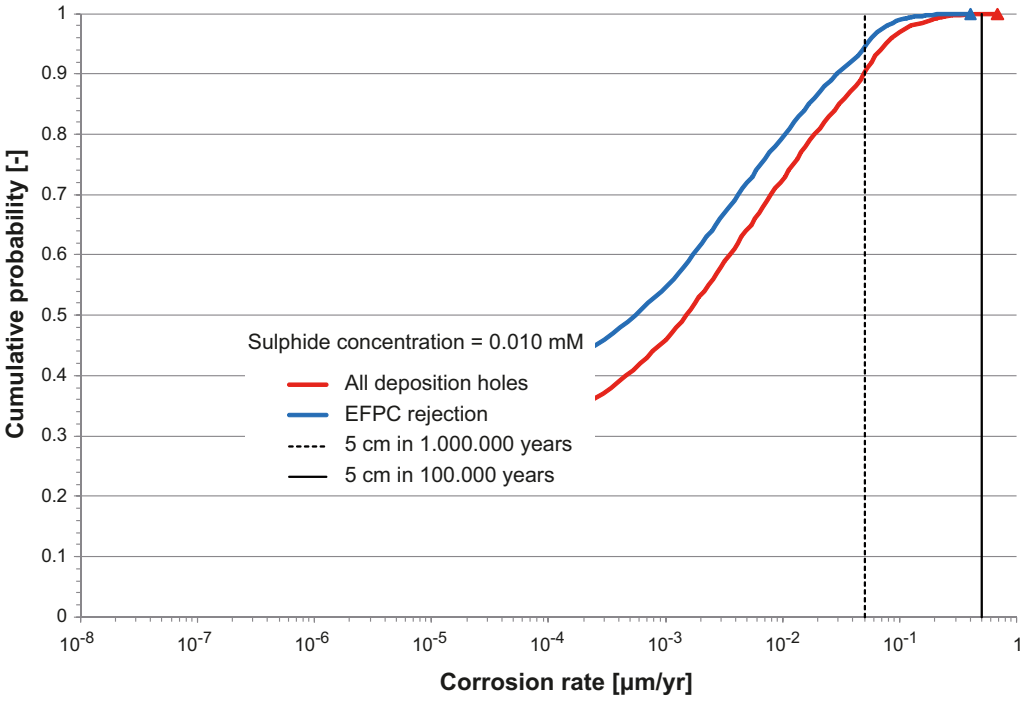

Figure 10-4. *Distribution of corrosion rates at Laxemar for the base case semi-correlated hydrogeological DFN model and assuming that all deposition holes have advective conditions. The vertical lines indicates the corrosion rates that correspond to corrosion of 47 mm copper in 10^6 (dashed line) and 10^5 (solid line) years respectively.*

A proper account of the distributions of flow rates and sulphide concentrations requires a probabilistic assessment. In a base case calculation, the elaborated hydrogeological DFN model, deposition hole rejection according to the EFPC criterion, the sulphide concentration distribution for temperate conditions at Laxemar and a cautious corrosion geometry are used. The distribution of sulphide concentrations for present and future conditions at Laxemar is presented in Chapter 6. This yields a mean number of failed canisters of 146 at one million years when the sulphide distribution is randomly combined with the flow rates for all the deposition holes.

As is demonstrated in the risk analysis presented in the next section, a failure of 146 canisters leads to unacceptable risk. In order to assess whether there are any design changes that could lead to reduction of the number of failures some hypothetical cases have also been assessed, where it is assumed that it would be possible to avoid deposition holes with high Darcy fluxes under future, saturated conditions. As is discussed in Section 10.2.3 of the **SR-Site main report** and assessed in detailed by /Selroos and Follin 2010, Section 7.1/, it may be conceivable to avoid deposition holes with Darcy flux above 0.01 m/yr, or maybe even down to 0.001 m/yr, since high Darcy fluxes in the future are correlated to high inflows during open conditions. By rejecting deposition holes with high inflow, or having potential for high inflow, the characteristics of the accepted deposition holes would thus be much better.

Table 10-1 shows the resulting number of failed canisters if applying different rejection criteria. As can be seen from the table, the impact from the rejection criteria is substantial. This suggests that it is conceivable to revise the repository design at Laxemar such that the potential number of canister failures would be reduced, but such an approach, implies further losses of deposition holes and also needs technical development and verification. (Applying such criteria at Forsmark would also reduce the failures, as is discussed in Section 14.2 of the **SR-Site main report**, but there the already existing reference design leads to an acceptable number of failures). It should also be noted that the loss of positions will be (much) larger than the number of rejected positions in the table since any practical inflow criterion is likely to also reject holes that would not have high Darcy flux during saturated conditions, see e.g. Table 5-6 suggesting that more the 50% of potential deposition holes at Laxemar would have inflows above 0.1 L/min.

Table 10-1. Number of failed canisters and loss of deposition holes at Laxemar, if applying some hypothetical deposition hole rejection criteria.

Criterion	Rejected positions [a)]	Mean number of failed canisters @ 10^6 yrs
No rejection	10[b)]	209
EFPC rejection	717	148
EFPC + T/L (avoid fractures with $T>10^{-6}$ and L > 443 m)	730	146
EFPC + T/L + avoiding deposition holes with Darcy flux U_0 > 0.01 m/yr	1,303	67
EFPC + T/L + U_0 > 0.001 m/yr	3,103	0

a) In practice this number will be much higher since any practical inflow criterion is likely to also reject holes that would not have high Darcy flux during saturated conditions.

b) Deposition holes erroneously positioned in deterministic fractures.

10.3 Analysis of retardation potential and risk estimates

The approach to modelling retardation and risk is outlined in Section 13.1 to 13.4 of the **SR-Site main report**. Those sections describe the approach for biosphere assessment with its derivation of landscape dose conversion factors for a glacial cycle and the models for radionuclide transport and dose calculations. The hydraulic data used are the same as in the containment assessment described above, additional transport data needed are provided in Appendix A8 of this report. The landscape dose conversion factors used are presented in Chapter 9 and in Appendix A9 of this report.

Forsmark

Figure 10-5 shows the resulting mean annual effective dose at Forsmark, for a probabilistic calculation with failure times and geosphere transport data from the ten realisations of the semi-correlated DFN model. The first releases occur after around 114,000 years when the first canister fails. The dose is dominated by Ra-226. It stays well below, almost by two orders of magnitude, the regulatory limit.

Laxemar

Figure 10-6 shows the resulting mean annual effective dose at Laxemar, for a probabilistic calculation with failure times and geosphere transport data from a realisation of the elaborated hydrogeological DFN model. The first releases occur already after 20,000 years when the first canister fails. The dose is dominated first by Nb-94 and later by Ra-226. Some time after 100,000 years the dose exceeds the regulatory limit and eventually grows to a level comparable to that due to the background radiation.

Following the assessment of some hypothetical cases where it is assumed that it would be possible to avoid deposition holes with high Darcy fluxes, presented in Table 10-1, the retardation potential and risk estimates have also been made for the case where it is assumed that deposition holes with higher Darcy flux than 0.01 m/yr are rejected, see Figure 10-7. The figure shows that applying such a criterion would reduce dose below the regulatory limit for the time when it is strictly applicable, but for later times the dose is still high. Applying an even stricter criterion, e.g. 0.001 m/yr will further reduce the mean annual dose, possibly even to very low values since Table 10-1 suggests that no canister would fail then, but the cost in terms of losses of potential deposition holes and methodology to be developed and verified is potentially quite high.

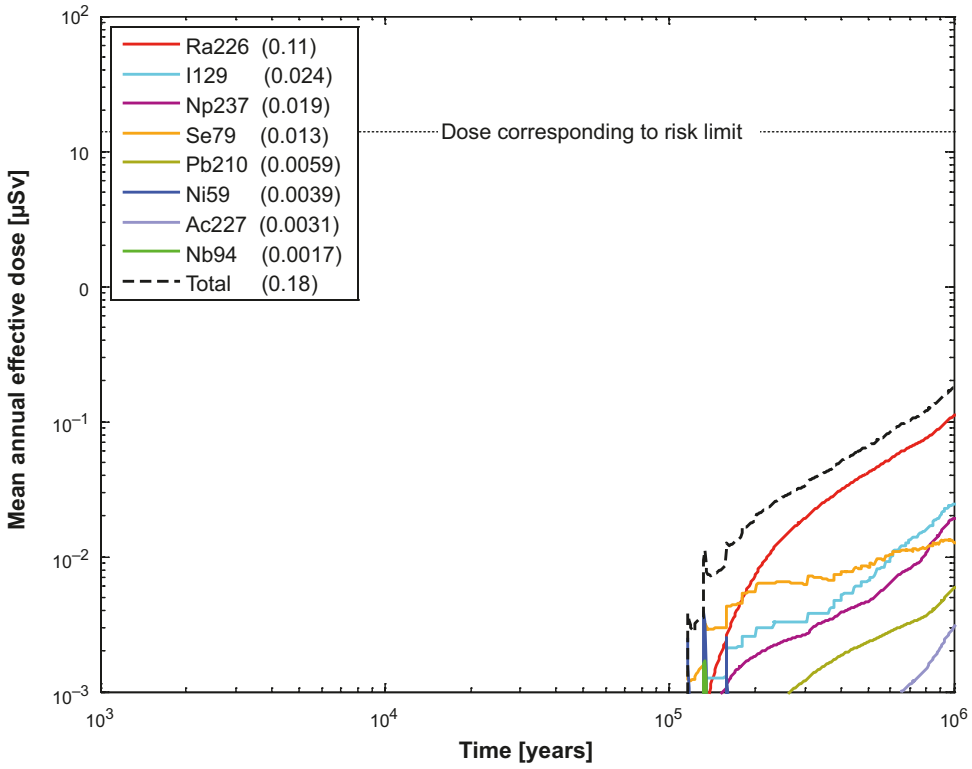

Figure 10-5. *Mean annual effective dose at Forsmark for a probabilistic calculation of the central corrosion case. The legends are sorted according to descending peak mean annual effective dose during one million years (given in brackets in μSv).*

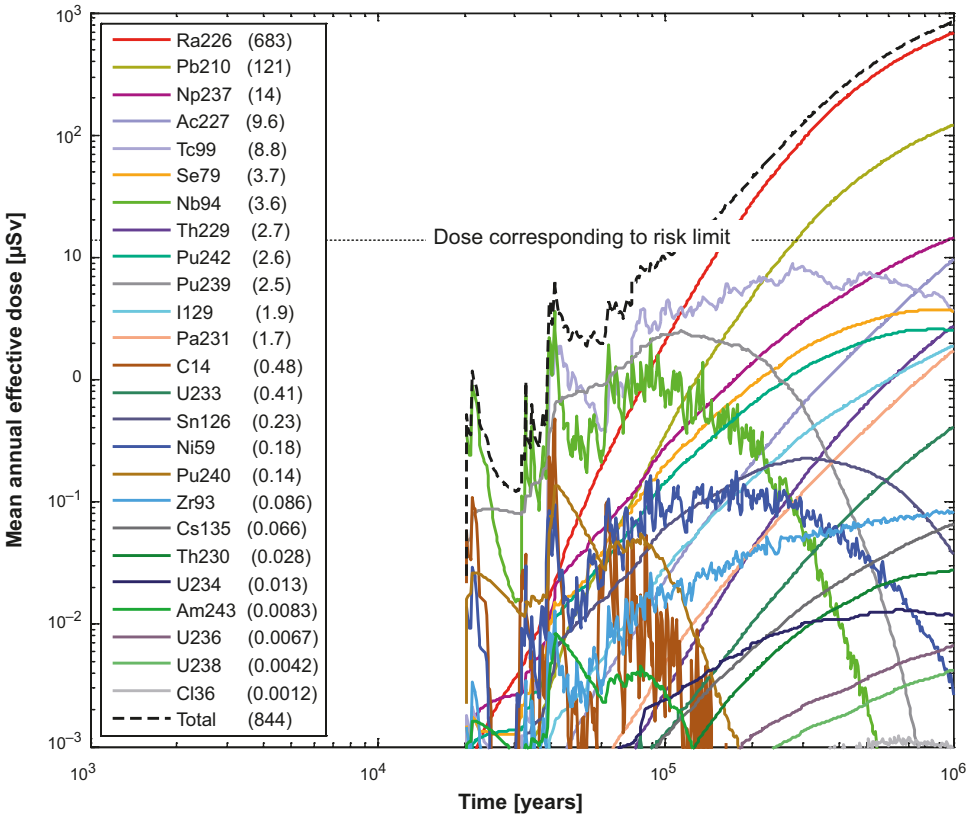

Figure 10-6. *Mean annual effective dose at Laxemar for a probabilistic calculation of the central corrosion case. The legends are sorted according to descending peak mean annual effective dose during one million years (given in brackets in μSv).*

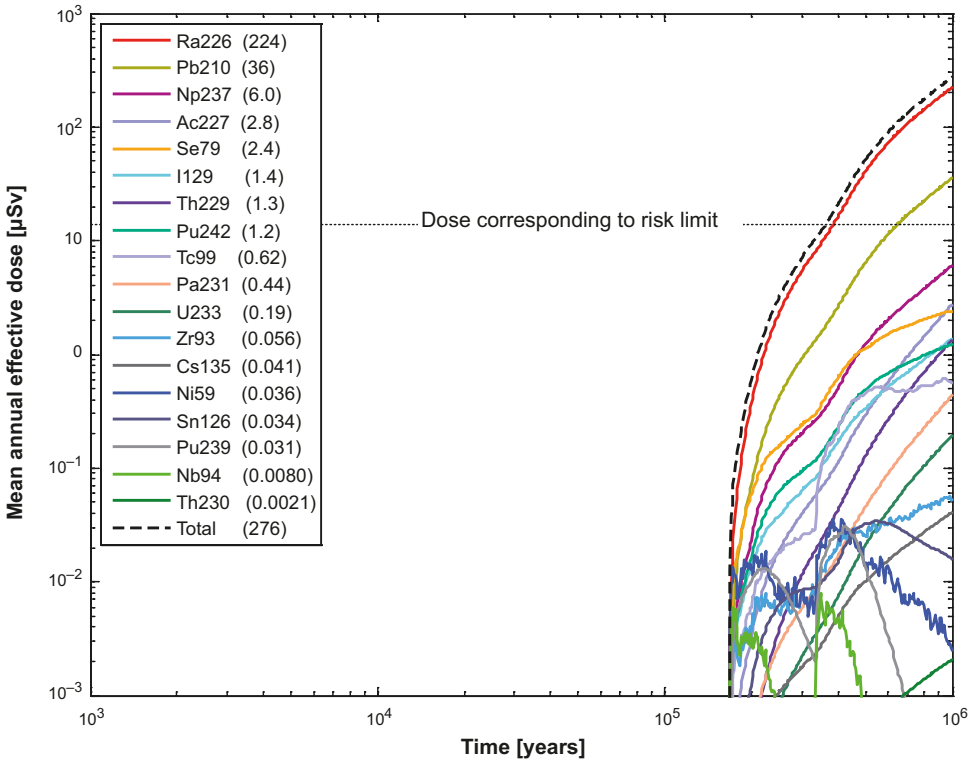

Figure 10-7. *Mean annual effective dose at Laxemar for a probabilistic calculation of assuming that all deposition holes with Darcy flux above 0.01 m/yr are rejected. The legends are sorted according to descending peak mean annual effective dose during one million years (given in brackets in μSv).*

10.4 Conclusions

According to the safety assessment methodology applied in SR-Site, the risk assessment is divided into two parts: analysis of containment potential and of retardation potential. For Forsmark, it is concluded in the **SR-Site main report** that the main contributor to risk is from the corrosion scenario, being the combination of loss of buffer due to ingress of dilute groundwater leading to advective conditions in some deposition holes, followed by enhanced potential for canister corrosion, which in turn leads to a few canister failures and subsequent release and transport of radionuclides. Furthermore, this risk is essentially captured within the assessment of the main scenario, although there are some risk contributions from the additional cases considered in the canister corrosion scenario. For comparison between the sites it is thus judged fully sufficient to only compare the risk contributions arising from the main scenario and only for the issues of loss of buffer material and canister corrosion.

The analyses presented show that the safety functions for the buffer and the canister are breached for many more deposition holes at Laxemar than at Forsmark. This also implies that the calculated risk for Forsmark will be considerably lower than that for Laxemar. This is a central result from the point of view of long-term safety since the calculated risk is the primary acceptance measure according to Swedish regulations.

Furthermore, the risk assessment for Laxemar, even if it is not complete, suggests that for a repository constructed at Laxemar, according to the current reference design, some time after 100,000 years the dose exceeds the regulatory limit and eventually grows to a level comparable to that due to the background radiation. However, this does not necessarily mean that a safe repository could not be constructed at Laxemar, but then design changes would be needed. As a demonstration of this latter conclusion, some hypothetical cases where it is assumed that it would be possible to avoid deposition holes with high Darcy fluxes are also analysed. Applying such criteria might reduce dose, potentially such that it meets the regulatory limit. Another theoretical possibility would be to place the repository at great depth, much below 700 m where the frequency of water conducting fractures possibly is much lower than at higher elevation. However, in practice the cost in terms of losses of potential deposition holes and methodology to be developed and verified is potentially quite high.

11 Confidence in the site descriptive models

11.1 Introduction

As set out in the geoscientific programme for investigation and evaluation of sites /SKB 2000/, the site investigations should continue until the reliability of the site description has reached such a level that the body of data is sufficient to adequately support safety assessment and repository engineering, or until the body of data shows that the site does not satisfy the requirements. Uncertainty and confidence assessments have been an integral part of the site descriptive modelling. For SDM-Site these assessments are reported in special reports for Forsmark /SKB 2008b/ and Laxemar /SKB 2009e/, respectively.

11.2 Safety relevance

As already discussed in previous chapters, only some site properties are important for the long-term safety. But it is also essential to develop sufficient understanding of the processes and mechanisms governing the general evolution of the site. This means that it is necessary to assess the uncertainties and the confidence in the modelling and address whether the confidence in the site descriptive model, with its uncertainties, is sufficiently high for this intended purpose.

11.3 Forsmark

The site descriptive modelling of the Forsmark site /SKB 2008a, Chapter 11/, generally judged that key aspects of the Forsmark site descriptive model, i.e. information needed for repository design and safety assessment, have a high level of confidence. Furthermore, in **SR-Site main report**, Section 15.3.6, it is concluded that the knowledge is sufficient for the assessment of long-term safety. The overall reason for this confidence is the relative wealth of data from the target volume and the consistency between independent data from different disciplines. It may also be added that the relative simplicity and homogeneity of the site, the lack of surprises and the consistent interpretations made from different disciplines enhances confidence.

Some uncertainties remain in the Forsmark site descriptive model as described in /SKB 2008b/. Most of the uncertainties concerning properties and processes inside the target volume are quantified or at least bounded by alternative models or assumptions. These uncertainties are propagated to repository engineering and safety assessment and are also assessed in previous chapters of this report. Uncertainties outside the potential repository volume are more substantial, but are judged to be of less importance for the design and long-term safety of the repository.

11.4 Laxemar

The site descriptive modelling of the Laxemar site /SKB 2009a, Chapter 11/, generally judged that key aspects of the Laxemar site descriptive model, i.e. information needed for repository design and safety assessment, have a high level of confidence even if details of the spatial variability are left unknown. The overall reason for this confidence is the spatial distribution of the data and the consistency between independent data from different disciplines and the relatively robust geological model. However, the relatively heterogeneous geology and the high frequency of water conducting fractures make detailed predictions of local properties uncertain.

Some uncertainties remain in the Laxemar site descriptive model as described in /SKB 2009e/. Most of the uncertainties concerning properties and processes inside the target volume are quantified or at least bounded by alternative models or assumptions. These uncertainties are propagated to repository engineering and safety assessment and are also assessed in previous chapters of this report. Uncertainties outside the potential repository volume are more substantial, but are judged to be of less importance for the design and long-term safety of a potential repository.

11.5 Conclusion

There is good confidence in the SDM at both sites. Confidence could only be significantly enhanced by data obtained from underground excavations. However, it must also be noted that the potential repository volume at Forsmark is more homogeneous, both in rock type distribution and in occurrence of water conductive fractures, than the Laxemar site. Heterogeneity is handled and described by stochastic modelling, but the smaller variability at Forsmark implies less uncertainty in the specific properties of a given location at Forsmark compared with Laxemar.

12 Conclusions

Based on experiences from SR-Can a number of issues related to long-term safety need to be considered in the context of comparing sites. For many issues the differences between the sites are small or insignificant for the site selection. This applies to:

- Changing climate conditions may imply that during cold periods without ice sheets at the sites, permafrost and freezing of ground water reach greater depths at Forsmark than at Laxemar, but these differences have little significance for site selection.
- Rock mechanics conditions imply there is potential for thermally induced spalling at both sites. The likelihood and extent of the spalling is much less at Laxemar, but this adds little to risk.
- Earthquake-triggered, fast, shear movements along fractures intersecting a canister can affect the containment of the canister, but the risk contribution from earthquakes is judged similar for both sites.
- Neither of the sites has potential for ore, industrial minerals or commercial stones.
- Chemical conditions affect the physical stability of bentonite, the corrosion of canisters and the transport of radionuclides. Very dilute groundwater may result in erosion of the buffer. At present there are samples with lower salinity at Laxemar when comparing the candidate repository depths of the two sites. In the future, most climatic changes will induce groundwater dilutions. Due to the low hydraulic conductivity of the repository volume at Forsmark it is possible that the groundwater salinity at the target repository volume in Forsmark could remain at the present levels over the whole glacial cycle, whereas at Laxemar as a whole, and in the fracture zones at Forsmark there will be a larger impact of the dilution processes resulting in lower salinities. At present the sulphide levels at Laxemar and Forsmark are not significantly different. The future evolution of sulphide concentrations is expected to be similar at both sites. Both sites have pH-buffering minerals in the fracture filling minerals, mainly calcite, indicating a good pH buffering capacity in the fractures of both sites. The content of Fe(II) in the rocks at Laxemar is about twice as high as that at Forsmark. However, the conceptual models of O2 consumption by Fe(II) in the rock matrix show that the larger reducing capacity is more than off-set by lower transmissivity of the fractures at Forsmark.
- There are several site specific biosphere aspects that are important for the dose assessment but LDF values for Forsmark and indicatory LDF values for Laxemar are very similar. However, there are some differences between the sites that can be of relevance for their comparison. The assessment indicates that the Forsmark site will be submerged under sea or covered by ice for longer periods than Laxemar, most likely giving considerable lower doses for long time periods. Moreover, the potential for future agriculture in areas potentially affected by released radionuclides islower for Forsmark.
- There is good confidence in the site descriptive model at both sites.

In contrast, there are important differences between the sites with respect to hydraulic properties. The *hydrogeological conditions* affect the stability of the buffer and the canister, and constitute direct input for radionuclide transport calculations. Hence these conditions affect radionuclide discharges from near-field and far-field, as well as associated doses in biosphere and the resulting risk.When the average conductive fracture frequency of the rock mass volumes between the deterministically modelled deformation zones is considered, it is observed that at Forsmark a clear distinction can be made between the rock above- and below 400 m elevation respectively, where the rock above is significantly more fractured than below. At Laxemar, the average conductive fracture frequency is greater at repository depth and there is also a considerable spatial variability between different parts of the considered rock mass volume. When hydraulic characteristics at repository depth are compared in detail, it is found that Forsmark has a much lower average conductive fracture frequency (less than 0.01 m^{-1} compared with 0.06 m^{-1} to 0.23 m^{-1} at Laxemar). Mainly due to this difference, all hydrogeological measures and entities considered in this comparison are in favour of Forsmark. For example, in the temperate period simulations, the Darcy flux at the deposition hole locations (for fractures intersecting deposition holes) is approximately two orders of magnitude larger at Laxemar than at Forsmark. These conditions also affect the *initial state*, where it is expected that there will be a substantially greater loss of potential deposition positions at the Laxemar site. Furthermore there would be many more accepted deposition positions that would have inflows near the acceptability criterion at the Laxemar site, which has consequences for safety.

Due mainly to the difference in hydraulic conditions, the safety functions for the buffer and the canister are breached for many more deposition holes at Laxemar than at Forsmark. Furthermore, the risk assessment for Laxemar suggests that for a repository at Laxemar, constructed according to the current reference design, the doses will exceed the regulatory limit already some time after 100,000 years and eventually grows to a level comparable to that due to the background radiation. However, this does not necessarily mean that a safe repository could not be constructed at Laxemar, but then design modifications would be needed. To illustrate this option, hypothetical cases assuming that deposition holes with high Darcy fluxes could be completely avoided have also been analysed. This could in theory reduce dose, potentially enough to meet the regulatory limit. Another theoretical possibility would be to locate the repository at a depth, exceeding 700 m, where the frequency of water conducting fractures possibly is much lower than at higher elevation. However, in practice the cost in terms of losses of potential deposition holes and methodology to be developed and verified is potentially quite high.

In summary, there are a number of safety related site characteristics for which the analyses do not show any decisive differences in terms of implications on safety, between the sites Forsmark and Laxemar. However, the frequency of water conducting fractures at repository depth is much larger at Laxemar than at Forsmark. This difference, in turn, affects the future stability of current favourable groundwater composition, which combined with the much higher flows at Laxemar would lead to a breach in the safety functions for the buffer and the canister for many more deposition positions at Laxemar than at Forsmark. Thereby the calculated risk for Forsmark will be considerably lower than that for Laxemar. From the safety perspective, therefore, Forsmark is clearly the most favourable site.

13 References

SKB's (Svensk Kärnbränslehantering AB) publications can be found at www.skb.se/publications.

Adams J, Wetmiller R J, Drysdale J, Hasegawa H S, 1991. The first surface rupture from an earthquake in eastern North America. Current Research, Geological Survey of Canada, 91-1C, pp 9–15.

Andersson E (ed), 2010. The limnic ecosystems at Forsmark and Laxemar-Simpevarp. SKB TR-10-02, Svensk Kärnbränslehantering AB.

Andersson J, Ström A, Svemar C, Almén K-E, Ericsson L-O, 2000. What requirements does the KBS-3 repository make on the host rock? Geoscientific suitability indicators and criteria for siting and site evaluation. SKB TR-00-12, Svensk Kärnbränslehantering AB.

Aquilonius K (ed), 2010. The marine ecosystems at Forsmark and Laxemar-Simpevarp. SKB TR-10-03, Svensk Kärnbränslehantering AB.

Avila R, Ekström P-A, Åstrand P-G, 2010. Landscape dose conversion factors used in the safety assessment SR-Site. SKB TR-10-06, Svensk Kärnbränslehantering AB.

Brydsten L, Engqvist A, Näslund J-O, Lindborg T, 2009. Förväntade extremvattennivåer för havsytan vid Forsmark och Laxemar-Simpevarp fram till år 2100. [Expected extreme sea water levels at Forsmark and Laxemar-Simpevaprt until the year 2100] (in Swedish). SKB R-09-06, Svensk kärnbränslehantering AB.

Böðvarsson R, 2002. Swedish National Seismic Network (SNSN). SKB P-02-04, Svensk Kärnbränslehantering AB.

Böðvarsson R, 2002–2009. Swedish National Seismic Network (SNSN). Series of short reports on recorded earthquakes during the period 2002-2008. Svensk Kärnbränslehantering AB.

Böðvarsson R, Lund B, Roberts R, Slunga R, 2006. Earthquake activity in Sweden. Study in connection with a proposed nuclear waste repository in Forsmark or Oskarshamn. SKB R-06-67, Svensk Kärnbränslehantering AB.

Carlsten S, Stråhle A, 2000. Borehole radar and BIPS investigations in boreholes at the Boda area. SKB TR-01-02, Svensk Kärnbränslehantering AB.

Cosgrove, J, Stanfors R, Röshoff K, 2006. Geological characteristics of deformation zones and a strategy for their detection in a repository. SKB R-06-39, Svensk Kärnbränslehantering AB.

Cowie P A, Scholz C H, 1992. Growth of faults by accumulation of seismic slip. Journal of Geophysical Research, 97, pp 11085–11095.

Crawford J, 2008. Bedrock transport properties Forsmark. Site descriptive modelling, SDM-Site Forsmark. SKB R-08-48, Svensk Kärnbränslehantering AB.

Crawford J, Sidborn M, 2008. Bedrock transport properties Laxemar. Site descriptive modelling, SDM-Site Laxemar. SKB R-08-94, Svensk Kärnbränslehantering AB.

Delos A, Trinchero P, Richard L, Molinero J, Dentz M, Pitkänen P, 2010. Quantitative assessment of deep gas migration in Fennoscandian sites. SKB R-10-61, Svensk Kärnbränslehantering AB.

Drake H, Tullborg E-L, 2009. Fracture mineralogy Laxemar. Site descriptive modelling, SDM-Site Laxemar. SKB R-08-99, Svensk Kärnbränslehantering AB.

Fenton C H, Adams J, Halchuk S, 2006. Seismic hazards assessment for radioactive waste disposal sites in regions of low seismic activity. Geotechnical and Geological Engineering, 24, pp 579–592.

Follin S, 2008. Bedrock hydrogeology Forsmark. Site descriptive modelling, SDM-Site Forsmark. SKB R-08-95, Svensk Kärnbränslehantering AB.

Follin S, Levén J, Hartley L, Jackson P, Joyce S, Roberts D, Swift B, 2007a. Hydrogeological characterisation and modelling of deformation zones and fracture domains, Forsmark modelling stage 2.2. SKB R-07-48, Svensk Kärnbränslehantering AB.

Follin S, Johansson P-O, Hartley L, Jackson P, Roberts D, Marsic N, 2007b. Hydrogeological conceptual model development and numerical modelling using CONNECTFLOW, Forsmark modelling stage 2.2. SKB R-07-49, Svensk Kärnbränslehantering AB.

Follin S, Hartley L, Jackson P, Roberts D, Marsic N, 2008. Hydrogeological conceptual model development and numerical modelling using CONNECTFLOW, Forsmark modelling stage 2.3. SKB R-08-23, Svensk Kärnbränslehantering AB.

Fälth B, Hökmark H, 2006. Seismically induced slip on rock fractures. Results from dynamic discrete fracture modeling. SKB R-06-48, Svensk Kärnbränslehantering AB.

Fälth B, Hökmark H, Munier R, 2007. Seismically induced shear displacements in repository host rock fractures. In: Proceedings of the 9th Canadian Conference on Earthquake Engineering, Ottawa, 26–29 June 2007.

Fälth B, Hökmark H, Munier R, 2008. Seismically induced slip on rock fractures – expanded study with particular account of large earthquakes. In: Proceedings of the 42nd U.S. Rock Mechanics Symposium, San Fransisco, 29 June–2 July 2008. Madison, Wis.: Omnipress.

Fälth B, Hökmark H, Munier R, 2010. Effects of large earthquakes on a KBS-3 repository. Evaluation of modelling results and their implications for layout and design. SKB TR-08-11, Svensk Kärnbränslehantering AB.

Gimeno M J, Auqué L F, Gómez J, Salas J, Molinero J, 2010. Hydrogeochemical evolution of the Laxemar site. SKB R-10-60, Svensk Kärnbränslehantering AB.

Glamheden R, Fälth B, Jacobsson L, Harrström J, Berglund J, Bergkvist L, 2010. Counterforce applied to prevent spalling. SKB TR-10-37, Svensk Kärnbränslehantering AB.

Gómez J B, Laaksoharju M, Skårman E, Gurban I, 2009. M3 version 3.0: verification and validation. SKB TR-09-05, Svensk Kärnbränslehantering AB.

Hallbeck L, Pedersen K, 2008a. Explorative analyses of microbes, colloids, and gases together with microbial modelling. Site description model, SDM-Site Laxemar. SKB R-08-109, Svensk Kärnbränslehantering AB.

Hallbeck L, Pedersen K, 2008b. Explorative analysis of microbes, colloids and gases. SDM-Site Forsmark. SKB R-08-85, Svensk Kärnbränslehantering AB.

Hallbeck L, Pedersen K, 2008c. Characterization of microbial processes in deep aquifers of the Fennoscandian Shield. Applied Geochemistry, 23, pp 1796–1819.

Hartikainen J, Kouhia R, Wallroth T, 2010. Permafrost simulations at Forsmark using a numerical 2D thermo-hydro-chemical model. SKB TR-09-17, Svensk Kärnbränslehantering AB.

Hedin A, 2008. Semi-analytic stereological analysis of waste package/fracture intersections in a granitic rock nuclear waste repository. Mathematical Geosciences, 40, pp 619–637.

Hora S, Jensen M, 2005. Expert panel elicitation on seismicity following glaciation. SSI Rapport 2005:20, Statens strålskyddsinstitut (Swedish Radiation Protection Authority).

Hökmark H, Lönnqvist M, Fälth B, 2010. THM-issues in repository rock. Thermal, mechanical, thermo-mechanical and hydro-mechanical evolution of the rock at the Forsmark and Laxemar sites. SKB TR-10-23, Svensk Kärnbränslehantering AB.

Joyce S, Simpson T, Hartley L, Appelgate D, Hoek J, Jackson P, Swan D, Marsic N, Follin S, 2010. Groundwater flow modelling of periods with temperate climate conditions – Forsmark. SKB R-09-20, Svensk Kärnbränslehantering AB.

Joyce S, Simpson T, Hartley L, Appelgate D, Hoek J, Swan D, Marsic N, Rhén I, 2011. Groundwater flow modelling of periods with temperate climate conditions – Laxemar. SKB R-09-24, Svensk Kärnbränslehantering AB.

Kim Y-S, Sanderson D J, 2008. Earthquake and fault propagation, displacement and damage zones. In: Landowe S J, Hammler G M (eds). Structural geology: new research. New York: Nova Science Publishers.

Kim Y-S, Peacock D C P, Sanderson D J, 2004. Fault damage zones. Journal of Structural Geology, 26, pp 503–517.

Kjellström E, Strandberg G, Brandefelt J, Näslund J-O, Smith B, Wohlfarth B, 2009. Climate conditions in Sweden in a 100,000-year time perspective. SKB TR-09-04, Svensk Kärnbränslehantering AB.

La Pointe P R, Cladouhos T, Follin S, 1999. Calculation of displacement on fractures intersecting canisters induced by earthquakes: Aberg, Beberg and Ceberg examples. SKB TR-99-03, Svensk Kärnbränslehantering AB.

Laaksoharju M, Skårman C, Skårman E, 1999. Multivariate mixing and mass balance (M3) calculations, a new tool for decoding hydrogeochemical information. Applied Geochemistry, 14, pp 861–871.

Laaksoharju M, Smellie J, Tullborg E-L, Gimeno M, Hallbeck L, Molinero J, Waber N, 2008. Bedrock hydrogeochemistry Forsmark. Site descriptive modelling, SDM-Site Forsmark. SKB R-08-47, Svensk Kärnbränslehantering AB.

Laaksoharju M, Smellie J, Tullborg E-L, Wallin B, Drake H, Gascoyne M, Gimeno M, Gurban I, Hallbeck L, Molinero J, Nilsson A-C, Waber N, 2009. Bedrock hydrogeochemistry Laxemar. Site descriptive modelling, SDM-Site Laxemar. SKB R-08-93, Svensk Kärnbränslehantering AB.

Lagerbäck R, Sundh M, 2008. Early Holocene faulting and paleoseismicity in northern Sweden. Research Paper C 836, Geological Survey of Sweden.

Lagerbäck R, Sundh M, Svedlund J-O, Johansson H, 2005. Forsmark site investigation. Searching for evidence of late- or postglacial faulting in the Forsmark region. Results from 2002–2004. SKB R-05-51, Svensk Kärnbränslehantering AB.

Lagerbäck R, Sundh M, Svantesson S-I, 2006. Oskarshamn site investigation. Searching for evidence of late- or postglacial faulting in the Oskarshamn region. Results from 2005. SKB P-06-160, Svensk Kärnbränslehantering AB.

Lindborg T (ed), 2010. Landscape Forsmark – data, methodology and results for SR-Site. SKB TR-10-05, Svensk Kärnbränslehantering AB.

Lindroos H, 2004. The potential for ore, industrial minerals and commercial stones in the Simpevarp area. SKB R-04-72, Svensk Kärnbränslehantering AB.

Lindroos H, Isaksson H, Thunehed H, 2004. The potential for ore and industrial minerals in the Forsmark area. SKB R-04-18, Svensk Kärnbränslehantering AB.

Lund B, 2005. Effects of deglaciation on the crustal stress field and implications for endglacial faulting: a parametric study of simple Earth and ice models. SKB TR-05-04, Svensk Kärnbränslehantering AB.

Lund B, 2006. Stress variations during a glacial cycle at 500 m depth in Forsmark and Oskarshamn: Earth model effects. SKB R-06-95, Svensk Kärnbränslehantering AB.

Lund, B, Schmidt P, Hieronymus C, 2009. Stress evolution and fault stability during the Weichselian glacial cycle. SKB TR-09-15, Svensk Kärnbränslehantering AB.

Löfgren A (ed), 2010. The The terrestrial ecosystems at Forsmark and Laxemar-Simpevarp. SR-Site Biosphere. SKB TR-10-01, Svensk Kärnbränslehantering AB.

Munier R, 2006. Using observations in deposition tunnels to avoid intersections with critical fractures in deposition holes. SKB R-06-54, Svensk Kärnbränslehantering AB.

Munier R, 2007. Demonstrating the efficiency of the EFPC criterion by means of sensitivity analyses. SKB R-06-115, Svensk Kärnbränslehantering AB.

Munier R, 2010. Full perimeter intersection criteria. Definitions and implementations in SR-Site. SKB TR-10-21, Svensk Kärnbränslehantering AB.

Munier R, Hökmark H, 2004. Respect distances. Rationale and means of computation. SKB R-04-17, Svensk Kärnbränslehantering AB.

Munier R, Stenberg L, Stanfors R, Milnes A G, Hermanson J, Triumf C-A, 2003. Geological Site Descriptive Model. A strategy for the model development during site investigations. SKB R-03-07, Svensk Kärnbränslehantering AB.

Munier R, Hökmark H, Fälth B, 2008. Respect distances: rationale and means of computation. In: Proceedings of the 33rd International Geologial Congress (33IGC). Oslo, 6–14 August 2008.

Mörner N-A, 1989. Postglacial faults and fractures on Äspö. SKB HRL Progress report 25-89-24, Svensk Kärnbränslehantering AB.

Mörner N-A, 2003. Paleoseismicity of Sweden – a novel paradigm. Stockholm: N-A Mörner.

Neretnieks I, 2006. Flow and solute transport in a zone damaged due to spalling. SKB R-06-91, Svensk Kärnbränslehantering AB.

Neretnieks I, Liu L, Moreno L, 2009. Mechanisms and models for bentonite erosion. SKB TR-09-35, Svensk Kärnbränslehantering AB.

Neretnieks I, Liu L, Moreno L, 2010. Mass transfer between waste canister and water seeping in rock fractures. Revisiting the Q-equivalent model. SKB TR-10-42, Svensk Kärnbränslehantering AB.

Olofsson I, Simeonov A, Stephens M, Follin S, Nilsson A-C, Röshoff K, Lindberg U, Lanaro F, Fredriksson A, Persson L, 2007. Site descriptive modelling Forsmark, stage 2.2. A fracture domain concept as a basis for the statistical modelling of fractures and minor deformation zones, and interdisciplinary coordination. SKB R-07-15, Svensk Kärnbränslehantering AB.

Olvmo M, 2010. Review of denudation processes and quantification of weathering and erosion rates at a 0.1 to 1 Ma time scale. SKB TR-09-18, Svensk Kärnbränslehantering AB.

Rhén I, Hartley L, 2009. Bedrock hydrogeology Laxemar. Site descriptive modelling, SDM-Site Laxemar. SKB R-08-92, Svensk Kärnbränslehantering AB.

Rhén I, Forsmark T, Hartley L, Jackson P, Roberts D, Swan D, Gylling B, 2008. Hydrogeological conceptualisation and parameterisation. Site descriptive modelling, SDM-Site Laxemar. SKB R-08-78, Svensk Kärnbränslehantering AB.

Rhén I, Forsmark T, Hartley L, Joyce S, Roberts D, Gylling B, Marsic N, 2009. Bedrock hydrogeology. Model testing and synthesis. Site descriptive modelling, SDM-Site Laxemar. SKB R-08-91, Svensk Kärnbränslehantering AB.

Salas J, Gimeno M J, Auqué L F, Molinero J, Gómez J, Juárez I, 2010. SR-Site – hydrogeochemical evolution of the Forsmark site. SKB TR-10-58, Svensk Kärnbränslehantering AB.

Sandström B, Tullborg E-L, Smellie J, MacKenzie A B, Suksi J, 2008. Fracture mineralogy of the Forsmark site. SDM-Site Forsmark. SKB R-08-102, Svensk Kärnbränslehantering AB.

Scholz C H, 2002. The mechanics of earthquakes and faulting. 2nd ed. Cambridge: Cambridge University Press.

Selroos J-O, Follin S, 2010. Forsmark - Groundwater flow modelling methodology, setup and results. SKB R-09-22, Svensk Kärnbränslehantering AB.

Sidborn M, Sandström B, Tullborg E-L, Delos A, Molinero J, Hallbeck L, Pedersen K, 2010. SR-Site: Oxygen ingress in the rock at Forsmark during a glacial cycle. SKB TR-10-57, Svensk Kärnbränslehantering AB.

SKB, 1990. Granskning av Nils-Axel Mörners arbete avseende postglaciala strukturer på Äspö. SKB AR 90-18, Svensk Kärnbränslehantering AB.

SKB, 2000. Geoscientific programme for investigation and evaluation of sites for the deep repository. SKB TR-00-20, Svensk Kärnbränslehantering AB.

SKB, 2006a. Long-term safety for KBS-3 repositories at Forsmark and Laxemar – a first evaluation. Main Report of the SR-Can project. SKB TR-06-09, Svensk Kärnbränslehantering AB.

SKB, 2006b. Climate and climate-related issues for the safety assessment SR-Can. SKB TR-06-23, Svensk kärnbränslehantering AB.

SKB, 2008a. Site description of Forsmark at completion of the site investigation phase. SDM-Site Forsmark. SKB TR-08-05, Svensk Kärnbränslehantering AB.

SKB, 2008b. Confidence assessment. Site descriptive modelling, SDM-Site Forsmark. SKB R-08-82, Svensk Kärnbränslehantering AB.

SKB, 2009a. Site description of Laxemar at completion of the site investigation phase. SDM-Site Laxemar. SKB TR-09-01, Svensk Kärnbränslehantering AB.

SKB, 2009b. Underground design Laxemar. Layout D2. SKB R-09-16, Svensk Kärnbränslehantering AB.

SKB, 2009c. Design premises for a KBS-3V repository based on results from the safety assessment SR-Can and some subsequent analyses. SKB TR-09-22, Svensk Kärnbränslehantering AB.

SKB, 2009d. Underground design Forsmark. Layout D2. SKB R-08-116, Svensk Kärnbränslehantering AB.

SKB, 2009e. Confidence assessment. Site descriptive modelling, SDM-Site Laxemar. SKB R-08-101, Svensk Kärnbränslehantering AB.

SKB, 2010a. Design and production of the KBS-3 repository. SKB TR-10-12, Svensk Kärnbränslehantering AB.

SKB, 2010b. Design, construction and initial state of the underground openings. SKB TR-10-18, Svensk Kärnbränslehantering AB.

SKB, 2010c. Climate and climate related issues for the safety assessment SR-Site. SKB TR-10-49, Svensk Kärnbränslehantering AB.

SKB, 2010d. Data report for the safety assessment SR-Site. SKB TR-10-52, Svensk Kärnbränslehantering AB.

SKB, 2010e. Ramprogram för detaljundersökningar vid uppförande och drift av slutförvar för använt kärnbränsle. [Framework programme for detailed investigations during construction and operation of final repository for spent nuclear fuel] (in Swedish). R-10-08, Svensk Kärnbränslehantering AB.

SKB, 2010f. Biosphere analyses for the safety assessment SR-Site – synthesis and summary of results. SKB TR-10-09, Svensk Kärnbränslehantering AB.

SKB, 2010g. Buffer, backfill and closure process report for the safety assessment SR-Site. SKB TR-10-47, Svensk Kärnbränslehantering AB.

SKB, 2011. Long-term safety for the final repository for spent nuclear fuel at Forsmark. Main report of the SR-Site project. SKB TR-11-01, Svensk Kärnbränslehantering AB.

SSMFS 2008:21. Strålsäkerhetsmyndighetens föreskrifter och allmänna råd om säkerhet vid slutförvaring av kärnämne och kärnavfall (The Swedish Radiation Safety Authority's Regulations concerning Safety in connection with the Disposal of Nuclear Material and Nuclear Waste) (in Swedish). Stockholm: Strålsäkerhetsmyndigheten (Swedish Radiation Safety Authority).

SSMFS 2008:37. Strålsäkerhetsmyndighetens föreskrifter och allmänna råd om skydd av människors hälsa och miljön vid slutligt omhänder-tagande av använt kärnbränsle och kärnavfall (The Swedish Radiation Safety Authority's Regulations on the Protection of Human Health and the Environment in connection with the Final Management of Spent Nuclear Fuel and Nuclear Waste) (in Swedish). Stockholm: Strålsäkerhetsmyndigheten (Swedish Radiation Safety Authority).

Stephens M B, Fox A, La Pointe P, Simeonov A, Isaksson H, Hermanson J, Öhman J, 2007. Geology Forsmark. Site descriptive modelling Forsmark stage 2.2. SKB R-07-45, Svensk Kärnbränslehantering AB.

Stephens M B, Bergman T, Isaksson H, Petersson J, 2008a. Bedrock geology Forsmark. Modelling stage 2.3. Description of the bedrock geological map at the ground surface. SKB R-08-128, Svensk Kärnbränslehantering AB.

Stephens M B, Simeonov A, Isaksson H, 2008b. Bedrock geology Forsmark. Modelling stage 2.3. Implications for and verification of the deterministic geological models based on complementary data. SKB R-08-64, Svensk Kärnbränslehantering AB.

Svensson U, Follin S, 2010. Groundwater flow modelling of the excavation and operation phases – Forsmark. SKB R-09-19, Svensk Kärnbränslehantering AB.

Svensson U, Rhén I, 2011. Groundwater flow modelling of the excavation and operation phases – Laxemar. SKB R-09-23, Svensk Kärnbränslehantering AB.

Tullborg E-L, Smellie J, Nilsson A-C, Gimeno M J, Auqué L F, Brüchert V, Molinero J, 2010a. SR-Site: Sulphide contents in the groundwater at Forsmark. SKB TR-10-39, Svensk Kärnbränslehantering AB.

Tullborg E-L, Smellie J, Nilsson A-C, Gimeno M J, Brüchert V, Molinero J, 2010b. Sulphide contents in the groundwater at Laxemar. SKB R-10-62, Svensk Kärnbränslehantering AB.

Vidstrand P, Follin S, Zugec N, 2010. Groundwater flow modelling of periods with periglacial and glacial climate conditions – Forsmark. SKB R-09-21, Svensk Kärnbränslehantering AB.

Vidstrand P, Rhén I, Zugec N, 2011. Groundwater flow modelling of periods with periglacial and glacial climate conditions – Laxemar. SKB R-09-25, Svensk Kärnbränslehantering AB.

Wahlgren C-H, Curtis P, Hermanson J, Forssberg O, Öhman J, Fox A, La Pointe P, Drake H, Triumf C-A, Mattsson H, Thunehed H, Juhlin C, 2008. Geology Laxemar. Site descriptive modelling, SDM-Site Laxemar. SKB R-08-54, Svensk Kärnbränslehantering AB.

Wänstedt S, 2000. Geophysical and geological investigations of the Boda area. SKB R-00-23, Svensk Kärnbränslehantering AB.

Appendix A

Geosphere and biosphere data as input to the Comparative analysis of safety related site characteristics

This appendix covers assessment and selection of Laxemar related input data used in the analyses presented in this report. Appendices A1 to A10 should be seen as complements to the SR-Site Data report /SKB 2010/ and provide Laxemar data, while the SR-Site Data report provides Forsmark data. These appendices only deal with site specific geosphere and biosphere data, while data on the spent fuel and engineered barrier, which are general, should be taken from the SR-Site Data report. As the Comparative analysis of safety related site characteristics has different objectives than SR-Site, these appendices do not necessarily provide all corresponding data to those found in the SR-Site Data report. Throughout these appendices the phrase "Comparative analysis" is used as short for "Comparative analysis of safety related site characteristics".

Contents

A1 Groundwater chemical composition

This appendix describes the groundwater chemical composition data for Laxemar used in the Comparative analysis of safety related site characteristics. This appendix does not aim to present a complete set of groundwater chemical composition data, but only data of extra importance for the Comparative analysis.

There are two types of modelling activities that deal with groundwater chemical compositions: models that have as main purpose to *calculate* groundwater chemical compositions, and models that *use* groundwater chemical compositions *as input conditions*. From the perspective of assessing the long-term safety of a KBS-3 repository, the most important parameters are the main chemical components which affect salinity and ionic strength, as well as sulphide, acidity, and redox parameters. The associated data are described in this appendix.

An especially important parameter is the concentration of sulphide in the groundwater, as it affects copper corrosion which in turn affects the lifetime of the copper canisters. Because the amount of sulphide is affected by bacterial sulphate reduction, the sulphide concentration is evaluated using a different methodology than for the other species. The resulting data are discussed in this appendix.

The corresponding data for Forsmark, used in the SR-Site analysis, are reported in Section 6.1 of the SR-Site Data report /SKB 2010/. We have chosen not to repeat aspects and methodologies that are general for both sites, but instead to refer to the corresponding Forsmark text. Therefore, we recommend the reader to first examine Section 6.1 of the SR-Site Data report, and thereafter read this present text.

A1.1 Modelling as input to the Comparative analysis of safety related site characteristics

This section describes what data are expected from the supplier, and in what modelling activity the data are to be used.

Defining the data requested from the supplier

Groundwater chemical compositions at the Laxemar site are generally calculated using the Phreeqc computational code /Charlton and Parkhurst 2002, Parkhurst and Appelo 1999/. This modelling requires mixing proportions and compositions of end-member groundwater components. The mixing proportions are obtained directly from, or are based on the results of, hydrogeological modelling described in Chapters A6 and A7. In addition, a thermodynamic database is needed, which is described in Section 3.4 and 6.1 of the SR-Site Data report /SKB 2010/**.** The same database has been used for both the Laxemar and Forsmark sites. As input to the Phreeqc modelling the supplier should deliver:

- The compositions of end-member groundwater components of Laxemar.

As output from the Phreeqc modelling the supplier should deliver:

- Results from the Phreeqc calculations, giving the concentrations of the main chemical components, for the rock volume surrounding the assumed repository.

Models that use groundwater chemical compositions as input to the Comparative analysis require the following data concerning the main components:

- Statistics on the sum of the concentrations of main cations, expressed in charge equivalents as $\Sigma q[Mq+]$, where q is the cation charge number and M is the cation concentration (mol/m^3).
- Maximum ionic strength (mol/m^3).
- Minimum and maximum ratio of Ca/Na concentrations.
- Minimum and Maximum *pH.*
- Minimum and maximum total inorganic carbon concentration (mol/m^3).
- Redox potential statistics, *Eh* (V).
- Sulphide concentration statistics (mol/m^3).

The sulphide concentration is affected by bacterial processes. Although the sulphide concentration is modelled with Phreeqc, different assumptions give different data ranges. Therefore, the results need to be complemented by measurement data and observations from the site investigation and the monitoring programmes.

Other data related to groundwater compositions, which are used as input to the Comparative analysis, are taken directly from the Laxemar site description reports /Drake and Tullborg 2009, Gimeno et al. 2009, Hallbeck and Pedersen 2008, Kalinowski 2009, Laaksoharju et al. 2009, Waber et al. 2009/ and are not discussed in this appendix.

Modelling activities in which data will be used

Groundwater compositions under different climatic conditions can be estimated using chemical mixing and equilibrium reaction calculations performed with the Phreeqc computational code. This modelling activity needs mixing proportions from the hydrogeological modelling, end-member compositions, and thermodynamic data as inputs. For the temperate period, mixing proportions from the hydrogeological modelling are taken directly from the Hydrogeological base case /Joyce et al. 2010/, which is based on the SDM-Site version of the Laxemar site-descriptive modelling /Rhén and Hartley 2009/. As described in Chapter A6, it has later been chosen to propagate the Elaborated Hydro-DFN case, and not the Hydrogeological base case. This inconsistency has been judged to be acceptable. For the periglacial and glacial periods, the outputs from the hydrogeological modelling /Vidstrand et al. 2010/ are salinities, which have been transformed into mixing proportions by /Gimeno et al. 2010/.

The Phreeqc modelling has been performed for different times of the temperate period and for different events (depending mainly on the ice location) of the periglacial and glacial period /Gimeno et al. 2010/. The choices of these times and events are determined by previous hydrogeological modelling (cf. Chapter A6).

The output from the Phreeqc modelling, in terms of concentrations of the main components, is mainly use as a basis for estimating erosion of the bentonite buffer. It is also used as supporting data when estimating radionuclide sorption parameters for a few radioelements (cf. Chapter A8). The concentrations can also be used for assessing solubility limits of radioelements inside of a failed canister, which may subsequently be used for assessing the source term in radionuclide transport modelling.

In the case of sulphide, the groundwater data obtained during the site investigation and the monitoring programmes are evaluated to provide a set of selected data. The data, presented as a statistical distribution, are used as input to assess the corrosion of copper canisters. These data are complemented with data from Phreeqc modelling of sulphide for the complete glacial cycle in Laxemar.

A1.2 Supplier input on use of data in the Comparative analysis

The supplier notes that for the main groundwater chemical components, the provided variability of compositions and ionic strengths is highly conditioned by the results of the hydrogeological models, but that they nevertheless reflect on qualitatively the conceptual models of the Laxemar site. The results indicate somewhat more diluted groundwaters at the Laxemar site compared to the Forsmark site. The sulphide concentrations are taken from selected measured values at present day conditions. These concentrations are similar to those measured at the Forsmark site.

A1.3 Sources of information and documentation of data qualification

Sources of information

The main sources of information are the hydrogeochemical modelling performed for Laxemar and reported in /Gimeno et al. 2010/, as well as the selection of representative sulphide data reported in /Tullborg et al. 2010/. The full references of these reports are given in Table A1-1.

The thermodynamic database used in the calculations of groundwater chemical compositions is the same for both Laxemar and Forsmark, and is discussed in Sections 3.4 and 6.1 of the SR-Site Data report /SKB 2010/ and is not further discussed here.

Table A1-1. Main sources of information used in data qualification.

Gimeno M J, Auqué, L, Gómez J, Salas J, Molinero J, 2010. Hydrogeochemical evolution of the Laxemar site. SKB R-10-60, Svensk Kärnbränslehantering AB.
Tullborg E-L, Smellie J, Nilsson A-C, Gimeno M J, Brüchert V, Wallin B, Molinero J, 2010. Sulphide contents in the groundwater at Laxemar. SKB R-10-62, Svensk Kärnbränslehantering AB.

The hydrogeological modelling results /Joyce et al. 2010, Vidstrand et al. 2010/ , which are used as input for the mixing calculations reported in /Gimeno et al. 2010/, are discussed in Chapters A6 and A7.

Categorising data sets as qualified or supporting data

The most important data sets related to groundwater chemistry are listed in Table A1-2, wherein arguments are provided for the categorisation into qualified or supporting data sets.

Excluded data previously considered as important

Concerning the sulphide concentration, the categorisation of all samples from the site investigation and monitoring programmes /Smellie and Tullborg 2009/ has been revised in /Tullborg et al. 2010/ with emphasis on the Fe(II) and sulphide data. In some cases, data previously labelled as representative when considering only major groundwater components have been deemed as less representative for trace elements such as Fe(II), sulphide, Mn(II), dissolved organic carbon, etc.

No other data have been excluded that previously had a significant impact on the perception of the appropriate choice of data values or of modelling approaches.

Table A1-2. Qualified and supporting data sets.

Qualified data sets	Supporting data sets
1. /Gimeno et al. 2010/, Table 4-3: Equilibrated end- members compositions, calculated with the coupled database used for the geochemical simulations. Used for Base case and variant cases 1 and 2. 2. /Gimeno et al. 2010/, Table 7-1 and appendix 2: Maximum and minimum values and statistics of the main geochemical parameters obtained from Phreeqc calculations for the Base case over the complete glacial cycle in Laxemar. 3. /Gimeno et al. 2010/, section 7.4.2 and appendix 2: Eh values for the complete glacial cycle in Laxemar. 3. /Gimeno et al. 2010/, section 7.2 and appendix 2: Cation charge equivalents for the complete glacial cycle in Laxemar. 4. /Tullborg et al. 2010/, set of sulphide concentrations selected as representative of the present day groundwater compositions at Laxemar.	5. The ChemNet data[1] 6. Sicada delivery[2] all groundwater data from Laxemar containing sulphide analyses.

Items 1-4: /Gimeno et al. 2010/ and /Tullborg et al. 2010/ are SKB reports for the Laxemar site that are produced and reviewed in accordance with the SKB's quality assurance system, and therefore these data are judged as qualified.

Items 5-6 are the complete data sets on which the selection of representative sulphide data in /Tullborg et al.2010/ is based. These data sets are quality assured /Smellie and Tullborg 2009/ but not qualified for the purpose of directly performing a comparative analysis of sulphide concentrations between the Laxemar and Forsmark sites.

[1] Simon Database: file "Laxemar 2_3_2008_28May(PROJECTPLACE).xls" (access might be given on request).

[2] Sicada Data Delivery, 10-093 (access might be given on request).

A1.4 Conditions for which data are supplied

Concerning the main geochemical parameters, estimated through Phreeqc modelling, the data are highly conditioned by the hydrogeological modelling providing mixing proportions /Joyce et al. 2010/ or salinities /Vidstrand et al. 2010/. Conditions for the hydrogeological modelling are outlined in Chapters A6 and A7. The hydrogeological modelling dictates the coordinates for the Phreeqc modelling. However, only subsets of all the coordinates are used in the Phreeqc modelling, representing three different rock volumes /Gimeno el at. 2010, Section 4.1.3/:

- All data points (coordinates) at repository depth, which means a complete horizontal slice at 500 ± 60 m depth.
- A subset of the above data including the data points within the candidate repository volume (included in the domain inside the following coordinates: [1546.40, 6367.62, –0.5]; [1550.05, 6367.62, –0.5]; [1550.05, 6365.00, –0.5]; and [1546.40, 6365.00, –0.5]). These data are used when presenting statistics for the main components.
- A vertical slice approximately parallel to the shoreline (NW: 1,544,500 m / 6,370,000; SE: 1,551,500 m / 6,363,025), through boreholes KLX13A, KLX18A, the entrance to the repository, and boreholes KLX12A and KLX056.

The data are also conditioned by the used end-member compositions. For Laxemar the following five end members are used /Gimeno et al. 2010, Section 4.2/:

- Deep Saline end member.
- The Old Meteoric end member.
- Glacial end member.
- Littorina end member.
- Altered Meteoric end member.

A basis for defining the end-member compositions are the assumptions of with which minerals the water is equilibrated. Examples of such minerals are calcite, hematite, quartz etc. Conditions for each end member are discussed in /Gimeno et al. 2010, Section 4.2.2.2/.

The redox potential is sensitive to equilibration with different minerals, and also to the presence of absence of sulphate-reducing bacteria. The use of hematite or FeS(am) as equilibrating minerals represents two alternative groundwater states. Equilibrium with hematite implies a situation where the redox state is not affected by sulphate-reducing bacteria, while equilibrium with FeS(am) characterises a situation with significant activity of sulphate-reducing bacteria. The existence of hematite has been described at all depths in the fracture fillings /Drake and Tullborg 2009/ and FeS(am) equilibrium situations have been identified in the groundwaters from Laxemar /Gimeno et al. 2009/. Thus, both geochemical cases have been evaluated through two geochemical variant cases. It should also be pointed out that both phases coexist in some sections in Laxemar (and Forsmark), so the poising of the redox state by one of them is a matter of choice rather than the result of sulphate reducing bacteria activity. Apart from these two cases, an additional variant has also been tested considering the possible control of Eh by the $Fe(OH)_3/Fe^{2+}$ redox pair mantaining homogeneous redox disequilibrium and, therefore, using the un-coupled thermodynamic database. See /Gimeno et al. 2010/ for details.

Concerning sulphide concentrations, data are based on on measurements and observations from the site investigation and monitoring programmes. Thus the data represent present day conditions. To assure that the representativity of the measured data is as good as possible, a selection of data has been performed in /Tullborg et al. 2010/, with focus on Fe(II) and sulphide data.

The sulphide concentrations over the complete glacial cycle have been modelled using Phreeqc. Figure A1-1 (upper left) shows how well modelling results at year 2000 AD correspond to measurement results (red dots). Variant case 1 modelling results are displayed by light grey symbols while variant case 2 results are displayed by dark grey symbols. Figure A1-1 (upper right) shows box-and-whisker plots for the sulphide concentration of the three variant cases at 2000 AD, as compared to the Base case (including both variant cases 1 and 2). The boxes represent the 25 and 75% percentiles while the whiskers represent the 5 and 95% percentiles. Figure A1-1 (lower) shows box-and-whisker plots for the Base case sulphide concentrations at 2000, 5000, 10,000 and 15,000 AD, as well as for different glacial events.

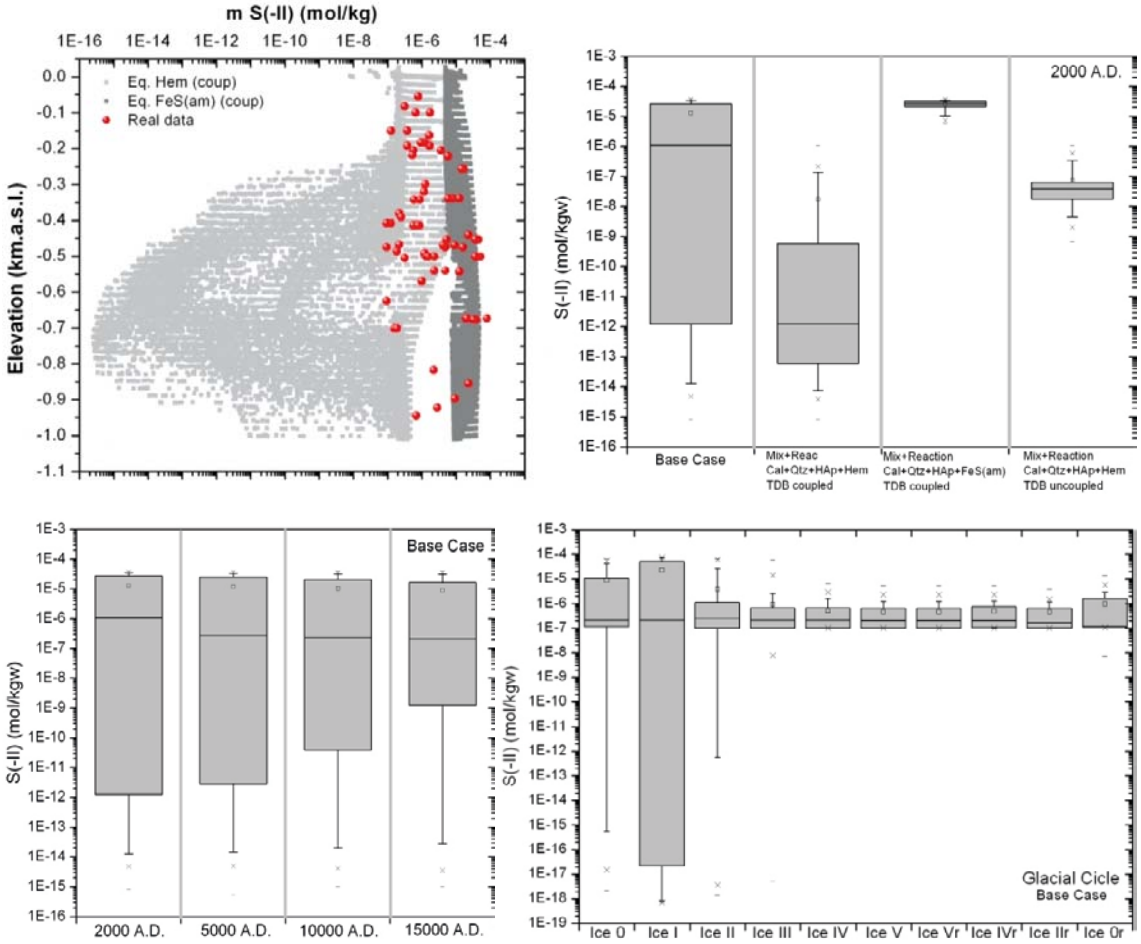

Figure A1-1. *Upper left: Measured sulphide concentrations (red dots) vs. modelling results at 2000 AD. Upper right: Modelled sulphide concentrations at 2000 AD for the Base case and variant cases 1, 2, and 3. Lower left: Modelled sulphide concentrations for the Base case during the temperate period. Lower right: Modelled sulphide concentrations for the Base case during the different glacial events. Reproduced from Figures 5-17, 5-18, 5-19, and 5-21 of /Gimeno et al. 2010/.*

Figure A1-1 aims to illustrate that the measured present day sulphide concentrations bracket the upper sulphide concentration range over the glacial cycle, including the periglacial and submerged periods (cf. Figures 5-20 to 5-24 of /Gimeno et al. 2010/). Therefore, it would be cautious to assume that sulphide concentrations in the upper concentration range at present day conditions prevail throughout the glacial cycle.

A1.5 Conceptual uncertainty

There is no conceptual uncertainty that is specific for the Laxemar site. Therefore, the reader is referred to the conceptual uncertainty discussion in Section 6.1.6 of the SR-Site Data report /SKB 2010/.

A1.6 Data uncertainty due to precision, bias, and representativity

General data uncertainty issues associated with groundwater chemical composition data are described in detail in Section 6.1.7 of the SR-Site Data report. Overall it is judged that the data supplied for Laxemar and Forsmark have a similar degree of data uncertainty. Sources of data uncertainty are shortly outlined in the below bullet list, wherein site specific references are given.

- *Uncertainty in the mixing proportions:* Mixing proportions, or salinities which are subsequently transferred into mixing proportions, are provided by the hydrogeological modelling. Uncertainties associated with the hydrogeological modelling are discussed in Sections A6.6 and A7.6, but also in Sections 6.6.7 and 6.7.7 of the Site Data report /SKB 2010/. The hydrogeological modelling of the temperate period in Laxemar is discussed in /Joyce et al. 2010/, while the modelling of the periglacial and glacial periods is discussed in /Vidstrand et al. 2010/. In /Gimeno et al. 2010/ this modelling is discussed in the context of groundwater chemical composition modelling.
- *Uncertainty in the compositions of end-member groundwater components:* Uncertainties in the composition of end members directly influence the uncertainty of the simulated groundwater compositions. The chemical composition of the end members has been updated in /Gimeno et al. 2010, Section 4.2/ using those estimated for SR-Can and reported in /Auqué et al. 2006/ as the starting point. As a basis for estimating the compositions are assumptions on with which minerals the groundwater is equilibrated.
- *Uncertainties in the thermodynamic database:* Such uncertainty is discussed in Sections 3.4 and 6.1 of the SR-Site Data report /SKB 2010/, which is referred to.
- *Uncertainty in site investigation data:* Groundwater chemical composition data from the site investigations are used to calibrate the hydrogeological modelling, as well as for estimating the composition of end members, which are in turn used to assess the future groundwater composition. Therefore, such uncertainty is propagated in an indirect manner to the output of Phreeqc modelling. General uncertainty in site investigation data is outlined in the SR-Site Data report /SKB 2010, Section 6.1/ and in the site-description modelling report /Laaksoharju et al. 2009/ and references therein.
- *Uncertanities in redox conditions:* Redox parameters are sensitive to equilibration with certain minerals, as well as to sulphate reducing bacterial processes. This is handled by intruding three variant cases in the Phreeqc modelling (cf. Section A1.4), whereof variant cases 1 and 2 are included in the Base case.
- *Uncertainties in sulphide concentration:* The sulphide data set is based on selected sulphide concentrations obtained in the site investigation and monitoring programmes, which means that they should represent present day conditions. In the process of selecting the data, some data points have been discarded, as they are judged to be contaminated or otherwise non-representative. Some of these discarded data points show higher sulphide concentrations than those finally selected, and therefore a detailed discussion on the selection procedure is given in /Tullborg et al. 2010/. It is judged that this selection procedure should constrain the degree of bias in the data, and assure that they represent the in situ groundwater to the best degree possible. There is a representativity issue concerning whether the data may be used for entire safety assessment period. Based on Phreeqc modelling (cf. Section A1.4) it is judged that the measured data in the upper sulphide concentration range bracket the upper sulphide concentrations over the glacial period.

A1.7 Spatial and temporal variability of data

Spatial variability

The spatial variability of the concentrations of main components is handled by modelling groundwater compositions for tens of thousands of coordinates in the rock volume surrounding the repository /Gimeno et al. 2010/. This modelling is performed by using Phreeqc using mixing proportions as inputs. The grid providing the coordinates is determined by the hydrogeological modelling /Joyce et al. 2010, Vidstrand et al. 2010/. Table A1-3 shows an excerpt of an output file of a Phreeqc simulation, where selected data for seven, out of the tens of thousands, modelled coordinates are displayed. The upper left field shows the coordinates and the upper right field the mixing proportions supplied from the hydrogeological modelling. The lower field shows resulting concentrations of the some

Table A1-3. Example of results from Phreeqc calculations, showing groundwater data for seven out of tens of thousands of coordinates. The complete results include more columns with other data not specifically requested in this appendix.

Row	X(km)	Y(km)	Z(km)	Brine	Littorina	DGW	Glacial	PoreWater
1	1,549.55	6,365.01	–0.4403	$5.4\cdot10^{-03}$	$7.8\cdot10^{-03}$	$9.6\cdot10^{-01}$	$1.3\cdot10^{-02}$	$1.1\cdot10^{-02}$
2	1,549.83	6,365.01	–0.441	$9.2\cdot10^{-04}$	$2.5\cdot10^{-03}$	$9.9\cdot10^{-01}$	$3.9\cdot10^{-03}$	$1.9\cdot10^{-03}$
3	1,549.87	6,365.01	–0.4411	$9.4\cdot10^{-04}$	$2.5\cdot10^{-03}$	$9.9\cdot10^{-01}$	$3.9\cdot10^{-03}$	$1.9\cdot10^{-03}$
4	1,549.91	6,365.01	–0.4411	$1.0\cdot10^{-03}$	$2.6\cdot10^{-03}$	$9.9\cdot10^{-01}$	$4.2\cdot10^{-03}$	$2.1\cdot10^{-03}$
5	1,549.55	6,365.05	–0.4405	$6.0\cdot10^{-03}$	$7.3\cdot10^{-03}$	$9.6\cdot10^{-01}$	$1.4\cdot10^{-02}$	$1.1\cdot10^{-02}$
6	1,548.91	6,365.09	–0.4403	$1.5\cdot10^{-02}$	$1.1\cdot10^{-02}$	$9.1\cdot10^{-01}$	$3.2\cdot10^{-02}$	$3.0\cdot10^{-02}$
7	1,549.55	6,365.09	–0.4403	$6.0\cdot10^{-03}$	$8.1\cdot10^{-03}$	$9.6\cdot10^{-01}$	$1.5\cdot10^{-02}$	$1.2\cdot10^{-02}$
	mCa	**mCl**	**mNa**	**mHS^-**	**mC**	**pH**	**Pe**	**IonicStr**
1	$2.6\cdot10^{-03}$	$9.5\cdot10^{-03}$	$8.0\cdot10^{-03}$	$9.3\cdot10^{-05}$	$3.9\cdot10^{-03}$	7.33	–3.60	$1.71\cdot10^{-02}$
2	$6.4\cdot10^{-04}$	$2.4\cdot10^{-03}$	$5.5\cdot10^{-03}$	$7.7\cdot10^{-05}$	$4.2\cdot10^{-03}$	7.82	–4.19	$8.44\cdot10^{-03}$
3	$6.5\cdot10^{-04}$	$2.4\cdot10^{-03}$	$5.5\cdot10^{-03}$	$7.7\cdot10^{-05}$	$4.2\cdot10^{-03}$	7.81	–4.18	$8.47\cdot10^{-03}$
4	$6.9\cdot10^{-04}$	$2.6\cdot10^{-03}$	$5.6\cdot10^{-03}$	$7.7\cdot10^{-05}$	$4.2\cdot10^{-03}$	7.79	–4.15	$8.67\cdot10^{-03}$
5	$2.9\cdot10^{-03}$	$1.0\cdot10^{-02}$	$8.1\cdot10^{-03}$	$9.1\cdot10^{-05}$	$3.9\cdot10^{-03}$	7.30	–3.56	$1.79\cdot10^{-02}$
6	$7.1\cdot10^{-03}$	$2.3\cdot10^{-02}$	$1.2\cdot10^{-02}$	$1.0\cdot10^{-04}$	$3.5\cdot10^{-03}$	7.06	–3.09	$3.46\cdot10^{-02}$
7	$2.9\cdot10^{-03}$	$1.0\cdot10^{-02}$	$8.2\cdot10^{-03}$	$9.4\cdot10^{-05}$	$3.9\cdot10^{-03}$	7.30	–3.56	$1.81\cdot10^{-02}$

X (km), Y (km), Z (km) are the coordinates for the simulated groundwater composition.

Brine, Littorina, DGW, Glacial, PoreWater are the mixing proportions of the end-member groundwater components (note that the names mismatch those used in /Gimeno et al. 2010/).

mCa, mCl, mNa, and mHS^- are the concentrations (mol/dm^3) of the solutes. mC is the concentration of total inorganic carbon.

pH, pe, and IonicStr are the pH, redox potential, and ionic strength (mol/dm^3).

of the concerned main component (in this example Ca^{2+}, Cl^-, Na^+, HS^- and total inorganic carbon are shown), as well as the *pH*, *pe* and ionic strength. The complete output file includes many more columns than shown in Table A1-3 (cf. /Gimeno et al. 2010/).

The chemical compositions of groundwaters in a fractured rock such as Laxemar may show a strong spatial variability over short distances (tens of metres), as some of the data from the Äspö Hard Rock Laboratory indicate. However, over longer distances overall patterns may appear, for example the general salinity increase with depth. Such general trends are illustrated in Figure A1-2, showing concentrations of Ca^{2+} and Na^+ for the Laxemar site. The red dots shows measured data, while the grey squares show Base case modelling results at 2000 AD.

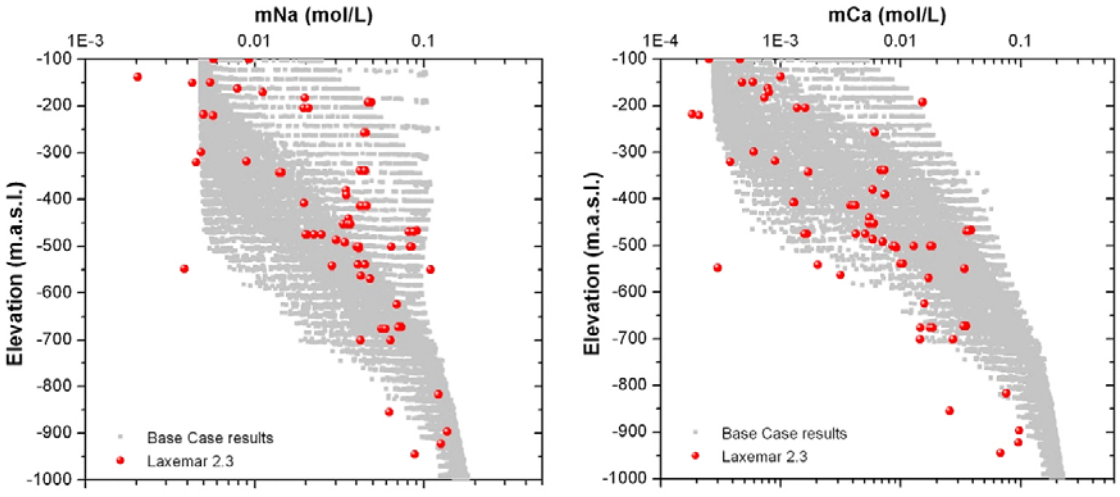

Figure A1-2. *Distribution of sodium and calcium concentrations in the groundwater at Laxemar with respect to depth. Measured data from groundwater samples in red dots and modelled data for the year 2000 AD in grey squares.*

From the results of the Phreeqc simulations the spatial variability of the concentrations can be examined. In /Gimeno et al. 2010/ a multitude of figures can be found illustrating this. The spatial variability of the Phreeqc modelling results reflects on the spatial variability of the flow field in the hydrogeological modelling.

The sulphide concentrations being selected as representative in /Tullborg et al. 2010/ indicate a significant spatial variability, over four orders of magnitude, but no apparent trend can been seen. Figure A1-3 illustrates this by showing the sulphide concentration vs. elevation. This apparent absence of trends perhaps reflects on that the processes controlling the sulphide concentrations are widely distributed, and that the data are distributed over a relatively large rock volume.

Temporal variability

The temporal variability is handled by performing Phreeqc simulations at a number of different times and different climate domains, as dictated by the hydrogeological modelling. The approach used in Laxemar is quite similar to that used for Forsmark, and therefore Section 6.1.8 in the SR-Site Data report /SKB 2010/ is referred to.

For the sulphide concentrations, it is argued in Section A1.4 that the same set of sulphide data can cautiously be used throughout the glacial cycle.

A1.8 Correlations

There is no correlation that needs to be propagated to subsequent copper corrosion or radionuclide transport modelling.

A1.9 Supplier's qualified data sets

End-member compositions

The end-member components used for the Laxemar site are justified in /Gimeno et al. 2010, Section 4.2/ and shown in Table A1-4. The data are reproduced from Table 4-3 of /Gimeno et al. 2010/.

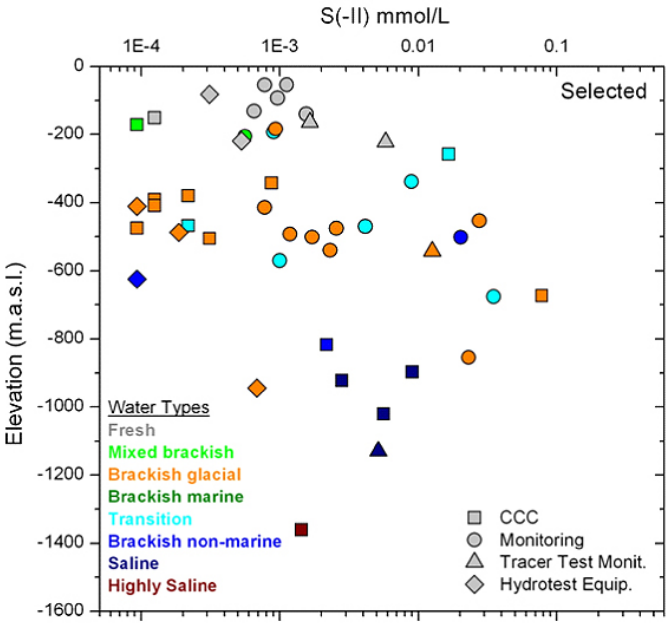

Figure A1-3. *The concentration of sulphide vs. elevation at the Laxemar site. Only the selection of representative samples is displayed in the plot.*[3]

[3] SKBdoc 1262945 (access might be given on request).

Table A1-4. Equilibrated end members, calculated with the coupled database used for the geochemical simulations. Units in molal (mol/kg) except for pH, temperature (°C), and pe. Data are reproduced from /Gimeno et al. 2010, Table 4-3/.

	Deep Saline	Old Meteoric	Glacial	Littorina	Altered Meteoric
pH	8.00	8.64	9.30	7.95	7.84
T	15	15	15	15	15
pe	–4.45	–5.12	–5.26	–4.42	–1.05
Al	$7.37 \cdot 10^{-9}$	$1.21 \cdot 10^{-6}$	$5.21 \cdot 10^{-6}$	$3.25 \cdot 10^{-7}$	$2.03 \cdot 10^{-7}$
Br	$4.16 \cdot 10^{-3}$			$2.81 \cdot 10^{-4}$	
C	$3.68 \cdot 10^{-5}$	$6.91 \cdot 10^{-4}$	$8.52 \cdot 10^{-5}$	$1.63 \cdot 10^{-3}$	$4.26 \cdot 10^{-3}$
Ca	0.49	$5.26 \cdot 10^{-4}$	$7.18 \cdot 10^{-5}$	$3.87 \cdot 10^{-3}$	$1.79 \cdot 10^{-4}$
Cl	1.37	$6.49 \cdot 10^{-4}$	$1.41 \cdot 10^{-5}$	0.19	$6.49 \cdot 10^{-4}$
F	$8.64 \cdot 10^{-5}$	$2.03 \cdot 10^{-4}$		$2.61 \cdot 10^{-5}$	$2.03 \cdot 10^{-4}$
Fe_{Tot}	$2.53 \cdot 10^{-7}$	$5.72 \cdot 10^{-9}$	$8.00 \cdot 10^{-7}$	$8.26 \cdot 10^{-6}$	$1.79 \cdot 10^{-6}$
K	$8.22 \cdot 10^{-4}$	$7.60 \cdot 10^{-5}$	$1.02 \cdot 10^{-5}$	$3.47 \cdot 10^{-3}$	$7.60 \cdot 10^{-5}$
Li	$6.86 \cdot 10^{-4}$	$1.59 \cdot 10^{-6}$		$1.02 \cdot 10^{-5}$	$1.59 \cdot 10^{-6}$
Mg	$8.95 \cdot 10^{-5}$	$1.48 \cdot 10^{-4}$	$4.11 \cdot 10^{-6}$	$1.87 \cdot 10^{-2}$	$1.48 \cdot 10^{-4}$
Mn	$2.62 \cdot 10^{-6}$	$1.06 \cdot 10^{-6}$			$1.06 \cdot 10^{-6}$
Na	0.38	$4.79 \cdot 10^{-3}$	$7.40 \cdot 10^{-6}$	0.16	$4.79 \cdot 10^{-3}$
SO_4^{2-}	$9.68 \cdot 10^{-3}$	$3.73 \cdot 10^{-4}$	$5.31 \cdot 10^{-6}$	$9.39 \cdot 10^{-3}$	$3.73 \cdot 10^{-4}$
Si	$8.81 \cdot 10^{-5}$	$1.42 \cdot 10^{-4}$	$1.67 \cdot 10^{-4}$	$1.28 \cdot 10^{-4}$	$1.35 \cdot 10^{-4}$
Sr	$3.95 \cdot 10^{-3}$			$3.10 \cdot 10^{-5}$	

Main chemical components

The Phreeqc results from the numerous of modelling cases presented in /Gimeno et al. 2010/ are stored as tabulated data files in /SKBdoc 1262945/. Table A1-3 shows an excerpt of one of these output files. Statistical results from the different cases are tabulated in appendix 2 of /Gimeno et al. 2010/. Based on the statistical results, box-and-whisker plots can be made. Figure A1-4 shows the sum of concentrations of the main cations expressed as charge equivalents $\Sigma q[M^{q+}]$ for different time periods and events of the glacial cycle.

The following specific parameters concerning the main chemical components are requested in Section A1.1: Minimum and maximum ratio of Ca/Na concentrations; minimum and maximum *pH*, minimum and maximum total inorganic carbon concentration, and maximum ionic strength. These data are reproduced from /Gimeno et al. 2010, Table 7-1/ in Table A1-5. The data represents the Base case for the complete glacial cycle inside the candidate repository volume at Laxemar.

In /Gimeno et al. 2010/, many more modelling cases than those shown in Table A1-5 are presented. However, the cases of Table A1-5 are judged to be representative for the complete glacial cycle in /Gimeno et al. 2010, Chapter 7/.

Redox potential

Figure A1-5 shows box-and-whisker plots of the redox potential *Eh* for different time periods and events of the glacial cycle. The underlying numerical data are found in appendix 2 of /Gimeno et al. 2010/.

Sulphide concentration

The sulphide concentration, based on selected measurement data /Tullborg et al. 2010/, is presented in as a cumulative distribution function in Figure A1-6. The numerical data are found in /SKBdoc 1262945/. The maximum sulphide concentration in the figure is $7.5 \cdot 10^{-5}$ mol/l. For comparison, the cumulative distribution function of SR-Can is shown.

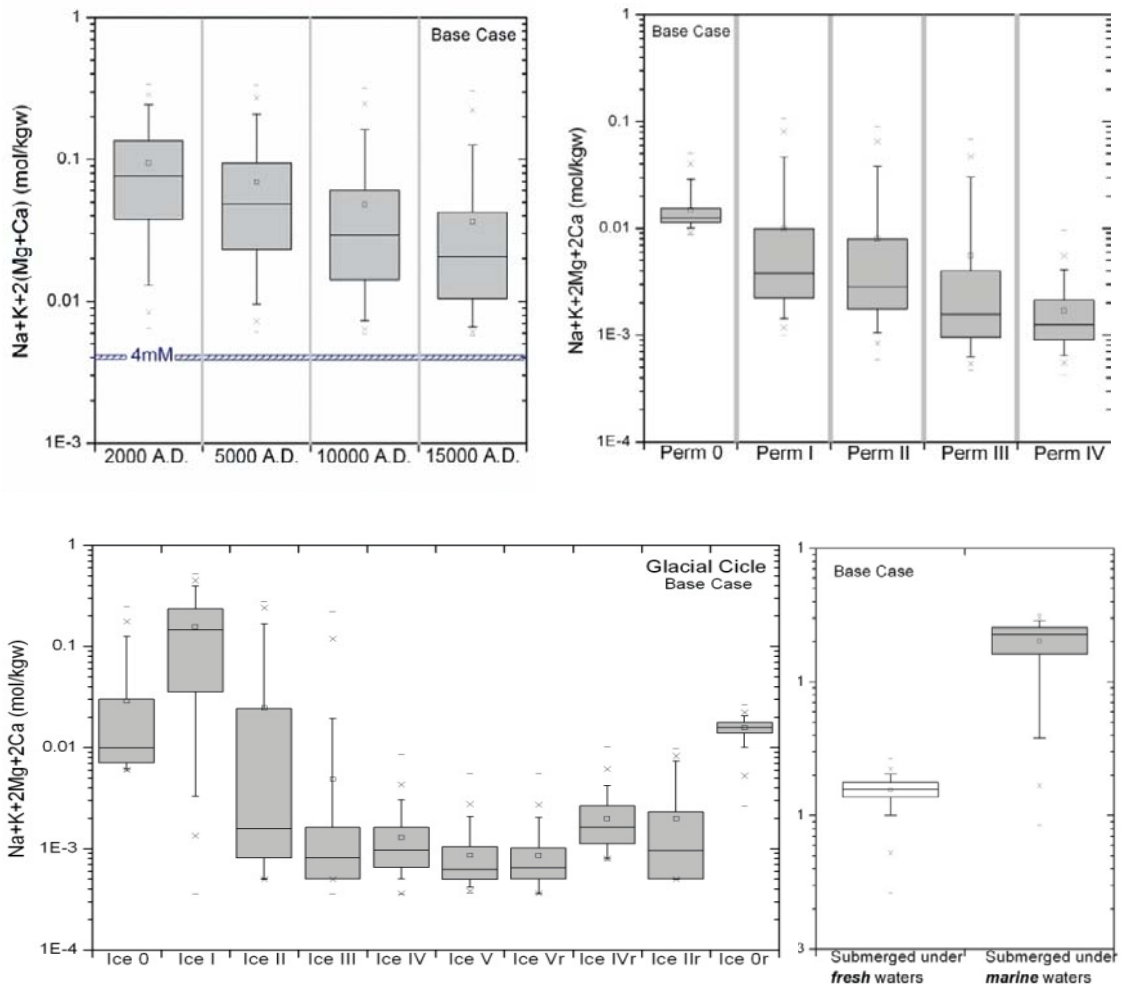

Figure A1-4. *Concentration of the main cations expressed as charge equivalents $\Sigma q[M^{q+}]$ obtained for the Base case over the complete glacial cycle. Concentrations are modelled for the temperate (upper left), glacial (lower left), glacial + permafrost (upper right), and submerged (lower right) periods for the groundwaters located within the candidate repository volume at Laxemar. The safety function indicator criteria of $\Sigma q[M^{q+}] > 4$ mM is indicated in the upper left figure. Boxes represent 25 and 75% percentiles. Whiskers represent 5% and 95% percentile. The crosses and horrizontal bars represent the 1% and 99% percentiles and the min and max values, respectively. Modified from Figure 7-1 of /Gimeno et al. 2010/. Numerical data are found in appendix 2 of /Gimeno et al. 2010/.*

Table A1-5. Minimum and maximum values of the main geochemical parameters obtained for the Base case over the complete Glacial Cycle in Laxemar. Data reproduced from Table 7-1 of /Gimeno et al. 2010/.

	Max Ca/Na	Min Ca/Na	Max pH	Min pH	Max total inorganic carbon (kmol/m^3)	Min total inorganic carbon (kmol/m^3)	Max ionic strength (kmol/m^3)
Temperate 2000 AD	1.25	0.105	8.14	6.77	$4.24\cdot10^{-03}$	$5.61\cdot10^{-05}$	$4.63\cdot10^{-01}$
Temperate 15,000 AD	1.205	0.063	8.11	6.8	$4.33\cdot10^{-03}$	$6.84\cdot10^{-05}$	$4.13\cdot10^{-01}$
Glacial (stage IIa)	3.7	0.076	9.64	6.54	$4.31\cdot10^{-03}$	$4.84\cdot10^{-05}$	$3.75\cdot10^{-01}$
Glacial (stage Vr)	25	0.093	9.7	8.03	$3.83\cdot10^{-03}$	$8.75\cdot10^{-05}$	$6.53\cdot10^{-03}$
Permafrost 0 (before onset of glaciation)	0.93	0.23	7.54	6.84	$4.12\cdot10^{-03}$	$3.49\cdot10^{-03}$	$6.69\cdot10^{-02}$
Permafrost IV (before onset of glaciation	4.166	0.425	9.66	7.84	$1.32\cdot10^{-03}$	$1.44\cdot10^{-04}$	$1.30\cdot10^{-02}$
Submerged glacial lake	1.388	0.725	9.26	7.25	$1.78\cdot10^{-03}$	$5.92\cdot10^{-05}$	$3.65\cdot10^{-02}$
Submerged seawater	1.265	0.051	8.29	6.83	$3.96\cdot10^{-03}$	$5.38\cdot10^{-05}$	$4.38\cdot10^{-01}$

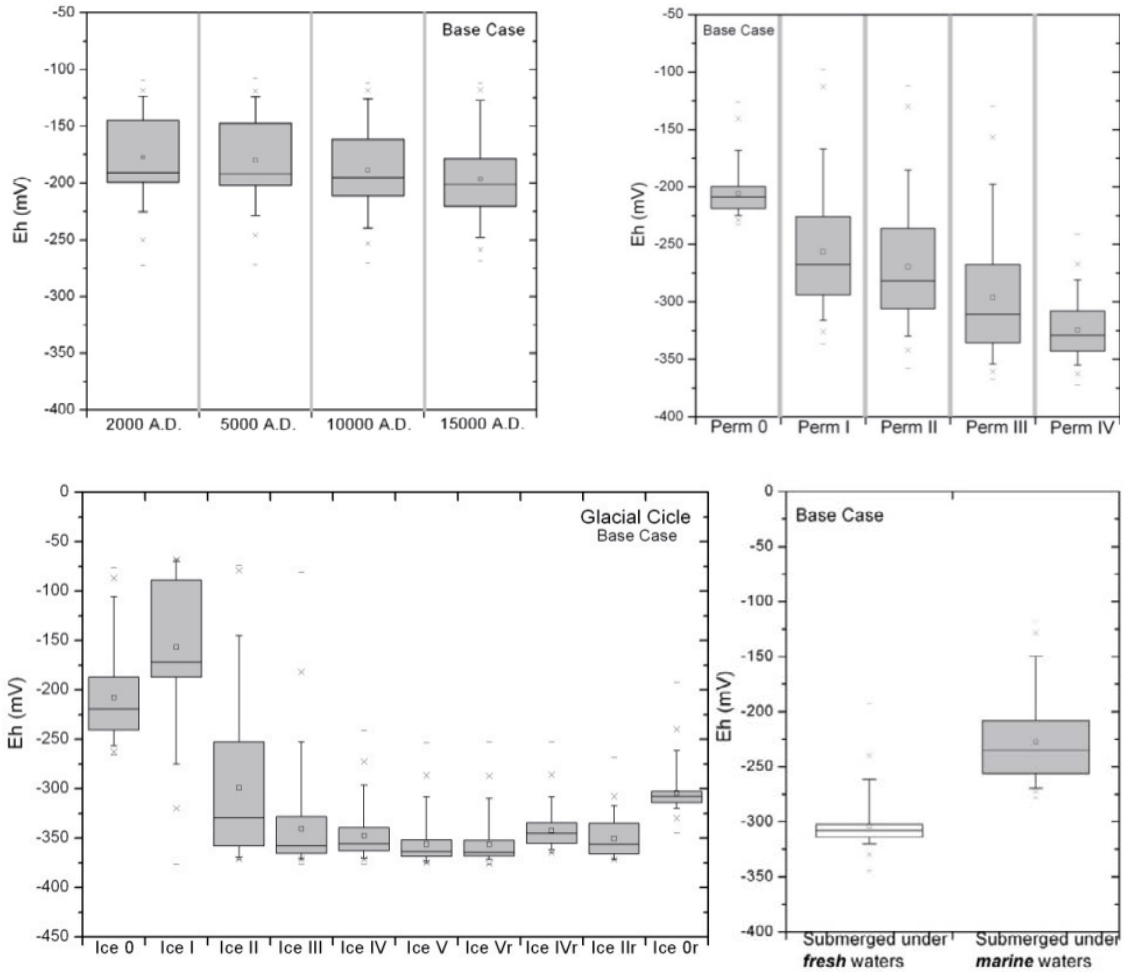

Figure A1-5. *Redox potential Eh (mV) obtained for the Base case over the complete glacial cycle. Data are modelled for the temperate (upper left), glacial (lower left), glacial + permafrost (upper right), and submerged (lower right) periods for the groundwaters located within the candidate repository volume at Laxemar. Legends are explained in Figure A1-3. Modified from Figure 7-5 of /Gimeno et al. 2010/. Numerical data are found in appendix 2 of /Gimeno et al. 2010/.*

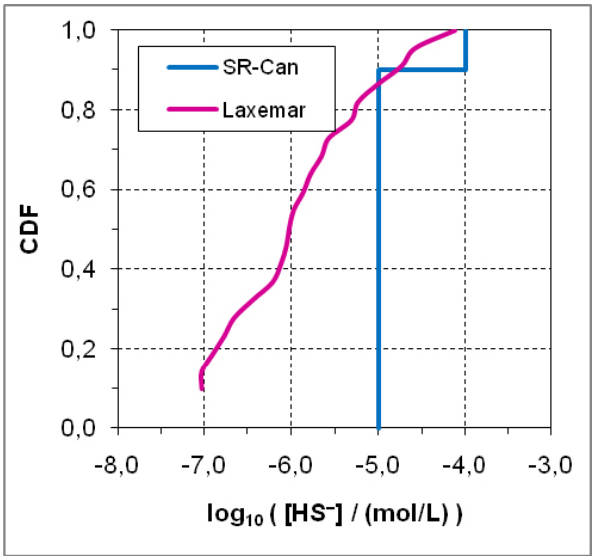

Figure A1-6. *The cumulative distribution function of sulphide concentrations (in mol/L) at Laxemar for the samples selected as being representative in /Tullborg et al. 2010/.*

A1.10 Data recommended for use in the Comparative analysis

Table A1-4 presents the Laxemar end-member compositions used as input in the Phreeqc modelling. The output results from the Phreeqc modelling presented in /Gimeno et al. 2010/ are stored in SKBdoc 1262945.

Table A1-5 presents requested minimum and maximum values of main chemical components. Figure A1-3 and Figure A1-4 present box-and-whiskers plots of the sum of the concentrations of main cations expressed as charge equivalents, and of the redox potential *Eh*. Underlying numerical data are found in appendix 2 of /Gimeno et al. 2010/.

Figure A1-6 shows the cumulative distribution function of sulphide. The numerical data are stored in SKBdoc 1262945.

All of these data are recommended for use in the Comparative analysis.

References A1.11

SKB's (Svensk Kärnbränslehantering AB) publications can be found at www.skb.se/publications.

Auqué L, Gimeno M J, Gómez J B, Puigdomenech I, Smellie J, Tullborg E-L, 2006. Groundwater chemistry around a repository for spent nuclear fuel over a glacial cycle. Evaluation for SR-Can. SKB TR-06-31, Svensk Kärnbränslehantering AB.

Charlton S R, Parkhurst D L, 2002. PHREEQCI – A graphical user interface to the geochemical model PHREEQC. USGS Fact Sheet FS-031-02. Denver, Colorado: U.S. Geological Survey.

Drake H, Tullborg E-L, 2009. Fracture mineralogy Laxemar. Site descriptive modelling, SDM-Site Laxemar. SKB R-08-99, Svensk Kärnbränslehantering AB.

Gimeno M J, Auqué L F, Gómez J B, Acero P, 2009. Water-rock interaction modelling and uncertainties of mixing modelling. Site descriptive modelling, SDM-Site Laxemar. SKB R-08-110, Svensk Kärnbränslehantering AB.

Gimeno M J, Auqué L F, Gómez J, Salas J, Molinero J, 2010. Hydrogeochemical evolution of the Laxemar site. SKB R-10-60, Svensk Kärnbränslehantering AB.

Hallbeck L, Pedersen K, 2008. Explorative analyses of microbes, colloids, and gases together with microbial modelling. Site description model, SDM-Site Laxemar. SKB R-08-109, Svensk Kärnbränslehantering AB.

Joyce S, Simpson T, Hartley L, Applegate D, Hoek J, Jackson P, Roberts D, Swan D, Gylling B, Marsic N, Rhén I, 2010. Groundwater flow modelling of periods with temperate climate conditions – Laxemar. SKB R-09-24, Svensk Kärnbränslehantering AB.

Kalinowski B E (ed), 2009. Background complementary hydrogeochemical studies. Site descriptive modelling, SDM-Site Laxemar. SKB R-08-111, Svensk Kärnbränslehantering AB.

Laaksoharju M, Smellie J, Tullborg E-L, Wallin B, Drake H, Gascoyne M, Gimeno M, Gurban I, Hallbeck A, Molinero J, Nilsson A-C, Waber N, 2009. Bedrock hydrogeochemistry Laxemar. Site descriptive modelling, SDM-Site Laxemar. SKB R-08-93, Svensk Kärnbränslehantering AB.

Parkhurst D L, Appelo C A J, 1999. User's guide to PHREEQC (Version 2): a computer program for speciation, batch-reaction, one-dimensional transport, and inverse geochemical calculations. Denver, Co: U.S. Geological Survey. (Water- resources investigations report 99-4259)

Rhén I, Hartley L, 2009. Bedrock hydrogeology Laxemar. Site descriptive modelling, SDM-Site Laxemar. SKB R-08-92, Svensk Kärnbränslehantering AB.

SKB, 2010. Data report for the safety assessment SR-Site. SKB TR-10-52, Svensk Kärnbränslehantering AB.

Smellie J, Tullborg E-L, 2009. Quality assurance and categorisation of groundwater samples from the Laxemar-Simpevarp area. In: Kalinowski B E (ed). Background complementary hydrogeochemical studies. Site descriptive modelling, SDM-Site Laxemar. SKB R-08-111, Svensk Kärnbränslehantering AB, pp 163–347.

Tullborg E-L, Smellie J, Nilsson A-C, Gimeno M J, Brüchert V, Wallin B, Molinero J, 2010. Sulphide contents in the groundwater at Laxemar. SKB R-10-62, Svensk Kärnbränslehantering AB.

Vidstrand P, Rhén I, Zugec N, 2010. Groundwater flow modelling of periods with periglacial and glacial climate conditions – Laxemar. SKB R-09-25, Svensk Kärnbränslehantering AB.

Waber H N, Gimmi T, deHaller A, Smellie J A T, 2009. Porewater in the rock matrix. Site descriptive modelling, SDM-Site Laxemar. SKB R-08-112, Svensk Kärnbränslehantering AB.

A2 Bedrock thermal properties

In the present appendix, thermal properties of the rock, that is rock thermal conductivity, rock heat capacity, thermal diffusivity, and thermal expansion coefficient, as well as the temperature at repository depth, are presented. These data are mainly needed for evaluating the impact of the thermal load from the spent fuel, which has bearing on the spacing between canister positions in the repository. The bentonite buffer temperature must not exceed 100°C for any canister deposited. A temperature margin including uncertainties is therefore also presented.

The thermal properties of the rock are also needed when assessing the long-term thermal evolution of the repository, caused by climate changes. In this appendix, data on thermal rock properties, including geothermal gradient, geothermal surface heat flow and internal heat generation, will also be discussed also in this context.

Furthermore, analyses of the thermo-hydro-mechanical (THM) evolution of the repository require thermo-mechanical parameters. The coefficient of thermal expansion is one such parameter, and is given in this section, whereas other mechanical input data are discussed in Chapter A4.

In the SR-Site Data report /SKB 2010, Section 6.2/ the corresponding data are given for the Forsmark site.

A2.1 Modelling as input to the Comparative analysis of safety related site characteristics

This section describes what data are expected from the supplier, and in what modelling activities the data are to be used.

Defining the data requested from the supplier

The following data should be delivered for the potential repository area at the Laxemar site by the supplier:

- Spatial distribution of the thermal conductivity λ (W/(m·K)) and its potential anisotropy, with correction for temperature and with uncertainty estimates. Different data sets may have to be given for different rock volumes. Especially the lower tail of the distribution is of concern since this is of central importance for assessing the canister spacing with respect to the temperature criterion.
- Spatial distribution of heat capacity C (J/(m³·K)), with correction for temperature and with uncertainty estimates. Different data sets may have to be given for different rock volumes.
- In situ temperature T (°C) at repository depth, with uncertainty estimates.
- Thermal expansion coefficients α (m/(m·K)) for significant rock types, with uncertainty estimates.
- Site-specific temperature margin (°C) data (margin up to 100°C) in the thermal dimensioning of the repository. The margin constitutes of both general and site-specific uncertainties. Different data sets may have to be given for different rock volumes. The value given constitutes the uncertainty.

In addition the following data should be delivered for the long-term evaluation caused by climate changes by the supplier:

- Mean value of the thermal conductivity λ (W/(m·K)) and its potential anisotropy, with correction for temperature and with uncertainty estimates. Different data sets may have to be given for different rock volumes, inside and outside the focused area at Laxemar.
- Mean value of the heat capacity C (J/(m³·K)) with correction for temperature and with uncertainty estimates. Different data sets may have to be given for different rock volumes, inside and outside the focused area.
- Mean value of the thermal diffusivity κ (m²/s). Different mean values may have to be given for different rock volumes.
- Mean value of the internal heat generation (μW/m³) with uncertainty estimates. Different data sets may have to be given for different rock types.
- Mean value of the geothermal gradient (°C/m).
- Mean value of the geothermal surface heat flow (mW/m²) with uncertainty estimates.

The data should originate from the site investigations and from the assessment of the site investigation data presented in Chapter 6 of the Laxemar site-descriptive model report, SDM-Site /SKB 2009a/, and its lower level references. Note that pessimistic considerations taken when assessing the peak temperature of the buffer may not necessarily be pessimistic when assessing the in situ temperature as impacted by climate change.

Modelling activities in which data will be used

Modelling the thermal evolution of the repository is focused on assessing the impact of the heat generated by the spent nuclear fuel. Of particular concern is to assess the peak temperature of the buffer, since it must not exceed 100°C. The temperature field around a canister is dependent on the rock thermal conductivity and the distance to neighbouring canisters. Rock having low thermal conductivity will require larger distances between canisters than high conductivity rock. There are uncertainties associated with calculation of the peak buffer temperature, so that a margin to the design threshold (100°C) must be established. Establishing a safe, yet not overly pessimistic, margin is an important issue.

The modelling of the thermal evolution of the near-field is based on a combination of analytical and numerical approaches as further described by /Hökmark et al. 2009/. The peak buffer temperature is calculated as a function of the canister spacing, the tunnel spacing, and the rock thermal properties, whereas a set of fixed assumptions are made for the conditions in the interior of the deposition holes (cf. Section 6.2.1 of the SR-Site Data report /SKB 2010/). These assumptions are relevant for dry deposition holes in which the temperatures will tend to be particularly high. This modelling approach has been used for dimensioning the repository, as further described in the Site engineering report for Laxemar /SKB 2009b/. However, as input to the Comparative analysis the objective of this appendix is to assess the thermal evolution for this selected design, and also to provide input to the THM analyses of the rock presented by /Hökmark et al. 2010/. The overall thermal evolution during the glacial cycle is in the THM-analyses assessed by the 3DEC code, as further described by /Hökmark et al. 2010/. The thermal property input needs to this modelling is covered by the input needs of the buffer peak temperature modelling. Thermo-mechanical models used in the Comparative analysis are described in Chapter A4.

The thermal properties are also used to assess the large-scale and long-term thermal evolution caused by climate changes. Note that thermal data for this purpose are required for a much larger area and at a larger scale compared to modelling of the peak buffer temperature in the repository. The demands, e.g. on describing the spatial distribution, are on the other hand much lower. Only mean and uncertainty estimates are required. The thermal evolution of the repository, as impacted by climate changes, is discussed in Chapter 3 of this present report.

A2.2 Supplier input on use of data in the Comparative analysis

The data supplied in this section depend on the rock and mineral composition as well as the spatial variability of these properties. In the context of thermal properties, the rock and mineral composition of the two sites is rather different. Therefore, the data supplied for Laxemar are different to those recommended for Forsmark in Section 6.2 of the SR-Site Data report /SKB 2010/.

A2.3 Sources of information and documentation of data qualification

Sources of information

Main sources of information on thermal properties used in data qualification are described in Table A2-1. In the thermal site descriptive modelling (SDM-Site) a large number of realisations of thermal properties are produced from stochastic modelling. These realisations are the basis for the description of thermal properties on domain level in the site descriptive modelling reports, see Table A2-1. However, the thermal property realisations (see Table A2-8 in Section A2.9) are directly used in the thermal dimensioning as described in Section A2.1.

Within the publications listed in Table A2-1, references to relevant lower level documents can be found.

Table A2-1. Main sources of thermal property information used in data qualification.

Sundberg J, Wrafter J, Back P-E, Rosén L, 2008. Thermal properties Laxemar. Site descriptive modelling, SDM-Site Laxemar. SKB R-08-61, Svensk Kärnbränslehantering AB.
Sundberg J, Back P-E, Ländell M, Sundberg A, 2009. Modelling of temperature in deep boreholes and evaluation of geothermal heat flow at Forsmark and Laxemar. SKB TR-09-14, Svensk Kärnbränslehantering AB.
SKB, 2009a. Site description of Laxemar at completion of the site investigation phase. SDM-Site Laxemar. SKB TR-09-01, Svensk Kärnbränslehantering AB. (Chapter 5: Bedrock geology and Chapter 6: Bedrock thermal properties).
SKB 2009b. Site engineering report Laxemar. Guidelines for underground design. Step D2. SKB R-08-88, Svensk Kärnbränslehantering AB.

Categorising data sets as qualified or supporting data

Qualified and supporting thermal data sets are displayed in Table A2-2 and numbered from 1 to 15. Detailed comments to the data sets are given in Table A2-3 and Table A2-4. Where different data sets are required for different rock volumes, these are described for the rock domains RSMA01, RSMM01 and RSMD01. Data outside the focused area are described for a number of different rock domains.

Most data sets have a priori been considered to be qualified. They have thereafter been judged to be qualified based on the criteria in the instruction for supplying data for the SR-Site Data report /SKB 2010, Section 2.3/. The exceptions are a few supporting data sets accounted for in Table A2-2.

Table A2-2. Qualified and supporting data sets.

Qualified data sets	Supporting data sets
1. Thermal conductivity: RSMA01, RSMM01, RSMD01: Table 6-7, 6-8 and 6-9 respectively in /Sundberg et al. 2008a/.	15. Temperature dependence for some rock types is taken from similar rock types in Forsmark and from the literature; see Table 3-31 in /Sundberg et al. 2008a/.
2. Heat capacity: RSMA01, RSMM01, RSMD01: Table 6-12 in /Sundberg et al. 2008a/.	
3. Spatial distribution of thermal conductivity and heat capacity in each rock domain and thermal subdomain. Up to 1000 realisations for each rock domain:	
4. Thermal conductivity and heat capacity for rock domains outside the focused area: properties based on modelling results and data for different rock types in the thermal site descriptive model version Site /Sundberg et al. 2008a/, Simpevarp model version 1.2 /Sundberg et al. 2005a/, Laxemar model version 1.2 /Sundberg et al. 2006/, Laxemar model stage 2.1 /Wrafter et al. 2006/ and geology from site descriptive model Simpevarp version 1.2 /SKB 2005/, Laxemar model version 1.2 /SKB 2006/ and the geology site descriptive model SDM-Site /Wahlgren et al. 2008/.	
5. Thermal diffusivity: Calculated from thermal conductivity and heat capacity data listed above.	
6. Anisotropy in thermal conductivity: section 6.5.3 in /Sundberg et al. 2008a/. Orientation in chapter 6 in /SKB 2009a/.	
7. Temperature dependence in thermal conductivity and heat capacity: Table 3-31 in /Sundberg et al. 2008a/.	
8. Pressure dependency in thermal conductivity: Section 3.12 in /Sundberg et al. 2008a/.	
9. Thermal expansion coefficient: Table 3-32 in /Sundberg et al. 2008a/.	
10. Temperature at repository level: Table 3-34 in /Sundberg et al. 2008a/.	
11. Geothermal gradient: Figure 3-36 in /Sundberg et al. 2008a/.	
12. Heat generation: Section 7.1.3 in /Sundberg et al. 2009a/.	
13. Heat flow: Mean in Section 7.2.2 with uncertainty estimates in section 8.1 in /Sundberg et al. 2009a/.	
14. Temperature margins are based on the principals in /Hökmark et al. 2009/ and site-specific data in /Sundberg et al. 2008a/.	

Table A2-3. Justification of the sorting of items 1-10 in Table A2-2.

1. The relevant thermal conductivity data as reported in chapter 3 in /Sundberg et al. 2008a/ are based on primary data acquired and refined within the Laxemar site description and site investigation phases. These phases have been conducted in conformance with relevant quality assurance routines. Lower level references are carefully listed, thus facilitating traceability (see e.g. chapter 3 in /Sundberg et al. 2008a/). Through lower level references, the traceability is ensured down to relevant quality assurance documents such as method descriptions, task descriptions, etc. In /Sundberg et al. 2008a/ issues such as data quality, variability, and representativity are discussed. Nonconformities and uncertainties are also discussed. Much of the thermal data delivered are derived from modelling. In /Back and Sundberg 2007/ and chapter 4 in /Sundberg et al. 2008a/, the modelling strategy, the modelling tools, and validity of the modelling are described. It is judged that the modelling approach is adequate.

2. The relevant heat capacity data reported in section 3.9 in /Sundberg et al. 2008a/ are based on primary data acquired and refined within the Laxemar site description and site investigation phases. The same considerations as for item 1 apply.

3. The spatial distribution of thermal conductivity and heat capacity are described in a large number of realisations for each rock domain, and based on data acquired and refined within the Laxemar site description and site investigation phases; see chapter 6 in /Sundberg et al. 2008a/. Item 1 and 2 above are based on these realisations. The same considerations as for item 1 apply.

4. The thermal conductivity and heat capacity data for rock domains outside the focused area at Laxemar are based on thermal properties of different rock types in the site descriptive model; see section 5.6.2 and section 3.9 respectively in /Sundberg et al. 2008a/. Similar considerations as for item 1 apply to the data for different rock types/TRCs (Thermal Rock Classes). However, the requirements are much lower compared to those for data from the focused volume. The mean thermal conductivity and heat capacity may be calculated from the proportions of different rock types or based on the dominant rock type /SKB 2006, Wahlgren et al. 2008/.

5. The thermal diffusivity data are calculated, in this present appendix, based on the data set for thermal conductivity (item 1 and 4) and heat capacity (item 2 and 4). As a consequence, the same considerations as for item 1 and 4 apply.

6. The anisotropy in thermal conductivity reported in section 3.8 in /Sundberg et al. 2008a/ is based on data acquired within the Laxemar site investigation phases. The same considerations as for item 1 apply. However, no advanced data refinement has been made. Focus has been on providing a relevant mean value for areas where the anisotropy is present. The orientation and strength of anisotropy is further described in chapter 6 in /SKB 2009a/.

7. The temperature dependence of thermal conductivity and heat capacity reported in section 3.11 in /Sundberg et al. 2008a/ are mainly based on data acquired within the Laxemar and Forsmark site investigation phases. The same considerations as for item 6 apply. The description has focused on the mean values for the dominant rock types. Data for subordinate rocks have been obtained from similar rock types in Forsmark /Sundberg et al. 2008b/ and from literature data given in /Sundberg et al. 2008a/. This approach has been judged to be adequate since the temperature dependence is moderate and has only minor influence on the maximum bentonite temperature.

8. The pressure dependence in thermal conductivity is described in section 3.12 in /Sundberg et al. 2008a/. The pressure dependence is small and has been neglected in the thermal conductivity modelling. Neglecting the pressure dependence has a slightly pessimistic effect on the results of the thermal conductivity modelling.

9. The thermal expansion coefficient reported in section 3.13 in /Sundberg et al. 2008a/ is based on data acquired within the Laxemar site investigation phases. The same considerations as for item 6 apply. Focus has been on providing a relevant mean value.

10. The temperature at repository level reported in section 3.14 in /Sundberg et al. 2008a/ is based on data acquired within the Laxemar site investigation phases. Similar considerations as for item 1 apply. In the thermal modelling, the reliability of temperature logging data has been evaluated in relation to calibration errors and disturbances from drilling. Only approved data has been used in the site descriptive model. Focus has been on providing both a relevant mean value for repository depth and a measure of variability.

Table A2-4. Justification of the sorting of items 11-15 in Table A2-2.

11. The geothermal gradient data reported in section 3.14 in /Sundberg et al. 2008a/ are based on the temperature logging data described in item 10. As a consequence, the same considerations as for item 10 apply.

12. The internal heat generation data are reported in section 7.1.3 in /Sundberg et al. 2009a/. It is based on data acquired within the Laxemar site investigation phases. Similar considerations as for item 1 apply. However, no advanced data refinement has been made. Focus has been on providing a relevant mean value.

13. The site-specific geothermal surface heat flow is reported in section 7.2.2 in /Sundberg et al. 2009a/. The heat flow is based on data acquired within the Laxemar site investigation phases together with data on the past climate evolution /Sundberg et al. 2009a/. The heat flow is determined indirectly from geothermal gradient (item 11), thermal conductivity (item 1), thermal diffusivity (item 5), internal heat generation (item 12) and past climate evolution. The uncertainty estimates have been evaluated from uncertainties in the above mentioned parameters together with the influence from e.g. temperature dependences (item 7) and anisotropy (item 6). Similar considerations as for the mentioned items apply (climate evolution and permafrost modelling is further discussed in chapter 3 of this present report). Focus has been on providing both a relevant mean for the site and an uncertainty estimate.

14. The temperature margin data are based on the principles and general data in /Hökmark et al. 2009/ and site-specific data in /Sundberg et al. 2008a/. The temperature margin consists of both uncertainties and under- and over-estimates in the calculation of the peak buffer temperature. The uncertainties are carefully discussed in /Hökmark et al. 2009/ and quantified in general terms with example values that are considered relevant for the different rock domains. In the site engineering report, site-specific data are used to define a margin for each rock domain /SKB 2009b/.

15. The supporting data on the temperature dependence (item 7) for subordinate rock types are either Forsmark data or are provided by articles in reputable scientific journals, which have been subjected to the customary review process before publication. As these data are not site specific they are considered as supporting.

Excluded data previously considered as important

No important data have been excluded from the analysis. Non-used thermal data are described in Section 2.2.3 in /SKB 2009c/.

A2.4 Conditions for which data are supplied

The thermal conductivity and heat capacity in the thermal properties realisations are provided at 20–25°C and at water saturated conditions. The natural temperature at repository depth is slightly lower. After deposition of the canisters the temperature will increase as a consequence of the heat generation in the canisters. However, the temperature dependence for the thermal conductivity and heat capacity is described in the thermal site descriptive models; Section 3.11 in /Sundberg et al. 2008a/.

The thermal conductivity measurements are made on stress-released samples. However, the pressure dependence is low when the samples are water saturated.

Further, the thermal transport is assumed to be conductive only. This is a relevant assumption since the thermal transport in the rock mass surrounding the canisters should have an insignificant contribution from convective heat transport.

The thermal expansion coefficients for different rock types are provided at 20–25°C.

The temperature loggings in water filled boreholes are assumed to correctly describe the temperature in the rock mass.

A2.5 Conceptual uncertainty

The major conceptual uncertainty of the thermal rock properties concerns correlations with density, since this correlation is used to assess the spatial correlation of thermal conductivity using high-spatial-resolution density data. Different correlations with density have been used in the thermal site descriptive modelling in order to: (1) define the spatial correlation structure for thermal conductivity and (2) subdivide certain TRC's (Thermal rock classes /Sundberg et al. 2008a/). Both the density and the thermal conductivity of rock is related to the mineralogical composition /Sundberg et al. 2009b/. The thermal modelling mentioned in this section refer to the thermal site descriptive model (SDM-Site) /SKB 2009a/, based on modelling in /Sundberg et al. 2008a/.

It has been assumed that thermal conductivity exhibits a similar correlation structure to density. The variogram models, used to describe the spatial correlation structure of the thermal conductivity in the thermal modelling, are primarily based on density loggings (approximately 0.1 m scale) in boreholes, supported by TPS (Transient Plane Source) data if a sufficient amount of data were available. A relationship between thermal conductivity and density has been established for some rock types (see Section 3.6 in /Sundberg et al. 2008a/ and 6.2.2 in /SKB 2009a/). Even for rock types where such a relationship is not evident, density logging data are used as input to the variogram modelling. It is reasonable to assume that any spatial dependence in density, as indicated by a variogram, also reflects spatial dependence in thermal conductivity /Sundberg et al. 2009b/. However, the associated uncertainty is not known. This uncertainty is handled by using slightly pessimistic variogram models in the stochastic modelling.

The relationship thermal conductivity and density has also been used in order to subdivide different TRC's when necessary.

Referring to the thermal conductivity/density relationship, it is reasonable to assume a corresponding relationship between density and heat capacity. Such a relationship has been established in Laxemar; see Figure 3-25 in /Sundberg et al. 2008a/. In thermal modelling of Forsmark /Sundberg et al. 2008a/, a relationship between heat capacity from direct measurements and thermal conductivity is described. The relationship was used to calculate heat capacity from the modelling results on thermal conductivity in order to complement the thermal conductivity realisations with heat capacity. However, in Laxemar no obvious relationship between thermal conductivity and heat capacity could be discerned /Sundberg et al. 2008a/. Instead, heat capacity was modelled based on realisations of the spatial distribution of TRC's, together with statistical distribution models for heat capacity for each TRC (see Section 5.9 in /Sundberg et al. 2008a/). There are uncertainties associated with the heat

capacity models used for 2 m scale because of the influence of scale. However, these uncertainties in heat capacity are judged to have only minor results on the calculated maximum buffer temperature (see Section A2.1).

The conceptual uncertainty in other parameters is judged to be low.

A2.6 Data uncertainty due to precision, bias, and representativity

The data uncertainty can be subdivided into precision, bias, and representativity. The data uncertainty can also be subdivided into uncertainties in primary data and model uncertainties. The discussion is focused on uncertainties in thermal properties inside the focused area but is partly also applicable to properties outside the focused area (mainly used for the thermal evolution of the repository due to climate changes). Uncertainties specifically related to data outside the focused area are explicitly described. The demands on data inside the focused area are much higher compared to those on data for permafrost modelling, see A2.1.

Data uncertainty due to precision and bias

Primary data in the site investigations

Data uncertainty due to precision is believed to have only minor influences for thermal conductivity determinations made by the TPS method. Heat capacity values calculated from simultaneously determined thermal conductivity and thermal diffusivity have a rather wide spread due to the combination of spatial variability and data precision. The latter is partly caused by anisotropy in the samples, which is present to a variable degree in the Laxemar area. However, in the thermal modelling, heat capacity data from calorimetric determinations have been used for the most common rock types. These data show a variability that is believed to be mainly caused by spatial variability. Significant bias in the thermal conductivity and heat capacity (calorimetric) determinations is not suspected.

The temperature loggings in boreholes are disturbed by water movements and the drilling of the borehole. In the SDM-Site model, the reliability of temperature loggings due to disturbance from drilling has been evaluated. As a result of this, only “approved” boreholes have been used in the description. However, uncertainties related to water movements are still present, especially at certain parts of the boreholes. However, the mean temperature at repository depth in different boreholes shows a rather small variability between different boreholes. Uncertainties in the temperature loggings are transferred into the determination of geothermal gradient and of heat flow, although the latter is not discussed here.

Uncertainties in temperature loggings due to calibration error have been evaluated /Wrafter et al. 2006, Sundberg et al. 2008a/. In some earlier loggings, rather large calibration errors occur. In the site version of the thermal site descriptive model, only temperature logging data that fulfils certain requirements regarding calibration have been used to describe the *in situ* temperature conditions /Sundberg et al. 2008a/. The variability between the temperature at the same relevant elevation in different boreholes is ±0.1°C about the mean (Table 2-6 in /Sundberg et al. 2008a/). For individual boreholes, the uncertainty is ±0.25°C (related to equipment).

The heat generation in the rock mass is calculated from the proportions of U, Th and K and summarised in Table 7-3 in /Sundberg et al. 2009a/. Uncertainties in the proportions in combination with sparse data for some rock types are transferred to uncertainties in the heat generation. These uncertainties can be rather large. However, the internal heat generation down to repository depth has only a minor influence on the calculated surface heat flow and the permafrost modelling.

Potential bias in the determination of the thermal expansion coefficient has been discussed in the thermal site descriptive model version Simpevarp 1.2 /Sundberg et al. 2005a/. The reason for potential bias was that the measurements are made on stress-released samples and the stress dependence had not been assessed. However, it is judged that this question can be ignored.

The uncertainties in the orientation of the boreholes and in the orientation of geological objects in the boreholes, documented by /Munier and Stigsson 2007/, are judged to have little or no effect on the results of thermal modelling.

Model uncertainties

There are several model uncertainties to consider in the thermal modelling of the spatial distribution of thermal conductivity and heat capacity. The five most important uncertainties identified in site descriptive model stage SDM Site /Sundberg et al. 2008a/ were associated with (1) the simulation scale, (2) the simulation volume, (3) the spatial statistical structure of TRC's (lithology), (4) the spatial statistical thermal models, and (5) the simulation technique.

A detailed discussion of the above mentioned uncertainties is performed in Section 7.2 in /Sundberg et al. 2008a/ and a summary is provided in /SKB 2009a/. Uncertainties associated with the simulation volume and the simulation scale are not believed to have had any major impact on the thermal modelling results. Geological heterogeneities were dealt with by dividing the domains into subdomains. This is believed to have reduced the uncertainty significantly. The remaining uncertainty concerning the variability in proportions is believed to be small. Based on confidence intervals for TRC proportions at borehole scale (see Section 5.5.5 in /Sundberg et al. 2008a/), this uncertainty has only a minor effect on the lower thermal conductivity tail (the 1-percentile may vary by about 1%). This is also discussed under "representativity".

Limited data for some TRC's result in uncertain spatial statistical models of thermal conductivity. In particular, modelling spatial dependence using variograms requires plentiful data. Assuming that thermal conductivity exhibits a similar correlation structure to density (see discussion above) means that variogram analysis of borehole density logs could justifiably be used to investigate the spatial correlation of thermal conductivity. Although there are uncertainties associated with this assumption, the spatial statistical thermal conductivity models are believed to be more reliable than in previous versions.

Uncertainties in the simulation technique are believed to have only a minor influence on the results. Uncertainties are also associated with the estimated mean anisotropy factor for thermal conductivity for the Ävrö granite (lineation/foliation), mainly due to few determinations. Furthermore, the spatial variability of thermal anisotropy, both with regard to orientation and magnitude, is largely unknown.

There are a number of uncertainties related to the determination of the site-specific heat flow. These uncertainties are related to uncertainties in geothermal gradient, thermal conductivity, thermal diffusivity, internal heat generation, and past climate evolution. A detailed discussion of the above mentioned uncertainties is performed in Section 8.1 in /Sundberg et al. 2009a/.

The temperature margin to the design criteria (100°C) consists of uncertainties as well as under- and overestimates in the calculation of the peak buffer temperature. The temperature margin data are based on the principles and general data carefully elaborated in /Hökmark et al. 2009/ and site-specific data in /Sundberg et al. 2008a/. The margins are optimised for the numerical method. Thus, the margin constitutes both general and site-specific uncertainties.

The uncertainties are discussed in detail in /Hökmark et al. 2009/. Here a short summary is provided and the temperature margin for different rock domains is justified from site-specific data. Non-site-specific uncertainties are not described here. Instead the reader is referred to /Hökmark et al. 2009/. In Table A2-5 and Table A2-6 the different uncertainties in the local solution and the numerically calculated rock wall temperature are summarised. The uncertainties and biases given in these tables represent realistic judgements for the individual parameters. In Table A2-7 the total temperature margin is presented.

Uncertainty U1 in Table A2-5 is site-specific and can be interpolated for different conductivities from /Hökmark et al. 2009/. The thermal conductivity at low percentiles of the thermal conductivity distribution are approx 2 W/(m·K) for rock domains RSMA01 and RSMM01, and 2.5 W/(m·K) for rock domain RSMD01. Uncertainties U2–U5 are not site-specific and are discussed in detail in /Hökmark et al. 2009/.

Uncertainties U6–U10 in Table A2-6 are site-specific. Item U6 is related to the anisotropy in the rock. It includes the effect of a foliated rock oriented in an unfavourable orientation compared with repository layout. The worst case scenario occurs when the foliation is vertical and parallel to the tunnel orientation. The anisotropy factor is assumed to be 15%. In rock domains RSMA01 and RSMM01, the orientation of the foliation (variable, often moderate, dip) in relation to the tunnel orientation is more

Table A2-5. Uncertainties in local solution. Modified from /Hökmark et al. 2009/ with site-specific data from /Sundberg et al. 2008a/.

DT_{tot}, difference between rock wall temperature and maximum bentonite temperature		Margin, °C, RSMA01	Margin, °C, RSMM01	Margin, °C, RSMD01
Uncertainties related to:				
U1	Geometry of air-filled canister/bentonite gap and variations in barrier conductivity	2.7	2.7	3
U2	Moisture redistribution in barrier	0.2	0.2	0.2
U3	Spalling	0.1	0.1	0.1
U4	Vertical variation of rock conductivity along deposition hole	0.25	0.25	0.25
U5	Vertical distribution of heat generation in the canisters	0.2	0.2	0.2
Sum ΔT_{tot}		3.45	3.45	3.75

Table A2-6. Uncertainties in numerically calculated rock wall temperature. Modified from /Hökmark et al. 2009/ with site-specific data from /Sundberg et al. 2008a/.

T_{wall} , Rock wall temperature at canister mid-height at the time of buffer temperature peak		Margin, °C, RSMA01	Margin, °C, RSMM01	Margin, °C, RSMD01
Uncertainties related to:				
U6	Anisotropy within rock type	0.3	0.3	0
U7	Bias in thermal properties	1.0	1.0	0.8
U8	Heterogeneity, site models (in the lower tail)	0.1	0.1	0.1
U9	Initial temperature	0.35	0.35	0.35
U10	Temperature dependence	0	0	0
U11	Pressure dependence	–0.2	–0.2	–0.2
U12	Tunnel backfill	0	0	0
U13	Strategy uncertainties	–	–	–
Sum (uncertainties)		1.55	1.55	1.05
Over/underestimate because of numerical model simplifications				
S1	Representation of canister	–0.7	–0.7	–0.7
S2-	Numerical precision	–0.8	–0.8	–0.8
S3	Boundary conditions	0.4	0.4	0.4
Sum (under/overestimates)		–1.1	–1.1	–1.1
Total T_{wall}		0.45	0.45	–0.05

Table A2-7. Total temperature margin in numerical solution to establish a definitive spacing.

Uncertainties related to:	Margin, °C, RSMA01	Margin, °C, RSMM01	Margin, °C, RSMD01
Local solution (Table A2-5)	3.45°C	3.45°C	3.75°C
Total T_{wall} Numerical solution (Table A2-6)	0.45°C	0.45°C	–0.05°C
Total Margin	3.9°C	3.9°C	3.7°C

favourable compared to the worst case in /Hökmark et al. 2009/. The temperature contribution is even lower for rock domain RSMD01 because foliation is generally subhorizontal. The uncertainty due to potential bias in the thermal properties is discussed in uncertainty U7. The temperature effect of the potential bias is interpolated from /Hökmark et al. 2009/ using site-specific data (1% percentile). The uncertainty U8 is related to the uncertainty in the lower tail of the thermal conductivity distribution (SDM-Site) due to uncertainties in rock type proportions. The temperature effect related to U8 is small.

Uncertainty U9 is related to uncertainties in the *in situ* temperature. The lowest and highest temperatures measured in different boreholes at 400 m depth vary by ±0.1°C about the mean /Sundberg et al. 2008a/. In addition there is possible bias in the measurements which is estimated to be in the order of 0.25°C. The initial temperature relevant for the dimensioning problem may differ from the present-day

rock temperature because of heat generated during tunnel excavation, ventilation etc. Presently it is not possible to estimate these effects or even to establish if the net effect will be a decreased or an increased effective background temperature /Hökmark et al. 2009/.

U10 is related to uncertainties due to the increased rock temperature and the temperature dependence in thermal properties. The uncertainty is very low and not site dependent when temperature dependent properties are included in the numerical approach for thermal dimensioning of the repository /Hökmark et al. 2009/. Data on temperature dependent properties are from /Sundberg et al. 2008a/.

Uncertainties U11–U13 are not site-specific. Over- and underestimations due to the representation of the canister and numerical precision in the numerical model are not site-specific (S1-S2). S3 includes the effect of boundary conditions in the numerical model. Since the dimensioning is made on the canister surrounded by rock with very low thermal conductivity, it is reasonable to believe that the thermal conductivity in the neighbouring tunnels is higher. 10% higher thermal conductivity in two neighbouring tunnels gives 0.4°C in temperature contribution /Hökmark et al. 2009/. The difference between the mean thermal conductivity and conductivity around a canister in low conductive rock is typically 35% for rock domains RSM0A1 and RSMM01 and 20% for RSMD01.

Data uncertainty due to representativity

Uncertainties in the proportions of rock types in bore map have an influence on the overall distribution of thermal conductivities for each domain. In /Sundberg et al. 2008a/ confidence intervals for TRC proportions have been calculated on the basis of the differences between different boreholes. The uncertainties are relatively small for rock domain RSMD01 (/Sundberg et al. 2008a/, Table 5-33) but larger for domains RSMA01 and RSMM01 (/Sundberg et al. 2008a/, Table 5-32 and Table 5-34 respectively) because of their higher degree of heterogeneity in geology and thermal properties. However, this uncertainty has only a minor effect on the lower thermal conductivity tail (the 1-percentile may vary by about 1%).

The samples used for determinations of thermal conductivity and heat capacity for the main rock types are from different sections in different boreholes and are judged to be representative for the different rock types. The representativity can be questioned for some subordinate rock types with only few determinations. However, the effect on the domain modelling results from subordinate rock types is small for obvious reasons.

The representativeness of samples selected for thermal expansion measurements can be questioned. The samples are few and focused to certain parts of the rock volume. However, the variability seems to be quite low.

Also the representativeness of the thermal anisotropy can be questioned since the investigations comprised only a few measurements in two rock types in the Laxemar area (Section 3.8 in /Sundberg et al. 2008a/).

The thermal data for permafrost modelling include rock domain data outside the focused area. The uncertainties in the mean and uncertainty estimates for the thermal conductivity, heat capacity and heat production are mainly related to the estimates in rock type proportions, if any, and if thermal data are available for the different rock types. For some rock domains outside the focused area, data are based on the dominant rock type, and the uncertainties may be particularly large. However, the uncertainties are not believed to have major influence on the permafrost modelling result since other uncertainties are judged to be larger.

The temperature loggings come from several boreholes and are judged to be representative for the site. The temperature data and geothermal gradient data are mainly available for the focused area but are judged to meet the needs for the large scale permafrost modelling, including areas outside the focused area.

The heat flow data are judged to be representative for the whole site, including areas outside the focused area used in permafrost modelling.

A2.7 Spatial and temporal variability of data

Spatial variability of data

The description of the spatial distribution of thermal conductivity and heat capacity has been the main objective of the thermal site descriptive modelling. Particular emphasis have been made on describing the lower tail of the thermal conductivity distribution since small uncertainties in the lower tail of the thermal conductivity distributions will have a significant impact on canister spacing in repository layout D2, in order to fulfil the maximum temperature criteria on the buffer. Also the uncertainty description in /Sundberg et al. 2008a/ focuses on the lower tail of the thermal conductivity distributions for the different rock domains. The models presented in the site descriptive modelling, SDM Site, are judged to represent the modelled rock domains and their variability in an appropriate way /SKB 2009a/. Confidence in the lower tails of the thermal conductivity distributions is generally high.

As an important part of the thermal modelling, data are upscaled from measurement scale to simulation scale (2 m in Laxemar). The temperature development around a canister is influenced by a number of different scales, approximately 2–20 m /Sundberg et al. 2005b/. When using the data to calculate an adequate spacing between canisters, the simulation scale is used (2 m) /Hökmark et al. 2009/. This means that an automatic upscaling is provided in the numerical modelling when calculating the maximum temperature from the data provided in the thermal realisations (see Section A2.1). However, in the site descriptive modelling report /Sundberg et al. 2008a/ there is a need to illustrate the upscaling effect. Upscaling is made to 5 m, a scale that is approximately relevant for the temperature development around the canister. The result of this upscaling is provided in the thermal site descriptive modelling report and used for trial values on canister spacing /Hökmark et al. 2009/ and uncertainty estimates.

The scale for the long term thermal evolution caused by climate changes is much larger compared to the scale for thermal evolution of the near field of individual canisters. Therefore the means of thermal conductivity, heat capacity, heat generation, anisotropy etc are relevant for this long term thermal evolution.

The description of the anisotropy in thermal conductivity has focused on determining a relevant mean anisotropy factor for the rock mass. Consequently, there are uncertainties in the spatial distribution of the anisotropy.

For the corresponding discussion of coefficient of thermal expansion, see Section A6.4.

Temporal variability of data

Except for the in situ temperature, none of the parameters exhibit temporal variability. The temperature loggings show a significant influence from drilling that is time dependent. If the loggings have been made shortly after the drilling, the results should be treated with caution. However, such temperature logging data have been excluded from the evaluation during an “approval” process, see Section 3.14 in /Sundberg et al. 2008a/. The natural temperature at repository depth is subject to long-term variability. However, this is a very slow process and the natural undisturbed variability is thus insignificant. The long-term thermal evolution of the repository is discussed in Chapter 3. However, the construction of the repository may influence the temperature at repository depth. This is discussed above in Section A2.6 in connection with the uncertainty discussion of the temperature margin.

For the corresponding discussion of coefficient of thermal expansion, see Chapter A4.

A2.8 Correlations

As described in Section A2.5, the spatial correlation structure for the thermal conductivity has been based on density logging data. Thermal conductivity measurements have been used to support the correlation structure when possible.

In contrast to Forsmark /Sundberg et al. 2008b/, no obvious relationship between thermal conductivity and heat capacity could be discerned in Laxemar. Thus, heat capacity (C) cannot be calculated from the thermal conductivity realisations produced by the thermal stochastic modelling, as was done in the case of Forsmark. However, a relationship between heat capacity and density is displayed by the rocks at Laxemar /Sundberg et al. 2008a/. This relationship has not been exploited in the thermal modelling.

A2.9 Result of supplier's data qualification

The data are presented in the site descriptive modelling reports /Sundberg et al. 2008a/. A summary is given here.

Thermal conductivity

The most reliable thermal conductivity data are mainly provided by laboratory measurements with the TPS-method. Thermal conductivity versus elevation for different rock types is illustrated in Figure A2-1 and Figure A2-2. From these figures it can be seen that three dominant rock types (Ävrö quartz monzodiorite, Ävrö granodiorite and quartz monzodiorite) have very different thermal conductivities. Ävrö granodiorite, the dominant rock type in domain RSMA01, has relatively high conductivities, whereas Ävrö quartz monzodiorite, the dominant rock type in domain RSMM01, is characterised by low conductivities. Quartz monzodiorite, the dominant rock type in domain RSMA01, has conductivities which fall between those of the above-mentioned rock types. As for subordinate rock types, some samples of diorite-gabbro and fine-grained diorite-gabbro display low thermal conductivities.

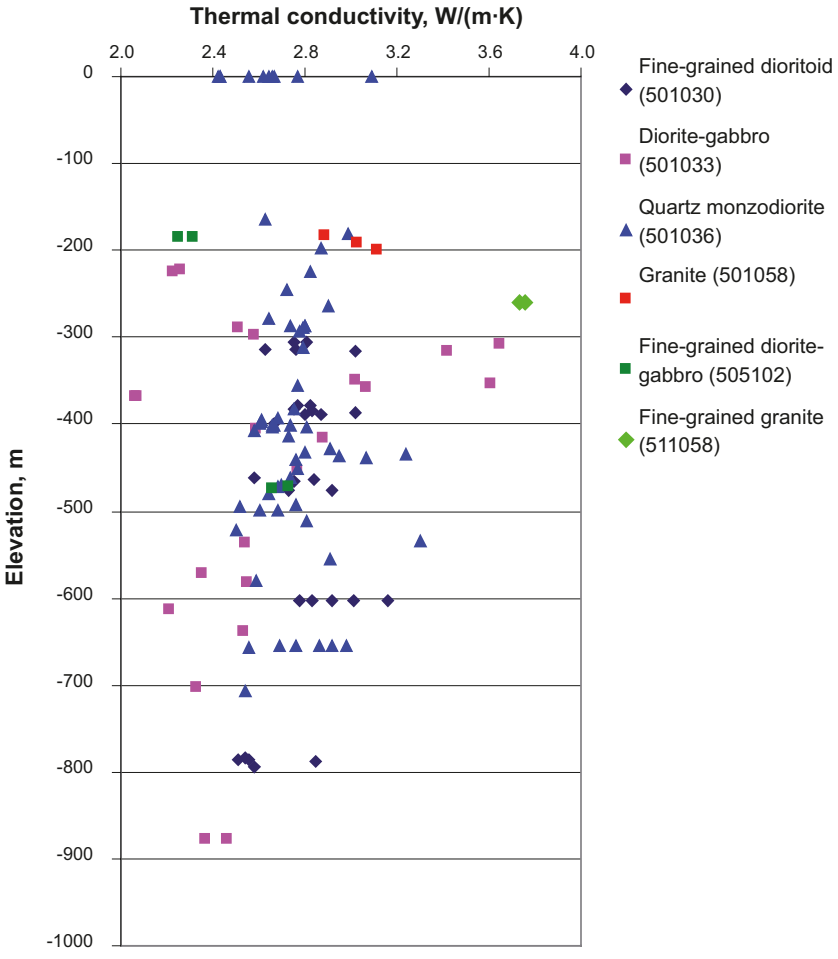

FigureA2-1. *Thermal conductivity versus elevation for different rock types. Samples measured using the TPS method. From /Sundberg et al. 2008a/.*

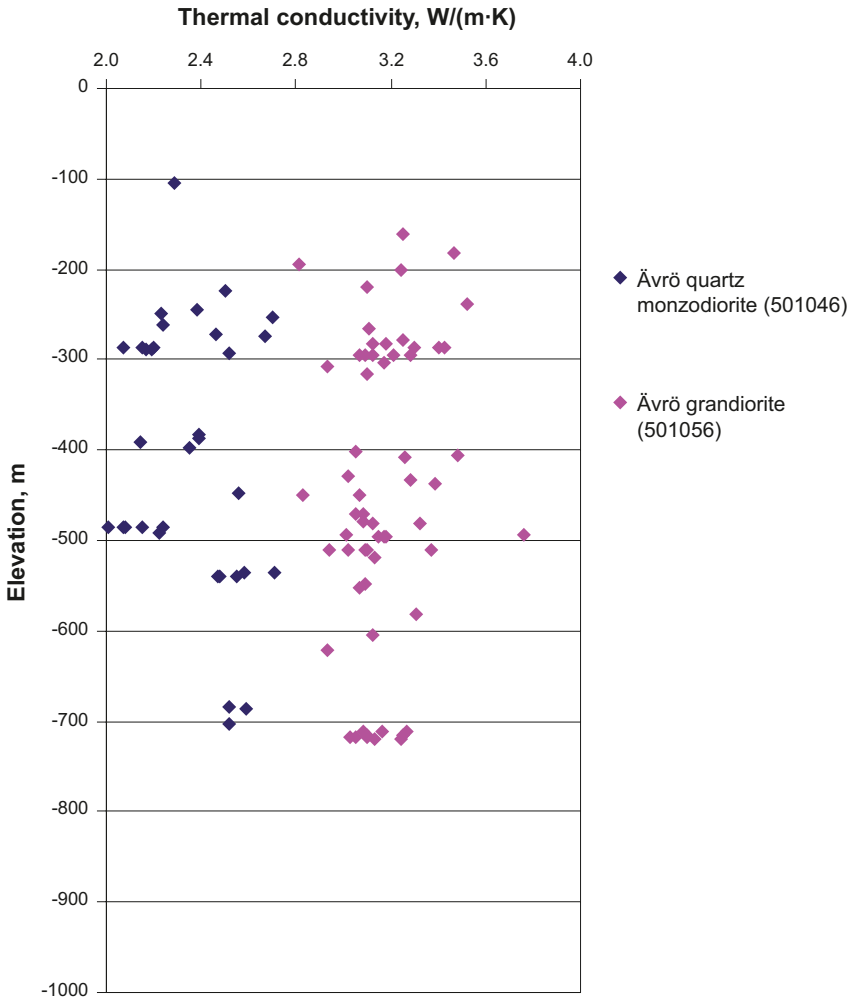

Figure A2-2. *Thermal conductivity versus elevation for Ävrö granodiorite and Ävrö quartz monzodiorite. Samples measured using the TPS method. From /Sundberg et al. 2008a/.*

The rock type distribution in boreholes is used as the basis for the stochastic modelling of geology. The distribution of thermal conductivity for each rock type and its spatial correlation structure are used as input for the stochastic modelling of thermal conductivity. The main result of the thermal modelling of a rock domain is a set of 1000 realisations of thermal conductivity at the 2 m scale. These realisations have been used in the design of the repository /SKB 2009b/ (see Section A2.1). Histograms of the realisations upscaled to 5 m are shown in Figure A2-3 for domains RSMA01, RSMM01 and RSMD01. The 5 m scale is judged to be more relevant for the temperature development around the canister and the peak temperature in the buffer. Summary statistics of the upscaled realisations to 5 m are presented in Table A2-8. The values in Table A2-8 are valid at 20°C.

The uncertainties in the lower tail of the modelled thermal conductivity distributions due to uncertainties in rock type proportions is estimated to be 1% (Section 7.2.4 in /Sundberg et al. 2008a/).

The thermal conductivity is influenced by the temperature, see Figure A2-4. Thermal conductivity at elevated temperature can be determined from Equation A2-1.

$$\lambda_1=\lambda_0(1+\alpha_\lambda(T_1-T_0)) \qquad \text{A2-1}$$

where,

λ_0 Thermal conductivity at 20°C, T_0, W/(m·K)

λ_1 Thermal conductivity at elevated temperature T_1, W/(m·K)

α_λ Temperature coefficient for thermal conductivity, 1/°C

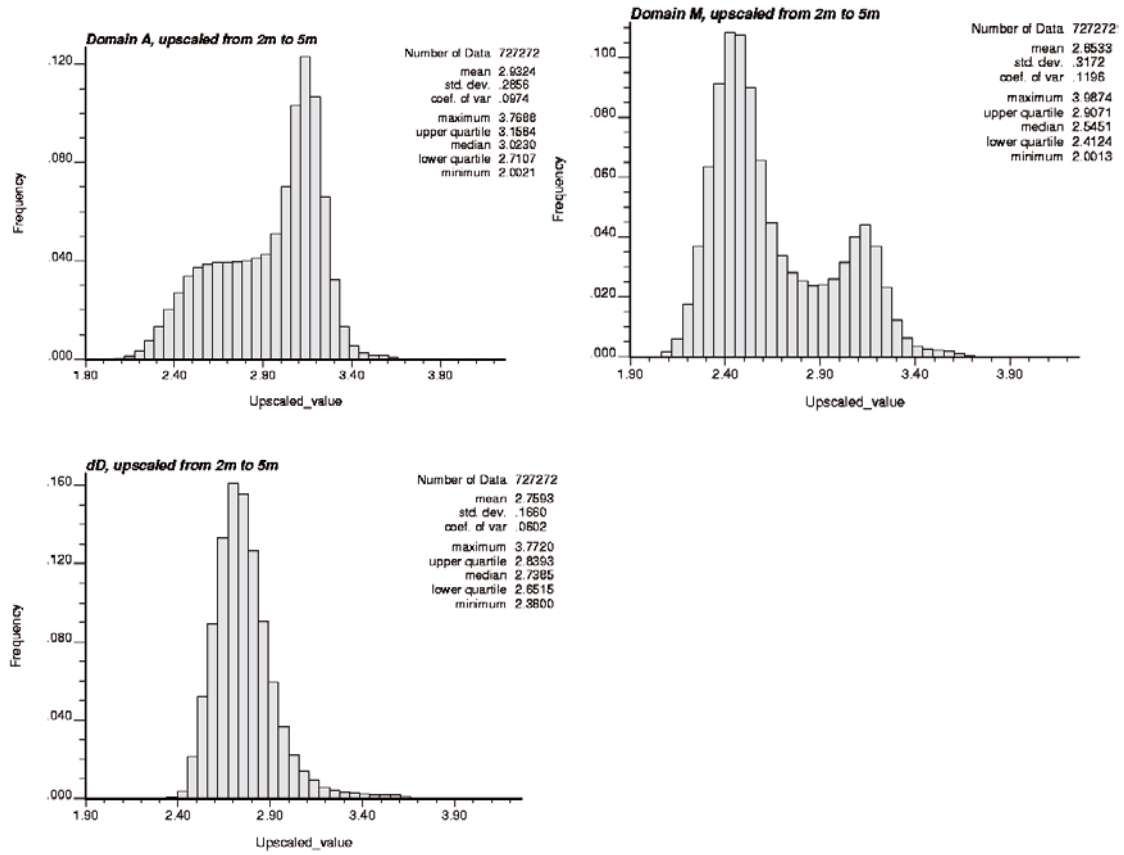

Figure A2-3. *Histogram of thermal conductivity of domains RSMA01, RSMM01 and RSMD01 (Figures 6-2, 6-10 and 6-23 respectively in /Sundberg et al. 2008a/) based on simulations at the 2 m scale followed by upscaling to 5 m.*

Table A2-8. Thermal conductivity (W/(m·K)) at 20°C for domains RSMA01, RSMM01 and RSMD01 based on simulations at the 2 m scale and upscaled to 5 m (Table 6-7, 6-8 and 6-9 respectively in /Sundberg et al. 2008a/). The 0.1–1.0-percentiles are intended to be used as first guess values for the canister spacing in the numerical modelling.

Statistical parameter	RSMA01 5 m scale	RSMM01 5 m scale	RSMD01 5 m scale
Mean	2.93	2.65	2.76
Standard deviation	0.286	0.317	0.166
0.1-percentile	2.16	2.11	2.41
1-percentile	2.27	2.19	2.48
2.5-percentile	2.34	2.23	2.50

Mean temperature coefficients for thermal conductivity in different rock types are estimated in Table A2-9 and the variability is indicated in Figure A2-5. For rock type fine-grained granite (511058), the temperature coefficient is based on a rock type with similar composition from the Forsmark site /Sundberg et al. 2008a/., The mean temperature coefficient of, for example, Ävrö granodiorite is –6.8% per 100°C. This means that the thermal conductivity at 20°C will be reduced by 3.4% if the temperature in the rock mass is raised to 70°C.

Anisotropy in thermal conductivity means that the conductivity (and the thermal diffusivity) is different in different directions. In a foliated rock the thermal conductivity is commonly higher parallel to the foliation plane compared to a direction perpendicular to the foliation. Measurements of thermal conductivity at seven outcrop locations in Laxemar /Mossmark and Sundberg 2007/, indicate that thermal conductivity parallel to the foliation plane is higher, by a factor of approximately 1.15, than conductivity perpendicular to the foliation /Sundberg et al. 2008a/.

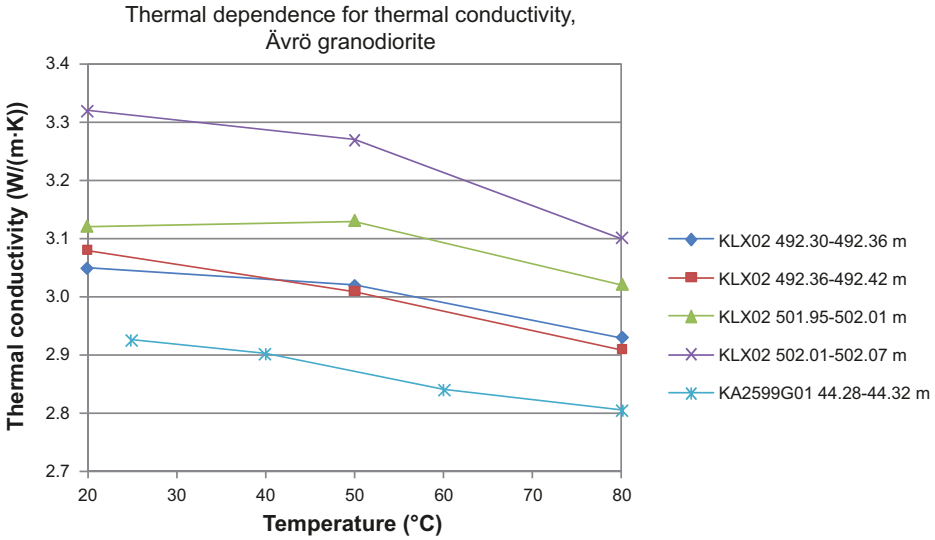

Figure A2-4. *Example of temperature dependence of thermal conductivity (rock type Ävrö granodiorite (501056)). From /Sundberg et al. 2008a/.*

Table A2-9. Estimated mean temperature coefficients for thermal conductivity in different rock types. The thermal rock class (TRC) to which the rock type has been assigned is also given (Table 3-31 in /Sundberg et al. 2008a/).

Name code	Rock name	TRC	Mean thermal conductivity at approx 20°C W/(m·K)	Mean temperature dependence % per 100°C	Thermal conductivity temperature coefficient, α_λ 1/°C	Comments
501030	Fine-grained dioritoid	30	2.79	–3.4%	$-3\cdot10^{-4}$	Measured
501036	Quartz monzodiorite	36	2.74	–1.1%	$-1\cdot10^{-4}$	Measured
501046	Ävrö quartz monzodiorite	46	2.36	–2.9%	$-3\cdot10^{-4}$	Measured
501056	Ävrö granodiorite	56	3.17	–6.8%	$-7\cdot10^{-4}$	Measured
511058	Fine grained granite	58	3.69	–10%	$-1\cdot10^{-3}$	Temperature dependence estimated from granite to granodiorite (101057) in Forsmark /Sundberg et al. 2008a/
	Gabbro	33/102		–3.1%	$-3\cdot10^{-4}$	Literature data /Mottaghy et al. 2005/

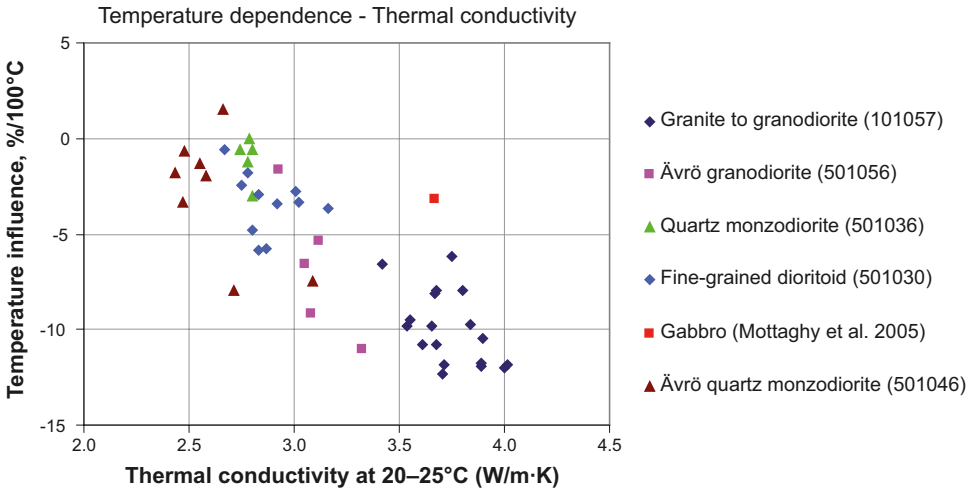

Figure A2-5. *Thermal conductivity (W/(m·K)) at 20–25°C versus the temperature coefficient (%/100°C) for the thermal conductivity in different rock types. Rock type granite to granodiorite (code 101057) is found in the Forsmark area (Figure 2-1 in /Sundberg et al. 2008a/).*

It is logical to assume a pressure dependence on the thermal conductivity. However, the pressure influence is low if the samples are water saturated, approximately 1–2% /Walsh and Decker 1966/, since any increased micro-crack porosity as a result of pressure release is water filled. All determinations of thermal conductivity in the site investigation programme have been made on water saturated samples. The pressure dependence has therefore been neglected in the evaluation /Sundberg et al. 2008a/.

For the large scale thermal evolution due to climate changes, thermal data are needed for a larger area, outside the focused area. Data on mean thermal conductivity and standard deviation is supplied in Table A2-10. It should not be assumed that a normal distribution adequately describes the data.

Heat capacity

Heat capacity distributions at rock domain level have been integrated in the thermal realisations (see Section A2.8) used in the Comparative analysis. The results for the 2 m scale for rock domains RSMA01, RSMM01 and RSMD01 are presented in Figure A2-6 and Table A2-11.

Table A2-10. Thermal conductivity (W/(m·K)) and temperature dependence ((%/100°C) for a number of rock domains both within and outside the focused area.

Rock domain	Dominant rock type /SKB 2006, Wahlgren et al. 2008/	Rock code (dominant)	Thermal conductivity (W/(m·K))		Temperature dependence (%/100°C)
			mean	Std	mean
RSMA01[1]	Ävrö granodiorite	501056	2.93	0.29	–7
RSMB06[2]	Fine-grained dioritoid	501030	2.74	0.20	–3
RSMBA03[3]	Ävrö granite[7]	501044	2.79	0.26	
RSMD01[4]	Quartz monzodiorite	501036	2.76	0.17	–1
RSME14[5]	Diorite to gabbro	501033	2.68	0.47	–3
RSMF01[6]	Fine- to medium-grained granite	511058	3.69	0.08	–10[8]
RSMM01[1]	Ävrö quartz monzodiorite	501046	2.65	0.32	–3
RSMP01-A01[9]	Ävrö granodiorite	501056	3.19		–3
RSMP01-D01[10]	Quartz monzodiorite	501036	3.15		–1

[1] Thermal conductivity has been modelled in SDM Laxemar Site /Sundberg et al. 2008a/. Temperature dependence is for dominant rock type /Sundberg et al. 2008a/.

[2] Thermal conductivity has been modelled in SDM Simpevarp 1.2 /Sundberg et al. 2005a/. Temperature dependence for dominant rock type /Sundberg et al. 2005a/.

[3] Thermal conductivity has been modelled in SDM Laxemar 2.1 /Wrafter et al. 2006/.

[4] Thermal conductivity has been modelled in SDM Laxemar Site /Sundberg et al. 2008a/. Temperature dependence is for dominant rock type /Sundberg et al. 2005a/.

[5] Thermal conductivity have been modelled in SDM Laxemar 2.1 /Wrafter et al. 2006/. Data applies to 1 m scale. Temperature dependence is for dominant rock type /Sundberg et al. 2008a/.

[6] No modelled thermal conductivity for domain. Thermal conductivity (TPS method) and temperature dependence for dominant rock type /Sundberg et al. 2008a/.

[7] Ävrö granite not subdivided into Ävrö quartz monzodiorite and Ävrö granodiorite /Appendix 11 in Wahlgren et al. 2008/

[8] Temperature dependence from Granite to granodiorite (101057) in Forsmark /Sundberg et al. 2008b/.

[9] Shear zone. No modelled thermal properties for domain. Thermal conductivity from RSMA01 but thermal conductivity increased 9% due to alteration. Temperature dependence for dominant rock type /Sundberg et al. 2008a/.

[10] Shear zone. No modelled thermal properties for domain. Thermal conductivity from RSMD01 but thermal conductivity increased 14% due to alteration. Temperature dependence for dominant rock type /Sundberg et al. 2008a/.

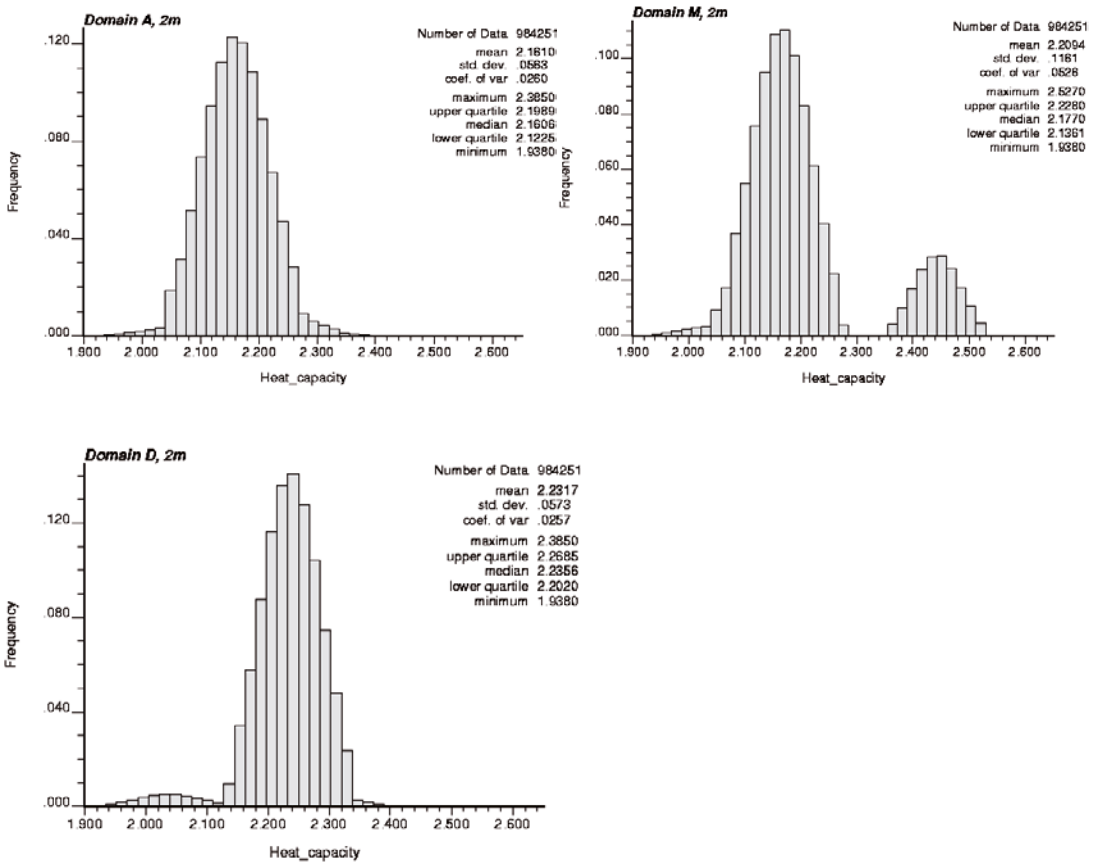

Figure A2-6. *Histogram of heat capacity for domains RSMA01, RSMM01 and RSMD01 based on the simulated TRC-distributions together with a statistical distribution model of heat capacity for each TRC at the 2 m scale (Figure 6-24, 6-27 and 6-32 in /Sundberg et al. 2008a/).*

Table A2-11. Heat capacity (MJ/(m³·K)) at 20°C for domains RSMA01, RSMM01 and RSMD01 based on the simulated TRC-distributions together with a statistical distribution model of heat capacity for each TRC at the 2 m scale (Table 6-6 in /Sundberg et al. 2008a/).

Statistical parameter	RSMA01 2 m scale	RSMM01 2 m scale	RSMD01 2 m scale
Mean	2.16	2.21	2.23
Standard deviation	0.06	0.12	0.06

The heat capacity is influenced by the temperature. The heat capacity at elevated temperature can be determined from Equation A2-2.

$$C_1 = C_0(1 + \alpha_C(T_1 - T_0)) \qquad \text{A2-2}$$

where,

C_0 Heat Capacity at room temperature T_0, MJ/(m³·K)

C_1 Heat Capacity at elevated temperature T_1, MJ/(m³·K)

α_C Temperature coefficient for heat capacity, 1/°C

The mean temperature coefficients for heat capacity in different rock types are estimated in Table A2-12 and the variability in Figure A2-7.

Table A2-12. Estimated mean temperature coefficients for heat capacity in different rock types. The thermal rock class (TRC) to which the rock type has been assigned is also given (Table 3-31 in /Sundberg et al. 2008a/).

Name code	Rock name	TRC	Mean heat capacity at approx 20°C MJ/(m³·K)	Mean temperature dependence % per 100°C	Heat capacity temperature coefficient, α_λ 1/°C	Comments
501030	Fine-grained dioritoid	30	2.22[1]	25.6%	$2.6 \cdot 10^{-4}$	Measured
501036	Quartz monzo-diorite	36	2.24	25.3%	$2.5 \cdot 10^{-4}$	Measured
501046	Ävrö quartz monzodiorite	46	2.17	26.0%	$2.6 \cdot 10^{-4}$	Measured
501056	Ävrö granodi-orite	56	2.12	23.8%	$2.4 \cdot 10^{-4}$	Measured
511058	Fine grained granite	58	2.04[1]	25%	$2.5 \cdot 10^{-4}$	Temperature dependence estimated from granite to granodiorite (101057) in Forsmark /Sundberg et al. 2008a/
	Gabbro	33/102		20.6%	$2.1 \cdot 10^{-4}$	Literature data /Mottaghy et al. 2005/

[1]Mean based on calculations from TPS data. Means for other rock types based on calorimetric measurements.

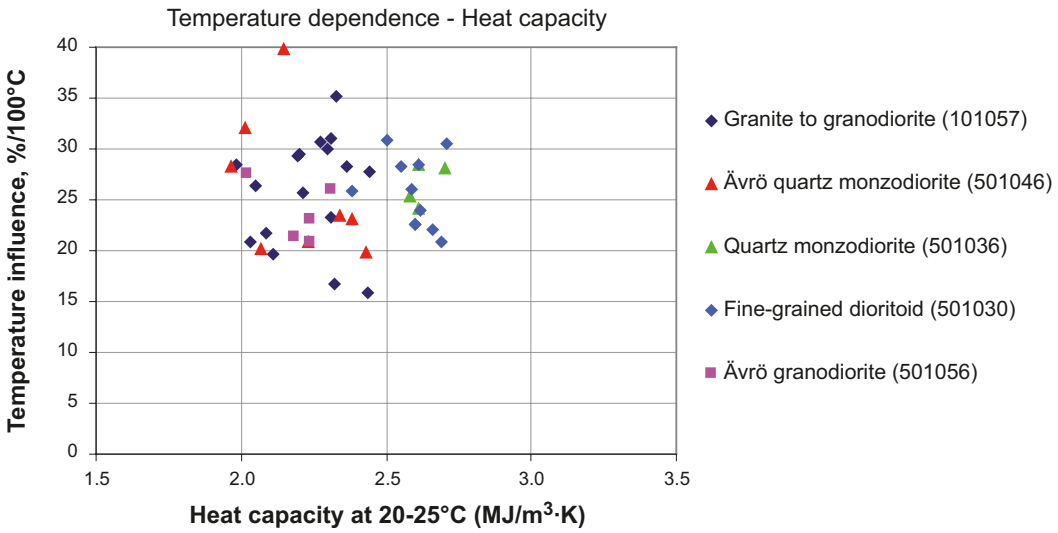

Figure A2-7. *Heat capacity (W/(m·K)) at 20–25°C versus the temperature coefficient (%/100°C) for the heat capacity in different rock types. Rock type granite to granodiorite (code 101057) is found in the Forsmark area (Figure 2-2 in /Sundberg et al. 2008a/).*

For the large scale thermal evolution due to climate changes, thermal data are needed for a larger area, outside the focused area. Data on mean heat capacity is supplied in Table A2-13. It should not be assumed that a normal distribution adequately describes the data.

Thermal diffusivity

Thermal diffusivity (m^2/s) is a measure of a material's ability to level out temperature differences. The thermal diffusivity (κ) for each domain can be calculated from the thermal conductivity (λ) and heat capacity (C) for each domain by the following equation:

$$\kappa = \lambda / C \qquad \text{A2-3}$$

In Table A2-14 the mean thermal diffusivity for each domain is calculated.

Table A2-13. Heat capacity (MJ/(m³·K)) and temperature dependence (%/100°C) for a number of rock domains both within and outside the focused area.

Rock domain	Dominant rock type /SKB 2006, Wahlgren et al. 2008/	Rock code (dominant)	Heat capacity (MJ/(m³·K)) mean	Std	Temperature dependence (%/100°C) mean
RSMA01[1]	Ävrö granodiorite	501056	2.16	0.06	24
RSMB06[2]	Fine-grained dioritoid	501030	2.23	0.10	26
RSMBA03[3]	Ävrö granite[6]	501044	2.23	0.12	25
RSMD01[4]	Quartz monzodiorite	501036	2.23	0.06	25
RSME14[5]	Diorite to gabbro	501033	2.44	0.04	21
RSMF01[5]	Fine- to medium-grained granite	511058	2.04	0.08	29[7]
RSMM01[1]	Ävrö quartz monzodiorite	501046	2.21	0.12	26
RSMP01-A01[8]	Ävrö granodiorite	501056	2.16		24
RSMP01-D01[9]	Quartz monzodiorite	501036	2.23		25

[1] Heat capacity has been modelled in SDM Laxemar Site /Sundberg et al. 2008a/. Temperature dependence is for dominant rock type /Sundberg et al. 2008a/.

[2] No modelled heat capacity for domain. Heat capacity and temperature dependence for dominant rock type /Sundberg et al. 2005a/.

[3] Heat capacity has been modelled in SDM Laxemar 1.2 /Sundberg et al. 2006/. Temperature dependence for dominant rock type /Sundberg et al. 2006/.

[4] Heat capacity has been modelled in SDM Laxemar Site /Sundberg et al. 2008a/. Temperature dependence is for dominant rock type /Sundberg et al. 2005a/.

[5] No modelled thermal conductivity for domain. Heat capacity and temperature dependence for dominant rock type /Sundberg et al. 2008a/.

[6] Ävrö granite not subdivided into Ävrö quartz monzodiorite and Ävrö granodiorite in /Appendix 11 in Wahlgren et al. 2008/.

[7] Temperature dependence from Granite to granodiorite (101057) in Forsmark /Sundberg et al. 2008b/.

[8] Shear zone. No modelled thermal properties for domain. Heat capacity from RSMA01. Temperature dependence for dominant rock type /Sundberg et al. 2008a/.

[9] Shear zone. No modelled thermal properties for domain. Heat capacity from RSMD01. Temperature dependence for dominant rock type /Sundberg et al. 2005a/.

Table A2-14. Mean thermal diffusivity (m²/s) at 20°C based on the heat capacity and thermal conductivity in Table A2-10 and Table A2-13 respectively.

Rock domain	Thermal diffusivity m²/s
RSMA01	$1.36 \cdot 10^{-6}$
RSMB06	$1.23 \cdot 10^{-6}$
RSMBA03	$1.25 \cdot 10^{-6}$
RSMD01	$1.24 \cdot 10^{-6}$
RSME14	$1.10 \cdot 10^{-6}$
RSMF01	$1.81 \cdot 10^{-6}$
RSMM01	$1.20 \cdot 10^{-6}$
RSMP01-A01	$1.48 \cdot 10^{-6}$
RSMP01-D01	$1.41 \cdot 10^{-6}$

Temperature and geothermal gradient

The mean *in situ* temperature measured at 400 m, 500 m and 600 m depth, based on 4 boreholes, is estimated at 13.3°C, 14.8°C, and 16.3°C respectively, see Table A2-15 and /Sundberg et al. 2008a/. The average gradient is approximately 13–16°C/km at repository depth. The temperature and the geothermal gradient versus elevation is displayed in Figure A2-8.

Table A2-15. Temperature (°C) for the "approved" boreholes at the Laxemar site, at different levels (modified from Table 3-34 in /Sundberg et al. 2008a/).

	Temperature (°C) at depth		
	400 m	**500 m**	**600 m**
Arithmetic mean	13.3	14.8	16.3
Uncertainty	+0.1/–0.2	±0.1	±0.1

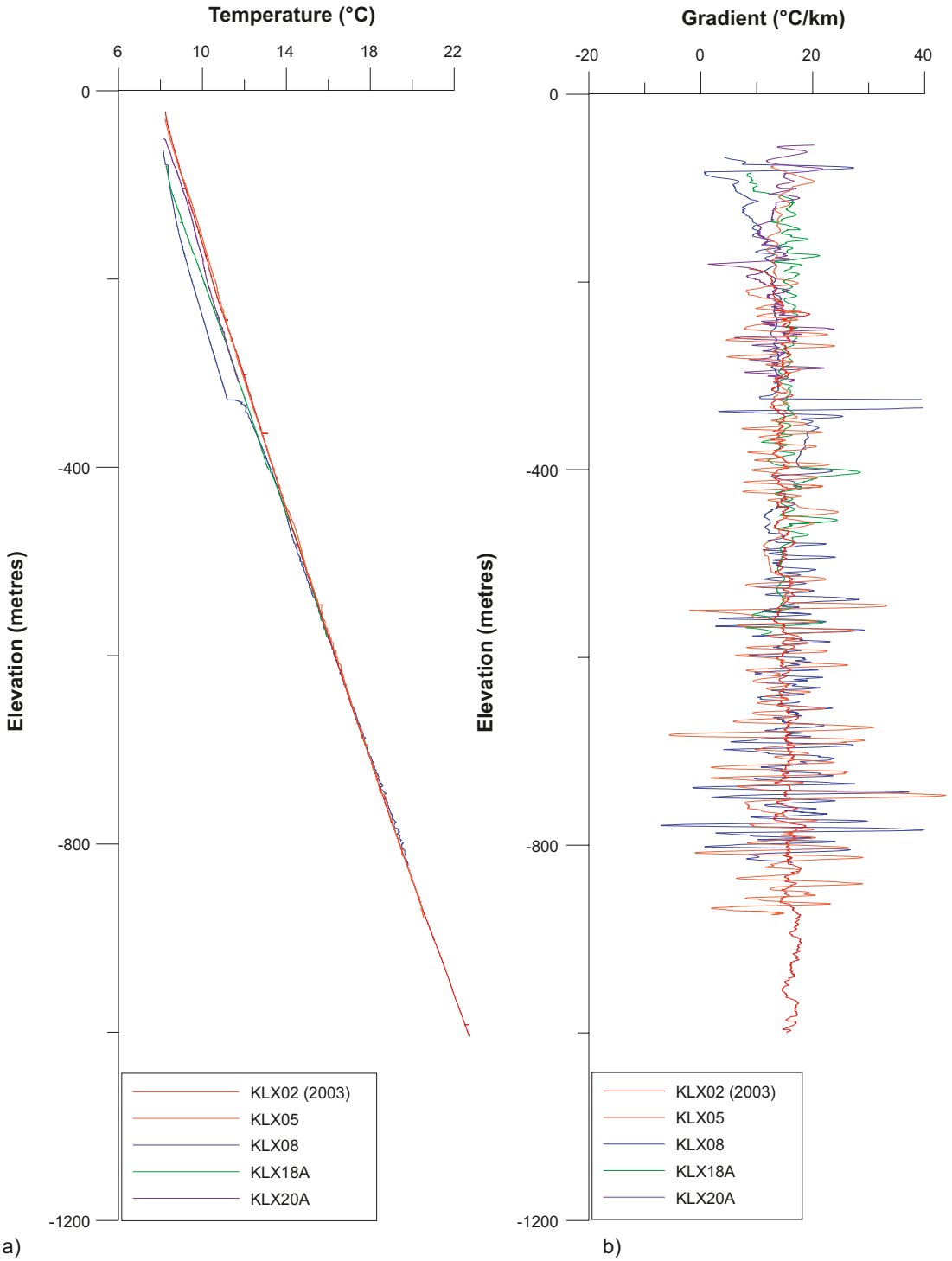

Figure. *A2-8 Summary of fluid temperature (a) and vertical temperature gradients calculated for nine metre intervals (b) for the five "approved" boreholes at Laxemar. Results from fluid temperature loggings from Figure 3-36 in /Sundberg et al. 2008a/.*

Heat generation

The heat generation based on mean proportions of different rock types in the rock and the content of U, Th and K is calculated to 2.13, 2.00 and 1.95μW/m^3 for domains RSMA01, RSMM01 and RSMD01 respectively (Section 7.1.3 in /Sundberg et al. 2009a/). The uncertainty is judged to be within ±30% based on ±1 std for the dominant rock types /Sundberg et al. 2009a/.

Heat flow

The palaeoclimatically corrected surface mean heat flow at Laxemar is suggested to be 56 mW/m^2 (Section 8.1 in /Sundberg et al. 2009a/). The heat flow determination is judged to be within +12% to –14%.

Thermal expansion coefficient

The mean thermal expansion coefficient for the main rock types in the Simepvarp-Laxemar area varies between $6.9 \cdot 10^{-6}$ and $7.4 \cdot 10^{-6}$ m/(m·K), see /Sundberg et al. 2008a/. The mean values of measured thermal expansion for the different rock types are rather similar.

Table A2-16. Measured thermal expansion (m/(m·K)) of different rock types (interval of temperature: 20–80°C) (Table 3-32 in /Sundberg et al. 2008a/).

Rock code	Rock name	Arithmetic mean	St. dev.	Min	Max	Number of samples
501030	Fine-grained dioritoid	$6.9 \cdot 10^{-6}$	$1.5 \cdot 10^{-6}$	$4.6 \cdot 10^{-6}$	$9.9 \cdot 10^{-6}$	17
501033	Diorite-gabbro	$7.4 \cdot 10^{-6}$	$1.0 \cdot 10^{-6}$	$5.9 \cdot 10^{-6}$	$8.3 \cdot 10^{-6}$	6
501036	Quartz monzodiorite	$7.3 \cdot 10^{-6}$	$1.1 \cdot 10^{-6}$	$5.8 \cdot 10^{-6}$	$9.3 \cdot 10^{-6}$	11
501046	Ävrö quartz monzodiorite	$7.1 \cdot 10^{-6}$	$1.4 \cdot 10^{-6}$	$4.3 \cdot 10^{-6}$	$9.1 \cdot 10^{-6}$	12
501056	Ävrö granodiorite	$7.3 \cdot 10^{-6}$	$1.9 \cdot 10^{-6}$	$4.5 \cdot 10^{-6}$	$1.2 \cdot 10^{-5}$	37

Temperature margin

There are uncertainties in input data as well as systematic over- and underestimates associated with the calculation of the peak buffer temperature in the thermal dimensioning of the repository. This is described in Section A2.6. The temperature margin up to the criteria is summarised in Table A2-7.

A2.10 Data recommended for use in the Comparative analysis

All data presented in Section A2.9 “Result of supplier’s data qualification” together with the realisations of thermal properties (see Table A2-2, item 3) and data in Table A2-7 are recommended for use in the Comparative analysis.

References A2.11

SKB’s (Svensk Kärnbränslehantering AB) publications can be found at www.skb.se/publications.

Back P-E, Sundberg J, 2007. Thermal Site Descriptive Model. A Strategy for the Model Development during Site Investigations. Version 2.0. SKB R-07-42, Svensk Kärnbränslehantering AB.

Hökmark H, Lönnqvist M, Kristensson O, Sundberg J, Hellström G, 2009. Strategy for thermal dimensioning of the final repository for spent nuclear fuel. SKB R-09-04, Svensk Kärnbränslehantering AB.

Hökmark H, Lönnqvist M, Fälth B, 2010. THM-issues in repository rock. Thermal, mechanical, thermo-mechanical and hydro-mechanical evolution of the rock at the Forsmark and Laxemar sites. SKB TR-10-23, Svensk Kärnbränslehantering AB.

Mossmark F, Sunberg J, 2007. Oskarshamn site investigation. Field measurements of thermal properties. Multi probe measurements in Laxemar. SKB P-07-77, Svensk Kärnbränslehantering AB.

Mottaghy D, Schellschmidt R, Popov Y A, Clauser C, Kukkonen I T, Nover G, Milanovsky S, Romushkevich R A, 2005. New heat flow data from the immediate vicinity of the Kola super-deep borehole: vertical variation in heat flow confirmed and attributed to advection. Tectonophysics, 401, pp 119–142.

Munier R, Stigsson M, 2007. Implementation of uncertainties in borehole geometries and geological orientation data in Sicada. SKB R-07-19, Svensk Kärnbränslehantering AB.

SKB 2005. Preliminary site description. Simpevarp subarea version 1.2, SKB R-05-08, Svensk Kärnbränslehantering AB.

SKB, 2006. Preliminary site description. Laxemar subarea – version 1.2. SKB R-06-10, Svensk Kärnbränslehantering AB.

SKB, 2009a. Site description of Laxemar at completion of the site investigation phase. SDM-Site Laxemar. SKB TR-09-01, Svensk Kärnbränslehantering AB.

SKB 2009b. Site engineering report Laxemar. Guidelines for underground design, step D2. SKB R-08-88, Svensk Kärnbränslehantering AB.

SKB, 2009c. Confidence assessment. Site descriptive modelling, SDM-Site Laxemar. SKB R-08-101, Svensk Kärnbränslehantering AB.

SKB, 2010. Data report for the safety assessment SR-Site. SKB TR-10-52, Svensk Kärnbränslehantering AB.

Sundberg J, Back P-E, Bengtsson A, Ländell M, 2005a. Thermal modelling. Preliminary site description. Simpevarp subarea – version 1.2. SKB R-05-24, Svensk Kärnbränslehantering AB.

Sundberg J, Back P-E, Hellström G, 2005b. Scale dependence and estimation of rock thermal conductivity. Analysis of upscaling, inverse thermal modelling and value of information with the Äspö HRL prototype repository as an example. SKB R-05-82, Svensk Kärnbränslehantering AB.

Sundberg J, Wrafter J, Back P-E, Ländell M, 2006. Thermal modelling. Preliminary site description. Laxemar subarea – version 1.2. R-06-13, Svensk Kärnbränslehantering AB.

Sundberg J, Wrafter J, Back P-E, Rosén L, 2008a. Thermal properties Laxemar. Site descriptive modelling, SDM-Site Laxemar. SKB R-08-61, Svensk Kärnbränslehantering AB.

Sundberg J, Wrafter J, Ländell M, Back P-E, Rosén L, 2008b. Thermal properties Forsmark. Modelling stage 2.3. Complementary analysis and verification of the thermal bedrock model, stage 2.2. SKB R-08-65, Svensk Kärnbränslehantering AB.

Sundberg J, Back P-E, Ländell M, Sundberg A, 2009a. Modelling of temperature in deep boreholes and evaluation of geothermal heat flow at Forsmark and Laxemar. SKB TR-09-14, Svensk Kärnbränslehantering AB.

Sundberg J, Back P-E, Ericsson L O, Wrafter J, 2009b. Estimation of thermal conductivity and its spatial variability in igneous rocks from in situ density logging. International Journal of Rock Mechanics and Mining Sciences, 46, pp 1023–1028.

Wahlgren C-H, Curtis P, Hermanson J, Forssberg O, Öhman J, Fox A, La Pointe P, Drake H, Triumf C-A, Mattsson H, Thunehed H, Juhlin C, 2008. Geology Laxemar. Site descriptive modelling, SDM-Site Laxemar. SKB R-08-54, Svensk Kärnbränslehantering AB.

Walsh J B, Decker E R, 1966. Effect of pressure and saturing fluid on the thermal conductivity of compact rock. Journal of Geophysical Research, 71, pp 3053–3061.

Wrafter J, Sundberg J, Ländell M, Back P-E, 2006. Thermal modelling. Site descriptive modelling. Laxemar – stage 2.1. SKB R-06-84, Svensk Kärnbränslehantering AB.

A3 Discrete-Fracture Network (DFN) models

The identification, mapping, modelling, and understanding of bedrock fractures at Laxemar are key components of the site description, which feeds directly into the Comparative analysis of safety related site characteristics. Fractures are important to both the design (available deposition volume, tunnelling and excavation stability) and the long-term performance (groundwater and heat flow, radionuclide transport in the event that a canister is compromised, and the question of post-glacial seismic safety) of a spent nuclear fuel repository.

The handling of fracture data from the site investigation can be divided into two general classes:

1. Description of the geometry, geology, morphology, genesis, and deformation history of brittle structures in the bedrock at Laxemar; and
2. Conceptual and mathematical representation of the fracture system in a format amenable to use in site characterisation, engineering design, and safety assessment efforts.

The description of the geometry and morphology of bedrock fractures includes the assessment of patterns of orientation, geometry and spatial arrangement, intensity, and size as functions of depth, spatial location, and geologic volumes (fracture- and rock domains). In addition, properties of importance to mechanical modelling, groundwater flow, and contaminant transport have also been assessed. These properties include aperture, mineral infilling, and fracture surface roughness.

SKB has chosen the discrete-fracture network (DFN) methodology /Munier 2004/ for the conceptual and mathematical representation of bedrock fractures (joints and faults) in repository design and numerical simulation. In a discrete-fracture network model, bedrock fractures are generally treated as infinitely thin planes of finite size (e.g. circular disks or n-sided planar polygons) in 3D-space. The geometric properties of the fractures can be considered either fixed (deterministic) or variable (stochastic) in space and/or time as probability functions /NRC 1996/. This is in contrast to the stochastic continuum approach, frequently used in numerical modelling of groundwater and heat flow, where the fracture system is treated as bulk volumetric properties (conductivity, storage, etc) of the rock mass and the geometries of individual features are largely ignored. The DFN methodology is well-suited to groundwater flow, contaminant transport, and mechanical modelling in rocks where the fractures dominate the bedrock structure and flow system, as in the massive igneous and metamorphic rocks that make up the bedrock at Laxemar.

A corresponding text for the Forsmark site is found in Section 6.3 of the SR-Site Data report /SKB 2010/. We have chosen not to repeat aspects that are general for both sites, but instead to refer to the corresponding Forsmark text. Therefore, we strongly recommend the reader to first examine Section 6.3 of the SR-Site Data report, and thereafter read this present text.

A3.1 Modeling as input to the Comparative analysis of safety related site characteristics

The elements of Discrete Fracture Network models are summarised in Section 6.3.1 of SR-Site Data report, where also a brief introduction to the discrete-fracture network terminology is given. For further readings on the DFN concept and the vocabulary associated with DFN modelling at Laxemar, readers are encouraged to consult SKB's DFN methodology document /Munier 2004/.

Defining the data requested from the supplier

The supplier is expected to provide a complete description of a stochastic model for fractures and minor deformation zones outside of deformation zones (DZ) and inside fracture domains at Laxemar.

The parameterisation of the stochastic model should be based on observed data. The minimum parameters necessary to define a geological DFN model are specified below:

- Domain: Refers to the volume for which the DFN parameters are valid, e.g. fracture domains, rock domains, hydraulic domains, and other relevant volumes as required;
- Set ID: Refers to the fracture set for which the parameters are valid. It is common practice to use the mean orientations of the planes, such as "ENE", "SubH", etc to identify sets;
- Trend (°): Refers to the trend of the mean fracture pole (normal) of a fracture set;
- Plunge (°): Refers to the plunge of the mean fracture pole (normal) of a fracture set;
- κ (–): The Fisher concentration parameter, for the univariate Fisher distribution;
- r_{min} (m): The minimum fracture radius for which the DFN model is valid. Unless stated differently, $r_{min} = r_0$;
- r_{max} (m): The maximum fracture radius for which the DFN model is valid. It has been common practice in the SDM work to use r_{max} = 564.2 m, which corresponds to a fracture with a one-sided surface area of 1 km^2. At Laxemar, a surface trace length cut-off of 1,000 m was used as the boundary between stochastic DFN models and deterministic DZ models. As such, r_{max} corresponds to the equivalent radius of a square fracture 1,000 long by 1,000 m deep.
- P_{32} (m^2/m^3): The intensity of fractures and minor deformation zones in the size range $r_{min} - r_{max}$.
- Fracture size distribution parameters: For a power-law distribution, this is the scaling exponent k_r and the minimum radius r_0; for a log-normal distribution of fracture size, it would be the distribution mean radius $\overline{r}$ (m) and standard deviation σ (–).

Modelling activities in which data will be used

DFN models will be used to:

- Estimate the intersection probabilities of fractures with canisters, deposition holes, and excavation structures. The fracture intersection probabilities control the degree of utilisation of the repository, which influences the rock volume required for a particular design /Hedin 2008, 2011, Munier 2010/;
- Understand the risks of buffer degradation, canister failure, and the compromise of repository integrity during a seismic event. The risk is quantified by the computation of the number of canisters that are intersected by critically-large fractures /Munier and Hökmark 2004, Hedin 2008, 2011, Fälth et al. 2010, Munier 2010/;
- Describe the saturated bedrock flow system at site and local scales. The groundwater flow model is a fundamental input to hydrochemical and solute transport models, which themselves are integral parts of the repository safety assessment and long-term safety calculations. Note that the hydrogeological DFN is a separate entity from the geological DFN (cf. Chapter A6) and is not discussed further within this present appendix; nevertheless, both conceptualisations are based on similar fracture data.

A3.2 Supplier input on use of data in the Comparative analysis

The Laxemar site generally has higher fracture intensity than the Forsmark site. The fracture network (DFN models) affects the assessed degree of utilisation of the repository; both by way of determining which rock volumes can be used for deposition tunnels, and for estimating the fraction of deposition holes that need to be discarded. As the Laxemar host rock is more fractured than the Forsmark host rock, this may result in a degree of utilisation that is lower in Laxemar than in Forsmark. Additionally, this implies that the groundwater flow through the postulated repository may be higher at the Laxemar site than at the Forsmark site, which may have implications for the canister integrity and radiological risk.

The objective of this appendix is to supply input data to the Comparative analysis for the selected design, with bearing on issues of long-term safety.

A3.3 Sources of information and documentation of data qualification

Sources of information

The geologic DFN models, derived as a component of the Laxemar site investigation, are presented as stand-alone reports for each modelling stage of the Laxemar site-descriptive modelling. For the Comparative analysis, the DFN work presented in /La Pointe et al. 2008/ are used together with relevant sections of the SDM-Site report /SKB 2009, pp 133–164/.

Summary tables of DFN parameters, including fracture orientation, size, and intensity statistical distributions, are archived as Microsoft Excel workbooks in SKB's model database. Other sources of information used for the derivation of the DFN models are declared in /La Pointe et al. 2008, Section 2.1, pp 15–24/.

Table A3-1. Main sources of information used in data qualification.

La Pointe P, Fox A, Hermanson J, Öhman J, 2008. Geological discrete fracture network model for the Laxemar site. Site Descriptive Modelling, SDM-Site Laxemar. SKB R-08-55, Svensk Kärnbränslehantering AB.
SKB, 2009. Site description of Laxemar at completion of the site investigation phase. SDM-Site Laxemar. SKB TR-09-01, Svensk Kärnbränslehantering AB.
SKB, 2010. Data report for the safety assessment SR-Site. SKB TR-10-52, Svensk Kärnbränslehantering AB.

Categorising data sets as qualified or supporting data

Geological discrete-fracture network models at Laxemar were constructed exclusively from qualified data extracted from SKB quality-assured databases (SICADA and SDE). The results of the site-descriptive modelling, in terms of geological DFN data, are stored in the SKB's model database. The full reference to these data, which are considered to be qualified, is shown in Table A3-2.

Table A3-2. Qualified and supporting data sets.

Qualified data sets	Supporting data sets
1. Modelldatabasen, 2008. Model: DFN LAX v2.3 (site).xls. Version 0.5. Approved 2008-08-19, Modeller: A. Fox. DatabaseID: GEO_HXXZNQSH. Svensk Kärnbränslehantering AB.	None.

1. The data in the SKB model database are considered to be qualified, as they result from the Laxemar site-descriptive modelling, which has been peer-reviewed. The data are obtained in a quality assured manner and are relevant for the site.

Excluded data previously considered as important

No data has been excluded as compared to previous versions of the DFN models.

A3.4 Conditions for which data are supplied

The DFN models are supplied for rock volumes within fracture domains FSM_C, FSM_EW007, FSM_N, FSM_NE005, FSM_S, and FSM_W (Figure A3-1), as defined in /SKB 2009, Section 5.6.1, pp 160 ff/.

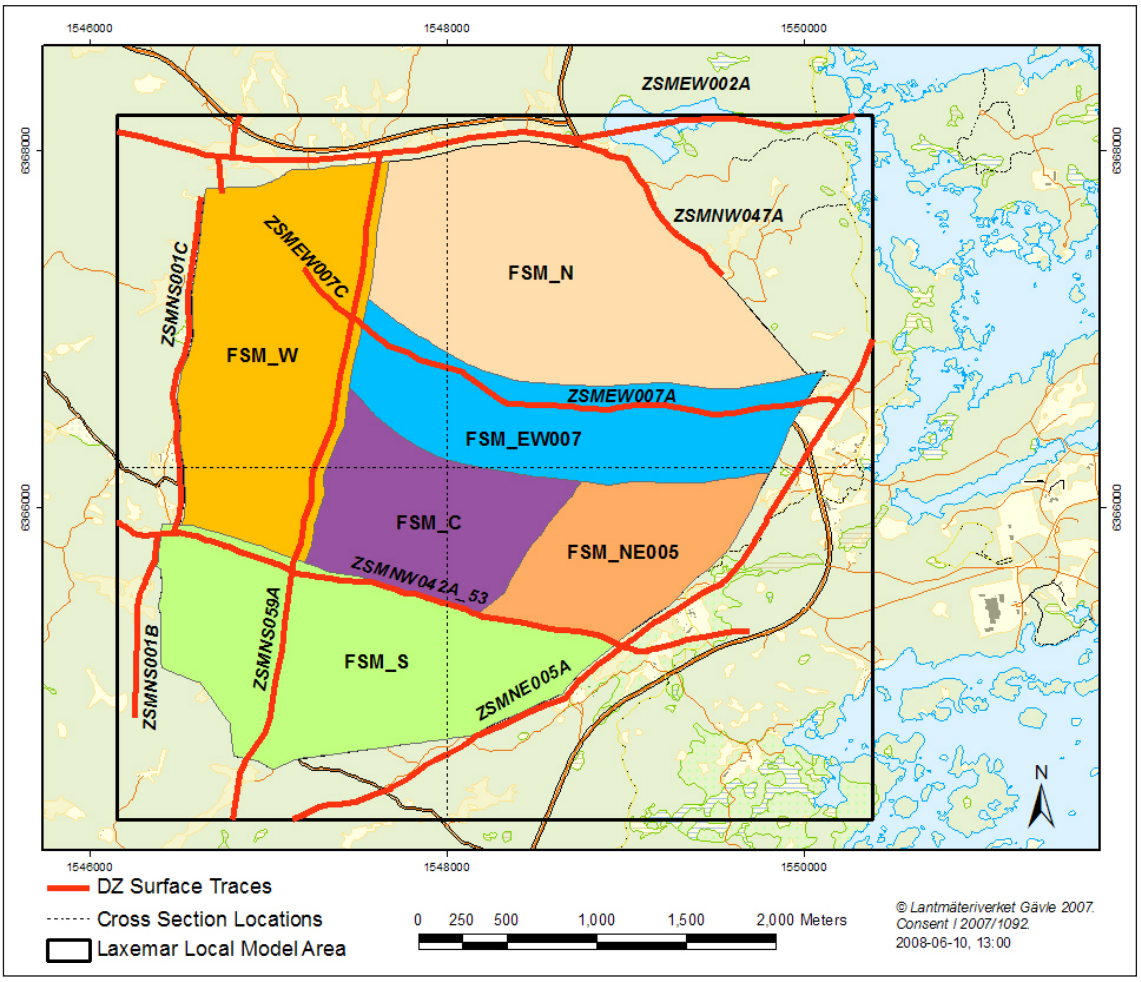

Figure A3-1. *Fracture domains and midplane of bounding deformation zones at Laxemar. Reproduced from /SKB 2009, Figure 5-57/.*

The DFN parameterisation is valid for fractures and minor deformation zones within a size range of r_0 m to 564.2 m; the latter represents the transition from stochastic fracture modelling to deterministic deformation zones (Figure A3-2), as interpreted in /Wahlgren et al. 2008, SKB 2009/. The geological DFN is defined for all fractures; no distinction is made between open, sealed, or hydraulically significant fractures.

Changes in fracture properties as functions of future processes (underground construction, de-watering, thermal loading, climate change, or additional mechanical loading from future glacial cycles) have not been assessed by the geological DFN team.

A3.5 Conceptual uncertainty

Most of the conceptual uncertainty that applies to the Forsmark site also applies to the Laxemar site. Therefore, the corresponding text in the SR-Site Data report /SKB 2010, Section 6.3.6/ is generally referred to. The conceptual uncertainties in the Laxemar DFN model resulted in a number of DFN model variants (see /La Pointe et al. 2008, Section 4.3.1/ for details). Of these, the so called "BM model" was used as base model for simulations in downstream models (e.g. intersection probabilities) and the alternative DFN models were used to bracket the uncertainty space.

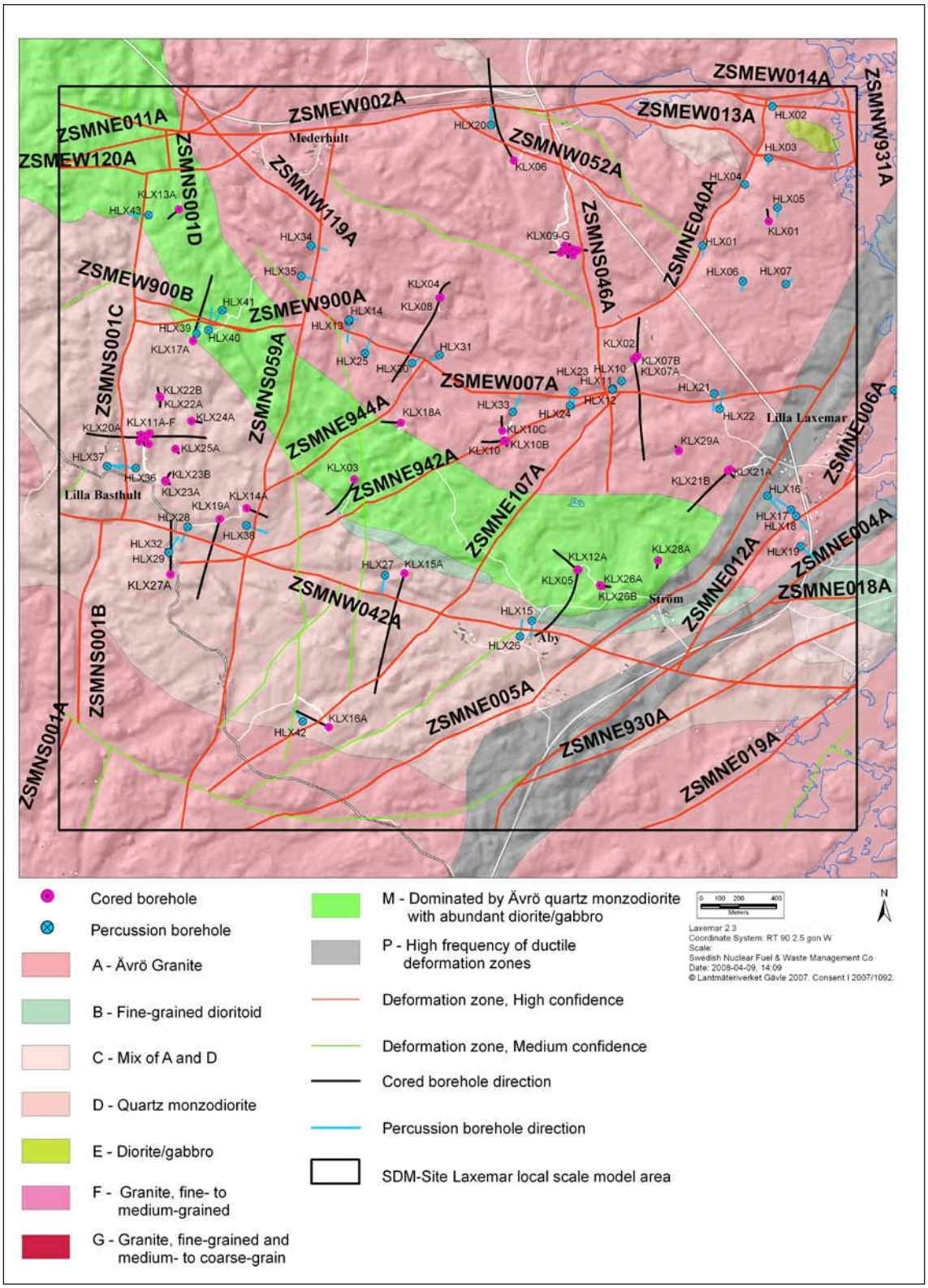

Figure A3-2. *An overview of deterministically modelled deformation zones in Laxemar. From /Wahlgren et al. 2008, Figure 5-30/.*

A3.6 Data uncertainty due to precision, bias, and representativity

Generally the data uncertainties that apply to the Forsmark site also apply to the Laxemar site. Therefore, the corresponding text in the SR-Site Data report /SKB 2010, Section 6.3.7/ is referred to.

A3.7 Spatial and temporal variability of data

The spatial variability of the fracture network is handled by assigning different DFN models to the different fracture domains.

Temporal variability of fracture data has not been taken into account during site-characterisation efforts or reporting. The temporal variability is judged to have little consequences for the site selection.

A3.8 Correlations

The same correlations are used for geological DFN modelling for the Forsmark site as for the Laxemar site. Therefore, the corresponding text in the SR-Site Data report /SKB 2010, Section 6.3.9/ is referred to.

A3.9 Result of supplier's data qualification

Based on the results of analyses performed during site characterisation, the outcome of discussions with reviewers associated to the site-descriptive modelling, and the professional judgement of the geological DFN team, the following data is recommended for use in the stochastic simulation of fractures and minor deformation zones in the Comparative analysis:

1. Each fracture domain has its own orientation model defined (sheet "orientation", in "DFN LAX v2.3 (site).xls" referred to in Table A3-2). For the calculation of P_{32}, the orientation model "FSM_Envelope" is used for all fracture domains.
2. DFN models are described for all fractures (open, partly open, and sealed) within a size range (equivalent radius) of 0.5–564.2 m; the DFN parameterisation is not valid outside those limits.
3. Size distribution models for each set, and each fracture domain, are provided in the sheets "CoupledSizeIntensity_Euclidean" and "CoupledSizeIntensity_Fractal" as a function of conceptual model.
4. Intensity models for each set, and each fracture domain, are provided in the sheets "CoupledSizeIntensity_Euclidean*"* and "CoupledSizeIntensity_Fractal" as a function of conceptual model.
5. Fracture set terminations for all fracture domains should be taken from worksheet "Termination Matrix".

A3.10 Data recommended for use in the Comparative analysis

The authoritative source for all parameters necessary to describe the geological DFN at Laxemar is the worksheet "DFN LAX v2.3 (site).xls" in the SKB model database, as referenced in Table A3-2. Specific considerations are given in Section A3.9.

References A3.11

SKB's (Svensk Kärnbränslehantering AB) publications can be found at www.skb.se/publications.

Fälth B, Hökmark H, Munier R, 2010. Effects of large earthquakes on a KBS-3 repository. Evaluation of modelling results and their implications for layout and design. SKB TR-08-11, Svensk Kärnbränslehantering AB.

Hedin A, 2008. Semi-analytic stereological analysis of waste package/fracture intersections in a granitic rock nuclear waste repository. Mathematical Geosciences, 40, pp 619–637.

Hedin A, 2011. Stereological method for reducing probability of earthquake-induced damage in a nuclear waste repository. Mathematical Geosciences, 43, pp 1–21.

La Pointe P, Fox, A, Hermanson J, Öhman J, 2008. Geological discrete fracture network model for the Laxemar site. Site descriptive modelling, SDM-Site Laxemar. SKB R-08-55, Svensk Kärnbränslehantering AB.

Munier R, 2004. Statistical analysis of fracture data, adapted for modelling Discrete Fracture Networks – Version 2. SKB R-04-66, Svensk Kärnbränslehantering AB.

Munier R, 2010. Full perimeter intersection criteria. Definitions and implementations in SR-Site. SKB TR-10-21, Svensk Kärnbränslehantering AB.

Munier R, Hökmark H, 2004. Respect distances. Rationale and means of computation. SKB R-04-17, Svensk Kärnbränslehantering AB.

NRC, 1996. Rock fractures and fluid flow: contemporary understanding and applications. Washington, D.C.: National Academy.

SKB, 2009. Site description of Laxemar at completion of the site investigation phase. SDM-Site Laxemar. SKB TR-09-01, Svensk Kärnbränslehantering AB.

SKB, 2010. Data report for the safety assessment SR-Site. SKB TR-10-52, Svensk Kärnbränslehantering AB.

Wahlgren C-H, Curtis P, Hermanson J, Forssberg O, Öhman J, Fox A, La Pointe P, Drake H, Triumf C-A, Mattsson H, Thunehed H, Juhlin C, 2008. Geology Laxemar. Site descriptive modelling, SDM-Site Laxemar. SKB R-08-54, Svensk Kärnbränslehantering AB.

A4 Rock mechanics

This appendix presents the mechanical properties of the rock and fractures (for fractures also hydro-mechanical properties) as wells as the stress conditions needed for the assessment of the thermo-hydro-mechanical (THM) evolution of the rock on different scales. These quantities are assessed from the Laxemar site-descriptive model reports (SDM-Site) and the version D2 repository layout.

In the SR-Site Data report /SKB 2010, Section 6.4/ the corresponding data are given for the Forsmark site. In a few instances, issues that are not site specific are detailed in the SR-Site Data report, to which references are made.

A4.1 Modelling as input to the Comparative analysis of safety related site characteristics

This section describes what data are expected from the supplier, and in what modelling activities the data are to be used.

Defining the data requested from the supplier

The modelling requires the following geosphere input data with estimates of spatial and temporal variability as well as associated uncertainties:

- Rock mass elastic properties for the different scales of importance (Young's modulus E (GPa) and Poisson ratio υ (–)).
- Rock mass density ρ (kg/m^3).
- Uniaxial compressive strength *UCS* (MPa) and spalling strength (% of *UCS*).
- Fracture friction angle φ (°) and cohesion c (MPa).
- Principal *in situ* stress magnitudes σ_1, σ_2, and σ_3 (MPa) and orientations of stress components in terms of plunge and trend (°).
- Evolution of stress additions during glacial cycle (glacially induced stresses), principal stress magnitudes σ_1, σ_2, and σ_3 (MPa) and orientations of stress components in terms of plunge and trend (°).
- Stress-transmissivity relations:
  - Parameter values for the continuously-yielding joint model /Itasca 2007/, *i.e. JKN* (MPa/mm) and *JEN* (–).
  - Joint roughness coefficient *JRC* (–).
  - Parameters for exponential expression of hydraulic apertures /Liu et al. 2004/, *i.e.* e_r (μm), e_{max} (μm) and α (–).

Modelling activities in which data will be used

The THM-evolution of the rock at Laxemar is assessed for the construction and operational phase, during the initial period of temperate climate after closure, and during the remaining part of the reference glacial cycle. The main results of these analyses concern:

1. Estimates of mechanically induced changes of the transmissivity of fractures that intersect the far-field, due thermal effects and effects of ice load.
2. Estimates of the scope and extent (time-frames and location) of fracturing around deposition holes (spalling), and based on this, a qualitative assessment of the potential hydraulic impact of this fracturing.

The mechanical and thermo-mechanical modelling is conducted using version 4.1 of the extensively tested *3DEC* code /Itasca 2007/. *3DEC* is a distinct element code, particularly developed to analyse the mechanical and thermo-mechanical behaviour of jointed media such as fractured rock. The results of the rock mechanics modelling are presented in the THM-report /Hökmark et al. 2010/.

In addition to the rock mechanics data given in this appendix, the modelling also needs the following thermal/thermo-mechanical (cf. Chapter A2) and hydraulic properties (cf. Chapter A6) of the rock mass. The data needed are listed below:

1. Rock mass thermal conductivity λ (W/(m·K)) and heat capacity C (J/(m^3·K)).
2. Rock mass thermal expansion coefficient α (m/(m·K)).
3. *In situ* temperature at repository depth T (°C).
4. Fracture transmissivity T (m^2/s).

Furthermore, the modelling needs

5. repository design, i.e. geometry and dimensions of deposition tunnels and deposition holes /SKB 2007/,
6. layout, i.e. coordinates of individual canister positions /SKB 2009c/,
7. Initial canister power and decay-rate of the spent nuclear fuel /Hökmark et al. 2009/.

A4.2 Supplier input on use of data in the Comparative analysis

The Comparative analysis presented in Chapter 4 focuses on the potential for thermally induced spalling and thus only needs a subset of the data presented in this Appendix. However, the rock mechanics modelling presented in the THM-report /Hökmark et al. 2010/ also considers estimates of mechanically induced changes of the transmissivity of fractures that intersect the far-field, due thermal effects and effects of ice load. The data presented in this appendix thus also serves a the formal basis for the input to the other Laxemar analyses in /Hökmark et al. 2010/.

A4.3 Sources of information and documentation of data qualification

Sources of information

The main sources of information used in the data qualification of rock mechanics data are presented in Table A4-1.

Categorising data sets as qualified or supporting data

The qualified and supporting data sets are presented in Table A4-2. Comments regarding each item are given in Table A4-3. Data sets taken from the site-descriptive modelling /Hakami et al. 2008/ (*i.e.* items 1–5) can a priori be categorised as qualified data. They have subsequently been judged to be qualified according to the instructions for supplying data to the SR-Site Data report (cf. /SKB 2010, Section 2.3/).

Table A4-1. Main sources of information used in data qualification.

Andersson C J, 2007. Äspö Hard Rock Laboratory. Äspö Pillar Stability Experiment, Final report. Rock mass response to coupled mechanical thermal loading. SKB TR-07-01, Svensk Kärnbränslehantering AB.
Hakami E, Fredriksson A, Lanaro F, Wrafter J, 2008. Rock mechanics Laxemar. Site descriptive modelling, SDM-Site Laxemar. SKB R-08-57, Svensk Kärnbränslehantering AB.
Jacobsson L, Flansbjer M, 2005a. Oskarshamn site investigation. Borehole KLX03A. Normal loading and shear tests on joints. SKB P-05-92, Svensk Kärnbränslehantering AB.
Jacobsson L, Flansbjer M, 2005b. Oskarshamn site investigation. Borehole KLX06A. Normal loading and shear tests on joints. SKB P-05-146, Svensk Kärnbränslehantering AB.
Jacobsson L, Flansbjer M, 2006a. Oskarshamn site investigation. Borehole KLX10. Normal loading and shear tests on joints. SKB P-06-39, Svensk Kärnbränslehantering AB.
Jacobsson L, Flansbjer M, 2006b. Oskarshamn site investigation. Borehole KLX12A. Normal loading and shear tests on joints. SKB P-06-75, Svensk Kärnbränslehantering AB.
Lund B, Schmidt P, Hieronymus C, 2009. Stress evolution and fault stability during the Weichselian glacial cycle. SKB TR-09-15, Svensk Kärnbränslehantering AB.
Martin D, 2005. Preliminary assessment of potential underground stability (wedge and spalling) at Forsmark, Simpevarp and Laxemar sites. SKB R-05-71, Svensk Kärnbränslehantering AB.
Rhén I, Forsmark T, Hartley L, Jackson P, Roberts D, Swan D, Gylling B, 2008. Hydrogeological conceptualisation and parameterisation. Site descriptive modelling, SDM-Site Laxemar. SKB R-08-78, Svensk Kärnbränslehantering AB.

Table A4-2. Qualified and supporting data sets.

Qualified data sets	Supporting data sets
1. Intact rock uniaxial compressive strength: Tables 3-2 and 3-13 /Hakami et al. 2008/	6. Spalling strength: Tables 3-2 and A.1 /Martin 2005/; Section 8.2 and Section 11 /Andersson 2007/.
2. Rock mass deformation properties: Table 5-11 /Hakami et al. 2008/	7. Rock mass density: Appendix 11 (pp. 353, 371 and 385) /Wahlgren et al. 2008/
3. Fracture friction angle and cohesion: Table 4-14 /Hakami et al. 2008/	8. Stress-transmissivity relations: • Model parameters JKN and JEN for the continuously-yielding joint model: Section 5.1 (normal stress-normal displacement curves based on direct measurements) in each of /Jacobsson and Flansbjer 2005a, b, 2006a, b/
4. Initial pre-mining stress magnitudes and orientations: Table 6-11 /Hakami et al. 2008/ and the major principal stress in Table 2-7 /Andersson 2007/	• Joint roughness coefficient: Table 4-2 /Hakami et al. 2008/
5. Evolution of stress additions during glacial cycle: Figure 7-18 /Lund et al. 2009/	• Initial (or residual) hydraulic aperture: Table 9-12 /Rhén et al. 2008/

Table A4-3. Justification for the sorting of items in Table A4-2.

1. Primary data for intact rock are obtained by laboratory (small) scale testing /Hakami et al. 2008/. Lower level references to test methods as well as discussions on uncertainties are also provided by /Hakami et al. 2008/.

2. The deformation properties of the rock mass are obtained from two different modelling approaches /Hakami et al. 2008/:

– An empirical approach, which is based on classification systems and empirical relationships.

– A theoretical approach, which is based on numerical modelling.

– The final estimate of the rock mass deformation properties is made by weighting the results together – a process known as “Harmonisation”. More detailed information regarding the process is provided by /Hakami et al. 2008/.

3. The Mohr-Coulomb strength properties of fractures reported in /Hakami et al. 2008/ are based on laboratory results from tilt tests and direct shear tests of discrete fractures and are expected to represent the majority of single open fractures. However, they do not represent sealed fractures and are also not expected to represent the highly water-conductive fractures. The latter ones were not represented in the population selected for mechanical testing /Hakami et al. 2008/. Lower level references to test methods as well as discussions on uncertainties are also provided by /Hakami et al. 2008/.

4. The stress additions during a glacial cycle are based on 3D simulations of the glacial isostatic adjustment /Lund et al. 2009/ due to a Fennoscandian ice model by Näslund /SKB 2006a/. The numerical model used to calculated glacially induced stresses has been extensively tested and verified against other, independent, codes as well as compared with GPS measurements of glacial isostatic adjustments (GIA) data /Lund et al. 2009/. Therefore, this data set can be judged to be qualified according to the instructions for supplying data to the Data report.

5. Stress-induced transmissivity changes are based on the continuously-yielding joint model (CY model) /Itasca 2007/, using lab-scale stress-stiffness data and average hydraulic apertures at repository depth, and an exponential relation /Liu et al. 2004/ to account for a residual aperture at high normal stress. The stress-transmissivity relations should therefore be considered a supporting data set.

6. The spalling strength is expressed as the range 52–62% of the uniaxial compressive strength (UCS) in each rock domain based on the findings from AECL’s Mine-by experiment (e.g./ Martin 2005/) and the Äspö Pillar Stability Experiment (APSE) /Andersson 2007/ and should therefore be considered a supporting data set.

7. The value of the rock mass density is generic (2,700 kg/m^3) and used to calculate the vertical stress component. It should therefore be considered a supporting data set.

8. The *in situ* stress model for Laxemar, *i.e.* initial pre-mining stress magnitudes and orientations, is based on direct measurements (overcoring, hydraulic fracturing and hydraulic testing on pre-existing fractures) and indirect observations (borehole breakouts, core disking and tests of microcrack porosity) from the site investigation as well as results from numerical modelling /Hakami et al. 2008/. An upper bound estimate of the major horizontal *in situ* stress is taken to be that of the back calculated *in situ* stress state from the Äspö Pillar Stability Experiment (APSE) /Andersson 2007/.

For the qualified data sets in Table A4-2, more extensive discussions on the uncertainties, variability and methodology used in the acquisition of data associated with each set of parameters are provide by the references given in Table A4-1 and Table A4-2; a summary is provided in the following sections. For the supporting data sets (with the exception of rock mass density), discussions regarding uncertainties and variability for each set of parameters are provided in the following sections.

Excluded data previously considered as important

No important data has been excluded from the analyses.

A4.4 Conditions for which data are supplied

All data supplied are valid at present-day conditions at the site and based on current knowledge of the site conditions, cf. Table A4-2. The rock volumes the data concern are clearly indicated throughout this appendix.

The stress additions during a glacial cycle, provided by /Lund et al. 2009/, are valid at 500 m depth, i.e. repository depth.

A4.5 Conceptual uncertainty

Strength properties of intact rock

The conceptual uncertainties relating to the uniaxial compressive strength are judged to be low. Factors contributing to the conceptual uncertainty of the spalling strength are:

- Relative humidity: Reduced humidity seems to increase the spalling strength /Glamheden et al. 2010/.
- Stress path: The Äspö Pillar Stability Experiment (APSE) /Andersson 2007/ was designed to give high tangential stresses after excavation. For a more gentle stress path, the spalling strength may be different.

Elastic properties of rock mass

The elastic properties of the rock mass are obtained from two independent modelling approaches /Hakami et al. 2008/. The main conceptual uncertainties associated with the two approaches are listed below:

- In the empirical approach, no explicit stress dependence in any of the parameters is assumed, whereas in the theoretical approach there is /Hakami et al. 2008/. Figure A4-1 shows an example of the rock mass deformation modulus evaluated at different levels of confining pressure. As seen in the figure, the stress-dependence is small.
- For both the empirical and theoretical approaches, it is assumed that the rock mass is isotropic /Hakami et al. 2008/. As there is no strong anisotropy in terms of fracturing in the different fracture domains /Hakami et al. 2008/, this assumption appears to be valid.
- Both modelling approaches involve a certain degree of subjectivity /Hakami et al. 2008/. For the empirical approach, factors such as the size of sample populations and subjectivity in the characterisation of the rock mass will contribute to the conceptual uncertainty. For the theoretical approach, there are conceptual uncertainties related to input data to the models, *i.e.* elastic properties of the rock, the mechanical properties of fractures, and the geological DFN model /La Pointe et al. 2008/.

A measure of the conceptual uncertainty can be found by examining the differences in results from the empirical and theoretical approaches. The mean values of Young's modulus obtained from the theoretical and empirical approaches deviate by 0.2–10.2 GPa from each other /Hakami et al. 2008/ with the largest difference in fracture domain FSM_W and smallest difference in fracture domain FSM_EW007, cf. Figure A4-2. Empirical characterisation, based on the *Q* and *RMR* systems, is not available for fracture domain FSM_W /Hakami et al. 2008/, which makes the uncertainty in this domain larger. It should also be noted that no theoretical modelling was performed for fracture domain FSM_N /SKB 2009b/. However, results from both methods indicate that the five fracture domains at Laxemar can be divided into two groups with similar properties /Hakami et al. 2008/. The group comprising fracture domains FSM_C, FSM_W and FSM_NE005 has a higher value of Young's modulus than the group comprising fracture domains FSM_N and FSM_EW007 /Hakami et al. 2008/. A corresponding comparison of the difference in Poisson's ratio is not relevant as the harmonised value for Poisson's ratio is based mainly on the theoretical approach /Hakami et al. 2008/, cf. section on uncertainty due to precision and bias.

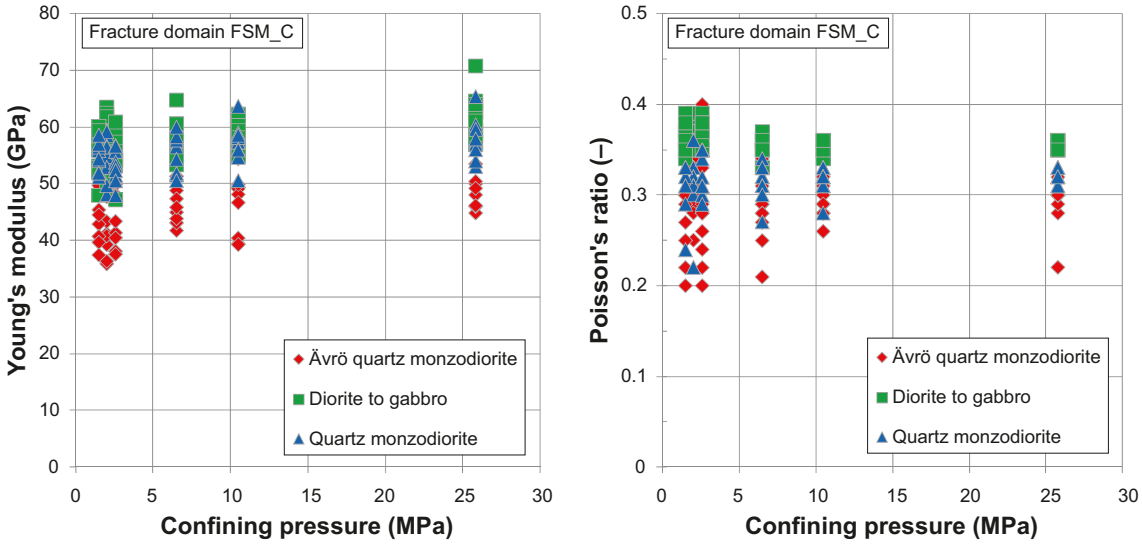

Figure A4-1. *Rock mass deformation modulus (left) and Poisson's ratio (right) evaluated at different levels of confining pressure by use of the theoretical approach in fracture domain FSM_C, data compiled from /Hakami et al. 2008, Tables A4-1 to A4-3, A4-5 to A4-7, A4-9 to A4-11, A4-13 to A4-15, A4-17 to A4-19 and A4-21 to A4-23/.*

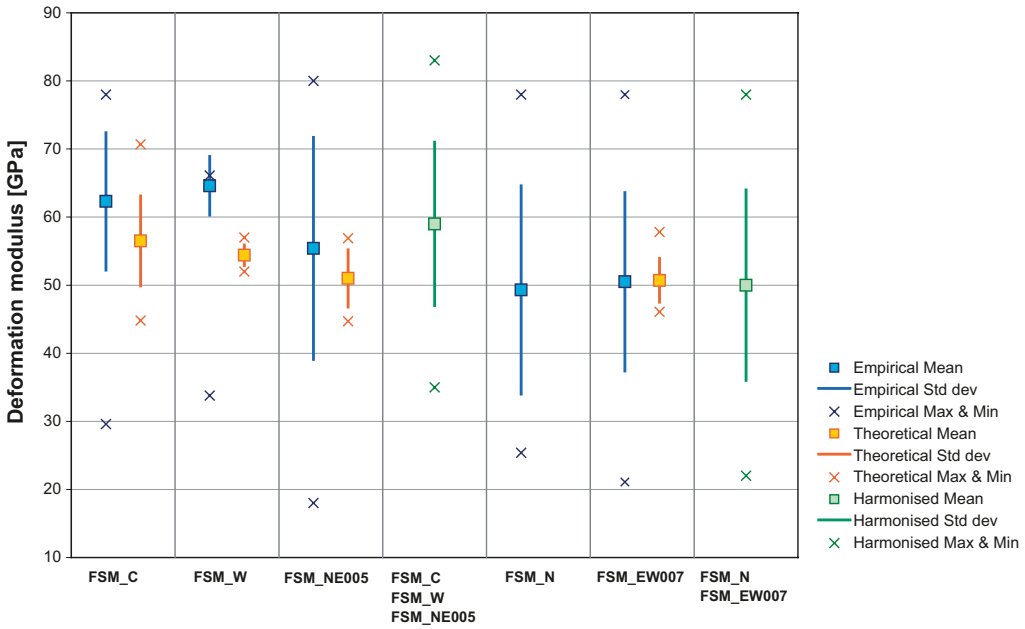

Figure A4-2. *Comparison between Young's modulus of the rock mass obtained by the empirical and theoretical approaches, from /Hakami et al. 2008, Figure 5-10/. Note that theoretical modelling of fracture domain FSM_N was not performed /SKB 2009b/.*

Mohr-Coulomb strength properties of fractures

The conceptual uncertainties relating to the lab-scale measurements of fracture strength properties are judged to be small. Uncertainties relating to scale effects are discussed in the subsection on uncertainty due to precision and bias (A4.6).

In situ stresses

The main conceptual uncertainty associated with hydraulic fracturing and hydraulic testing of pre-existing fractures (HTPF) methods is that in small-diameter boreholes (such as those used by SKB, it is assumed that the fracture orientation at the end of the test is the same as the measured orientation of the fracture at the injection-borehole wall /Martin 2007/.

Evolution of stress additions during a glacial cycle

The conceptual uncertainty associated with the evolution of the stress additions during a glacial cycle is judged to be large and is also, in comparison with uncertainties due to precision, bias and representativity, the largest uncertainty, see Section 6.4 in the SR-Site Data report /SKB 2010/ for a more extensive discussion. The uncertainties are related to the following:

- *The modelling approach:* /Lund et al. 2009/ do not consider the influence of tectonic strain, the shear impact of the ice, or thermo-mechanical effects during the glacial cycle. The total effect of the first two together is estimated to be at most 1 MPa /SKB 2010/. Estimates of the magnitude of the stress reductions due to the temperature reduction of the rock during permafrost conditions are made for the Forsmark site in the THM report /Hökmark et al. 2010/ and not quantified here.
- *The ice model:* SKB's reference ice model by Näslund /SKB 2006a/ is based on a reconstruction of the Weichselian glaciation. A different model of the latest glaciation /Lambeck 2005/ resulted in a thinner ice that covered the site for a much longer period in time than Näslund's ice. A comparison of the temporal evolution of the ice sheet thickness at Laxemar from the two models is shown in Figure A4-3. /Lund et al. 2009/ modelled the evolution of the glacially induced stresses due to Näslund's ice and found the magnitude of the horizontal stress components to be significantly smaller than the corresponding ones obtained by /Lambeck 2005/. /Lund et al. 2009/ attribute the higher stress magnitudes obtained from Lambeck's model to be a result of a combination of thinner lithosphere, lower upper mantle viscosity and longer duration of ice coverage.
- *The earth model*: /Lund et al. 2009/ consider a number of different earth models. Although there are quantitative differences in resulting stress magnitudes between these models, the temporal variations largely follow those of the ice model (Figure A4-3). In terms of fit to GPS data and sea level data, /Lund et al. 2009/ choose Model T9 (a horizontally stratified earth model) as their preferred model as its lithospheric elastic structure is in agreement with the Fennoscandian seismic investigation, cf. Section 6.4 in the SR-Site Data report /SKB 2010/. By inspection of the stress results /Lund et al. 2009, Figure 7-18/ during the last glacial advance and retreat (without considering results from the overly pessimistic Model 1), the glacially induced stresses from the different earth models appear to be within ±10 MPa of those from the preferred model (Model T9). The vertical stress is identical in all earth models and reflects the ice load, *i.e.* the thickness of the ice sheet.

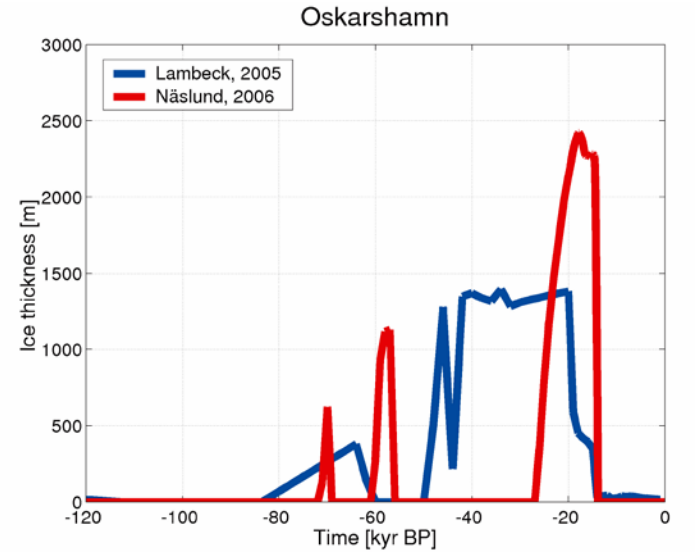

Figure A4-3. *Evolution of ice thickness at Laxemar from two different ice models, from /Lund et al. 2009/.*

Stress-transmissivity relations

The conceptual uncertainty associated with the stress-transmissivity relations is judged to be large and is also, in comparison with uncertainties due to precision, bias and representativity, the largest uncertainty, see the SR-Site Data report /SKB 2010/ for a more extensive discussion. The conceptual uncertainty is associated with:

- *The nature of stress-stiffness relations of individual fractures*: For the purpose of estimating the sensitivity of fracture transmissivities to variations in normal stress, the stress-dependence of the fracture normal stiffness is approximated by the continuously-yielding (CY) joint model /Itasca 2007/, cf. Section A4.8. Figure A4-4 (lower two rows) shows fracture normal stiffnesses at 1, 5 and 10 MPa estimated from stress-deformation plots in /Jacobsson and Flansbjer 2005a, b, 2006a, b/ with the CY model (straight lines) fitted to the data points. In the stress-range 1–10 MPa, there is reasonable agreement between the CY-model and the stress-stiffness data obtained from the measurements.
- *Estimates of the hydraulic aperture and fracture transmissivity*: The CY model does not account for a residual aperture, which is important at high normal stress (e.g. /Rutqvist and Tsang 2008/), and may therefore overestimate the joint normal closure at high normal stress. To account for this, an exponential expression suggested by /Liu et al. 2004/ is fitted to the hydraulic aperture. The relative transmissivity is calculated from hydraulic aperture assuming the cubic law to hold.
- Normal stiffness and hydraulic properties of individual fractures:
  - *Normal stiffness:* The tangent normal stiffness at a given level of normal stress is estimated from cyclic compression tests of core samples from Laxemar /Jacobsson and Flansbjer 2005a, b, 2006a, b/. Results from the laboratory scale tests are taken to be representative of fractures of all sizes, although, in reality, the normal stiffness may be scale-dependent In order to return a sample to a state that is representative for *in situ* conditions, several load-unload cycles are needed /Martin et al. 1990/. /Jacobsson and Flansbjer 2005a, b, 2006a, b/ performed two load-unload cycles at normal stress-levels up to 10 MPa, cf. Figure A4-4 (top row). Here, the CY-model parameters are evaluated after the second load cycle. By visual inspection of the graphs given in /Jacobsson and Flansbjer 2005a, b, 2006a, b/, it appears that the tangent normal stiffness, at a given level of normal stress, in the stress-range 1–10 MP does not vary in any significant way from the first unload cycle through the second load-unload cycle.
  - *Hydraulic properties:* /Hökmark et al. 2006/ concluded that fractures with high residual, or initial, apertures (i.e. high transmissivity) are less sensitive to variations in normal stress. This is supported by results from hydraulic jacking tests in borehole KLX02 at Laxemar described in e.g. /Rutqvist and Tsang 2008/ where it was found that pressure sensitivity was strongly dependent on the initial hydraulic permeability. The residual hydraulic aperture is not a parameter whose value can be estimated from present-day *in situ* transmissivity data presented in the site report, e.g. /Rhén et al. 2008/. By noting that there appears to be a trend of decreasing transmissivity values with depth, the residual aperture is here taken to be the average present-day hydraulic aperture at large depths (calculated from transmissivity values given by /Rhén et al. 2008/ through the cubic flow law).

Considering the uncertainties associated with the stress-transmissivity relations, it is not feasible to derive stress-transmissivity relations for individual fractures. Instead, two stress-transmissivity relations will be given: 1) One based on mean value fracture stiffness data to estimate the average response to variations in normal stress and 2) one based on fracture stiffness data that give an upper bound estimate to the sensitivity to variations in normal stress.

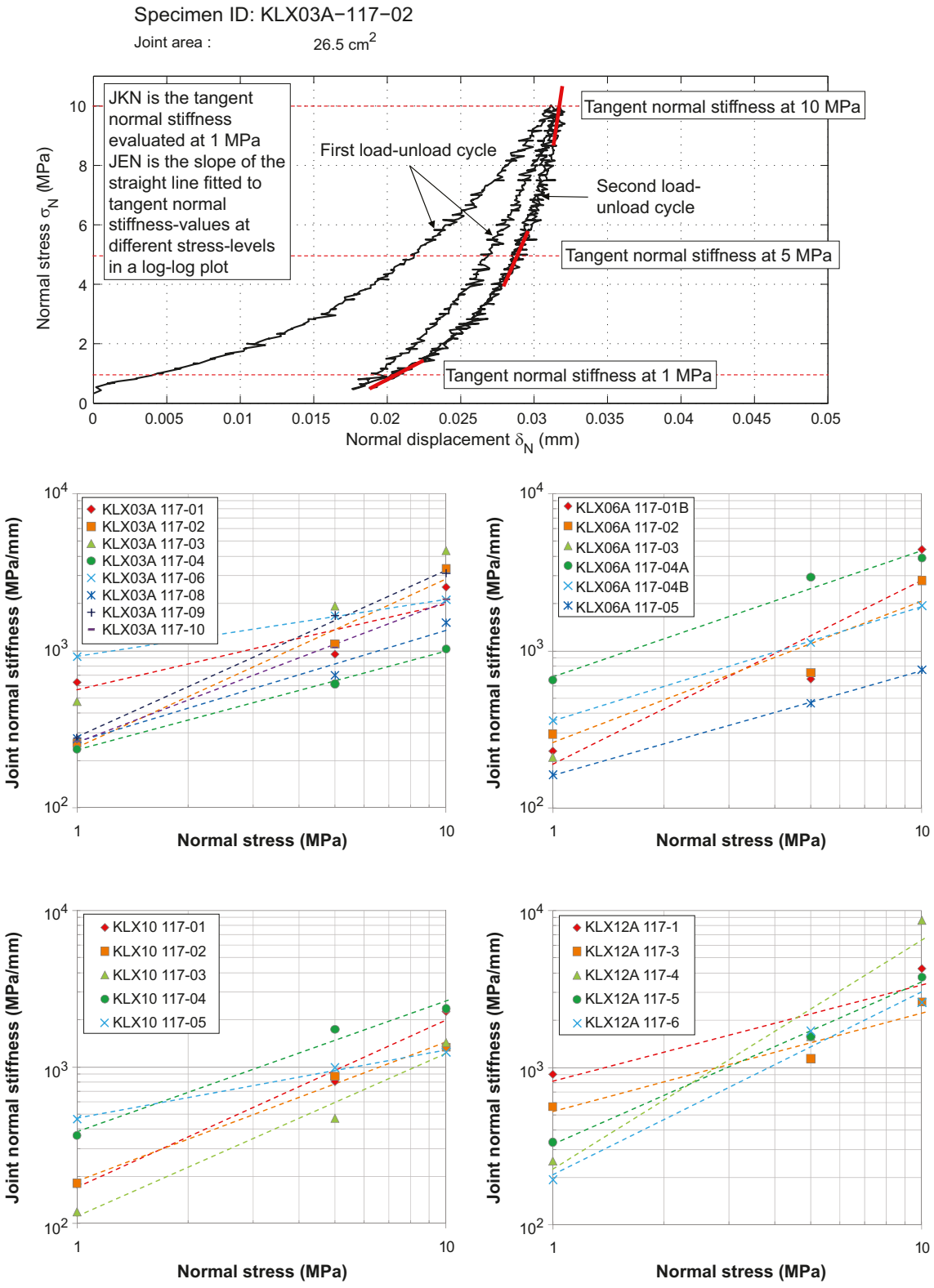

Figure A4-4. *Example of a cyclic loading compression test (top row), modified from /Jacobsson and Flansbjer 2005a/. CY model (straight lines) fitted to stress-stiffness estimates obtained from stress-deformation curves in /Jacobsson and Flansbjer 2005a, b, 2006a, b/. The value of JKN ranges between 119 and 918 MPa/mm (mean 367 MPa/mm); JEN ranges between 0.36 and 1.46 (mean 0.86).*

A4.6 Data uncertainty due to precision, bias, and representativity

Data uncertainty due to precision and bias

The following factors contribute to the uncertainty due to bias and apply for all rock mechanics parameters /SKB 2009a/:

- There could be directional bias, as most core samples were taken from sub-vertical boreholes.
- There is sparse data coverage in the southern subarea at Laxemar. Particularly for rock domain RSMM, there might be bias in the mechanical properties if samples from the available boreholes are not representative of the whole domain.

Strength properties of intact rock

The uncertainties due to precision and bias relating to the uniaxial compressive strength of intact rock are judged to be small based on the following:

- *Sampling strategy*: Samples were selected from all rock types expected to constitute more than 3% of the rock volume in each rock domain /Hakami et al. 2008/. For the most frequently occurring rock types a larger number of samples were taken /Hakami et al. 2008/. In total, 137 uniaxial tests were performed on core samples from 16 boreholes in the Laxemar local model area and at the Simpevarp peninsula together with 8 additional tests on samples containing sealed fractures /Hakami et al. 2008/. The number of tests was judged to be sufficient for reliable statistics, at least for the fresh and most frequent rock types, and the spatial distribution of sampling points (boreholes) was also adequate /Hakami et al. 2008/.
- *Altered rock*: /Hakami et al. 2008/ found that oxidisation leads to lower strength and saussuritisation leads to higher strength than unaltered rock, respectively. About 10% of rocks outside the deformation zones in rock domain RSMD01 and about 14% in rock domain RSMM01 are expected to be oxidised to some degree /Wahlgren et al. 2008/. For oxidised rock (Quartz monzodiorite and Ävrö quartz monzodiorite), /Hakami et al. 2008/ recommend that the mean values presented for *UCS* and crack initiation stress should be reduced by 7% and 8%, respectively.
- *Microcracking*: Observations of increasing slight core damage with depth were made based on microcrack volume determinations on samples from borehole KLX17A /Hakami et al. 2008/. However, this core damage did not appear to affect the strength of the samples as no depth trend was observed.
- *Interlaboratory differences*: Laboratory tests on core samples from borehole KSH01A located on the Simpevarp peninsula were performed by the Swedish National Testing and Research Institute (SP) /Jacobsson 2004/ and Helsinki University of Technology (HUT) /Eloranta 2004/. The results appear to be in good agreement, cf. Figure A4-5, although the sample population tested by HUT was significantly smaller (5 samples) than that tested by SP (20 samples of which 5 were discarded due to observed imperfections). Note that the results by /Eloranta 2004/ were not taken into account in the site model for Laxemar /Hakami et al. 2008/. A similar comparison was made on samples from Forsmark as part of the preliminary site description for that site. /Lanaro and Fredriksson 2005/ found that the mean uniaxial compressive strength determined by the two laboratories differed by about 5%.

No field experiments of the spalling strength of the rock types at Laxemar (other than APSE /Andersson 2007/) have been conducted. Therefore the uncertainty due to precision and bias cannot be quantified. However, /Andersson 2007/ suggested that the crack initiation stress could be used to assess the spalling strength. A correlation was found between the uniaxial compressive strength and the crack initiation stress /Hakami et al. 2008/. A few examples, for different rock types, are presented in Figure A4-6. For the tested samples, the ratio between crack initiation stress and uniaxial compressive strength was found to be in the range 0.52–0.57 /Hakami et al. 2008/. Therefore, the assumed lower bound spalling strength (52% of *UCS*, cf. Table A4-2) appears to be adequate.

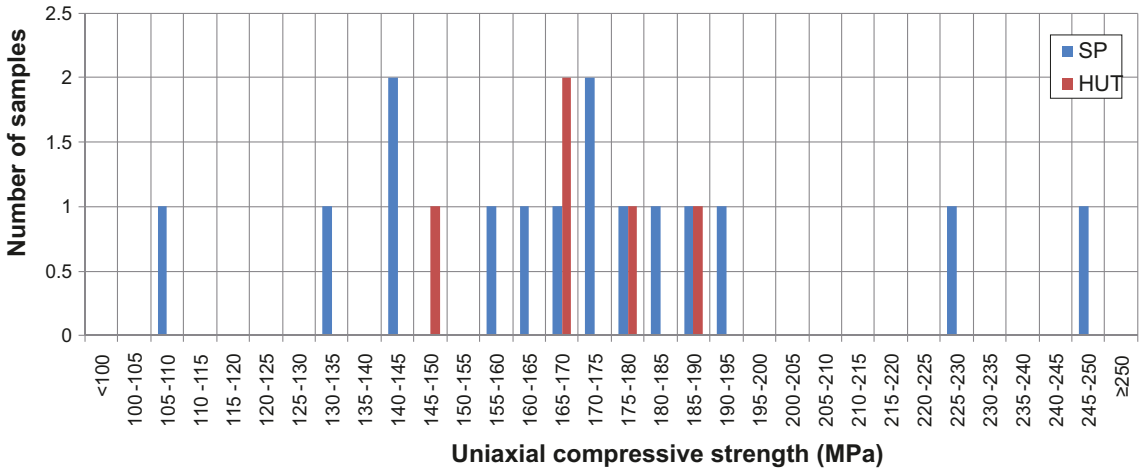

Figure A4-5. *Comparison between laboratory results of the uniaxial compressive strength from samples obtained from borehole KSH01A and tested at SP /Jacobsson 2004/ and HUT /Eloranta 2004/. Note that a further five samples were tested by SP. However, these were not considered representative of homogeneous rock due to observed imperfections (weakness zone, multiple cracks and failure in sealed fractures) /Jacobsson 2004/.*

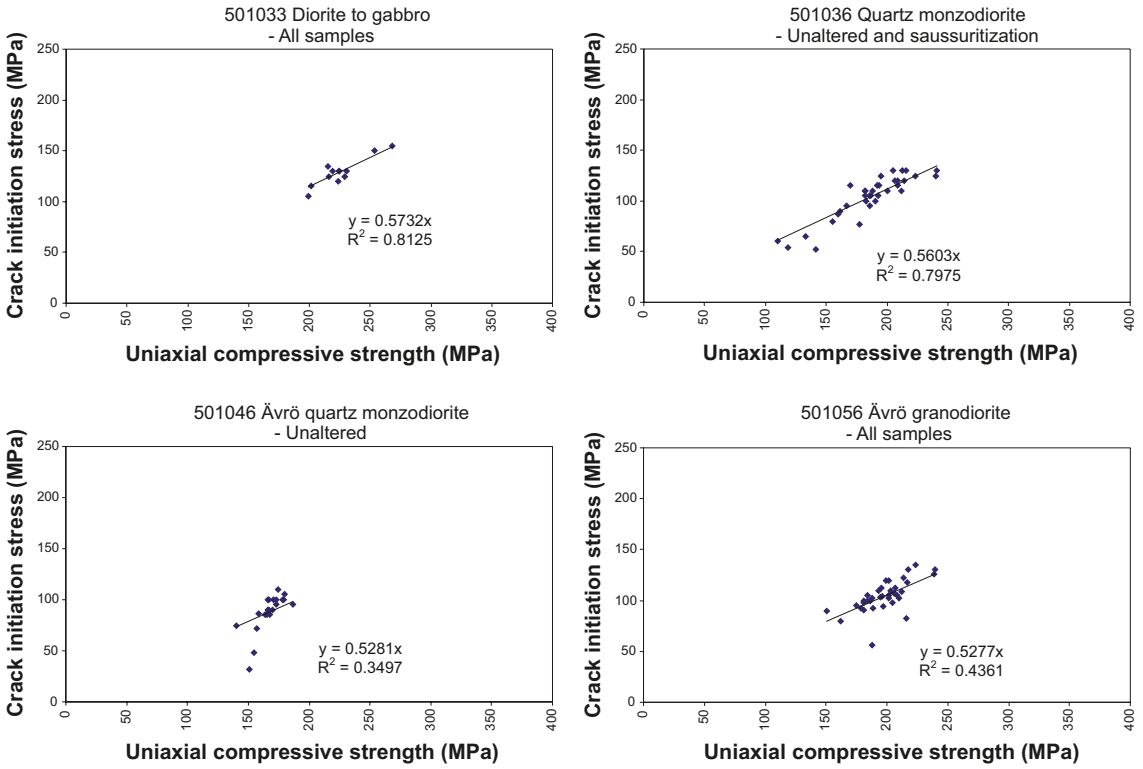

Figure A4-6. *Examples of correlations between UCS and crack initiation stress for different rock types, from /Hakami et al. 2008, Figure 3-10/.*

Elastic properties of rock mass

The elastic properties of the rock mass at Laxemar are based on harmonised results from two independent approaches /Hakami et al. 2008/, which are in reasonably good agreement with each other, cf. Figure A4-2. The harmonised value of the deformation modulus is based on results from both approaches with equal weighting. The value for Poisson's ratio based on the empirical approach is limited to that of intact rock, whereas the corresponding value based on the theoretical approach can be larger than that for intact rock /Hakami et al. 2008/. Therefore, the harmonised value for Poisson's ratio is based mainly on the theoretical approach. The estimates of the elastic properties from the theoretical approach do not include effects of deformation zones (including minor deformation zones). Therefore, the variation in mechanical properties may be underestimated /Hakami et al. 2008/.

Mohr-Coulomb strength properties of fractures

The Mohr-Coulomb strength properties are based on results from tilt tests and direct shear tests of fractures taken from drill core samples /Hakami et al. 2008/. There are significant differences in results from the tilt tests and the shear tests. However, results from the tilt tests are considered less reliable than corresponding ones from shear tests /Hakami et al. 2008/. Therefore, /Hakami et al. 2008/ recommend that results from the shear tests should be used as they are based on direct measurements at stress levels comparable with those expected at repository depth. As the tilt tests are more numerous (199 tests) compared with the shear tests (71 tests on open fractures), the former results have been used in the assessment of variability in the fracture properties /Hakami et al. 2008/. The following additional factors are also found to be contributing the uncertainties due to precision and bias /Hakami et al. 2008/, see also section on representativity:

- *Sampling strategy*:
  - Due to the small diameter of the drill cores, the fracture samples are biased towards smaller well-mated fractures (see corresponding sections on conceptual uncertainty and representativity).
  - The sampling for tilt tests was performed during the drill core logging. In order to ensure that different fracture orientations were represented in the sample population, fractures with a relative angle to its core axis in the range 0–30°, 30–60° and >60° were selected.
  - For the direct shear tests, samples were usually taken from gently dipping fractures or steeply dipping fractures with a small angle to the core axis. In the case of steeply dipping fractures, 2–3 samples could be taken from the same fracture.
  - No highly water-conductive fractures were among the tested population.
- *Scale effects*: It should be noted that the fracture properties relate to specimens of 50–60 mm in size. Large-scale properties are likely to deviate from lab-scale properties. It is likely that the shear strength will be reduced in magnitude compared with lab-results. Furthermore, it is possible that the properties of large-scale fractures will differ between fracture sets, although only insignificant differences were seen in the lab-scale tests, cf. also section on representativity.
- *Interlaboratory differences*: The tilt tests were performed at the Norwegian Geological Institute Laboratory (NGI), whereas the direct shear tests were performed at SP. No interlaboratory check has been made for samples from Laxemar. However, results from shear tests performed at NGI and SP of samples from Forsmark /Lanaro and Fredriksson 2005/ (see also the SR-Site Data report, Section 6.4 /SKB 2010/) indicated that the two laboratories might have different accuracy or testing procedures. For the Forsmark site, the shear test results obtained at SP were judged to best represent the fracture properties as they were more numerous and agreed well with the tilt tests /Lanaro and Fredriksson 2005, Glamheden et al. 2007/.

In situ stresses

The *in situ* stress model for Laxemar, i.e. initial pre-mining stress magnitudes and orientations, is based on direct and indirect results from the site investigation, as well as results from numerical modelling /Hakami et al. 2008/. In addition to the factors that apply for all rock mechanics parameters, the following factors are found to be contributing to the uncertainties due to precision and bias /Hakami et al. 2008/:

- For the direct measurements, only data from 1996 and onwards are used, which means that the quality of measurement procedures and documentation are well established.
- Overcoring data are usually ranked into categories depending on the quality or success of measurements. For the stress modelling, only data ranked Class A (highest confidence) and Class B (somewhat less confidence) were considered. Data points without ranking in SKB's database Sicada were assigned to Class B (data ranked Class C are not included in Sicada).
- For data from Äspö HRL, only measurement points located a minimum distance of 10 m from the excavations were considered to avoid influences by secondary stress fields from the openings.
- There are three boreholes (KLX02, KLX04 and KLX12A) in the Laxemar local model area where direct measurements have been made. Overcoring measurements were made in boreholes KLX04 and KLX12A, whereas hydraulic measurements were made in boreholes KLX02 and KLX12A. Of the three, KLX12A is the only borehole located entirely within the focused area and is also the only borehole where both overcoring measurements as well as hydraulic measurements have been made. For borehole KLX12A, there is reasonably good agreement between the results from the different methods.
- The hydraulic measurements were interpreted with the assumption that the principal *in situ* stresses are horizontal and vertical. Therefore, these methods do not give any information regarding the potential plunge in the stress field, cf. section on spatial variability. Estimates of the major horizontal *in situ* stress based on the HF method were not used due to low confidence in that approach.
- Observations of borehole breakouts give an estimate of the orientations of the horizontal stresses and, if breakouts are scarce, an upper limit of the expected stresses along the borehole, cf. Section A4.8. Due to the concentration of stresses around a borehole, the orientations of breakouts are expected to be perpendicular to the major horizontal *in situ* stress, cf. section on representativity. The confidence in the correlation between breakout orientation and in situ stress orientation is higher for vertical or sub-vertical boreholes. Borehole breakout data have been compiled from six boreholes at Laxemar, which are, with one exception (inclination around 54°), inclined between 75° and 85°. The occurrence of breakouts is limited and mostly observed at large depths and in subordinate rock types or in deformation zones.
- The amount of core disking in a borehole gives important indirect information to the stress modelling, as it is indicative of high stresses. The total extent of core disking at Laxemar is very limited and mostly observed at large depths.

Evolution of stress additions during glacial cycle

The following factors are found to be contributing to the uncertainties due to precision and bias:

- *The numerical code*: The code used in the modelling work has been extensively tested and verified and found to be in good agreement with other independent codes /Lund et al. 2009/.
- *The ice model*: SKB's reference ice model /SKB 2006a/ used in the modelling by /Lund et al. 2009/ is based on a reconstruction of the Weichselian glaciation. It is difficult to assess how well it would predict a future glaciation, cf. e.g Figure A4-3. However, there is no reason to believe that future ice sheets will be fundamentally different from previous Late Pleistocene Fennoscandian ice sheets /Lund et al. 2009/.
- *The earth model*: /Lund et al. 2009/ choose Model T9 (horizontally stratified earth model) as their preferred model in terms of fit to GPS data and sea level data and as its lithospheric elastic structure is in agreement with the Fennoscandian seismic investigation, cf. section on uncertainties due to representativity.

Stress-transmissivity relations

The uncertainties due to precision and bias are assumed to be large and stem from uncertainties in fracture mechanical and hydraulic data as well as uncertainties in the stress-aperture and transmissivity model. In terms of accurately estimating stress-induced transmissivity changes of individual fractures, precision is judged to be poor. However, for providing an upper bound estimate as well as a best estimate of the average sensitivity to stress changes of differently oriented fractures, it is judged that the stress-transmissivity relations provided by the CY-model and the exponential function /Liu et al. 2004/ (cf. Section A4.8) are adequate.

Data uncertainty due to representativity

Strength properties of intact rock

/Martin 2005/ suggested a spalling strength of 57 ± 2% of the uniaxial compressive strength (*UCS*) for coarse and medium grained crystalline rocks based on the findings from the Äspö Pillar Stability Experiment (APSE) /Andersson 2007/ and the Mine-by experiment /Martin 2005/, cf. Table A4-4. The spalling strength estimated for APSE appears to have been relevant for both the initial (non-heated) phase and the subsequent heated phase /Martin 2005/. Therefore, the proposed range in spalling strength (52–62% of *UCS*, cf. Table A4-2) appears to be representative for the excavation and operational phase and the heated phase of the initial temperate period.

Table A4-4. Estimates of spalling strength from the Äspö Pillar Stability Experiment (APSE) /Andersson 2007/ and the Mine-by experiment /Martin 2005/.

Experiment	Spalling strength (%)	Uncertainty span (%)
APSE	59	±3
Äspö Diorite		
Mine-by		
Lac du Bonnet granite	56	–
Granodiorite	65	–

Elastic properties of rock mass

The confidence in the rock mass mechanical properties within the fracture domains is high /Hakami et al. 2008/. The results from the empirical and theoretical approaches are in reasonably good agreement and indicate that the fracture domains can be divided into two groups with similar properties /Hakami et al. 2008/, cf. Figure A4-2. Note that the elastic properties given for the rock mass relate to the rock mass between interpreted deformation zones, i.e. the effects of deformation zones (including minor deformation zones) are not included in the estimates /Hakami et al. 2008/.

Mohr-Coulomb strength properties of fractures

The site model Mohr-Coulomb strength properties of fractures are representative for single open fractures in all fracture domains with the exception of sealed fractures and highly water-conductive fractures /Hakami et al. 2008/:

- Results from shear tests of sealed fractures that have been broken are similar to results from tests on open fractures.
- No mechanical tests were performed on highly water-conductive fractures. However, the cohesion and friction angle are estimated to be slightly lower than those given for non-conductive fractures.

In situ stresses

In the focused area at Laxemar, there are two boreholes with overcoring data – KLX04 and KLX12A /Hakami et al. 2008/. The data from KLX04 show a large spread in orientations (Figure A4-7, yellow triangles) and were suspected to be influenced by a deformation zone located not far from the measurement points in the borehole /SKB 2009b/. Therefore, the data from KLX12A (Figure A4-7, blue squares) were given more weight when selecting the most likely orientation value for the stress model /SKB 2009b/. However, both direct measurements and indirect observations indicate a general orientation of the major principal stress of 135±15° with respect to North (cf. Figure A4-7), which makes the confidence in the orientation of the major principal stress high /SKB 2009b/.

The overall uncertainty in the mean stress magnitudes is rather high /SKB 2009b/ due to the limited number of direct stress measurements within the focused volume and the fact that the area (or volume) where the stress model should apply is large, i.e. there is a risk that the measurements are not representative of the stresses in the domain as a whole. However, the confidence in the upper limit stress magnitudes is larger /SKB 2009b/ based on the fact that there are rather a large number of deep cored boreholes within the local model area but few observed borehole failures and that the two independent approaches (cf. Section A4.8), which have been applied to assess the upper limit of the *in situ* stresses give similar results.

Evolution of stress additions during glacial cycle

There is no reason to believe that future ice sheets will be fundamentally different from previous Late Pleistocene Fennoscandian ice sheets /Lund et al. 2009/. In the reference scenario /SKB 2006a/, the maximum thickness at Laxemar is around 2.5 km, cf. Figure A4-3. Based on modelling of the Saalian ice sheet the maximum ice sheet thickness at Laxemar (supported by geological observations) is 2,600 m; even for more extreme sensitivity cases it is unlikely to exceed 3,700 m /SKB 2006a/. This corresponds to an increase in thickness by about 7–50% compared with the reference case and an increase in vertical stress by about 1.5–11 MPa, as the vertical glacially induced stress reflects the ice load (e.g. /Lund et al. 2009/). Without explicit modelling work, it is difficult to estimate the impact on the magnitude of the horizontal stress components due to an ice sheet with larger thickness.

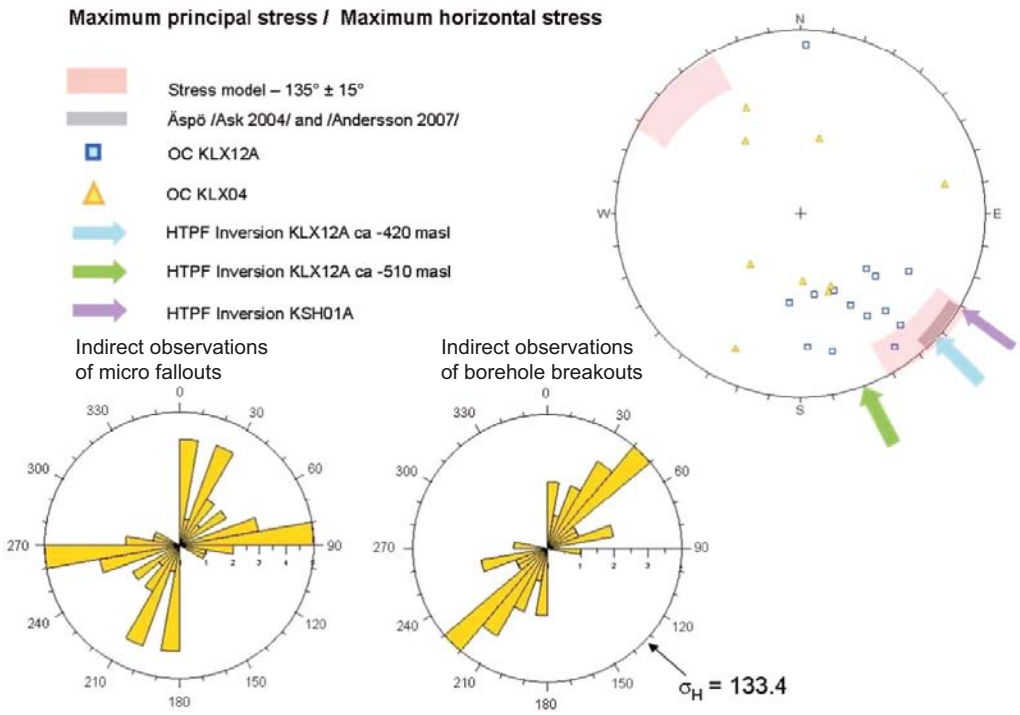

Figure A4-7. *Orientation of the major principal stress obtained from overcoring (OC) measurements and the major horizontal stress obtained from inversion of hydraulic testing on pre-existing fractures (HTPF) and indirect observations, modified from /SKB 2009b, Figure 11-12/.*

Stress-transmissivity relations

It should be noted that the stress-transmissivity relations become very uncertain as the effective normal stress approaches zero, i.e. at which the transmissivity becomes indefinite. Close to the repository openings, local transmissivity increases could be significant, e.g. because of shear displacements along fractures in very low compression. However, it is judged that for fractures in compression of a few MPa, the stress-transmissivity relations are relevant as upper bound estimates of the sensitivity to variations in effective normal stress.

It can easily be shown that the sensitivity to variations in normal stress is greatest for a combination of low values of both *JKN* and *JEN*. The distribution of *JKN* values (obtained from Figure A4-4) is shown in Figure A4-8 (left). The values of the normal stiffness vary between 119 and 918 MPa/mm with a seemingly higher proportion of samples with values in the lower part of the range although the sample population is quite small (24 samples). However, the results shown in Figure A4-8 (right) suggest that the value of *JEN* increases with decreasing values of *JKN*.

As there were no mechanical tests on highly water-conductive fractures at Laxemar /Hakami et al. 2008/, the stress-stiffness data presented here may, therefore, not be representative for these fractures. /Hakami et al. 2008/ refer to results from a (as of then unpublished) study by D. Mas Ivars and K.Norén in which shear-flow tests on samples from a highly water-conductive fracture at the APSE site (Äspö HRL) were made. The latter authors found that this fracture was about 10 times less stiff than the tested non-conductive fractures in the Laxemar boreholes. However, the highly water-conductive fractures only constitute a small fraction of the total open fractures at Laxemar /Hakami et al. 2008/.

Figure A4-9 (left) shows examples of stress-transmissivity relations obtained from hydraulic jacking tests in borehole KLX02 at Laxemar. However, the injection tests were carried out near high-flow zones of the borehole /Rutqvist and Tsang 2008/. Therefore, these stress-transmissivity relations may be representative of relatively permeable fractures /Rutqvist and Tsang 2008/. The two stress-transmissivity relations derived for Laxemar (Lax 1 and 2) in Figure A4-20 (right) are shown alongside the stress-transmissivity relation used in SR-Can /Hökmark et al. 2006/ in Figure A4-9 (right). /Rutqvist and Tsang 2008/ note that the stress-transmissivity relation used in SR-Can gave a similar response to variations in effective stress, i.e. in terms of a relative changes from a given stress-level, as the fractures at 266 m and 267 m. The “Lax 1” relation is based on lower-bound estimates of the CY-model parameters and also gives similar response to variations in effective stress as the fractures at 266 m and 267 m. The other relation (“Lax 2”) is based on mean value estimates of the CY-model parameters and gives similar response to variations in effective stress as the fractures at 315 m, 337 m and 338 m. A possible explanation for the sensitivity to variations in normal stress of the two fractures at 316 m and 336 m is that mineral filling would tend to clog the fractures at high normal stress /Rutqvist and Tsang 2008/.

A4.7 Spatial and temporal variability of data

Spatial variability of data

The rock at Laxemar is subdivided into rock domains and fracture domains as shown in Figure A4-10. In the focused area/volume, i.e. where a potential repository might be constructed, there are three main rock domains RSMA, RSMD and RSMM /SKB 2009b/ as indicated in the left figure. Furthermore, six fracture domains are recognised at the site: FSM_C, FSM_EW007, FSM_NE005, FSM_W, FSM_N and FSM_S /Wahlgren et al. 2008/ (Figure A4-10, right), of which the first four are located in the focused volume /SKB 2009b/.

Strength properties of intact rock

Figure A4-11 (upper left) shows locations of samples for and results of uniaxial compression tests in and around the Laxemar Local Area, cf. also Figure A4-10 (left). The right part of the figure shows the modelled distribution of the uniaxial compressive strength in each of the three main rock domains (RSMA01, RSMM01 and RSMD01). The modelling approach employed here is based on that for the thermal properties described in /Back and Sundberg 2007, Sundberg et al. 2008/, for details see /Hakami et al. 2008/. The modelled mean value *UCS* is of a similar magnitude in each of the three

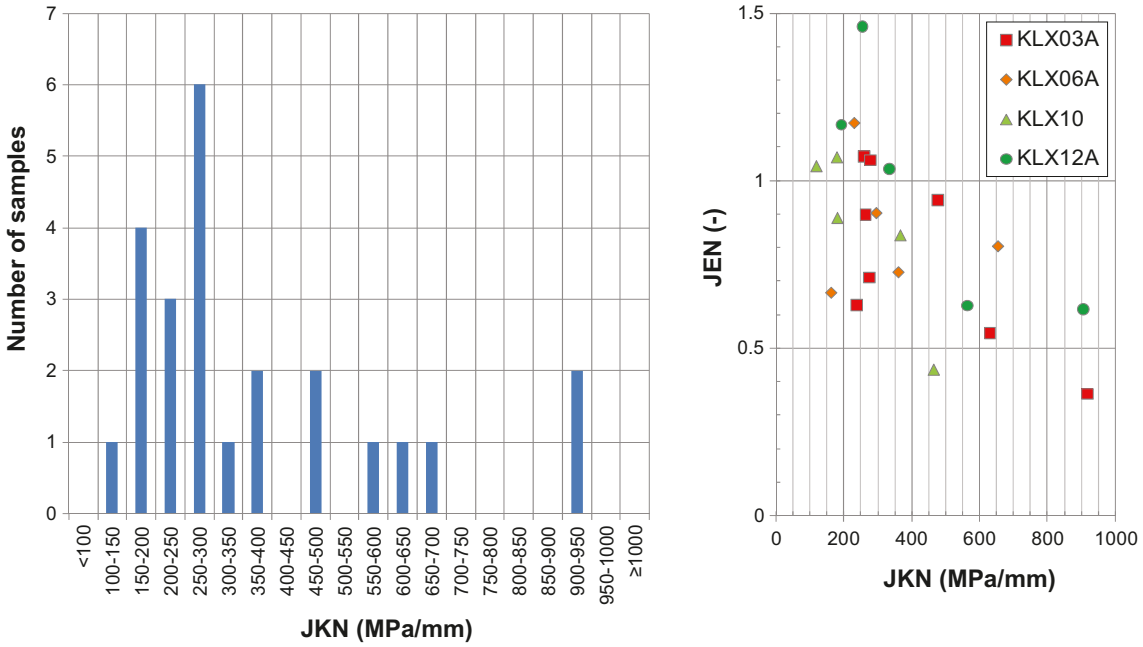

Figure A4-8. *Left: Distribution of JKN values obtained from the stress-stiffness estimates shown in Figure A4-6. Right: JEN as functions of JKN for each borehole in Figure A4-6.*

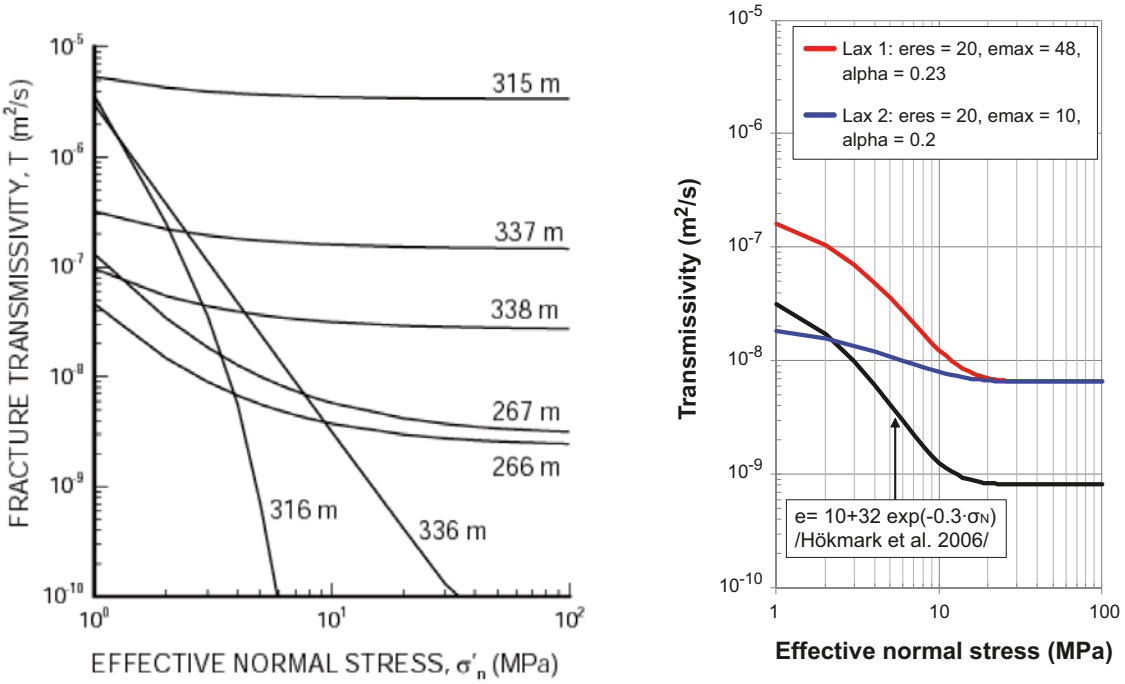

Figure A4-9. *Left: Example of stress-transmissivity relations estimated from hydraulic jacking tests in borehole KLX02 at Laxemar, from /Rutqvist and Tsang 2008, Figure 5.1-3/. Right: Stress-transmissivity relation based on the exponential expression suggested by /Liu et al. 2004/ used in SR-Can /Hökmark et al. 2006/ compared with corresponding relations derived for Laxemar in Figure A4-20 (right).*

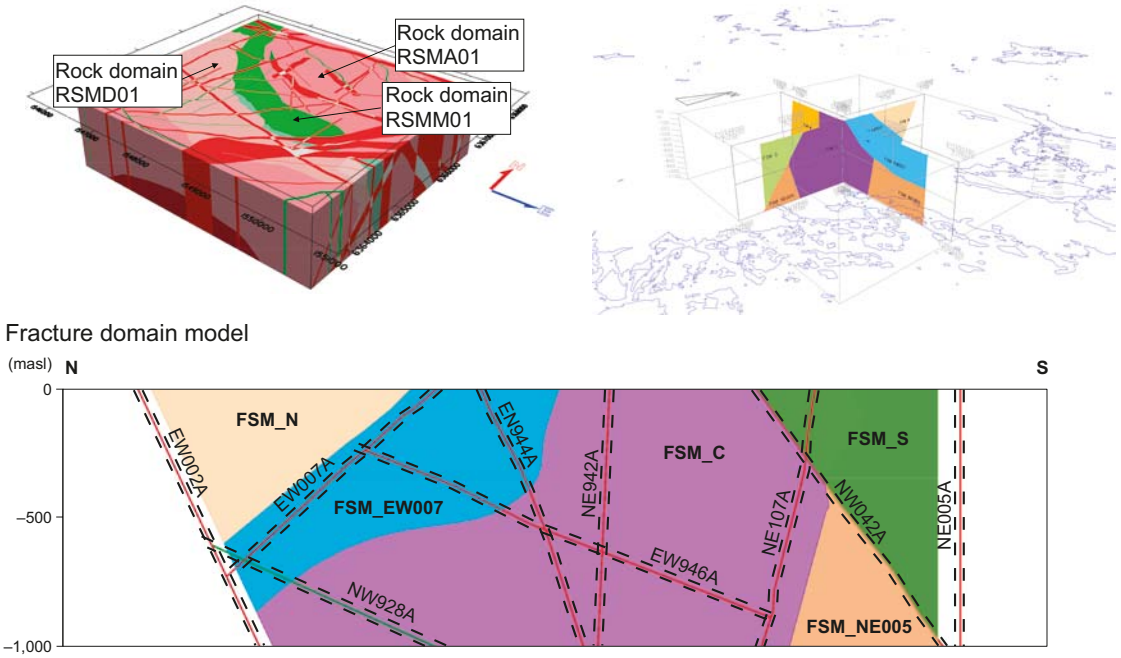

Figure A4-10. *Left: 3D view of rock domains in the Local model volume at Laxemar, modified from /SKB 2009b, Figure 5-61/. Right and lower: View of the fracture domains in the Local model volume, from /Wahlgren et al. 2008 (Figure 6-12), SKB 2009b (Figure 11-18)/. Fracture domains FSM_C, FSM_EW007, FSM_NE005 and FSM_W are located in the focused volume.*

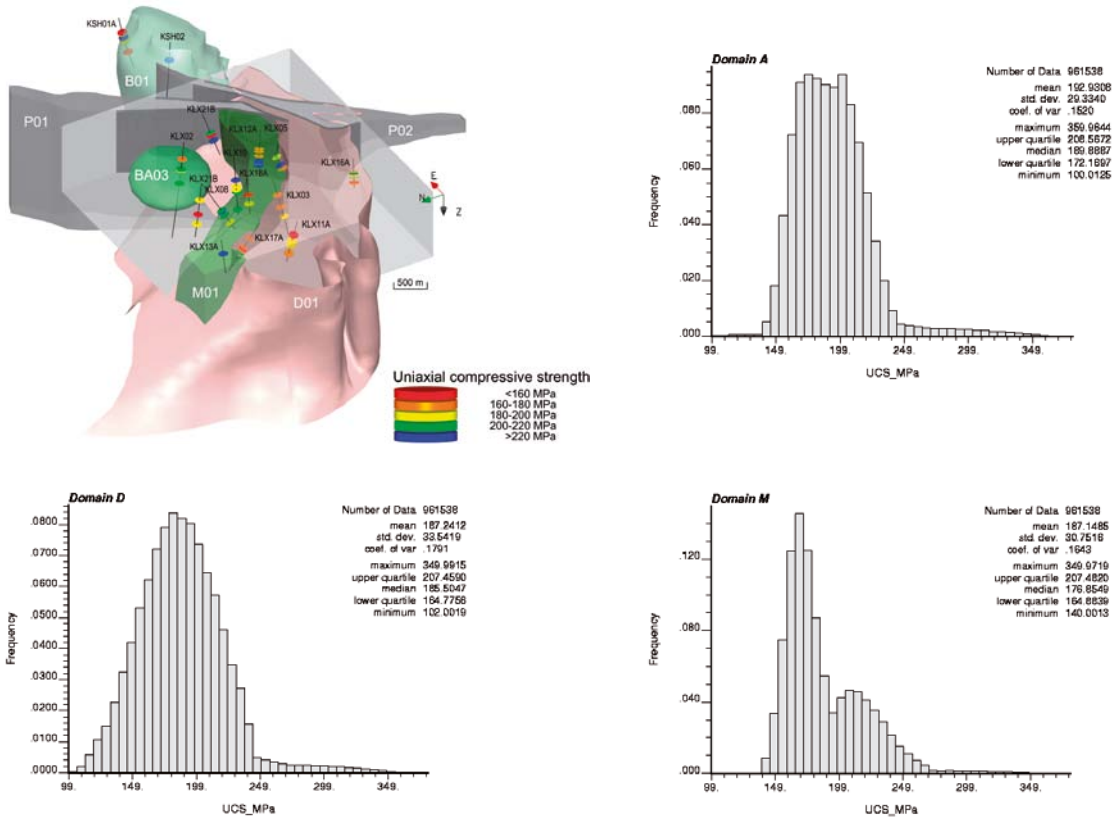

Figure A4-11. *Upper left: Locations of samples for and results of uniaxial compression tests in and around the Laxemar Local Area (grey box), from /SKB 2009b, Figure 7-1/. Note that fracture domain RSMA01 is made transparent. Lower left and right column: Distributions of uniaxial compressive strength in rock domains RSMA01, RSMM01 and RSMD01, from /Hakami et al. 2008, Figures A8-16 and A8-17/.*

rock domains /Hakami et al. 2008/. However, rock domain RSMD01 has a higher proportion of rock with low uniaxial strength. The lower tails of rock domains RSMA01 and RSMM01 is associated with Ävrö quartz monzodiorite , whereas the lower tail in rock domain RSMD01 is dominated by fresh and altered quartz monzodiorite /Hakami et al. 2008/. Note that the distributions given in Figure A4-11 are rather uncertain due to few data; in particular the tails of the distributions are influenced by the truncation levels /Hakami et al. 2008/.

There appears to be slight reduction in strength with for Ävrö granite, which could be explained by damaged samples due to drilling in rock with higher *in situ* stresses /Hakami et al. 2008/. However, there is a clear spatial variation, which makes the depth-trend uncertain /Hakami et al. 2008/.

Elastic properties of the rock mass

Due to availability of data, rock mass properties are evaluated for all fracture domains with the exception of fracture domain FSM_S /Hakami et al. 2008/. The variations in parameter values between the five fracture domains can be seen in Figure A4-2. Based on the results from the empirical and theoretical approaches, it was found that the fracture domains could be combined into two groups each with similar properties /Hakami et al. 2008/: One group comprises fracture domains FSM_C, FSM_W and FSM_NE005 and the other comprises fracture domains FSM_N and FSM_EW007. The expected spatial variation of each parameter within a given rock domain group is given by a truncated normal distribution /Hakami et al. 2008/, cf. Figure A4-12.

Mohr-Coulomb strength properties of fractures

Data from tilt tests and shear tests were each grouped into fracture sets according to the geological DFN model of Laxemar /La Pointe et al. 2008/ and plotted versus depth. Data that could not be assigned to any fracture sets because sampling took place outside the fracture domains, i.e. in Simpevarp, were assigned ‘not assigned’. /Hakami et al. 2008/ found that the data were so scattered that no clear trend with depth or between fracture sets could be distinguished.

In situ stresses

The measurement data and large-scale numerical model /Hakami et al. 2008/ indicated that there may be variations in stresses depending on location in the region /SKB 2009b/. For example, the stress measurements at Ävrö and Simpevarp indicate lower stress magnitudes than at Äspö HRL /SKB 2009b/. Therefore, differences between the Laxemar fracture domains, Simpevarp, Ävrö and Äspö can be expected /SKB 2009b/, although it is uncertain how large the differences are. A possible explanation

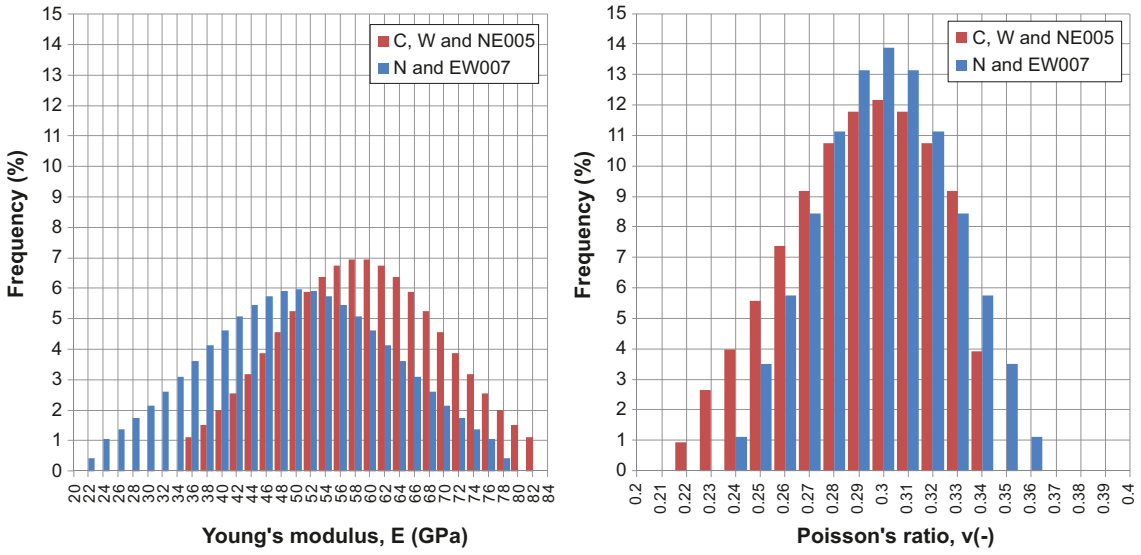

Figure A4-12. *Distribution of rock mass Young’s modulus (left) and Poisson’s ratio (right) in given fracture domains, data compiled from /Hakami et al. 2008, Table 5-11/. The width of each bar is the given value ±1 GPa for Young’s modulus and ±0.005 for Poisson’s ratio.*

for the differences is the distance between the measurement sites as well as the major deformation zones separating them /SKB 2009b/. Figure A4-13 shows the measured stress magnitudes as functions of depth in the Laxemar local model area (boreholes KLX04 and KLX12A) compared with corresponding measurements at Simpevarp, Äspö HRL and Oskarshamn. Table A4-5 shows a comparison between the best-estimate back-calculated stress magnitudes at the APSE site in Äspö HRL /Andersson 2007/ and the proposed stress model for Laxemar /Hakami et al. 2008/ at 450 m depth.

Results from numerical modelling support measurement data that some redistribution of the *in situ* stresses due to the major deformation zones in the area is to be expected /Hakami et al. 2008/. However, the variation should not be more than about ± 4 MPa in the focused volume, i.e. that defined by fracture domains FSM_C, FSM_W and FSM_NE005 /Hakami et al. 2008/, cf. Figure A4-10 (right). On the scale of single overcoring measurements, the stresses may vary by about 12% around the mean value due to fracturing /Hakami et al. 2008/.

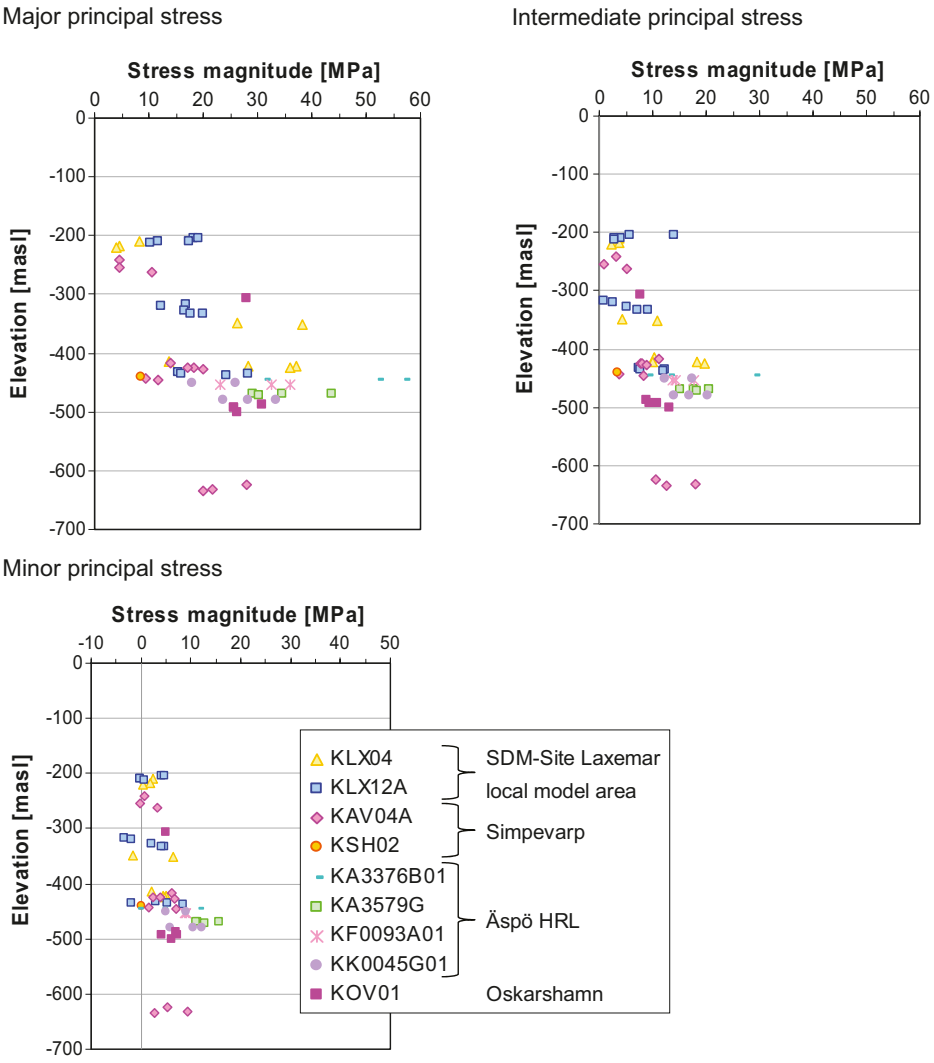

Figure A4-13. *Principal stress magnitudes obtained from the overcoring method in the Oskarshamn area as functions of depth, modified from /Hakami et al. 2008, Figure 6-4/.*

Table A4-5. Comparison between the best estimate back-calculated stress magnitudes at the APSE site in Äspö HRL /Andersson 2007/ and the proposed stress model for Laxemar /Hakami et al. 2008/ at 450 m depth.

Stress model	*σH* (MPa)	*σh* (MPa)	*σv* (MPa)
Äspö (APSE site)	30	10	15
Laxemar	20.6	10.9	12.2

As with the stress magnitudes (Figure A4-13), there is significant scatter in the orientations of the principal stresses, cf. Figure A4-13, although most measurements indicate that the major principal stress is reasonably horizontal /Hakami et al. 2008/. The numerical modelling indicates that the major principal stress (σ_1) may vary in orientation by ±9° due to discrete fractures /Hakami et al. 2008/. For the measurements in the two boreholes at Laxemar (Figure A4-14, left), there is a clear trend of the major principal stress in the NW-SE direction /Hakami et al. 2008/. The back-calculated orientation of the major principal stress (trend 310° in the Äspö96 coordinate system and zero plunge) at the APSE site in Äspö HRL /Andersson 2007/ is consistent with the measurements at Laxemar.

Evolution of stress additions during glacial cycle

On a large scale, there are large spatial variations in ice thickness, cf. Figure A4-15 (left). The spatial variations also vary with time. However, the ice model has a resolution of 50×50 km /Lund et al. 2009/. Any lateral spatial variations of the glacially induced stresses at the Laxemar site are unlikely to be of any relevance.

Figure A4-15 (right) shows the temporal evolution (note that the time scale is reversed compared with previous figures) of the glacially induced stresses evaluated at two different depths: 500 m and 1.5 km. In this depth-range the variations with depth are insignificant.

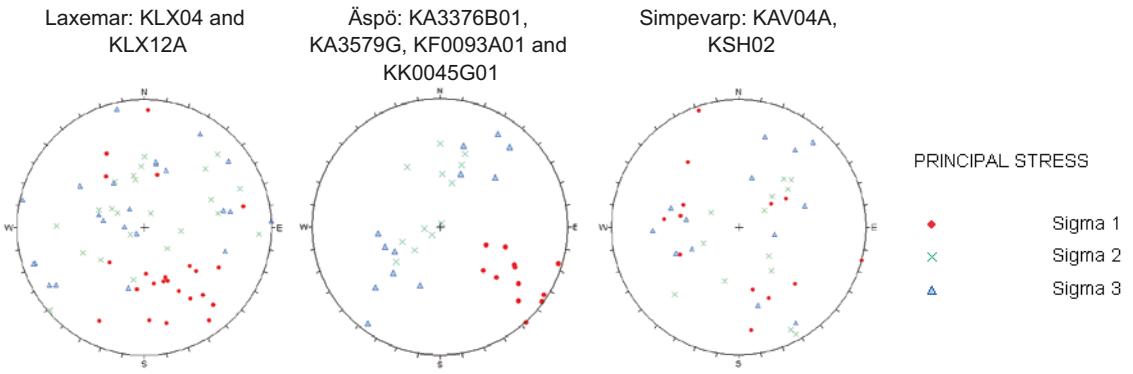

Figure A4-14. *Stereographic plots of principal stress orientations obtained from the overcoring method in given boreholes at Laxemar (left), Äspö (middle) and Simpevarp (right), from /Hakami et al. 2008, Figure 6-5/.*

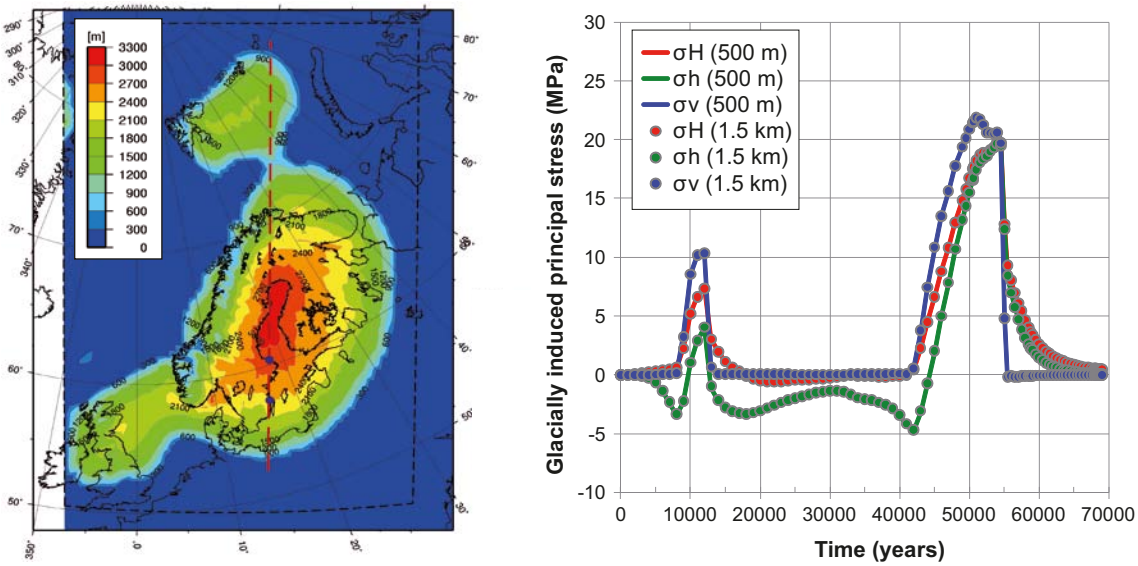

Figure A4-15. *Left: Height of the ice sheet at 18.4 kyr BP when the ice has its largest lateral extent, modified from /Lund et al. 2009, Figure 4-1/. Right: Temporal development of the glacially induced principal stresses at 500 m and 1.5 km depth at Laxemar, obtained from ice-crust-mantle analyses (model T9) performed by /Lund et al. 2009/.*

Stress-transmissivity relations

Figure A4-16 (left) shows values of *JKN* as functions of depth in boreholes KLX03A, –06A, –10 and –12A. The depth is estimated from the average value of the upper and lower (Secup and Seclow) sampling depths /Jacobsson and Flansbjer 2005a, b, 2006a, b/. The right part of the figure shows the corresponding values of *JEN* as functions of depth. No clear trend with depth or between boreholes can be observed in either of the two parameters.

Data for the joint roughness coefficient (***JRC***) obtained from tilt tests /Hakami et al. 2008/ were each grouped into fracture sets according to the geological DFN model of Laxemar /La Pointe et al. 2008/ and plotted versus depth. Data that could not be assigned to any fracture sets because sampling took place outside the fracture domains, i.e. in Simpevarp, were assigned 'not assigned'. /Hakami et al. 2008/ found that the data were so scattered that no clear trend with depth or between fracture sets could be distinguished.

Temporal variability of data

Deformation properties of the rock

Within the temperature range 0–150° the temperature dependence of elastic properties is negligible /Lau et al. 1991/.

/Hakami et al. 2008/ evaluated the rock mass deformation modulus and Poisson's ratio at different levels of confining pressure (cf. Figure A4-1) and found that, in the stress-interval 1.5–26 MPa, the stress-dependence was small.

Spalling strength

/Damjanac and Fairhurst 2010/ found that the long-term strength of intact rock without any pre-existing fractures should be equal to or greater than the crack initiation strength (40–60% of the compressive strength).

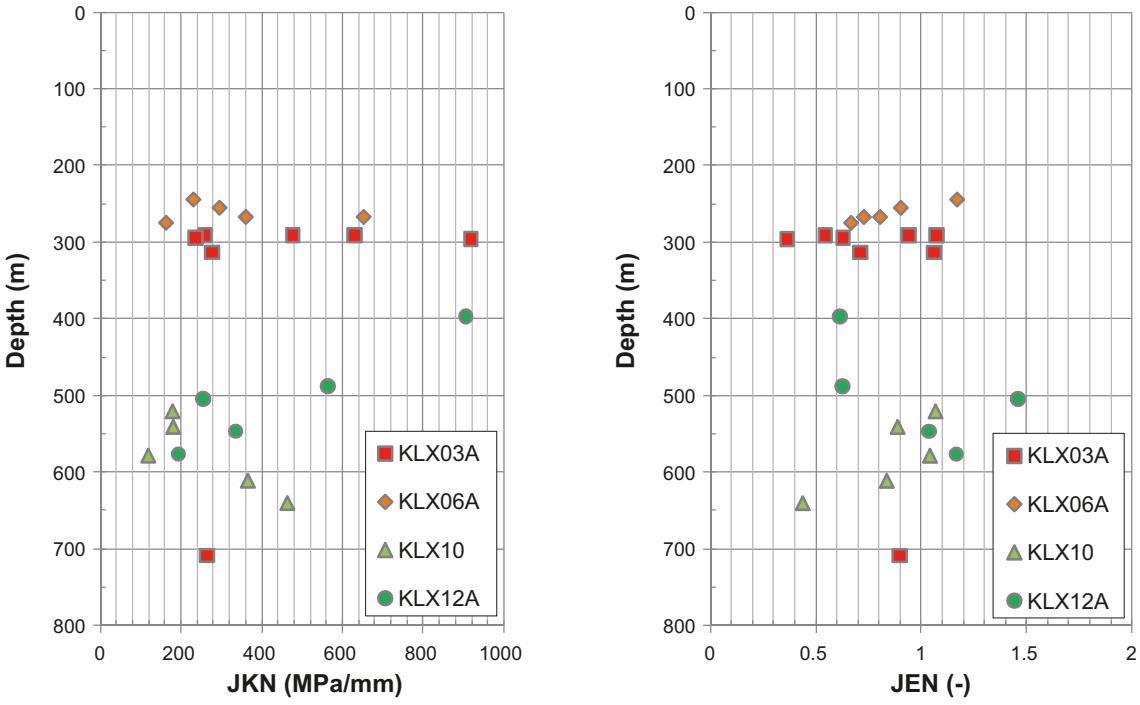

Figure A4-16. *Estimated values of JKN (left) and JEN (right) as functions of depth. Stress-stiffness data obtained from normal stress/normal deformation plots in /Jacobsson and Flansbjer 2005a, b, 2006a, b/.*

Mohr-Coulomb strength properties of fractures

The shear strength of a fracture depends on the normal stress. Direct shear tests were performed at three levels of normal stress, 0.5, 5 and 20 MPa /Hakami et al. 2008/. The Mohr-Coulomb strength properties (peak cohesion and peak friction angle/residual cohesion and residual friction angle) were determined by a least squares fit to the measured peak/residual shear stresses at the three levels of normal stress /Hakami et al. 2008/. The cohesion and friction angle do not vary with time or load.

In situ stresses

The present-day *in situ* stresses are taken to be representative of the long-term state of background stress in the Laxemar area. The changes in stress due to the still ongoing post-glacial rebound and the tectonic strain induced by the Mid-Atlantic ridge push /Muir Wood 1995/ are significantly smaller in magnitude than the thermal stresses induced by the deposited nuclear waste and stresses generated by the ice load during the subsequent glacial phase. Therefore any temporal variations in the *in situ* stresses are ignored.

Evolution of stress additions during glacial cycle

The temporal variations of the glacially induced stress additions 500 m below the ground surface at Laxemar are presented in Figure A4-15 (right). Although quantitatively the stress magnitudes depend on the earth model, the temporal variations largely follow those of the ice model (cf. Figure A4-3) /Lund et al. 2009/.

Stress-transmissivity relations

The stress-transmissivity relations give estimates of changes in transmissivity due to the loading and unloading of fractures that take place during the time-frame of the safety assessment. As there are no data to suggest otherwise, the stress-transmissivity relations are taken to be relevant for both the initial temperate phase and the glacial phase.

A4.8 Correlations used in data qualification

In situ stresses

An upper limit for the *in situ* stresses at repository depth (400–700 m) is assessed by use of two failure criteria /Hakami et al. 2008/: 1) an empirical criterion (Equation A4-1) employed in the Forsmark site investigation /Martin 2007/, and 2) the Mogi-Coulomb failure criterion (Equation A4-2) /Al-Ajmi and Zimmerman 2006/. In both criteria, the ratio between major and minor horizontal stress, σ_H/σ_h, was set to 3.7 based on the stress ratio at 500 m depth in the previous site model for Laxemar /SKB 2006b/.

The upper limit of stresses, based on the analyses of borehole stability, was used as a guide for selecting the uncertainty span of the stress model /Hakami et al. 2008/. The upper truncation limit of the *in situ* stresses was selected based on the upper limit stresses obtained from the Mogi-Coulomb criterion /Hakami et al. 2008/.

Empirical:
$$3\sigma_H - \sigma_h \geq UCS \cdot SR \qquad \text{A4-1}$$

Mogi-Coulomb:
$$(A+B)^2 - 3(A \cdot B) = (a + b \cdot A)^2, \text{ where}$$
$$A = 3\sigma_H - \sigma_h$$
$$B = \sigma_v + 2\nu(\sigma_H - \sigma_h) \qquad \text{A4-2}$$
$$a = 2c\cos(\varphi),\ b = \sin(\varphi)$$

Here, *UCS* is the uniaxial compressive strength of intact rock, *SR* is the spalling ratio (set to 0.56 based on suggestion by /Martin 2007/), υ is Poisson's ratio, σ_H, σ_h and σ_v are the three principal stress components and c and φ are cohesion and friction angle, respectively, obtained from triaxial testings at appropriate levels of confinement /Hakami et al. 2008/.

Stress-transmissivity relations

In the CY model, the relation between fracture stiffness and normal stress (σ_N) is defined as

$$K_N = JKN \cdot \sigma_N^{JEN} \quad \text{A4-3}$$

where *JKN* and *JEN* are a model parameters. *JKN* is defined as the tangent normal stiffness evaluated at 1 MPa, whereas *JEN* is the slope of straight lines fitted to stress-stiffness data in a log-log plot, cf. Figure A4-4.

The mechanical aperture (E) at a normal stress of σ is given by Equation A4-4, where the initial aperture is E_0 at a normal stress of σ_0. The hydraulic aperture (e) is estimated using an empirical relationship (Equation A4-5) /Barton 1982/ that relates the mechanical aperture (E (μm)) and hydraulic aperture (e (μm)) through the Joint Roughness Coefficient (*JRC*). The initial mechanical aperture, E_0, is estimated from Equation A4-5 using the reported mean value of JRC_0 /Hakami et al. 2008, Table 4-2/ and assuming that the corresponding hydraulic aperture is equal to the residual hydraulic aperture, e_r.

$$E = E_0 + \Delta E = E_0 - \frac{1}{JKN}\int_{\sigma_0}^{\sigma} \sigma'^{-JEN}\, d\sigma' \quad \text{A4-4}$$

$$e = \min\left(E, \frac{E^2}{JRC_0^{2.5}}\right) \quad \text{A4-5}$$

To account for a residual aperture, an exponential expression suggested by /Liu et al. 2004/ is fitted to the hydraulic apertures calculated from Equations A4-4 and A4-5. The exponential expression is given by Equation A4-6:

$$e = e_r + e_{\max} \exp(-\alpha \cdot \sigma_N) \quad \text{A4-6}$$

Here, e_r is the residual aperture and σ_N the effective normal stress, whereas e_{max} and α are model parameters. The relative transmissivity, T/T_0, is subsequently calculated from Equation A4-6 assuming the cubic law to hold:

$$T / T_0 = \left(e / e_0\right)^3 \quad \text{A4-7}$$

Here, e_0 is the hydraulic aperture at the reference effective normal stress σ_0.

A4.9 Result of supplier's data qualification

Strength properties of intact rock

The strength properties of intact rock for the main and subordinate rock types at Laxemar /Hakami et al. 2008/ are presented in Table A4-6. For oxidised rock (applies to Quartz monzodiorite and Ävrö quartz monzodiorite), the mean uniaxial compressive strength should be reduced by 7% and the mean crack initiation stress should be reduced by 8% /Hakami et al. 2008/. The variation of the UCS for each rock type is given as a truncated normal distribution with mean value, min–max truncation values and standard deviation based on results from the tested samples /SKB 2009b/.The uncertainty of the mean value is quantified for a 95% confidence interval /Hakami et al. 2008/.

The uniaxial strength of intact rock in each rock domain is presented in A4-7. For the distribution of values in each rock domain, see Figure A4-11.

Spalling is assumed to occur when the tangential stresses around an opening exceed a certain fraction of the uniaxial compressive strength (*UCS*). /Martin 2005/ suggested a spalling strength of 57 ± 2% of the *UCS* for coarse and medium grained crystalline rocks. Based on the estimates by /Martin 2005/ and values of the crack initiation stress presented in Figure A4-6 the spalling strength is assumed to be 57±5% of the *UCS*. Spalling strengths of intact rock in the three main rock domains RSMA01, RSMM01 and RSMD01 as well as for the main and subordinate rock types (cf. Table A4-6 and Table A4-7) are presented in Table A4-8.

Table A4-6. Strength properties of main and subordinate rock types /Hakami et al. 2008, Table 3-9/.

Parameter	501030 Fine-grained dioritoid	501033 Diorite/ gabbro	501036 Quartz monzodiorite, Unaltered	501046 Ävrö quartz monzodiorite, Unaltered	501056 Ävrö granodiorite	511058 Fine-grained granite
	Mean/stdev Min–Max *Uncertainty of mean*	Mean/stdev Min–Max *Uncertainty of mean*	Mean/stdev Min–Max *Uncertainty of mean*	Mean/stdev Min–Max *Uncertainty of mean*	Mean/stdev Min–Max *Uncertainty of mean*	Mean/stdev Min–Max *Uncertainty of mean*
Uniaxial compressive strength, UCS (MPa)	239/72 100-360 ±16%	225/20 200-270 ±5%	186/30 110-240 ±5%	167/11 140-190 ±3%	198/19 150-240 ±3%	280/45 210-350 ±11%

Table A4-7. Strength properties of intact rock in each rock domain /Hakami et al. 2008, Table 3-13/, cf. Figure A4-11.

Rock domain	Uniaxial compressive strength, *UCS* (MPa)	
	Mean	Stdev
RSMA01	193	29
RSMM01	187	31
RSMD01	187	34

Table A4-8. Estimated spalling strength (57±5% of mean *UCS*) of intact rock in rock domains RSMA01, RSMM01 and RSMD01 and of the main and subordinate rock types, cf. Table A4-6 and Table A4-7.

Rock domain	Spalling strength (MPa)
RSMA01	110±10
RSMM01	107±9
RSMD01	107±9
Rock type (rock type code)	Spalling strength (MPa)
Fine-grained dioritoid (501030)	136±12
Diorite/ gabbro (501033)	128±11
Quartz monzodiorite, Unaltered (501036)	106±9
Ävrö quartz monzodiorite, Unaltered (501046)	95±8
Ävrö granodiorite (501056)	113±10
Fine-grained granite (511058)	160±14

Elastic properties of the rock mass

The elastic properties of the rock mass in the different fracture domains /Hakami et al. 2008/ are presented in Table A4-9. Based on the results from the empirical and theoretical approaches, it was found that the fracture domains could be combined into two groups each with similar properties /Hakami et al. 2008/, cf. Figure A4-2. The expected spatial variation of each parameter within given rock domain groups is given by a truncated normal distribution (Figure A4-12) with mean, min–max truncation values and standard deviations as given in Table A4-9. The uncertainty of the mean values is based on differences between the empirical and theoretical approaches and a general confidence of the approaches for each parameter /Hakami et al. 2008/. Note that these values do not include effects due to minor deformation zones (MDZ's) /Hakami et al. 2008/.

Mohr-Coulomb strength properties of fracture

The Mohr-Coulomb strength properties of fractures reported in /Hakami et al. 2008/ are based on laboratory results from tilt tests and direct shear tests of discrete fractures and are expected to represent the majority of single open fractures, cf. Table A4-10. The uncertainties are expressed statistically as a range of variation in the evaluated mean values and quantified for a 95% confidence

Table A4-9. Rock mass properties in fracture domains FSM_C, FSM_W, FSM_NE005, FSM_N and FSM_EW007 /Hakami et al. 2008, Table 5-11/.

Parameters	Unit	FSM_C, FSM_W and FSM_NE005 Mean/std. dev Min–max *Uncertainty of mean*	FSM_N and FSM_EW007 Mean/std. dev Min–max *Uncertainty of mean*
Young's modulus (*E*)	GPa	59/12	50/14
		35–83	22–78
		±3%	±3%
Poisson's ratio (v)	–	0.3/0.04	0.3/0.03
		0.22–0.34	0.24–0.36
		±10%	±10%

Table A4-10. Mohr-Coulomb strength properties of single open fractures in all fracture domains at Laxemar, from /Hakami et al. 2008, Table 4-14/.

Peak friction angle ϕ_p (°) Mean/std. dev. Min–max *Uncertainty of mean*	Peak cohesion c_p (MPa) Mean/std. dev. Min–max *Uncertainty of mean*	Residual friction angle ϕ_r (°) Mean/std. dev. Min–max *Uncertainty of mean*	Residual cohesion c_r (MPa) Mean/std. dev. Min–max *Uncertainty of mean*
36.6/3.2	0.9/0.4	34.7/3.5	0.4/0.2
28.5–45.4	0.3–2.5	25.7–44.7	0.0–1.0
± 2%	± 11%	± 2%	± 14%

interval according to the "Central Limit Theorem" with min–max values based on observed minimum/maximum values of the tested samples /Hakami et al. 2008/. Note that the fracture properties presented in Table A4-10 do not represent sealed fractures and are also not expected to be representative for highly water-conductive fractures, cf. Section A4.6.

In situ stresses

The stress model for the Laxemar Local Model Area /Hakami et al. 2008/ for fracture domains FSM_C, FSM_W, FSM_NE005 and FSM_EW007 below ZSMEW007 in the depth-range 400–700 m is presented in Table A4-12, cf. Figure A4-17. The *in situ* stress model is given by the stress components σ_H (major horizontal stress), σ_h (minor horizontal stress) and σ_v (vertical stress). It is assumed that these can be approximated to be principal stresses, *i.e.* $\sigma_H = \sigma_1$, $\sigma_h = \sigma_3$ and $\sigma_v = \sigma_2$, although that may not be strictly the case, cf. Figure A4-14. The vertical stress is assumed to be equal to the weight of the overburden and is calculated using a generic value of the rock mass density, cf. Table A4-11. The uncertainty span (uncertainty of mean) is based on variations in measurement data and analyses of borehole stability /Hakami et al. 2008, SKB 2009b/. Small scale spread, at the scale of a single overcoring measurement, in stress magnitudes and orientations due to fracturing are given by normal distributions with mean values and standard deviations as presented in Table A4-12.

An extreme upper limit of the maximum stress based on observations of stable drill holes /Hakami et al. 2008, Table 6-11 and p 148/ is 31–34 MPa at 400 m depth and about 35–40 MPa at 700 m depth with the lower value in rock domain RSMM01 and the higher value in rock domain RSMD01, respectively.

Table A4-11. Generic rock mass density used to estimate the vertical stress gradient. This value is consistent with the densities given by /Wahlgren et al. 2008/ for the most common rock types in rock domains RSMA01, RSMM01 and RSMD01.

Parameter	Unit	Value
Density (ρ)	kg/m^3	2,700

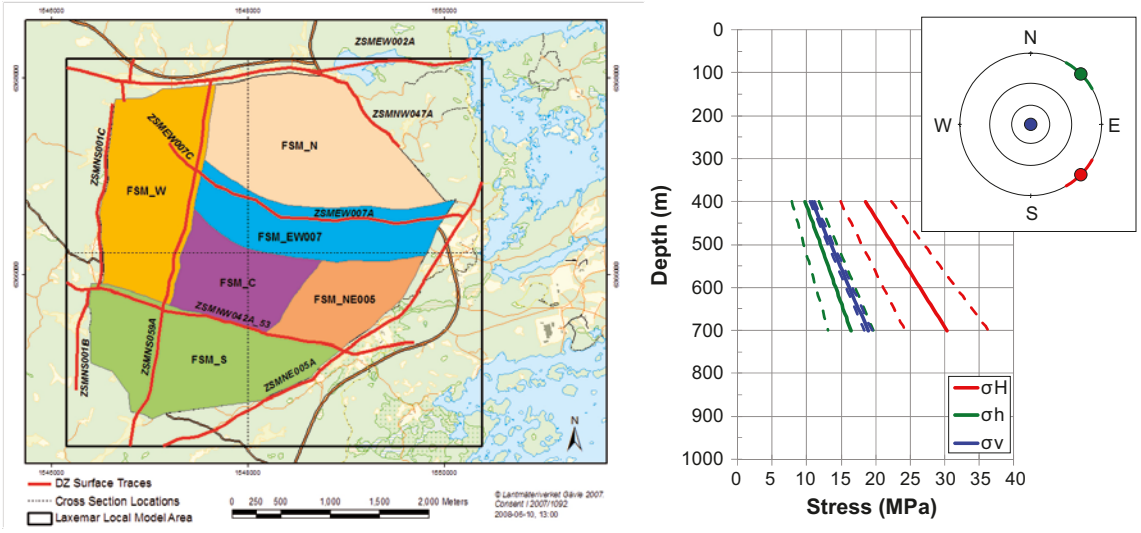

Figure A4-17. *Left: Fracture domains (FSMx) and surface traces of some of the major deterministic deformation zones (ZSMx) in the Laxemar Local Model Area, from /Hakami et al. 2008, Figure 2-10/. Right: Site model in situ stresses and orientations with uncertainty spans (dashed lines) /Hakami et al. 2008, SKB 2009b/ for fracture domains FSM_C, FSM_W, FSM_NE005 and FSM_EW007 below the deformation zone ZSMEW007, cf. left figure.*

Table A4-12. Stress model in the depth range 400–700 m for fracture domains FSM_C, FSM_W, FSM_NE005 and FSM_EW007 below the deformation zone ZSMEW007 at Laxemar /Hakami et al. 2008, Table 6-11, SKB 2009b, Table 7-7/.

Parameter	Mean/stdev	Uncertainty of mean
Major horizontal stress, σH (MPa)	3 + 0.039z/12%	± 20%
Minor horizontal stress, σh (MPa)	1 + 0.022z/13%	± 20%
Vertical stress, σv (MPa)	0.027z/15%	± 3%
Orientation of σH with respect to North (°)	135/±15°	± 15°

Evolution of stress additions during glacial cycle

/Lund et al. 2009/ choose a horizontally stratified earth model (Model T9) as their preferred model in terms of fit to GPS data, sea-level data and as the lithospheric elastic structure is in agreement with Fennoscandian seismic investigations. One principal stress component can be shown to be near vertical at all times. Therefore, the glacially induced stress components (σ_H, σ_h and σ_v) presented at repository depth (500 m) in Figure A4-18 are principal stresses. Furthermore, the variations with depth in the upper 1.5 km of the rock are negligible, cf. Figure A4-15 (right), i.e. the stress additions can be approximated to be constant with depth in the upper 1.5 km of the rock.

Stress-transmissivity relations

In addition to a stress-transmissivity model based on mean values of fracture normal stiffness data, it is recommended that a model with low values of *JKN* and *JEN* should also be considered. Mean values (and range in parameter values) for the CY model are presented in Table A4-13. By inspection of Figure A4-8 (right), the parameter combination *JKN* = 150 MPa/mm and *JEN* = 0.6 is judged to be sufficiently low. There are only small variations in the mean value of *JRC* between fractures sets (5.6–7.4 /Hakami et al. 2008/). It is therefore recommended that the mean value of *JRC* (approximately 6, cf. Table A4-13) be used in the models. Note that, similarly as for the Mohr-Coulomb strength properties, the values given in the table may not be representative of highly water-conductive fractures.

The residual hydraulic aperture is taken to be the average hydraulic aperture at large depth. It is here set to 20 µm based on reported fracture transmissivities below 650 m depth in fracture domains/hydraulic rock domains FSM_EW007/HRD_EW007, FSM_NE005, FSM_N/HRD/_N, FSM_W/HRD_W and HRD_C /Rhén et al. 2008/, cf. Figure A4-19.

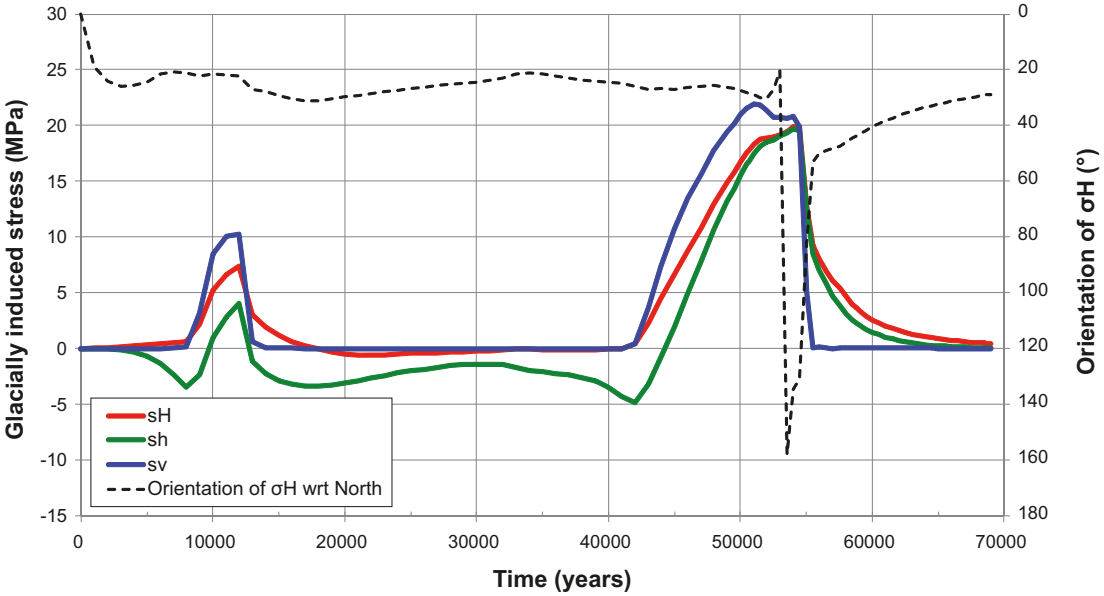

Figure A4-18. Stress additions and orientation of the major horizontal stress at 500 m depth during the Weichselian glacial cycle obtained from of ice-crust-mantle analyses (Model T9) by /Lund et al. 2009/. Here, 0° represents North and 180° South.

Table A4-13. Model parameters for the CY model (JKN and JEN) are derived from cyclic loading compression tests by /Jacobsson and Flansbjer 2005a, b, 2006a, b/, cf. Figure A4-4. The values of the joint roughness coefficient (JRC) are based on tilt tests on samples from Laxemar and Simpevarp /Hakami et al. 2008, Tables 4-2 and 4-3/.

Parameter	Mean	Min	Max
JKN (MPa/mm)	367	119	918
JEN (-)	0.86	0.36	1.46
JRC_{100} (-)	6.1	1.8	9.5

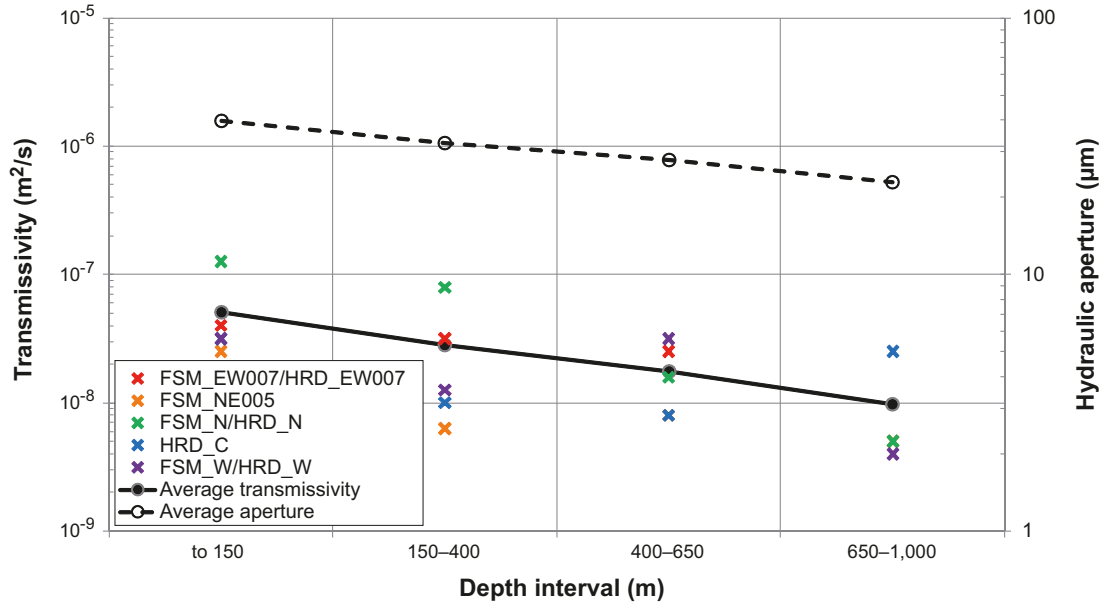

Figure A4-19. Summary of fracture transmissivities at different depth intervals in fracture domains/hydraulic rock domains FSM_EW007/HRD_EW007, FSM_NE005, FSM_N/HRD_N, FSM_W/HRD_W and HRD_C /Rhén et al. 2008, Table 9-12/ (marked with 'x'). The average transmissivity is here given by the average value of the reported transmissivities for the hydraulic rock domains/fracture domains at each depth interval. The corresponding average hydraulic apertures are calculated from the average transmissivity values through the cubic flow law.

Figure A4-20 shows the hydraulic aperture obtained by the CY model (Equations A4-3 and A4-4) using the two sets of fracture stiffness data described in the text above evaluated for the initial normal stress σ_0 set to the mean effective stress at repository depth (500 m), $\sigma_0 = (\sigma_H + \sigma_h + \sigma_v)/3 - p$, where σ_H, σ_h and σ_v are the three principal stress components and p is the hydrostatic pore pressure. The initial effective normal stress is here approximated to be 12 MPa based on the stress model by /Hakami et al. 2008/, cf. Table A4-12. For both sets of fracture stiffness data, an exponential fit to the hydraulic apertures (Equation A4-5) has been made and compared with corresponding relations suggested for Forsmark in Section 6.4 of the SR-Site Data report /SKB 2010/. Parameter values for the two sets of data for the CY model and corresponding values for the exponential expression are presented in Table A4-14.

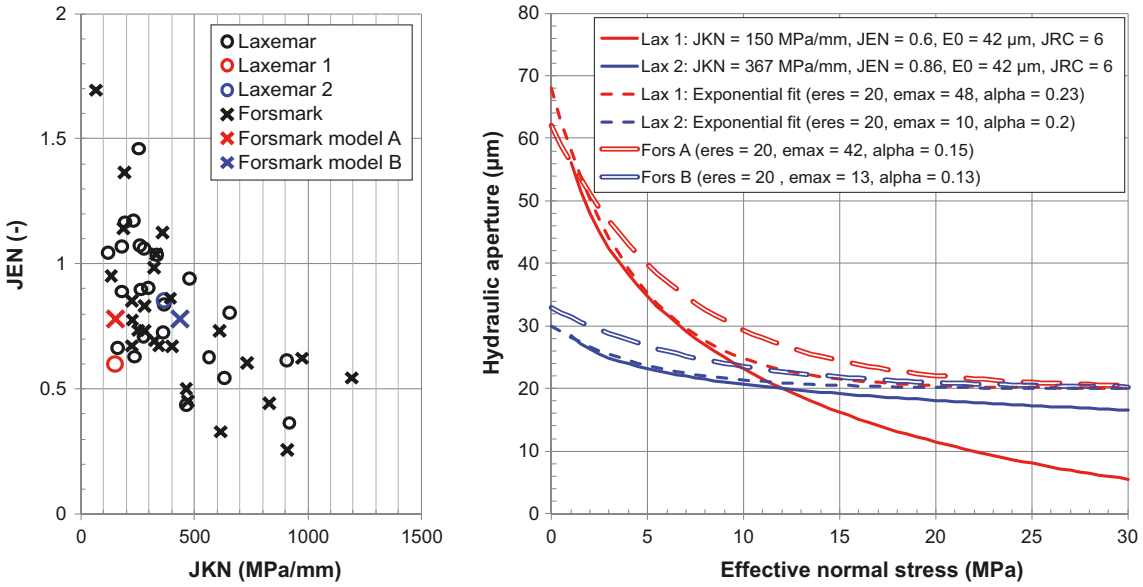

Figure A4-20. *Left: JKN and JEN values for Laxemar (see Figure A4-10, right) compared with Forsmark data compiled from Section 6.4 in the SR-Site Data report /SKB 2010/. The stress-aperture relations are based on the following parameter combinations: JKN = 150 MPa/mm, JEN = 0.6 (Laxemar 1), JKN = 367 MPa/mm, JEN = 0.86 (Laxemar 2), JKN = 150 MPa/mm, JEN = 0.78 (Forsmark model A), JKN = 436 MPa/mm, JEN = 0.78 (Forsmark model B). Right: Hydraulic apertures calculated using the CY model (Equations A4-3 and A4-4) with exponential fits to the apertures (EquationA4-5) compared with corresponding exponential relations suggested for Forsmark in Section 6.4 of the SR-Site Data report /SKB 2010/.*

Table A4-14. Recommended parameter values for the CY model (Equations A4-3 and A4-4) based on 1) average fracture stiffness data (Table A4-13) and 2) based on lower bound fracture stiffness data (alternative data set described in the text) with corresponding parameter values for the exponential expression (Equation A4-5).

Model	Parameter	Average	Alternative
CY-model	*JKN* (MPa/mm)	367	150
	JEN (-)	0.86	0.6
	JRC (-)	6.0	6.0
	E_0 (µm)	42	42
Exponential expression	e_r (µm)	20	20
	e_{max} (µm)	10	48
	α *(-)*	0.2	0.23

A4.10 Data recommended for use in the Comparative analysis of safety related site characteristics

All data provided in Section A4.9 are recommended for use in the analysis of safety related site characteristics. Reference parameter values for all models are given by the mean value of each parameter. To assess the influence of uncertainties, a small number of parameter values judged to represent the variability are selected and used in the modelling work. Note that the thermal and thermo-mechanical properties of the rock (*i.e.* thermal conductivity, heat capacity and heat expansion coefficient) are described in Chapter A2.

Thermal, mechanical and thermo-mechanical properties of the rock mass

The mechanical properties of the rock mass for the large-scale models are provided in Table A4-15. The corresponding mechanical properties of the rock mass for the near-field models are provided in Table A4-16.

Table A4-15. Thermal, mechanical and thermo-mechanical properties of the rock mass for large-scale THM-modelling, cf. Table A4-9.

Parameters	Value	Comment
Density, ρ (kg/m^3)	2,700	Generic value, cf. Table A4-11
Young's modulus, E (GPa)	55	Average value of mean E in each fracture domain group, cf. Table A4-9
Poisson's ratio, v (-)	0.3	Mean value in both fracture domain groups, cf. Table A4-9

Table A4-16. Mechanical properties of the rock mass in each fracture domain group for near-field THM-modelling, cf. Table A4-9.

Parameters	FSM_N and _EW007	FSM_C, _W and _NE005
Density, ρ (kg/m^3)	2,700	2,700
Young's modulus, E (GPa)	50	59
Poisson's ratio, v (-)	0.3	0.3

Spalling strength

The spalling strength is assumed to be 52–62% of the uniaxial compressive strength in each rock domain, cf. Table A4-17.

Table A4-17. Strength properties of intact rock in each rock domain, cf. Table A4-7 and Table A4-8.

Parameters	Unit	RSMA	RSMM	RSMD
Uniaxial compressive strength (*UCS*)	MPa	193	187	187
Spalling strength	MPa	100–120	97–116	97–116

In situ stresses

In situ stresses as function of depth for the large-scale modelling are provided in Table A4-18.

Table A4-18. In situ stresses as functions of depth for large-scale modelling, cf. Table A4-12. The orientation of the major horizontal in situ stress is given with respect to North.

Depth range (m)	σH (MPa)	σH orientation (°)	σh (MPa)	σv (MPa)
0–1,000	3 + 0.039z	135	1 + 0.022z	0.027z

In situ stresses at repository depth (500 m) for the small-scale near-field modelling are provided in Table A4-19. Uncertainty spans for each stress model are given in brackets.

Table A4-19. Most likely in situ stress magnitudes and orientation of σH (with respect to North) at repository depth (500 m) used in near-field modelling work. As an upper limit the magnitude of the major horizontal stress is given by that at Äspö /Andersson 2007/, cf. Table A.4-5. Uncertainty spans for each stress model are given in brackets based on the uncertainty spans given in the right column of Table A.4-12.

Stress model	*σH* (MPa)	*σH* orientation (°)	*σh* (MPa)	*σv* (MPa)
Most likely	22.5	135 (150)	12	13.5
Most likely (with Äspö σH)	30 (36)	135 (150)	12 (14.4)	13.5 (13.9)

Mohr-Coulomb strength properties of fractures

The Mohr-Coulomb strength properties (cohesion and friction angle) used in the modelling work are presented in Table A4-20.

Table A4-20. Mohr-Coulomb fracture strength properties obtained by taking the average value of their mean laboratory-determined peak and residual values, cf. Table A.4-10.

Property	Unit	Value
Cohesion	MPa	0.6
Friction angle	°	35.7

Glacially induced stresses and pore pressure

The glacially induced stresses (in excess of the present-day *in situ* stresses) at six selected points in time during the glacial cycle are presented in Table A4-21. The stress magnitudes and orientations given in the table do not vary with depth. The glacially induced pore pressure (in excess of hydrostatic pressure) is assumed to be 90% of the ice sheet thickness (or about 98% of the glacially induced vertical stress σ_v).

Table A4-21. Glacially induced stresses (orientation is given with respect to North) at selected points in time during the glacial cycle, cf. Figure A4-18.

Time	σH (MPa)	σH orientation (°)	σh (MPa)	σv (MPa)
First glacial maximum (12 kyr)	7.39	22	4.01	10.23
Edge passing(14 kyr)	1.94	28	–2.26	0.06
Stress reductions due to forebulge (42 kyr)	0.42	26	–4.85	0.47
Second glacial maximum, σv max (51 kyr)	18.31	29	17.49	21.97
Second glacial maximum, σH max (54.5 kyr)	19.84	131	19.49	19.94
Edge passing (55.5 kyr)	9.25	53	8.48	0.08

Stress-transmissivity relations

The two stress-transmissivity models (Models A and B) derived for Forsmark (cf. Section 6.4 of the SR-Site Data report /SKB 2010/) are chosen to estimate stress induced transmissivity changes based on the exponential relation suggested by /Liu et al. 2004/ (Equation A4-5) and the cubic flow law (Equation A4-6), cf. Figure A4-20 (right). The parameter values for each stress-transmissivity model are given in Table A4-22.

Table A4-22. Parameter values for the exponential expression, Equation A4-5 from Section 6.4.12 in the SR-Site Data report /SKB 2010/.

Parameter	Model A	Model B
er (μm)	20	20
emax (μm)	42	13
α (-)	0.15	0.13

References A4.11

SKB's (Svensk Kärnbränslehantering AB) publications can be found at www.skb.se/publications.

Al-Ajmi A M, Zimmerman R W, 2006. Stability analysis of vertical boreholes using the Mogi-Coulomb failure criterion. International Journal of Rock Mechanics and Mining Sciences, 43, pp 1200–1211.

Andersson J C, 2007. Äspö Hard Rock Laboratory. Äspö Pillar Stability Experiment, final report. Rock mass response to coupled mechanical thermal loading. SKB TR-07-01, Svensk Kärnbränslehantering AB.

Back P-E, Sundberg J, 2007. Thermal site descriptive model. A strategy for the model development during site investigations – version 2. SKB R-07-42, Svensk Kärnbränslehantering AB.

Barton N, 1982. Modelling rock joint behaviour from in situ block tests: implications for nuclear waste repository design. Technical Report ONWI-308, Office of Nuclear Waste Isolation, Columbus, Ohio.

Damjanac B, Fairhurst C, 2010. Evidence for a long-term strength threshold in crystalline rock. Rock Mechanics and Rock Engineering, 43, doi: 10.1007/s00603-00010-00090-00609.

Eloranta P, 2004. Drill hole KSH01A. Uniaxial compression test (HUT). Oskarshamn site investigation. SKB P-04-182, Svensk Kärnbränslehantering AB.

Glamheden R, Fredriksson A, Röshoff K, Karlsson J, Hakami H, Christiansson R, 2007. Rock mechanics Forsmark. Site descriptive modelling Forsmark stage 2.2. SKB R-07-31, Svensk Kärnbränslehantering AB.

Glamheden R, Fälth B, Jacobsson L, Harrström J, Berglund J, Bergkvist L, 2010. Counterforce applied to prevent spalling. SKB TR-10-37, Svensk Kärnbränslehantering AB.

Hakami E, Fredriksson A, Lanaro F, Wrafter J, 2008. Rock mechanics Laxemar. Site descriptive modelling, SDM-Site Laxemar. SKB R-08-57, Svensk Kärnbränslehantering AB.

Hökmark H, Fälth B, Wallroth T, 2006. T-H-M couplings in rock. Overview of results of importance to the SR-Can safety assessment. SKB R-06-88, Svensk Kärnbränslehantering AB.

Hökmark H, Lönnqvist M, Kristensson O, Sundberg J, Hellström G, 2009. Strategy for thermal dimensioning of the final repository for spent nuclear fuel. SKB R-09-04, Svensk Kärnbränslehantering AB.

Hökmark H, Lönnqvist M, Fälth B, 2010. THM-issues in repository rock. Thermal, mechanical, thermo-mechanical and hydro-mechanical evolution of the rock at the Forsmark and Laxemar sites. SKB TR-10-23, Svensk Kärnbränslehantering AB.

Itasca, 2007. 3DEC – 3-Dimensional Distinct Element Code, version 4.1, user's guide. Minneapolis, Minnesota: Itasca Consulting Group.

Jacobsson L, 2004. Drill hole KSH01A. Uniaxial compression test of intact rock. Oskarshamn site investigation. SKB P-04-207, Svensk Kärnbränslehantering AB.

Jacobsson L, Flansbjer M, 2005a. Borehole KLX03A. Normal loading and shear tests on joints. Oskarshamn site investigation. SKB P-05-92, Svensk Kärnbränslehantering AB.

Jacobsson L, Flansbjer M, 2005b. Borehole KLX06A. Normal loading and shear tests on joints. Oskarshamn site investigation. SKB P-05-146, Svensk Kärnbränslehantering AB.

Jacobsson L, Flansbjer M, 2006a. Borehole KLX10. Normal loading and shear tests on joints. Oskarshamn site investigation. SKB P-06-39, Svensk Kärnbränslehantering AB.

Jacobsson L, Flansbjer M, 2006b. Borehole KLX12A. Normal loading and shear tests on joints. Oskarshamn site investigation. SKB P-06-75, Svensk Kärnbränslehantering AB.

La Pointe P, Fox A, Hermanson J, Öhman J, 2008. Geological discrete fracture network model for the Laxemar site. Site descriptive modelling, SDM-Site Laxemar. SKB R-08-55, Svensk Kärnbränslehantering AB.

Lambeck K, 2005. Glacial load stresses: can existing faults or other zones of crustal weakness be reactivated during glacial cycles? In: Hora S, Jensen M (eds). Expert panel elicitation of seismicity following glaciation in Sweden. SSI Report 2005:20, Statens strålskyddsinstitut (Swedish Radiation Protection Authority), pp 85–106.

Lanaro F, Fredriksson A, 2005. Rock mechanics model – summary of the primary data. Preliminary site description Forsmark area – version 1.2. SKB R-05-83, Svensk Kärnbränslehantering AB.

Lau J O S, Jackson R, Gorski B, 1991. The effects of temperature and pressure on the mechanical properties of Lac du Bonnet grey granite. In: Roegiers J-C (ed). Rock mechanics as a multidisciplinary science: proceedings of the 32nd US Symposium on Rock Mechanics, the University of Oklahoma, Norma, 10–12 July 1991, Rotterdam: Balkema.

Liu H-H, Rutqvist J, Zhou Q, Bödvarsson G S, 2004. Upscaling of normal stress-permeability relationships for fracture networks obeying fractional Levy motion. In: Stephansson O, Hudson J A, Jing L (eds). Coupled thermo-hydro-mechanical-chemical processes in geosystems: fundamentals, modelling, experiments and applications. Amsterdam: Elsevier, pp 263–268.

Lund B, Schmidt P, Hieronymus C, 2009. Stress evolution and fault stability during the Weichselian glacial cycle. SKB TR-09-15, Svensk Kärnbränslehantering AB.

Martin C D, 2005. Preliminary assessment of potential underground stability (wedge and spalling) at Forsmark, Simpevarp and Laxemar sites. SKB R-05-71, Svensk Kärnbränslehantering AB.

Martin C D, 2007. Quantifying in situ stress magnitudes and orientations for Forsmark. Forsmark stage 2.2. SKB R-07-26, Svensk Kärnbränslehantering AB.

Martin C D, Davison C C, Kozak E T, 1990. Characterizing normal stiffness and hydraulic conductivity of a major shear zone in granite. In: Barton N, Stephansson O (eds). Rock joints: proceedings of the International Symposium on Rock Joints, Loen, Norway, 4–6 June 1990, Rotterdam: Balkema.

Muir Wood R, 1995. Reconstructing the tectonic history of Fennoscandia from its margins: the past 100 million years. SKB TR 95-36, Svensk Kärnbränslehantering AB.

Rhén I, Forsmark T, Hartley L, Jackson P, Roberts D, Swan D, Gylling B, 2008. Hydrogeological conceptualisation and parameterisation. Site descriptive modelling, SDM-Site Laxemar. SKB R-08-78, Svensk Kärnbränslehantering AB.

Rutqvist J, Tsang C-F, 2008. Review of SKB's work on coupled THM processes within SR-Can. External review contribution in support of SKI's and SSI's review of SR-Can. SKI Report 2008:08, Statens kärnkraftinspektion (Swedish Nuclear Power Inspectorate).

SKB, 2006a. Climate and climate-related issues for the safety assessment SR-Can. SKB TR-06-23, Svensk Kärnbränslehantering AB.

SKB, 2006b. Preliminary site description. Laxemar subarea – version 1.2. SKB R-06-10, Svensk Kärnbränslehantering AB.

SKB, 2007. Final repository facility. Underground design premises/D2. SKB R-07-33, Svensk Kärnbränslehantering AB.

SKB, 2009a. Confidence assessment. Site descriptive modelling, SDM-Site Laxemar. SKB R-08-101, Svensk Kärnbränslehantering AB.

SKB, 2009b. Site description of Laxemar at completion of the site investigation phase. SDM-Site Laxemar. SKB TR-09-01, Svensk Kärnbränslehantering AB.

SKB, 2009c. Underground design Laxemar. Layout D2. SKB R-09-16, Svensk Kärnbränslehantering AB.

SKB, 2010. Data report for the safety assessment SR-Site. SKB TR-10-52, Svensk Kärnbränslehantering AB.

Sundberg J, Wrafter J, Back P-E, Rosén L, 2008. Thermal properties Laxemar. Site descriptive modellin,g SDM-Site Laxemar. SKB R-08-61, Svensk Kärnbränslehantering AB.

Wahlgren C-H, Curtis P, Hermanson J, Forssberg O, Öhman J, Fox A, La Pointe P, Drake H, Triumf C-A, Mattsson H, Thunehed H, Juhlin C, 2008. Geology Laxemar. Site descriptive modelling, SDM-Site Laxemar. SKB R-08-54, Svensk Kärnbränslehantering AB.

A5 Spalling and the excavation damaged zone

Repository induced damages to the rock mass affect the groundwater flow and, as a consequence, the solute transport in the fractured rock. Assessments of these rock damages, in terms of spalling and the excavation damaged zone (EDZ), are therefore needed as input for the assessment of radiological risk, associated with radionuclide transport from the repository. The input data considered in the Comparative analysis are the resulting properties from these damages and alterations. These properties, in turn, are assessed from various sources and assessments, including detailed process modelling, as further described in this appendix.

The data presented in this appendix are used as input to Chapters A6 and A7, and associated activities, discussing hydraulic properties of the rock and flow related migration parameters.

In the SR-Site Data report /SKB 2010b, Section 6.5/ the corresponding data are given for the Forsmark site. In some instances concerning spalling and EDZ, issues that are not site specific are detailed in the SR-Site Data report, to which references are made.

A5.1 Modelling as input to the comparative analysis of safety related site characteristics

The excavation damaged zone is here defined as "the part of the rock mass closest to the underground opening that has suffered irreversible deformation where shearing of existing fractures as well as propagation and/or development of new fractures has occurred" /Bäckblom et al. 2004/. In the comparative analysis, the concern is on the remaining impact from the tunnelling, i.e. after re-saturation, on the hydraulic properties. The EDZ basically originates from:

- excavation damage (i.e. from the blasting or from a Tunnel Boring Machine, TBM, if this is used);
- the changes of the stress field and associated fracturing (spalling) and fracture dilation effects resulting from the changed stress boundary conditions compared to the undisturbed situation.

It should be noted that other definitions of the EDZ exist, but the one adopted here pragmatically focuses on the resulting impact on the rock – and not on the various causes for these impacts.

Defining the data requested from the supplier

Depending on the nature of the excavation damaged zone, the data which need to be supplied differ. If the EDZ is generally not connected on the tunnel scale:

- The absence of a connected EDZ should be justified based on experimental observations and data.

If the EDZ is connected on the tunnel scale, giving rise to altered hydraulic properties compared to the properties of the rock prior to construction, the following should be supplied:

- The axial transmissivity T (m^2/s) of the EDZ along the deposition tunnel, as averaged across the tunnel floor.
- The axial transmissivity T (m^2/s) of the EDZ along other tunnels and shafts, as averaged across the tunnel floor (and corresponding for shafts).

Concerning any volume around the deposition holes with altered hydraulic properties compared to the properties of the rock prior to construction (referred to as the spalled zone), the following should be supplied:

- The potential for spalling, with focus on the potential for thermally induced spalling.

If spalling occurs:

- The length L_{zone} (m) and location of the spalled zone along the deposition hole.
- The width W_{zone} (m), and thickness d_{zone} (m) of the spalled zone around the deposition hole.
- The tortuosity τ_y (–) and porosity ε_{zone} (–) of the spalled zone.
- The hydraulic conductivity K (m/s) of the spalled zones. If this conductivity cannot be shown to be small in relation to the transmissivity of the fracture intersecting the deposition hole, or if there is no fracture intersecting the deposition hole, it is sufficient to note that the hydraulic conductivity of the spalled zone is "high".

If no spalling occurs:

- The connected effective transmissivity T (m^2/s) of the deposition hole EDZ, integrated along the full length of the deposition hole wall, and as averaged around the hole. If no such fully connected zone would develop, arguments are needed to state this.

Modelling activities in which data will be used

The data will be incorporated in the groundwater flow models as well as in the migration models used in the Comparative analysis. These models are further described in Chapter A6 regarding hydraulic properties of the rock, and in Chapter A7 regarding flow related migration parameters. The potentials for an EDZ and for spalling are implemented in the following manner:

- The groundwater flow simulations, using ConnectFlow /Serco 2005/, implement the EDZ as a continuous fracture, with a prescribed transmissivity as input, under the floor of all deposition tunnels.
- The source term model, COMP23 /Cliffe and Kelly 2006/ considers the possibility of an EDZ with enhanced transmissivity intersecting the upper part of the deposition hole and uses an equivalent flow rate Q2, see Section 6.7, to handle the release from the buffer into the EDZ.
- The far-field radionuclide transport model FARF31 /Norman and Kjellbert 1990, Elert et al. 2004/ pessimistically neglects retention in the EDZ.

A5.2 Supplier input on handling of data in the comparative analysis

The potential for spalling, based on the findings by /Hökmark et al. 2010/, is assessed in Chapter 4 of this present report. In addition to being an issue by itself, the occurrence of spalling has implications for the radionuclide migration, but only in case the buffer is intact. A main issue for this appendix is thus to assess whether such conditions would occur. Also the other data listed above are needed as input for the migration calculations, being part of the assessment presented in Chapter 10, although not directly discussed in the main document of the Comparative analysis.

A5.3 Sources of information and documentation of data qualification

Sources of information

The main sources of information used in the data qualification of data on the EDZ and spalling are presented in Table A5-1.

Table A5-1. Main sources of information used in data qualification for EDZ and spalling.

Andersson C J, 2007. Äspö Hard Rock Laboratory. Äspö Pillar Stability Experiment, Final report. Rock mass response to coupled mechanical thermal loading. SKB TR-07-01, Svensk Kärnbränslehantering AB.

Bäckblom G, 2008. Excavation damage and disturbance in crystalline rock – results from experiments and analyses. SKB TR-08-08, Svensk Kärnbränslehantering AB.

Ericsson L O, Brinkhoff P, Gustafson G, Kvartsberg S, 2009. Hydraulic Features of the Excavation Disturbed Zone – Laboratory investigations of samples taken from the Q- and S-tunnels at Äspö HRL. SKB R-09-45, Svensk Kärnbränslehantering AB.

Glamheden R, Fälth B, Jacobsson L, Harrström J, Berglund J, Bergkvist L, 2010. Counterforce applied to prevent spalling. SKB TR-10-37, Svensk Kärnbränslehantering AB.

Hökmark H, Fälth B, Wallroth T, 2006. T-H-M couplings in rock. Overview of results of importance to the SR-Can safety assessment. SKB R-06-88, Svensk Kärnbränslehantering AB.

Hökmark H, Lönnqvist M, Fälth B, 2010. THM-issues in repository rock. Thermal, mechanical, thermo-mechanical and hydro-mechanical evolution of the rock at the Forsmark and Laxemar sites. SKB TR-10-23 Svensk Kärnbränslehantering AB.

Neretnieks I, Andersson J C, 2009. Characterisation of spalling fragments to obtain data for flow and transport in damaged zones. In: Hudson J, Tham L, Feng X-T, Kwong A (eds). Rock characterisation, modelling and engineering design methods: proceedings of the International Symposium on Rock Mechanics (SINOROCK 2009), University of Hong Kong, 19–22 May 2009.

Olsson M, Niklasson B, Wilson L, Andersson C, Christiansson R, 2004. Äspö HRL. Experiences of blasting of the TASQ tunnel. SKB R-04-73, Svensk Kärnbränslehantering AB.

Olsson M, Markström I, Pettersson A, Sträng M, 2009. Examination of the Excavation Damaged Zone in the TASS tunnel, Äspö HRL. SKB R-09-39, Svensk Kärnbränslehantering AB.

SKB, 2010a. Design, construction and initial state of the underground openings for operational and long-term safety. SKB TR-10-18, Svensk Kärnbränslehantering AB.

SKB, 2010b. Data report for the safety assessment SR-Site. SKB TR-10-52, Svensk Kärnbränslehantering AB.

Categorising data sets as qualified or supporting data

The qualified and supporting data sets are presented in Table A5-2. Comments regarding each item are given in Table A5-3. The following principles have been applied in this assessment:

- For obvious reasons there are no data from actually constructed tunnels at depth at either of the Forsmark or Laxemar sites. However, it is judged that the phenomena of forming EDZ and spalling depends on general rock mechanics processes, which means that data obtained from other sites, such as Äspö HRL, are applicable.
- Data obtained from SKB reports being reviewed and approved in accordance with the SKB QA Plan, can a priori be regarded as qualified data. However, since the report by /Bäckblom 2008/ is a compilation of data from various sources of varying quality, data regarding EDZ in tunnels presented by Bäckblom may partly be considered to be supporting.
- The assessment on the EDZ in the Underground opening construction report /SKB 2010a/, is based on the findings by (e.g. /Ericsson et al. 2009, Glamheden et al. 2010/). The conclusions reached have been reviewed and accepted by SKB's internal and external experts, and it is thus qualified from that respect.
- The conclusions drawn in the Underground opening construction report concerning spalling and the EDZ are judged to be as representative for the Laxemar site as for the Forsmark site.

Table A5-2. Qualified and supporting data sets.

Qualified data sets	Supporting data sets
1. Occurrence, location, and extent of any volume around the deposition tunnels, and other tunnels, with altered hydraulic properties compared to the properties of the rock prior to construction: /Olsson et al. 2009, Fig 7-9, 7-10/, /Olsson et al. 2004/, /SKB 2010a, Chapter 6/.	6. Published data on characterisation of the EDZ in drilled and blasted tunnels /Bäckblom, 2008, Table 3-3/.
2. Connected effective transmissivity (m2/s) along the deposition tunnel, or other tunnels, and averaged across the tunnel floor: /Olsson et al. 2009, Fig 7-9, 7-10/, /Ericsson et al. 2009, Chapter 4/, /SKB 2010a, Section 5.2.2/.	
3. Occurrence, location, and extent of any volume around the deposition holes, with altered hydraulic properties compared to the properties of the rock prior to construction: Appendix I in /Hökmark et al. 2010, Glamheden et al. 2010, Andersson 2007/.	
4. The connected effective transmissivity integrated along the full length of the deposition hole wall and as averaged around the hole (m^2/s): /Bäckblom 2008, Table 3-3, SKB 2010a, Section 5.2.3/.	
5. Local hydraulic conductivity, tortuosity, porosity and thickness of the spalled zones, if a spalled zone occurs: /Neretnieks and Andersson 2009, Glamheden et al. 2010/.	

Table A5-3. Justifications to the sorting of items in Table A5-2.

1./Olsson et al. 2009/ characterised natural and excavation induced fractures in rock blocks removed from a section of a tunnel wall at the Äspö HRL. /Olsson et al. 2004/ concern assessment of excavation induced fractures at the TASQ-tunnel at Äspö HRL. Generally, the Underground opening construction report /SKB 2010a, chapter 6/ concludes that it is possible to control the excavation of a drilled end blasted tunnel such that excavation induced fractures would not form a continuous network. These reports, apart from /Olsson et al. 2004/, are reviewed and accepted according to the SKB QA-plan. Furthermore, it is judged that the work of /Olsson et al. 2004/ was carried with a similar quality as their later report. Thus data presented in these reports are judged to be qualified.
2. The excavation induced fractures in the rock side-walls characterised by /Olsson et al. 2009/ are dominantly radial and does not form a continuous network along the axial direction of the tunnel over any significant distance. /Ericsson et al. 2009/ performed laboratory permeability tests of the fractures in the rock blocks characterised by /Olsson et al. 2009/. By numerical analyses and analytical expressions, /Hökmark et al. 2010/ assess the change in fracture transmissivity due to the impact of changing mechanical loads. Generally, the /SKB 2010a, section 5.2.2/ concludes that it is possible to control the excavation of a drilled end blasted tunnel such that the excavation induced fractures would not form a continuous network. These reports are reviewed and accepted according to the SR-Site QA-plan and the presented data are thus judged to be qualified.
3. /Hökmark et al. 2010/ performed numerical analyses of the potential for, and the geometrical extension of, thermally induced spalling in deposition holes. /Andersson 2007/ presents the Äspö Pillar Stability Experiment (APSE) carried out to examine the failure process in a heterogeneous and slightly fractured rock mass when subjected to coupled excavation-induced and thermal-induced stresses. /Glamheden et al. 2010/ present a field experiment at Äspö HRL, where 0.5 m diameter boreholes are exposed to a thermal load, with and without a confining pressure. These reports, apart from /Andersson 2007/, are reviewed and accepted according to the SR-Site QA-plan. However, the work of /Andersson 2007/ was part of a doctoral dissertation and has been subject to an extensive scientific review. Thus data presented in these reports are judged to be qualified.
4. /Bäckblom 2008, Table 3-3/ compiles published data on characterisation of the EDZ in mechanically excavated tunnels and boreholes. These data are judged to be of more controllable quality and are thus judged to be qualified.
5. /Neretnieks and Andersson 2009/ assessed the tortuosity (-) of the spalled rock fragments obtained from spalling tests at the Äspö Pillar Stability Experiment (APSE) /Andersson 2007/. /Glamheden et al. 2010/ performed hydraulic tests of the thermally spalled zones in one of their tests. These reports are reviewed and accepted according to the SR-Site QA-plan and the presented data are thus judged to be qualified.
6. /Bäckblom 2008, Table 3-3/ compiles published data on characterisation of the EDZ in drilled and blasted tunnels. The data are of various origin and quality, and it is not evident that there is a clear separation between natural and induced fractures and are thus judged to be supporting.

Excluded data previously considered as important

No important data have been excluded from the analyses.

A5.4 Conditions for which data are supplied

The field data on the excavation induced fracturing /Olsson et al. 2009, Ericsson et al. 2009, Bäckblom 2008/, concern conditions resulting after rock excavation. The field data on thermally induced spalling /Neretnieks and Andersson 2009, Glamheden et al. 2010/ concern conditions after heating, with and without a small counter pressure on the rock wall.

The numerical results by /Hökmark et al. 2010/ relate to the situation after excavation and the impact of the thermal load.

A5.5 Conceptual uncertainty

There is no conceptual uncertainty regarding the assessment of spalling that is specific for the Laxemar site. Therefore, the reader is referred to the conceptual uncertainties described in Section 6.5.5 of the SR-Site Data report /SKB 2010b/.

/Hökmark et al. 2010/ does not assess transmissivity changes of fractures in the near-field for the Laxemar site. However, in the near-field, the geometry of individual fractures and how they intersect repository openings and interact with other fractures are much more important than details in the background stress field. Therefore, the estimates given in SR-Can /Hökmark et al. 2006/ are relevant also for the Laxemar site. For a general discussion on uncertainties regarding estimates of transmissivity changes in the near-field, the reader is referred to Section 6.5 of the SR-Site Data report /SKB 2010b/.

A5.6 Data uncertainty due to precision, bias, and representativity

Data uncertainty due to precision

The extent of the EDZ around the tunnels excavated using careful drill-and-blast techniques at Äspö HRL was found to vary from a few cm to a few tens of cm /Ericsson et al. 2009/. /Ericsson et al. 2009/ observed a distribution of discontinuous fractures and microcracks and a slightly increased matrix porosity within this zone. Given the heterogeneous nature of this zone it is difficult to know if the transmissivity values reported by /Ericsson et al. 2009/ for the fractures in individual cored samples taken from this zone are representative, or represent an upper bound value. In addition the transmissivity values of the very small discontinuous fractures were not measured. The precision of the reported transmissivity values of the individual fractures is judged to be adequate but may overestimate the transmissivity of the EDZ and hence may not be representative.

/Hökmark et al. 2010/ consider a number of cases regarding magnitudes and orientations of the *in situ* stresses and variations in the thermal properties of the rock (cf. Chapter A4). Results from all models indicate that spalling during the excavation and operational phase would not take place other than by exception. Unlike the Forsmark site, where the majority of the deposition holes will have thermally induced spalling at some point during the heated phase, the number of deposition holes with thermally induced spalling at the Laxemar site is more uncertain. This is related to:

- Uncertainties regarding in the *in situ* state of stress (cf. Table A4-19 in Chapter A4).
- Spatial variations in the rock mass Young's modulus (cf. Table A4-16 in Chapter A4).
- Distribution of rock mass thermal conductivity values (cf. Chapter A2).

Although assuming that there will be thermally induced spalling in all deposition holes would be a safe upper bound estimate, this approach may significantly exaggerate the actual number of deposition holes with spalling. Therefore, an attempt to quantify the number of deposition holes with thermally induced spalling, taking uncertainties and spatial variations into account, is made (cf. Section A5.10).

Data uncertainty due to bias

There is no known bias in the data characterisation by /Olsson et al. 2009/. The methodology developed for the fracture characterization was specifically designed to eliminate the bias created by two-dimensional fracture mapping typically carried out in tunnels. Extracting large blocks and slicing the blocks into 10 cm slabs (see Figure A5-1) to develop a three-dimensional fracture pattern eliminated any mapping bias. The wire saw cutting of the blocks and their removal, and the slab cutting likely allowed closed fractures to open and caused some fractures to extend. Therefore the 3D mapped fractures likely overestimate the fracture pattern in situ. It is believed that they have carefully characterised all fractures in the excavated rock blocks and have created a new standard for fracture mapping in the EDZ. Any bias introduced by this new technique is judged to be extremely small.

/Ericsson et al. 2009/ used well-established laboratory methods to measure the transmissivity of discrete fractures. The bias associated with such laboratory techniques is not considered significant. The selection of fractures for testing can be biased since closed or partially closed fractures are not sampled. Therefore the fracture sampling produces a bias that results in upperbound transmissivity values. This bias is considered acceptable.

/Glamheden et al. 2010/ concluded that the hole scale used in CAPS project (Counterforce Applied to Prevent Spalling) was too small to be fully representative for the heterogeneous rock conditions encountered at Äspö. The depth of spalling is dependent on hole size, i.e. the larger the hole the greater the depth for given stress conditions, and therefore the conclusions by /Glamheden et al. 2010/ may be biased by this factor.

CAPS hydraulic testing was carried out using standard testing procedures used for borehole testing. Complete saturation during testing could not be ensured. However, it is unlikely these conditions affected the conclusions by /Glamheden et al. 2010/ regarding the relative transmissivity of the spalled zone. The absolute transmissivity values for the spalled zone may be biased by the test conditions, but the uncertainties due to this bias are judged to be small.

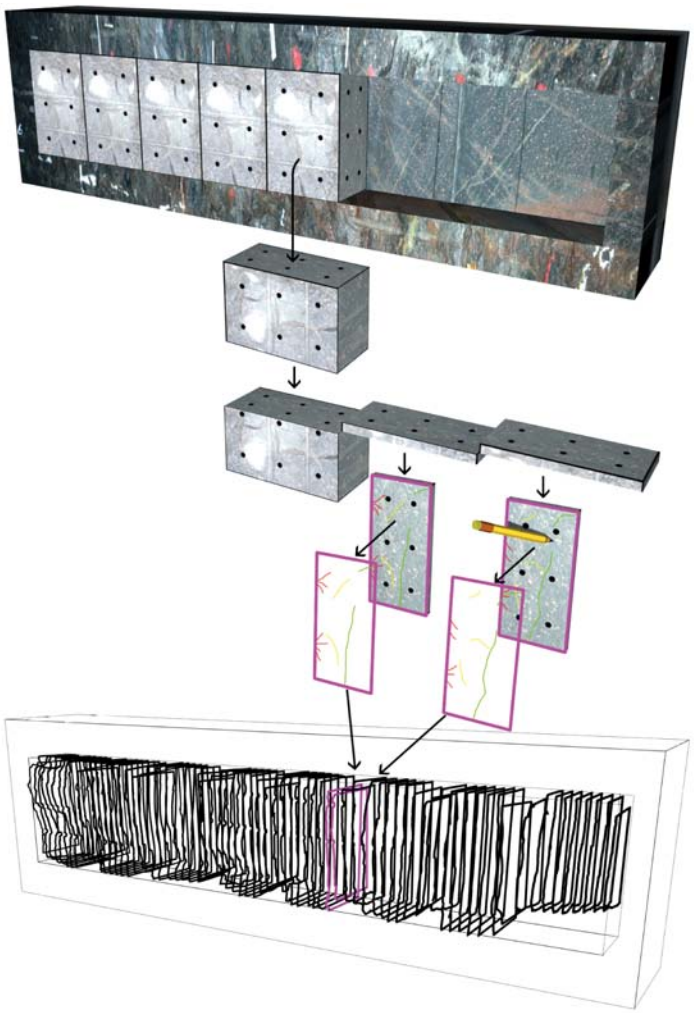

Figure A5-1. *Schematic view of the process of extracting blocks from the tunnel wall, sawing the block into slabs and making a digital 3D model of the tunnel. Reproduced from /Olsson et al. 2009, Figure 4-6/.*

The uncertainties due to bias associated with the numerical models analysed by /Hökmark et al. 2010/ are judged to be small. In the analyses for the Laxemar site; /Hökmark et al. 2010/ assess the potential for spalling during two out of the four repository phases: the excavation and operational phase and the subsequent heated phase of initial temperate phase. Similarly to the analyses conducted for the Forsmark site, these phases are analysed independently of each other, cf. Section 6.5.7 of the SR-Site Data report /SKB 2010b/:

- It is assumed that transition from *in situ* conditions to excavated state takes place in undisturbed rock.
- For the heated part of the temperate phase, the projected deposition sequence /Leander et al. 2009/ is approximated by simultaneous deposition of all canisters.

Data uncertainty due to representativity

The results documented by /Olsson et al. 2009/ were obtained from a tunnel excavation in fractured rock that utilised careful-blasting techniques. While the data produced by /Olsson et al. 2009/ represent conditions of a carefully blasted tunnel wall, it must be recognised that there are few as carefully conducted characterisations from other underground excavations. It has been demonstrated by /Kuzyk and Martino 2008/ that careful blasting techniques can essentially eliminate the connected fracture characteristics that are frequently associated with an EDZ created using traditional drill and blast techniques. Therefore, while the /Olsson et al. 2009/ data set is unique, it is believed that their findings are applicable to hard rock masses where careful blasting techniques are applied.

As already stated above, it is difficult to know if the transmissivity values reported by /Ericsson et al. 2009/ for the fractures in individual cored samples taken from this zone are representative, or represent an upper bound value. In addition the transmissivity values of the very small discontinuous fractures were not measured.

The spalling criteria and EDZ data have been obtained from Äspö HRL. The rock mass at Äspö HRL is considered typical of the rock masses found in Fennoscandia. The EDZ fracturing is composed of natural fracturing and excavation-induced fractures. The excavation-induced fractures are a function of the blast design and are hence controlled. The natural fractures are a characteristic of the rock mass and may locally vary. However, at the repository depth this variability is not judged to be significant. The spalling strength developed by /Anderssson 2007/ at Äspö HRL has been normalised to the laboratory uniaxial compressive strength, which has been measured for all the major rock types at Laxemar and Forsmark.

Estimates of the spalling potential are based on results from linear elastic models /Hökmark et al. 2010/ without considering structurally controlled failures. As part of the safety assessment SR-Can, /Fälth and Hökmark 2007/ found that slipping low strength-fractures intersecting the deposition hole tend to increase the tangential stresses between the intersection and the floor and to reduce them below the intersection. However, /Hökmark et al. 2006, 2010/ concluded that sporadic local, structurally controlled failures should not be considered important for the overall assessment of the spalling potential. This means that, for sparsely fractured rock, the linear elastic models analysed by /Hökmark et al. 2010/ are judged to be adequate.

A5.7 Spatial and temporal variability of data

Spatial variability of data

Spatial variations of the potential for spalling depend mainly on the spatial variability of the thermal, thermo-mechanical, and mechanical properties of the rock. These variations are assessed in Chapters A2 and A4 of this report. In order to quantify the number of deposition holes that will have thermally induced spalling, the following approximations regarding the spatial variability of data are made:

- *Distribution of thermal conductivity:* The value of the thermal conductivity (i.e. mean or dimensioning value) was found to have an impact on the potential for thermally induced spalling /Hökmark et al. 2010/. Usually, the dimensioning value of the thermal conductivity is within the 0.1–2 percentile of the low-conductivity tail of the conductivity distribution /Hökmark et al. 2009/. For the purpose of the quantifying the number of deposition holes with thermally induced spalling, it is assumed that 10% of all deposition holes in a given rock domain are located within rock in which the dimensioning value of the thermal conductivity is representative and that the remaining deposition holes are located within rock in which the mean value thermal conductivity is representative.
- *Variation in Young's modulus:* The variation in the magnitude of Young's modulus between the fracture domains was found to have an impact on the potential for spalling /Hökmark et al. 2010/. However, it is not possible to deduce from the layout itself how many potential canister positions are located within each fracture domain (the number of potential canister positions in each rock domain is known, see /Hökmark et al. 2010, section I2.2/). Therefore, based on a qualitative assessment of how the repository is located in relation to the fracture domains (see Figure A5-2), all deposition holes located within rock domain RSMA are approximated to be located within fracture domain FSM_EW007, which has a lower value of Young's modulus. The remaining canister positions are assumed to be located within fracture domains FSM_W, FSM_NE005 and FSM_C, which all have the same (higher) value of Young's modulus.

The following additional factors contribute to the spatial variability of the potential for spalling:

- *Repository layout, i.e. tunnel orientation with respect to the major horizontal in situ stress:* It is well known that the tangential stresses in the walls of a deposition hole are minimised if the deposition tunnel is aligned with the major horizontal *in situ* stress. In the layout version considered by /Hökmark et al. 2010/, all deposition tunnels have a small deviation (approx. 5°) from the most likely orientation of the major horizontal *in situ* stress.

- *The location within the repository region (applies for the heated part of the temperate phase):* Canister positions located near a tunnel end or beginning have lower temperatures than more centrally located canister positions /Hökmark et al. 2009/. Consequently, the stresses in the walls of the former deposition holes would also be lower. However, the potential for spalling in the walls of such deposition holes has not been analysed by /Hökmark et al. 2010/. Furthermore, the thermally induced stresses around deposition holes located close to rejected canister positions will also be lower. For the purpose of providing upper bound estimates of the potential for spalling, /Hökmark et al. 2010/ assumes that no potential canister positions are rejected.

Temporal variability of data

In the numerical modelling, it is assumed that the thermal, thermo-mechanical, and mechanical properties of the rock mass do not vary with time (cf. Chapters A2 and A4).

The potential for spalling varies with the induced loads during the different repository phases /Hökmark et al. 2010/:

- *Construction and operational phase:* Spalling in the walls of deposition holes during the construction and operational phase will occur only by way of exception.
- *Heated period of the temperate phase:* The potential for thermally induced spalling, in a given rock domain, depends on the state of *in situ* stress and the thermal and mechanical properties in that rock domain (see also sections on precision and spatial variability. For a discussion on the temporal evolution of the spalled zone, see Section 6.5.6 of the SR-Site Data report /SKB 2010b/.

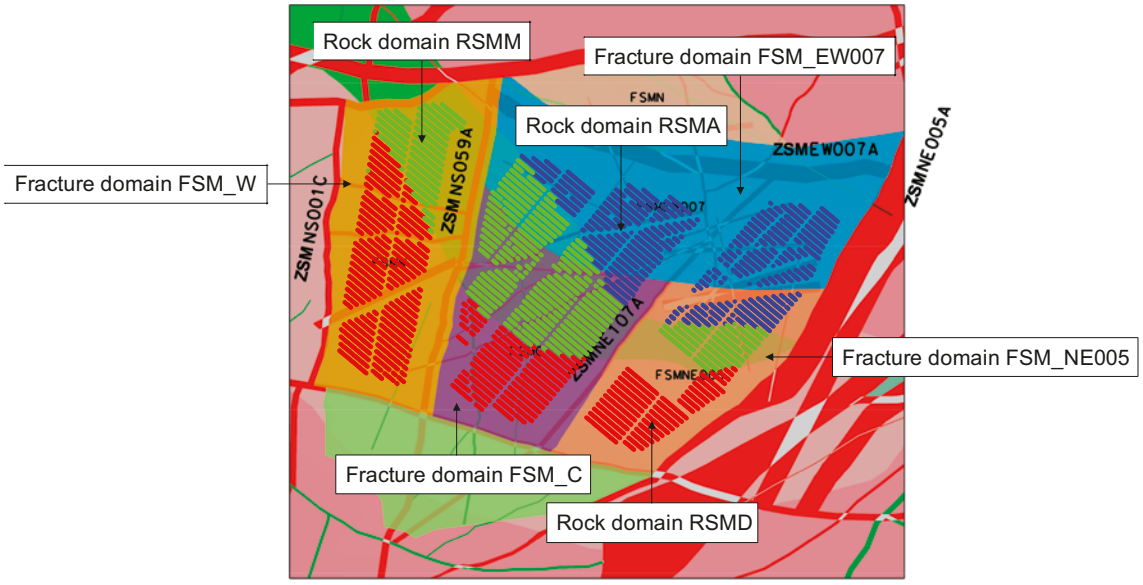

Figure A5-2. *Repository layout superimposed on map showing outlines of the fracture domains at 500 m depth. The layout is colour coded according to rock domain (RSMA is blue, RSMM is green and RSMD is red). Fracture domains (FSM_x) are represented by coloured blocks (FSM_EW007 is light blue, FSM_W is yellow, FSM_C is lilac and FSM_NE005 is beige). Background map modified from /SKB 2009, Figure 5-62/.*

A5.8 Correlations

The potential for spalling depends on the properties of the rock mass (elastic properties, heat transport properties, and the coefficient of thermal expansion), the magnitude and orientations of the *in situ* stresses, as well as the near-field design of deposition tunnels and deposition holes. The potential for spalling is assessed by comparison of the calculated tangential stresses /Hökmark et al. 2010/ with the estimated spalling strength. The parameter values used in the modelling work are described in Section A4.10 of this report. Similarly to the assessment for SR-Can /Hökmark et al. 2006/, the possibility that the swelling pressure from the bentonite buffer may suppress spalling is ignored.

There is no correlation that needs to be considered in subsequent hydrogeological or radionuclide transport modelling.

A5.9 Result of supplier's data qualification

Data for the tunnels

In this appendix, the absence of an EDZ that is connected on the tunnel scale is argued, as motivated based on experimental observations and data. This does not necessarily mean that transmissivity in the EDZ is as low as in the undisturbed rock, wherefore the axial transmissivity T (m^2/s) of the EDZ along deposition tunnels, other tunnels, and shafts is given.

As stated in the Underground opening construction report /SKB 2010a, Chapter 6/, it is possible to control the drill and blasting of the tunnels such that a continuous fracturing along the axial direction of the tunnel will not develop. This was stated already in SR-Can, based on experiences from the excavation of the TASQ tunnel at ÄSPÖ HRL /Olsson et al. 2004/, and has been further confirmed by the intermediate results from the demonstration trial of smooth blasting techniques at the ÄSPÖ HRL /Olsson et al. 2009, Ericsson et al. 2009/. These indicate that blast induced fractures in the rock side-walls are dominantly radial and that such fractures will not be continuous along the axial direction of the tunnel over any significant distance, see Figure A5-3.

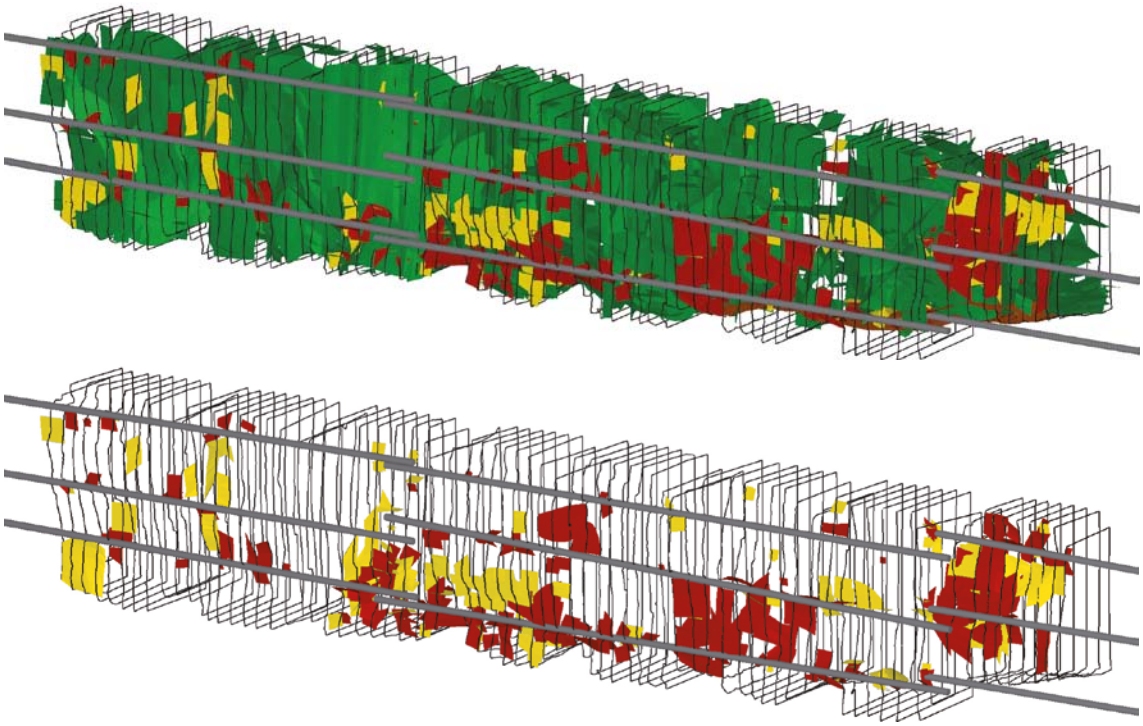

Figure A5-3. *Top: Boreholes, slabs and all interpreted fractures. Bottom: Ditto but only with blast and blast-induced fractures. The colours indicate different fractures according to: Green = natural, red = blast, and yellow = blast induced. Reproduced from /Olsson et al. 2009, Fig 7-9 and 7-10/. The length of the test area is 8 m and the height is 1.5 m.*

Furthermore, available literature suggests that the hydraulic conductivity in drilled and blasted tunnels is on the order of 10^{-8} m/s /Bäckblom 2008/ although these conductivities could possibly be very local and may not necessarily be created by the excavation activities.

In the near-field, the geometry of individual fractures and how they intersect repository openings and interact with other fractures are much more important than details in the background stress field. Therefore, the estimates given in SR-Can /Hökmark et al. 2006/, *i.e.* an increase in transmissivity of about two orders of magnitude 1–2 m from the tunnel openings and no significant change elsewhere, are relevant also for the Laxemar site (see also Section 6.5.10 of the SR-Site data report /SKB 2010b/).

An increase of the transmissivity by two orders of magnitude, as compared to the pristine rock with a transmissivity of about 10^{-10} m^2/s, would suggest an axial transmissivity of about 10^{-8} m^2/s in the EDZ.

Very close to the periphery of the tunnel, the normal stress could be low enough that, theoretically, the transmissvity increase could be even larger than that suggested in SR-Can for fractures that are almost parallel to the tunnel axis. However, in reality fractures will not be persistently parallel to the tunnel where there are deposition holes, especially since deposition holes intersected by fractures intersecting more than four deposition holes will be rejected according to the EFPC criterion. This means that this effect can be discarded, or at least captured within the EDZ assumption of $T = 10^{-8}$ m^2/s along the tunnel.

Data for the deposition holes

The data that should be supplied are listed in Section A5.1. This is addressed in the following.

Potential for spalling

The potential occurrence of spalling is site and repository design specific, as it depends on the *in situ* stress, the intact rock mechanical strength, and on the repository layout (*i.e.* orientation of deposition tunnels and near-field design of deposition tunnels and deposition holes). For the heated part of the initial temperate phase, additional parameters such as the elastic properties, the heat transport properties, and the thermo-mechanical properties of the rock mass become important. Spalling is the only fracturing mechanism identified as relevant during the initial temperate period.

/Hökmark et al. 2010/ have revised the assessment of potential for thermally induced spalling presented in SR-Can, using a detailed near-field model geometry that incorporates one tunnel segment with seven canisters, three of which have explicitly modelled deposition holes. The model calculates the tangential stress in the wall of the deposition hole resulting from the excavation, and the subsequent thermal load. The calculated stress is in turn compared with the spalling strength of the rock, which is assumed to be in the range 52–62% of the uniaxial compressive strength (UCS) of intact rock in each rock domain (cf. Table A4-17 in Chapter A4). /Hökmark et al. 2010/ studied a number of cases with different assumptions regarding the value of the thermal conductivity, and magnitudes and orientations of the *in situ* stress. An attempt to quantify the number of deposition holes with thermally induced spalling is made in Table A5-4 and Table A5-5. /Hökmark et al. 2010/ estimate the potential for spalling in one or two locations in each rock domain at Laxemar. For each model, two assumptions are made regarding the thermal conductivity (mean or dimensioning value) and two assumptions are made regarding the most likely *in situ* stress magnitudes and orientations (cf. Table A4-19 of Chapter A4). The result from each model, in terms of potential for spalling, is subsequently taken to be representative of all deposition holes in a given rock domain with the same assumption regarding thermal conductivity and state of *in situ* stress.

Table A5-4. Esimate of number of deposition holes with thermally induced spalling (Yes = model results predict that there will be thermally indced spalling, No = model results predict that there will not be any thermally induced spalling, see Figures I-29, I-30, I-31 and I-33 in /Hökmark et al. 2010/). Most likely in situ stress magnitudes and orientations as given in the site description of Laxemar, cf. Table A4-19 in Chapter A4.

Rock domain	Thermal conductivity		Deposition holes with spalling (% of total)
	Mean	Dimensioning	
RSMA	No	No	0.0
RSMD	Yes	Yes	44.0
RSMM	No	Yes	3.1
Deposition holes with spalling (% of total)	39.6	7.5	47.1

Table A5-5. Esimate of number of deposition holes with thermally induced spalling (Yes = model results predict that there will be thermally indced spalling, No = model results predict that there will not be any thermally induced spalling, see Figures I-29, I-30, I-31 and I-33 in /Hökmark et al. 2010/). Most likely in situ stress magnitudes and orientations with the major horizontal stress as in Äspö, cf. Table A4-19 in Chapter A4.

Rock domain	Thermal conductivity		Deposition holes with spalling (% of total)
	Mean	Dimensioning	
RSMA	Yes	Yes	35.0
RSMD	Yes	Yes	44.0
RSMM	Yes	Yes	31.0
Deposition holes with spalling (% of total)	90.0	10.0	100.0

A summary of the results is provided by the following:

- All models predict that spalling after excavation will occur only by exception.
- For the most likely stress model given in the Laxemar site description report, thermally induced spalling is likely in about 50% of the deposition holes, cf. Table A5-4.
- With the major principal stress as in Äspö, thermally induced spalling is likely in the great majority of the deposition holes, cf. Table A5-5.

Geometry and location of the spalled zone

Examples of the magnitude of the major principal stress and its location on the deposition hole perimeter at stress maximum are provided in Figure A5-4 (most likely *in situ* stress model as given in the site report for Laxemar) and Figure A5-5 (*in situ* stress model with the major principal stress as in Äspö). These examples apply for a typical deposition hole in rock domain RSMD, which according to the model results provided in /Hökmark et al. 2010/ is the rock domain that has the highest potential for thermally induced spalling. Note that the stress perturbation at approximately 2 m depth is due to the fact that the location of the maximum stress in the deposition hole wall coincides with the location of the deposition hole wedge (cf. Section 9.3 in /Hökmark et al. 2010/).

As seen in Figure A5-4 and Figure A5-5, for these cases representing the most likely stress magnitudes and orientations, the length of the spalled zone is highly dependent on the assumed state of *in situ* stress. If the major horizontal stress can be assumed to be equal to that at Äspö, spalling is likely to occur along the great majority of the deposition hole (Figure A5-5). Therefore it is reasonable to assume, as an upper bound estimate, a length of the spalled zone L_{zone} of 8 m, located along the entire length of the deposition hole.

According to /Hökmark et al. 2010/ there is, at present, no way of directly calculating the actual shape or depth of thermally induced failures. Experience from the APSE /Andersson 2007/ indicates that the failures will be notch-shaped and that the notch will self-stabilise at some depth that depends on the stress that prevailed at the time of the failure. Once the notch is stable, subsequent increases in stress will not significantly increase the depth of the failure. The notch developed at APSE was typically 0.5 m wide /Andersson 2007, Figure 6-17/ and 0.1 m deep (thick) /Andersson 2007, Figure 6-18/. Based on this W_{zone} = 0.5 m and d_{zone} = 0.1 m is suggested.

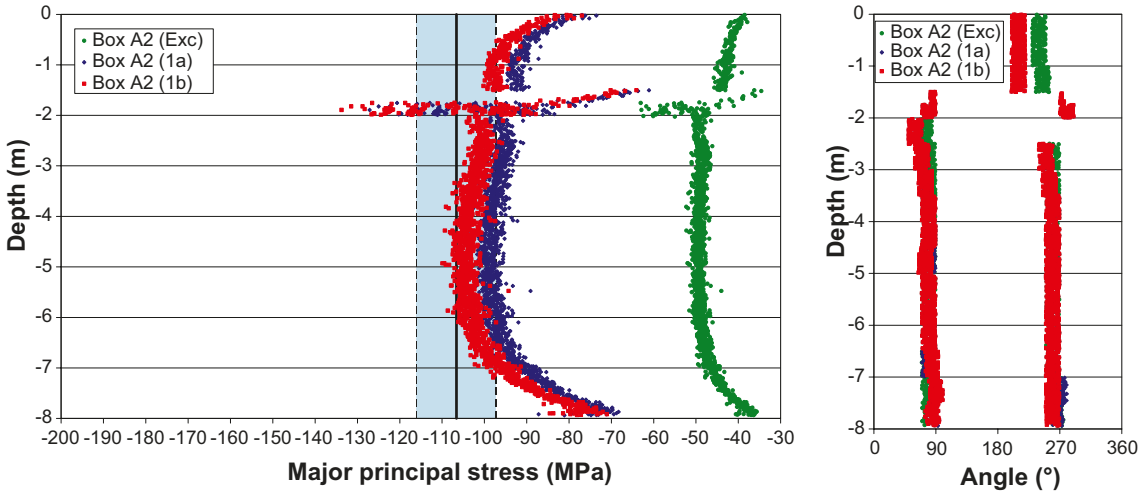

Figure A5-4. *Left: Simulated maximum tangential stress along the deposition hole wall for the most likely in situ stress magnitudes and orientations given in the site report for Laxemar after excavation (Exc) and after 50 years of heating for two assumptions regarding the thermal conductivity – mean value (1a) and dimensioning value (1b). Blue area represents spalling strength in rock domain RSMD (52-62% of UCS). Right: Location of maximum stress on deposition hole perimeter. Both figures are obtained from Figure I-34 in /Hökmark et al. 2010/.*

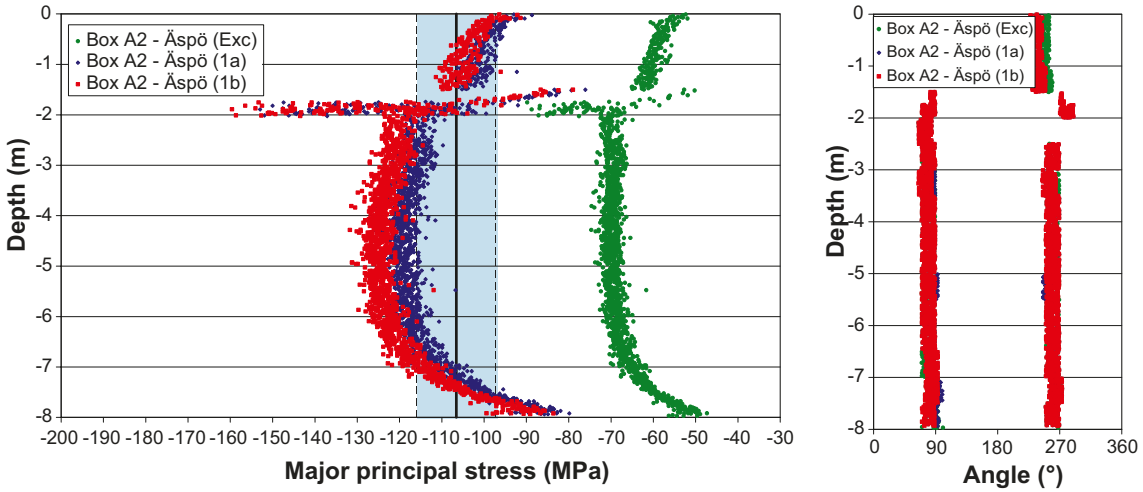

Figure A5-5. *Left: Simulated maximum tangential stress along the deposition hole wall for the most likely in situ stress magnitudes and orientations (major horizontal in situ stress as in Äspö) after excavation (Exc) and 50 yearsof heating for two assumptions regarding the thermal conductivity – mean value (1a) and dimensioning value (1b). Blue area represents spalling strength in rock domain RSMD (52–62% of UCS). Right: Location of maximum stress on deposition hole perimeter. Both figures are obtained from Figure I-35 in /Hökmark et al. 2010/.*

Tortuosity and porosity of the spalled zone

The data concerning tortuosity and porosity of the spalled zone were obtained in the Äspö Pillar Stability Experiment /Neretnieks and Andersson 2009, Andersson 2007, Neretnieks et al. 2010/. These data are applied for both the Forsmark and Laxemar sites. As justified in the corresponding section of the SR-Site Data report /SKB 2010b/, $\tau_y = 10$ and $\varepsilon_{zone} = 0.02$ are suggested.

Hydraulic conductivity

The data on the hydraulic conductivity of the spelled zone are obtained at the Äspö HRL. These data are applied for both the Forsmark and Laxemar sites. As justified in the corresponding section of the SR-Site Data report /SKB 2010b/, the hydraulic conductivity of the spalled zone is suggested to be "high".

The connected effective transmissivity T (m^2/s) of the deposition hole EDZ

As justified in the SR-Site Data report, based on the findings in /Bäckblom 2008, SKB 2010a/ the transmissivity associated with EDZ in deposition holes is less than 10^{-10} m^2/s. This is under the pre-requisite that no spalling occurs. This data are judged to be applicable for the Laxemar site.

A5.10 Data recommended for use in comparative analysis

Hydraulic properties along tunnel walls and floor

Table A5-6 lists the recommended axial transmissivity value along tunnel walls. The recommended value is based on the value given as a design premises. However, some variant transmissivity values are also suggested as input for exploring how transmissive an EDZ need to be in order to significantly impact other safety functions, as well as exploring the impact of no axially continuous EDZ at all.

Table A5-6. Recommended axial transmissivity data along deposition tunnels, other tunnels, and shaft.

Parameter	Recommended value	Variant values
Tunnel and shaft EDZ transmissivity	10^{-8} m^2/s	0, 10^{-7}, 10^{-6} m^2/s

Hydraulic properties in deposition hole wall

Table A5-7 lists recommended hydraulic data along the deposition hole walls, and properties of the spalled zone. Two variants are recommended, assuming no spalling or spalling in all deposition holes. However, it should be observed that in case the buffer is lost, there is no impact from spalling. The occurrence of spalling should not affect the potential for loss of buffer or for canister corrosion (see SR-Site Main report /SKB 2011, Section 10.3.11/).

Table A5-7. Recommended data for deposition hole walls.

Parameter	Value	Variant values
Potential for spalling	High	–
Length of spalled zone, L_{zone}	8 m	No spalling
Thickness of spalled zone, d_{zone}	0.1 m	No spalling
Width of spalled zone, W_{zone}	0.5 m	No spalling
Tortuosity of spalled zone, τ_y	10	No spalling
Spalled zone porosity, ε_{zone}	0.02	No spalling
Hydraulic conductivity of spalled zone, K	High	No spalling
Connected effective transmissivity of deposition hole wall EDZ, in holes where no spalling occurs	10^{-10} m^2/s	–

References A5.11

SKB's (Svensk Kärnbränslehantering AB) publications can be found at www.skb.se/publications.

Andersson J C, 2007. Äspö Hard Rock Laboratory. Äspö Pillar Stability Experiment, final report. Rock mass response to coupled mechanical thermal loading. SKB TR-07-01, Svensk Kärnbränslehantering AB.

Bäckblom G, 2008. Excavation damage and disturbance in crystalline rock – results from experiments and analyses. SKB TR-08-08, Svensk Kärnbränslehantering AB.

Bäckblom G, Christiansson R, Lagerstedt L, 2004. Choice of rock excavation methods for the Swedish deep repository for spent nuclear fuel. SKB R-04-62, Svensk Kärnbränslehantering AB.

Cliffe K A, Kelly M, 2006. COMP23 version 1.2.2 user's manual. SKB R-04-64, Svensk Kärnbränslehantering AB.

Elert M, Gylling B, Lindgren M, 2004. Assessment model validity document FARF31. SKB R-04-51, Svensk Kärnbränslehantering AB.

Ericsson L O, Brinkhoff P, Gustafson G, Kvartsberg S, 2009. Hydraulic Features of the Excavation Disturbed Zone. Laboratory investigations of samples taken from the Q- and S-tunnels at Äspö HRL. SKB R-09-45, Svensk Kärnbränslehantering AB.

Fälth B, Hökmark H, 2007. Mechanical and thermo-mechanical discrete fracture near-field analyses based on preliminary data from the Forsmark, Simpevarp and Laxemar sites. SKB R-06-89, Svensk Kärnbränslehantering AB.

Glamheden R, Fälth B, Jacobsson L, Harrström J, Berglund J, Bergkvist L, 2010. Counterforce applied to prevent spalling. SKB TR-10-37, Svensk Kärnbränslehantering AB.

Hökmark H, Fälth B, Wallroth T, 2006. T-H-M couplings in rock. Overview of results of importance to the SR-Can safety assessment. SKB R-06-88, Svensk Kärnbränslehantering AB.

Hökmark H, Lönnqvist M, Kristensson O, Sundberg J, Hellström G, 2009. Strategy for thermal dimensioning of the final repository for spent nuclear fuel. SKB R-09-04, Svensk Kärnbränslehantering AB.

Hökmark H, Lönnqvist M, Fälth B, 2010. THM-issues in repository rock. Thermal, mechanical, thermo-mechanical and hydro-mechanical evolution of the rock at the Forsmark and Laxemar sites. SKB TR-10-23, Svensk Kärnbränslehantering AB.

Kuzyk G W, Martino J B, 2008. Development of excavation technologies at the Canadian underground research laboratory. In: Bäckblom G (ed). Proceedings of the International Conference Underground Disposal Unit Design & Emplacement Processes for a Deep Geological Repository, Prague, Czech Republic, 16–18 June 2008. Paris: Andra.

Leander M, Nyborg M, Lundqvist A, Eriksson M, Petersson J, 2009. Underground design Laxemar. Layout D2. Layout and construction plan. SKB R-09-08, Svensk Kärnbränslehantering AB.

Neretnieks I, Andersson J C, 2009. Characterisation of spalling fragments to obtain data for flow and transport in damaged zones. In: Hudson J, Tham L, Feng X-T, Kwong A (eds). Rock characterisation, modelling and engineering design methods: proceedings of the International Symposium on Rock Mechanics (SINOROCK 2009), University of Hong Kong, 19–22 May 2009.

Neretnieks I, Liu L, Moreno L, 2010. Mass transfer between waste canister and water seeping in rock fractures. Revisiting the Q-equivalent model. SKB TR-10-42, Svensk Kärnbränslehantering AB.

Norman S, Kjellbert N, 1990. FARF31 – A far field radionuclide migration code for use with the PROPER package. SKB TR 90-01, Svensk Kärnbränslehantering AB.

Olsson M, Niklasson B, Wilson L, Andersson C, Christiansson R, 2004. Äspö HRL. Experiences of blasting of the TASQ tunnel. SKB R-04-73, Svensk Kärnbränslehantering AB.

Olsson M, Markström I, Pettersson A, Sträng M, 2009. Examination of the Excavation Damaged Zone in the TASS tunnel, Äspö HRL. SKB R-09-39, Svensk Kärnbränslehantering AB.

Serco, 2005. CONNECTFLOW Release 9.0. Technical summary document. Report SA/ ENV/ CONNECTFLOW/15, Serco Assurance.

SKB, 2009. Site description of Laxemar at completion of the site investigation phase. SDM-Site Laxemar. TR-09-01, Svensk Kärnbränslehantering AB.

SKB, 2010a. Design, construction and initial state of the underground openings. SKB TR-10-18, Svensk Kärnbränslehantering AB.

SKB, 2010b. Data report for the safety assessment SR-Site. SKB TR-10-52, Svensk Kärnbränslehantering AB.

SKB, 2011. Long-term safety for the final repository for spent nuclear fuel at Forsmark. Main report of the SR-Site project. SKB TR-11-01, Svensk Kärnbränslehantering AB.

A6 Quantities for groundwater flow modelling

The use of hydrogeological models in the Comparative analysis allows for simulations of groundwater flow from a deep disposal facility to the biosphere. It also allows for the calculation of performance measures that will provide an input to a safety assessment.

This appendix provides site specific data of the quantities associated with the stochastic fracture network realisations for use in the discrete fracture network (DFN) and equivalent continuous porous medium (ECPM) groundwater flow modelling. This appendix only concerns quantities and properties of the rock mass volumes found in between deterministically modelled deformation zones (DZ). The flow and transport properties of the latter, as well as of the regolith found on top of the rockhead, are given in /Rhén and Hartley 2009/.

The hydrogeological data presented in this appendix feed into the assessment of flow related migration properties. The usage of flow related migration properties in the Comparative analysis is described in Chapter A7.

Similar types of calculations have been performed in SR-Site based on Forsmark data. A corresponding text for the Forsmark site is found in Section 6.6 of the SR-Site Data report /SKB 2010/. In instances concerning uncertainties and methodologies that are general for both sites, we have chosen to refer to the corresponding Forsmark text instead of repeating the information. Therefore, we recommend the reader to examine Section 6.6 of the SR-Site Data report prior to reading this present text.

A6.1 Modelling as input to the Comparative analysis of safety related site characteristics

In the Comparative analysis, groundwater flow in the repository host rock is conceptualised to occur in a discrete fracture network. Hydrogeological DFN models explicitly model the fractures through which the groundwater flows, and are characterised by quantities associated with these fractures, such as orientation, size, intensity, transmissivity, and aperture. Hydrogeological DFN modelling invokes Monte Carlo simulations (multiple realisations) as the fracture quantities are described statistically. They often represent a local rock volume, due to the high demands of computational capacity. The central part of the site scale model is commonly represented by a using an explicit DFN concept.

In order to assess the implications of DFN models on flow and transport on scales larger than that encompassed by the immediate repository host rock, it is often necessary for practical reasons to convert DFN models to models with appropriate continuum flow and transport properties. These properties include hydraulic conductivity, fracture kinematic porosity, and flow wetted fracture surface area per unit volume of rock. On a regional model scale, i.e. in rock mass volumes far away from the repository, the ECPM approach with heterogeneous flow and transport properties is used. The ECPM properties are derived by means of up-scaling the underlying DFN realisation. Since each ECPM model is based on a particular underlying stochastic DFN realisation, the flow and transport properties of the ECPM models are also stochastic. That is, uncertainties relating to the spatial variability are quantified by means of multiple realisations. On an intermediate model scale, i.e. on a site scale, the equivalent continuous porous medium approach with heterogeneous flow and transport properties is used.

In conclusion, in the modelling of Laxemar for the Comparative analysis, the groundwater flow modelling on the repository and site scales is performed using the DFN and ECPM approaches, respectively. On a regional scale, groundwater flow modelling is performed using the ECPM approach. The rational for using this mixture of flow concepts in SR-Site is summarised in /Selroos and Follin 2010/. The same rational is used for the Comparative analysis.

Defining the data requested from the supplier

The following quantities associated with the generation of stochastic fracture network realisations for use in the DFN and ECPM groundwater flow modelling are requested from the supplier:

- The fracture orientation model statistics for each suggested fracture set, in terms of the Fisher distribution mean pole trend (°), plunge (°) and concentration κ (–).
- The fracture size model statistics for each suggested fracture set in terms of the Pareto distribution location parameter r_0 (m) and shape parameter k_r (–).

- Statistics for the fracture intensity model, in terms of the open fracture surface intensity per unit volume of rock $P_{32,o}[r_0,564\text{m}]$ (m^2/m^3), for each suggested fracture set. The largest fracture radius considered for these data should be 564.2 m (cf. Chapter A3).
- The constants a, b, and σ_{logT}, for a semi-correlated transmissivity model. Constants for correlated and uncorrelated transmissivity models are presented in the SDM-Site Laxemar report by /Rhén and Hartley 2009/, but only the semi-correlated concept is used in the Comparative analysis.

All these data should be given for each suggested fracture set. Judged as appropriate by the supplier, different fracture sets should be suggested for different rock mass volumes of the host rock. In addition, the repository system should be taken into account, in case it affects how discrete fractures are connected.

Modelling activities in which data will be used

Groundwater flow modelling for the Laxemar site is performed in the Comparative analysis with the purpose of:

- Estimating the inflow rate to the repository and the potential for upconing of saline groundwater during open repository conditions.
- Assessing exit locations of downstream flow paths as well as entrance locations of upstream flow paths starting at different deposition hole positions. In addition their associated flow-related transport properties are assessed, such as Darcy fluxes at repository depth, advective travel times, and transport resistances during saturated temperate, periglacial, or glacial conditions (cf. Chapter A7).
- Delivering input data to hydrogeochemical modelling during saturated temperate, periglacial, and glacial conditions (cf. Chapter A1).

The following groundwater flow modelling studies are performed in the Comparative analysis:

- *Excavation and operation phases:* During the excavation and operation phases of the repository, the system is characterised by the tunnels being at atmospheric pressure. Simulations of the excavation and operation periods are performed by /Svensson and Follin 2010/ using the DarcyTools code /Svensson et al. 2010/. For the inflow calculations, saturated groundwater flow below the groundwater table, and a simplified description of unsaturated flow above the groundwater table, are used. Additional simulations of near-surface effects are done using the hydrogeological modelling tool MIKE-SHE /Mårtensson et al. 2009/. The objective of these latter studies is primarily to assess the interaction between the near-surface and deep rock groundwater systems. Also, the near-surface modelling can provide information to Environmental Impact Assessment studies.
- *Periods with temperate climate conditions:* The simulations that deal with temperate climate conditions address an approximately 20,000 year long period, extending from repository saturation up till the initiation of the next permafrost-glaciation event. Saturated groundwater flow is modelled including the shoreline displacement as a transient boundary condition. The backfilled tunnels are explicitly included in the models that are based on a nesting of different scales (from regional to site to canister scales) using a mixture of continuum and discrete fracture network representations of the rock mass. Simulations of the temperate period are performed by /Joyce et al. 2010/ using the ConnectFlow code /Hartley and Holton 2004/. The strategy for identifying the most important and/or critical hydrogeological variants to be addressed in the temperate period simulations is to propagate a number of SDM-Site variants to the regional scale simulations. The Comparative analysis simulations for Laxemar differ from the SDM-Site calculations in that they cover the time period from the end of the last glaciation up till the onset of the next glacial period, whereas the SDM-Site models end at present day conditions. The variants with greatest impact on performance measures are propagated to detailed site and repository scale calculations involving an explicit hydrogeological DFN representation.
- *Periods with periglacial and glacial climate conditions:* The main objective of the periglacial and glacial simulations is to assess the groundwater flow pattern during periods when the upper part of the geosphere may be frozen, thus restricting flow, and/or when a glacial load (glaciation advance and retreat) may imply different recharge and stress conditions. Input is obtained from an ice-sheet model that provides the glacial conditions. A second objective is to study the possible movement of salt due to up-coning during glacial conditions. Simulations of the permafrost and glacial conditions are performed by /Vidstrand et al. 2010/ using the DarcyTools code. The modelling strategy is to identify important parameter combinations of climatological and rock property conditions, and then implement 3-D models on a large, supra-regional scale.

A6.2 Supplier input on use of data in the Comparative analysis

The Laxemar site generally has a higher frequency of flowing fractures at depth than the Forsmark site. Furthermore, in the hydrogeological modelling it has been found that the groundwater flow rates in deformation zones and background fractures at depth are higher in Laxemar than in Forsmark. The groundwater flow rates through the repository host rock have a large influence on the safety assessment and therefore these data, together with the data delivered in Chapter A7, may prove valuable for the Comparative analysis.

A6.3 Sources of information and documentation of data qualification

Sources of information

The main sources of information are listed in Table A6-1. The publications referred to provide important input to the groundwater flow modelling studies carried out in the Comparative analysis.

Table A6-1. Main sources of information used in data qualification.

Joyce S, Simpson T, Hartley L, Applegate D, Hoek J, Jackson P, Roberts D, Swan D, Gylling B, Marsic N, Rhén I, 2010. Groundwater flow modelling of periods with temperate climate conditions – Laxemar. SKB R-09-24, Svensk Kärnbränslehantering AB.
Rhén I, Hartley L, 2009. Bedrock Hydrogeology Laxemar, Site descriptive modelling, SDM-Site Laxemar. SKB R-08-92, Svensk Kärnbränslehantering AB.
SKB, 2006. Climate and climate-related issues for the safety assessment SR-Can. SKB TR-06-23, Svensk Kärnbränslehantering AB.
SKB, 2009a. Site description of Laxemar at completion of the site investigation phase. SDM-Site Laxemar. SKB TR-09-01, Svensk Kärnbränslehantering AB.
SKB, 2009b. Underground design Laxemar. Layout D2. SKB R-09-16, Svensk Kärnbränslehantering AB.
SKB, 2010. Data report for the safety assessment SR-Site. SKB TR-10-52, Svensk Kärnbränslehantering AB.
Svensson U, Rhén I, 2010. Groundwater flow modelling of the excavation and operation phases – Laxemar. SKB R-09-23, Svensk Kärnbränslehantering AB
Vidstrand P, Rhén I, Zugec N, 2010. Groundwater flow modelling of periods with periglacial and glacial conditions – Laxemar. SKB R-09-25, Svensk Kärnbränslehantering AB.

The SDM-Site version of site description Laxemar /SKB 2009a/ summarises the results of modelling activities in several disciplines. /Rhén and Hartley 2009/ is the key reference document on bedrock hydrogeology at Laxemar and summarises the results of a chain of groundwater flow modelling activities carried out on behalf of site description Laxemar.

/SKB 2009b/ provides the geometry of the repository system (Layout D2) that is taken into account in the analyses of how discrete fractures are connected to the repository system. The SR-Site Data report /SKB 2010/ provides important data on the engineered barrier system, such as the hydraulic properties of the backfill. These data support the hydrogeological modelling of Laxemar in the Comparative analysis.

The SR-Can Climate report /SKB 2006/ provides a description of past and future climate conditions at the Laxemar site (also reported in Chapter 3 of this present report). The understanding of historic data and the suggested reference evolution of the future is used as input to the groundwater flow modelling that handles periods with temperate climate conditions /Joyce et al. 2010/ and periglacial and glacial climate conditions /Vidstrand et al. 2010/.

/Joyce et al. 2010/ provides a description of the chosen methodology for groundwater flow modelling of Laxemar in the Comparative analysis, and the corresponding simulation results. /Svensson and Rhén 2010/ provides a description of the inflow calculations to the repository during the excavation and operation phases.

Categorising data sets as qualified or supporting data

The data requested in this appendix have been produced during a chain of site-descriptive modelling activities and also in activities of the Comparative analysis, taking the repository layout into account.

Most data sets in this appendix are reproduced from tables or equivalents of background reports, which are referenced in Table A6-2. Data sets that are produced for the Laxemar site within site-descriptive modelling or Comparative analysis activities are generally considered as qualified. The sorting of data sets as qualified or supporting is justified in Table A6-3.

Table A6-2. Qualified and supporting data sets.

Qualified data sets	Supporting data sets
1. /Joyce et al. 2010/, Table E-1: The fracture orientation, size, and intensity statistics, as well as the fracture transmissivity model constants for the fraction of the repository rock mass volume coinciding with the hydraulic rock domain HRD_C. 2. /Joyce et al. 2010/, Table E-2: As in 1. but for the fraction of repository rock mass volume coinciding with the rock domain HRD_EW007. 3. /Joyce et al. 2010/, Table E-3: As in 1. but for the site-scale rock mass volume coinciding with the rock domains HRD_W. 4. /Joyce et al. 2010/, Table 2-2: The hydraulic conductivity for the rock mass volumes far away from the repository host rock mass volume (outside HRD_C, HRD_EW007, and HRD_W).	5. /Joyce et al. 2010/, Equation 3-2: The fracture aperture model constants.

Table A6-3. Justification of the sorting of items in Table A6-2.

1–3: For the repository host rock mass volume and the site-scale rock mass volume, the fracture orientation model statistics, the fracture size model statistics, the fracture intensity model statistics, and the fracture transmissivity model constants coinciding with rock domains HRD_C, HRD_EW007, and HRD_W were derived and applied within the site-descriptive modelling through a chain of different modelling activities that were each peer reviewed. These modelling activities comply with the SKB quality assurance system and thus the data are judged as qualified. 4: The rock mass in the regional model, outside the defined HRDs mentioned above, is based on the material property assignments made in model version Laxemar 1.2 (summarised in /Rhén et al. 2009/) and assessments of similarities between regional HRDs and the newly developed HRDs inside the Laxemar local model volume; HRD_C, HRD_EW007, HRD_N and HRD_W. These modelling activities comply with the SKB quality assurance system and thus the data are judged as qualified.	5: For the host rock mass volume, the fracture aperture model constants (reported in /Hjerne et al. 2010/) were applied within the site-descriptive modelling through a chain of different modelling activities that were each peer-reviewed. Although these modelling activities comply with the SKB quality assurance system, the model parameters are not based on investigations at Laxemar. These data are therefore sorted as supporting.

Excluded data previously considered as important

Throughout the modelling chain of the site descriptions and Comparative analysis there have been modifications of the hydrogeological models (e.g. /Rhén et al. 2008/). Different models may utilise different data collected in the site investigation.

A6.4 Conditions for which data are supplied

Six fracture domains, (FSM_C, FSM_EW007, FSM_N, FSM_NE005, FSM_S, FSM_W), are defined in the geological DFN modelling based on spatial differences in the fracture frequency of *all* fractures /La Pointe et al. 2008/. In the hydrogeological DFN modelling, hydraulic rock domains (HRD's) were introduced /Rhén and Hartley 2009/ based on the differences observed in the frequency of flowing fractures versus depth. HRD_C is corresponding to FSM_C, FSM_NE005, and FSM_S in combination. HRD_EW007 is corresponding to FSM_EW007, HRD_N to FSM_N, and HRD_W to FSM_W with exclusion of data from KLX13A /Rhén et al. 2008/. Figure A6-1 shows two cartoons of the rock domains at Laxemar that constitute the rock mass volumes on the repository and site scales.

The assignment of the rock mass in the regional model, outside the defined four HRD's mentioned above, is based on the material property assignments made in model version Laxemar 1.2 (summarised in /Rhén et al. 2009/) and assessments of similarities between regional HRD's and the newly developed HRD's inside the Laxemar local model volume; HRD_C, HRD_EW007, HRD_N and HRD_W.

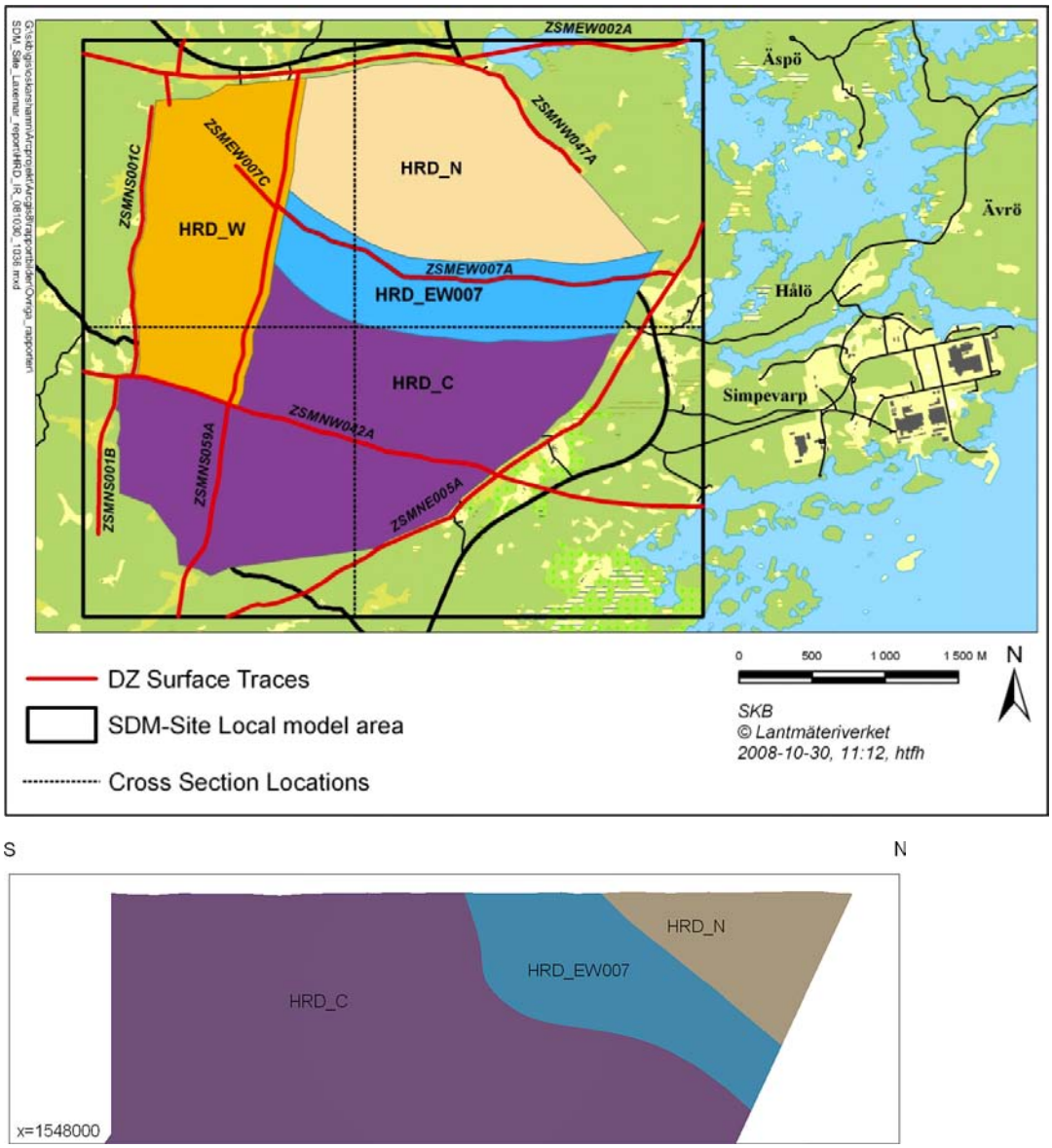

Figure A6-1. *Cartoons showing the rock domains at Laxemar that constitute the bedrock surrounding the repository. The key rock domains forming the repository host rock are labelled HRD_C, HRD_EW007, and HRD_W. Labels beginning with ZSM are names of major deformation zones. Reproduced from Figures 5-4 and 5-5 in /Rhén and Hartley 2009/. Note that in the cross-sectional cartoon, left represents south and right represents north (as opposed to the direction in e.g. Figure A6-2).*

Structural-hydraulic data from cored boreholes gathered during the site investigations at Laxemar /Rhén et al. 2009/ are used in the hydrogeological DFN modelling in the Comparative analysis. The boreholes are drilled at different locations and in different orientations in the rock mass volumes surrounding the repository. A comparison of conceptual models for fracture domains, hydrogeological DFN, and associated hydraulic rock mass domains is shown in Figure A6-2.

The structural data gathered in the boreholes are analysed for each fracture domain sub-unit based on the analyses of fracture frequency, the spatial arrangement of fractures, fracture orientation, and fracture size, as described in the geological DFN modelling. In order to construct the hydrogeological DFN model representation for the Comparative analysis, the same methodology was initially used as the one described in the SR-Site Data report /SKB 2010, Section 6.6/. However, the upscaled hydrogeological DFN models based on the methodology used in the SDM-Site Laxemar seem to overestimate the hydraulic properties of the rock of Laxemar. In order to improve the representation, an Elaborated hydrogeological DFN methodology was developed /Joyce et al. 2010/.

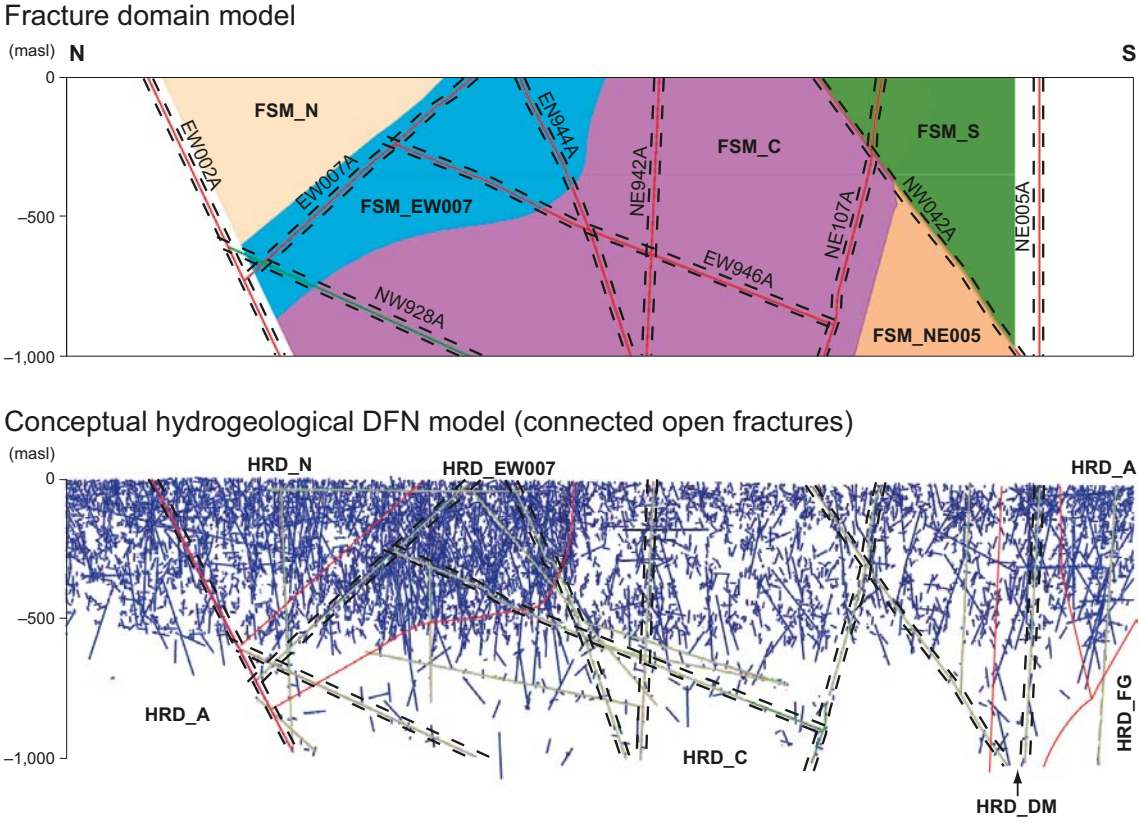

Figure A6-2. *Comparison of conceptual models for fracture domains, hydrogeological DFN, and associated hydraulic rock mass domains along the N-S cross section (cf. Figure A6-1). The length of the cross section is ~ 4,300 m. Reproduced from Figure 2-10 in /Joyce et al. 2010/.*

The key changes used for the Elaborated Hydro-DFN methodology compared to the methodology detailed in /Rhén et al. 2009/, as used for SDM-Site, are the following:

- Representative boreholes were modelled explicitly, and HCD's included in these models.
- Particular care was taken with the fracture size to transmissivity relationship assigned to the WNW set in DZ3.
- Particular care was taken to calibrate the fracture sets individually.
- A maximum Terzaghi correction of 100 was used in the modelling, compared to a value of 7 used in the SDM-Site Hydro-DFN calibration /Rhén et al. 2008/.

A6.5 Conceptual uncertainty

In the hydrogeological DFN modelling associated with the Comparative analysis, three key assumptions have been made:

1. The fracture surface area per unit volume of rock of *all fractures* greater than the borehole radius $P_{32,a}[r \geq r_{BH}]$ can be estimated from the Terzaghi corrected linear (1-D) borehole fracture frequency of *all fractures*, i.e.:

$$P_{32,a}[r \geq r_{BH}] \geq P_{10,a,\,corr} \qquad \text{A6-1}$$

By the same token, it is assumed that for the *open fractures*, that:

$$P_{32,o}[r \geq r_{BH}] \geq P_{10,o,corr} \qquad \text{A6-2}$$

2. The fracture surface area per unit volume of rock (fracture intensity) of *all fractures* is greater than the fracture intensity of *open fractures*, which in turn is greater than the fracture intensity of *connected open fractures*, which in turn is greater than the measured intensity of *flowing fractures* (*pfl fractures*) detected with the PFL method, i.e.:

$$P_{32,all} \geq P_{32,open} \geq P_{32,cof} \geq P_{32,pfl} \qquad \text{A6-3}$$

3. The sizes of *all* and *open* fractures, from the smallest fractures to the largest, are both power-law distributed (tectonic continuum).

The second and third working hypotheses are illustrated in Figure A6-3.

Another key assumption is the assignment of fracture transmissivity. In the quantitative calibration of fracture transmissivity it is attempted to establish the parameters shown in Table A6-4. Monte-Carlo realisations are studied for each set of parameter values as a mean to address variability between realisations. For each hydrogeological DFN realisation, a pumping test simulation has been carried out.

Table A6-4. Transmissivity model used for the Elaborated hydrogeological DFN modelling.

Type	Description	Relationship	Parameters
Semi-correlated	Log-normal distribution about a power-law correlated mean	$\log(T) = \log(a \cdot r^b) + \sigma_{log(T)}\, N(0,1)$	a , b, $\sigma_{log(T)}$

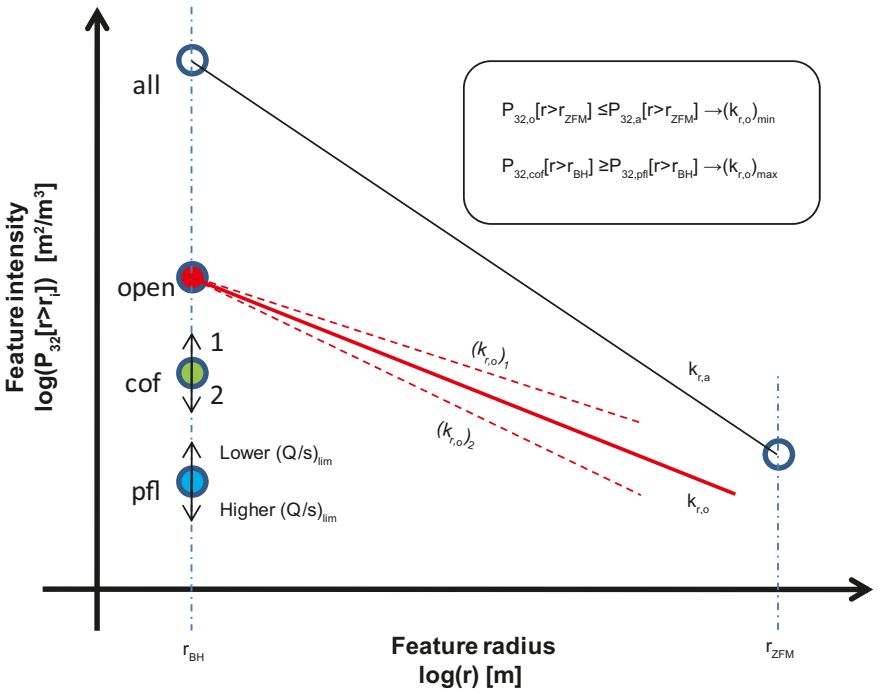

Figure A6-3. *Cartoon showing the working hypothesis of tectonic continua for* ***all*** *fractures and for open fractures, respectively. Given this hypothesis, the possible minimum and maximum limits of the shape parameter for the open fractures, $(k_{r,o})_{min}$ and $(k_{r,o})_{min}$, can be defined as shown. Details on how to read the figure are given in /SKB 2010, Section 6.6/, from where the figure is reproduced.*

A6.6 Data uncertainty due to precision, bias, and representativity

The heterogeneous nature of the flowing fractures in cored boreholes creates uncertainties in the hydrogeological understanding and modelling. To mitigate these uncertainties, a large number of cored boreholes were drilled at different locations and orientations in the fractured bedrock at Laxemar. Most of the cored boreholes were hydraulically investigated with two types of test methods, in order to better understand the spatial differences in the near-field and far-field hydraulic properties. The two test methods employed were:

- difference flow logging with the Posiva Flow Log (PFL) method during long-term pumping conditions; and
- short-term double-packer injection tests with the Pipe String System (PSS) method.

The shortest length of the borehole interval tested is 0.1 m with the PFL method and 5 m with the PSS method. This difference in spatial resolution affects the interpretation of the measured frequency of flow anomalies, $P_{10,pfl}$, in particular where this frequency is high (small spacing). This is the most important reason why the PFL method was selected as the major single-hole hydraulic test method in SDM-Site Laxemar.

The data uncertainty is similar for Laxemar data as for Forsmark data, which is described in Section 6.6.7 of the SR-Site Data report /SKB 2010/.

A6.7 Spatial and temporal variability of data

Spatial variability of data

Figure A6-4 shows Terzaghi-corrected frequencies of open and partly open (OPO) fractures, and of the flowing fractures detected with the PFL method, of different fracture sets. The data come from the cored drilled boreholes at different locations and orientations in hydraulic rock domain HRD_C. The figure is based on data in Table 9-10 of /Rhén et al. 2008/, where the corresponding data for the other hydraulic rock domains can be found.

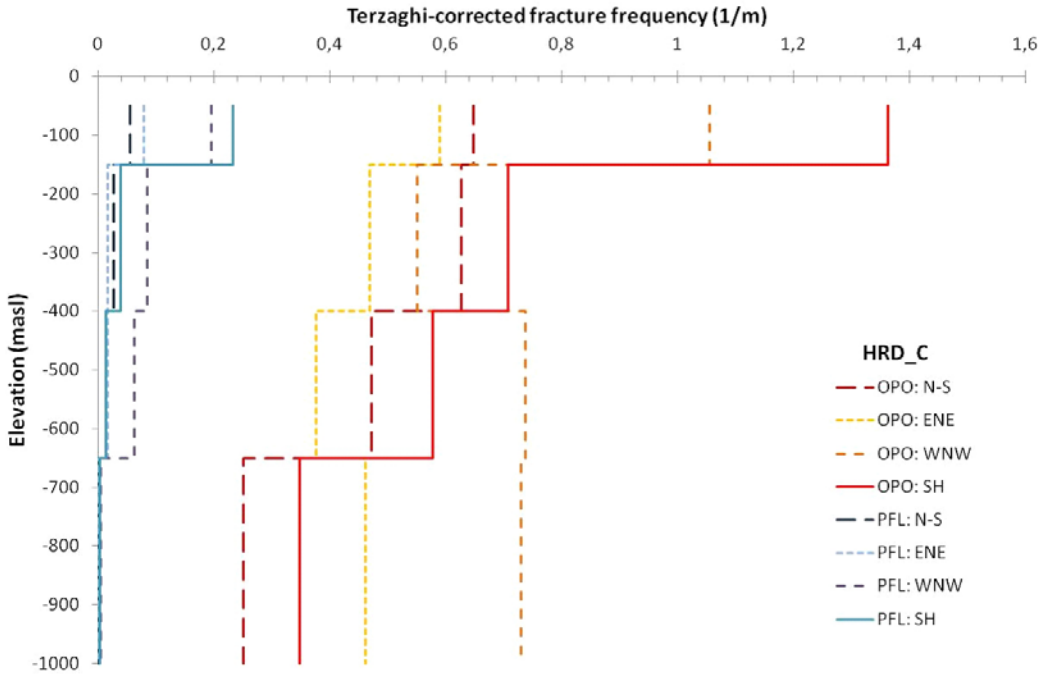

Figure A6-4. *Terzaghi-corrected fracture intensities for open and partly open (OPO) fractures, and PFL-f features for the depth zones and fracture sets of HRD_C as an example. Depths zones are defined in terms of elevation (masl). Based on Table 9-10 in /Rhén et al. 2008/*

Figure A6-5 shows transmissivity values of the flowing fractures detected with PFL method in hydraulic rock domain HRD_C. The red line represents the geometric mean over the boreholes and the dashed blue lines represent the spread between individual boreholes. The figure is based on data in Table 9-12 of /Rhén et al. 2008/, where the corresponding data for the other hydraulic rock domains can be found.

Temporal variability of data

The geometrical and hydraulic properties reported in /SKB 2009a/ describe the present-day hydraulic properties. It is advocated that the present-day properties are reasonable for the groundwater modelling of the excavation and operation periods as well as for the temperate period. For the groundwater flow modelling of the periglacial and glacial periods, temporal changes in the hydraulic properties seem more plausible, e.g. due to the potential impact of freezing and mechanical deformation. The temporal changes in the hydraulic properties to be used for Laxemar in the Comparative analysis are described in /Vidstrand et al. 2010/.

A6.8 Correlations

In the Comparative analysis, particle transport calculations are made in studies dealing with groundwater flow modelling during periods with temperate climate conditions /Joyce et al. 2010/ and periglacial and glacial climate conditions /Vidstrand et al. 2010/. These flow simulations will employ a mixture of DFN and ECPM representations of the rock mass volumes depending on scale and computer code.

With respect to the flow related migration parameters discussed in Chapter A7, in particular the flow-related transport resistance (F [TL^{-1}]), the following correlations are noted:

- On a repository scale, a DFN representation will be used in the transport calculations. The flow-related transport resistances along flow paths in a DFN representation is calculated as:

$$F = \sum_f \left(\frac{2\,t}{e_t} \right)_f \qquad \text{A6-4}$$

where t is the advective travel time [T] in a fracture f along the flow path and e_t is the fracture transport aperture [L]. The latter is in SDM-Site assumed to be correlated to the fracture transmissivity as:

$$e_t = a\ T^b \qquad \text{A6-5}$$

The values of the constants a and b used in SDM-Site are a = 0.705 and b = 0.404 /Hjerne et al. 2010/.

- On a site scale, the continuation of the DFN representation is upscaled to an ECPM finite-element representation, provided that the distance from the repository is still within the range of the hydrogeological DFN modelling of the six fracture domains. Outside the bounds of these fracture domains, an ECPM approach is employed. The hydraulic soil domain is modelled using a CPM approach. The flow-related transport resistances along flow paths in the ECPM and CPM finite-element representations is calculated as:

$$F = \sum_l \left(\frac{a_r\ \Delta l}{q} \right) \qquad \text{A6-6}$$

where a_r is the fracture surface area per unit volume of rock (L^{-1}), Δl (L) is a step distance along the flow path, e.g., through one finite-element, and q (LT^{-1}) is the Darcy flux in the same finite-element.

Within the range of the ECPM representation, the fracture surface area per unit volume of rock will be calculated as:

$$a_r\,(x, y, z) = 2\ P_{32,\ element}\,(x, y, z) \qquad \text{A6-7}$$

That is, a_r is treated as a stochastic quantity that varies in space in accordance to a particular realisation of the underlying hydrogeological DFN model.

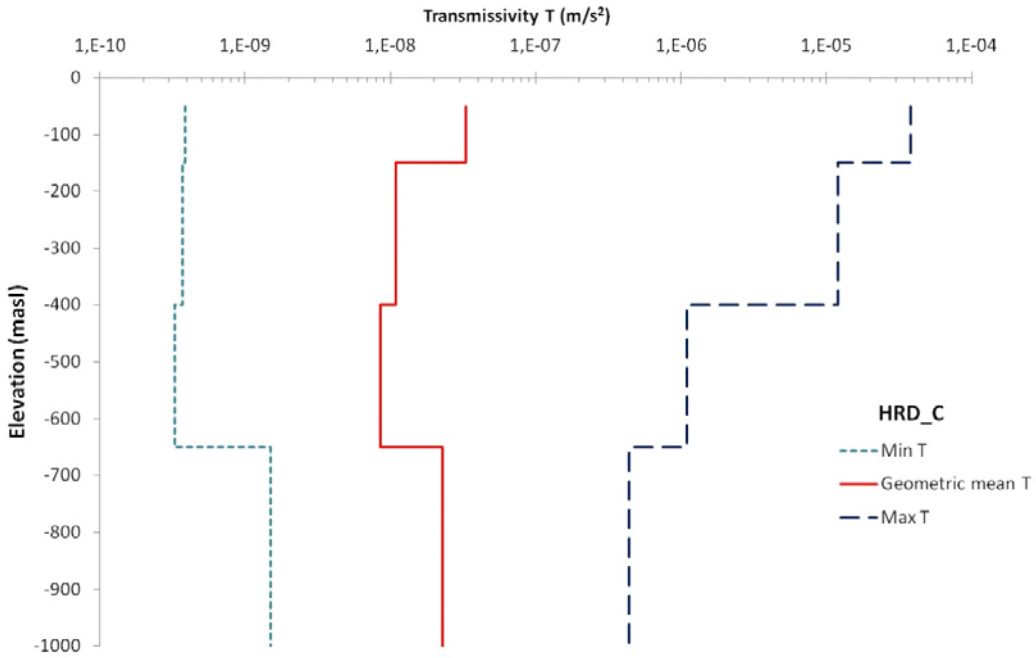

Figure A6-5. *Meassured transmissivity values for flowing features in HRD_C, which is used as an example, detected by PFL in the borehole intervals outside of interpreted deterministic deformation zones. The red line represents the geometric mean over the boreholes and the dashed blue lines represent the spread between individual boreholes, i.e. the minimum and maximum values observed in the borehole. Based on Table 9-12 in /Rhén et al. 2008/.*

A6.9 Result of supplier's data qualification

In the SDM-Site Laxemar work /Rhén et al. 2009/, calibrated Hydro-DFN models were developed for the different hydraulic rock domains. These Hydro-DFN models can be used as input data for DFN models used in the Comparative analysis, e.g. in the site scale models or as input to the upscaled blocks used in regional scale ECPM models.

As mentioned above, the upscaled hydrogeological DFN models based on the methodology used in SDM-Site Laxemar seem to overestimate the hydraulic properties of the rock of Laxemar. In order to improve the representation of the hydraulic properties of the hydraulic rock domains, an Elaborated hydrogeological DFN methodology was developed /Joyce et al. 2010/. The results from this improved concept are generally propagated to the Comparative analysis.

In the Elaborated Hydro-DFN methodology, a set of 'representative boreholes' were chosen for each of the hydraulic rock domains HRD_C, HRD_W, and HRD_EW007. A criterion for choosing the representative boreholes was that they have a significant length in the relevant HRD. The following boreholes were modelled: KLX11A, KLX17A, and KLX19A in HRD_W; KLX03, KLX05, KLX15A, and KLX21B in HRD_C; and KLX07A and KLX08 in HRD_EW007.

The recommended hydrogeological DFN parameters, based on the Elaborated Hydro-DFN methodology, to be used for HRD_C are tabulated in Table A6-5. Table A6-6 and Table A6-7 show the parameters to be used for HRD_EW007 and HRD_W, respectively.

The rock mass in the regional model, outside the defined four HRD's mentioned above, is based on the material property assignments made in model version Laxemar 1.2 (summarised in /Rhén et al. 2009/) and assessments of similarities between regional HRD's and the newly developed HRD's inside the Laxemar local model volume. Table A6-8 shows from which of the hydraulic rock domains HRD_C, HRD_EW007, HRD_N, and HRD_W data should be taken from.

Table A6-5. Description of the Elaborated Hydro-DFN input parameters for HRD_C with fixed r_0=0.038 m and intensity of open fractures based on OPO. Data are reproduced from Table E-1 in /Joyce et al. 2010/.

Depth interval (masl)	Set	Orientation set pole: (trend, plunge), conc.	Fracture radius model power-law (k_r, r_0)	Intensity P_{32} (m^2/m^3) of open fractures	Semi-correlated transmissivity model (a, b, σ)
–150 to 0	ENE	(155.1,3.4), 9.6	(2.70, 0.038)	0.52	($2{\cdot}10^{-7}$, 0.7, 0.4)
	WNW	(204,1.6), 12	(2.49, 0.038)	0.95	($2{\cdot}10^{-7}$, 0.9, 0.6)
	N-S	(270.2,8.4), 7.8	(2.80, 0.038)	0.54	($8{\cdot}10^{-8}$, 0.5, 0.4)
	SubH	(46.3,84.7), 12	(2.59, 0.038)	1.20	($6{\cdot}10^{-8}$, 0.7, 0.5)
–400 to –150	ENE	(155.1,3.4), 9.6	(3.00, 0.038)	0.47	($6{\cdot}10^{-7}$, 0.7, 0.9)
	WNW	(204,1.6), 12	(2.44, 0.038)	0.55	($1{\cdot}10^{-8}$, 0.5, 0.7)
	N-S	(270.2,8.4), 7.8	(2.91, 0.038)	0.63	($1{\cdot}10^{-8}$, 0.7, 0.2)
	SubH	(46.3,84.7), 12	(2.87, 0.038)	0.71	($3.5{\cdot}10^{-8}$, 1.2, 0.9)
–650 to –400	ENE	(155.1,3.4), 9.6	(2.87, 0.038)	0.38	($8{\cdot}10^{-8}$, 0.8, 0.6)
	WNW	(204,1.6), 12	(2.54, 0.038)	0.74	($3{\cdot}10^{-9}$, 0.8, 0.6)
	N-S	(270.2,8.4), 7.8	(2.87, 0.038)	0.47	($6{\cdot}10^{-9}$, 0.4, 0.4)
	SubH	(46.3,84.7), 12	(3.00, 0.038)	0.58	($2{\cdot}10^{-7}$, 0.8, 0.7)
–1,000 to –650	ENE	(155.1,3.4), 9.6	(2.96, 0.038)	0.46	($1{\cdot}10^{-8}$, 0.7, 0.4)
	WNW	(204,1.6), 12	(3.00, 0.038)	0.73	($3{\cdot}10^{-7}$, 0.7, 0.4)
	N-S	(270.2,8.4), 7.8	(3.00, 0.038)	0.25	($1{\cdot}10^{-8}$, 0.7, 0.4)
	SubH	(46.3,84.7), 12	(2.97, 0.038)	0.35	($1{\cdot}10^{-7}$, 0.7, 0.4)

Table A6-6. Description of the Elaborated Hydro-DFN input parameters for HRD_EW007 with fixed r_0=0.038 m and intensity of open fractures based on OPO. Data are reproduced from Table E-2 in /Joyce et al. 2010/.

Depth interval (masl)	Set	Orientation set pole: (trend, plunge), conc.	Fracture radius model power-law (k_r, r_0)	Intensity P_{32} (m^2/m^3) of open fractures	Semi-correlated transmissivity model (a, b, σ)
–150 to 0	ENE	(162.8,1.4), 10.7	(2.77, 0.038)	0.55	($3{\cdot}10^{-8}$, 0.6, 0.4)
	WNW	(25.3,0.2), 16.4	(2.30, 0.050)	1.01	($3{\cdot}10^{-8}$, 0.6, 0.3)
	N-S	(88.9,3.9), 8.8	(2.53, 0.038)	0.33	($1{\cdot}10^{-7}$, 0.8, 0.3)
	SubH	(138.7,81.3), 9.7	(2.76, 0.038)	1.72	($2.3{\cdot}10^{-7}$,0.8,0.5)
–400 to –150	ENE	(162.8,1.4), 10.7	(2.83, 0.038)	0.60	($2{\cdot}10^{-7}$, 0.6, 0.6)
	WNW	(25.3,0.2), 16.4	(2.41, 0.038)	1.15	($3{\cdot}10^{-8}$, 0.6, 0.4)
	N-S	(88.9,3.9), 8.8	(2.60, 0.038)	0.54	($3{\cdot}10^{-7}$,0.8, 0.4)
	SubH	(138.7,81.3), 9.7	(2.84, 0.038)	0.82	($5{\cdot}10^{-8}$, 0.8, 0.4)
–650 to –400	ENE	(162.8,1.4), 10.7	(2.93, 0.038)	0.69	($1{\cdot}10^{-8}$, 0.5, 0.2)
	WNW	(25.3,0.2), 16.4	(2.62, 0.038)	1.43	($1.2{\cdot}10^{-7}$, 0.3, 0.2)
	N-S	(88.9,3.9), 8.8	(3.00, 0.038)	0.64	($8{\cdot}10^{-8}$, 0.4, 0.2)
	SubH	(138.7,81.3), 9.7	(2.99, 0.038)	0.92	($1.5{\cdot}10^{-7}$, 0.7, 0.3)
–1,000 to –650	ENE	(162.8,1.4), 10.7	(2.96, 0.038)	0.33	($1{\cdot}10^{-8}$, 0.7, 0.4)
	WNW	(25.3,0.2), 16.4	(3.00, 0.038)	0.89	($3{\cdot}10^{-7}$, 0.7, 0.4)
	N-S	(88.9,3.9), 8.8	(3.00, 0.038)	0.21	($1{\cdot}10^{-8}$, 0.7, 0.4)
	SubH	(138.7,81.3), 9.7	(2.97, 0.038)	0.80	($1{\cdot}10^{-7}$, 0.7, 0.4)

Table A6-7. Description of the Elaborated Hydro-DFN input parameters for HRD_W with fixed r_0=0.038 m and intensity of open fractures based on OPO. Data are reproduced from Table E-3 in /Joyce et al. 2010/.

Depth interval (masl)	Set	Orientation set pole: (trend, plunge), conc.	Fracture radius model power-law (k_r, r_0)	Intensity P_{32} (m^2/m^3) of open fractures	Semi-correlated transmissivity model (a, b, σ)
–150 to 0	ENE	(340.3,1.2), 15	(2.59, 0.038)	0.44	($2.1 \cdot 10^{-8}$, 0.7, 0.6)
	WNW	(208.9,2.2), 10.9	(2.54, 0.038)	0.61	($7 \cdot 10^{-8}$, 0.8, 1.0)
	N-S	(272.8,12), 11.5	(2.52, 0.038)	0.54	($4 \cdot 10^{-8}$, 0.7, 0.8)
	SubH	(277.1,84.3), 11.1	(2.50, 0.038)	1.03	($8 \cdot 10^{-8}$, 0.7, 0.7)
–400 to –150	ENE	(340.3,1.2), 15	(2.54, 0.038)	0.28	($2.2 \cdot 10^{-9}$, 0.5, 0.4)
	WNW	(208.9,2.2), 10.9	(2.65, 0.038)	0.38	($1.5 \cdot 10^{-8}$, 0.5, 1.2)
	N-S	(272.8,12), 11.5	(3.00, 0.038)	0.40	($5 \cdot 10^{-9}$, 0.4, 0.3)
	SubH	(277.1,84.3), 11.1	(2.72, 0.038)	0.50	($1.2 \cdot 10^{-7}$, 0.7, 1.2)
–650 to –400	ENE	(340.3,1.2), 15	(3.00, 0.038)	0.17	($3 \cdot 10^{-9}$, 0.6, 0.4)
	WNW	(208.9,2.2), 10.9	(2.61, 0.038)	0.33	($1.5 \cdot 10^{-8}$, 0.5, 0.3)
	N-S	(272.8,12), 11.5	(2.53, 0.038)	0.30	($5 \cdot 10^{-8}$, 0.2, 0.2)
	SubH	(277.1,84.3), 11.1	(2.72, 0.038)	0.38	($2 \cdot 10^{-7}$, 0.8, 0.8)
–1,000 to –650	ENE	(155.1,3.4), 9.6	(3.00, 0.038)	0.12	($1 \cdot 10^{-8}$, 0.7, 0.4)
	WNW	(208.9,2.2), 10.9	(3.00, 0.038)	0.09	($3 \cdot 10^{-8}$, 0.7, 0.4)
	N-S	(272.8,12), 11.5	(2.53, 0.038)	0.14	($1 \cdot 10^{-8}$, 0.7, 0.4)
	SubH	(277.1,84.3), 11.1	(3.00, 0.038)	0.65	($3 \cdot 10^{-8}$, 0.7, 0.4)

Table A6-8. Hydraulic properties to be used for the rock mass volumes outside the rock domains HRD_C, HRD_EW007, HRD_N, and HRD_W /Rhén et al. 2008/.

Regional hydraulic rock mass domain	Suggested hydraulic properties based on hydrogeological DFN
HRD_A	HRD_N
HRD_A2	HRD_N, but rock below –650 masl is the same as –400 to –650 masl
HRD_D-E-M	HRD_C
HRD_B-C	HRD_C
HRD_F-G	HRD_N, 10 times higher T
HRD_P	HRD_N

A6.10 Data recommended for use in the Comparative analysis

The Hydrogeological base case is based on the SDM-Site parameterisation /Joyce et al. 2010/. However, it is recommended that the model parameterisations for the Elaborated hydrogeological DFN concept /Joyce et al. 2010/ should be used to the greatest extent possible in the modelling of groundwater flow. Hence, the data presented in Table A6-5 to Table A6-8 are recommended for use in the Comparative analysis.

It is noted that for the particular case of hydrogeochemical modelling for the temperate domain, which uses results from the hydrogeological modelling as input (cf. Chapter A1), the Hydrogeological base case has been propagated.

Clearly, for the model application of the glacial period, a model domain much larger than the SDM model is needed, and here the recommendation is to follow the approach outlined above, i.e. an extrapolation of the ECPM properties into the larger domain is utilised.

Furthermore, it is recommended that discrete hydrogeological DFN models should be utilised at as large scales as possible within the Comparative analysis application. Only at scales larger than computationally feasible for the discrete DFN approach, or at scales for which a DFN parameterisation does not exist, should continuum representations be used.

The parameters provided are judged representative for both present day and future conditions except for the period when permafrost conditions prevail.

References A6.11

SKB's (Svensk Kärnbränslehantering AB) publications can be found at www.skb.se/publications.

Hartley L J, Holton D, 2004. CONNECTFLOW (Release 8.0). Technical summary document. Report SA/ERRA C/TSD02V1, Serco Assurance.

Hjerne C, Nordqvist R, Harrström J, 2010. Compilation and analyses of results from cross-hole tracer tests with conservative tracers. SKB R-09-28, Svensk Kärnbränslehantering AB.

Joyce S, Simpson T, Hartley L, Applegate D, Hoek J, Jackson P, Roberts D, Swan D, Gylling B, Marsic N, Rhén I, 2010. Groundwater flow modelling of periods with temperate climate conditions – Laxemar. SKB R-09-24, Svensk Kärnbränslehantering AB.

La Pointe P, Fox A, Hermanson J, Öhman J, 2008. Geological discrete fracture network model for the Laxemar site. Site descriptive modelling, SDM-Site Laxemar. SKB R-08-55, Svensk Kärnbränslehantering AB.

Mårtensson E, Gustafsson L-G, Bosson E, 2009. Effects on surface hydrology and near-surface hydrogeology of an open repository in Laxemar. Results of modelling with MIKE SHE. SKB R-09-36, Svensk Kärnbränslehantering AB.

Rhén I, Forsmark T, Hartley L, Jackson P, Roberts D, Swan D, Gylling B, 2008. Hydrogeological conceptualisation and parameterisation. Site descriptive modelling, SDM-Site Laxemar. SKB R-08-78, Svensk Kärnbränslehantering AB.

Rhén I, Forsmark T, Hartley L, Joyce S, Roberts D, Gylling B, Marsic N, 2009. Bedrock hydrogeology. Model testing and synthesis. Site descriptive modelling, SDM-Site Laxemar. SKB R-08-91, Svensk Kärnbränslehantering AB.

Rhén I, Hartley L, 2009. Bedrock hydrogeology Laxemar. Site descriptive modelling, SDM-Site Laxemar. SKB R-08-92, Svensk Kärnbränslehantering AB.

Selroos J-O, Follin S, 2010. SR-Site groundwater flow modelling methodology, setup and results. SKB R-09-22, Svensk Kärnbränslehantering AB.

SKB, 2006. Climate and climate-related issues for the safety assessment SR-Can. SKB TR-06-23, Svensk kärnbränslehantering AB.

SKB, 2009a. Site description of Laxemar at completion of the site investigation phase. SDM-Site Laxemar. SKB TR-09-01, Svensk Kärnbränslehantering AB.

SKB, 2009b. Underground design Laxemar. Layout D2. SKB R-09-16, Svensk Kärnbränslehantering AB.

SKB, 2010. Data report for the safety assessment SR-Site. SKB TR-10-52, Svensk Kärnbränslehantering AB.

Svensson U, Follin S, 2010. Groundwater flow modelling of the excavation and operation phases – SR-Site Forsmark. SKB R-09-19, Svensk Kärnbränslehantering AB.

Svensson U, Ferry M, Kuylenstierna H-O, 2010. DarcyTools, Version 3.4. Concepts, methods, and equations. SKB R-07-38, Svensk Kärnbränslehantering AB.

Svensson U, Rhén I, 2010. Groundwater flow modelling of the excavation and operation phases – Laxemar. SKB R-09-23, Svensk Kärnbränslehantering AB

Vidstrand P, Rhén I, Zugec N, 2010. Groundwater flow modelling of periods with periglacial and glacial climate conditions – Laxemar. SKB R-09-25, Svensk Kärnbränslehantering AB.

A7 Flow related migration properties

Several of the parameters controlling radionuclide transport are related to the amount and distribution of groundwater flow. The values of these flow related migration parameters are essentially obtained by numerical simulation of groundwater flow using the hydrogeological models described in Chapter A6. Hence, before reading this appendix it is recommended to read Chapter A6, and possibly also Section 6.6 of the SR-Site Data report /SKB, 2010a/, where many issues of relevance for this present text are detailed.

A corresponding text for the Forsmark site is found in Section 6.7 of the SR-Site Data report.

A7.1 Modelling as input to the Comparative analysis of safety related site characteristics

This section describes what data are expected from the supplier, and in what modelling activities the data are to be used.

Defining the data requested from the supplier

In radionuclide transport modelling, transport from the canister in the nearfield is assumed to occur along three release paths. These are the Q1 path, with transport in a fracture intersecting the deposition hole; the Q2 path, with transport in the excavation damaged zone (EDZ); and the Q3 path, with transport in the deposition tunnel to an intersecting fracture (cf. Figure 9-16 of SR-Can Main report /SKB 2006a/). There are thus three release paths from the nearfield into the farfield of the geosphere; it is the farfield parameters that are dealt with in this appendix.

The following flow-related migration parameters are requested for each deposition hole location within the repository:

- Darcy flux q (m/yr) for the Q1, Q2, and Q3 release paths. Also equivalent flow rates Q_{eq} (m^3/year) corresponding to the Q1, Q2, and Q3 release paths (Q_{eq1}, Q_{eq2}, and Q_{eq3}) are needed, which in turn are related to the groundwater flow rates for the Q1, Q2, and Q3 release paths. The Darcy fluxes and flow rates are calculated in fractures intersecting the deposition holes, in the EDZ in the tunnel floor adjacent to the deposition holes, and in fractures intersecting the deposition tunnel for the Q1, Q2, and Q3 release paths, respectively. The relation between flow rate, Darcy flux and equivalent flow rate for the Q1, Q2, and Q3 release paths are detailed in Chapter 3.2.6 and Appendix D of /Joyce et al. 2010/.
- Recharge and discharge coordinates in the biosphere along flow paths from the Q1, Q2, and Q3 release paths.
- Advective travel time t_w (yr) along flow paths to the recharge and discharge locations for the Q1, Q2, and Q3 release paths.
- Flow related transport resistance F (yr/m) along flow paths to the recharge and discharge locations for the Q1, Q2, and Q3 release paths.

In addition the following parameters, which are not related to the paths, should be supplied:

- Measures of longitudinal dispersion Pe (–).
- Maximum penetration depth for solute diffusion into the rock matrix L_D (m), in case the fracture spacing is limiting (as opposed to the connectivity of the microporous system discussed in Chapter A8).

Comparative analysis models in which data will be used

The flow related migration parameters described in this appendix are used in radionuclide transport calculations. These calculations are performed using different computer codes for the nearfield and farfield, respectively. The nearfield code is COMP23/Compulink /Romero et al. 1999, Cliffe and Kelly 2006, Vahlund and Hermansson 2006/, and for the farfield the code FARF31 /Norman and Kjellbert 1990, Elert et al. 2004/ is used. The codes use the following flow related migration parameters:

COMP23:

- Equivalent flow rates Q_{eq1}, Q_{eq2}, and Q_{eq3} for three possible release paths Q1, Q2, and Q3. The equivalent flow rates are obtained based on the calculated flow rates in the groundwater flow models described in /Joyce et al. 2010/.

FARF31:

- Flow related transport resistance F.
- Advective travel time t_w.
- Peclet number Pe.
- Maximum penetration depth L_D into the matrix if a finite matrix is considered.

Biosphere assessment:

- Coordinates (x, y, z) at the end of each flow path connecting canister positions with exit locations.

The flow-related transport resistance and advective travel time are integrated parameters along flow paths obtained through particle tracking in the flow models described in Chapter A6. Particles are released at each of the locations corresponding to the Q1, Q2, and Q3 release paths, see above.

A7.2 Supplier input on use of data in Comparative analysis

The flow related migration properties are results of the groundwater flow simulations presented in Chapter A6. Thus, all data pertinent for defining the groundwater flow simulations are also relevant for the results presented in this appendix. As stated in Section A6.2, hydrogeological modelling shows that the groundwater flow rates in deformation zones and background fractures at depth are higher in Laxemar than in Forsmark. This is of consequence for subsequent radionuclide transport modelling using data from this present appendix.

A7.3 Sources of information and documentation of data qualification

Sources of information

All the data presented in this appendix result from the groundwater flow simulations. The sources of information and data qualification of the data needed for these simulations are described in detail in Chapter A6 and in the individual modelling reports /Joyce et al. 2010/ and /Vidstrand et al. 2010/.

The simulations done are performed as two separate studies, one for the temperate period /Joyce et al. 2010/, and one for the periglacial and glacial period /Vidstrand et al. 2010/. Full references are given in Table A7-1. These reports summarise the different cases modelled and the justification of these cases.

Table A7-1. Main sources of information used in data qualification.

Joyce S, Simpson T, Hartley L, Applegate D, Hoek J, Jackson P, Roberts D, Swan D, Gylling B, Marsic N, Rhén I, 2010. Groundwater flow modelling of periods with temperate climate conditions – Laxemar. SKB R-09-24, Svensk Kärnbränslehantering AB.
Vidstrand P, Rhén I, Zugec N, 2010. Groundwater flow modelling of periods with periglacial and glacial climate conditions – Laxemar. SKB R-09-25, Svensk Kärnbränslehantering AB.

The Excavation and Operation period is hydrogeologically analysed in /Svensson and Rhén 2010/; this report is not further discussed in the present context since that analysis does not produce flow related migration data for use in subsequent assessment calculations.

Categorising data sets as qualified or supporting data

In this document the hydrogeological subject area is divided on the two Chapters A6 and A7. This present appendix gives results from the hydrogeological modelling of Laxemar in the Comparative analysis, whereas Chapter A6 supplies the most important inputs to such modelling (although other inputs are also needed). Because of this, a deliberate deviation from the instruction given in Section 2.3.4 of the SR-Site Data report /SKB 2010a/ is made, and no sorting of input data as qualified or supporting is made in this section. What could be said in general concerning input data to hydrogeological modelling is the following:

The data sets used as input to the groundwater flow simulations are detailed in the individual reports referenced in Table A7-1. The main data set is related to the parameterisation of the hydrogeological discrete fracture network model detailed in Chapter A6. Additional data sets needed for the hydrogeological modelling, e.g. parameterisation of hydraulic conductor domains (deformation zones) and hydrogeological soil domains (regolith), as well as formulation of initial and boundary conditions for both flow and transport of salt and reference waters, are summarised in /Rhén and Hartley 2009/.

Excluded data previously considered as important

No such data have been excluded but the considerations given in Section A6.3 apply.

A7.4 Conditions for which data are supplied

Data are supplied for temperate period conditions, and for different combinations of periglacial (permafrost) and glacial period conditions, respectively. For the glacial period, also submerged conditions are included. The temperate period is modelled as a continuation of today's conditions including the future shoreline displacement process and projected changes in salinity in the Baltic Sea. The present conditions are described in detail in the bedrock hydrogeology report of SDM-Site Laxemar /Rhén and Hartley 2009/. The periglacial and glacial periods are more hypothetical; rather than trying to predict the future evolution, the models have been set up to bound the hydrogeological consequences associated with these climatic conditions. The future evolution of the climate is described the SR-Can Climate report /SKB 2006b/ and in Chapter 3 of this present report.

In the model of temperate conditions /Joyce et al. 2010/, the repository is explicitly included in the model. The repository description includes deposition holes, deposition tunnels, transport and main tunnels, as well as the central area including ramp and shafts. Also the excavated damaged zone (EDZ) is included. All tunnels are assumed to be backfilled. In the model of periglacial and glacial periods /Vidstrand et al. 2010/, the repository is not included. This is justified by the much larger scale (super-regional) considered in these simulations.

Conditions in terms of geological and other settings governing the hydrogeological data are further described in Section A6.4 and in /Rhén and Hartley 2009/.

A7.5 Conceptual uncertainty

The conceptual uncertainties associated with the hydrogeological modelling are summarised in Section A6.5.

A few uncertainties with specific relevance for the flow-related transport properties are highlighted here. First, it is noted that the advective travel time and flow related transport resistance are calculated along flow paths in steady-state velocity fields, i.e. a snapshot-in-time approach is used. Clearly, different results would be obtained in transient flow fields, but the resulting uncertainty is judged small given that steady-state flow fields bounding the transient evolution are used.

Second, the combination of model scales within the hydrogeological applications as detailed in /Selroos and Follin 2010/ implies an uncertainty in some cases. This applies to the Comparative analysis as well. Models in ConnectFlow may be combined in two ways: First, models can be embedded in each other in which case they are formally nested such that the whole flow system is solved simultaneously using constraint equations on the model interfaces, resulting in continuity of both pressure and velocity over the interfaces. Second, models may be solved separately using boundary conditions from the larger scale model on the boundaries of the smaller scale model. In this case, velocities are not necessarily continuous, and particles are manually moved from the smaller scale model to the larger scale model at the boundary. This implies an uncertainty in the flow path characteristics.

An uncertainty stems also from the fact that individual fractures in the hydrogeological DFN model are modelled as homogeneous, whereas in reality there is some spatial variation of the aperture field within each fracture. In SR-Can, this uncertainty was dealt with by reducing all calculated flow related transport resistance values F by a factor of ten. In the Comparative analysis, the F values are left unmodified based on arguments compiled in SR-Site Radionuclide transport report /SKB 2010b/. In short, it is argued that aperture variability, leading to channelised flow, creates the possibility for more interaction with the matrix through diffusion processes. This is due to the formation of stagnant (immobile) water in the fracture plane between the channels. Solutes may easily diffuse from the mobile channels to the immobile fracture water, and subsequently into the rock matrix.

Finally, the assumed relationship between fracture transmissivity and aperture will affect the calculated advective travel times. However, the uncertainty is considered small; moreover, the advective travel times do not have a strong influence on subsequently calculated entities within the compliance calculations.

A7.6 Data uncertainty due to precision, bias, and representativity

Since the temperate period model resolves fractures at smaller scales and also has an explicit representation of the repository structures relative to the glacial period model, one may argue that a higher degree of precision is present in the former model. There is thus a relative difference in precision between the two models.

Since the super-regional periglacial/glacial model is set up to bound hydrogeological consequences for periglacial/glacial climate conditions rather than to provide a detailed prediction of the future, the results (performance measures) of these analyses are biased towards pessimism relative to the temperate period results.

There may be judged to be differences between the different performance measures concerning precision (accuracy) and bias in results. The two flow measures Darcy flux q and equivalent flow rate Q_{eq} depend primarily on the permeability and connectivity of the fractures system and applied boundary conditions. The accuracy of these measures is thus as good as the underlying description of the bedrock and knowledge of boundary conditions. When it comes to advective travel time, t_w, additional assumptions need to be made concerning porosity and/or transport aperture, both of which are highly uncertain entities. Hence, the advective travel time is associated with much more uncertainty than the flow measures. The flow-related transport resistance F also requires additional assumptions concerning the flow-wetted surface along the flow path. This entity can be estimated with greater certainty than the aperture or porosity, but is still subject to great uncertainty. However, in an explicit discrete fracture network model, the flow-wetted surface is explicitly defined through the network properties, and thus the uncertainty in flow-wetted surface is given by the uncertainty in the discrete fracture network model, see Chapter A6. The resulting uncertainty in F is judged to be greater than the uncertainty in q or Q_{eq}, but smaller than in t_w.

The provided values on Peclet number, and maximum penetration depth do not originate from the modelling described above, but are based on judgement and underlying data. The uncertainty can be judged minor for Peclet number; also, the chosen values of these parameters generally have a small effect on calculated radionuclide transport characteristics. The uncertainty in maximum penetration depth is related to the uncertainty in fracture frequency, and is thus smaller than other uncertainties discussed here.

It is not possible to provide detailed quantitative measures of the uncertainties listed above (combination of conceptual, precision, bias, and representativity). However, it is judged that the greatest uncertainty is associated with the periglacial/glacial model, followed by the uncertainty discussed in relation to the performance measures of the temperate model, and finally followed by the uncertainties associated with Peclet number and maximum penetration depth. For the temperate period calculations, uncertainties are handled by performing two realisations based on the Elaborated Hydro-DFN model, which probably are too few realisations to properly address the uncertainty. However, the cumulative distributions of the performance measures are relatively similar for the performed realisations (see Figure A7-1 in Section A7.9), and because of this only one of the realisations based on the Elaborated Hydro-DFN model is propagated. The uncertainties related to Peclet number and maximum penetration depth are so small that no variants are deemed necessary to propagate.

A7.7 Spatial and temporal variability of data

Spatial variability of data

The calculated Darcy fluxes are point values in space; one point (three points, if a distinction is made between release paths Q1, Q2, and Q3) for each canister deposition hole position is considered. Depending on the underlying variability of the hydraulic properties and the boundary conditions for the assumed flow, the Darcy fluxes will display a variation.

The advective travel time and flow-related transport resistance are Lagrangian quantities integrated along flow paths within the FARF31 application. The integration implies an averaging; i.e. the order between high and low values along the path does not matter as long as the cumulative result is the same. However, it is noted that the integrated values obtained at the end of each flow path will vary between flow paths even though averaging takes place. Specifically, there tends to be large variability in t_w and F values due to the varying nature of the flow path distribution; i.e. some flow paths are short and primarily located in high permeability features such as deformation zones, whereas other flow paths are long and characterised by low permeability conditions.

In Table A7-2, statistics of the Darcy flux and flow related transport resistance are exemplified in tabulated form for the central case of the Comparative analysis for the temperate period at 2000 AD. Hence, the table is based on the Elaborated Hydro-DFN case with stochastic fractures but homogeneous deformation zones (including a depth trend). The table thus reflect a single realisation. There is some variability in the entities in Table A7-2 between realisations (not shown in table), indicating that the spatial variability results in uncertainty. Two realisations are considered within the temperate period only; within the periglacial/glacial period, the conceptual uncertainties are judged to dominate over the uncertainty implied by spatial variability.

Table A7-2. Resulting statistics of Darcy flux at deposition hole locations, and flow-related transport resistance F for the temperate period at 2000 AD for the three release paths Q1, Q2, and Q3 of the Elaborated Hydro-DFN case. Fraction of particles in the last row indicates the fraction of released particles discharging at the top surface of the model; the statistics for F in the table are based on this fraction.

Log(*q*[m/y]), Log(*F*[y/m])	*q* (Q1)	*q* (Q2)	*q* Q(3)	*F* (Q1)	*F* (Q2)	*F* (Q3)
Mean	$-2.94\cdot10^{0}$	$-1.67\cdot10^{0}$	$-4.67\cdot10^{0}$	$5.29\cdot10^{0}$	$5.22\cdot10^{0}$	$5.23\cdot10^{0}$
Median	$-2.91\cdot10^{0}$	$-1.64\cdot10^{0}$	$-4.69\cdot10^{0}$	$5.29\cdot10^{0}$	$5.23\cdot10^{0}$	$5.25\cdot10^{0}$
5th percentile	$-4.63\cdot10^{0}$	$-2.62\cdot10^{0}$	$-5.77\cdot10^{0}$	$3.96\cdot10^{0}$	$3.88\cdot10^{0}$	$3.92\cdot10^{0}$
10th percentile	$-4.20\cdot10^{0}$	$-2.38\cdot10^{0}$	$-5.52\cdot10^{0}$	$4.25\cdot10^{0}$	$4.20\cdot10^{0}$	$4.23\cdot10^{0}$
25th percentile	$-3.58\cdot10^{0}$	$-2.02\cdot10^{0}$	$-5.12\cdot10^{0}$	$4.73\cdot10^{0}$	$4.68\cdot10^{0}$	$4.71\cdot10^{0}$
75th percentile	$-2.64\cdot10^{0}$	$-1.30\cdot10^{0}$	$-4.24\cdot10^{0}$	$5.82\cdot10^{0}$	$5.76\cdot10^{0}$	$5.76\cdot10^{0}$
90th percentile	$-1.70\cdot10^{0}$	$-9.93\cdot10^{-01}$	$-3.79\cdot10^{0}$	$6.32\cdot10^{0}$	$6.21\cdot10^{0}$	$6.22\cdot10^{0}$
95th percentile	$-1.34\cdot10^{0}$	$-8.05\cdot10^{-01}$	$-3.52\cdot10^{0}$	$6.59\cdot10^{0}$	$6.49\cdot10^{0}$	$6.49\cdot10^{0}$
Std deviation	$1.01\cdot10^{0}$	$5.51\cdot10^{-01}$	$6.98\cdot10^{-01}$	$8.05\cdot10^{-01}$	$7.90\cdot10^{-01}$	$7.74\cdot10^{-01}$
Variance	$1.02\cdot10^{0}$	$3.03\cdot10^{-01}$	$4.88\cdot10^{-01}$	$6.48\cdot10^{-01}$	$6.24\cdot10^{-01}$	$5.99\cdot10^{-01}$
Max value	$-4.05\cdot10^{-01}$	$-7.54\cdot10^{-01}$	$-5.52\cdot10^{-01}$	$8.13\cdot10^{0}$	$8.02\cdot10^{0}$	$7.75\cdot10^{0}$
Min value	$-7.20\cdot10^{0}$	$-3.75\cdot10^{0}$	$-7.01\cdot10^{0}$	$2.38\cdot10^{0}$	$2.52\cdot10^{0}$	$2.53\cdot10^{0}$
Fraction of particles	0.706	0.996	1.000	0.604	0.856	0.848

The advective travel time is generally strongly correlated to the flow related transport resistance. Also, the equivalent flow rate is directly related to the Darcy flux, so the results shown in Table A7-2 provide a good overview of the characteristics of the different cases.

A Peclet number is provided as an effective value for the whole model domain; hence judgement concerning the spatial variability is not relevant. Maximum penetration depth depends on average fracture spacing, see Section A7.9 for details. The fracture spacing clearly varies in space; specifically the fracture frequency tends to decrease with depth. However, for the modelling in the Comparative analysis, a single value of maximum penetration depth representative for the rock volume between –400 and –650 m depths is chosen.

Temporal variability of data

Temporal variability is handled by using different model set-ups for the different climate domains, i.e. temperate and periglacial/glacial, respectively, and also by representing a time evolution within the different climate domains.

In the temperate domain modelling, the triplets (Darcy flux or equivalent flow rate, advective travel time, and flow related transport resistance) are calculated at snapshots-in-time. The chosen snapshots are 2000 BC, 2000 AD, 5000 AD and 15,000 AD. The differences in calculated triplets are due to the fact that the snapshots-in-time are characterised by different shoreline positions. There is very little variation in any of the performance measures in the rock with release time. This is because the particle pathways are dominated by the deformation zones rather than the location of the retreating shoreline.

During the glacial period, both higher and lower flow conditions are experienced. When the ice front is in close proximity to the repository (located right above the repository), Darcy fluxes are high and advective travel times and flow related transport resistance values are low. However, these conditions only last for a short time period. Conversely, when the site is completely ice covered, Darcy fluxes are lower and advective travel times and flow related transport resistance values are higher, as compared to the temperate period. This time period may last for tens of thousands of years (cf. Chapter 3). Also the period with submerged conditions, when the ice sheet has retreated, is characterised by lower Darcy fluxes than during the temperate period. The periglacial/glacial simulations are described in detail in /Vidstrand et al. 2010/.

A7.8 Correlations

There is no correlation related to these data that needs to be propagated to subsequent modelling.

A7.9 Result of supplier's data qualification

Below, references are made to the resulting triplets for the different cases considered within the temperate, periglacial, and glacial period simulations. Within each period, the importance of the cases for subsequent assessment calculations is discussed.

At the end of the section, the suggested Peclet number and maximum penetration depth are presented.

Temperate period

In Table A7-3 the temperate period cases analysed in /Joyce et al. 2010/ that result in input for the radionuclide transport models are listed. Furthermore, references are made to where tabulated results can be found for each case.

Table A7-3. Modelling cases and references to tabulated results.
Tabulated results are stored in SKBdoc 1263831 (access might be given on request).

Hydrogeological modelling case
Hydrogeological Base Case
Elaborated Hydro-DFN case
Elaborated Hydro-DFN case with no MDZs
Stochastic continuum case

For each modelling case, a data file is delivered for each Q1, Q2, and Q3 release path. Table A7-4 shows an excerpt of such a data file, displaying four out of 8,031 rows (one row for each deposition hole).

The so-called Hydrogeological Base Case is a representation of site conditions based on the understanding as expressed in the SDM-Site model /Rhén et al. 2009/. It is here argued that the Elaborated Hydro-DFN Case, implemented in /Joyce et al. 2010/, is the central case to propagate to Comparative analysis calculations. It is the case that best represents perceived site conditions.

Table A7-4. Excerpt from resulting data file from hydrogeological modelling of release path Q1 for the Elaborated Hydro-DFN case. Four out of 8,031 rows are displayed. The resulting data files also feature other columns than shown in the excerpt, with data not specifically requested in this present appendix.

POINT	XS	YS	ZS	XE	YE	ZE	OKFLAG
1	1549759.56	6366770.40	–509.72	1550329.88	6366047.99	0.65	0
2	1549752.87	6366776.43	–512.14	1550489.71	6366322.04	–1.01	0
3	1549745.48	6366781.71	–514.16	1550434.64	6366169.93	1.30	0
4	1549737.58	6366788.55	–510.15	1550489.38	6366319.01	–1.03	0
POINT	**T0**	**U0**	**QEQ**	**TW**	**F**	**L**	
1	$2.00 \cdot 10^{3}$	$4.62 \cdot 10^{-02}$	$4.28 \cdot 10^{-03}$	$9.44 \cdot 10^{0}$	$1.43 \cdot 10^{4}$	$1.38 \cdot 10^{3}$	
2	$2.00 \cdot 10^{3}$	$5.54 \cdot 10^{-02}$	$1.23 \cdot 10^{-02}$	$3.98 \cdot 10^{0}$	$5.20 \cdot 10^{3}$	$1.36 \cdot 10^{3}$	
3	$2.00 \cdot 10^{3}$	$7.89 \cdot 10^{-03}$	$3.20 \cdot 10^{-03}$	$6.14 \cdot 10^{0}$	$5.84 \cdot 10^{3}$	$1.21 \cdot 10^{3}$	
4	$2.00 \cdot 10^{3}$	$1.88 \cdot 10^{-02}$	$1.95 \cdot 10^{-03}$	$1.20 \cdot 10^{1}$	$1.59 \cdot 10^{4}$	$1.40 \cdot 10^{3}$	

Point indicates path number

XS, YS and ZS are coordinates for start of flow path

XE, YE and ZE are coordinates for exit location

OKFLAG indicates whether or not a particle reached the model boundary

T0 is release time

U0 is Darcy flux (m/yr) for Q1 and Q2; UR is used for Q3 (not shown in this excerpt)

QEQ is the equivalent flow rate for Q1 and Q2; QEQR is used for Q3 (not shown in this excerpt)

TW is the advective travel time in the rock, i.e. in the DFN (yr)

F is the flow related transport resistance for the rock, i.e. in the DFN (yr/m)

L is the path length in the rock, i.e. in the DFN (m)

It is noted that also a stochastic continuum case is presented in /Joyce et al. 2010/. This case is not recommended for further use in the Comparative analysis since measurable site characteristics are believed to be less well represented in this case relative to the DFN model applications. Also, tails in resulting performance measure distributions are believed to be less well quantified in the continuum representation.

In Figure A7-1, cumulative distribution functions of the Darcy flux, advective travel time, and flow related transport resistance for a snapshots-in-time are exemplified.

Periglacial and glacial period

In Table A7-5 the periglacial and glacial period cases analysed in /Vidstrand et al. 2010/ are listed. Furthermore, references are made to where tabulated results can be found for each case.

The variant with a North-South ice profile direction addresses the uncertainty in ice direction, (see /Vidstrand et al. 2010/ for details).

In addition to the cases listed in Table A7-5, results can be extracted for a case with permafrost but no ice (i.e. permafrost has developed but the ice sheet has not yet arrived), and for a submerged case (i.e. when the ice sheet has completely retreated and the site is covered by a sea). Results for these two cases are contained within the glacial case without permafrost for the submerged case, and within results for the glacial case with permafrost for the permafrost only case. The set-up of these modelling cases is described in more detail in /Vidstrand et al. 2010/. It is noted that the glacial case without permafrost and glacial cases with permafrost together constitute a base case; i.e. during glacial advance permafrost and an ice sheet exist together, while during retreat no permafrost is present and the glacier is warm based.

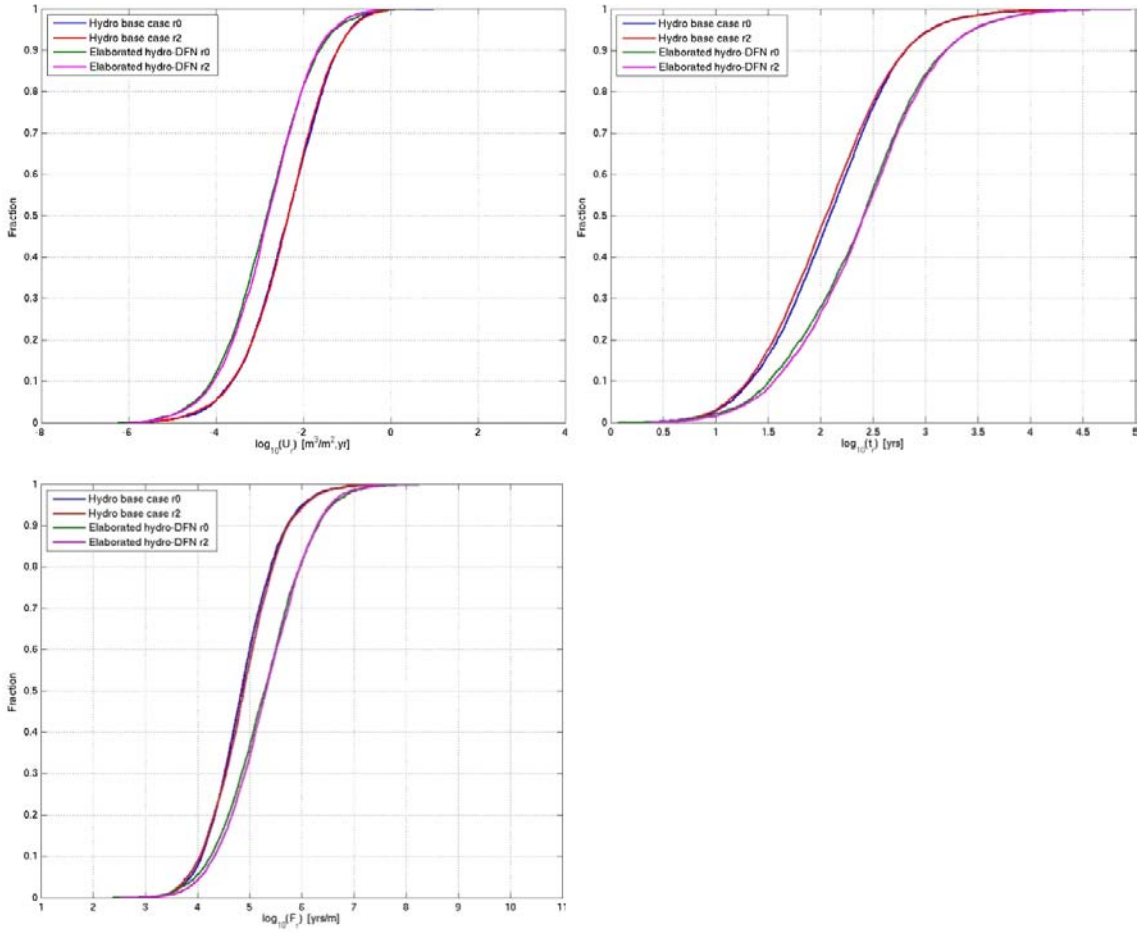

Figure A7-1. *Cumulative distribution function plots of Darcy flux q (denoted U_r in figure caption,) t_w, and F (denoted t_r and F_r in figure captions to indicate that t_w and F are calculated in the bedrock described as a DFN only) in the hydrogeological base case and the Elaborated Hydro-DFN case, including one additional realisation of each, for the Q1 particles successfully reaching the model top boundary (60%–69%) released at 2000 AD. Reproduced from Figures 6-23 through 6-25 in /Joyce et al. 2010/.*

Table A7-5. Modelling cases and references to tabulated results.
Tabulated results are stored in SKBdoc 1263831 (access might be given on request).

Hydrogeological modelling case
Glacial case without permafrost
Glacial case without permafrost and North-South ice profile
Glacial case with permafrost – 2 km permafrost tongue.

The glacial case without permafrost, with an ice front location above the repository, yields the most unfavourable results. For the other ice front locations, the results are much more favourable. Figure A7-2 shows the normalised Darcy flux calculated in the super-regional model for the glacial case without permafrost in a few observation points at repository depth during a glacial advance and retreat. Values are normalised to the flux value for temperate conditions. It is clearly seen that high groundwater flow conditions are experienced during the two ice front passages, while during ice coverage the Darcy flux in most observation locations are comparative to the corresponding temperate value.

The alternative cases considered, i.e. the North-South ice profile, do not provide substantially different results and are not suggested to be propagated.

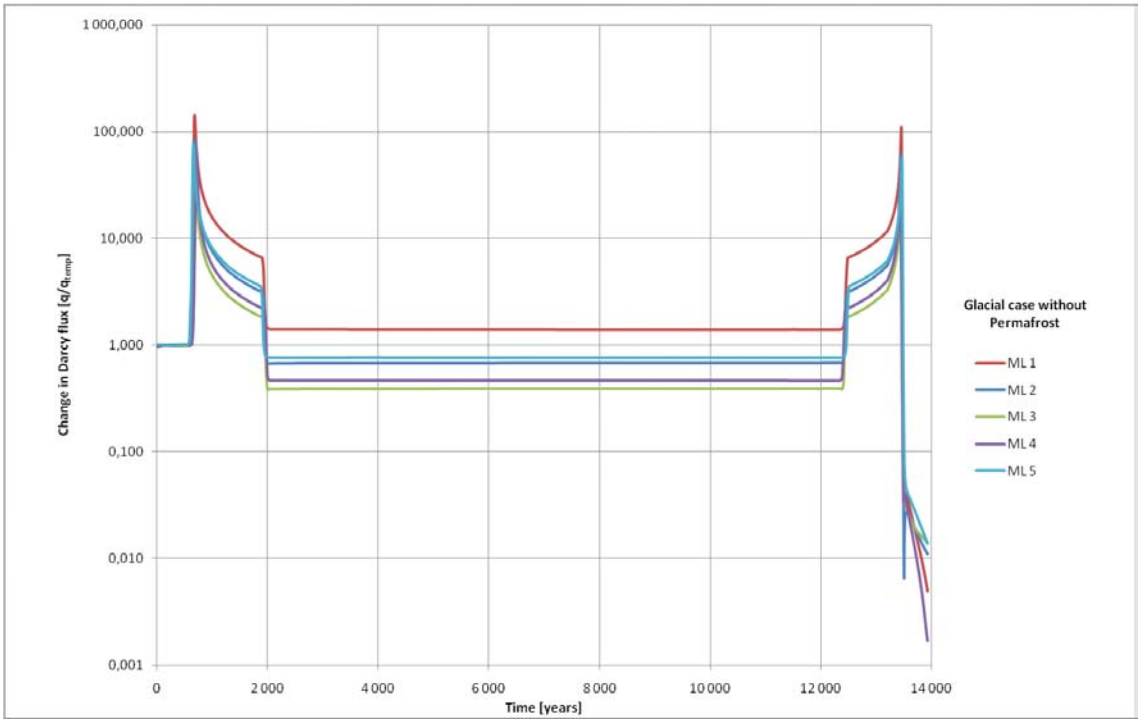

Figure A7-2. *Change in Darcy flux ratio, (q/q_{temp}) during a cycle of approximately 18ka. Between the two ice front passages, the model domain is completely covered by ice. The time scale represents the model simulation time rather than calendar time. Figure from /Vidstrand et al. 2010/.*

In Figure A7-3, the median as well as maximum and minimum Darcy flux values representing the full set of deposition hole locations are shown as obtained in /Vidstrand et al. 2010/. The results indicate that the situation with permafrost only, i.e. the period before onset of the glacial advance, and the glacial maximum case, i.e. when the site is fully covered by an ice sheet, provides slightly less favourable conditions than the temperate case. The Glacial case without permafrost provides the highest fluxes, while the cases with combined permafrost and ice sheet provide somewhat more favourable conditions than the pure glacial case. The submerged case provides more favourable conditions than the temperate case.

Peclet number and maximum penetration depth

The Peclet number /Norman and Kjellbert 1990/ which relates to the relative importance of advective versus dispersive transport mechanisms along the individual flow paths, through a dimensionless ratio, has not been further addressed since the SR-Can safety assessment. The central value recommended in SR-Can, which is 10, is recommended for use as a single point value in the Comparative analysis. The justification is twofold:

- Large scale dispersion is handled through multiple flow paths in the groundwater flow models. Longitudinal dispersion along individual flow paths has a minor effect on breakthrough characteristics. Field evidence from tracer tests suggests that the dispersion length typically is 10 percent of the distance of a tracer test; this yields a Peclet number of 10.
- Since dispersion is more of a model concept than a strict process, it is hard to justify shapes of distributions.

Concerning the maximum penetration depth, the matrix pore space is connected over all distances of interest within the assessment (cf. Chapter A8). Thus, the maximum penetration depth is given by the average fracture spacing. This is reported in the site-descriptive model /Rhén et al. 2008, Table 9-13/ and is approximately 9 m for the rock in the depth interval (depth zone 3) –400 m to –650 m in fracture domain HRD_C. The maximum penetration depth is half the fracture spacing, i.e. 4.5 m. It is suggested that this value is used as a deterministic value in the Comparative analysis

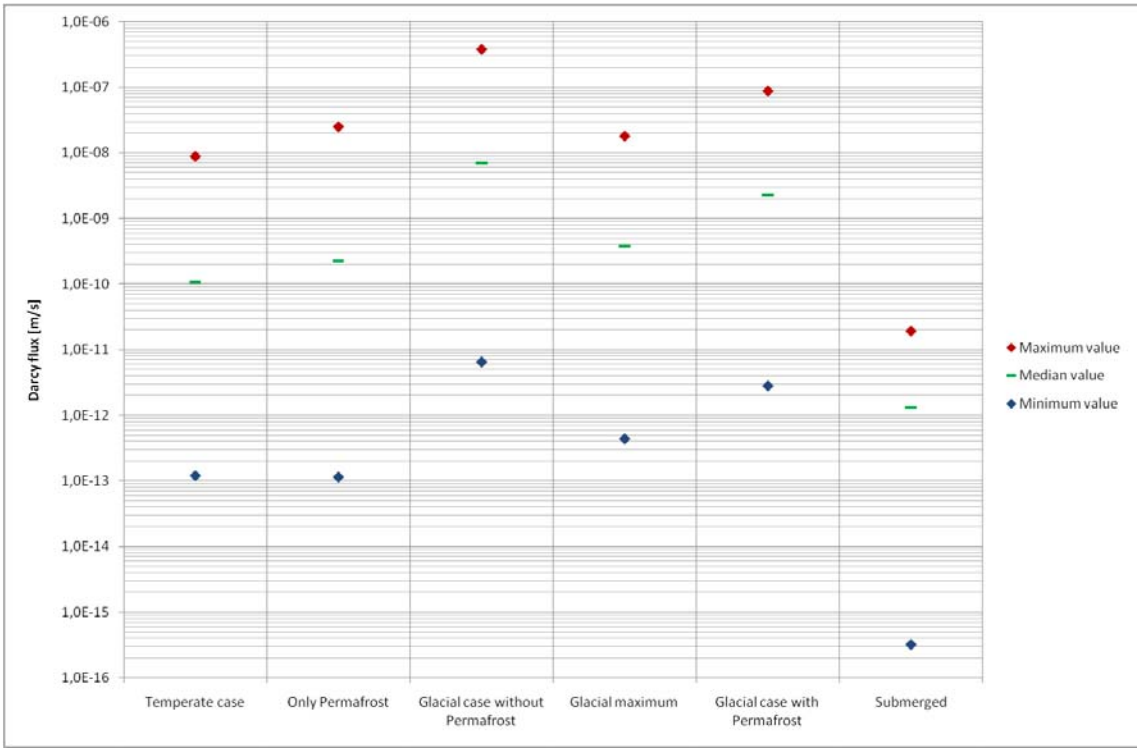

Figure A7-3. *Estimated Darcy fluxes for the main climate situations considered in a full glacial cycle. Minimum, maximum, and median values based on all deposition holes are shown for each situation.*

A7.10 Data recommended for use in the Comparative analysis

It is recommended that the following cases, out of those tabulated in Table A7-3 and Table A7-5, are propagated to the Comparative analysis.

- *Temperate period:* Elaborated Hydro-DFN Case.
- *Periglacial and Glacial period:* Glacial case without permafrost.

References to data files providing Q_{eq}, F, t_w, and q are given in Table A7-3 and Table A7-5. Furthermore, the Peclet number and maximum penetration depth recommended for use in the Comparative analysis are listed in Table A7-6.

Table A7-6. Data recommended for use in SR-Site.

Parameter	Recommended data
Peclet number, *Pe* (–)	10
Maximum penetration depth, L_D (m)	4.5

References A7.11

SKB's (Svensk Kärnbränslehantering AB) publications can be found at www.skb.se/publications.

Cliffe K A, Kelly M, 2006. COMP23 version 1.2.2 user's manual. SKB R-04-64, Svensk Kärnbränslehantering AB.

Elert M, Gylling B, Lindgren M, 2004. Assessment model validity document FARF31. SKB R-04-51, Svensk Kärnbränslehantering AB.

Joyce S, Simpson T, Hartley L, Applegate D, Hoek J, Jackson P, Roberts D, Swan D, Gylling B, Marsic N, Rhén I, 2010. Groundwater flow modelling of periods with temperate climate conditions – Laxemar. SKB R-09-24, Svensk Kärnbränslehantering AB.

Norman S, Kjellbert N, 1990. FARF31 – A far field radionuclide migration code for use with the PROPER package. SKB TR 90-01, Svensk Kärnbränslehantering AB.

Rhén I, Hartley L, 2009. Bedrock Hydrogeology Laxemar. Site descriptive modelling, SDM-Site Laxemar. SKB R-08-92, Svensk Kärnbränslehantering AB.

Rhén I, Forsmark T, Hartley L, Jackson P, Roberts D, Swan D, Gylling B, 2008. Hydrogeological conceptualisation and parameterisation. Site descriptive modelling, SDM-Site Laxemar. SKB R-08-78, Svensk Kärnbränslehantering AB.

Rhén I, Forsmark T, Hartley L, Joyce S, Roberts D, Gylling B, Marsic N, 2009. Bedrock hydrogeology. Model testing and synthesis. Site descriptive modelling, SDM-Site Laxemar. SKB R-08-91, Svensk Kärnbränslehantering AB.

Romero L, Thompson A, Moreno L, Neretnieks I, Widén H, Boghammar A, 1999. Comp23/ Nuctran user´s guide – Proper version 1.1.6. SKB R-99-64, Svensk Kärnbränslehantering AB.

Selroos J-O, Follin S, 2010. SR-Site groundwater flow modelling methodology, setup and results. SKB R-09-22, Svensk Kärnbränslehantering AB.

SKB, 2006a. Long-term safety for KBS-3 repositories at Forsmark and Laxemar – a first evaluation. Main report of the SR-Can project. SKB TR-06-09, Svensk Kärnbränslehantering AB.

SKB, 2006b. Climate and climate-related issues for the safety assessment SR-Can. SKB TR-06-23, Svensk kärnbränslehantering AB.

SKB, 2010a. Data report for the safety assessment SR-Site, TR-10-52, Svensk Kärnbränslehantering AB.

SKB, 2010b. Radionuclide transport report for the safety assessment SR-Site. SKB TR-10-50, Svensk Kärnbränslehantering AB.

Svensson U, Rhén I, 2010. Groundwater flow modelling of the excavation and operation phases – Laxemar. SKB R-09-23, Svensk Kärnbränslehantering AB.

Vahlund F, Hermansson H, 2006. A direct numerical approach to solving the transport equations for radionuclide transport in fractured rock. SKB R-04-50, Svensk Kärnbränslehantering AB.

Vidstrand P, Rhén I, Zugec N, 2010. Groundwater flow modelling of periods with periglacial and glacial climate conditions – Laxemar. SKB R-09-25, Svensk Kärnbränslehantering AB.

A8 Non-flow related migration properties

Migration of solutes through fractured rock depends on several parameters. The data handled in this appendix, concerning the effective diffusivity, diffusion available porosity, and sorption partitioning coefficient, are related to the rock matrix properties themselves. These data are site specific, depending on the geological settings and groundwater composition.

Other parameters of importance for solute transport are closely related to the groundwater flow, i.e. are "flow related", and are discussed in Chapter A7.

A corresponding text for the Forsmark site is found in Section 6.8 of the SR-Site Data report /SKB 2010a/. We have chosen not to repeat aspects and methodologies that are general for both sites, but instead to refer to the corresponding Forsmark text. Therefore, we strongly recommend the reader to first examine Section 6.8 of the SR-Site Data report, and thereafter read this present text.

A8.1 Modelling as input to the Comparative analysis of safety related site characteristics

This section describes what data are expected from the supplier, and in what modelling activity the data are to be used.

Defining the data requested from the supplier

The following data should be delivered by the supplier:

- The diffusion available porosity ε (–), also commonly referred to as the porosity, for the undisturbed rock matrix. Different species may experience different diffusion available porosity. When necessary, different porosities should be delivered for different rock volumes, judged as appropriate by the supplier.
- The effective diffusivity D_e (m^2/s) for radioelements of the selected inventory. The D_e should represent the undisturbed rock matrix. In estimating the effective diffusivity, it may be necessary to discuss the formation factor F_f (–). When necessary, different effective diffusivities should be delivered for different rock volumes, judged as appropriate by the supplier.
- The scale on which the porous system is connected L (m), thus allowing for matrix diffusion.
- The sorption partitioning coefficient K_d (m^3/kg) for the radioelements of the selected inventory. The uncertainty estimate of K_d data should encompass the underlying uncertainties in groundwater compositions that are likely to be encountered (cf. Chapter A1). When possible and necessary, different K_d data should be delivered for different rock volumes, judged as appropriate by the supplier.

The radioelements of the selected inventory, for which transport parameters are required, are: H (assumed as HTO), C (inorganic and organic compounds), Cl, Ni, Se, Sr, Zr, Nb, Mo, Tc, Pd, Ag, Cd, Sn, I, Cs, Sm, Eu, Ho, Pb, Ra, Ac, Th, Pa, U, Np, Pu, Am, and Cm (cf. the SR-Site Data report /SKB 2010a, Section 2.2/).

Modelling activities in which data will be used

Migration of dissolved radionuclides in the rock matrix occurs predominantly by diffusive transport, which is modelled by using Fick's laws. The diffusive transport will occur in the porewater that saturates the microporous system of rock at depth. Species will also, to different degrees, interact with the mineral surfaces surrounding the microporous system. Sorption of radionuclides in the far-field is modelled using a linear relation (justified by a low radionuclide concentration and equilibrium) between sorbed species and solute concentrations. The proportionality coefficient is the sorption partitioning coefficient K_d.

Radionuclide migration through the far-field is in the Comparative analysis modelled analytically or by the transport simulation code FARF31 /Norman and Kjellbert 1990/. The general approach taken when modelling radionuclide transport in the far-field is described in the SR-Site Radionuclide transport report /SKB 2010b/. This approach is also valid for the Comparative analysis, although the scope of the Comparative analysis is limited.

A8.2 Supplier input on use of data in the Comparative analysis

The data supplied in this appendix depend on the properties of the rock matrix, and on the chemical composition of the groundwater and rock matrix porewater. In the context of non-flow related migration properties, the rock matrix at the two sites is very similar. In addition, the groundwater compositions at the sites share similar characteristics, where the variations during the glacial cycle are so large that it overshadows present day differences in groundwater compositions. As a result, the data supplied for Laxemar are similar to those recommended for Forsmark. There is no indication of differences in data that would be of major importance for the site selection.

In SR-Site Data report /SKB 2010a, Section 6.8/, the qualification process of non-flow related migration properties for Forsmark is detailed. The same considerations apply for Laxemar data, unless explicitly stated.

A8.3 Sources of information and documentation of data qualification

Sources of information

Laboratory porosity data from the Laxemar site investigation are compiled in the SDM-Site report /Crawford and Sidborn 2009/. A way to transfer laboratory to in situ porosities is given in the SR-Site Data report /SKB 2010a, Section 6.8/. Apparent in situ formation factors from four boreholes in Laxemar are presented in /Löfgren 2007/. A way to transfer apparent formation factors to formation factors is given in the SR-Site Data report. In addition, a way to correct the D_e data for anion exclusion is given in the SR-Site Data report. K_d data, also for Laxemar, are compiled in a dedicated SR-Site report /Crawford 2010/. The above mentioned publications are listed in Table A8-1.

Table A8-1. Main sources of information used in data qualification.

Crawford J, Sidborn M, 2009. Bedrock transport properties Laxemar. Site descriptive modelling, SDM-Site Laxemar. SKB R-08-94, Svensk Kärnbränslehantering AB.
SKB, 2010a. Data report for the safety assessment SR-Site. SKB TR-10-52, Svensk Kärnbränslehantering AB.
Löfgren M, 2007. Oskarshamn site investigation. Formation factor logging in situ by electrical methods in KLX07A, KLX08, KLX10 and KLX12A. SKB P-06-288, Svensk Kärnbränslehantering AB.
Crawford J, 2010. Bedrock Kd data and uncertainty assessment for application in SR-Site geosphere transport calculations. SKB R-10-48, Svensk Kärnbränslehantering AB.

Categorising data sets as qualified or supporting data

The most important data sets used in qualifying the diffusion available porosity, effective diffusivity, and sorption partitioning coefficient are listed in Table A8-2. For the porosity and effective diffusivity the data originates from the Laxemar site investigation, but may have been modified in the Laxemar site-descriptive modelling or in this present text. The recommended K_d data represent a mix of data obtained during the site investigations at Forsmark and Laxemar, as well as data obtained from literature sources deemed of sufficient quality. These data are compiled in /Crawford 2010/. Comments on the sorting of these data sets are given in the table.

Table A8-2. Qualified and supporting data sets.

Qualified data sets	Supporting data sets
1. /Crawford and Sidborn 2009/, Tables 4-7 and 4-27: Laboratory porosities of unaltered rock matrix in Laxemar.	
2. /SKB 2010a/, Section 6.8.7: Reduction factor of 0.8 used for correcting laboratory porosity to in situ porosity.	
3. /Löfgren 2007/, Equations 4-5 to 4-8: The estimated electrical conductivity profiles of the pore water in KLX07A, KLX08, KLX10, and KLX12A.	
4. /Löfgren 2007/, Appendix B: The rock matrix apparent formation factors of boreholes KLX07A, KLX08, KLX10, and KLX12A (numerical data taken from corresponding SICADA files).	
5. /SKB 2010a/, Section 6.8.7: Equation used to correct apparent formation factors to formation factors. Equation used to transfer D_e for cations and non-charged solutes to D_e for anions.	
6. /Crawford 2010/, Table 6-2: Recommended K_d data for the Laxemar site.	
7. /Vilks et al. 2005/, Tables 1 and 2. D_e for HTO and iodide of 16 samples from the LTDE-SD experiment at Äspö Hard Rock Laboratory. For use in evaluating the effect of anion exclusion.	

Item 1–6 are site investigation reports, site-descriptive modeling reports, or SR-Site reports. These are all produced and reviewed in accordance with the SKB quality assurance system. The data are judged as qualified. Item 7 is a report produced by Atomic Energy of Canada Limited, presenting results from rock samples from Äspö. The data are judged to be representative and accurate, but it should be noted that all samples are taken from a very local rock volume.

Excluded data previously considered as important

The same considerations apply as given in the corresponding section in the SR-Site Data report. There is no additional consideration for Laxemar data.

A8.4 Conditions for which data are supplied

Generally, the same considerations apply as given in the corresponding section in the SR-Site Data report, where the following conditions are discussed:

- Rock type and degree of alteration/disturbance.
- Groundwater composition.
- In-situ temperature.
- In-situ stress.

Concerning these conditions, the sites differ as following.

- The common rock types at the Laxemar site have, on average, a somewhat larger CEC (cation exchange capacity) than those at Forsmark. This affects the K_d of certain radioelements.

The rock mass at the Laxemar site has a higher frequency of open fractures than at Forsmark. Therefore, it is likely that a larger portion of the rock mass is affected by water-bearing fractures, and that the alteration is greater. However, as data are required for the unaltered rock mass, this should not affect the data. The fracturing and alteration may, however, give rise to slightly larger data uncertainty.

- The groundwater compositions at Laxemar and Forsmark at repository depth are similar, in the context of how they affect non-flow related migration properties. The variations over the glacial cycle are so large that they overshadow present day differences in groundwater compositions.
- Differences between the in situ temperatures at depth at the two sites are small enough to have an insignificant impact on the data.
- Differences between the in situ stresses at the two sites are small enough to only have a minor effect on the data. This effect is judged to be so small that no special treatment is made for Laxemar, but instead information from the Forsmark site is used.

A8.5 Conceptual uncertainty

There is no conceptual uncertainty that is specific for the Laxemar site. Therefore, the reader is referred to the conceptual uncertainties described in the SR-Site Data report /SKB 2010a, Section 6.8.6/.

A8.6 Data uncertainty due to precision, bias, and representativity

Diffusion available porosity

There is no additional uncertainty regarding the porosity for the Laxemar site, comparing to the Forsmark site. Therefore, the corresponding data uncertainty discussion given in the SR-Site Data report /SKB 2010a, Section 6.8.7/ is referred to.

Effective diffusivity

In the SR-Site Data report, two methods of estimating the effective diffusivity are used. The first method is based on D_e data from through diffusion experiments in the laboratory, where the data are corrected for the fact that the samples are stress released in the laboratory. In the second method, in situ apparent formation factors F_f^{app} (-) based on downhole electrical resistivity loggings are used. These apparent formation factors are corrected into formation factors by use of Equation A8-1.

$$F_f = F_f^{app} - \frac{0.0012 \cdot F_f^{0.415}}{\kappa_w} \qquad \text{A8-1}$$

where κ_w is the electrical conductivity of the pore water of the rock matrix. From the formation factor, the effective diffusivity is calculated according to:

$$D_e = D_w \cdot F_f \qquad \text{A8-2}$$

Where D_w (m^2/s) is the diffusivity in unconfined porewater. Equation A8.2 is valid under the prerequisite that there is no exclusion effect or enhancing effect, such as surface diffusion. If such effects are present, further corrections are needed. In this text, such corrections are made to account for anion exclusion. It should be noted that the empirical constants in Equation A8-1 is predominantly based on measurements on rock samples from the Oskarshamn site investigation area (for example from the borehole KLX02).

As shown in the SR-Site Data report, these two methods give very similar data, and for Forsmark, the final choice of data has been based on the second method, utilising downhole electrical resistivity measurements. For Laxemar, the somewhat simplified approach of only basing the recommended data on the second method has been chosen. This induces some extra uncertainty, compared with the Forsmark data, but this extra uncertainty is judged to be small.

Data from the four boreholes KLX07A, KLX08, KLX10, and KLX12A are the foundation of the suggested data /Löfgren 2007/. These boreholes are chosen as the data evaluation was refined during the site investigation, and as these boreholes were evaluated last. Also the knowledge on how the groundwater composition varies within the site evolved with time. This suggests that these four boreholes was handled somewhat more accurately that boreholes of earlier reports.

In borehole KLX08, the estimated profile of the electrical conductivity of the porewater versus borehole length is based on both the electrical conductivity of freely flowing groundwater, and on data estimated from porewater extraction/leaching of drill core samples in the laboratory. Therefore, the methodology of obtaining these data matches that used in the SR-Site Data report. For the other boreholes, the estimated profiles are based only on measurement on freely flowing water. This induces extra uncertainty, compared to in Forsmark, especially as the groundwater composition appears to be more heterogeneous in Laxemar than in Forsmark.

Figure A8-1 (upper graph) shows the electrical conductivity of freely flowing fracture water, as measured in packed off sections in seven boreholes including KLX07A, KLX10 and KLX12A. The lower graph shows the electrical conductivity as measured on freely flowing fracture water (“EC in situ”) and as estimated from porewater extraction/leaching data (“Matrix fluid EC”) in KLX08.

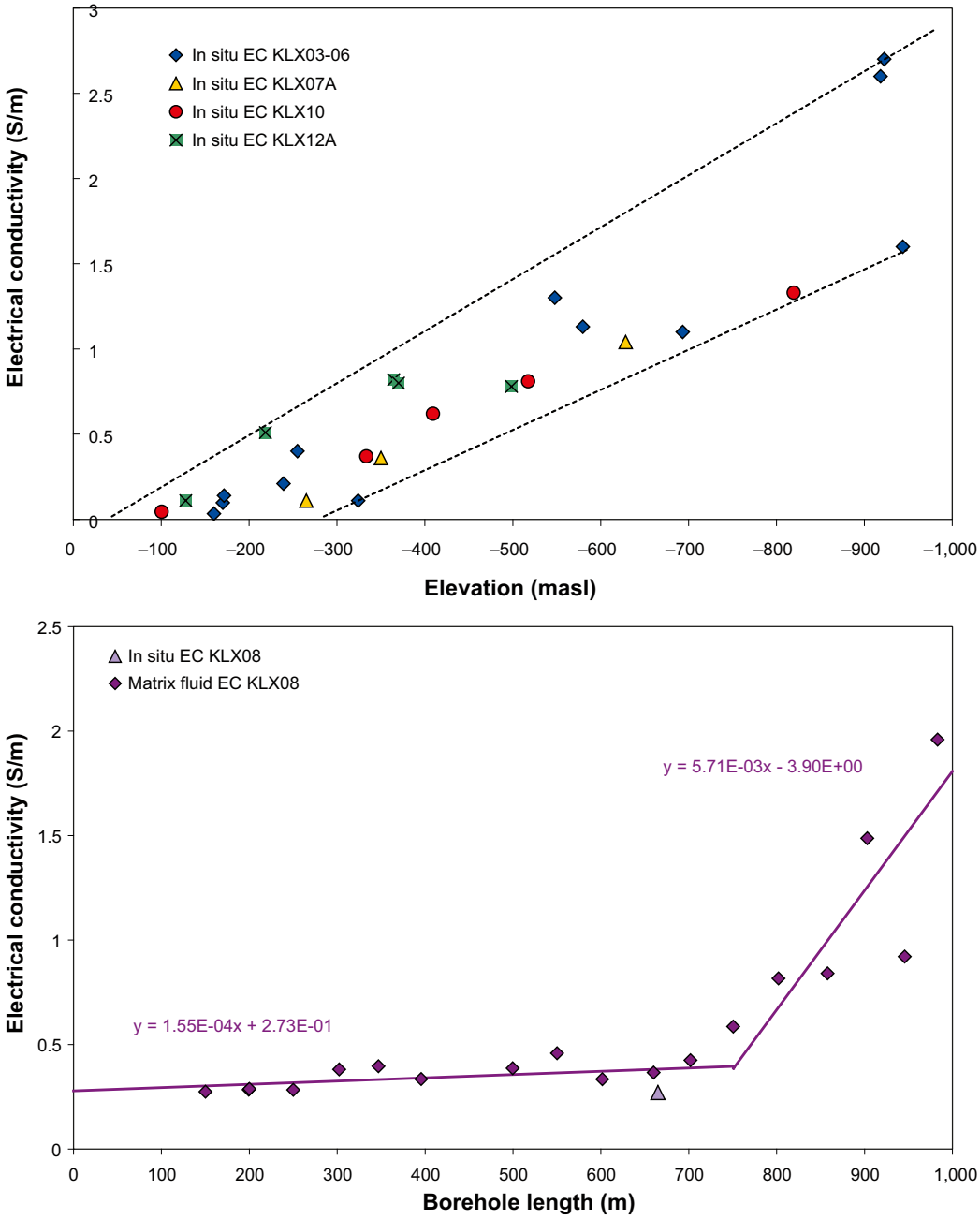

Figure A8-1. *Electrical conductivity of freely flowing groundwater and matrix pore water at Laxemar. Figures reproduced from Figure 4-18 and 4-20 of /Löfgren 2007/. Inclination at ground surface for KLX08 is ~ –60° . For KLX08, the estimated profiles of electrical conductivity vs. borehole length are shown by the purple lines and equations.*

The uncertainty in suggested $\boldsymbol{D_e}$ data due to the lack of porewater extraction/leaching data is, on average, judged to be contained within a few tens of percents.

Other considerations on data uncertainty for the effective diffusivity, such as the uncertainty in D_w used in Equation A8-2, are discussed in Section 6.8.7 of the SR-Site Data report.

Anion exclusion

In the SR-Site Data report /SKB 2010a, Section 6.8.7/ it is argued that the D_e for anions can be obtained from the D_e of cations and non-charged solutes by the following equation:

$$\log_{10}(D_e, anions) = \log_{10}(D_e) - 0.5 \qquad \text{A8-3}$$

The same considerations apply for Laxemar data, and the same correction is suggested for use in the Comparative analysis. The justification of Equation A8-3 is partly based on data from the Äspö Hard Rock Laboratory /Vilks et al. 2005/, which lends creditability to the equation's applicability at Laxemar. The existence of anion exclusion has recently been indicated in the in situ tracer test Long Term Sorption Diffusion Experiment (LTDE-SD) at the Äspö HRL /Nilsson et al. 2010/.

The scale on which the porous system is connected

As for Forsmark, it is suggested that the porous system at Laxemar is connected on all scales relevant for the safety assessment (at least decametre scale), and that there is little uncertainty or variability.

Sorption partitioning coefficient

Data uncertainties associated with K_d estimations is summarised in the SR-Site Data report and detailed in /Crawford 2010/. The recommended data are based on data from both sites, as well as on literature data. No uncertainty that is specifically related to the Laxemar site exists. Accordingly the discussion in the SR-Site Data report is referred to.

It can be worth noting that out of the transfer factors used (cf. /Crawford 2010/) only that for CEC (cation exchange capacity) is assigned different values for the Laxemar and Forsmark site. As discussed in Chapter 5 of /Crawford 2010/, Laxemar rock types generally have a higher biotite content than Forsmark rocks, and can be expected to have a proportionately larger CEC. Otherwise the same data derivation is used for the two sites.

In the derivation of K_d data for the Laxemar site it is assumed that the variation in future groundwater compositions over the glacial cycle overshadows present day differences between the Forsmark and Laxemar sites. Implicitly it is also assumed that the groundwater compositions at the sites follow the same systematic trends as response to shore-level displacement and climatic changes. Based on these assumptions, groundwater compositions that are valid for the Forsmark site have been used in the derivation of Laxemar data. This induces additional uncertainty. However, this uncertainty is judged to be overshadowed by the general uncertainty involved in estimating K_d values representative for different groundwater compositions over the glacial cycle (cf. /Crawford 2010/).

A8.7 Spatial and temporal variability of data

In Section 4.4.1 of /Crawford and Sidborn 2009/, the porosity measured in the site investigation laboratory programme is summarised (cf. Table 4-6, 4-7 and 4-27 of /Crawford and Sidborn 2009/). By comparing the porosity of different rock types, in deformation zones and non-deformed rock, it can be concluded that the spatial variability is fairly small, although it is generally larger than in Forsmark.

In Table A8-3, the data for the unaltered rock matrix given in Table 4-27 of /Crawford and Sidborn 2009/ are reproduced. The data could be used as representative, best estimate laboratory porosities for the main rock types within rock domains RSMA01, RSMD01, RSMM01, and RFMBA03.

Table A8-3. Laboratory porosities of unaltered rock matrix for main rock types in Laxemar. Data from Table 4-7 and 4-27 in /Crawford and Sidborn 2009/.

Rock type	Rock type code	Arithmetic mean (%)	Standard deviation (%)	Number of data points (samples)
Fine-grained dioritoid	501030	0.20	0.22	73
Quartz monzodiorite	501036	0.19	0.19	61
Ärvö quartz monzodiotite	501046	0.36	0.14	27
Ärvö granodiorit	501056	0.30	0.10	53
Fine-grained diorite-gabbro	505102	0.16	0.06	8
Granite, fine- to medium-grained	511058	0.24	0.07	24

The data of Table A8-3 are illustrated in Figure A8-2 for the different rock types. The triangle marks the arithmetic mean and the error bars the standard deviation.

As can be seen in Figure A8-2, the variation in the arithmetic mean porosity between different rock types is minor. The porosity should be flowpath averaged before use in solute transport modelling in the Comparative analysis. This means that all porosities encountered along the flowpath should be averaged, by way of taking their arithmetic mean. As the natural variability of local porosities is relatively small, the flowpath averaged porosity can for safety assessment purposes be regarded to feature no significant spatial variability. Furthermore, the porosity is suggested to feature no significant temporal variability.

Figure A8-3 shows how the apparent formation factor varies in different boreholes within the Oskarshamn site investigation area. In the image, the 10 m running average of the apparent rock matrix formation factor is shown.

The great majority of the apparent formation factors are found within a one order of magnitude range, which is also the case for the formation factor. As the formation factor and effective diffusivity should be flowpath averaged before use in solute transport modelling, the spatial variability between flowpaths is suggested to be minor. The temporal variability in the data is also judged to be minor and the suggested data ranges in Section A8.9 encompass these effects.

The considerations on natural variability for K_d given in the SR-Site data report (Section 6.8.9) are valid also for Laxemar data. The data ranges given in Section A8.9 of this present report aim to encompass these effects. A discussion on the natural variability of K_d data due to external conditions (mainly the impact of the glacial cycle) and due to the physical state of the rock matrix is given in /Crawford 2010, Chapter 4/.

A8.8 Correlations

The same correlations and functional relationships as discussed in the SR-Site Data report /SKB 2010a, Section 6.8.9/ apply for the Laxemar data. Correlation groups for K_d of different radioelements are given in Table A8-4.

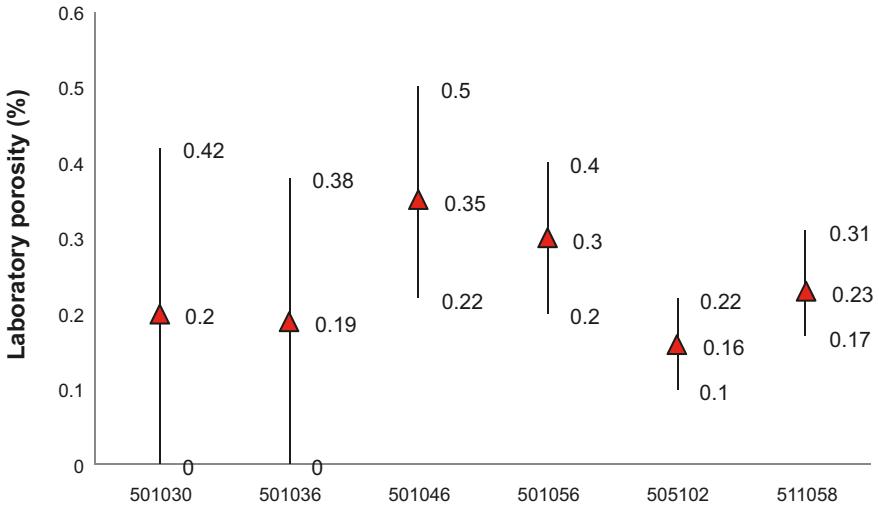

Figure A8-2. *Laboratory porosities of unaltered rock matrix for main rock types in Laxemar. Triangle marks the arithmetic mean and the error bars the standard deviation.*

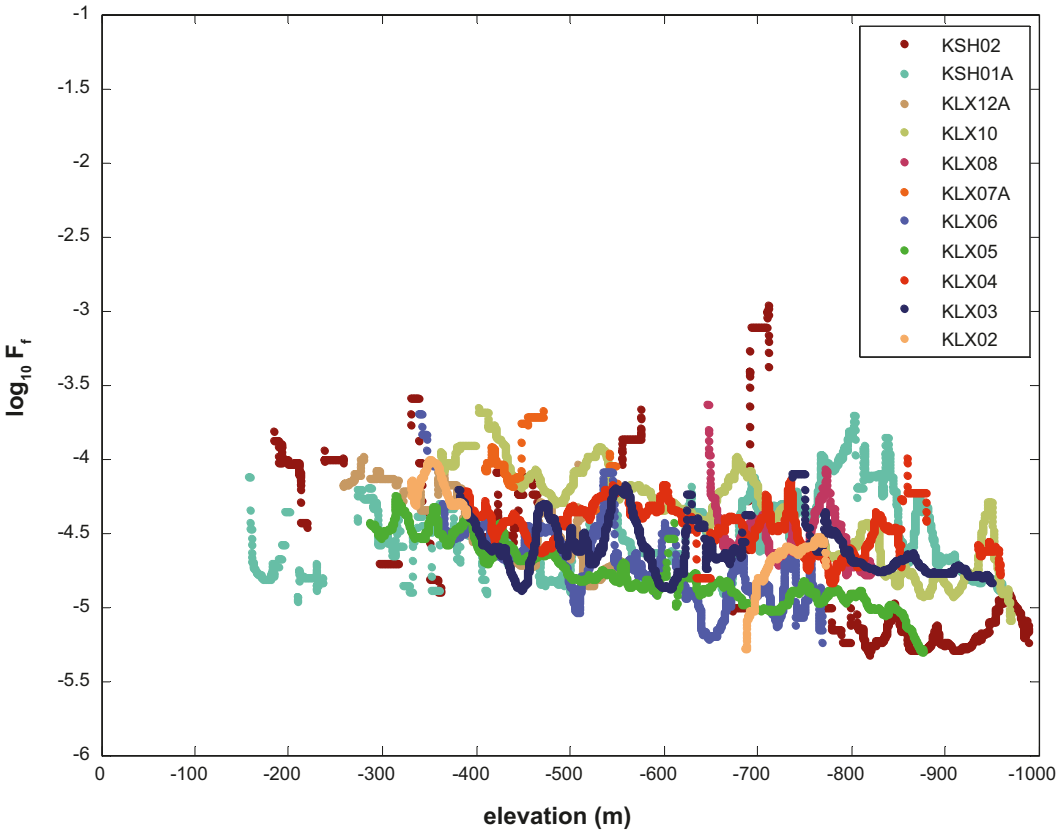

Figure A8-3. *Variation of the in situ apparent rock matrix formation factor (10 m running averages) plotted as a function of elevation for all reported boreholes from the Laxemar-Simpevarp area. Measurement points less than 0.5 m distant from mapped open fractures are excluded. Reproduced from Figure D-2 of /Crawford and Sidborn 2009/.*

A8.9 Result of supplier's data qualification

Diffusion available porosity

Laboratory porosities for different rock types are summarised in Table A8-3. The arithmetic mean of all 246 samples that Table A8-3 is based upon is 0.24%. To correct for the fact that the laboratory samples are stress released, the same correction factor is used as argued for in the SR-Site Data report, i.e. 0.8. By multiplying 0.24% with 0.8, the recommended in situ porosity becomes 0.19%. The porosity should be flowpath averaged, and this single point value is recommended for use in all flowpaths at the site, with no associated uncertainty range.

As discussed in the SR-Site Data report, it is judged that there is no significant anion exclusion on the porosity. Accordingly the diffusion available porosity is the same for cations, non-charged solutes, and anions.

Formation factor and effective diffusivity

The apparent formation factors of borehole KLX07A, KLX08, KLX10, and KLX12A are corrected into formation factors by used of Equation A8-1. In doing this, the electrical conductivities of the porewater at different depths are needed. Electrical conductivity versus borehole length profiles are described by Equations 4-5 to 4-8 of /Löfgren 2007/. These profiles are based on the data illustrated in Figure A8-1, where one can see such estimated profiles for borehole KLX08.

Figure A8-4 shows the cumulative density functions (CDF) of the formation factors of the individual boreholes, as well as that including all formation factors of the four boreholes (blue curve).

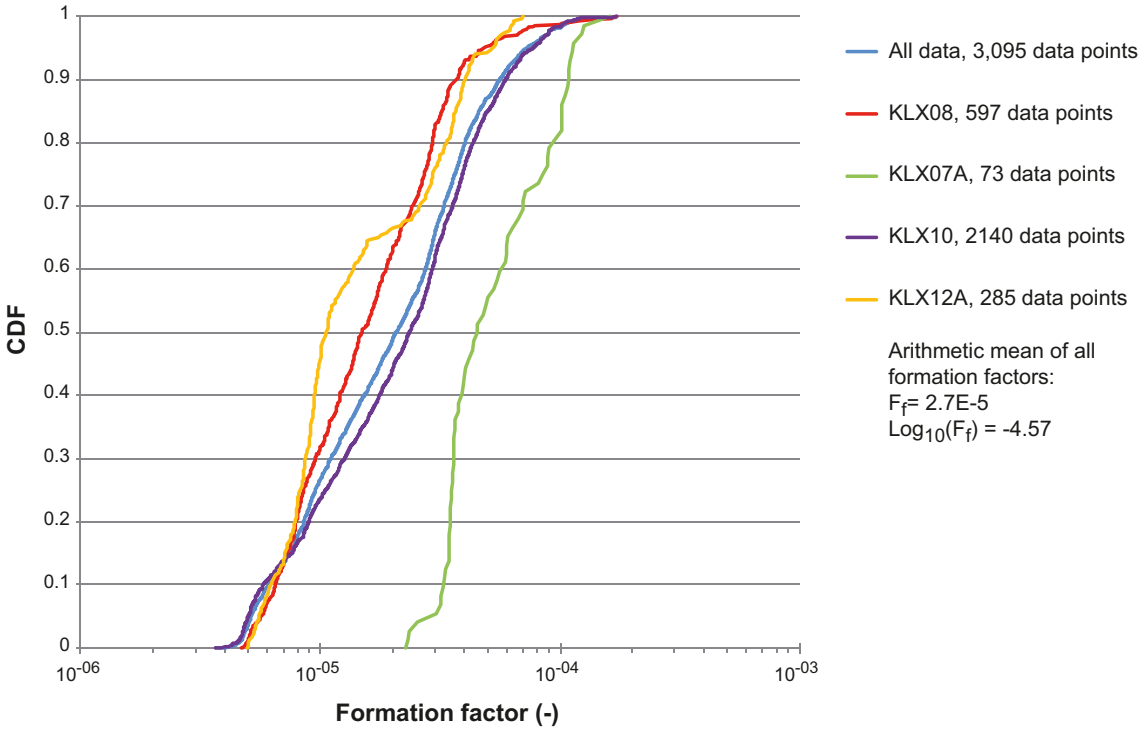

Figure A8-4. *CDF of F_f data points from boreholes KLX07A, KLX08, KLX10, and KLX12A in Laxemar. Blue CDF is based on all 3,095 formation factors of the four boreholes. Arithmetic mean of all 3,095 formation factors is $2.7 \cdot 10^{-5}$.*

It should be noted that the borehole KLX07A was drilled in highly fractured rock, which is the reason that only 73 data points out of 4,780 possible were selected between the borehole lengths 367–845 m. This may suggest that the formation factors that were not discarded due to the proximity to open fractures (see /Löfgren 2007/ for methodology of discarding data) are somewhat affected by the fracturing, which is also indicated by their relatively enhanced values.

Recommended data: For the flowpath averaged in situ formation factor, we recommend using the arithmetic mean value of the 3,095 data points from borehole KLX07A, KLX08, KLX10, and KLX12A. This equals $2.7 \cdot 10^{-5}$. If using a D_w of $1 \cdot 10^{-9}$ m^2/s, the corresponding D_e becomes $2.7 \cdot 10^{-14}$ m^2/s. As justified in the SR-Site Data report; for cations and non-charged solutes the $\log_{10}$ of this value is used as μ in a normal distribution, with the standard deviation of 0.25:

- $\text{Log}_{10}(D_e)$ normal distribution parameters: $\mu = -13.6$, $\sigma = 0.25$.

The standard deviation relates to uncertainty and not to natural variability. For anions, this distribution is shifted downwards by half an order of magnitude, by use of Equation A8-3.

- $\text{Log}_{10}(D_e)$ normal distribution parameters (anions): $\mu = -14.1$, $\sigma = 0.25$.

One could argue for a slightly larger uncertainty range for Laxemar data than for Forsmark data, as the spatial variability of the formation factor is larger at Laxemar. However, this fact has only a very minor impact on the uncertainty in the flowpath averaged effective diffusivity, and the effect is disregarded. It is cautioned that as the suggested standard deviation is due to conceptual and data uncertainty, and not due to natural variability of the rock matrix, the distributions cannot again be flowpath averaged.

It should be noted that a radioelement may have a speciation allowing for cationic, neutral, and anionic forms. Therefore, in case of a radionuclide transport modelling code that only allows for one D_e per radioelement, one must choose whether the radioelement predominantly is in its cationic, neutral, or anionic form.

Sorption partitioning coefficient, K_d

Based on the data extrapolation and qualification procedures described in /Crawford 2010/, K_d data have been estimated for application conditions in Laxemar.

The K_d data are given in the form of log-normal distributions which implicitly include the combined impact of uncertainty as well as spatial and temporal variability. The median of the log-transformed K_d uncertainty may be taken to be the best estimate value for central case deterministic calculations. Although flowpath averaging effects would normally suggest the use of the arithmetic mean K_d value, the use of the median is deemed a more cautious choice given that uncertainty (rather than natural variability) is the dominant contribution to the statistical dispersion of the K_d ranges. For stochastic simulations, it is recommended that the log-normal distributions are sampled uniformly between the 2.5% and 97.5% percentiles (that is the distribution should be truncated).

The recommended K_d data for the Laxemar site are supplied in Table A8-4. These data are recommended for all rock volumes throughout repository evolution. The table also gives two correlation groups for the radioelements.

Table A8-4. Recommended sorption partitioning coefficient, K_d values, for use in Comparative analysis of the Laxemar site. The predominant species for redox sensitive elements are highlighted in bold text. Values are given for the best estimate (median), parameters for the log-normal distribution (m and s), as well as lower and upper limits corresponding to the 2.5% and 97.5% percentiles, respectively. For each row a correlation group (1 or 2) or no correlation group (-) is assigned.

Radionuclide (Redox State)	Best estimate K_d (m^3/kg)	$\log_{10}K_d$ – m	$\log_{10}K_d$ – s	Lower K_d limit (m^3/kg)	Upper K_d limit (m^3/kg)	Corr. Group
Ac(III)	$1.48\cdot10^{-2}$	–1.83	0.72	$5.74\cdot10^{-4}$	$3.83\cdot10^{-1}$	2
Ag(I)	$6.54\cdot10^{-4}$	–3.18	0.51	$6.49\cdot10^{-5}$	$6.60\cdot10^{-3}$	1
Am(III)	$1.48\cdot10^{-2}$	–1.83	0.72	$5.74\cdot10^{-4}$	$3.83\cdot10^{-1}$	2
C, HCO_3^-	0.0	–	–	0.0	0.0	–
C, CH_4	0.0	–	–	0.0	0.0	–
C, $-CO_2H$	0.0	–	–	0.0	0.0	–
Cd(II)	$2.07\cdot10^{-3}$	–2.68	0.65	$1.12\cdot10^{-4}$	$3.83\cdot10^{-2}$	1
Cl(-I)	0.0	–	–	0.0	0.0	–
Cm(III)	$1.48\cdot10^{-2}$	–1.83	0.72	$5.74\cdot10^{-4}$	$3.83\cdot10^{-1}$	2
Cs(I)	$6.54\cdot10^{-4}$	–3.18	0.51	$6.49\cdot10^{-5}$	$6.60\cdot10^{-3}$	1
Eu(III)	$1.48\cdot10^{-2}$	–1.83	0.72	$5.74\cdot10^{-4}$	$3.83\cdot10^{-1}$	2
H(I)	0.0	–	–	0.0	0.0	–
Ho(III)	$1.48\cdot10^{-2}$	–1.83	0.72	$5.74\cdot10^{-4}$	$3.83\cdot10^{-1}$	2
I(-I)	0.0	–	–	0.0	0.0	–
Mo(VI)	0.0	–	–	0.0	0.0	–
Nb(V)	$1.98\cdot10^{-2}$	–1.70	0.64	$1.11\cdot10^{-3}$	$3.53\cdot10^{-1}$	2
Ni(II)	$2.07\cdot10^{-3}$	–2.68	0.65	$1.12\cdot10^{-4}$	$2.83\cdot10^{-2}$	1
Np(IV)	$\mathbf{9.92\cdot10^{-2}}$	**–1.00**	**0.65**	$\mathbf{5.33\cdot10^{-3}}$	$\mathbf{1.85\cdot10^{0}}$	**2**
Np(V)	$7.75\cdot10^{-4}$	–3.11	0.65	$2.78\cdot10^{-5}$	$2.16\cdot10^{-2}$	2
Pa(IV)	$5.92\cdot10^{-2}$	–1.23	0.48	$6.76\cdot10^{-3}$	$5.18\cdot10^{-1}$	2
Pa(V)	$\mathbf{5.92\cdot10^{-2}}$	**–1.23**	**0.48**	$\mathbf{6.76\cdot10^{-3}}$	$\mathbf{5.18\cdot10^{-1}}$	**2**
Pb(II)	$2.52\cdot10^{-2}$	–1.60	0.56	$2.05\cdot10^{-3}$	$3.10\cdot10^{-1}$	2
Pd(II)	$5.20\cdot10^{-2}$	–1.28	0.83	$1.22\cdot10^{-3}$	2.21	2
Pu(III)	$\mathbf{2.78\cdot10^{-2}}$	**–1.56**	**0.72**	$\mathbf{1.08\cdot10^{-3}}$	$\mathbf{7.19\cdot10^{-1}}$	**2**
Pu(IV)	$9.92\cdot10^{-2}$	–1.00	0.65	$5.33\cdot10^{-3}$	$1.85\cdot10^{0}$	2
Pu(V)	$1.71\cdot10^{-2}$	–1.77	0.60	$1.16\cdot10^{-3}$	$2.53\cdot10^{-1}$	2
Pu(VI)	$1.71\cdot10^{-2}$	–1.77	0.60	$1.16\cdot10^{-3}$	$2.53\cdot10^{-1}$	2
Ra(II)	$4.53\cdot10^{-4}$	–3.34	0.41	$7.26\cdot10^{-5}$	$2.83\cdot10^{-3}$	1
S(-II)	0.0	–	–	0.0	0.0	–
Se(-II)	$\mathbf{2.95\cdot10^{-4}}$	**–3.53**	**0.55**	$\mathbf{2.50\cdot10^{-5}}$	$\mathbf{3.48\cdot10^{-3}}$	**–**
Se(IV)	$2.95\cdot10^{-4}$	–3.53	0.55	$2.50\cdot10^{-5}$	$3.48\cdot10^{-3}$	–
Se(VI)	$2.95\cdot10^{-4}$	–3.53	0.55	$2.50\cdot10^{-5}$	$3.48\cdot10^{-3}$	–
Sm(III)	$1.48\cdot10^{-2}$	–1.83	0.72	$5.74\cdot10^{-4}$	$3.83\cdot10^{-1}$	2
Sn(IV)	$1.59\cdot10^{-1}$	–0.80	0.28	$4.51\cdot10^{-2}$	$5.58\cdot10^{-1}$	2
Sr(II)	$6.42\cdot10^{-6}$	–5.19	0.99	$7.21\cdot10^{-8}$	$5.71\cdot10^{-4}$	1
Tc(IV)	$\mathbf{9.92\cdot10^{-2}}$	**–1.00**	**0.65**	$\mathbf{5.33\cdot10^{-3}}$	$\mathbf{1.85\cdot10^{0}}$	**2**
Tc(VII)	0.0	–	–	0.0	0.0	–
Th(IV)	$5.29\cdot10^{-2}$	–1.28	0.65	$2.84\cdot10^{-3}$	$9.84\cdot10^{-1}$	2
U(IV)	$\mathbf{9.92\cdot10^{-2}}$	**–1.00**	**0.65**	$\mathbf{5.33\cdot10^{-3}}$	$\mathbf{1.85\cdot10^{0}}$	**2**
U(VI)	$\mathbf{2.00\cdot10^{-4}}$	**–3.70**	**0.66**	$\mathbf{1.04\cdot10^{-5}}$	$\mathbf{3.84\cdot10^{-3}}$	**2**
Zr(IV)	$2.13\cdot10^{-2}$	–1.67	0.35	$4.48\cdot10^{-3}$	$1.02\cdot10^{-1}$	2

A8.10 Data recommended for use in the Comparative analysis

Porosity data recommended for use in the Comparative analysis are summarised in Table A8-5. It should be noted that the suggested values are flowpath averaged.

Table A8-5. in situ diffusion available porosity suggested for use in Comparative analysis for the Laxemar site.

Type of solute	e (%)
Cations and non-charged solutes	0.19
Anions	0.19

The effective diffusivity data recommended for use in the Comparative analysis are summarised in Table A8-6. It should be noted that the probability density function reflects on uncertainty, and not on spatial variability. Spatial variability is already handled by suggesting flowpath averaged values. The D_e values for different elements should be correlated (cf. Section 6.8.9 of the SR-Site Data report).

Table A8-6. Flowpath averaged in situ effective diffusivity suggested for use in Comparative analysis for the Laxemar site.

Type of solute	Best estimate D_e (m^2/s)	$Log_{10}D_e$ (m^2/s) – μ	$Log_{10}D_e$ (m^2/s) – σ	Probability density function
Cations and non-charged solutes	$2.7 \cdot 10^{-14}$	–13.6	0.25	Log-normal
Anions	$8.5 \cdot 10^{-15}$	–14.1	0.25	Log-normal

Concerning the scale on which the porous system is connected *L (m)*, it is suggested to be connected on all scales relevant for the safety assessment (at least on the decametre scale). This means that the maximum penetration depth L_D (m) for matrix diffusion is dependent on half the spacing between hydraulically conductive fractures, as discussed in Chapter A7.

Sorption data recommended for use in the Comparative analysis are summarised in Table A8-4. The K_d data are given in the form of log-normal distributions characterised by a mean (μ) and standard deviation (σ). For stochastic simulations, it is suggested that the distributions are sampled uniformly between the upper and lower limits defined by the 2.5% and 97.5% percentiles. The best estimate K_d value for use in deterministic calculations is given as the median of the K_d distribution. K_d data of the same correlation group (1 or 2) should be correlated.

References A8.11

SKB's (Svensk Kärnbränslehantering AB) publications can be found at www.skb.se/publications.

Crawford J, 2010. Bedrock Kd data and uncertainty assessment for application in SR-Site geosphere transport calculations. SKB R-10-48, Svensk Kärnbränslehantering AB.

Crawford J, Sidborn M, 2009. Bedrock transport properties Laxemar. Site descriptive modelling SDM-Site Laxemar. SKB R-08-94, Svensk Kärnbränslehantering AB.

Löfgren M, 2007. Formation factor logging in situ by electrical methods in KLX07A, KLX08, KLX10 and KLX12A. Oskarshamn site investigation. SKB P-06-288, Svensk Kärnbränslehantering AB.

Nilsson K, Byegård J, Selnert E, Widestrand H, Höglund S, Gustafsson E, 2010. Äspö Hard Rock Laboratory. Long Term Sorption Diffusion Experiment (LTDE-SD). Results from rock sample analyses and modelling. SKB R-10-68, Svensk Kärnbränslehantering AB.

Norman S, Kjellbert N, 1990. FARF31 – A far field radionuclide migration code for use with the PROPER package. SKB TR 90-01, Svensk Kärnbränslehantering AB.

SKB, 2010a. Data report for the safety assessment SR-Site. SKB TR-10-52, Svensk Kärnbränslehantering AB.

SKB, 2010b. Radionuclide transport report for the safety assessment SR-Site. SKB TR-10-50, Svensk Kärnbränslehantering AB.

Vilks P, Miller N H, Stanchell F W, 2005. Laboratory program supporting SKB's long term diffusion experiment. Report 06819-REP-01300-10111-R00, Ontario Power Generation, Nuclear Waste Management Division, Canada.

A9 Landscape dose conversion factors

In the Comparative analysis, doses to humans are assessed for by multiplying radionuclide activity release rates to the biosphere by radionuclide specific landscape dose conversion factors (*LDF*). In this appendix the *LDF's* for Laxemar, used in the Comparative analysis, are supplied.

For the Laxemar site, there is no dedicated report providing *LDF's* that would correspond to /Avila et al. 2010/, reporting the Forsmark *LDF's* used in SR-Site. Therefore, the source for the *LDF's* used in the Comparative analysis is this appendix. Furthermore, for Laxemar there is no dedicated report describing the landscape development, which would correspond to the SR-Site Biosphere synthesis report /SKB 2010a/. Instead the Laxemar landscape development is outlined in Chapter A10 of this present report.

As the documentation describing the modelling of *LDF's* for Laxemar is limited, no proper site specific uncertainty discussion can be given. Instead, for methodology issues /Avila et al. 2010, SKB 2010a/ are referred to, while for uncertainty issues /Avila et al. 2010/ is referred to. Site specific conditions used to model the landscape development of Laxemar are presented in Chapter A10. Before studying this appendix, the reader is strongly recommended to first study the corresponding text in the SR-Site Data report /SKB 2010b, Section 7.2/ to gain a better understanding of the uncertainties associated with the *LDF*.

A9.1 Modelling as input to the Comparative analysis of safety related site characteristics

This section describes what data are expected from the supplier and in which modelling activities the data are to be used.

Defining the data requested from the supplier

For the Comparative analysis, the following data should be delivered by the supplier:

- Radionuclide-specific basic landscape dose conversion factors, *LDF's* (Sv/y per Bq/y) for the temperate climate domain. The exposure should be calculated for a representative individual of the most exposed group, as averaged over the lifetime of an individual.

The *LDF's* should be supplied for the following radionuclides of the selected inventory, where the justification provided in the SR-Site Radionuclide transport report /SKB 2010c/ is also valid for the comparative analysis:

- Ac-227, Ag-108m, Am-241, Am-243, C-14, Ca-41, Cl-36, Cm-244, Cm-245, Cm-246, Cs-135, Cs-137, Ho-166m, I-129, Nb-94, Ni-59, Ni-63, Np-237, Pa-231, Pb-210, Pd-107, Po-210, Pu-239, Pu-240, Pu-242, Ra-226, Se-79, Sm-151, Sn-126, Sr-90, Tc-99, Th-229, Th-230, Th-232, U-233, U-234, U-235, U-236, U-238, and Zr-93.

Modelling activities in which data will be used

The chain of models used to calculate the release rates, as well as the application of the *LDF's* in the dose calculations, are described in detail in the SR-Site Radionuclide transport report /SKB 2010c/ for the Forsmark site. The same descriptions apply for the Comparative analysis and the Laxemar site, although the scope of the radionuclide transport modelling is limited in the Comparative analysis.

Basically, the activity release rate to the biosphere is calculated either analytically or using the computational programs COMP23/Compulink /Romero et al. 1999, Cliffe and Kelly 2006, Vahlund and Hermansson 2006/, for the nearfield, and FARF31 /Norman and Kjellbert 1990, Elert et al. 2004/ for the farfield. By multiplying the release rates by the *LDF's*, the maximum annual effective doses to a representative individual of the most exposed group can be calculated. To estimate annual exposure during the lifetime of an individual, predicted doses have been averaged over a period of 50 years, which is the integration period used by ICRP in the derivation of dose coefficients for adults.

A9.2 Supplier input on use of data in the Comparative analysis

LDF values have been delivered by the SR-Site biosphere modelling team to the Comparative analysis project, where the dose assessments are performed. In this text the SR-Site biosphere modelling team is acknowledged as the supplier and the Comparative analysis project as the customer. Supplier inputs, partly based on the authorities' comments on SR-Can, have been given at an early stage and have already been incorporated in the Comparative analysis.

The supplier acknowledges that documentation on the supplied *LDF's* is better for the Forsmark site than for the Laxemar site. Also, it is recognised that for Laxemar, the uncertainties have not been investigated in the same degree as for Forsmark. However, the identical methodology has been applied in obtaining *LDF's* for both sites. Furthermore, the input data to the *LDF* modelling have roughly the same uncertainties for both sites. Therefore, the data supplied in this appendix have approximately the same degree of adequacy as those supplied in the SR-Site Data report /SKB 2010b, Section 7.2/.

A9.3 Sources of information and documentation of data qualification

Sources of information

The *LDF's* supplied in this appendix are calculated based on c 140 input parameters. Many of these are site specific and thus the *LDF's* are dependent on site specific characteristics and future landscape development (cf. Chapter A10). The surface systems at the two sites differ with regard to ecosystem specific characteristics, e.g. differences in hydrology, chemistry, and species composition. The surface ecosystems are thoroughly described in /Andersson 2010, Aquilonius 2010, Löfgren 2010/. Detailed descriptions of the hydrological and hydrochemical conditions in the Laxemar area are presented in /Werner 2009, Bosson et al. 2009, Tröjbom et al. 2008/. The site description of the Laxemar surface systems is presented in /Söderbäck and Lindborg 2009/.

The main sources of information providing input data to the *LDF* modelling are /Andersson 2010, Aquilonius 2010, Löfgren 2010, Nordén et al. 2010/. The methodology of the *LDF* modelling is described in /SKB 2010a, Avila et al. 2010/ for the Forsmark site. The methodology used to derive the *LDF's* is identical for Forsmark and Laxemar. Data qualification and uncertainty discussions for Forsmark data are given in /SKB 2010b, Section 7.2/ and similar descriptions apply t the Laxemar site. The full references to these reports are provided in Table A9-1.

Table A9-1. Main sources of information used in data qualification.

Andersson E (ed), 2010. The limnic ecosystems at Forsmark and Laxemar-Simpevarp. SKB TR-10-02, Svensk Kärnbränslehantering AB.
Aquilonius K (ed), 2010. The marine ecosystems at Forsmark and Laxemar-Simpevarp. SKB TR-10-03, Svensk Kärnbränslehantering AB.
Avila R, Ekström P-A, Åstrand P-G, 2010. Landscape dose conversion factors used in the safety assessment SR-Site. SKB TR-10-06, Svensk Kärnbränslehantering AB.
Löfgren A (ed), 2010. The terrestrial ecosystems at Forsmark and Laxemar-Simpevarp. SKB TR-10-01, Svensk Kärnbränslehantering AB.
Nordén S, Avila R, de la Cruz I, Stenberg K, Grolander S, 2010. Element-specific and constant parameters used for dose calculations in SR-Site, SKB TR-10-07, Svensk Kärnbränslehantering AB.
SKB, 2010a. Biosphere analyses for the safety assessment SR-Site – synthesis and summary of results. SKB TR-10-09, Svensk Kärnbränslehantering AB.
SKB, 2010b. Data report for the safety assessment SR-Site. SKB TR-10-52, Svensk Kärnbränslehantering AB.

In addition, the Laxemar biosphere objects and future landscape development are described in Chapter A10.

Categorising data sets as qualified or supporting data

The radionuclide model used to calculate *LDF values* relies on nearly 140 input parameters, of which of which one third represent radionuclide- or element-specific properties. In order to summarise the number and types of parameters that are used to model transport and accumulation of radionuclides in the biosphere, and the potential exposure to organisms, the parameters have been sorted into a number of categories (see Table A9-2).

Parameters used in the radionuclide model reflect important processes concerning transport, accumulation, and exposure to radionuclides at the site over time, thus including the effects of site development and site specific characteristics.

Parameters that are used to describe ecosystem characteristics used in the *LDF* calculations are presented in the ecosystems reports /Andersson 2010, Aquilonius 2010, Löfgren 2010/. Additional parameters are presented in /Nordén et al. 2010/. Landscape geometries and landscape development parameters are described in /Lindborg 2010/. The descriptions are also relevant for the Comparative analysis but the parameters values for the Laxemar site may differ from those for the Forsmark site. The Laxemar data are stored in /SKBdoc 1263189/.

No sorting of the c 140 input parameters as supporting or qualified has been made, which is a deviation from the instruction on data qualification given in /SKB 2010b, Section 2.3/.

Table A9-2. Parameters used in the radionuclide model. The references are given in the footnote below the table.

Type of parameters	N	Example	Source	Reference
Radionuclide specific[a]	1	Radionuclide half life	Literature	TR-10-07
Landscape geometries[c]	13	Size of biosphere objects and catchment areas, sedimentation and resuspension rate	Site investigation, site modelling	SKBdoc 1263189
Regolith[c]	27	Depth, density and porosity of sediments and soil	Site investigation, site modelling	TR-10-01 TR-10-02 TR-10-03
Ecosystem properties – aquatic ecosystems[c]	17 34	Biomass, productivity, gas exchange	Site investigation, site modelling	TR-10-02 TR-10-03
Ecosystem properties – terrestrial ecosytems		Biomass, productivity, gas exchange	Site investigation, site modelling	TR-10-01 TR-10-07
Surface hydrology and water exchange[c]	9	Runoff, vertical and horizontal advective fluxes, marine water exchange	Site investigation, site modelling	TR-10-01 TR-10-02 TR-10-03
Distribution coefficients and diffusivity[b]	10	Element-specific solid/liquid distribution coefficients (Kd) for regolith and particulate matter	Site investigation, literature	TR-10-07
Concentration ratios, retention and release[b]	19	Element-specific ratios between environmental media and organisms (CR)	Site investigation, literature	TR-10-07
Human characteristics	5	Life span, energy and water consumption	Literature	TR-10-07
Dose coefficients[a]	4	Radionuclide specific factors for radiation exposure through external irradiation, inhalation and ingestion	Literature	TR-10-07

[a] Each parameter estimated for 48 radionuclides.

[b] Each parameter estimated for 31 stable elements.

[c] Time dependent parameters for which a separate parameter value is given for each time step and object (8 landscape geometry parameters, 4 regolith parameters, 8 aquatic ecosystem parameters and 1 surface hydrology and water exchange parameter).

References: TR-10-01 /Löfgren 2010/, TR-10-02 /Andersson 2010/, TR-10-03 /Aquilonius 2010/, TR-10-07 /Nordén et al. 2010/.

Excluded data previously considered as important

Seven biosphere objects in Laxemar are excluded from calculations deriving *LDF's*, as their transition times from marine to terrestrial stages are not adequately described (cf. Section A10.2).

A9.4 Conditions for which data are supplied

As seen in Table A9-2, the *LDF* modelling uses a number of input data where some are universal and some are assumed, but where a great number of surface system data are site specific and also dependent on the future landscape development. A description of the various basins, biosphere objects, and the landscape development in Laxemar is given in appendix A10. Figure A9-1 shows the Laxemar site and the associated biosphere objects. Note that only a subset of the biosphere objects is used in the *LDF* modelling. This subset includes objects 201, 203, 206, 207, 208, 210, 211, 213, 214, and 215.

The *LDF* values are derived for a long-term constant release to the landscape during the whole simulation period. The *LDF* values should therefore only be used in scenarios with long-term continuous releases. If applied to scenarios where the concentrations in the biosphere have not reached equilibrium, the calculated doses might be substantially overestimated.

The *LDF* values supplied in this appendix are modelled for the temperate domain, also referred to as the interglacial period, i.e. the period from the deglaciation to the onset of periglacial conditions (cf. Chapter 3). As land emerges sufficiently from the sea, wetlands are assumed to be converted to arable land. Drinking water for humans and livestock during the terrestrial stage of this period is assumed to be supplied in equal parts from surface water and from a contaminated well drilled into the bedrock (cf. Chapter 8 in SR-Site Biosphere synthesis report /SKB 2010a/). The calculation period starts at the time of the deglaciation, when the landscape is covered by the sea (i.e. submerged conditions). The length of the submerged period differs between biosphere objects since it takes thousands of years from the emergence of the first object from the sea, until the shoreline has passed over the whole model area.

The *LDF's* have been calculated over time for each of the biosphere objects listed above. Important inputs to assess the succession of the objects are the shore-level changes and climate data discussed in Chapter 3. Other conditions and inputs are described in /Avila et al. 2010/, where the general descriptions apply to Laxemar as well as to Forsmark, but where details and numerical values may differ.

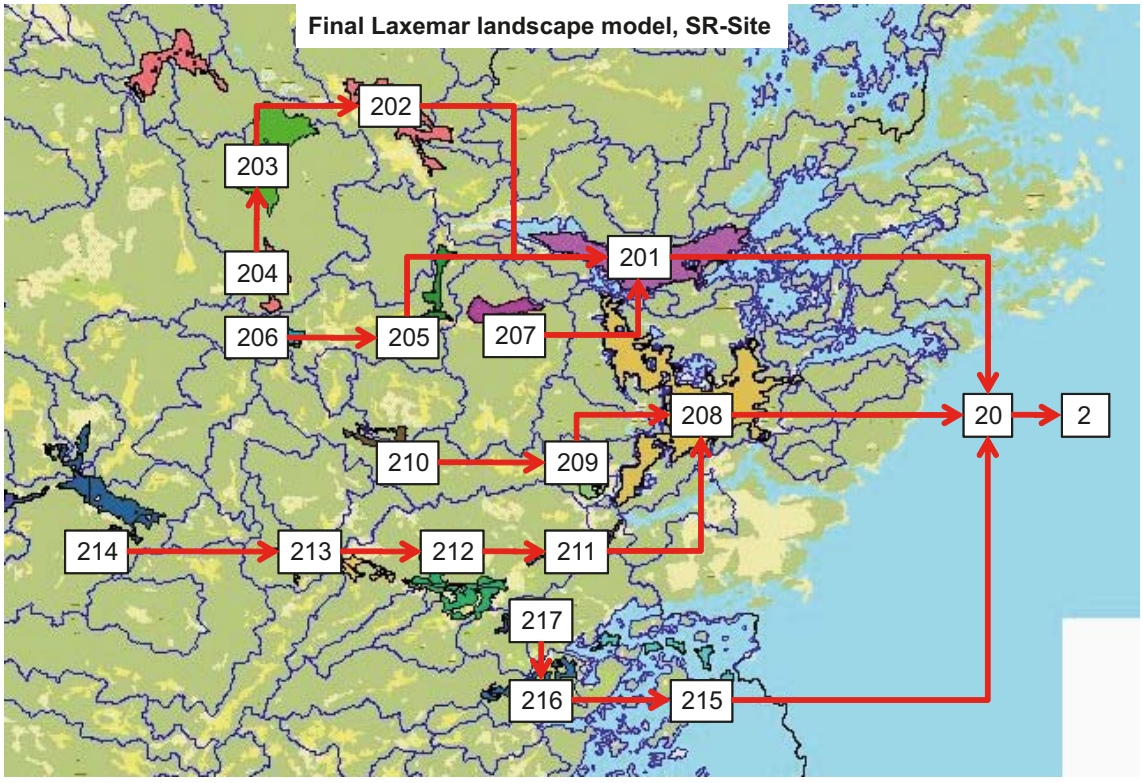

Figure A9-1. *Biosphere objects in Laxemar. Basin 216 and 217 is merged to one basin (216) in the modelling. Basins 201, 203, 206, 207, 208, 210, 211, 213, 214, and 215 are used in the calculation of LDF's for Laxemar.*

The rational for supplying *LDF's* only for the temperate climate domain in the Comparative analysis is that they are generally higher for the temperate domain than for the periglacial and glacial domains (cf. *LDF's* for the Forsmark site for the different climate domains /SKB 2010b, Section 7.2.10/). Furthermore, in SR-Site many of the scenario calculations use only the temperate factors in reporting the results.

A9.5 Conceptual uncertainty

The same conceptual uncertainties apply for Laxemar as for Forsmark, so the corresponding text in the SR-Site Data report /SKB 2010b, Section 7.2.6/ is applicable.

A9.6 Data uncertainty due to precision, bias, and representativity

No uncertainty analysis has been performed for the *LDF's* supplied for the Laxemar site, which would correspond to that for the Forsmark site presented in /Avila et al. 2010/ and /SKB 2010b, Section 7.2.7/. It should especially be noted that no probabilistic simulation has been performed for the Laxemar area that could underpin an evaluation of data uncertainties.

However, the same parameters and the identical methodology are used for *LDF* calculations in Forsmark and Laxemar. Therefore, it is reasonable to assume that ranges in uncertainty would be similar for the two sites. Accordingly the uncertainty discussion given in the SR-Site Data report /SKB 2010b, Section 7.2.7/ is broadly applicable. Furthermore, the descriptions of data uncertainty in the SR-Site Biosphere synthesis report /SKB 2010a/ and /Avila et al. 2010/ are relevant.

There is one Laxemar specific uncertainty worth mentioning. Since not all possible biosphere objects (cf. Figure A9-1) are included in the *LDF* modelling, there are uncertainties relating to how representative the calculated *LDF* values are. The included biosphere objects are distributed within the model area and cover a wide range of sizes, and are therefore judged to be a relevant representation of possible biosphere objects at the Laxemar site.

A9.7 Spatial and temporal variability of data

The *LDF's* represent the highest values for each radionuclide over all biosphere objects during the whole simulation time period corresponding to the temperate climate domain. Hence, the delivered *LDF's* are constant in time and space. However, the *LDF* values are derived on the basis of time dependent doses per unit release rate, obtained from simulations for different biosphere objects with their different properties. These underlying data for different times and objects provide an indication of the data uncertainty (natural variability) of the *LDF*, associated with spatial and temporal variations.

Figure A9-2, Table A9-3, and Table A9-4 show the *LDF* for the individual biosphere objects at the Laxemar site, as modelled during the interglacial period. The value for each radionuclide that is cautiously suggested for the Comparative analysis is the maximum value over all objects. As can be seen, variations between objects range between factors of a few to almost two orders of magnitude. Generally, for radionuclides where exposure from food is the dominant exposure pathway (i.e. C-14, Cl-36, I-129, Nb-94, Np-237, Se-79, Sn-126, and Tc-99), the *LDF's* typically have a larger variation than for radionuclides where drinking water is an important exposure pathway (e.g. Am-241, Pa-231, Pu-239, Pu-242, Ra-226 and Th-229). This was also found to be the case for Forsmark.

No figure is provided to illustrate the underlying temporal variability within the temperate domain. For such an illustration /SKB 2010b, Figure 7-4/ can be consulted.

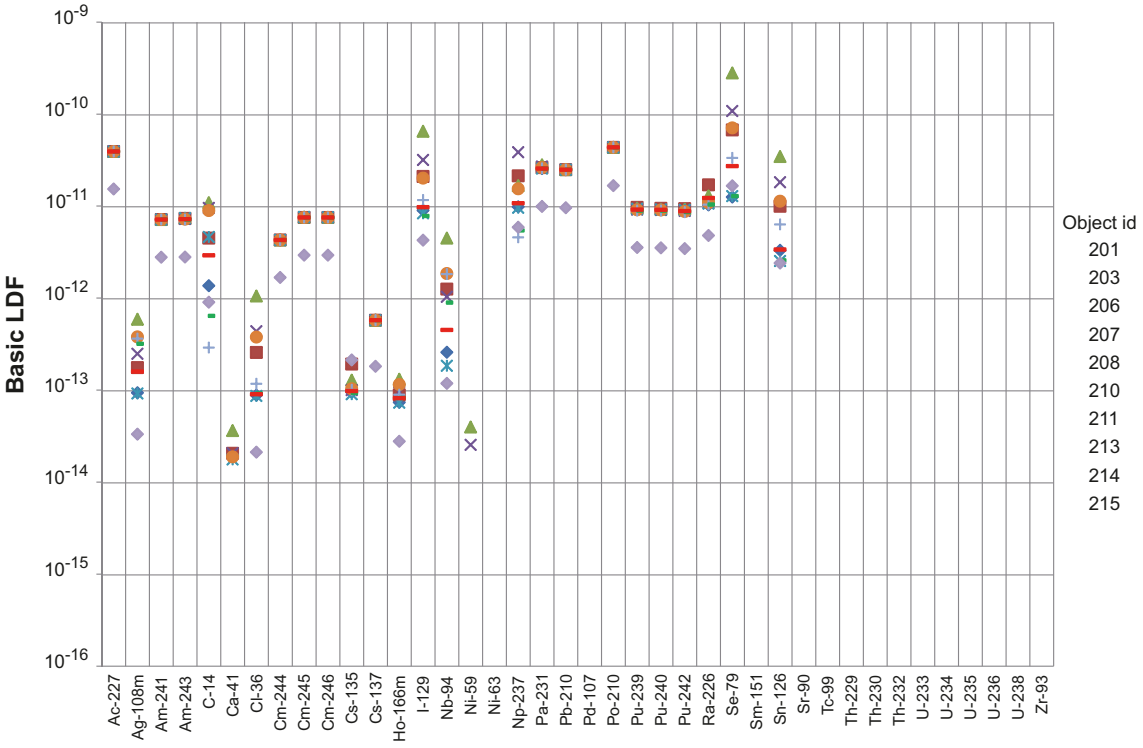

Figure A9-2. *LDF's for the modelled biosphere objects during the interglacial period (–9000 to 9400 AD), at the time of the maximum value for each radionuclide. Underlying numerical data are provided in Table A9-3 and Table A9-4.*

A9.8 Correlations

The supplied *LDF's* have been obtained from independent deterministic simulations for each radionuclide. As a result, there is no correlation that needs to be propagated to subsequent modelling steps using the *LDF's* as inputs.

A9.9 Result of supplier's data qualification

The recommended *LDF's* for different radionuclides for the interglacial period (submerged and temperate conditions) are supplied in Table A9-5. In the table, the timing and biosphere object where the maximum *LDF* is reached for each radionuclide are presented. Also the number of persons that the relevant object can sustain at the time of the maximum *LDF* is shown.

A9.10 Data recommended for use in the Comparative analysis

The *LDF's* for Laxemar presented in Table A9-5 are recommended for used in the Comparative analysis. These data are representative for the temperate climate domain and should strictly be used for assessing the radiological risk for this domain only. Generally, *LDF's* are higher for the temperate domain than for the periglacial and glacial domains. However, for Forsmark this proved not to be the case for Cs-135 due to a strong retention (Kd) and half-life of this nuclide (cf. /SKB 2010b, Section 7.2.10), wherefore caution should be used if applying these data to other climate domains.

The *LDF* values should only be used in scenarios with long-term continuous releases. If applied to scenarios where the concentrations in the biosphere have not reached equilibrium (i.e. in pulse release scenarios), the calculated doses might be substantially overestimated.

Table A9-3. Maximum LDFs for different radionuclides obtained in the modelled biosphere objects for Laxemar during an interglacial period (-9000 to 9400 AD), modelled with a well.

Radionuclide	Object id 201	203	206	207	208
Ac-227	$3.92 \cdot 10^{-11}$	$3.92 \cdot 10^{-11}$	$3.92 \cdot 10^{-11}$	$3.92 \cdot 10^{-11}$	$3.92 \cdot 10^{-11}$
Ag-108m	$9.33 \cdot 10^{-14}$	$1.75 \cdot 10^{-13}$	$5.88 \cdot 10^{-13}$	$2.48 \cdot 10^{-13}$	$9.17 \cdot 10^{-14}$
Am-241	$7.12 \cdot 10^{-12}$	$7.12 \cdot 10^{-12}$	$7.13 \cdot 10^{-12}$	$7.13 \cdot 10^{-12}$	$7.12 \cdot 10^{-12}$
Am-243	$7.29 \cdot 10^{-12}$	$7.33 \cdot 10^{-12}$	$7.36 \cdot 10^{-12}$	$7.23 \cdot 10^{-12}$	$7.39 \cdot 10^{-12}$
C-14	$1.36 \cdot 10^{-12}$	$4.48 \cdot 10^{-12}$	$1.09 \cdot 10^{-11}$	$9.54 \cdot 10^{-12}$	$4.61 \cdot 10^{-12}$
Ca-41	$1.1 \cdot 10^{-14}$	$2.05 \cdot 10^{-14}$	$3.63 \cdot 10^{-14}$	$2.05 \cdot 10^{-14}$	$1.76 \cdot 10^{-14}$
Cl-36	$8.81 \cdot 10^{-14}$	$2.56 \cdot 10^{-13}$	$1.05 \cdot 10^{-12}$	$4.35 \cdot 10^{-13}$	$8.64 \cdot 10^{-14}$
Cm-244	$4.28 \cdot 10^{-12}$	$4.28 \cdot 10^{-12}$	$4.28 \cdot 10^{-12}$	$4.28 \cdot 10^{-12}$	$4.28 \cdot 10^{-12}$
Cm-245	$7.53 \cdot 10^{-12}$	$7.52 \cdot 10^{-12}$	$7.59 \cdot 10^{-12}$	$7.55 \cdot 10^{-12}$	$7.61 \cdot 10^{-12}$
Cm-246	$7.51 \cdot 10^{-12}$	$7.51 \cdot 10^{-12}$	$7.55 \cdot 10^{-12}$	$7.53 \cdot 10^{-12}$	$7.56 \cdot 10^{-12}$
Cs-135	$9.47 \cdot 10^{-14}$	$1.92 \cdot 10^{-13}$	$1.28 \cdot 10^{-13}$	$1 \cdot 10^{-13}$	$8.99 \cdot 10^{-14}$
Cs-137	$5.74 \cdot 10^{-13}$	$5.75 \cdot 10^{-13}$	$5.75 \cdot 10^{-13}$	$5.75 \cdot 10^{-13}$	$5.75 \cdot 10^{-13}$
Ho-166m	$7.35 \cdot 10^{-14}$	$8.87 \cdot 10^{-14}$	$1.31 \cdot 10^{-13}$	$9.46 \cdot 10^{-14}$	$7.3 \cdot 10^{-14}$
I-129	$8.96 \cdot 10^{-12}$	$2.1 \cdot 10^{-11}$	$6.51 \cdot 10^{-11}$	$3.17 \cdot 10^{-11}$	$8.31 \cdot 10^{-12}$
Nb-94	$2.58 \cdot 10^{-13}$	$1.25 \cdot 10^{-12}$	$4.49 \cdot 10^{-12}$	$1.03 \cdot 10^{-12}$	$1.84 \cdot 10^{-13}$
Ni-59	$6.61 \cdot 10^{-15}$	$1.64 \cdot 10^{-14}$	$3.96 \cdot 10^{-14}$	$2.54 \cdot 10^{-14}$	$5.42 \cdot 10^{-15}$
Ni-63	$5.61 \cdot 10^{-15}$	$5.64 \cdot 10^{-15}$	$5.74 \cdot 10^{-15}$	$5.65 \cdot 10^{-15}$	$5.61 \cdot 10^{-15}$
Np-237	$9.81 \cdot 10^{-12}$	$2.13 \cdot 10^{-11}$	$1.67 \cdot 10^{-11}$	$3.84 \cdot 10^{-11}$	$9.59 \cdot 10^{-12}$
Pa-231	$2.55 \cdot 10^{-11}$	$2.61 \cdot 10^{-11}$	$2.81 \cdot 10^{-11}$	$2.69 \cdot 10^{-11}$	$2.55 \cdot 10^{-11}$
Pb-210	$2.48 \cdot 10^{-11}$	$2.48 \cdot 10^{-11}$	$2.48 \cdot 10^{-11}$	$2.48 \cdot 10^{-11}$	$2.48 \cdot 10^{-11}$
Pd-107	$1.76 \cdot 10^{-15}$	$3.97 \cdot 10^{-15}$	$4.44 \cdot 10^{-15}$	$3.28 \cdot 10^{-15}$	$1.64 \cdot 10^{-15}$
Po-210	$4.33 \cdot 10^{-11}$	$4.33 \cdot 10^{-11}$	$4.33 \cdot 10^{-11}$	$4.33 \cdot 10^{-11}$	$4.33 \cdot 10^{-11}$
Pu-239	$9.3 \cdot 10^{-12}$	$9.66 \cdot 10^{-12}$	$9.48 \cdot 10^{-12}$	$9.16 \cdot 10^{-12}$	$9.38 \cdot 10^{-12}$
Pu-240	$9.13 \cdot 10^{-12}$	$9.46 \cdot 10^{-12}$	$9.24 \cdot 10^{-12}$	$9.05 \cdot 10^{-12}$	$9.2 \cdot 10^{-12}$
Pu-242	$9.02 \cdot 10^{-12}$	$9.36 \cdot 10^{-12}$	$9.24 \cdot 10^{-12}$	$8.85 \cdot 10^{-12}$	$9.09 \cdot 10^{-12}$
Ra-226	$1.03 \cdot 10^{-11}$	$1.7 \cdot 10^{-11}$	$1.29 \cdot 10^{-11}$	$1.08 \cdot 10^{-11}$	$1.06 \cdot 10^{-11}$
Se-79	$1.25 \cdot 10^{-11}$	$6.7 \cdot 10^{-11}$	$2.79 \cdot 10^{-10}$	$1.08 \cdot 10^{-10}$	$1.28 \cdot 10^{-11}$
Sm-151	$3.5 \cdot 10^{-15}$	$3.5 \cdot 10^{-15}$	$3.5 \cdot 10^{-15}$	$3.5 \cdot 10^{-15}$	$3.5 \cdot 10^{-15}$
Sn-126	$3.3 \cdot 10^{-12}$	$9.96 \cdot 10^{-12}$	$3.44 \cdot 10^{-11}$	$1.81 \cdot 10^{-11}$	$2.53 \cdot 10^{-12}$
Sr-90	$1.06 \cdot 10^{-12}$	$1.06 \cdot 10^{-12}$	$1.06 \cdot 10^{-12}$	$1.06 \cdot 10^{-12}$	$1.06 \cdot 10^{-12}$
Tc-99	$5.21 \cdot 10^{-14}$	$3.28 \cdot 10^{-13}$	$8.54 \cdot 10^{-13}$	$3.38 \cdot 10^{-13}$	$5.61 \cdot 10^{-14}$
Th-229	$1.75 \cdot 10^{-11}$	$1.75 \cdot 10^{-11}$	$1.76 \cdot 10^{-11}$	$1.75 \cdot 10^{-11}$	$1.75 \cdot 10^{-11}$
Th-230	$1.06 \cdot 10^{-11}$	$2.73 \cdot 10^{-11}$	$2.03 \cdot 10^{-11}$	$1.26 \cdot 10^{-11}$	$1.02 \cdot 10^{-11}$
Th-232	$8.2 \cdot 10^{-12}$	$8.24 \cdot 10^{-12}$	$8.35 \cdot 10^{-12}$	$8.23 \cdot 10^{-12}$	$8.2 \cdot 10^{-12}$
U-233	$2.21 \cdot 10^{-12}$	$2.59 \cdot 10^{-12}$	$4.26 \cdot 10^{-12}$	$3.17 \cdot 10^{-12}$	$2.14 \cdot 10^{-12}$
U-234	$2.67 \cdot 10^{-12}$	$3.14 \cdot 10^{-12}$	$5.04 \cdot 10^{-12}$	$3.87 \cdot 10^{-12}$	$2.23 \cdot 10^{-12}$
U-235	$2.02 \cdot 10^{-12}$	$2.36 \cdot 10^{-12}$	$3.97 \cdot 10^{-12}$	$3.04 \cdot 10^{-12}$	$1.97 \cdot 10^{-12}$
U-236	$1.95 \cdot 10^{-12}$	$2.21 \cdot 10^{-12}$	$3.17 \cdot 10^{-12}$	$2.55 \cdot 10^{-12}$	$1.91 \cdot 10^{-12}$
U-238	$1.87 \cdot 10^{-12}$	$2.12 \cdot 10^{-12}$	$3.11 \cdot 10^{-12}$	$2.49 \cdot 10^{-12}$	$1.84 \cdot 10^{-12}$
Zr-93	$4.08 \cdot 10^{-14}$	$4.54 \cdot 10^{-14}$	$5.96 \cdot 10^{-14}$	$5.03 \cdot 10^{-14}$	$4.04 \cdot 10^{-14}$

Table A9-4. Maximum LDFs for different radionuclides obtained in the modelled biosphere objects for Laxemar during an interglacial period (-9000 to 9400 AD), modelled with a well.

Radionuclide	Object id 210	211	213	214	215
Ac-227	$3.92 \cdot 10^{-11}$	$3.92 \cdot 10^{-11}$	$3.92 \cdot 10^{-11}$	$3.92 \cdot 10^{-11}$	$1.53 \cdot 10^{-11}$
Ag-108m	$3.79 \cdot 10^{-13}$	$3.63 \cdot 10^{-13}$	$3.18 \cdot 10^{-13}$	$1.59 \cdot 10^{-13}$	$3.31 \cdot 10^{-14}$
Am-241	$7.13 \cdot 10^{-12}$	$7.12 \cdot 10^{-12}$	$7.12 \cdot 10^{-12}$	$7.12 \cdot 10^{-12}$	$2.78 \cdot 10^{-12}$
Am-243	$7.19 \cdot 10^{-12}$	$7.14 \cdot 10^{-12}$	$7.13 \cdot 10^{-12}$	$7.19 \cdot 10^{-12}$	$2.79 \cdot 10^{-12}$
C-14	$8.91 \cdot 10^{-12}$	$2.89 \cdot 10^{-13}$	$6.39 \cdot 10^{-13}$	$2.91 \cdot 10^{-12}$	$9.02 \cdot 10^{-13}$
Ca-41	$1.88 \cdot 10^{-14}$	$1.29 \cdot 10^{-14}$	$1.13 \cdot 10^{-14}$	$1.35 \cdot 10^{-14}$	$5.35 \cdot 10^{-15}$
Cl-36	$3.76 \cdot 10^{-13}$	$1.17 \cdot 10^{-13}$	$9.18 \cdot 10^{-14}$	$9 \cdot 10^{-14}$	$2.11 \cdot 10^{-14}$
Cm-244	$4.28 \cdot 10^{-12}$	$4.28 \cdot 10^{-12}$	$4.28 \cdot 10^{-12}$	$4.28 \cdot 10^{-12}$	$1.67 \cdot 10^{-12}$
Cm-245	$7.52 \cdot 10^{-12}$	$7.5 \cdot 10^{-12}$	$7.49 \cdot 10^{-12}$	$7.49 \cdot 10^{-12}$	$2.92 \cdot 10^{-12}$
Cm-246	$7.51 \cdot 10^{-12}$	$7.49 \cdot 10^{-12}$	$7.49 \cdot 10^{-12}$	$7.49 \cdot 10^{-12}$	$2.92 \cdot 10^{-12}$
Cs-135	$1.03 \cdot 10^{-13}$	$1.01 \cdot 10^{-13}$	$9.3 \cdot 10^{-14}$	$9.75 \cdot 10^{-14}$	$2.12 \cdot 10^{-13}$
Cs-137	$5.75 \cdot 10^{-13}$	$5.75 \cdot 10^{-13}$	$5.75 \cdot 10^{-13}$	$5.75 \cdot 10^{-13}$	$1.81 \cdot 10^{-13}$
Ho-166m	$1.15 \cdot 10^{-13}$	$8.91 \cdot 10^{-14}$	$8.19 \cdot 10^{-14}$	$8.16 \cdot 10^{-14}$	$2.78 \cdot 10^{-14}$
I-129	$2.01 \cdot 10^{-11}$	$1.16 \cdot 10^{-11}$	$7.81 \cdot 10^{-12}$	$9.71 \cdot 10^{-12}$	$4.26 \cdot 10^{-12}$
Nb-94	$1.85 \cdot 10^{-12}$	$1.82 \cdot 10^{-12}$	$8.93 \cdot 10^{-13}$	$4.49 \cdot 10^{-13}$	$1.18 \cdot 10^{-13}$
Ni-59	$1.33 \cdot 10^{-14}$	$8.44 \cdot 10^{-15}$	$4.74 \cdot 10^{-15}$	$4.42 \cdot 10^{-15}$	$4.13 \cdot 10^{-15}$
Ni-63	$5.67 \cdot 10^{-15}$	$5.66 \cdot 10^{-15}$	$5.63 \cdot 10^{-15}$	$5.62 \cdot 10^{-15}$	$2.09 \cdot 10^{-15}$
Np-237	$1.54 \cdot 10^{-11}$	$4.57 \cdot 10^{-12}$	$5.44 \cdot 10^{-12}$	$1.07 \cdot 10^{-11}$	$5.88 \cdot 10^{-12}$
Pa-231	$2.61 \cdot 10^{-11}$	$2.56 \cdot 10^{-11}$	$2.55 \cdot 10^{-11}$	$2.55 \cdot 10^{-11}$	$9.89 \cdot 10^{-12}$
Pb-210	$2.48 \cdot 10^{-11}$	$2.48 \cdot 10^{-11}$	$2.48 \cdot 10^{-11}$	$2.48 \cdot 10^{-11}$	$9.6 \cdot 10^{-12}$
Pd-107	$2.28 \cdot 10^{-15}$	$1.74 \cdot 10^{-15}$	$1.53 \cdot 10^{-15}$	$1.9 \cdot 10^{-15}$	$8.92 \cdot 10^{-16}$
Po-210	$4.33 \cdot 10^{-11}$	$4.33 \cdot 10^{-11}$	$4.33 \cdot 10^{-11}$	$4.33 \cdot 10^{-11}$	$1.67 \cdot 10^{-11}$
Pu-239	$9.09 \cdot 10^{-12}$	$8.93 \cdot 10^{-12}$	$8.95 \cdot 10^{-12}$	$9.13 \cdot 10^{-12}$	$3.55 \cdot 10^{-12}$
Pu-240	$9.06 \cdot 10^{-12}$	$8.92 \cdot 10^{-12}$	$8.94 \cdot 10^{-12}$	$9.08 \cdot 10^{-12}$	$3.51 \cdot 10^{-12}$
Pu-242	$8.74 \cdot 10^{-12}$	$8.57 \cdot 10^{-12}$	$8.59 \cdot 10^{-12}$	$8.79 \cdot 10^{-12}$	$3.45 \cdot 10^{-12}$
Ra-226	$1.09 \cdot 10^{-11}$	$1.04 \cdot 10^{-11}$	$1.04 \cdot 10^{-11}$	$1.22 \cdot 10^{-11}$	$4.79 \cdot 10^{-12}$
Se-79	$7.06 \cdot 10^{-11}$	$3.33 \cdot 10^{-11}$	$1.28 \cdot 10^{-11}$	$2.71 \cdot 10^{-11}$	$1.66 \cdot 10^{-11}$
Sm-151	$3.5 \cdot 10^{-15}$	$3.5 \cdot 10^{-15}$	$3.5 \cdot 10^{-15}$	$3.5 \cdot 10^{-15}$	$1.36 \cdot 10^{-15}$
Sn-126	$1.13 \cdot 10^{-11}$	$6.3 \cdot 10^{-12}$	$2.57 \cdot 10^{-12}$	$3.37 \cdot 10^{-12}$	$2.4 \cdot 10^{-12}$
Sr-90	$1.06 \cdot 10^{-12}$	$1.06 \cdot 10^{-12}$	$1.06 \cdot 10^{-12}$	$1.06 \cdot 10^{-12}$	$3.89 \cdot 10^{-13}$
Tc-99	$3.06 \cdot 10^{-13}$	$8.07 \cdot 10^{-14}$	$5.27 \cdot 10^{-14}$	$1.09 \cdot 10^{-13}$	$3.02 \cdot 10^{-14}$
Th-229	$1.75 \cdot 10^{-11}$	$1.75 \cdot 10^{-11}$	$1.75 \cdot 10^{-11}$	$1.75 \cdot 10^{-11}$	$6.82 \cdot 10^{-12}$
Th-230	$1.11 \cdot 10^{-11}$	$9.44 \cdot 10^{-12}$	$8.77 \cdot 10^{-12}$	$1.18 \cdot 10^{-11}$	$1.79 \cdot 10^{-11}$
Th-232	$8.26 \cdot 10^{-12}$	$8.25 \cdot 10^{-12}$	$8.22 \cdot 10^{-12}$	$8.2 \cdot 10^{-12}$	$3.2 \cdot 10^{-12}$
U-233	$2.62 \cdot 10^{-12}$	$2.36 \cdot 10^{-12}$	$2.1 \cdot 10^{-12}$	$2.14 \cdot 10^{-12}$	$1.57 \cdot 10^{-12}$
U-234	$2.67 \cdot 10^{-12}$	$2.29 \cdot 10^{-12}$	$2.05 \cdot 10^{-12}$	$2.05 \cdot 10^{-12}$	$2.49 \cdot 10^{-12}$
U-235	$2.44 \cdot 10^{-12}$	$2.14 \cdot 10^{-12}$	$1.95 \cdot 10^{-12}$	$1.94 \cdot 10^{-12}$	$6.57 \cdot 10^{-13}$
U-236	$2.22 \cdot 10^{-12}$	$2.05 \cdot 10^{-12}$	$1.91 \cdot 10^{-12}$	$1.92 \cdot 10^{-12}$	$6.54 \cdot 10^{-13}$
U-238	$2.15 \cdot 10^{-12}$	$1.97 \cdot 10^{-12}$	$1.83 \cdot 10^{-12}$	$1.84 \cdot 10^{-12}$	$6.26 \cdot 10^{-13}$
Zr-93	$4.52 \cdot 10^{-14}$	$4.18 \cdot 10^{-14}$	$4.03 \cdot 10^{-14}$	$4.04 \cdot 10^{-14}$	$1.59 \cdot 10^{-14}$

Table A9-5. Maximum LDFs for the Laxemar site for the interglacial period (-9000 to 9400 AD) modelled with well. Time refers to the time at which the maximum LDF is reached in the interglacial. N is the number of persons that can be sustained in the biosphere object at the time for the maximum LDF.

Radionuclide	LDF	Time	N	Object
Ac-227	$3.92 \cdot 10^{-11}$	–2,250	69	206
Ag-108m	$5.88 \cdot 10^{-13}$	–1,150	69	206
Am-241	$7.13 \cdot 10^{-12}$	–2,750	69	206
Am-243	$7.39 \cdot 10^{-12}$	3,350	1	208
C-14	$1.09 \cdot 10^{-11}$	–4,150	<1	206
Ca-41	$3.63 \cdot 10^{-14}$	9,400	69	206
Cl-36	$1.05 \cdot 10^{-12}$	8,850	69	206
Cm-244	$4.28 \cdot 10^{-12}$	–2,750	69	206
Cm-245	$7.61 \cdot 10^{-12}$	3,350	1	208
Cm-246	$7.56 \cdot 10^{-12}$	3,350	1	208
Cs-135	$2.12 \cdot 10^{-13}$	9,400	<1	215
Cs-137	$5.75 \cdot 10^{-13}$	–2,750	69	206
Ho-166m	$1.31 \cdot 10^{-13}$	–2,450	69	206
I-129	$6.51 \cdot 10^{-11}$	–2,750	69	206
Nb-94	$4.49 \cdot 10^{-12}$	9,400	69	206
Ni-59	$3.96 \cdot 10^{-14}$	9,400	69	206
Ni-63	$5.74 \cdot 10^{-15}$	–2,750	69	206
Np-237	$3.84 \cdot 10^{-11}$	150	<1	207
Pa-231	$2.81 \cdot 10^{-11}$	9,400	69	206
Pb-210	$2.48 \cdot 10^{-11}$	–2,750	69	206
Pd-107	$4.44 \cdot 10^{-15}$	9,400	69	206
Po-210	$4.33 \cdot 10^{-11}$	–2,750	69	206
Pu-239	$9.66 \cdot 10^{-12}$	–1,100	1	203
Pu-240	$9.46 \cdot 10^{-12}$	–1,100	1	203
Pu-242	$9.36 \cdot 10^{-12}$	–1,100	1	203
Ra-226	$1.70 \cdot 10^{-11}$	–800	1	203
Se-79	$2.79 \cdot 10^{-10}$	–2,750	69	206
Sm-151	$3.50 \cdot 10^{-15}$	–2,750	69	206
Sn-126	$3.44 \cdot 10^{-11}$	9,400	69	206
Sr-90	$1.06 \cdot 10^{-12}$	–2,150	69	206
Tc-99	$8.54 \cdot 10^{-13}$	–600	69	206
Th-229	$1.76 \cdot 10^{-11}$	9,400	69	206
Th-230	$2.73 \cdot 10^{-11}$	–750	1	203
Th-232	$8.35 \cdot 10^{-12}$	9,400	69	206
U-233	$4.26 \cdot 10^{-12}$	9,400	69	206
U-234	$5.04 \cdot 10^{-12}$	9,400	69	206
U-235	$3.97 \cdot 10^{-12}$	9,400	69	206
U-236	$3.17 \cdot 10^{-12}$	9,400	69	206
U-238	$3.11 \cdot 10^{-12}$	9,400	69	206
Zr-93	$5.96 \cdot 10^{-14}$	9,400	69	206

References A9.11

SKB's (Svensk Kärnbränslehantering AB) publications can be found at www.skb.se/publications.

Andersson E (ed), 2010. The limnic ecosystems at Forsmark and Laxemar-Simpevarp. SR-Site Biosphere. SKB TR-10-02, Svensk Kärnbränslehantering AB.

Aquilonius K (ed), 2010. The marine ecosystems at Forsmark and Laxemar-Simpevarp. SR-Site Biosphere. SKB TR-10-03, Svensk Kärnbränslehantering AB.

Avila R, Ekström P-A, Åstrand P-G, 2010. Landscape dose conversion factors used in the safety assessment SR-Site. SKB TR-10-06, Svensk Kärnbränslehantering AB.

Bosson E, Sassner M, Gustafsson L-G, 2009. Numerical modelling of surface hydrology and near-surface hydrogeology at Laxemar-Simpevarp. Site descriptive modelling, SDM-Site Laxemar. SKB R-08-72, Svensk Kärnbränslehantering AB.

Cliffe K A, Kelly M, 2006. COMP23 version 1.2.2 user's manual. SKB R-04-64, Svensk Kärnbränslehantering AB.

Elert M, Gylling B, Lindgren M, 2004. Assessment model validity document FARF31. SKB R-04-51, Svensk Kärnbränslehantering AB.

Lindborg T (ed), 2010. Landscape Forsmark – data, methodology and results for SR-Site. SKB TR-10-05, Svensk Kärnbränslehantering AB.

Löfgren A (ed), 2010. The terrestrial ecosystems at Forsmark and Laxemar-Simpevarp. SR-Site Biosphere. SKB TR-10-01, Svensk Kärnbränslehantering AB.

Nordén S, Avila R, de la Cruz I, Stenberg K, Grolander S, 2010. Element-specific and constant parameters used for dose calculations in SR-Site. SKB TR-10-07, Svensk Kärnbränslehantering AB.

Norman S, Kjellbert N, 1990. FARF31 – A far field radionuclide migration code for use with the PROPER package. SKB TR 90-01, Svensk Kärnbränslehantering AB.

Romero L, Thompson A, Moreno L, Neretnieks I, Widén H, Boghammar A, 1999. Comp23/ Nuctran user's guide. Proper version 1.1.6. SKB R-99-64, Svensk Kärnbränslehantering AB.

SKB, 2010a. Biosphere analyses for the safety assessment SR-Site – synthesis and summary of results. SKB TR-10-09, Svensk Kärnbränslehantering AB.

SKB, 2010b. Data report for the safety assessment SR-Site. SKB TR-10-52, Svensk Kärnbränslehantering AB.

SKB, 2010c. Radionuclide transport report for the safety assessment SR-Site. SKB TR-10-50, Svensk Kärnbränslehantering AB.

Söderbäck B, Lindborg T, 2009. Surface system Laxemar-Simpevarp. Site descriptive modelling, SDM-Site Laxemar. SKB R-09-01, Svensk Kärnbränslehantering AB.

Tröjbom M, Söderbäck B, Kalinowski B, 2008. Hydrochemistry of surface water and shallow groundwater. Site descriptive modelling, SDM-Site Laxemar. SKB R-08-46, Svensk Kärnbränslehantering AB.

Vahlund F, Hermansson H, 2006. A direct numerical approach to solving the transport equations for radionuclide transport in fractured rock. SKB R-04-50, Svensk Kärnbränslehantering AB.

Werner K, 2009. Description of surface hydrology and near-surface hydrogeology at Laxemar-Simpevarp. Site descriptive modelling, SDM-Site Laxemar. SKB R-08-71, Svensk Kärnbränslehantering AB.

A10 Laxemar landscape development and biosphere objects

The modelling of LDF's, as discussed in Chapter A9, are dependent on site specific properties of the surface systems and are thus also on the landscape development. In addition, input to the comparison between the two sites is not limited to LDF values; other aspects can play a role in the optimisation of the disposal system and the site selection. For example, the duration of the periods when the potential exposure is the highest, the extent of the area that potentially can be affected by releases, and the viable use of potentially affected areas are aspects that are discussed in Chapter 9.

A site description of the present Laxemar is found in /SKB 2009/ but the landscape development at Laxemar is not presented in a separate report. Instead the landscape development of the Laxemar area, and identification and description of biosphere objects used in calculations of LDF's for Laxemar is presented in this appendix. The methodology used for identification of biosphere objects in Forsmark and Laxemar is identical (with the exception of hydrodynamic modelling, which is described below).

This appendix does not give a full description methodology or processes involved in landscape development, but cover instead the site-specific conditions and aspect used to model the landscape development of Laxemar. For thorough descriptions of the methodology and terminology regarding the modelling of landscape development (e.g. shoreline displacement and succession of ecosystems from marine to limnic to terrestrial), the reader is guided to the SR-Site reports for Forsmark /SKB 2010a, Lindborg 2010/. This appendix does not include a comparison between the sites, but is a report of the landscape development and of the site-specific conditions used to calculate the Laxemar LDF's. The comparison between Laxemar and Forsmark is given in Chapter 9.

A10.1 Topography and landscape development

The topography has an effect on many processes in the landscape, such as lake formation, groundwater hydrology, surface hydrology, sediment dynamics in the sea, and therefore also on dynamics of radionuclides. The topography of a landscape is often described with a digital elevation model (DEM). The DEM is constantly changing throughout in the glacial–interglacial cycle. Many processes control these changes such as the glacial isostatic adjustment (GIA) and the transport of sediments.

The future development of the Forsmark and Laxemar sites is modelled using the DEM together with a model of GIA, a coupled regolith model, and a model of the present and future streams. The modelling of the future landscape at Forsmark is thoroughly described in /Lindborg 2010/. The same methodology is used to model the future landscape development of Laxemar. Below follows a brief description of the modelling (whereas the description of the methodology is given in /Lindborg 2010/), i.e. the reader is guided to this report for an explanation of the use of different parameters and to get a general picture of the future landscape development. Herein the emphasis is on identification of differences in modelling between the sites, and a short description of the future landscape at Laxemar.

DEM

The DEM is a required input to most models describing the surface systems. A high accuracy of the DEM is therefore important for the accuracy of many different types of results produced within the surface modelling. The description of the DEM's for Laxemar is given in /Strömgren and Brydsten 2008/.

Glacial isostatic adjustment and relative sea level

Glacial isostatic adjustment (GIA) is the response of the solid earth to mass redistribution during a glacial cycle /Whitehouse 2009/. During glacial periods the ice sheets at higher latitudes grow and the relative sea level falls. The opposite occurs during interglacial periods, i.e. the ice sheets melt and the relative sea level rises. The relative sea level (RSL) is defined as the elevation of the contact between the ocean surface and land. The relative sea level has been modelled for a glacial cycle, i.e. 120,000 years applying the SR-Site Biosphere project assumptions that the next 120,000 years will be a repetition of the last 120,000 years (the Weichsel period). The RSL for this period at Forsmark is presented in /SKB 2010b/.

For Laxemar the RSL for the period was presented in /SKB 2006/. However, since then, an updated version of the RSL has been produced. The development of this updated RSL is described below.

The present RSL change rate in Laxemar is approximately 1 mm per year with a north-south gradient of c 0.5 mm 100 km^{-1} with increasing rate to the north /Freden 1994/. In /Påsse 2001/ there is a compilation of RSL data for Fennoscandia and one of the stations is located in Oskarshamn. /Påsse 2001/ also gives a method for transforming RSL data (altitude and age) into an equation that simplifies the use of the RSL in mathematical models.

The small increase in the RSL curve for Laxemar c –10,000 AD coincides with the first lacustrine phase of the Baltic, the Baltic Ice lake. The abrupt rise in of the RSL curve (c. –8600 AD) coincides with the second of the lacustrine phases of the Baltic, the Ancylus stage. During the Ancylus stage the eustatic part of the RSL equation is replaced by the RSL equation for the lake thresholds places /Påsse 2001/. In the beginning of the stage the lake outlet was at Degerfors and during the late stage through the Danish sounds the so called Darss Sill.

The Holocene RSL model can probably be extended into the future for a limited time period, but not longer than to the beginning of next glacial stage because only the remaining uplift after Weichsel is included in the equation. Future eustatic changes due to degradation of ice sheets (Greenland and West Antarctica) and the thermal expansion of seawater following global warming is not considered for Laxemar. For Forsmark this was considered in a special case, global warming case. In the base case, the model of future glacial stages presented in /Kjellström et al. 2009/ states that next glacial stage will begin at c 57,000 AD. In the same report, the RSL curve for Laxemar covering the complete Weichsel glacial cycle, is presented (the so called Whitehouse curve).

However, the curve from Whitehouse shows errors early in the period, while the Holocene curve has errors after c. 50,000 AD. For these reasons a combination of the two curves has been produced. The updated curve involves fixed RSL values of c 0 m at 2009 AD and 122,009 AD. The period from 110,500 AD to 122,000 AD (corresponding to 9500 BC – 2000 AD) is best represented by the RSL equation from 2001 since this is based on measured values /Påsse 2001/. The RSL equation does not involve parameters for the future glaciations, so for the period from the next glaciations to 110,500 AD, the Whitehouse curve provides the only data that are available, and thus, the values from Whitehouse curve are used for the period 20,000 – 110,500 AD. The Whitehouse curve is nearly constant at c 20,000 AD (at c 45 m). Finally, the period from 2000 AD to 20,000 AD is calculated with a change rate of –0.00122 m per year at 2000 AD and a subsequently decreasingchange rate to connect to –18 m at 20,000 AD, since there are no processes during that period that can cause an increasing RSL change rate under a constant climate. The updated RSL-curve is shown in Figure A10-1.

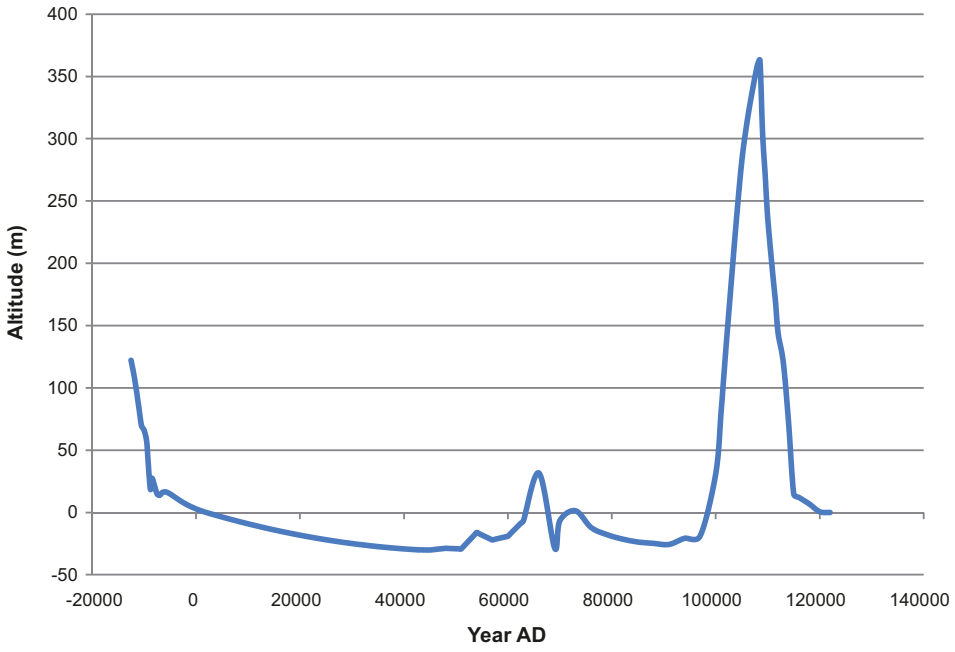

Figure A10-1. *The updated RSL curve for Laxemar for the next glacial-interglacial cycle.*

A coupled model for regolith-lake development

A coupled model for regolith-lake development (RLDM) has been constructed that can model the surface geology, stratigraphy, and thickness of different strata in the Forsmark area at any time during the studied glacial cycle /Brydsten and Strömgren 2010/. The same methodology was applied to the Laxemar area using the updated RSL curve for Laxemar (described above) and using a map of Quaternary deposits /Sohlenius and Hedenström 2008/ and a regolith depth model (RDM) for Laxemar /Nyman et al. 2008/.

Methods to model present and future streams

Essentially, the methodology employed for modelling present and future streams in Forsmark, as described in /Lindborg 2010/, is applied also to Laxemar. For both sites, most existing streams are mapped by walking along the streams with GPS equipment /Brunberg et al. 2004a, b, Carlsson et al. 2005a, b, Strömgren et al. 2006/. Remaining existing streams are copied from the official cadastral or terrain maps. Future streams are modelled with the ArcGis hydrological function using the DEM for 35,000 AD as input for Forsmark. For Laxemar, the DEM for 10,000 AD was used instead. Besides that, the methodology was identical.

Future landscape

Only three lakes are modelled in the study of Laxemar; the existing lake Frisksjön and the future lakes Inre Granholmsfjärden and Borholmsfjärden. All three lakes are (or will be) relatively deep and will be completely infilled in 13,000 to 24,000 years. The identification of biosphere objects and characteristics of those is further described in the next section.

A10.2 Identification and description of biosphere objects

Biosphere objects are areas with potential discharge of deep groundwater from the repository. The methodology for identifying biosphere objects in the landscape is the same for both sites. The derivation of biosphere objects for Forsmark is described in /Lindborg 2010/, where the terminology regarding landscape objects is described (e.g. geometries such as watersheds and sub-catchments, and processes connected with landscape development such as sedimentation and resuspension). The derivation of biosphere objects for Laxemar is described below, in which context the reader is referred to /Lindborg 2010/ for detailed descriptions and definitions. In order to identify biosphere objects, the landscape has to be partitioned into basins. Biosphere objects are then chosen as those basins that contain discharge exit points from the repository. Below follows a description of the identification of basins, discharge points, and resulting biosphere objects for the Laxemar area.

Delineation of basins in Laxemar

The Laxemar landscape is divided into basins /Brunberg et al. 2004b, Brydsten 2006/, as shown in Figure A10-2.

Each basin includes a single lake (existing or future), or one single wetland (possible a completely infilled lake). The basin is defined as the catchment of the outlet of the object minus the catchment of the outlet of the next upstream object. The extents of the basins were established by field mapping of the water divides in the land part of the model area /Brunberg et al. 2004b/, and by GIS modelling using the DEM for the water divides that presently are beneath the sea /Brydsten 2006/.

Lake basins are linked together by streams (Figure A10-3). The basins are grouped into three major branches: a northern branch with 8 basins (41% of the total area), a central branch with 8 basins (51% of the area) and a southern branch with 3 basins (8% of the area).

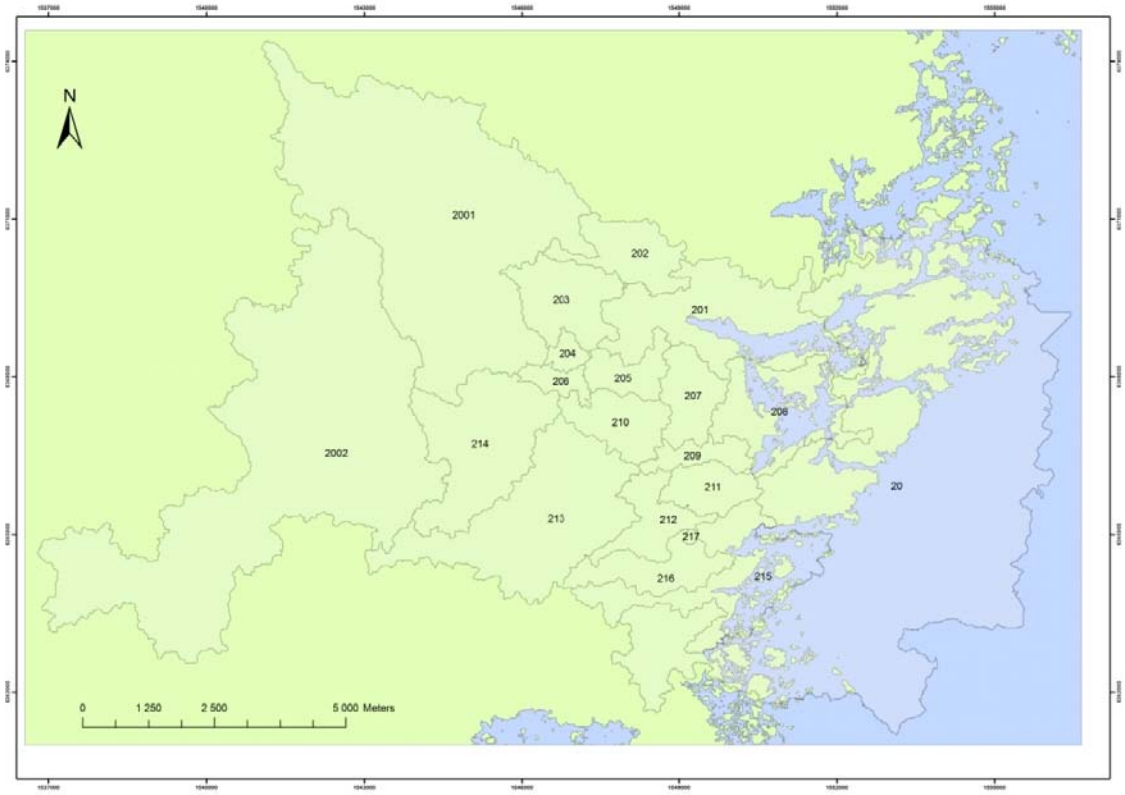

Figure A10-2. *Laxemar basins identified in /Brunberg et al. 2004b/ and /Brydsten 2006/.*

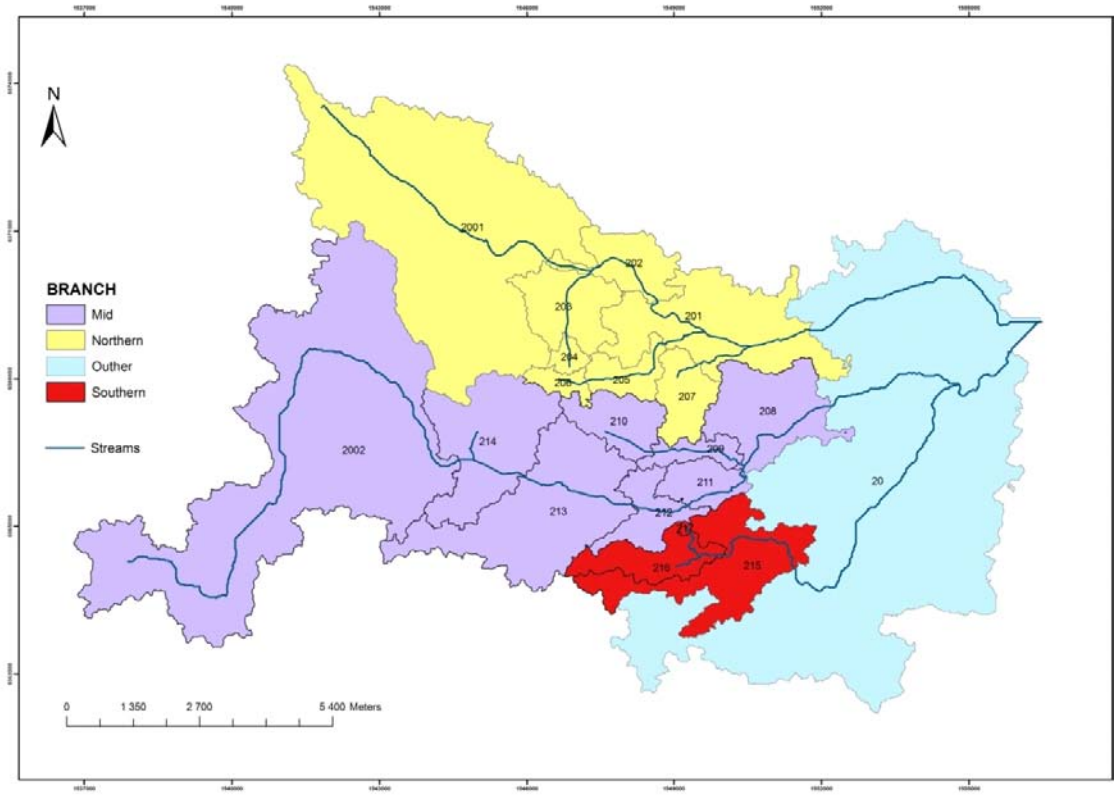

Figure A10-3. *The hydrological network in the landscape model area for Laxemar.*

Characteristics of discharge points

The hydrogeological model traces the transport of water by following "water parcels" or "particles" from each canister position within the repository volume through the bedrock and soils up to the ground surface, see /Joyce et al. 2010/ for details. The positions where the particle traces reach the surface are called "discharge points". The methodology to identify discharge points is the same for Laxemar as for Forsmark.

Discharge points have been used for the selection of basins treated in the landscape model. The data set holds c 40,000 records. Many of the traces never reach the surface and many enter the surface when the Laxemar area is covered by an ice sheet (at times later than 62,600 AD); these records are deleted from the data set. The number of records left after this deletion is 31,441. This methodology is cautious as it allows discharge also during permafrost conditions but is the same methodology as for Forsmark.

The spatial distribution of the discharge points of the regional model is shown in Figure A10-4. Most of the discharge points are found close to the repository and a minor fraction are displayed in a NE direction. The most distant discharge points are located approximately 10 km from the repository. The spatial distributions of discharge points on basins are shown in Table A10-1 and Table A10-2.

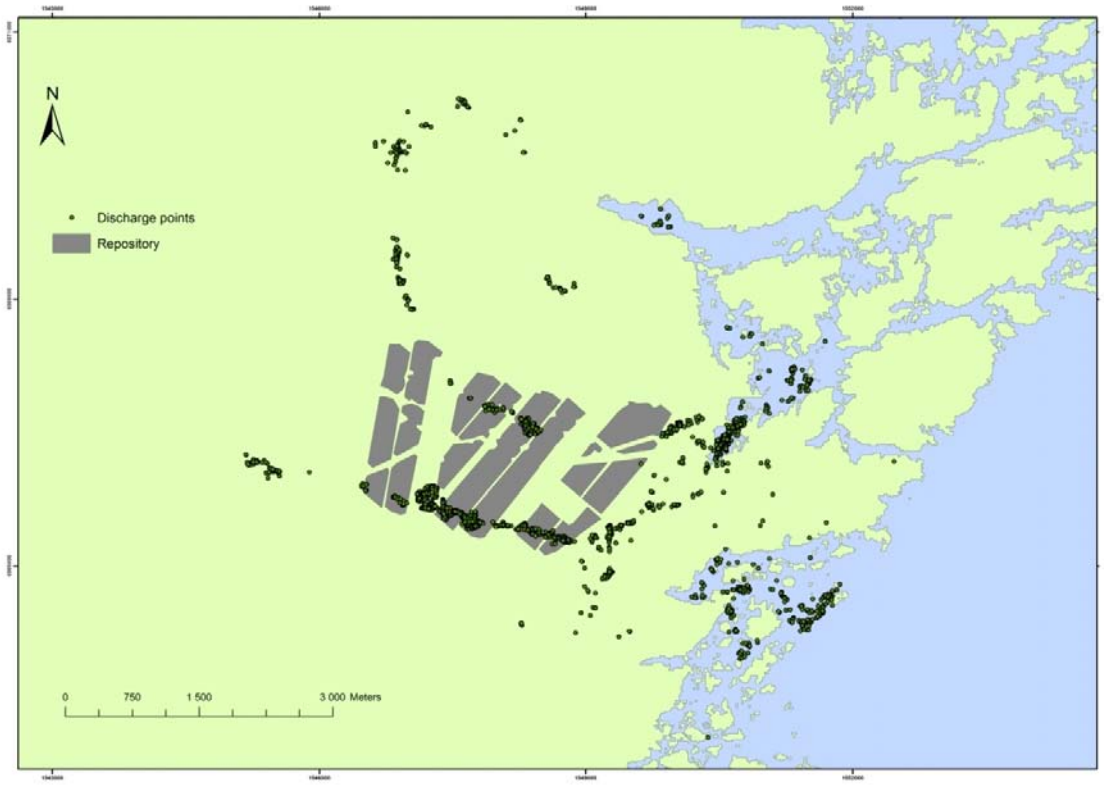

Figure A10-4. *Distribution of discharge points calculated using the hydrogeological model /Joyce et al. 2010/. The area of the proposed repository is marked with grey.*

Table A10-1. Discharge points in the northern, central and southern branches basins identified in the landscape modelling.

Branch	No. discharge points	%
Northern	1,336	4.2
Central	27,945	88.9
Southern	2,087	6.6
Other	73	0.2

Table A10-2. Number of discharge points by basin.

Basin	No. discharge points	%
20	73	0.2
201	82	0.3
202	42	0.1
203	238	0.8
204	787	2.5
205	132	0.4
206	31	0.1
207	24	0.1
208	6,095	19.4
209	1,972	6.3
210	1,863	5.9
211	2,249	7.2
212	2,962	9.4
213	12,590	40.0
214	214	0.7
215	1,046	3.3
216	109	0.3
217	932	3.0

The discharge locations are mostly situated at low-points in the landscape (groundwater discharge areas), but no more than c 20% of the points are situated in lakes (Table A10-3) of which almost all are situated in the future lake Borholmsfjärden. One explanation for this is that the three model lakes in this study are located far from the proposed repository volume.

Table A10-3. Number of discharge points in lakes and % of total number of points. The only lake with high number of discharge points is Borholmsfjärden.

Lake id	Lake	No. of discharge points	% of total
201	Inre Granholmsfjärden	65	0.2
207	Frisksjön	0	0.0
208	Borholmsfjärden	6,043	19.2

Resulting biosphere objects in the landscape model

In total there are 19 basins in the Laxemar landscape model (the Baltic Proper basin included, see Figure A10-2). Basins that are treated in the landscape model are only those significant for the biosphere radionuclide model. These are either basins that contain discharge exit points (“primary basins”) or basins that are receiving surface water from primary basins but do not contain discharge points(“secondary basins”). Basins without discharge points and that are placed upstream primary basins are designated “tertiary basins”.

In the Laxemar model area there are no secondary basins except the most downstream basin 2, which is the Baltic Proper (see Figure A10-5).

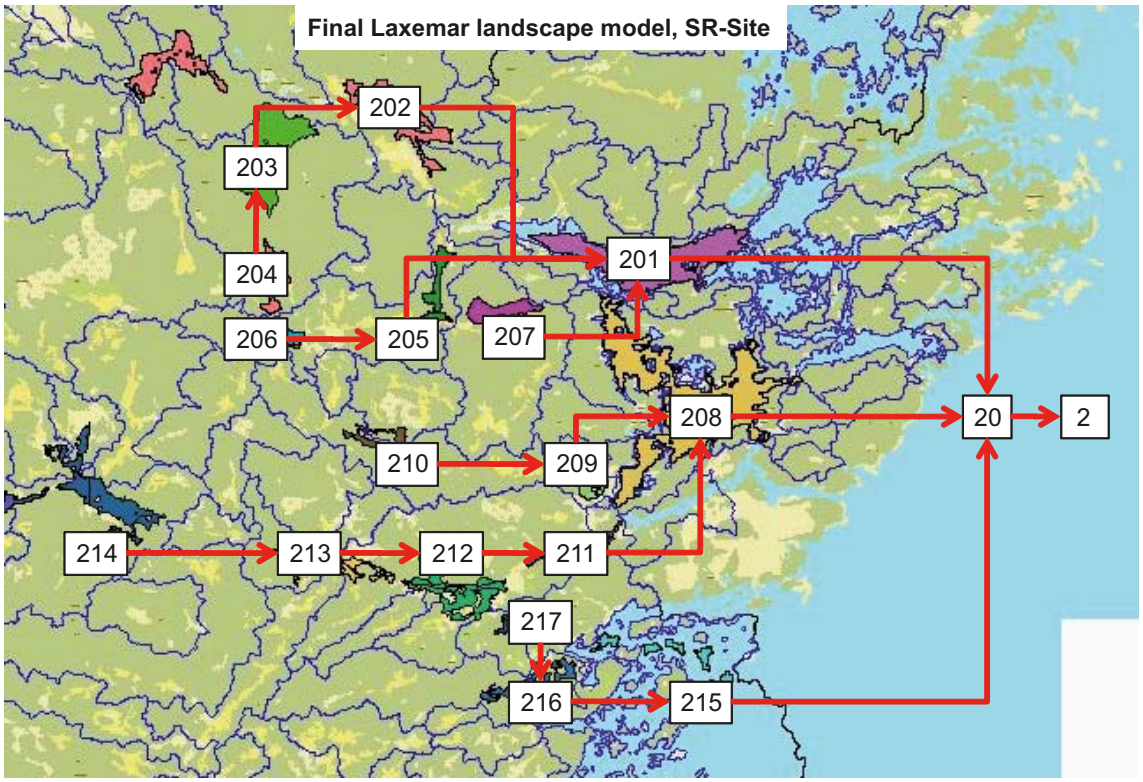

Figure A10-5. *Biosphere objects in Laxemar. Basin 216 and 217 is merged to one basin (216) in the modelling. Basins 201, 203, 206, 207, 208, 210, 211, 213, 214, and 215 are used in the calculation of LDF's for Laxemar.*

Due to the shore line displacement, objects originating as marine basins are transformed to lakes and terrestrial areas. Lake isolation is a gradual process because of the transient sea level changes. The methodology for calculating isolation times for the Laxemar area is the same as used for Forsmark /Lindborg 2010/. The sea level at Laxemar is monitored at several places, but for the present assessment data from Kungsholms Fort (1887–1983), situated to the south of the model area, are judged to best represent the whole model area.

The lowest recorded level at Kungsholms Fort is –0.94 m (adjusted for shore line displacement to the national elevation system RH70) and the highest recorded level is +1.33 m /Sjöfartsverket 1992/. With the present shore line displacement rate (0.100 mm per year), a lake isolation period will be c 2,300 years. This means that it will take 2,300 years from the first time the lake is isolated from the sea at an extremely low sea level until the last time when brackish water is flowing into the lake at an extremely high sea level.

Assuming that these extreme sea levels are constant over time, it is possible to use the shore line displacement equation to calculate the isolation period for each lake (existing and future, Figure A10-4) Since the shore line displacement rate in the Laxemar area has been continuously decreasing during the Holocene, the lake isolation durations are shorter for higher situated lakes. For objects without a lake stage, i.e. those forming streams and wetlands directly from marine basins, the same length of the isolation period as for Frisksjön has been used in the modelling.

Only one lake or wetland in each basin is treated in the landscape model. The extension of the only existing lake (Frisksjön) is mapped in the field /Brunberg et.al. 2004b/. The extensions of future lakes are modelled with GIS using the DEM /Brydsten 2006/.

Seven biosphere objects in Laxemar were excluded from calculations deriving LDF's. The transition from the marine to the terrestrial stage without passing through a lake stage is not handled optimally in the model. Thus, for some objects the transition time is not adequately described. Therefore it was chosen to calculate LDF's for the ten objects where there is a realistic description of the transforma-

tion between the marine and terrestrial stages. These objects are distributed within the model area and cover a wide range of sizes, and are therefore a relevant representation of possible biosphere objects at the Laxemar site. The calculations of LDF's are based on objects 201, 203, 206, 207, 208, 210, 211, 213, 214, and 215.

Characteristics of the objects, such as isolation times from marine to terrestrial/limnic stages, altitudes, and geometries of the lakes are found in Table A10-4 to Table A10-7. A number of parameter values (e.g. geometries and regolith depths) for a number of time steps for each biosphere object are obtained using the DEM and the RLDM. The parameter values are stored at /SKBdoc 1263189/.

Table A10-4. Summary of significant dates for lakes treated in the landscape model. The Start parameter is the date of the earliest time that the lake is isolated from the sea, the Isolation parameter is the date when the lake threshold is at the mean sea level and the Stop parameter is the last date when brackish water flows into to the lake. The Ter-parameters are dates for successive lake infilling values where Ter 100% is the date when a wetland is fully developed.

Object id	Name	Start (AD)	Isolation (AD)	Stop (AD)	Ter 50% (AD)	Ter 75% (AD)	Ter 100% (AD)
201_1	Inre Granholmsfjärden	3610	5040	6225	8200	11,600	29,200
207_1	Frisksjön	–1080	–380	170	3800	5900	14,600
208_1	Borholmsfjärden	1450	2490	3340	5000	7300	16,100

Table A10-5. Physical characteristics of lakes used in the landscape model.

Object id	207_1	201_1	208_1
Name	Frisksjön	Inre Granholmsfjärden	Borholmsfjärden
Area (m^2)	126,432	592,000	1,083,344
Altitude RH70 (m)	3.54	–3.24	–0.64
Mean depth (m)	3.77	4.58	1.47
Max depth (m)	4.83	14.83	7.38
Volume (m^3)	495,653	2,711,360	1,599,360

Table A10-6. Characteristic values for the basins used in the landscape model. The First land parameter is the first date for the basin to hold land and the Last Sea parameter is the last date for sea within the basin(see figures above for maps of basins and biosphere objects).

Object id	Branch	First Land (AD)	Last Sea (AD)	Max Alt. (masl)	Min Alt. (masl)
20	Other	–8670	> 30,000	17.92	–44.70
201	Northern	–8830	5170	21.00	–3.30
202	Northern	–8990	–510	27.92	3.78
203	Northern	–8920	–1540	24.40	5.83
204	Northern	–8920	–3550	24.57	10.83
205	Northern	–8950	–1900	25.80	6.61
206	Northern	–9050	–4060	30.83	12.28
207	Northern	–8940	–380	25.49	3.54
208	Central	–8860	2500	21.88	–0.65
209	Central	–8880	1910	23.37	0.07
210	Central	–9030	–4320	29.69	13.04
211	Central	–8820	2100	20.73	–0.17
212	Central	–8620	–450	21.15	3.67
213	Central	–9160	–1740	37.95	6.26
214	Central	–9100	–2900	33.29	9.05
215	Southern	–8810	17,620	20.30	–9.29
216	Southern	–8890	1370	23.33	0.79
217	Southern	–7630	–1790	16.61	6.38
2001	Northern	–9340	–1540	48.23	5.83
2002	Central	–9645	–3020	62.88	9.37

Table A10-7. Characteristics of the biosphere objects that develop from marine to terrestrial (with stream) objects without passing a lake stage.

Object id	Name	Area (m²)	Comment	Altitude (m)	Hydrology
202_1	Gässhult	270,800	Modelled	5.3	Kärrviksån
203_1	Gäster	368,251	Property map	5.8	Kärrviksån
204_1	Brandegöl	94,400	Modelled	10.8	Kärrviksån
205_1	Olofskärr	88,800	Modelled	6.6	Mederhultsån
206_1	Marstrand	78,400	Modelled	12.3	Mederhultsån
209_1	Rågängarna	92,800	Modelled	2.4	Ekerumsån
210_1	Skettkärret	115,762	Modelled	13.0	Ekerumsån
211_1	Röängen	58,105	Modelled	2.9	Laxemarån
212_1	Bredängen	216,984	Modelled	6.9	Laxemarån
213_1	Klotängen	136,016	Property map	6.4	Laxemarån
214_1	Västregård	293,961	Modelled	9.7	Laxemarån
215_1	Storesund	109,600	Modelled	–6.2	Glostadsbäcken
216_1	Glostad	98,786	Modelled	1.8	Glostadsbäcken
217_1	Svartekärret	12,800	Modelled	6.6	Glostadsbäcken

A10.3 Differences in hydrodynamic modelling used as input to LDF calculations

The same methodology has been used in the biosphere modelling for Laxemar as for Forsmark. However, some differences in methodology to derive input parameter values for LDF calculations exist, e.g. in the hydrodynamic modelling of the water residence times of the sea basins. The realism of both methods are similar and the differences will have small impact on LDF's since it is generally the terrestrial objects that determine the LDF. Nevertheless, a brief description of the differences between the sites in methodology to derive hydrological retention times is presented below.

Differences in hydrodynamic modelling

Hydrodynamic models have been applied to estimate the residence times of the water in the marine basins in Forsmark and Laxemar during an interglacial /Karlsson et al. 2010, Engqvist 2010/. The residence time (here calculated as the average age of a water parcel, AvA days) is an important input parameter in the radionuclide transport modelling. It was calculated for a time span representing a landscape development of the regional model area from completely submerged stage to a terrestrial stage with lakes. In the Forsmark modelling, the AvA days-parameter was calculated for 13 years representative of various landscape stages between 6500 BC and 9000 AD. For each of the 13 years during the period, a hydrodynamic model was run for one year using the same external forcing from the atmosphere, the surrounding sea, and the runoff from land. The difference between the years was the bathymetry, as determined from /Brydsten 2006/.

The method for calculating the residence time parameter for Laxemar was basically the same; calculations were made for the time span 3000 BC to 9000 AD, for 13 representative years, using the same forcing of the model. However, instead of the high-resolution three-dimensional model used for Forsmark, a numerical two-dimensional model, computing the AvA days for a set of discrete hydraulically coupled basins, was used /Engqvist 2010/. In addition to having a higher spatial resolution, the three-dimensional model calculates gradients within a basin, while the two-dimensional basin model calculates gradients in between basins. It has been shown that the realism of these two methods is similar /Engqvist and Stenström 2004, Engqvist et al. 2006/. The resulting AvA days values for Laxemar and Forsmark are presented in /Engqvist 2010, Karlsson et al. 2010/.

References A10.4

SKB's (Svensk Kärnbränslehantering AB) publications can be found at www.skb.se/publications.

Brunberg A-K, Carlsson T, Blomqvist P, Brydsten L, Strömgen M, 2004a. Identification of catchments, lake-related drainage parameters and lake habitats. Forsmark site investigation. SKB P-04-25, Svensk Kärnbränslehantering AB.

Brunberg A-K, Carlsson T, Brydsten L, Strömgren M, 2004b. Identification of catchments, lake-related drainage parameters and lake habitats. Oskarshamn site investigation. SKB P-04-242, Svensk Kärnbränslehantering AB.

Brydsten L, 2006. A model for landscape development in terms of shoreline displacement, sediment dynamics, lake formation, and lake choke-up processes. SKB TR-06-40, Svensk Kärnbränslehantering AB.

Brydsten L, Strömgren M, 2010. A coupled regolith-lake development model applied to the Forsmark site. TR-10-56, Svensk Kärnbränslehantering AB.

Carlsson T, Brunberg A-K, Brydsten L, Strömgren M, 2005a. Characterisation of running waters, including vegetation, substrate and technical encroachments. Oskarshamn site investigation. SKB P-05-40, Svensk Kärnbränslehantering AB.

Carlsson T, Brunberg A-K, Brydsten L, Strömgren M, 2005b. Characterisation of running waters, including vegetation, substrate and technical encroachments. Forsmark site investigation. SKB P-05-150, Svensk Kärnbränslehantering AB.

Engqvist A, 2010. Estimation of residence times (Average Age) of coastal basins in the Laxemar-Simpevarp coastal area for one-year physical forcing cycles equitemporally interspersed between 3000 BC and 9000 AD employing a coupled discrete basins numerical model. SKB R-10-57, Svensk Kärnbränslehantering AB.

Engqvist A, Stenström P, 2004. Archipelago strait exchange processes – an overview. Deep Sea Research II: Topical Studies in Oceanography, 51, 371–392.

Engqvist A, Stenström P, Pierce K, 2006. Modelling the effects of a pumping program for increasing water circulation in a semi-enclosed bay in the Stockholm archipelago. In: Spaulding M (ed). Proceedings of the 9th International Conference on Estuarine and Coastal Modeling, Charleston, South Carolina, 31 October–2 November 2005. New York: American Society of Civil Engineers, pp 253–269.

Freden C (ed), 1994. Sveriges nationalatlas. Berg och jord. Högnäs: Bra böcker (in Swedish).

Joyce S, Simpson T, Hartley L, Applegate D, Hoek J, Jackson P, Roberts D, Swan D, Gylling B, Marsic N, Rhén I, 2010. Groundwater flow modelling of periods with temperate climate conditions – Laxemar. SKB R-09-24, Svensk Kärnbränslehantering AB.

Karlsson A, Eriksson C, Borell Lövstedt C, Liungman O, Engqvist A, 2010. High-resolution hydrodynamic modelling of the marine environment at Forsmark between 6500 BC and 9000 AD. SKB R-10-09, Svensk Kärnbränslehantering AB.

Kjellström E, Strandberg G, Brandefelt J, Näslund J-O, Smith B, Wohlfarth B, 2009. Climate conditions in Sweden in a 100,000-year time perspective. SKB TR-09-04, Svensk Kärnbränslehantering AB.

Lindborg T (ed), 2010. Landscape Forsmark – data, methodology and results for SR-Site. SKB TR-10-05, Svensk Kärnbränslehantering AB.

Nyman H, Sohlenius G, Strömgren M, Brydsten L, 2008. Depth and stratigraphy of regolith. Site descriptive modelling, SDM-Site Laxemar. SKB R-08-06, Svensk Kärnbränslehantering AB.

Påsse T, 2001. An empirical model of glacio-isostatic movements and shore-level displacement in Fennoscandia. SKB R-01-41, Svensk Kärnbränslehantering AB.

Sjöfartsverket, 1992. Svensk lots. D. A, Allmänna upplysningar. Norrköping: Sjöfartsverket (in Swedish).

SKB, 2006. Climate and climate-related issues for the safety assessment SR-Can. SKB TR-06-23, Svensk Kärnbränslehantering AB.

SKB, 2009. Site description of Laxemar at completion of the site investigation phase. SDM-Site Laxemar. SKB TR-09-01, Svensk Kärnbränslehantering AB.

SKB, 2010a. Biosphere analyses for the safety assessment SR-Site – synthesis and summary of results. SKB TR-10-09, Svensk Kärnbränslehantering AB.

SKB, 2010b. Climate and climate-related issues for the safety assessment SR-Site. SKB TR-10-49, Svensk Kärnbränslehantering AB.

Sohlenius G, Hedenström A, 2008. Description of regolith at Laxemar-Simpevarp. Site descriptive modelling, SDM-Site Laxemar. SKB R-08-05, Svensk Kärnbränslehantering AB.

Strömgren M, Brydsten L, 2008. Digital elevation models of Laxemar-Simpevarp. SDM-Site Laxemar. SKB R-08-63, Svensk Kärnbränslehantering AB.

Strömgren M, Brydsten L, Lindgren F, 2006. Measurements of brook gradients. Oskarshamn site investigation. SKB P-06-05, Svensk Kärnbränslehantering AB.

Whitehouse P, 2009. Glacial isostatic adjustment and sea-level change. State of the art report. SKB TR-09-11, Svensk Kärnbränslehantering AB.